Research Performance Progress Report (RPPR)

Project Title:	"Baseload Nitrate Salt Central Receiver Power Plant Design"
Project Period:	9/1/10 – 9/30/14
Project Budget:	$6,649,331
Submission Date:	10/31/14
Recipient:	Abengoa Solar LLC
Address:	1250 Simms St Unit 101
	Lakewood, CO 80401
Award Number:	DE-EE0003596
Project Team:	Tietronix
	Foster Wheeler
	Sandia National Lab
Contacts:	Drake Tilley
	Project Manager
	Phone: 303-323-9489
	Email: drake.tilley@solar.abengoa.com
	Bruce Kelly
	Technical Lead
	Email: bruce.kelly@solar.abengoa.com

Executive Summary:

The objectives of the work were to demonstrate that a 100 MWe central receiver plant, using nitrate salt as the receiver coolant, thermal storage medium, and heat transport fluid in the steam generator, can 1) operate, at full load, for 6,400 hours each year using only solar energy, and 2) satisfy the DOE levelized energy cost goal of $0.09/kWhe (real 2009 $). To achieve these objectives the work incorporated a large range of tasks relating to many different aspects of a molten salt tower plant.

The first Phase of the project focused on developing a baseline design for a Molten Salt Tower and validating areas for improvement. Tasks included a market study, receiver design, heat exchanger design, preliminary heliostat design, solar field optimization, baseline system design including PFDs and P&IDs and detailed cost estimate. The baseline plant met the initial goal of less than $0.14/kWhe, and reinforced the need to reduce costs in several key areas to reach the overall $0.09/kWhe goal. The major improvements identified from Phase I were: 1) higher temperature salt to improve cycle efficiency and reduce storage requirements, 2) an improved receiver coating to increase the efficiency of the receiver, 3) a large receiver design to maximize storage and meet the baseload hours objective, and 4) lower cost heliostat field.

The second Phase of the project looked at advancing the baseline tower with the identified improvements and included key prototypes. To validate increasing the standard solar salt temperature to 600 ˚C a dynamic test was conducted at Sandia. The results ultimately proved the hypothesis incorrect and showed high oxide production and corrosion rates. The results lead to further testing of systems to mitigate the oxide production to be able to increase the salt temperature for a commercial plant.

Foster Wheeler worked on the receiver design in both Phase I and Phase II looking at both design and lowering costs utilizing commercial fossil boiler manufacturing. The cost and design goals for the project were met with this task, but the most interesting results had to do with defining the failure modes and looking at a “shakedown analysis” of the combined creep-fatigue failure. A separate task also looked at improving the absorber coatings on the receiver tubes that would improve the efficiency of the receiver. Significant progress was made on developing a novel paint with a high absorptivity that was on par with the current Pyromark, but shows additional potential to be optimized further. Although the coating did not meet the emissivity goals, preliminary testing the new paint shows potential to be much more durable, and potential to improve the receiver efficiency through a higher average absorptivity over the lifetime. Additional coatings were also designed and modeled results meet the project goals, but were not tested. Testing for low cycle fatigue of the full length receiver tubes was designed and constructed, but is still currently undergoing testing.

A novel small heliostat was developed through an extensive brainstorming and down select. The concept was then detailed further with inputs from component testing and eventually a full prototype was built and tested. This task met or exceeded the accuracy and structure goals and also beat the cost goal. This provides a significant solar field costs savings for Abengoa that will be developed further to be used in future commercial plants. Ultimately the $0.09/kWhe (real 2009 $) and 6,400 hours goals of the project were met.

Table of Contents

Background:

Molten Salt Tower technology has been around for over 30 years. One of the first molten salt demonstrations in the mid-1980s was the Category B experiment, which included the design, fabrication, and operation of a 5 MWt salt cavity in Albuquerque and ran for about 1 year. The second was the Molten Salt Electric Experiment, also in Albuquerque, that included a 5 MWt salt cavity receiver, a 3 MWt salt steam generator, and a 750 kWe steam turbine and also ran for about 1 year. Much of the equipment selection and arrangement at Solar Two was based on the results of the Molten Salt Electric Experiment. Solar Two was a 10 MWe molten salt tower which started operation in 1996 and ran for 3 years. Abengoa has an active development program in nitrate salt technology, including the development of the 115 MWe Atacama 1 project in Chile, the design and operation of the 5 MWt nitrate salt receiver and steam generator for the CRS Sales R&D project in Seville, and several corrosion studies of stainless steel and nickel alloys in nitrate salt at temperatures in the range of 600 to 625 ˚C. In parallel, a wide range of international organizations are also developing systems and components for salt tower technology. Examples include the following: DLR – Advanced receiver designs, using bayonet tubes with annular liquid flows, and enhanced dry cooling systems for heat rejection; Sandia – Nitrate salt corrosion studies of aluminized stainless steels, the development of reliable pressure and flow instruments for high temperature salt service, and the verification of heliostat tracking error correction algorithms; NREL – Electric grid stability and economic assessments of the value of thermal storage to utilities in the Southwest United States; Indian Institute of Science – Studies of trans- and supercritical steam and CO_2 power conversion cycles; CNRS – Development of high temperature selective surface coatings for absorber tubes; Bertrams-Heatec – Development of advanced nitrate salt steam generators, with high allowable rates of temperature change.

Introduction:

The aim of this project was to build on previous molten salt tower efforts such as Solar Two and develop a current baseline molten salt tower and then advance the technology for a cost competitive solar thermal plant with storage. The project was been set up to include all major aspects of a molten salt tower in order to realize system improvements rather than just optimization of one component. The major improvements identified from Phase I were: 1) higher temperature salt to improve cycle efficiency and reduce storage requirements, 2) an improved receiver coating to increase the efficiency of the receiver, 3) a large receiver design to maximized storage and incorporate items 1 and 2, and 4) lower cost heliostat field. Phase II was set up to tackle these improvements and provide verification through testing and prototypes.

The final deliverables for the project were the following:

1) Develop, prototype, and test an advanced heliostat to achieve a 30 percent solar field cost reduction over the baseline design to reach a $121/m^2 cost target and demonstrate system efficiency benefits of close-packed field and improved optical reflector surface that additionally reduces the cost by an effective $10/m^2.

2) Increase the receiver outlet temperature to 600 °C, which allows a 1.1 percentage point improvement in annual net Rankine cycle efficiency to 41.0 percent (at a condenser pressure of 170 mbar) relative to baseline cycle efficiency of 39.9 percent, and a 15 percent reduction in unit thermal storage mass per MWhe, relative to the baseline of 25,200 kg/MWhe.

3) Develop an advanced receiver selective surface, which demonstrates a thermal efficiency of 92 percent at 600 °C, a 4 percentage point improvement in receiver thermal efficiency, relative to baseline receiver efficiency of 88 percent at an outlet temperature of 600 °C with Pyromark.

4) Conduct salt thermal stability tests, which will provide the corrosion data on which to base a commercial plant design. Publish corrosion data in the open literature.

5) Validate receiver design meets requirements for a 30 year plant lifetime.

6) Report of the Advanced Plant capital cost estimate and the LCOE analysis using Abengoa commercial financial parameters.

Project Results and Discussion:

Phase I

Phase I of the project was focused on developing a current baseline design for a Molten Salt Tower and validating areas for improvement. Tasks included a market study, receiver design, preliminary heliostat design, solar field optimization, baseline system design and cost estimate. Phase I set a baseline for measuring improvements to be made in Phase II and did not identify any technical barriers to advancements proposed in Phase II. The baseline design showed an LCOE below $0.14/kWhe for a 100 MW net plant with 6 hours of storage.

Phase II

Task 2.1 – Advanced Receiver Design

The receiver was designed to meet the criteria defined in the Receiver Specification. The key design basis parameters include:

- **Coolant** Nitrate salt; 60 percent $NaNO_3$ and 40 percent KNO_3 (by wt.)
- **Process Temperatures** 308 °C inlet and 600 °C outlet
- **Process Flow Rate** 1,790 kg/sec
- **Thermal Duty** 795 MWt
- **Design Point Radiation** 950 W/m^2 at noon on the vernal equinox
- **Peak Incident Heat Flux** 1,287 kW/m^2
- **Design Life** 30 years
- **Ambient Temperature** 25^{o}C (for heat loss calculations)
- **Wind Velocity** 17.9 m/sec (for heat loss calculations)

40.2 m/sec (for structural design)

- **Seismic** 0.30 g

The solar receiver consists of 24 tube panels located at the top of and positioned along the outside circumference (external arrangement) of a tower. Each panel consists of 56 tubes that are 40.9 mm in outside diameter, have an average wall thickness of 1.65 mm, and are longitudinally welded together to form a 2.29 m wide flat panel. The tubes have an effective heat transfer length of 22.6 m and are supported on their back side by 3 equally spaced buckstays. Jumper tubes provided at the top and bottom connect the panel to flow distribution headers and provide flexibility for thermal expansion; when assembled the top header to bottom header centerline spacing is 29.9 m. The tubes receive high solar fluxes and are therefore furnished in Haynes 230, as this material has excellent creep to rupture properties and is resistant to nitrate salt corrosion and stress corrosion cracking. An isometric view of the receiver is shown Figure 1

Figure 1 Isometric View of the Receiver

Circuit Flow Arrangement

In the Phase I study, several potential flow arrangements were considered. Tube diameters were selected to maintain a nominal 4 m/s salt velocity for a high heat transfer rate, and there was a cross-over from East Pass to West Pass, and West Pass to East Pass, to minimize the variation in the thermal inputs to each circuit in the morning and in the afternoon. The preferred arrangement used 45.7 mm tubes, with eight (8) panels in series and two (2) parallel flow paths.

For Phase II, the starting point for the design was to use the same approach selected in Phase I. Limiting the panel width to ~3 m for shipping purposes would require a minimum of 18 panels for the selected receiver diameter. The number of panels per circuit would thereby increase form the Phase I value of 8 to a new value of 9. Average salt velocity through the panels also increased to ~4.7 m/sec and the resulting total pressure loss was greater than 28 bar. Velocities greater than 4 m/sec can lead to high erosion losses, and an inlet pressure greater than 25 bar can result in tube hoop stresses exceeding ASME allowable values. As such, it was decided to increase the number of panels to 24. The flow arrangement consisted of 4 independently controlled circuits, with 6 panels per circuit, as illustrated in Figure 2.

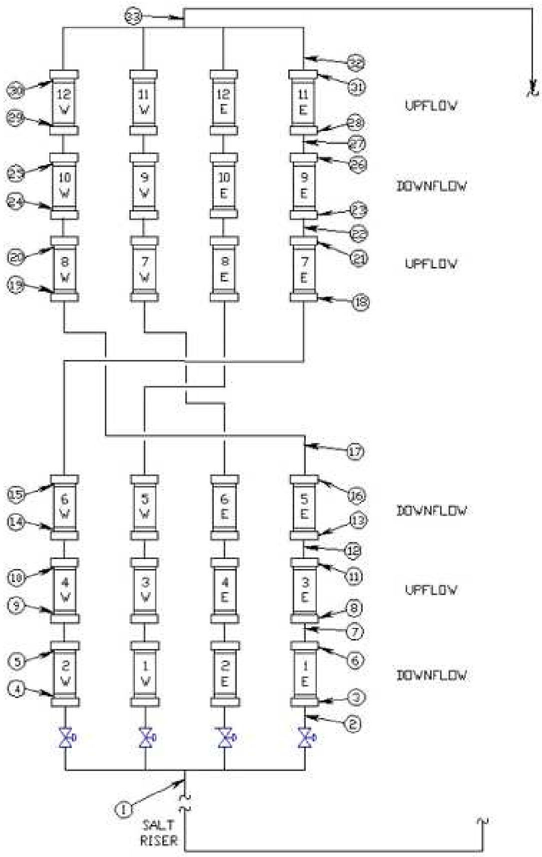

Figure 2 Receiver Circuit Arrangement

Thermal Efficiency

The incident heat flux maps have each panel divided into a grid of 96 nodes. An iterative calculation was performed to match the assumed and the computed incident and absorbed heat fluxes for each node based on the computed tube surface temperature. Receiver losses were based on the following parameters:

- Ambient temperature 25 ^{o}C
- Wind velocity 17.9 m/sec

- Receiver surface emissivity Table 1
- Receiver surface reflectivity 0.0388
- Convection losses Table 2

Table 1 Tube Coating Emissivity as a Function of Coating Temperature

Temp (°C)	Emissivity
0	0.2688
50	0.2737
100	0.2802
150	0.2886
200	0.2991
250	0.3118
300	0.3266
350	0.3434
400	0.3619
450	0.382
500	0.4033
550	0.4256
600	0.4486

Table 2 Receiver External Forced and Natural Convection Coefficients

CONVECTION HEAT LOSS	
NATURAL CONVECTION COEFFICIENT CHURCHILL & CHU CORRELATION (1975) For the heat transfer coefficient calculation based on natural convection with turbulent external flow on a flat vertical surface	$Nu_{nc} = \frac{h_{nc}L}{k} = \left[0.825 + \frac{0.387Ra^{1/6}}{\left[1 + \left(\frac{0.492}{Pr}\right)^{9/16}\right]^{8/27}}\right]^2$
FORCED CONVECTION COEFFICIENT SOURCE UNKNOWN	$Nu_{fc} = \frac{h_{fc}D}{k} = 0.0266Re^{0.805}Pr^{1/3}$
MIXED CONVECTION COEFFICIENT SANDIA REPORT: SAND84-8717 (1984)	$h = \left(h_{fc}^{3.2} + h_{nc}^{3.2}\right)^{1/3.2}$

The optical properties of the absorptive coating are based on a coating applied by plasma deposition. It is assumed that vacuum deposition machines, normally used for applying a coating to a continuous sheet of stainless steel, can be modified to handle a round, rather than a flat, geometry. For sheet application, the supply roll is outside the vacuum chamber, as is the take-up roll. Sliding seals, between the moving sheet and the stationary machine, are available to isolate the vacuum chamber from the ambient. The sliding seals would be modified to handle the round tube geometry.

The maximum efficiency for all of the cases analyzed was on Day 154 at 10:00 am.

- Total incident power 870 MWt
- Total absorbed power 795 MWt
- Receiver thermal efficiency 91.36 percent

Combined Creep-Fatigue Analysis

During normal operation, the crown of the receiver tubes experience temperatures sufficiently high to be within the material creep regime. Further, due the cyclic nature of the receiver, fatigue life is also a principal design consideration. The receiver must be designed in such a fashion as to survive a combination of creep damage and fatigue damage.

An additional challenge has been the lack of detailed material data required to solve creep-fatigue problems. Very limited data are available for Haynes 230 alloy on creep-fatigue interaction, traditionally used to design pressure parts using ASME Section III, Division 1, Subsection NH methods.

After consultation with experts in the field, Foster Wheeler employed an alternate method, which is a simplification of the method described in a paper entitled, “Application of Shakedown Analysis to Evaluation of Creep-Fatigue Limits”, by Peter Carter (Stress Engineering Services Inc.). This evaluation method may be summarized as follows:

1. Define a temperature-dependent “pseudo” yield stress. Pseudo yield stress is the lesser of 1) the tabulated yield stress and 2) the stress to cause rupture, due to creep, in the time of interest.
2. Use the pseudo yield stress, instead of the actual yield stress, for finite element analysis.
3. Use an elastic-perfectly plastic material model in the finite element analysis.
4. Perform cyclic elastic-plastic analysis to demonstrate shakedown. Shakedown refers to the achievement of cyclic elastic behavior in the material based on the pseudo yield stress.

If shakedown is achieved in the finite element analyses using the pseudo yield stress and elastic-perfectly plastic material model, it can be concluded that the real cyclic rupture time is greater than the selected time. Application of these methods, for the single receiver tube model, resulted in the conclusion that the receiver tubes will meet the design life criteria.

Stress to rupture was calculated using the Modified Power Law method, as presented by M. Katcher, et. al. [1]. The calculated stress value was multiplied by 0.67, where 0.67 is the safety factor used by ASME.

For temperatures of 1,100 ˚F and below, the yield stress for Haynes 230, as per ASME Section 2, is lower than the stress to rupture. The resultant pseudo yield stress is tabulated in Table 3 below.

Table 3 Pseudo Yield Strength of Haynes 230 (1000 psi)

Temperature (F)	Design Life		
	44,000 hrs (10 yrs)	88,000 hrs (20 yrs)	132,000 hrs (30 yrs)
100	31.30	31.30	31.30
500	31.30	31.30	31.30
1100	31.30	31.30	31.30
1125	29.66	28.17	27.33
1150	24.28	22.71	21.84
1175	19.84	18.27	17.40
1200	16.52	15.00	14.18
1225	14.25	12.82	12.06
1250	12.77	11.45	10.74
1275	11.78	10.56	9.91
1300	11.01	9.90	9.30
1325	10.31	9.31	8.77
1350	9.62	8.72	8.23

It is assumed that the solar receiver will be in operation for 12 hours a day. Consequently, 30 years of operation results in approximately 132,000 hours of operation.

A load cycle was constructed of two simple steps:

1. Operating load: Deadweight of metal and salt, internal pressure, and thermal load
2. Shutdown load: Dead weight of metal only; i.e., the receiver is drained.

Considering one start up and one shut down per day, a 30 year design life would mean 10,950 full cycles in total. This does not account for partial cycles encountered due to cloud cover. A conservative assumption of 3 full cycles per day to account for cloud cover, and any other transient situation, will result in approximately 33,000 cycles during a 30 year design life.

Figure 3 shows plots of the maximum plastic strain versus the number of load cycles. Strain values associated with only the operating load are plotted for clarity. It can be seen that in all the cases, plastic strain increases for the initial few cycles. However, after a relatively small number of cycles, no increase in plastic strain is seen between consecutive cycles. Shakedown is reached in all cases in less than 60 cycles.

Equivalent strain ranges were calculated as per ASME Sec III, Division 1, Subsection NH – Non Mandatory Appendix T – Paragraph T-1414: Equation for Equivalent Strain Range.

Fatigue lives of the receiver tubes were calculated based on the fatigue curves for Haynes 230, as presented in Figure 4.

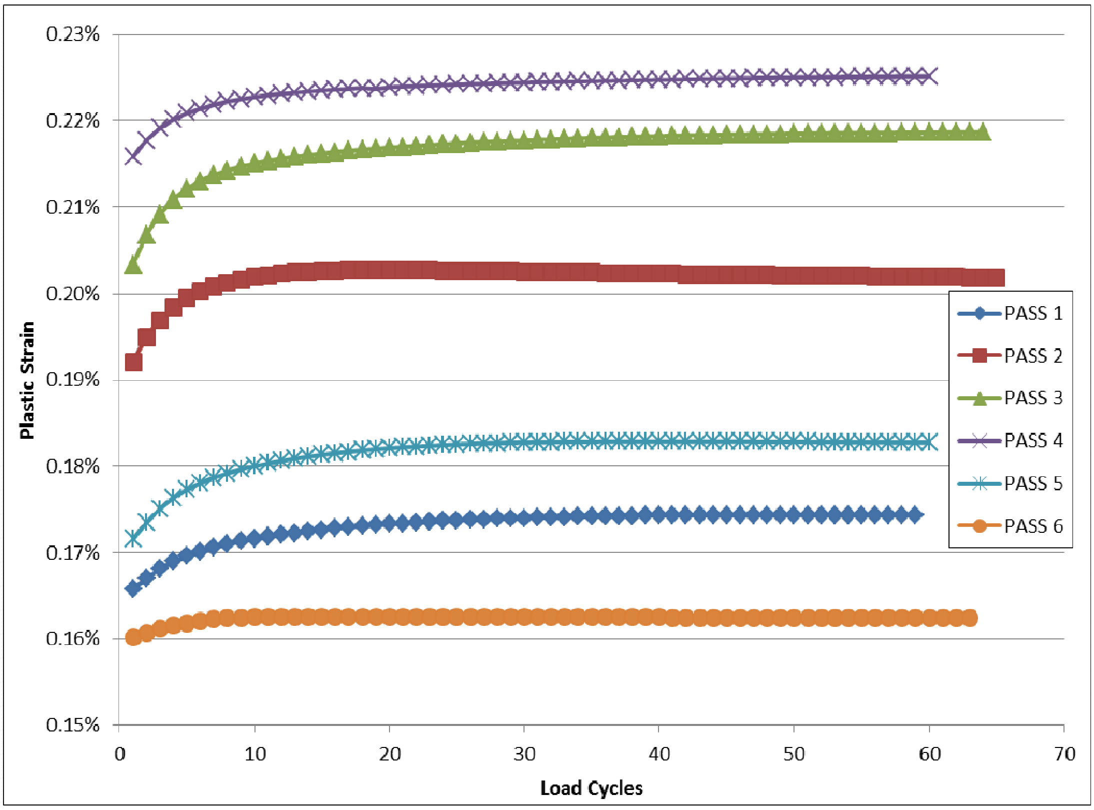

Figure 3 Maximum Plastic Strain versus Load Cycles at Various Panel Locations

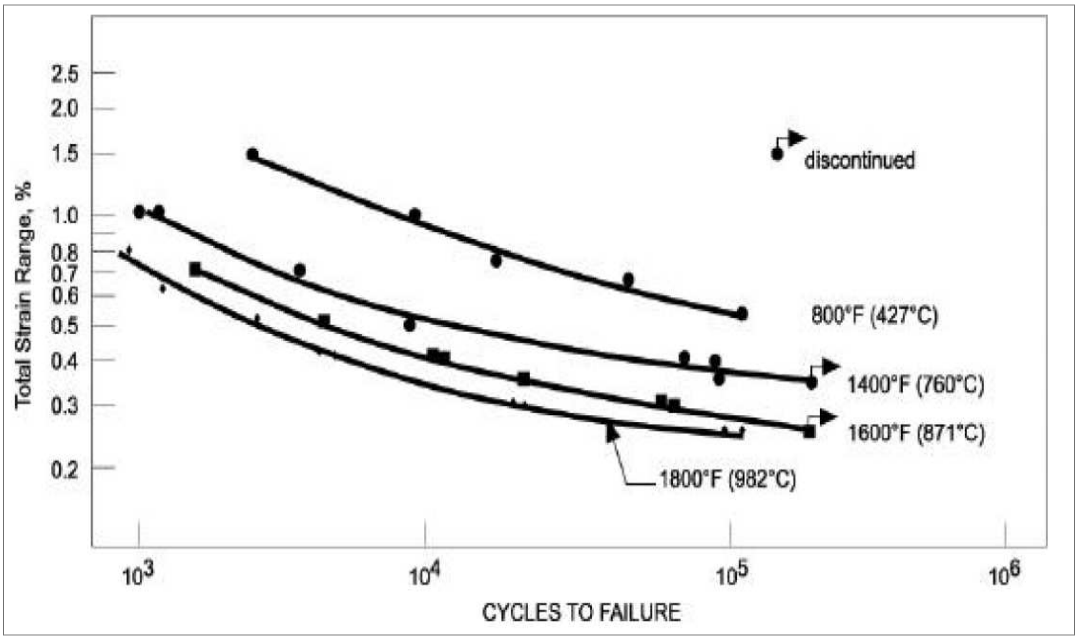

Figure 4 Fatigue Characteristics of Haynes 230

For each of the receiver panels, two points were selected to evaluate the fatigue life. The first point was selected as the location of highest strain. This point also coincided with peak flux point on the tube. The second point was the location of highest temperature. For up-flow panels, the second point with highest temperature was the same as first point with highest strain. For the down-flow panels, there were generally two separate points used in the evaluation.

As per the ASME Boiler and Pressure Vessel Code, a factor of two was applied on calculated strain range. For each given temperature and strain range, the fatigue life was estimated, using some interpolation and some extrapolation, from the Haynes 230 fatigue curves. Results of fatigue life are given Table 4.

Table 4 Estimated Panel Fatigue Lives

DESIGN POINT		PANEL	Results			
DAY	TIME			Temp, ˚F	2 x Strain Range	Life (Cycles)
8	12:00	1W	*Max Strain Point*	1,055	0.52 percent	47,000
			Max Temp Point	1,082	0.48 percent	65,000
300	10:30	3E	*Max Strain Point* / *Max Temp Point*	1,181	0.52 percent	31,000
300	10:30	5E	*Max Strain Point*	1,213	0.51 percent	30,000
			Max Temp Point	1,251	0.48 percent	35,000
81	10:00	7E	*Max Strain Point* / *Max Temp Point*	1,244	0.46 percent	42,000
154	10:00	9E	*Max Strain Point*	1,252	0.42 percent	80,000
			Max Temp Point	1,282	0.38 percent	160,000
154	10:00	11E	*Max Strain Point* / *Max Temp Point*	1,345	0.35 percent	260,000

With the limited material data available, the results presented are considered to be a good approximation. The panels in pass 2 and pass 3 have the shortest lives of approximately 30,000 cycles. Note that Panel 11E, although operating at the highest metal temperatures, has the longest fatigue life. This is due to a relatively low incident flux on Panel 11, and a corresponding reduction in the tube strains.

Several items can be noted from the creep and fatigue analyses:

1) A factor of safety of 0.67 was applied to the allowable stress values in the creep analysis, and a factor of 2 was applied to the strain range in the fatigue analysis. As noted in Figure 4, applications of these factors results in a very conservative estimate of fatigue life.
2) Offsetting this conservatism, to some degree, is the source of the data in Figure 4. Specifically, fatigue data are often developed with a test specimen in the shape of a solid bar, with fully reversed loadings in compression only. A typical test rate is 20 cycles per minute. In contrast, a receiver uses hollow tubes, rather than a solid bar, and hold times in compression normally lasting at least 2 hours. In general, for a given strain, the fatigue life of a hollow tube with a long hold time is noticeably less than the fatigue life of a solid bar with a short hold time. Unfortunately, to replicate the data in Figure 4 with hold times on the order of 2 hours would require a test period of several years, and tube suppliers have yet to undertake such an extensive test program.

As a consequence, there are still some uncertainties regarding the actual fatigue life of a tube in a receiver. To some extent, the receivers in operation at Gemasolar and Crescent Dunes may be the best methods for providing accurate information on tube lifetimes.

Task 2.2 – Advanced Heliostat Design

Specifications

Molten Salt Tower heliostat brainstorming and specifications development began in May 2012. Overall optical and structural performance specifications are those of the SunShot goal and are similar to Abengoa design criteria:

Table 5 MST heliostat design requirements

Beam error under 5 m/s winds	≤ 3 mrad
Beam error under windy conditions (12 m/s)	≤ 4 mrad
Wind speed at which to go to stow	≥ 15.6 m/s
Wind speed at which heliostat must survive in any orientation	≥ 22.4 m/s
Wind speed heliostat must survive in stow orientation	≥ 40 m/s
Lifetime	≥ 30 years
Cost	≤ 120 $/m^2 (≤ 220 $/kWth with MST project assumptions)

All winds speeds above are 3 second-average gusts and measured at 10 m height.

The optical requirements are stringent. Prior to brainstorming heliostat designs, a rough optical error budget for the heliostat field was created and is summarized below.

Table 6 MST Optical error budget guideline

Beam error type	5 m/s wind loading Isolated (mrad)	5 m/s wind loading **Field average (mrad)**	12 m/s wind loading Isolated (mrad)	12 m/s wind loading **Field average (mrad)**
Reflector	2	**2**	2	**2**
Structure deflection	1	**0.3**	4	**1.3**
Assembly	1	**1**	1	**1**
Tracking	1.5	**1.5**	1.5	**1.5**
Other	1	**1**	1	**1**
Convolved total:	3.0	**2.9**	4.9	**3.2**

Optical errors are presented as beam errors, i.e. 2x slope and pointing errors. Error budgets at two wind speeds, 5 m/s (11 mph) and 12 m/s (27 mph) are presented for "isolated" and "field average" heliostat values. 5 m/s is the DNI weighted wind speed at the Nevada design site, while 12 m/s wind speed is the maximum wind speed at which the heliostat must maintain optical accuracy. The "isolated" heliostat error budget reflects structural deflection values associated with worst-case orientation and wind-loading, while the "field average" represents the average structural deflection for the heliostat field over the course of the year due to average orientation and wind loading. The field average is used in annual performance models. The heliostat was designed to meet isolated heliostat requirements, and then its field average value was approximated from it.

The values shown in the optical error budget table were a guide, with the understanding that the value associated with each line item should not be regarded as "set-in-stone" though the convolved field average totals, both near 3 mrad, should be according to present performance standards.

Wind loading was calculated using the methodology described by Peterka [2] to determine the required stiffness of structural members and torques of the drives.

Brainstorming and Downselect

Brainstorming began once the specifications were in place. Designs from the brainstorming were compared on a $/m^2 basis using costing rules-of-thumb, experience, and vendor quotes. If it was believed that a design would offer better (or worse) optical performance than specified, an annual plant performance model was used to translate the change in performance into a $/m^2 benefit or disadvantage.

Figure 5 illustrates and describes the five most promising designs from the brainstorming process that were the subject of the downselect in December 2012. It was believed that optical performance would be similar for these designs.

The five heliostats range in size from 15 m^2 to 200 m^2 with installed costs from 97 to 108 $/m^2. Their cost is compared to a baseline Sandia National Laboratory stretched membrane heliostat. Low cost enablers for the larger heliostats were hydraulic drives, efficient support structures, and the large reflection area possible with minimal material using a stretched membrane design, while cost enablers for the small heliostats were recent reductions in control and motor costs, the use of PV panels and batteries for power instead of conventional field wiring, and the reduction in structure due to reduced wind loading on a per square meter basis. Thus, both approaches were viable for reaching the cost target.

The purpose of the downselect was to pick one design for further development. Though it was agreed that $\$/m^2$ was the most important evaluation metric, the cost of the five heliostats were similar within our ability to accurately assess cost at this stage. The next criterion was risk. Large heliostat designs tend to rely heavily on field labor, and field labor costs can vary from \$20/hr to \$180/hr depending on location and specialty. This was determined to be a large risk, especially in markets like the USA with higher labor rates. In the case of the smaller heliostats, the cost on a $\$/m^2$ basis depends more on the cost of all the different components that make up the heliostat (drives, control, power, structure) and if any one component is significantly more expensive than projected, it can eliminate the potential savings relative to the baseline quickly.

Multiple vendor bids associated with cost-sensitive components (such as the controller and drives) as well as perceived automated manufacturing advantages associated with a smaller heliostat led to its selection in the end. At the smaller size, the stretched membrane did not have a cost advantage relative to the composite facet, and so for lower risk and commercial relevance the 18 m^2 composite facet heliostat was selected.

This heliostat, named the ROP 18, is the subject of the remainder of this report. At Abengoa Solar, this development process has been perceived as successful and steps are being taken to commercialize it. The Abengoa Solar heliostat development team wishes to thank DOE for their support and critical review of this task.

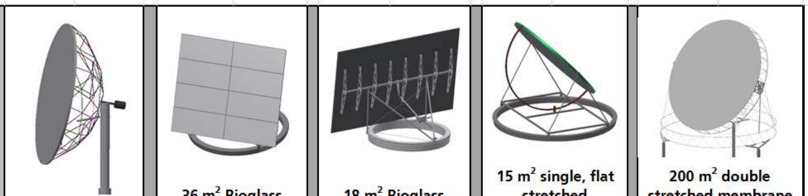

Component	Baseline 140 m^2 heliostat Cost	150 m^2 Heliodesic double stretched membrane on a pedestal with hydraulic cylinder drives		36 m^2 Rioglass panels (8) on pre-cast concrete ring ballast foundation with electromechanical drives		18 m^2 Rioglass panels (4) on pre-cast concrete ring ballast foundation with electromechanical drives		15 m^2 single, flat stretched membrane on pre-cast concrete ring ballast foundation with electromechanical drives		200 m^2 double stretched membrane supported by truss ring and carousel driven by rotary hydraulic drives, with concrete pylon foundations	
Heliostat Cost	**$\$/m^2$**	**Cost**	**+/- to BL**	**Cost**	**+/- to BL**	**Cost**	**+/- to BL**	**Cost**	**+/- to BL**	**Cost**	**+/- to BL**
Azimuthal Drive	$28.37	$6.50	-$21.88	$9.22	-$19.15	$10.50	-$17.87	$12.38	-$15.99	$4.00	-$24.37
Support Structure	$23.73	$12.94	-$10.79	$12.37	-$11.37	$7.47	-$16.26	$0.00	-$23.73	$14.23	-$9.50
Heliostat Structure	$27.08	$13.64	-$13.44	$7.31	-$19.76	$5.43	-$21.65	$15.07	-$12.01	$0.00	-$27.08
Membranes	$17.53	$12.80	-$4.73	$0.00	-$17.53	$0.00	-$17.53	$5.00	-$12.53	$12.93	-$4.61
Focus System	$13.68	$6.00	-$7.68	$0.00	-$13.68	$0.00	-$13.68	$0.00	-$13.68	$7.00	-$6.68
Mirror	$11.27	$10.18	-$1.09	$35.00	$23.73	$35.00	$23.73	$15.50	$4.23	$7.50	-$3.77
Elevation Drive	$9.45	$6.50	-$2.96	$11.61	$2.16	$9.79	$0.34	$11.76	$2.31	$7.20	-$2.25
Field Wiring	$8.71	$2.78	-$5.93	$4.92	-$3.79	$6.80	-$1.91	$7.00	-$1.71	$2.39	-$6.32
Ring	$6.80	$4.32	-$2.48	$0.00	-$6.80	$0.00	-$6.80	$11.07	$4.27	$9.68	$2.88
Labor	$5.12	$5.12	$0.00	$5.12	$0.00	$5.12	$0.00	$5.12	$0.00	$5.12	$0.00
Field Assembly	$2.63	$2.63	$0.00	$2.63	$0.00	$2.63	$0.00	$2.63	$0.00	$2.63	$0.00
Foundation	$2.60	$5.57	$2.97	$14.17	$11.57	$12.89	$10.29	$14.54	$11.94	$15.75	$13.15
Drive Electrical	$2.02	$0.00	-$2.02	$0.00	-$2.02	$0.00	-$2.02	$0.00	-$2.02	$0.00	-$2.02
Controls	$1.94	$7.47	$5.53	$2.00	$0.06	$3.07	$1.13	$3.50	$1.56	$5.75	$3.81
Tooling	$1.58	$1.58	$0.00	$1.58	$0.00	$1.58	$0.00	$1.58	$0.00	$1.58	$0.00
Feedback	$2.58	$1.95	-$0.63	$1.31	-$1.27	$2.70	$0.12	$2.70	$0.12	$1.15	-$1.43
Total Capital Cost	**$165.10**	**$99.97**	**-$65.13**	**$107.25**	**-$57.85**	**$102.98**	**-$62.12**	**$107.85**	**-$57.25**	**$96.91**	**-$68.20**

Figure 5 Downselect options as of December 2012

Design Development

Structure

The heliostat had to meet strength (stress) and deflection (optical error) criteria. Strength criteria means that stresses in the structural members should not exceed a predetermined stress based on material properties, geometry, and desired safety factors. The deflection criterion corresponds to maximum structural deflections that translate to angular deviations that affect the direction of the reflected beam towards the receiver. Finite-Element-Analysis (FEA) was used to assess both for candidate heliostat structures undergoing various wind loading scenarios.

Early in the analysis it became clear that acceptable structural deflection associated with 12 m/s wind gusts incident on a heliostat structure with its facet array pointed 30° from zenith was going to be the most difficult design criterion to meet, and would therefore dictate the design of the structure and the size of its members. The structure changed little-by-little to meet it, and a snapshot showing some aspects of the progress is shown in Figure 6. At the end of the design process, the amount of structural steel in the heliostat was compared to the Sandia [3] semi-empirical analysis that relates the amount of structural steel per square meter of the heliostat to its area. This comparison is shown in Figure 7, along with data from other heliostats.

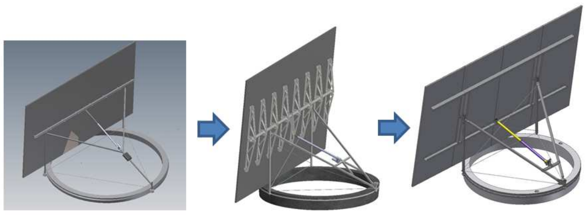

Figure 6 MST heliostat design progression

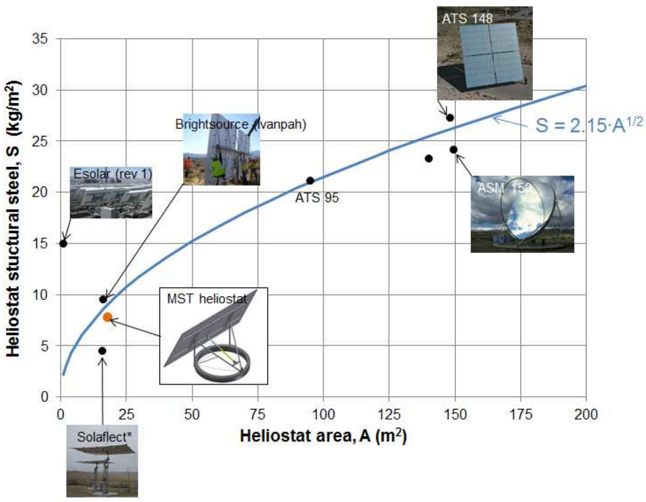

Figure 7 Comparison of the amount of structural steel in the MST heliostat compared to Sandia's structural steel curve, with other heliostats for reference

Concrete Ring

The concrete ballast foundation serves multiple purposes: prevention of motion under significant wind loading, ease of installation, structural enhancement through the enablement of a tensioned steel structure, and drive cost reduction through gear reduction. For it to fill these functions, however, it had to pass some strict shape and deflection criteria.

An accurate roll-formed form for the concrete was procured by Lindsay Precast, as was a roll-formed V steel track. After the pour the shape of both was inspected by photogrammetry. The track radius varied by ± 2.0 mm (± 0.080 in) to 95 percent confidence, while the concrete radius varied by ± 1.0 mm (± 0.040 in). Both were within specification, though prototyping efforts continue to attempt to reduce the variation in the track radius as this influences the required excursion of the tension rods in the ROP structure.

Also of interest was potential deflection of the concrete ring and embedded track due to non-uniform ground support. In a field installation, it is envisioned that the concrete ring will be placed on the ground quickly with little-to-no ground preparation. The ring may just be supported by three unevenly spaced points. If the ring and track deflect, then an angular error may result, especially in elevation.

The shape of the track as a function of support was investigated using photogrammetry. Figure 8 shows three support conditions - ground supported, evenly on 3 points, and support on 2 ends - where the shape of the ring and track were quantified.

Figure 8 Photogrammetric evaluation of concrete ring and track deflection as a function of support condition

Vertical deviations in the track cause an angular error, mostly in elevation, of the reflected beam. Figure 9 quantifies the deviation relative to the ground supported case. The maximum deviation would result in an angular error of approximately 0.4 mrad, which is a small overall contributor in the error budget and therefore acceptable.

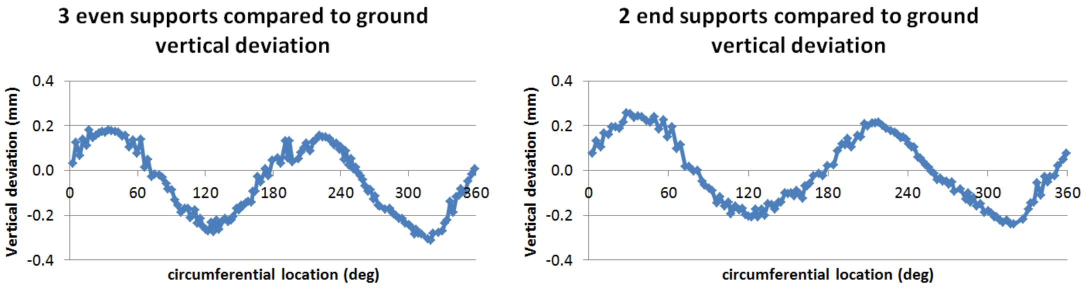

Figure 9 Vertical deviation of track relative to the ground supported base case for 3 and 2 point support cases

Azimuth drive

Early simulation work suggested that wind loading would cause enough contact stress and wear between the wheels and the concrete that a steel-on-steel interface was required. Steel wheels and a steel track were selected for testing. A succession of tests was carried out: coefficient of friction, accuracy, and wheel wear. Overviews of each are presented below.

Coefficient of friction

Figure 10 shows how the coefficient of friction between the steel wheel and track varied as a function of loading, but most importantly, track soiling condition.

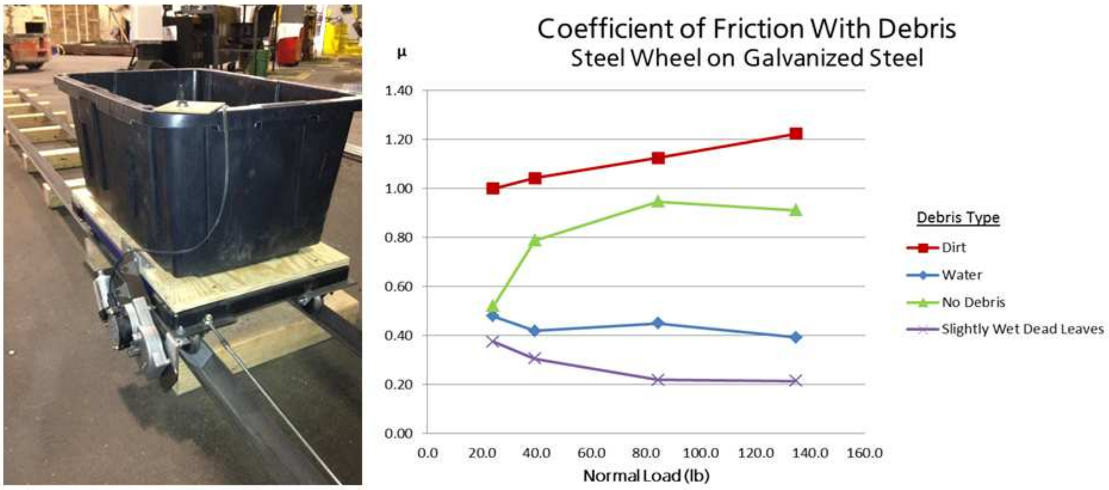

Figure 10 Coefficient of friction testing between drive wheel and track

Accuracy

The challenge of obtaining accurate tracking from cheap, inaccurately manufactured components was foremost on the project team's mind from the beginning. For astronomical telescopes and robotics, friction drives are common because they offer gear reduction, are energy efficient, have no backlash, and require only controlled radii for accuracy. The ROP's small radius steel wheel operating on the large radius roll-formed steel V-track supported by the concrete ring is a friction drive.

Figure 11 Testing of azimuth track friction drive showing proximity sensor and laser-cut encoder

Even so, there was a concern that wheel slippage on the track, or a drive wheel radius that varies with time, would require some form of error-correction in the azimuth track. Therefore a strip with laser cut holes was manufactured and envisioned to be a large radius encoder whose edges are detected by an inductive sensor. The assembly is show in Figure 11.

ISO 230-2 [4] was selected as the methodology to determine the accuracy of the drives. In this method, 5 target positions are approached in both forward and backward directions. Each time a target position is reached, its location relative to a reference position is measured externally (in this case, by laser radar) and compared to the programmed target distance. As described by the standard, the accuracy can be summarized as a function of the deviations between the true external reference and the programmed set point. An example of the application of this test standard to a candidate azimuth drive is shown in Figure 12. An accuracy of ± 1.5 mm at 95 percent confidence on the test track corresponds to an acceptable azimuth beam tracking accuracy of ± 1 mrad on the heliostat considering the geometric gear reduction.

82° from zenith: 4519 N (1016 lb) Avg. rod tension: 5720 N (1286 lb) Avg. DC power: 6.7 W Accuracy: ± 1.5 mm		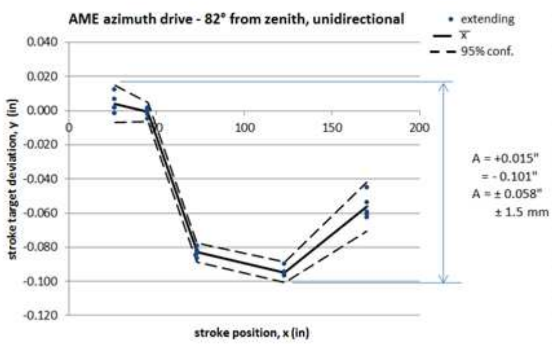

Figure 12 Unidirectional accuracy test of azimuth drive in the laboratory

<u>Wear</u>

It was theorized that the large normal force between the wheel and the track would cause the drive wheel to wear, but the rate of the wear far exceeded calculations. After the accuracy testing, the azimuth track was put through 24 hour, 5 day/week continuous duty cycling to simulate "years" of typical operation. Testing was stopped after 2 months, the equivalent of 20 years. Figure 13 shows how the profile of the drive wheel changed with time.

The reason for the fast wear rate was determined to be a slightly non-orthogonal drive axis relative to the planar axis of the steel track. This misalignment causes the wheel to attempt to ride up or down the track, depending on direction. This misalignment is invisible to the eye and will be an obvious result of typical manufacturing. The heliostat presently uses the "year 8" profile to start, as the rate of wear from this point on is reduced.

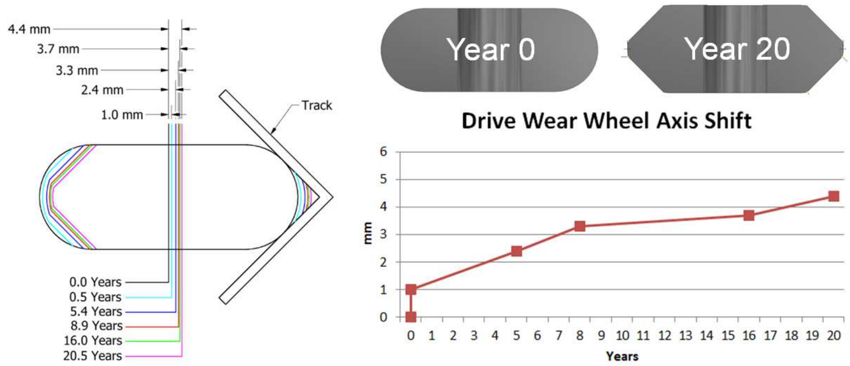

Figure 13 The changing profile of the steel drive wheel with lifecycle testing

<u>Elevation drive</u>

The linear actuators from several prospective vendors were evaluated based on the aforementioned ISO accuracy test. An indoor test stand was constructed and the actuators were tested in turn.

Figure 14 shows the results of the most promising actuator, custom developed by AME, and compares its results to two other commercial actuators. The accuracy of ± 0.4 mm to 95 percent confidence equates to an elevation beam tracking error of ± 0.8 mrad, which is within specification for the drive. Of the other actuators, the Schaeffler actuator could have also met specification if its uniform lead screw error could have been calibrated out, however its projected cost was near double that of the AME drive. The Joyce Dayton actuator is used in tracking PV systems and was not expected to perform well in the tests.

For both Azimuth and Elevation drives, AM Equipment (http://www.amequipment.com) was selected based on performance and projected commercial cost to provide drives for the ROP. This company specializes in high volume manufacturing and supply of brushed DC motors to the automotive industry, and they were eager to apply their manufacturing and design expertise to a new application.

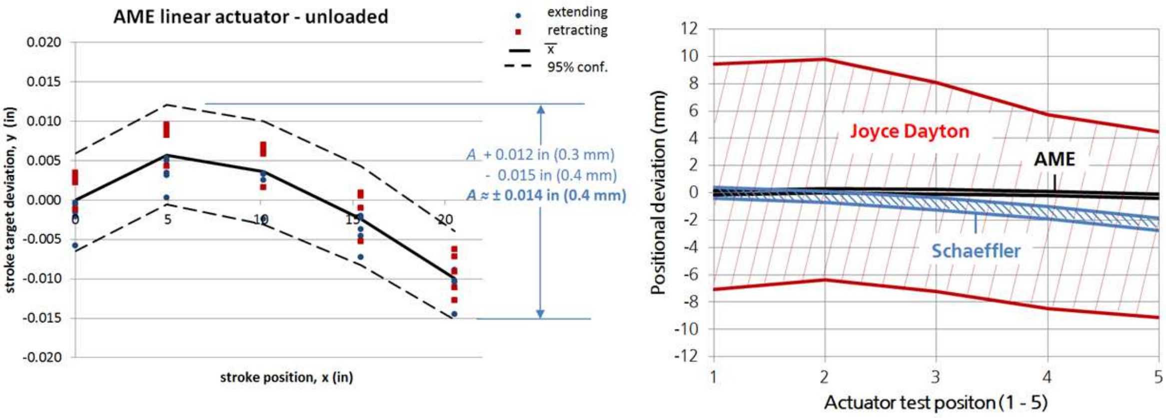

Figure 14 Accuracy testing of prospective linear actuators

Like the azimuth drive, the elevation drive was also subjected to life cycle testing. Its accuracy was within specification until year 20. Work continues to ready this drive for commercial application.

Prototype Construction and Deployment

With component evaluation complete, a design for the structure, and control hardware and algorithms demonstrated, the first ROP prototype was assembled and deployed at SolarTAC at the end of 2013. Pictures of the assembly are shown below.

Figure 15 Construction of the first prototype

The heliostat was put on-sun successfully for the first time in February 2014.

Figure 16 ROP tracking the sun on to the beam characterization target

<u>Tracking</u>

Though Figure 16 shows the beam centered on the target, initial tracking was not so successful. However, a calibration method described by Guo [5] was adapted to the ROP geometry. Subsequent tracking showed that the orientation of the heliostat and many of its inherent optical misalignments can be determined from deviations of the beam centroid from the target, and then corrected for by the tracking algorithm, as shown below.

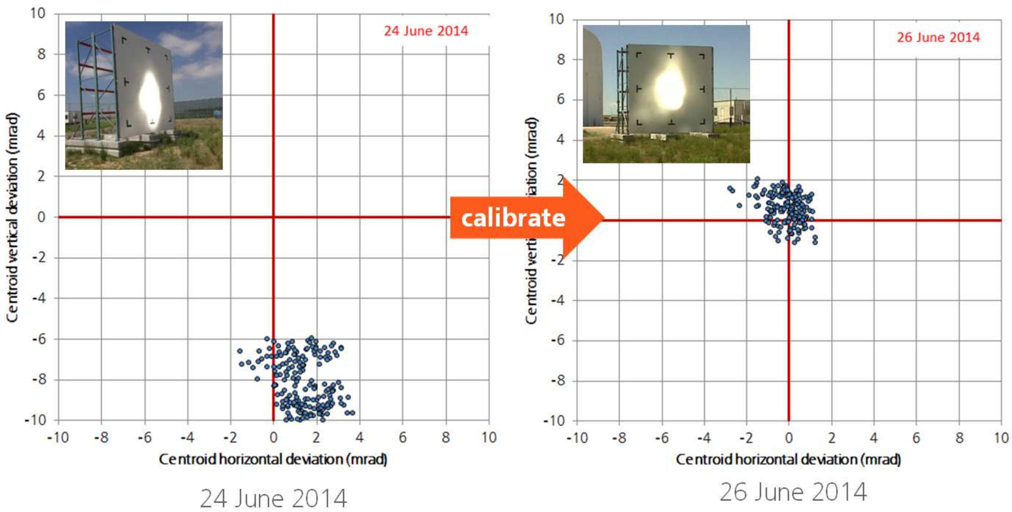

Figure 17 ROP tracking, before and after calibration. Points indicate beam centroid at 1 minute intervals

To quantify the accuracy of tracking, circles indicating 1σ and 2σ confidence intervals are overlaid on the after-calibration tracking data. Recall from Table 6 that the allowable 1σ tracking error budget was 1.5 mrad. Figure 18 shows a tracking accuracy of 1.3 mrad, which is within specification.

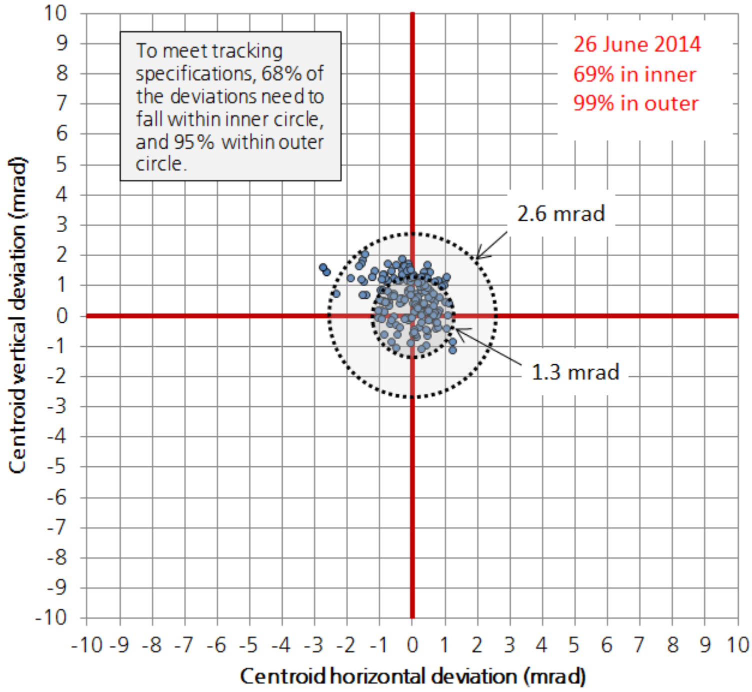

Figure 18 Tracking accuracy of the ROP

Commercial Cost Estimate

A 100 MWe plant with 6 hours of thermal energy storage will require about 60,000 ROP heliostats. Vendors' quotes were based on this volume, often with significant discounts relative to single unit prices. Abengoa Research - Consulting performed the assembly, installation, and manufacturing study, leveraging knowledge gained through their involvement in SolarMat. Figure 19 describes the heliostat cost as a function of material costs and assembly and installation costs. The installed heliostat cost in Nevada is projected to be 114 $\$/m^2$. This is less than the 120 $\$/m^2$ project goal.

Qty	Description	$/heliostat	$/m²
1	ROP Heliostat, materials, 18m²	$1,809.04	$100.64
1	Concrete and Track Assembly	$276.41	$15.38
1	Concrete ring	$250.00	$13.91
1	Track & encoder ring	$26.41	$1.47
1	Heliostat Structure	$215.91	$12.01
1	Leg Assembly	$41.38	$2.30
1	Leg Assembly Mirror	$41.38	$2.30
1	Elevation Actuator Mounts	$3.06	$0.17
1	Gear Drive Wheel Assembly	$20.83	$1.16
1	Wye	$50.61	$2.82
1	Tension rod assemblies	$14.29	$0.80
	Fasteners	$43.15	$2.40
1	Heliostat Facet Assembly	$828.70	$46.10
1	Facet Frame Assembly	$144.24	$8.02
4	Reflective facets, 1406 mm x 3216 mm	$636.94	$35.43
	Fasteners	$47.52	$2.64
1	Controller	$110.34	6.14
1	Level I and Level II controllers	$41.12	$2.29
1	Trinamic control box (Level III)	$69.22	$3.85
1	Power and energy storage	$111.18	$6.18
1	12 V, 50 W PV Panel	$52.50	$2.92
1	Battery	$49.00	$2.73
1	Wiring	$6.18	$0.34
2	Connectors	$3.50	$0.19
1	Drives	$266.50	$14.83
1	Elevation Drive	$155.57	$8.65
1	Azimuth drive	$110.93	$6.17

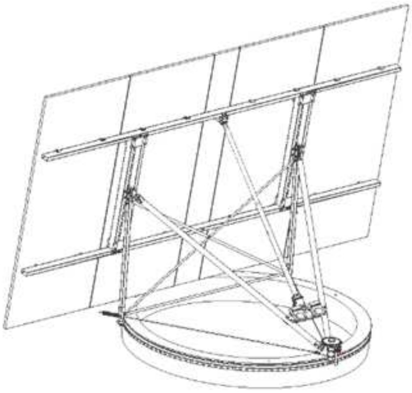

Heliostat line item cost	$/heliostat	$/m²	Basis
Materials & components	$1,809	$100.64	Vendor quotes and representative steel costs
Shipping components to site within U.S.	$27	$1.52	Shipping cost study by ARC
Assembly building and tools	$25	$1.41	ARC manufacturing study for ROP
Field installation equipment rental	$114	$6.36	ARC manufacturing study for ROP
Assembly, installation, and check-out labor	$80	$4.44	ARC manufacturing study for ROP 2.66 man-hr @ 30$/hr, 0.15 man-hr/m²
Total installed heliostat	**$2,056**	**$114**	

Figure 19 ROP commercial cost breakdown, 60,000 units, Nevada installation

Conclusions

Below Table 7 evaluates each task goal according to desired DOE task metrics. In all cases, except one (Lifetime), project goals were met. Development work continues on the drives, control, and PV panel and battery to bring this heliostat to commercialization.

Table 7 - Heliostat task evaluation

Task description	Evaluation metric	Achieved (Y/N)	Basis	If not achieved, pending solution
Beam error under 5 m/s winds	≤ 3 mrad	Y	Convolved error of all sub-components, FEA deflection, tracking results, ARC structural study	-
Beam error under windy conditions (12 m/s)	≤ 4 mrad	Y	Convolved error of all sub-components, FEA deflection, tracking results	-
Wind speed at which to go to stow	≥ 15.6 m/s	Y	FEA, drive testing	-
Wind speed at which heliostat must survive in any orientation	≥ 22.4 m/s	Y	FEA, ARC structural study, survival at SolarTAC	-
Wind speed heliostat must survive in stow orientation	≥ 40 m/s	Y	FEA, ARC structural study, survival at SolarTAC	-
Lifetime	≥ 30 years	N	Reduction of drive accuracy year 20, intermittent drive & control failures, excessive wheel wear	Continued development
Cost	≤ 120 $/m^2	Y	Vendor quotes and ARC manufacturing study	-

Task 2.3 – Selective Coating

During the lifetime of this project several samples were examined with varying levels of success. Both paints and thermal spray coatings have been analyzed with the most encouraging results coming from paints. The goals of this task were to find a coating that was air stable at 750 °C with an absorbance >95 percent and an emissivity <30 percent. These very aggressive goals were based off a patent from NREL using TiSi2 based coating stack. Initially work was planned with NREL to develop this coating but due to budget cuts both parties decided it would be better to work on the coatings individually. NREL pursued the PVD based coatings and Abengoa looked into other types of coatings that are easy to apply in the field. Initially thermal spray was analyzed due to the durability of thermal spray coatings and the ability to apply in the field. Several coatings were testing during this process with very little success. Our initial goal was to try and reach the highest absorbance possible and then try and lower the emittance values. Models suggested that absorbance values have a greater effect on the efficiency of the plant than the emittance at temperatures between 650 °C and 750 °C. As the temperature rises above 750 °C, the emittance has an increased effect on the plant efficiency.

The initial investigation ruled out several different coatings based on complexity of the coating, oxidation resistance and absorbance characteristics. Since thermal spray and paint processes were used, the coating had to be single layer film roughly between 20 um and 100 um thus layered coating stacks could not be applied. In addition, only commercially available materials were chosen in the starting process. The initial screening was for absorbance values >93 percent. Most commercially available thermal spray coatings for high temperature resistance do not have a high optical absorbance.

In an attempt to locate the best coating several companies were contacted. NDAs with Sandia National Lab, UCSD, Nevada Thermal Spray and Forrest Paint were completed. UCSD was developing a unique coating, but had problems meeting the absorptivity for the full solar weighted spectrum. Additionally, UCSD was working on a way to test emissivity and absorbance at temperatures greater than 700 °C. This development however never reached the point where Abengoa samples could be tested.

Thermal spray samples tested during the project lifetime were deposited by Nevada Thermal Spray and University of Rey Juan Carlos. Samples that were deposited by NTST are labeled with a NT before the sample number and samples from URJC are labeled with a UZ before the sample number. Finally, Forrest Paint was contacted as a possible paint vendor for solar selective coatings. Forrest Paint has a few commercially available high temperature paints, and was willing to devote internal research funds to develop a product to meet our needs. Forrest Paint is currently working on a coating idea but has not yet revealed any data or samples for us to test.

Results

Throughout the project several different types of samples were coated and analyzed. Table 8 lists the most promising coatings from this project. Many other samples were deposited but either had issues with delamination or had very low absorbance values thus were not included in Table 8. Measurements of the samples were carried out at NREL and University of Zaragoza (UZ) in Spain, with several samples tested at both facilities. Overall the results from the two facilities correlated well in terms of relative values, but with samples measured at UZ observed to have a higher absorptivity value than the same sample measured at NREL by roughly 0.3-1.2 percent. Samples are organized by the type of coating, paint or thermal spray, labeled on the top of each section. In addition to the absorbance and emissivity measurements, efficiencies were calculated for MST at different temperatures (565 °C and 700 °C) using a model created internally. Furthermore, the Figure of Merit (FOM) was calculated for each sample.

The FOM can be calculated by the following formula:

$$\eta = \frac{\alpha Q - \varepsilon \sigma T^4}{Q}$$

Where α is the solar weighted absorbance, ε is the solar weighted emittance, σ is the Boltzmann's constant (1.38E-23 m^2 k g s^{-2} K^{-1}), T is the temperature and Q is the irradiance on the receiver.

Some of the more promising coatings were heat treated. In Table 8 heat treated samples are noted with an (a) by the name of the sample, with the type of thermal treatment found in the far right column. Highlighted in yellow are samples measured at NREL whereas all the other samples were measured in Spain at the University of Zaragoza (UZ). Additionally, samples in red represent the highest efficiency samples per coating type. For samples with paint coatings, the highest absorbance prior to heat treatment was found on sample C-7300 which is a commercially available paint. Unfortunately, this paint also had a very high emissivity value. Samples SS-B-14 and 15 were paints created by Abengoa. The samples initially had a slightly lower absorbance than the three commercially available paints (labeled with a C before the sample number). However after thermal treatment both samples had absorbance values greater than the commercial paints. Additionally, both Abengoa paint samples have showed an increase in performance after 40 cycles at 650 °C. After 40 cycles, sample SS-B-14a, was observed to have a dramatic increase in performance from 94.69 percent to 95.90 percent. Sample SS-B-15 was also observed to have an increase in absorbance from 94.62 percent to 95.06 percent. Samples SS-B-14 and SS-B-15 were coated using the same paint formula but coated on different days. The difference in absorbance between the two samples was likely due to the application of the paint. Sample SS-B-14 has a more uniform surface coating whereas SS-B-15 has some areas where the coating is lighter in color. Taking three points on each sample the standard deviations for both paints were 0.11 percent and 0.56 percent for SS-B-14 and SS-B-15, respectively. These paints are provide the most promising coating and are comparable with data collected for Pyromark at NREL.

In addition to paint samples, thermal spray samples were tested and heat treated. Of the thermal spray samples examined, the NT-B samples were observed to have the highest absorbance value with an average absorbance value greater than 95 percent. The NT-B samples also had the highest emissivity values. The lowest emissivity value was observed on UZ-AT samples at roughly 0.75 which unfortunately also had the lowest absorbance value at around 90 percent. A selected few thermal spray samples were also heat treated.

Table 8 Samples measured during the MST project lifetime

Sample Number	Sample	Absorbance (α)	Emisivity at 700°C (ε)	MST ~(565°C)	MST ~(700°C)	FOM (700°C)	Thermal treatment
Paint							
1	C-138	94.81%	93.84%	91.74%	90.18%	0.87	None
2	C-7300-1	94.90%	94.54%	91.82%	90.25%	0.87	None
3	C-7300-2	94.96%	95.20%	91.87%	90.29%	0.87	None
4	SS-B-14	94.69%	95.40%	91.61%	90.02%	0.87	None
	SS-B-14a	95.90%	95.30%	92.80%	91.21%	0.88	40 cycles at 650°C
5	SS-B-15	94.62%	93.80%	91.56%	89.99%	0.87	None
	SS-B-15a	95.10%	95.70%	92.01%	90.41%	0.87	40 cycles at 650°C
Thermal Spray							
6	NT-C-1	94.80%	94.03%	91.73%	90.16%	0.87	None
7	NT-CA-20-1	94.75%	93.12%	91.69%	90.14%	0.87	None
8	UZ-CA-20-1	89.18%	89.87%	86.26%	84.76%	0.82	None
9	UZ-CA-20-2	88.90%	89.54%	85.99%	84.50%	0.81	None
10	UZ-CA-20-3	91.40%	93.96%	88.39%	86.83%	0.83	None
11	NT-B-1	93.96%	94.12%	90.90%	89.34%	0.86	None
	NT-B-1a	97.30%	94.45%	94.18%	92.60%	0.89	Annealed at 700°C for 2 hrs
12	NT-B-2	95.40%	95.56%	92.30%	90.71%	0.87	None
	NT-B-2a	95.80%	95.65%	92.69%	91.10%	0.88	Annealed at 650°C for 10 cycles
13	NT-B-3	95.49%	95.96%	92.39%	90.79%	0.87	None
14	NT-B-4	95.17%	95.70%	92.07%	90.48%	0.87	None
	NT-B-4a	93.26%	95.40%	90.20%	88.62%	0.85	Annealed at 650°C for 20 cycles
15	NT-BT-5-1	90.92%	94.81%	87.91%	86.34%	0.83	None
	NT-BT-5-1a	94.93%	95.02%	91.85%	90.26%	0.87	Annealed at 650°C for 10 cycles
16	NT-BT-5-2	95.28%	96.10%	92.18%	90.58%	0.87	None
17	NT-BT-15-1	94.70%	93.56%	91.64%	90.07%	0.87	None
	NT-BT-15-1a	94.70%	93.08%	91.64%	90.09%	0.87	Annealed at 700°C for 2 hrs
18	NT-BT-30-1	93.20%	91.82%	90.19%	88.65%	0.85	None
	NT-BT-30-1a	91.80%	92.06%	88.81%	87.27%	0.84	Annealed at 700°C for 2 hrs
19	NT-BTA-1	94.19%	95.09%	91.12%	89.54%	0.86	None
	NT-BTA-1a	94.82%	95.40%	91.73%	90.15%	0.87	Annealed at 650°C for 10 cycles
20	NT-BTA-2	94.59%	95.71%	91.50%	89.91%	0.86	None
21	NT-AT-1	90.92%	90.51%	87.96%	86.45%	0.83	None
22	UZ-AT-1	90.50%	75.54%	87.73%	86.42%	0.84	None
23	UZ-AT-2	88.80%	74.66%	86.07%	84.78%	0.82	None
24	Pyromark	96.19%	88.09%	93.17%	91.67%	0.89	None
	Pyromark	94.99%	89.40%	91.97%	90.46%	0.87	None

Legend

	Absorbance	Emittance
(light orange)	90-93%	85-90%
(light green)	>93%	<85%
(yellow)	Samples measured at NREL	
(a) =	annealed	
red =	best samples	

The samples that were thermal treated were NT-C-1, NT-CA-20-1, NT-B-2, NT-B-4, NT-BTA-1, NT-BT-5-1, NT-BT-15-1 and finally NT-BT-30-1. Samples NT-C-1 and NT-CA-20-1 delaminated during the thermal cycling thus the results could not be obtained. All of the samples that survived the thermal cycling showed an increase in absorbance and emissivity values. The highest absorbance value post thermal treatment was observed on sample NT-B-1, 97.30 percent. With the increase in absorbance, an increase in emissivity was also observed. After sitting for a month, the coating turned a lighter color and the absorbance value was found to be 81.44 percent. A second annealing was conducted and found the absorbance value increased from 81.44 percent to 96.49 percent. The absorbance values post cycling increased roughly 0.4 percent and emissivity increased between 0.1 to 0.4 percent. The one exception was from NT-BT-5-1, which was observed to have a change of roughly 4 percent, from 90.92 percent to 94.93 percent. The reason for the large increase may be due to an error in the initial absorbance measurements pre thermal cycle. A large difference is also observed for the NT-BT-5-1 coating when measured at NREL versus UZ (as seen in red).

Additionally, NT-BT-5-2, which was coated at the same time using the same material, was observed to have a much higher absorbance value of 95.28 percent. Both of these factors combined suggest a possible error in measurement of the NT-BT-5-1 sample. After 20 cycles at 650 °C, NT-B-4 showed a significant decrease in performance. Additionally, the coating appeared to be thinning to the point where the substrate could be observed through the coating.

Table 9 Results from Paint and Thermal Spray coating as measured by NREL and Universidad Zaragoza

Sample	Type	Measured at Universidad Zaragoza (UZ)		As measured at NREL		Change in α	FOM (UZ)	FOM (NREL)
		α (%)	$\varepsilon_{700°C}$ (%)	α (%)	$\varepsilon_{700°C}$ (%)	(%)		
C-138	Paint	94.81	93.84	93.92		0.47	0.87	
C-7300-1	Paint	94.90	94.54	94.05	94.00	0.45	0.87	0.86
C-7300-2	Paint	94.96	95.20	94.08		0.47	0.87	
NT-C-1	Plasma Spray	94.80	94.03	94.15		0.34	0.87	
NT-CA-20-1	Plasma Spray	94.75	93.12	93.88	90.10	0.46	0.87	0.86
NT-B-2	Plasma Spray	95.40	95.56	94.96		0.23	0.87	
NT-B-2a	Plasma Spray	95.80	95.65	NA			0.88	
NT-B-3	Plasma Spray	95.49	95.96	94.79		0.37	0.87	
NT-BTA-1	Plasma Spray	94.19	95.09	93.74	94.10	0.24	0.86	0.86
NT-BTA-2	Plasma Spray	94.59	95.71	93.30		0.69	0.86	
NT-BTA-2a	Plasma Spray	94.82	95.40	NA			0.87	
NT-AT-1	Plasma Spray	90.92	90.51	89.50		0.79	0.83	
NT-BT-5-1	Plasma Spray	90.92	94.81	93.14		1.21	0.83	
NT-BT-5-1a	Plasma Spray	94.93	95.02	NA			0.87	
NT-BT-5-2	Plasma Spray	95.28	96.10	94.50		0.41	0.87	
Pyromark	Paint	96.19	88.09	94.99	89.21	0.63	0.89	0.87

A select few samples were analyzed via SEM before thermal cycling and after thermal cycling, Table 10. Samples NT-B-2a, NT-B-3, NT-BT-5-1a, NT-BT-5-2, NT-BTA-1 and BT-BTA-2a were analyzed via SEM. The SEM images did not show a significant loss in thickness after heating the sample. It does however appear that the images show an increase in pinholes after heating which may signify volatility in the thermal spray coating.

Table 10 SEM images of thermal spray samples on stainless steel before and after thermal treatment

Sample	Anneal Conditions	Thickness (um)		SEM images
		Avg	Stdev	
NT-B-3	None	47.52	7.13	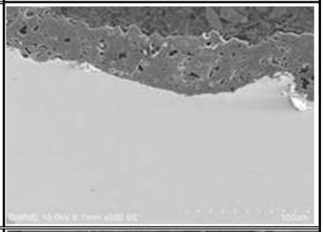
NT-B-2a	Thermal cycled at 650°C for 10 cycles	43.47	10.52	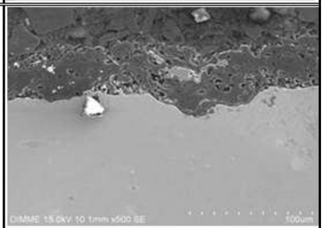
NT-BT-5-2	None	44.18	9.07	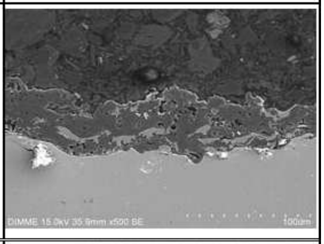
NT-BT-5-1a	Thermal cycled at 650°C for 10 cycles	47.77	8.26	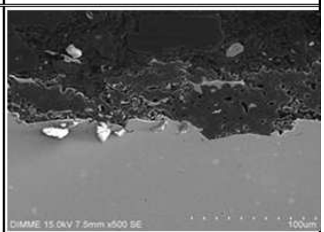
NT-BTA-2	None	37.41	6.54	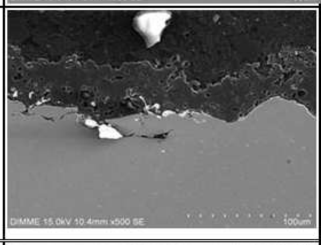
NT-BTA-1a	Thermal cycled at 650°C for 10 cycles	35.67	6.38	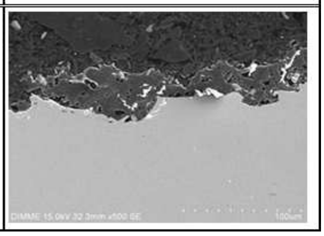

In addition to thermal cycling the samples, a water drop test was conducted on samples NT-B-4 and SS-B-15 after the first thermal cycle. The water drop test was used to determine the reaction of the thermal spray sample in comparison with a SS-B-15 mixed paint. In the past, applying a water drop to the thermal spray samples created a whitish water mark. Figure 20 and Figure 21 show the results of the water drop test with the red circle highlighting where the water drop was placed. Sample NT-B-4 is the thermal sprayed sample and sample SS-B-15 is the painted sample.

The water mark on sample 2 appears to be very distinct with defined barriers. The surface appeared to be hydrophobic causing the water drop to have a very high contact angle. Additionally, a reaction does appear to occur, marking a white distinct water mark with well-defined barriers. The hydrophobic appearance is likely due to the rough surface of the thermal sprayed in combination with the high surface tension of the water droplet, causing the water droplet to maintain its form. The white discoloration was likely from the reaction of the thermal spray coating and water, possibly forming a hydrate.

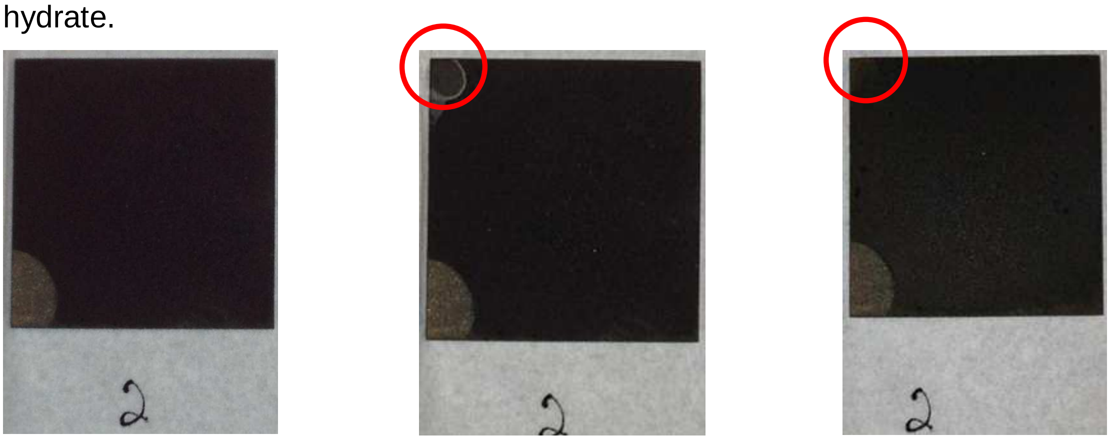

(a) (b) (c)

Figure 20 Images of sample 2 after thermal cycling, (a) post 10 cycles @ 650°C, (b) post 10 cycles at 650°C with a drop of water (c) post 20 cycles at 650°C. The water drops are highlighted in red circles

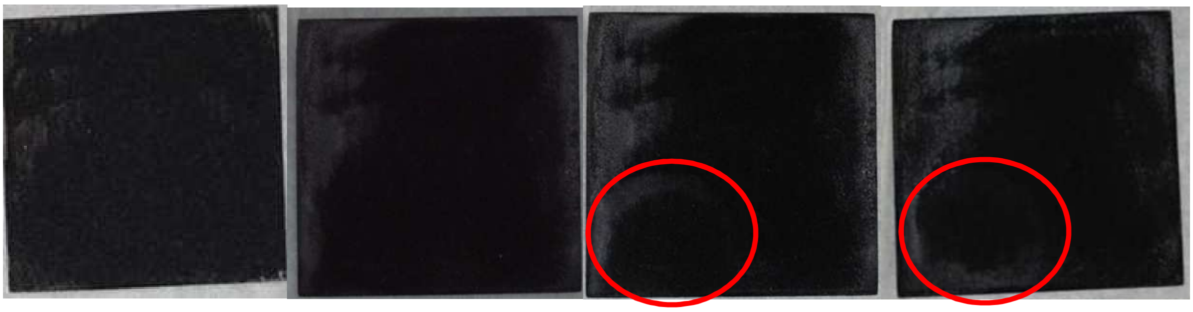

(a) (b) (c) (d)

Figure 21 Images of sample 15 in different stages of thermal cycling, (a) post cure, (b) post 10 cycles at 650°C, (c) post 10 cycles at 650°C with water drop (in the red circle), (d) post 20 cycles at 650°C. The red circles highlight the mark left from the water drop.

Sample SS-B-15 on the other hand, the water drop appeared to soak into the coating suggesting a hydrophilic nature. Additionally, the water marking was not as distinct as observed on NT-B-4. The water drop also did not change the color of the coating of the painted surface. It is important to note that both samples (paint and thermal spray) used the same powder. The powder that was used for the thermal spray samples was blended with a binder to create the paint.

It is also important to note that when the binder and powder are mixed together, the mixture is black, but when the binder is applied as a top coating on the thermal sprayed coating, the coating turns light grey. This might suggest an unstable oxide formation on the thermal spray samples that does not exist in the powder. After thermal cycling the color of the droplet disappears on sample NT-B-4 which would suggest the hydration occurs at the surface of the coating and not throughout the coating. At high temperature a dehydration reaction occurs thus eliminating the top layer of the film. Sample SS-B-15 does not appear to change in appearance after thermal cycling. After 20 cycles the thermal spray sample began to degrade. Visually, the substrate appeared to be visible through the coating, thus the thermal cycling was stopped after 20 cycles.

In addition to thermal cycling, optical modeling was conducted on some coating ideas, Table 11. Macleod software was used to model different coatings varying from 10 layers to 3 layers. The first coating tried was a multilayer coating using high temperature stable materials. After five revisions of the coating, a coating with 10 layers and an absorbance value of 96.5 percent was created (labeled ASI-5). The emissivity of the coating was calculated to be 0.32 at 750 °C. Unfortunately, the coating is likely limited to PVD/CVD due to the thickness of each coating and the number of coatings. To reduce the number of layers, cermets were created using the software.

Initially, cermet 1 was created using two different types of absorbers while also varying the metal volume in each layer, with the highest metal fraction closest to the substrate. Cermet 1 consists of a substrate/high volume metal fraction (HVMF)/mid volume metal fraction (MVMF)/low volume metal fraction (LVMF) with an antireflective layer configuration. Cermet 2, used a similar technique but without the MVMF layer, thus reducing the layers from 4 to 3. Cermet 3 has a similar structure but uses the same absorber throughout thus will be easier during the deposition process. Additionally, Cermets 2 and 3 have layers which vary from roughly 400 nm to 530 nm in thickness. All three cermets consisted of an antireflective layer roughly 40 nm thick. The absorbance values of the cermets show an increase over the 10 layer coating but at the cost of a higher emissivity value. Cermet 3 has the highest absorbance at 97.8 percent but also has the highest emissivity at 0.85 at 750 °C. In comparison with Pyromark, all of the coatings modeled have higher FOM values, with the 10 layer stack having the highest. More modeling needs to be conducted to determine if a single coating can be obtained with a high FOM value.

The reflectance for ASI-5, cermet 1 and cermet 3 was plotted versus wavelength in Figure 22. In addition, the Blackbody (purple line) and AM1.5 (dark blue line) spectrums were added to the figure. The red line indicates the idea properties of a solar selective coating. ASI-5 is the closest to following this line thus the emissivity measurements are lower than both cermets. The cermets have a greater absorbance in the near IR to mid IR range giving them higher weighted absorbance however this also increases the emissivity values.

Table 11 Modeled coatings using Macleod optical software to for solar selective coating analysis. Pyromark is added on the bottom for comparison purposes

Coating	Layers	α (%)	ε(25°C)	FOM (25°C)	ε(450°C)	FOM (450°C)	ε(750°C)	FOM (750°C)
ASI-5	10	96.50%	0.368	0.965	0.340	0.958	0.320	0.932
Cermet 1	4	97.10%	0.300	0.971	0.604	0.959	0.710	0.898
Cermet 2	3	97.10%	0.390	0.971	0.710	0.957	0.802	0.888
Cermet 3	3	97.80%	0.580	0.978	0.780	0.963	0.850	0.890
Pyromark	1	96.10%	0.780	0.960	0.815	0.945	0.880	0.870

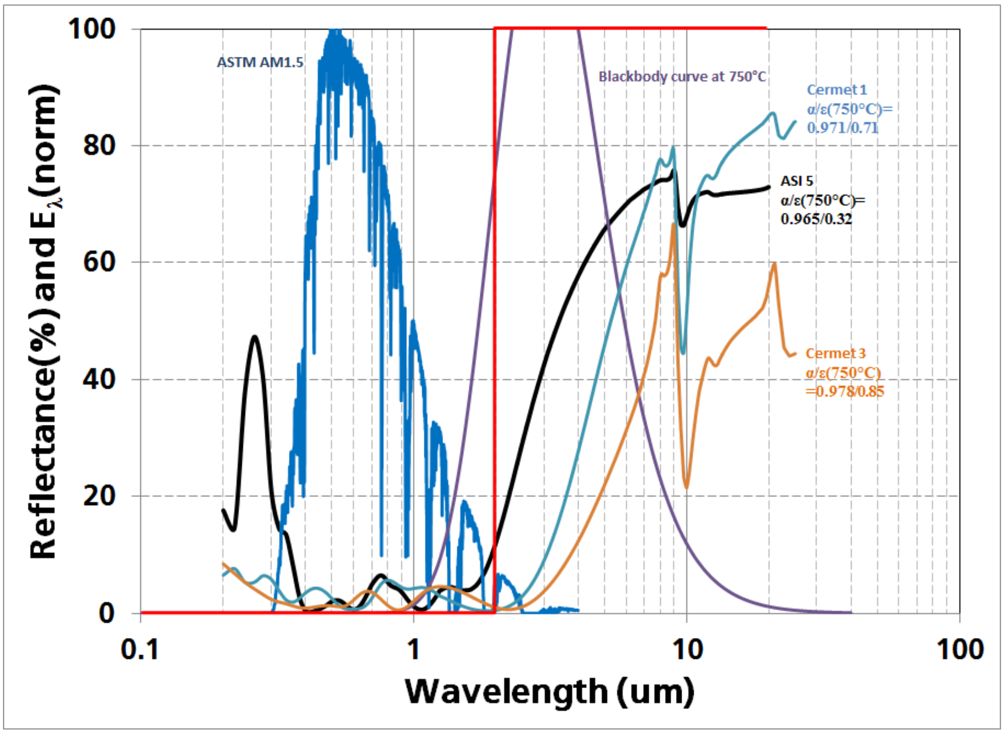

Figure 22 Reflectance versus wavelength of the modeled solar selective coatings. Included in the figure is both the normalized ASTM 1.5 spectrum and Blackbody curve at 750°C.

Conclusion

Thus far the coating that has shown the most promise is the mixed paint SS-B. After 40 cycles, the absorbance value of the paint was measured at 95.1 percent and 95.9 percent for samples SS-B-14 and SS-B-15, respectively. In comparison, Pyromark measured at the same time had an absorbance of 94.99 percent. If the mixed SS-B paint continues to be thermally stable after 1000 hrs, this might be a good replacement for Pyromark. With an 8 hr cure process and an easy application method, the downtime for application of the paint would be minimal compared to the roughly 2 day application of Pyromark. With further optimization, the absorptivity could be increased to further improve the receiver efficiency. Additionally with less degradation the yearly average absorptivity would be significantly better than Pyromark in a commercial plant. The emissivity could potentially be decreased as well with the addition of IR reflective materials in the paint, but only if it does not significantly affect the absorptivity.

Thermal spray on the other hand was found to be a difficult process to obtain selective materials. Thermal spray coatings are typically not uniform in either structure or chemical composition thus the optical properties are difficult to alter. Additionally, the thermal spray coatings tested for this project were observed to have issues with thermal stability likely due to unstable oxide formation during the thermal spray process. An Argon curtain during the thermal spray may prevent some of the oxide formation from occurring. Further research is needed to determine whether different procedures or materials will help the thermal spray coatings.

Thermal cycling will be continued on samples 14 and 15 with the addition of the Pyromark sample as a control sample. The thermal cycling will be continued at NREL, as NREL is well suited for this type of experiment. Furthermore, new mixed paints will be created on both stainless steel and Haynes 230. The Haynes 230 will be used to test the samples at higher temperatures (~750 °C). Additionally, other pigments will be tried using the binder solution used in the SS-B samples. Additionally, optimizing the painting technique will be investigated. SEM and EDX cross-section analysis is also recommended for future coatings.

Although the aggressive specific goals of the task were not reached on this task, good progress was made towards an improved coating. Additionally the work showed that the higher receiver efficiency may be better achieved through increased absorptivity rather than a reduced emissivity. This work highlighted the importance and potentials of an improved coating. Tower receiver coatings are very applicable for Abengoa, and work on this will continue after the project. Currently Abengoa is in the process of executing a CRADA with Sandia National Lab for a 2 year development of selective coatings. Sandia's facilities will allow SEM/EDX analysis and on-sun testing as mentioned above. This CRADA will build upon the work developed in this project and work developed by Sandia for a separate DOE project to ultimately develop a commercial coating.

Task 2.4 – Advanced Salt Technology

The receiver outlet temperature in Phase II is 600 °C. To achieve a bulk salt temperature of 600 °C, the salt film temperature must be about 670 °C. At 670 °C, the salt will thermally decompose, producing nitric oxide (NO), in the form of a gas, and oxide ions, which remain in the salt inventory. However, the residence time of the salt in the film region is believed to be too short for the decomposition reaction to proceed to completion.

Since the decomposition reaction is not believed to be 'fast', the decomposition process accelerates when the salt moves from the bulk region to the film region, but then quickly slows when the salt moves from the film region back into the bulk region. To simulate the rate of decomposition which will be experienced in a commercial project, an experiment was conducted, which emulated the temperature and hydraulic conditions in the last panel of a commercial receiver.

Experiment Design

The experiment includes a circulation pump, a heated test section, various instruments, and a control system. A piping and instrument diagram is shown in Figure 23.

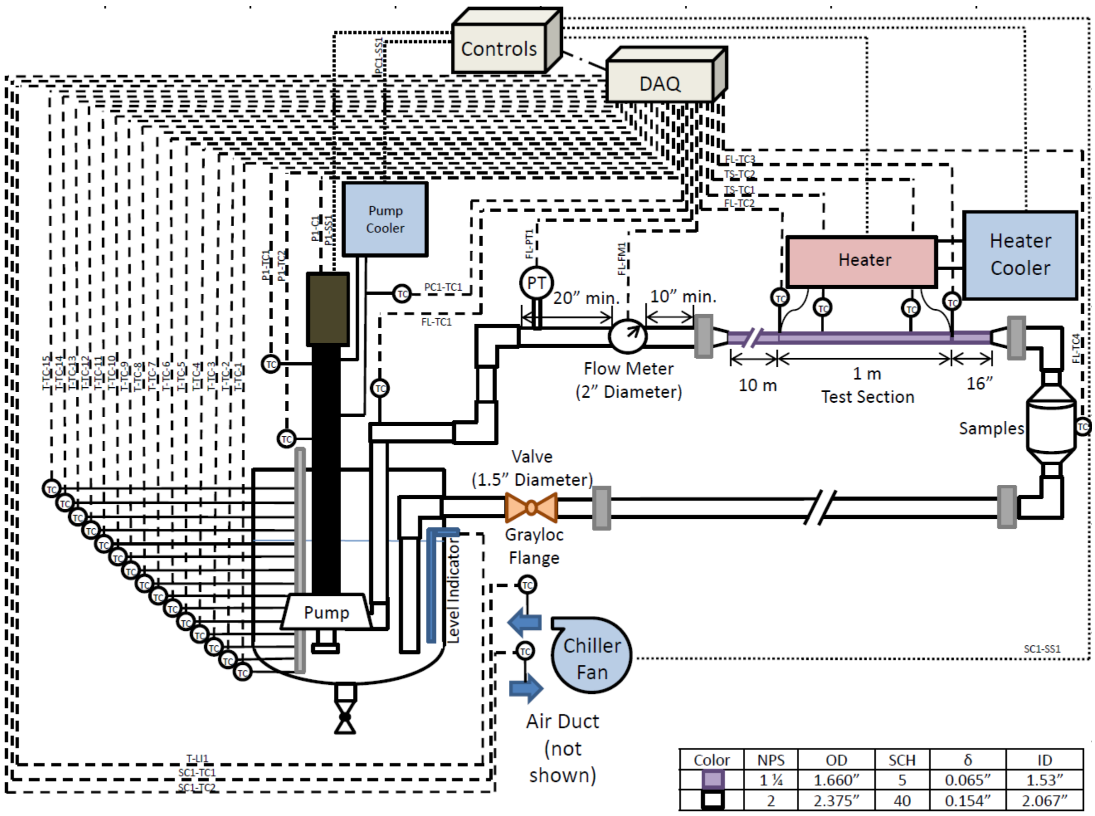

Color	NPS	OD	SCH	δ	ID
(purple)	1 ¼	1.660″	5	0.065″	1.53″
(white)	2	2.375″	40	0.154″	2.067″

Figure 23 Salt Thermal Stability Experiment Piping and Instrument Diagram

The pump draws suction from a pump sump, circulates the salt through the test section, and returns the salt to the pump sump. A chiller fan circulates air to and around the pump sump. The pump sump is maintained at a nominal temperature of 600 °C by balancing the heat input from the test section with the heat removed by the fan.

The experiment uses a tube with an inside diameter equal to that of the commercial receiver (41 mm), and operates with a nominal salt velocity of 3 m/sec. An unheated section of pipe, with a diameter of 41 mm and a length of 11 m, is installed upstream of the test section. A conceptual equipment arrangement is shown in Figure 24.

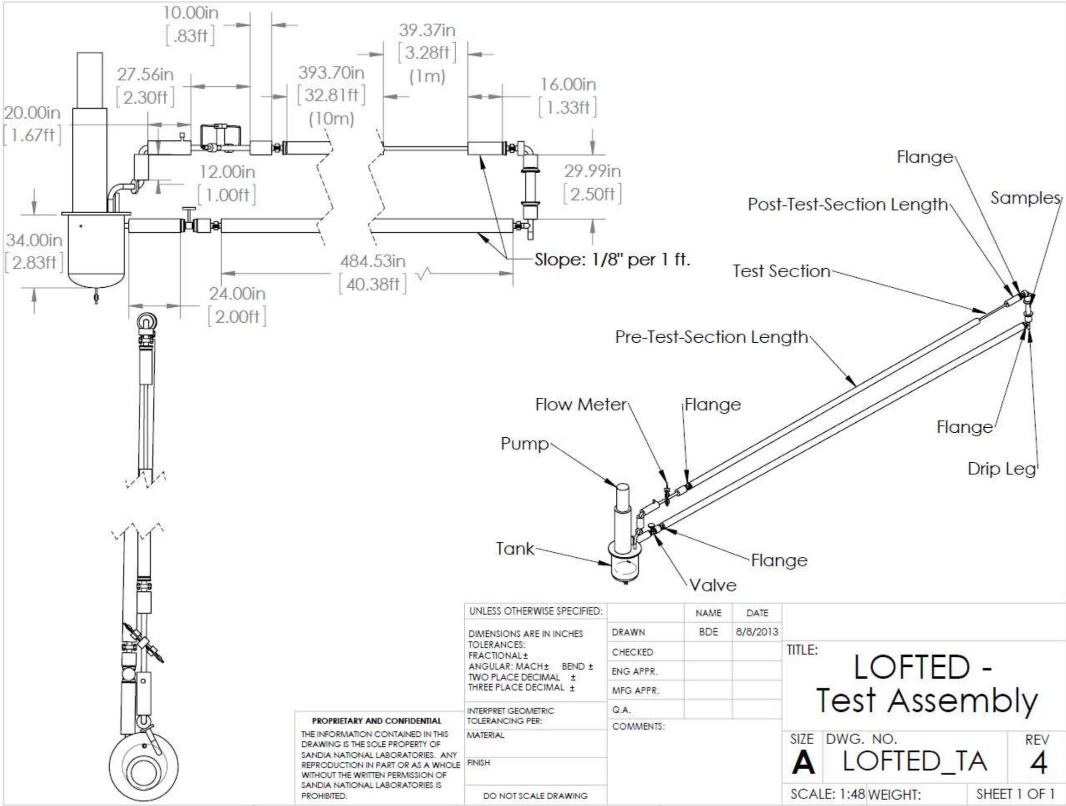

Figure 24 Salt Thermal Stability Experiment Equipment Arrangement

The purpose of the 11 m unheated section is to establish a hydraulic boundary layer similar to that at the mid-point of a commercial receiver panel. As such, the commercial receiver and the test section will have comparable values for the Reynolds number, the velocity profile across the tube diameter, the fluid temperature profile across the tube diameter, and, ideally, the oxide production rate per kg of flow.

Experiment Operation

The salt thermal stability test was concluded after 62 days of operation. In general, the equipment has operated as intended, with two exceptions:

1) The Inductoheat unit is cooled with a cooling water circuit, which, in turn, rejects heat to the ambient in a water-to-air heat exchanger. On hot days, the temperature of the water returning to the Inductoheat unit exceeded the limits set by the vendor, and the electric power supply to the Inductoheat was automatically turned off. However, salt circulation continued to prevent the salt from freezing in the supply line to the alloy test section. When the ambient temperature dropped later in the day, electric power was again supplied to the Inductoheat unit.

2) A salt leak developed in the transition piece which connects the pump sump with the mounting flange for the pump. On Day 6 of the experiment, the salt level had decreased to the point where the circulation pump tripped on low level. A salt capture system was installed at the transition piece, which returned the majority of the leakage

back to the pump sump. On Days 38, 45, and 50, a total of approximately 283 kg of salt was added to the pump sump. At the conclusion of the experiment, the salt inventory was estimated to be 356 kg, which was within a few percent of the initial salt inventory.

Oxide Production

It can be noted that the additions of salt to the experiment resulted in some fraction of the salt that was heated by the Inductoheat unit more than other portions of the salt. To estimate the rate of oxide production in the complete inventory as a function of time, a calculation method was developed, based on the following assumptions:

1) The nitrate ions and the nitrite ions in the salt reached equilibrium conditions by the start of the test. The equilibrium reaction is:

$$NO3^{-} \leftrightarrow NO2^{-} + ½\ O2 \quad \textit{Equation 1}$$

2) The oxide ions are formed from the equilibrium reaction:

$$NO2^{-} \leftrightarrow NO + O^{- -} \quad \textit{Equation 2}$$

3) The oxide ion is a proxy for a mixture of oxide, peroxide ($O_2^{- -}$), and superoxide (O^{-}) ions. (Unfortunately, the relative contributions of the 3 oxide species are currently unknown.) None of the oxide species reach their respective saturation limits. (The saturation limits are also unknown.)
4) The oxide ion production rate is a linear function of the nitrite ion concentration.
5) The nitrate ion concentration is much larger than the nitrite ion concentration; i.e., there is a surplus of nitrate ions to replenish the nitrite ions converted to oxide ions.
6) The nitrite ions which are converted to the oxide ions are replenished by the nitrate / nitrite equilibrium reaction at a rate which is high enough to ensure that the nitrite ion concentration does not limit the production rates of the oxides.
7) The oxide ion production rate is a constant value of 23 ppm per hour of Inductoheat operation

Based on these assumptions, the rate of oxide production is as shown in Figure 25.

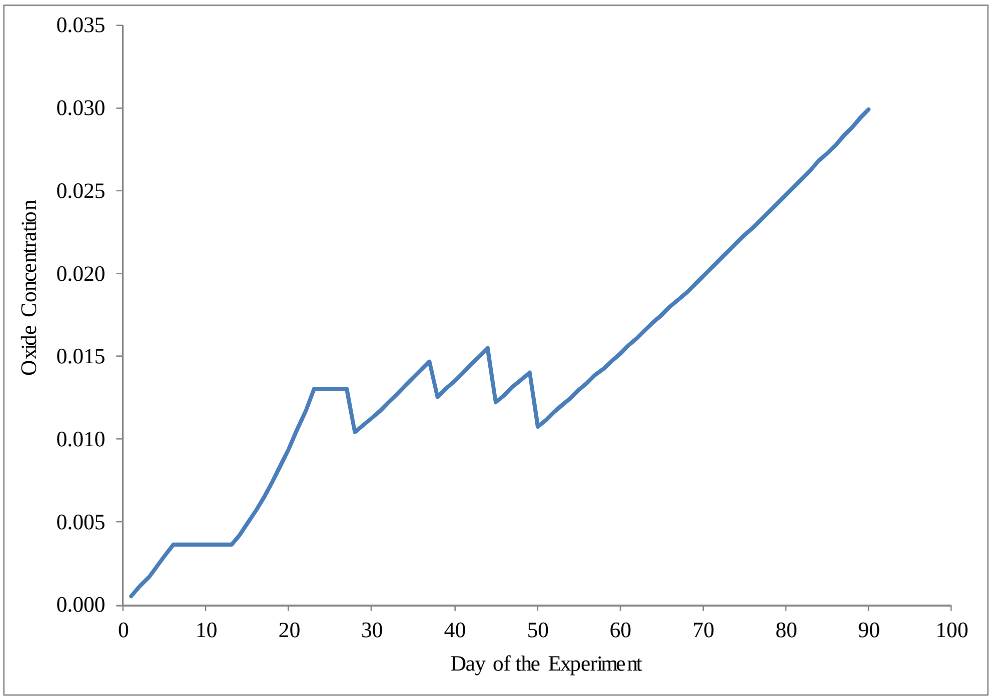

Figure 25 Oxide production rate as a function of time

The horizontal lines represent outage days, the portions of the line with negative slopes represent the addition of salt to the inventory, and the portions of the line with positive slopes represent the addition of oxides to the inventory based on the operation of the Inductoheat unit.

The total operating period of the Inductoheat unit was some 1,480 hours, which is equivalent to a nominal 12 years of operation in a commercial receiver.

It should be noted that the oxide production rate of 23 ppm per hour was not measured directly. The value was, in essence, back-calculated from the oxide concentration of 3.1 percent measured at the end of the experiment.

Although the oxide concentration increases in a roughly linear manner, after accounting for additions of salt to the inventory, Sandia believes that the oxide concentration may reach a steady state value on the order of 4 to 4.5 percent. Specifically, the principal reaction which produces the oxide ion is Equation 1. Simultaneously, there are several reactions which consume oxide ions, such as the formation of the following:

Sodium carbonate: $2\ Na^{+} + O^{--} + CO_2 \rightarrow Na_2CO_3$ *Equation 3*

Various iron oxides, such as: $2\ Fe^{+} + 3\ O^{--} \rightarrow Fe_2O_3$ *Equation 4*

Nickel oxide: $Ni^{++} + O^{--} \rightarrow NiO$ *Equation 5*

Various chromium oxides, such as: $2\ Cr^{+++} + 3\ O^{--} \rightarrow Cr_2O_3$ *Equation 6*

As such, there may be an equilibrium concentration of oxides, in which the rate of formation equals the rate of consumption. To a first order, the equilibrium value might be reached after a commercial plant has been in operation for about 15 years.

Coupon Corrosion Analyses

The results of the coupon corrosion analyses, conducted by Sandia, are shown in Figure 26. Note that the ordinate of the chart is a log scale.

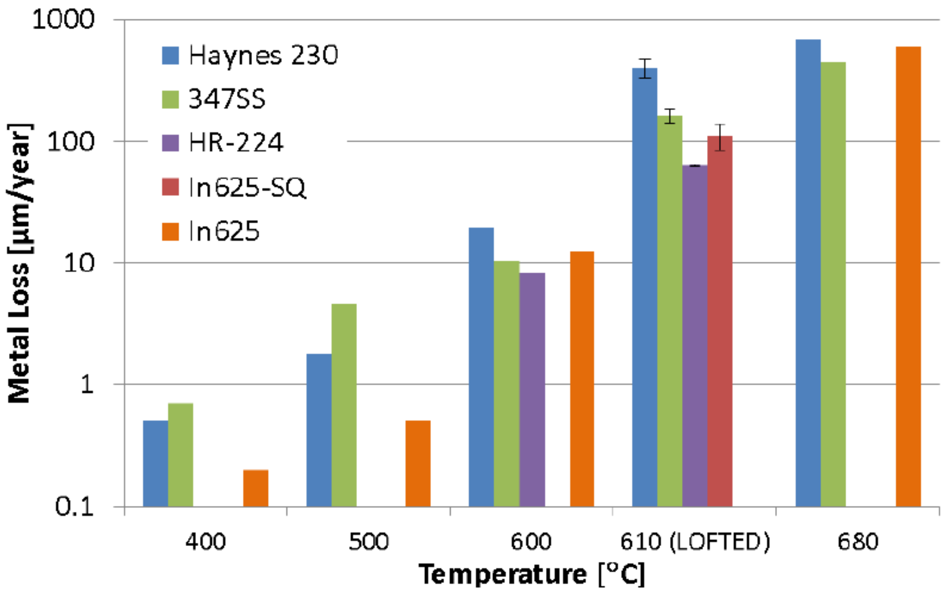

Figure 26 Metal Loss Rates for Corrosion Coupons

Several observations can be made from the data, as follows:

1) The corrosion rates in the experiment were a factor of 8 to 20 times higher than the corrosion rates measured in previous static test at 600 ˚C. The corrosion coupons were exposed to salt at a nominal temperature of 610 ˚C. However, the 10 ˚C increase in temperature over the previous studies would not account for the difference in the corrosion rates. The higher corrosion rates were likely due to i) higher oxide concentrations, and ii) continuous circulation of the oxides.

2) Compared to a typical static corrosion test at 610 ˚C, the higher oxide concentrations in the Sandia experiment are due to the periodic exposure of the salt to the tube internal film temperature of 670 ˚C.

Minor spalling was also observed in the Haynes 230 and the Inconel 625SQ coupons. In general, spalling is an undesirable corrosion characteristic, as it implies the oxide layer is not adherent. If the oxide layer is not adherent, the parent alloy below the oxide layer is exposed to the salt after spalling, and a new oxide layer must be formed. This has the potential for a significant increase in the corrosion rate.

The high corrosion rates observed in the experiment, together with the onset of spalling, implies that an acceptable limit of corrosion for a commercial project has been reached, and perhaps crossed. In the absence of some mechanism for limiting oxide levels, operation of a salt central receiver project at 600 ˚C is likely to too risky for commercial consideration.

Oxide Control

As noted in Reactions 3 through 6, oxide ions are continuously consumed due to reactions with carbon dioxide in the storage tank ullage gas, the iron in carbon steel, and the nickel and the chromium in stainless steel. In principle, the expected long-term equilibrium oxide concentration of perhaps 4 percent can be reduced by promoting one or more of these reactions. Potential methods for doing so include the following:

1) In a reaction column, establish a counter flow of carbon dioxide and salt. Because the storage tanks are vented to the atmosphere, the salt is continuously exposed to carbon dioxide in the ullage gas. However, the surface-to-volume ratio in the reaction column will be several orders of magnitude greater than the surface-to-volume ratio in the storage tanks, which should accelerate the reaction to a considerable degree.
2) Introduce carbon steel filing into the cold salt tank. Various forms of iron oxides will quickly form, producing an insoluble precipitate at the bottom of the tank.
3) In a reaction column, establish a counter flow of nitric oxide and salt. The nitric oxide reacts with the oxide ion to form the nitrite ion, as noted in Equation 2.

Based on the high corrosion rates shown in Figure 26, some form of salt treatment system to control the long term oxide concentration will likely be necessary in a commercial project. If the oxide concentration can be reduced to a level representing a continuous salt temperature of 600 ˚C, rather than an intermittent salt film temperature of 670 ˚C, then the corrosion rates should be low enough for commercial consideration.

Task 2.5 – Advanced Receiver Prototype

To validate the receiver design, and to reduce the risks in a large commercial project, an experiment was developed to test full-length receiver tubes under thermal cycling conditions.

Piping and Instrument Diagram

A piping and instrument diagram for the test panel is shown in Figure 27.

A total of 8 radiant heaters are located above the panel. The thermal output of each heater is controlled individually, which allows the tube strain distribution along the length of a tube to nominally match that of a commercial receiver panel.

Individual inlet and outlet air dampers allow the forced convection cooling during the cooling period to match the heat input during the heating period.

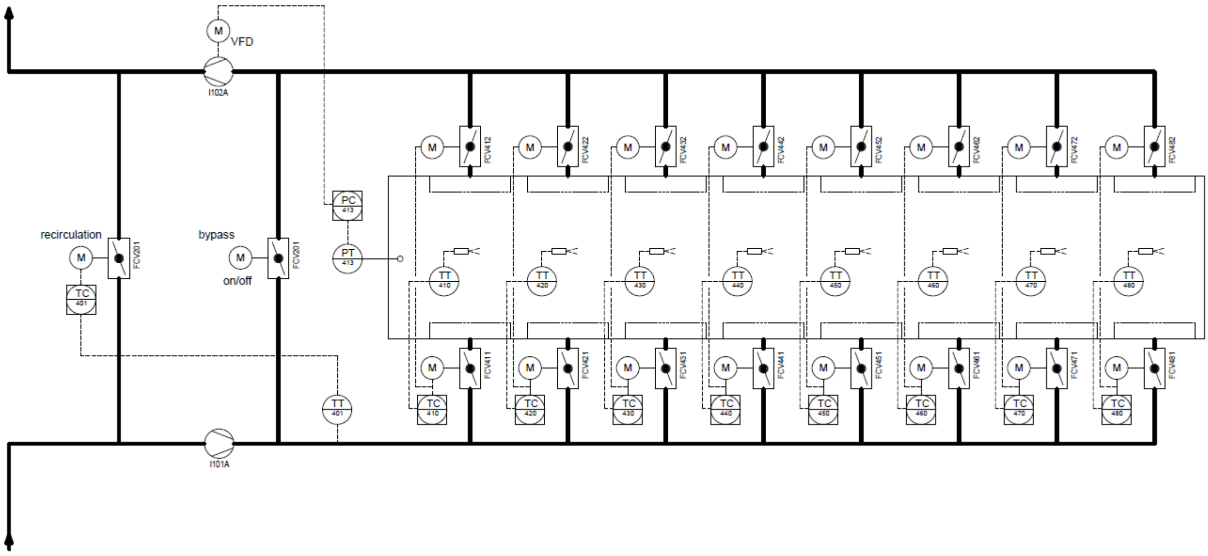

Figure 27 Test Panel Piping and Instrument Diagram

Test Panel Fabrication

A sketch of the test panel is shown in Figure 28. Since the panel consists of only 5 tubes, the length-to-width ratio of the absorber is about 100:1. In a commercial receiver, the ratio is closer to 6.5.

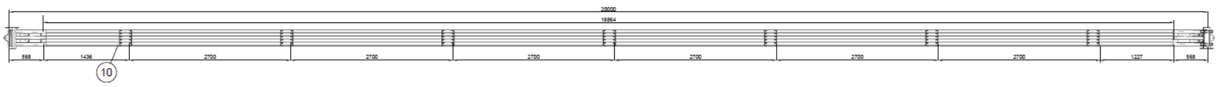

Figure 28 Test Panel Plan View

An isometric view of the panel headers is shown in Figure 29. The header is a 6 in. diameter, Sch 40 section of Type 316L stainless steel. The tubes connect to the header in two planes to provide the access necessary to weld the tubes to the header. Since both the header and the tube-to-header connections operate at a constant temperature of 245 °C, there is no need to provide sophisticated tapered nozzles between the tubes and the headers. The tubes are welded directly to the header wall.

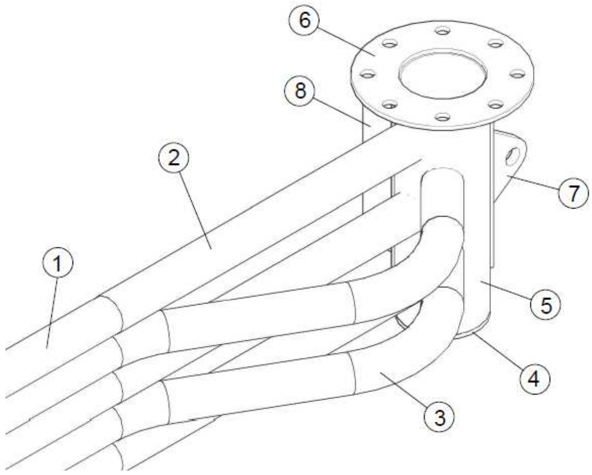

Figure 29 Isometric View of Tube-to-Header Connections

A lug on the header (Item 7) allows a horizontal load to be applied to the panel. The horizontal load simulates the dead weight of the tubes, the salt, and the headers in a commercial panel.

Oven Configuration

An elevation view of the selected oven design is shown in Figure 30. A small cooling air flow is needed during the heating cycle to help establish the required tube front-to-back temperature gradient.

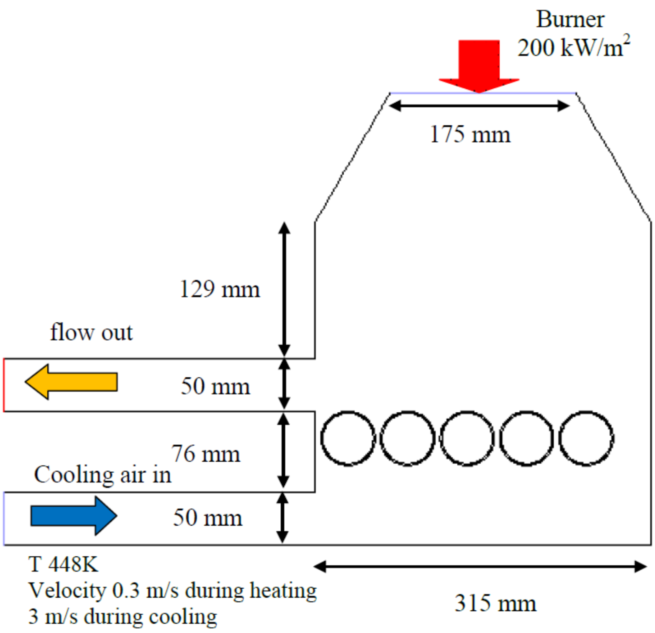

Figure 30 Vertical Section of Oven Geometry

Tube Fatigue Life

The tubes are subjected to an incident flux on only the front of the tubes. Due to the finite thermal conductivity of the tube alloy, and due to the finite internal convection heat transfer coefficient, two temperature distributions are established: a circumferential distribution; and a through-the-tube crown distribution. The tube strains associated with the temperature distributions are near, and in some cases, greater than, the yield stress. Further, the tubes are subjected to large strains for hold times in a commercial receiver which are on the order of hours. As such, the tubes eventually fail due a combination of low cycle fatigue and creep. Unfortunately, there are little data available on the combined effects of creep and fatigue for the hold times of interest (hours), and for the shapes of interest (thin wall tubes). As a result, there is considerable uncertainty in the calculated life of the receiver.

To provide data on the topic, the experiment operates through the following cycle:

1) The entire tube is at a uniform temperature of 250 ˚C.

2) The burners are started, and operate for about 30 seconds. The front of the tube reaches a temperature of about 585 ˚C, while the back of the tube reaches a temperature of about 300 ˚C. The circumferential and radial temperature distribution establishes a strain profile nominally equivalent to a tube in the first panel in the receiver.

3) The burners are shutoff for a period of 90 seconds. Forced air cooling, from the back of the tubes, returns the tube temperature to 250 ˚C.

4) The process is repeated for 30,000 cycles, or until a tube fails due to a crack or a rupture.

Computational Flow Dynamics Models

Figure 31 shows the temperature profiles expected within the oven at the end of the heating period. The temperatures shown are in °K, rather than °C.

The top of the tubes are heated by a combination of radiation and convection heat transfer from the burners. The bottoms of the tubes are heated only by the limited heat transfer from the front of the tube to the back of the tubes. Further, the bottoms of the tubes are cooled by a small flow of ambient air entering the bottom of the oven. At the end of the heating period, the required front-to-back temperature gradient of 250 °C has been established.

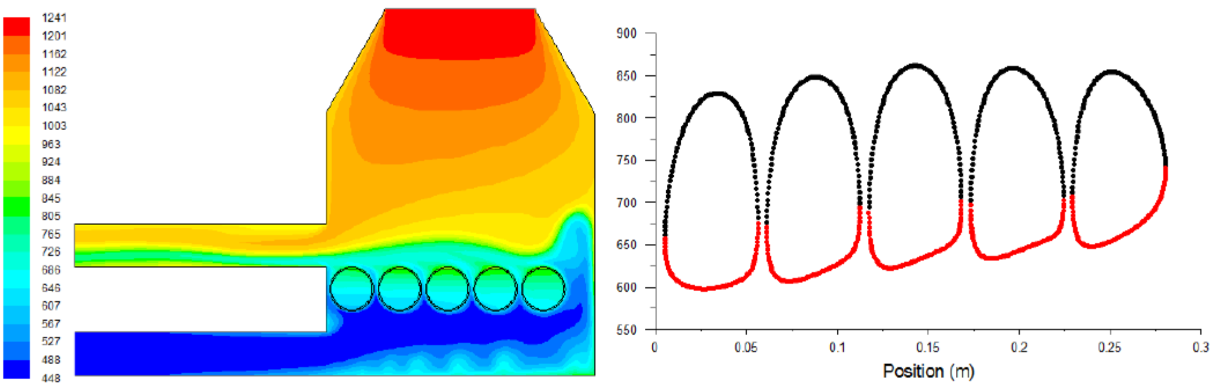

Figure 31 Temperature Profiles at the End of the Heating Period

Figure 32 shows the temperature profiles expected at the end of the cooling period. The cold ambient air entering at the bottom left is heated by the relatively warmer tubes and the walls in the oven. The front-to-back temperature gradient has decreased to about 60 °C. The associated tube strain is about 0.00075, or one-fourth that at the end of the heating period. Ideally, the front-to-back temperature profile, and the associated strain, would both be zero at the end of the cooling period. However, with a nominal metal temperature of 300 °C, the allowable fatigue life at a strain of 0.00075 is in excess of 7,000,000 cycles. As such, the residual fatigue damage associated with not reaching the desired front-to-back temperature gradient of 0 °C is believed to be negligible, and will not influence the results of the test. Nonetheless, it will be possible to establish a temperature gradient of 0 °C during the test by 1) extending the duration of the cooling period, or 2) increasing the flow of ambient air to the bottom of the tubes during the heating period.

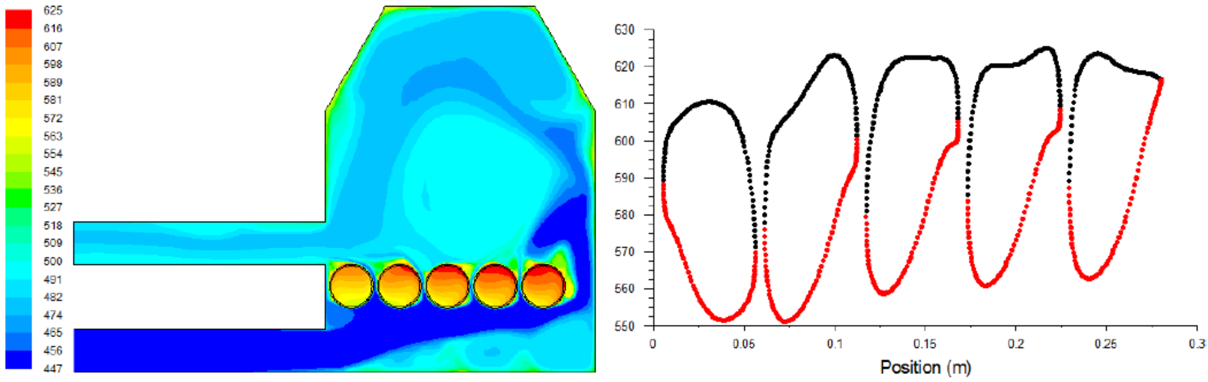

Figure 32 Temperature Profiles at the End of the Cooling Period

Weld Characteristics

In terms of uniform alloy chemistry and grain size, a seamless tube is preferred for a commercial receiver. However, seamless tubes are not available in the combination of diameter (~40 mm), wall thickness (1.65 mm), and length (>20 m) required for a commercial plant. As such, tubes must be fabricated through one of the following methods:

Class 1) Starting with a flat strip, in the solution annealed condition; a tube is formed by rolling, and then welding at the seam. The welding process form intermetallic compounds, such as nickel-niobium, which disrupt the lattice, and reduce the ductility of the alloy. The tube is solution annealed a second time to dissolve the intermetallic compounds. The tube is then forced through a series of dies to reduce the diameter and to reduce the wall thickness. The minimum cold work is 20 percent. The cold work process mechanically breaks apart the large grains formed during the welding and the second annealing processes. The tube is solution annealed a third time to remove the residual stresses from the cold work, and to control the grain size.

Class 2) Starting with a flat strip, in the solution annealed condition; a tube is formed by rolling, and then welding at the seam. The weld is bead worked to mechanically break apart the large grains formed during welding. The tube is then solution annealed a second time.

Class 3) Starting with a flat strip, in the solution annealed condition; a tube is formed by rolling, and then welding at the seam.

Class 3 tubes are generally considered not acceptable for commercial use due to the disruption of the alloy chemistry and the grain size at the weld zone.

In the experiment, the tube material is Alloy 230, with the types of tubes selected as follows:

1) Three of the Class 3 tubes. The tubes are single piece, with no butt welds in the heated zone.

2) Two of the Class 2 tubes. The tubes are fabricated from short pieces, each 3 to 4 m in length. The tubes are joined by butt welds, using a filler material suitable for Alloy 230.

In general, butt welds in the flux zone are undesirable, as it is not possible to cold work a butt weld. As such, the metal chemistry and the grain size in the weld zone can be markedly different than in the parent tube, and the fatigue properties at the weld zone are likely to be inferior to the parent alloy. However, it is not known to what extent the fatigue properties have been influenced. The oven test will provide some useful data on the topic. Specifically, does a butt weld have a fatigue life of 1,000 cycles, or a fatigue life of 10,000 cycles? If the former, the use of butt welds in a commercial receiver can be excluded from consideration.

Currently the test is starting up and a supplemental report will be provided at the conclusion of the testing with results.

Task 2.6 – Economic Analysis

Two of the motivations in increasing the receiver outlet temperature from 565 C in Phase I to 600 C in Phase II was to improve the efficiency of the Rankine cycle, and to reduce the unit cost of the storage system, in $/kWhe.

Rankine Cycle

In Phase I, the Rankine cycle was a single reheat design, with live steam conditions of 125 bar and 540 ˚C and hot reheat steam conditions of 17 bar and 540 ˚C. The design point for the cycle was a summer day, with an ambient dry bulb temperature of 42.8 C. With an air cooled condenser for heat rejection, the condenser pressure was 170 mbar and the gross cycle efficiency was 0.409. With an ambient temperature of 15 ˚C, the condenser pressure decreased to 44 mbar, and the gross cycle efficiency improved to 0.436.

In Phase II, a single reheat cycle was retained. However, the higher salt temperature allowed an increase in the live steam conditions to 170 bar and 585 ˚C, and an increase in the hot reheat steam conditions to 18 bar and 585 ˚C. The design point for the cycle was, again, a summer day, with an ambient dry bulb temperature of 42.8 C. With an air cooled condenser for heat rejection, the condenser pressure was 170 mbar and the gross cycle efficiency was 0.429. With an ambient temperature of 15 ˚C, the condenser pressure decreased to 44 mbar, and the gross cycle efficiency improved to 0.456.

To a first order, the increase in the receiver outlet temperature for Phase II provided an increase in the Rankine cycle efficiency of 2 percentage points. This, in turn, leads to a nominal decrease in the required heliostat area of 4.5 percent. Assuming that the heliostat field represents 40 percent of the cost of the project, a reduction of 4.5 percent in the reflector area translates to a 2 percent reduction in the levelized cost of energy.

Thermal Storage System

In Phase I, the nominal hot salt and cold salt temperatures were 565 ˚C and 292 ˚C, respectively. These values resulted in nominal salt enthalpies of 842.7 kJ/kg and 429.3 kJ/kg, respectively. At the design point Rankine cycle efficiency of 0.409, the mass of salt required to store the equivalent of 1 MWhe of electric energy production was 21,300 kg.

In Phase II, the nominal hot salt and cold salt temperatures were 600 ˚C and 304 ˚C, respectively. These values resulted in nominal salt enthalpies of 896.8 kJ/kg and 446.4 kJ/kg, respectively. At the design point cycle efficiency of 0.429, the mass of salt required to store the equivalent of 1 MWhe of electric energy production was 18,600 kg. As a result, the unit cost of storage in Phase II was about 12 percent less than the unit cost in Phase I.

Annual Plant Performance

The annual plant performance was calculated using Abengoa’s MSTowerSim program. The principal inputs to the program include the following:

1) Lathrop Well, Nevada, project site, and an annual direct normal radiation of 2,783 kWh/m^2.
2) A heliostat field consisting of 1,525,370m^2 of collector area. The total beam error of the heliostat, at the average wind speed of the site (3.0 m/sec), was estimated to be 2.87 mrad.
3) During the year, 12 scheduled outage days and 6 forced outage days.

A summary of the plant performance is shown in Table 12. The abbreviation RCSBTSp represents mirror reflectivity, cosine losses, shading losses, blocking losses, atmospheric transmission losses, and receiver spillage.

Table 12 Annual Plant Performance

	Energy, GWh	Efficiency, %
Gross Solar Energy	4,245.3	
Gross Available Solar Energy (Maintenance, wind speed, bad days)	4,228.1	99.60%
Solar Field Energy RCSBTSp	2,267.1	53.40%
Solar Field Energy RCSBTSp and Degradation	2,267.1	100.00%
Solar Field Energy RCSBTSp, Degradation and Wind	2,258.1	99.60%
Solar Field Defocused Energy	325.0	14.33%
Receiver Incident Total Energy	1,933.1	85.61%
Receiver Incident Energy for Startup and Drainage	32.7	1.69%
Receiver Incident Energy with Molten Salts	1,900.4	98.31%
Receiver Absorbed Energy	1,736.8	89.84%
Energy to Hot Tank From Receiver	1,720.3	
Energy to Steam Generator System from Hot Tank	1,714.6	
Energy to Steam Generator System from Cold Tank	11.9	
Absorbed Energy by Steam Generator System	1,726.4	99.40%
Gross Production	764.2	44.26%
Gross Production with degradation	764.2	100.00%
Online Parasitics	81.3	10.64%
Offline Parasitics	11.0	1.44%
Net Production	671.9	

Note that the Solar Field Defocused Energy represents about 14 percent of the theoretical energy available to the receiver. Energy is defocused because 1) the incident power on the receiver exceeds the maximum thermal rating of the receiver, or 2) the storage system is full. On clear summer days, the storage system often reaches maximum capacity as early as 2:00 pm, and a significant fraction of the heliostat field must be defocused for the balance of the day. However, an annual defocus loss of approximately 14 percent is an economic choice. Specifically, if heliostats are inexpensive relative the Rankine cycle, then the lowest levelized cost of energy is reached if some of the energy available from the heliostat field is lost in an effort to operate the Rankine cycle at full load for more hours each year.

Plant Capital Cost

A summary of the plant capital cost, in current year dollars, is shown in Table 13. The percentage values for contingencies, engineering, construction management, project development, land, and sales tax are those specified in the original FOA.

Table 13 Plant Capital Cost Summary, 2014 Dollars

Item	$1,000	Contingency	$1,000
Land	0	10%	0
Structures and Improvements	19,369	10%	21,306
Collector System	184,646	10%	203,111
Receiver System	89,958	10%	98,954
Thermal Storage System	91,275	10%	100,403
Steam Generation System	15,181	10%	16,699
Electric Power Generation System	147,936	10%	162,729
Master Control System	6,224	10%	6,847
	-----------		-----------
Subtotal - Total Field Cost	554,589		610,048
Indirect Capital Costs			
Engineering, Procurement, Home Office, Construction Management, Field Procurement, Startup and Checkout		16%	97,608
Project Development, Land, and Miscellaneous		3.5%	21,352
Sales Tax		7.75%	37,823

Total Indirect Capital Cost			156,782
Total Capital Cost			766,830

Annual Operation and Maintenance Cost

The development of the annual operation and maintenance cost is shown in Table 14

The plant requires a full-time staff of 39 personnel. The wages shown in the table are direct wages only. To the direct wages, 39 percent is added for payroll additives; i.e., federal and state taxes, unemployment insurance, disability insurance, vacation, sick leave, and holidays. To the sum of the direct wages plus payroll additives costs, is added 45 percent for the contractor’s overhead and profit.

Table 14 Annual Operation and Maintenance Cost Estimate

Position	Number of personnel	Direct wage, $/hr	Total cost
Plant Manager	1	$50	$210,000
Operations Manager	1	$40	$168,000
- Senior Operators	4	$35	$587,000
- Control Operators	4	$30	$503,000
- Plant Equipment Operators	4	$28	$470,000
- Assistant Plant Equipment Operators	0	$0	$0
Maintenance Supervisor	1	$40	$168,000
- Electricians	2	$31	$260,000
- Instrument Technicians	2	$31	$260,000
- Mechanics	2	$30	$252,000
- Mechanics Helpers	0	$0	$0
- Machinist / Welder	1	$32	$134,000
- Vehicle Mechanic	1	$25	$105,000
- Heliostat Washers	12	$12	$604,000
- Warehouse Clerk	1	$15	$63,000
Plant Engineer	1	$35	$147,000
Chemical Technician	1	$28	$117,000
Water Treatment Technician	0	$0	$0
Secretary	1	$18	$75,000
	-----		---------------
	39		$4,123,000
Non-labor costs			
- Heliostat field (0.5 percent of system cost)			$1,100,000
- Receiver system (2.0 percent of system cost)			$1,750,000
- Thermal storage system (0.5 percent of system cost)			$450,000
- Steam generation system (1.5 percent of system cost)			$230,000
- Electric power generation system (1.5 percent of system cost)			$2,190,000
- Service contracts			$500,000
- Water			$125,000
- Miscellaneous			$350,000
- Capital equipment			$140,000

Subtotal: Non-labor costs			$6,835,000
Total: Labor and Non-labor Costs			$10,958,000

The non-labor costs represent allowances for spare parts, vehicle maintenance, and periodic expenses for specialty subcontract services, such as turbine overhauls.

Levelized Cost of Energy

An estimate of the levelized cost of energy was developed using cash flow analysis in the Solar Advisor Model. The principal financial inputs to the model include the following parameters, as specified in the FOA:

- Federal and state income tax rates of 34.0 and 6.0 percent, respectively, resulting in an effective rate of 38.0 percent
- Property insurance and property tax rates of 0.5 and 0.0 percent, respectively
- State sales tax rate of 7.75 percent, applied to 80 percent of the direct costs
- Federal investment tax credit of 10 percent
- Modified accelerated capital recovery, with a 6 year depreciation period
- Debt interest rate and term of 8.0 percent and 20 years, respectively
- Debt fraction of 50 percent
- Power purchase agreement annual escalation rate in the energy sales price of 1 percent
- Minimum debt service coverage ratio of 1.40
- No supplemental investments past the commercial operation date
- Minimum internal rate of return of 12 percent.

The calculated cost of energy is $0.124/kWhe, in nominal 2014 dollars, and $0.102/kWhe, in real 2014 dollars.

The estimated escalation factor, to bring nominal 2014 dollars back to the level of nominal 2009 dollars, is 0.820. The estimated energy cost, in nominal 2009 dollars, is $0.102/kWhe. In the SAM financial model, the conversion factor from real dollars to a nominal dollars is 111 / 134 = 0.828. As such, the estimated cost of energy, in real 2009 dollars, is $0.084/kWhe, and the LCOE satisfies the requirement in the Statement of Project Objectives for a maximum LCOE of $0.090/kWhe.

Conclusions:

This project was very large and incorporated many different aspects that all needed to work together to get a significant reduction in the cost of a molten salt tower. All of the critical milestones of Phase I which included: $0.14/kWhe (real 2009 $) LCOE, technical and economic projections for a baseload plant, identification and understanding of technical barriers related to raising salt temperature, and identification of “key” components for prototypes, were all met and provided the path forward to Phase II. Most of the overall project goals were met, with a few falling a bit short, but still providing valuable knowledge on the concepts.

The initial hypothesis of being able to increase the salt temperature to 600 ˚C was tested and valuable knowledge was gained from the dynamic test. The results were significant and proved the initial hypothesis, that high temperatures in the film region would have limited effect on oxide production, wrong. These results show that in order to reach 600 ˚C salt temperature further development would be needed on a system for controlling the oxides and corrosion. The overall efficiency gains from a 600 ˚C salt temperature were still shown in the economic analysis, but practical implementation needs additional work.

The improvement of receiver efficiency due to a solar selective coating was shown with modeling, but still needs additional work for commercial implementation. Much of the coating work focused on developing a coating that would be easy to apply to 18 m or longer receiver tubes through thermal spray or paint. Coatings were screened for high absorptivity and stability in air at 750 ˚C, and then could be optimized for lower emissivity. Although emissivity is a loss, absorptivity plays a much bigger factor in receiver efficiency. This is best illustrated by the fact that the absorptivity relates to the aperture of the entire solar field, while emissivity only relates to the aperture of the receiver.

The heliostat task was very successful and met all of the goals to achieve over a 30 percent solar field cost reduction over the baseline design. This work allowed Abengoa to develop a completely new and novel small heliostat that ran counter to the traditional large heliostats used which will provide benefit to future towers constructed by Abengoa. This is especially significant since Abengoa is the largest energy provider using solar thermal technology.

The receiver design showed that although a large receiver was more difficult, it is feasible. The work also showed a reasonable method for calculating the combined creep fatigue and highlighted additions needed to ASME codes accounting for the specialty metals. Once the receiver prototype cycle fatigue testing is completed it will also verify reliability of long tubes and butt-welded tubes, which will be important for reducing risk for financing.

Budget and Schedule:

The budget for the project was $6,649,331 with a 20 percent recipient cost share for most tasks, 50 percent cost share for prototyping tasks, and $200,000 paid directly to Sandia by DOE. The DOE cost share for the project was fully spent and additional costs were covered by Abengoa. The final cost share based on a total cost of $6,843,468 was 69 percent DOE (including money to Sandia) and 31 percent Abengoa (and cost share partners). A majority of the additional spending was due to increased labor needed for pre prototype heliostat tasks and additional costs for starting up the receiver prototype oven. Many of the tasks slipped from the original schedule, but were ok within the overall schedule. The major task that slipped and required a no cost project extension of 3 months was task 2.5, the receiver prototype. This task was delayed from the start due to difficulty finding a vendor to provide the necessary equipment, which was originally assumed to happen in an existing oven facility. Once a vender was found to construct a custom oven there was a delay due to modifying the contract to move equipment cost from the heliostat task to the receiver. The order was placed with the vendor before the contract was fully approved to meet the minimum time needed for the task to be completed within the project period. The task saw further delays due to difficulty acquiring the specialty metals needed for the receiver tubes and failure of the annealing equipment for the tubes. Additional delays in Task 2.4 salt testing also took advantage of the short project extension. Delays due to reduced staff at Sandia extended the construction period of the test equipment. Additionally there were large salt leaks with the test that required additional rework time and extended testing to account for the leak replacement salt.

Path Forward:

Abengoa has reached financial closure on a large commercial salt tower project in the Atacama Desert of Chile. The plant has a nominal receiver rating of 690 MWt, a thermal storage capacity of 14 hours, and a gross turbine rating of 115 MWe. As such, the plant will provide baseload power during much of the Spring and the Fall, and during all of the Summer, months. The baseline plant from Phase I helped build the knowledge to design the basis for this plant. Additionally a number of plant design features developed in Phase II, such as the use of seam welded Alloy 230 receiver tubes, have been adopted for the project in Chile.

The receiver coating work will continue further to develop a commercial solution through a CRADA with Sandia. This can be used in any of the existing plants and new plants such as the one in Chile, since Pyromark has to be replaced yearly.

The ROP Heliostat is being refined and further testing is planned in Spain next year on the path to commercialization.

As discussed in Task 2.4, increasing the salt temperature from 565 ˚C in Phase I to 600 ˚C in Phase II results in measureable increases in both the oxide concentrations and the alloy corrosion rates. Some form of oxide control is likely to be needed in a commercial project. The development of an experiment, which examines various methods for reducing the oxide concentration, could be conducted with the staff at Sandia, either in Livermore or in Albuquerque.

Appendix A – Foster Wheeler report

Appendix B – Sandia Report

References:

[1] Katcher, M., Pike, L. M., and Ishwar, V. R., "Modified Power Law – Haynes 230 Alloy Creep Rupture", 12th International Conference on Creep and Fracture of Engineering Materials and Structures, May 2011, Kyoto, Japan

[2] Peterka, J.A., Derickson, R.G. *Wind Load Design Methods for Ground-Based Heliostats and Parabolic Dish Collectors*, New Mexico : Sandia National Laboratories, 1992. Sandia Report SAND92-7009

[3] Kolb, G.J., Jones, S.A., Donnnelly, M.W., Gorman, D., Thomas, R., Davenport, R., Lumia, R., *Heliostat Cost Reduction Study*, New Mexico : Sandia National Laboratories, 2007. Sandia Report SAND2007-3293

[4] "Test code for machine tools – Part 2: Determination of accuracy and repeatability of positioning numerically controlled axes", ISO 230-2-2006(E), Third Edition, 2006-03-15, International Organization for Standardization, Geneva, Switzerland.

[5] Guo, M. et al. "Determination of the angular parameters in the general altitude-azimuth tracking angle formulas for a heliostat with a mirror-pivot offset based on experimental tracking data," Solar Energy 86 (2012) pp 941-950.

DEVELOPMENT of BASELOAD CSP ADVANCED NITRATE SALT CENTRAL RECEIVER POWER PLANT

Phase 2: Engineering Design and Prototyping of Advanced Technologies

FINAL REPORT

Prepared by:

William Cannon **Horst Hack** **Robert Seltzer**
Jack Desmond **Peter Jansen** **Marifae Tibay**
Stephen Goidich **Sanjay Patel** **Richard Virgilio**
Andrew Seltzer

Issued November 2014

Work Performed Under
U.S. Department of Energy
Cooperative Agreement No. DE-EE0003596

Foster Wheeler North America Corp.
53 Frontage Road PO 9000
Hampton, NJ 08827-9000

Disclaimer

Abstract

A concentrating solar power system (CSP), consisting of a solar receiver and a series of heat exchangers, has been conceptually designed and cost estimated by Foster Wheeler (FW). The solar receiver absorbs 795 MWt of incident solar energy and heats molten nitrate salt from 308 to 600 °C (588 to 1112 °F) with a flow rate of 1790 kg/sec ($14.21x10^6$ lb./hr.); using the hot salt the heat exchangers generate 585 °C (1085 °F) 170 bara (2465 psia) steam to power a steam turbine for electrical power generation. The solar receiver consists of 24 tube panels located at the top of and positioned along the outside circumference (external arrangement) of a tower. Each panel consists of 56 tubes that are 40.9 mm (1.61 in) in outside diameter, have an average wall thickness of 1.65 mm (0.065 in), and are longitudinally welded together to form a 2.29 m (7.5 ft.) wide flat panel. The tubes have an effective heat transfer length of 22.6 m (74.2 ft.) and are supported on their back side by 6 equally spaced buckstays. Jumper tubes provided at the top and bottom connect the panel to flow distribution headers and provide flexibility for thermal expansion; when assembled the top header to bottom header centerline spacing is 29.9 m (98.1 ft.). The tubes receive high solar fluxes and are therefore furnished in Haynes 230 as this material has excellent creep to rupture properties and is resistant to nitrate salt corrosion and stress corrosion cracking. The design of the CSP is described herein along with the thermal, mechanical, creep, and fatigue analyses that were the basis for its design.

Table of Contents

Table of Contents (Cont'd.)

Table Number Page

1.0 Introduction

The objective of this Department of Energy (DOE) funded study is to develop and evaluate Concentrating Solar Power (CSP) components and/or systems that could lead to the development of utility-scale baseload CSP power plants with a capacity factor of 75%, capable of generating electricity at costs competitive with fossil-fired generators and estimated to be 8 to 9 ¢/kWh adjusted for real 2009$ (Ref. 1).

A CSP consists of a Thermosolar Power Plant that uses Tower Technology to receive the focused sunlight and heat the Heat Transfer Fluid (HTF). The Thermosolar Power Plant is characterized by a tower mounted cylindrical receiver (heat exchanger) using nitrate salt as the heat transfer fluid. The cold nitrate salt is heated from 308 ºC (588 °F) to 600 ºC (1112 °F) in the receiver by reflected solar energy from a field of sun tracking mirrors-heliostat.

The hot salt flows from the hot salt tank to a steam generation system. The superheated steam produced is delivered to a steam turbine to produce electricity.

This report will focus on the Receiver and the Heat Exchangers which make up the boiler portion of the Thermosolar Power Plant.

Figure 1 shows a typical *Central Receiver Solar Power Plant* arrangement.

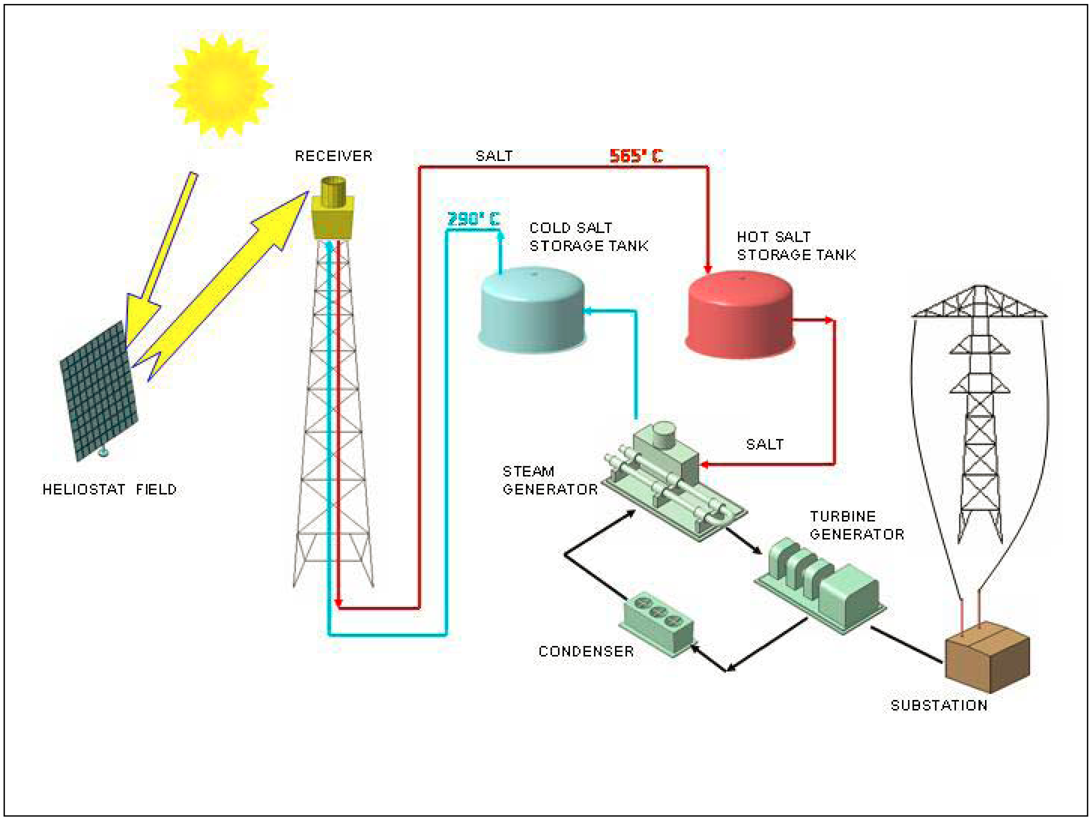

Figure 1. Molten Salt Central Receiver System Power Plant

The Steam Generator System (SGS) uses at least four separate heat exchangers for feedwater preheating, evaporation, superheating and reheating. Usually, all four heat exchangers are shell and tubes type, with salt on the shellside and steam/water on the tubeside (excluding some types of evaporator).

Hot salt from a storage tank is pumped in parallel to the reheater and superheater shells. After transferring heat to the reheat and main steam lines, the salt streams leaving the reheater and superheater, combine with a by-pass stream and enter the evaporator where the hot salt gives up its heat to evaporate water. The salt is then routed to the preheater, where the feedwater is heated. The salt from the preheater is sent to a cold-salt storage tank for recycling to the solar tower receiver system.

Treated feedwater is supplied to the preheater by a pump and is heated before it enters the evaporator. Saturated steam is generated in the evaporator and routed to the superheater (after separating water droplets), where it is superheated before it enters the high-pressure turbine for power generation. Intermediate pressure steam from the turbine is brought to the reheater for further superheating and sent to the low pressure turbine for additional work extraction. The exiting steam goes to the condenser, and the condensed water is then recycled through the feedwater pump to the feedwater heaters before restarting the cycle.

Typical SGS consists of four components: preheater/economizer, steam generator, superheater, and reheater, as shown in the preliminary functional diagram (Figure 2).

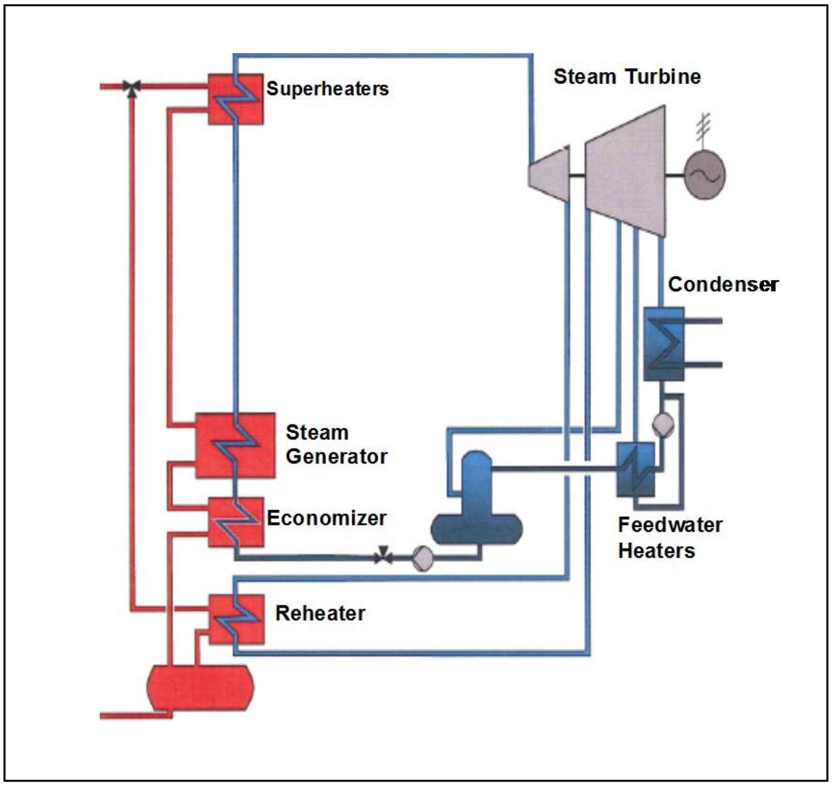

Figure 2. Typical Steam Generator System

The 100 MW_e Central Receiver Solar Power Plant SGS has been designed with two (2) 50 MW_e identical trains consisting of two (2) preheaters operating in series, one (1) forced circulation evaporator plus steam drum, one (1) superheater, and one (1) reheater, both hairpin type.

The Solar Receiver consists of twenty-four (24) individually fabricated panels which are arranged in four (4) passes flowing in a North to South direction. These panels will have an internal east west cross over after the third panel. These panels make up the receiver which is mounted on top of a tower to allow the heliostat field to radiate directly on their surface. After the last panel the system is vented to atmosphere thereby allowing the hot salt to gravity feedback to grade.

2.0 Executive Summary

A concentrating solar power system (CSP), consisting of a solar receiver and a series of heat exchangers, has been conceptually designed and cost estimated by Foster Wheeler (FW). The solar receiver heats molten nitrate salt from 308 to 600 °C (588 to 1112 °F) at a rate of 1790 kg/sec ($14.21x10^6$ lb./hr.) and via the heat exchangers generates 585 °C (1085 °F) 70 bara (2465 psia) steam to power a steam turbine for electrical power generation. The solar receiver consists of 24 tube panels located at the top of and positioned along the outside circumference (external arrangement) of a tower. Each panel consists of 56 tubes that are 40.9 mm (1.61 in) in outside diameter, have an average wall thickness of 1.65 mm (0.065 in), and are longitudinally welded together to form a 2.29 m (7.5 ft.) wide flat panel. The tubes have an effective heat transfer length of 29.9 m (98.1 ft.) and are supported on their back side by 6 equally spaced buckstays. Jumper tubes provided at the top and bottom connect the panel to flow distribution headers and provide flexibility for thermal expansion; when assembled the top header to bottom header centerline spacing is 23.9 m (78.4 ft.). The tubes receive high solar fluxes and are therefore furnished in Haynes 230, as this material has excellent creep to rupture properties and is resistant to nitrate salt corrosion and stress corrosion cracking.

A field of heliostats surrounding the tower focuses 870 MWt of sunlight on the panels at mid-day (full load condition). The panel faces are painted with a high-temperature black coating (similar to Pyromark) to increase their absorption and, operating with an efficiency of 91.36%, the receiver absorbs 795 MWt of the incident heat flux. The peak incident heat flux is 1287 kW/m^2 (408.1 Btu/ft^2).

Pumps located at grade draw salt from a cold storage tank and pump it to a surge tank provided atop the tower. From the surge tank, the salt splits into two streams, and each flows through twelve (12) panels. To provide a tube side velocity of approximately 4 m/sec (13.1 ft./sec) the twelve panels are grouped into two (2) parallel circuits (a total of four parallel circuits for the receiver), each with six (6) panels. Flow enters the top of the inlet panel for each circuit and flows up and down in a serpentine arrangement with transfer piping connecting the inlet and outlet headers for each panel. After passing through the six panels, the four salt streams join and proceed down the tower to a hot salt storage tank. Since the nitrate salt freezes at 230 °C (446

°F), each header is enclosed within an insulated and electrically heated “oven box” that preheats the headers at start-up (before cold salt enters the panel) and maintains a minimum temperature overnight after shutdown. Similarly all transfer piping and the inlet surge tank are insulated and electrically heat traced.

The steam generators consist of heat exchangers that transfer salt heat to the steam cycle. Since the steam cycle pressure is much greater than the salt pressure, the boiler feedwater and steam are placed inside the tubes; excepting for the steam drum, this places the salt on the shell side and, because of its much lower pressure, results in reduced vessel weights and costs. The evaporator and feedwater preheater vessels each possess a U tube bundle and, to accommodate the high steam cycle pressure, a bonnet head (integral cover) is provided welded to a tubesheet which in turn is welded to the shell. The superheater and reheater vessels are similar excepting that the U tubes are welded to separate tubesheets loaded into a hairpin shaped shell.

The salt and water/steam flow countercurrent to each other through the vessels. Hot salt pumped from the storage tank splits into two streams, one to the superheater and the other to the reheater; after passing though those units the salt streams combine, proceed through the evaporator, pass through the second and then the first stage feedwater preheaters, and onto the cold salt storage tank. Boiler feedwater is pumped through the first and second stage preheater vessels and proceeds to the steam. A recirculation pump draws saturated water from the drum, passes it through the evaporator, and returns a low quality steam-water mixture to the drum. From the drum, saturated steam proceeds through the superheater vessel and onto the steam turbine; intermediate pressure steam from the turbine is reheated in the reheater vessel and returned to the steam turbine. The exteriors of all the vessels, piping, valves, etc. are insulated and electric heat tracing is provided to warm them before salt is admitted.

Using the specified midday, full load incident heat flux distribution, the temperature differences and stresses that will exist within a tube and across the operating receiver panels were calculated. Tube side pressure, wind load, dead weight, salt weight, and seismic conditions were taken into consideration and structural elastic and non-linear analyses were conducted to determine stresses and strains. Results from the non-linear structural analysis were used to calculate fatigue damage using methods of ASME Section Vlll Division 2. The geometry of the tubes with the given heat flux distribution satisfied ASME Code allowables for strain limits and fatigue and the panels should be suitable for approximately 30 years of service.

3.0 Solar Receiver Design and Analysis

3.1 Design Basis. The receiver was designed to meet the criteria defined in the Receiver Specification document included in Reference 2. The key design basis parameters include:

- **Coolant** Nitrate salt 60% $NaNO_3$ and 40 % KNO_3 (by wt.)
- **Process Temperatures** 308 °C (588 °F) inlet and 600 °C (1112 °F) outlet
- **Process Flow Rate** 1790 kg/sec (14.21×10^6 lb./hr.)
- **Thermal Duty** 795 MWt
- **Design Point Radiation** 950 W/m^2 (301.2 Btu/hr./ft^2) at noon on the vernal equinox
- **Peak Incident Heat Flux** 1287 kW/m^2 (408.1×10^3 Btu/hr./ft^2)
- **Design Life** 30 years
- **Ambient Temperature** 25^{o}C (77 °F) (for heat loss calculations)
- **Wind Velocity** 17.9 m/sec (58.7 ft./sec) (for heat loss calculations)
  40.2 m/sec (131.9 ft./sec) (for structural design)
- **Seismic** 0.30 g

3.2 Concept Selection.

3.2.1 Receiver Configuration. Since the mid 1970's numerous CSP studies have been conducted with the conclusion that the optimum heliostat field shape for large scale Northern hemisphere units (>100 MW_t] is a surrounding field as illustrated in Figure 3 [Ref. 3, 4]. The heliostat field for this study is therefore a surrounding field.

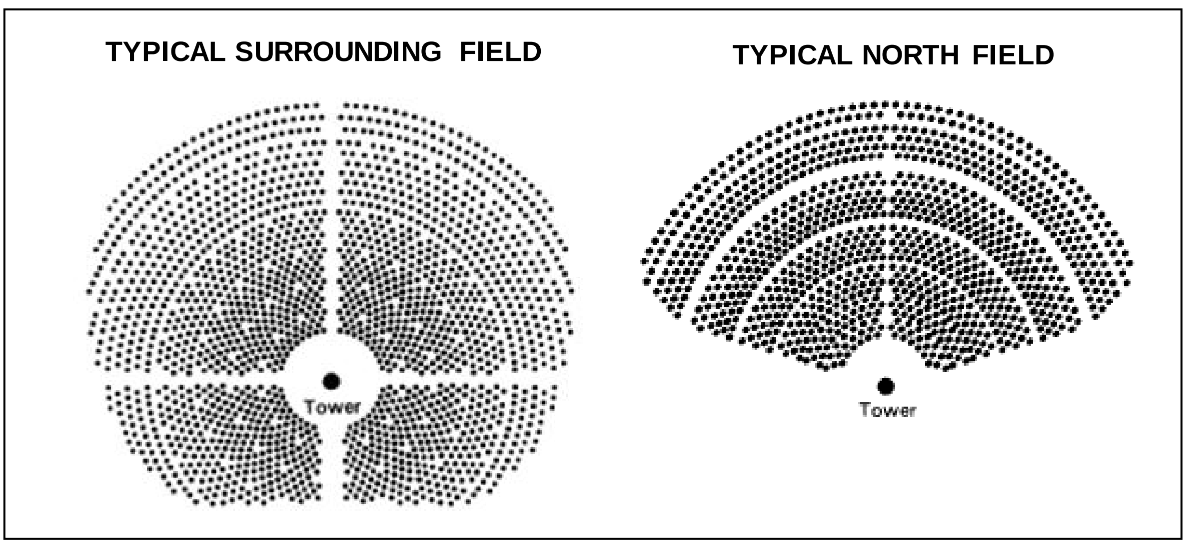

Figure 3. Typical Heliostat Field Arrangements

With a surrounding heliostat field, options for the receiver include a multi-aperture, quad cavity type or external type configuration as illustrated in Figure 4. The external type configuration is typically a multi-panel polyhedron approximating a cylinder as shown in Figure 4. Another option is a multi-panel square configuration with beveled corners.

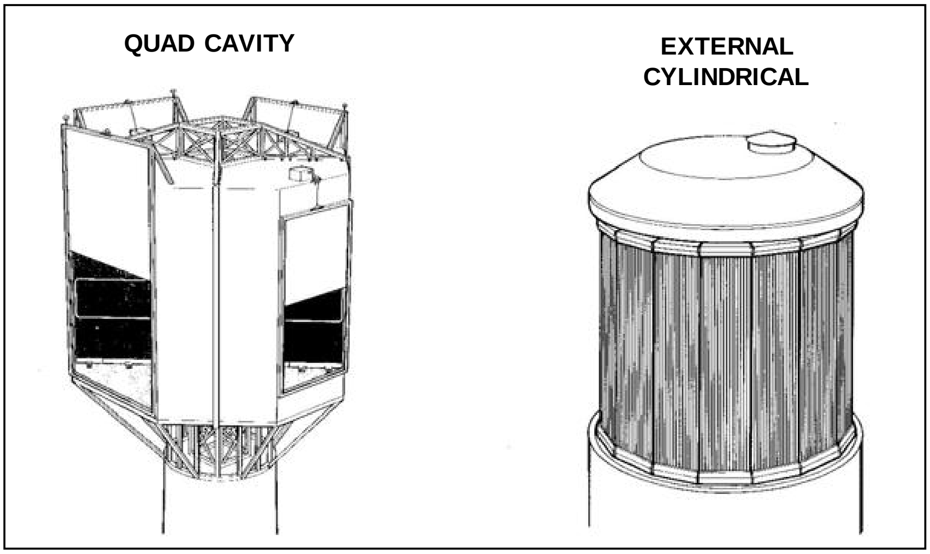

Figure 4. Receiver Configurations for a Surrounding Heliostat

Figure 5. Gemasolar Molten Salt Receiver

In general the external receiver is smaller, lighter, and less costly, but suffers greater thermal losses than a cavity receiver [Ref. 3, 4]. Evaluation from numerous tradeoff studies and the experiences with the external cylindrical receiver tested at Solar Two resulted in DOE guidelines [Ref. 5] for molten salt receivers preferring the external cylindrical configuration for large scale applications. This type configuration was used for the 120 MW_t Gemasolar project (Figure 5) which began commercial operation in May 2011 and was defined as the preferred configuration for this study.

3.2.2 Receiver Circuitry

- **Flow Direction.** The DOE guidelines [Ref. 5] for molten salt receiver design identify a serpentine path for the molten salt alternating from upflow to downflow through the panels. As described in Ref. 8 for a 470 MWt molten salt receiver, this type of arrangement minimizes the length of interconnecting piping between panels and can reduce overall pressure part weight by ~13%, salt weight by ~26%, and total pressure part/salt weight by ~22%. By minimizing piping length, overall pressure drop can be reduced which reduces design pressure which also further reduces pressure part weight. However, analysis of non-uniformly heated downflow molten salt circuits [Ref. 6] has shown that at low receiver heat input, with low salt flow rates, buoyancy force differences within a panel can potentially cause flow stagnation or flow reversal. As conceptually shown in Figure 6 for a downflow panel, the average circuit dictates the total pressure drop (Point 1) between inlet (upper) header and the outlet (lower) header. A strongly heated tube can have a reduced flow (Point 2) and a resulting higher fluid temperature. Another possible pressure balance is a reversed flow (Point 3) where the hot, lighter salt gravity head is less than the total pressure drop and an upward flow is required to achieve the total pressure drop. FWNAC historical cost/risk approach has been to keep all heated panels with upward flowing salt. For the Phase I study described in Ref. 8, all heated panels have upward flowing salt. For the Phase II study described in the report, additional investigation, analysis, and modification to the design were done to give confidence that a safe and reliable design can be done with both down and upflow panels. Refer to Appendix A for additional details.

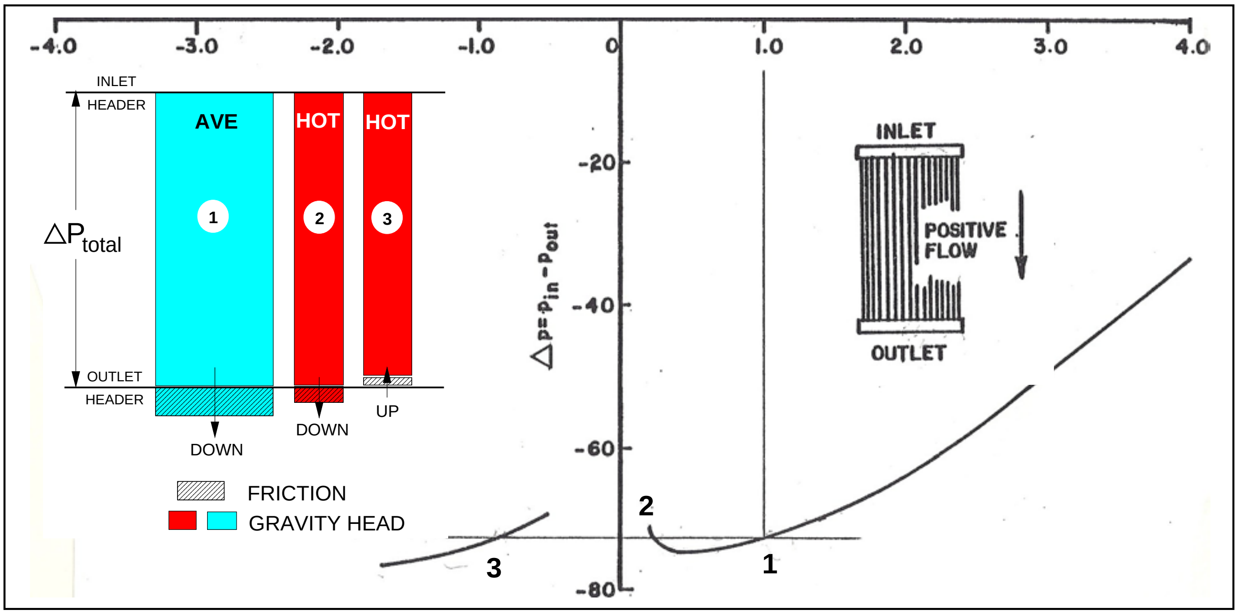

Figure 6. Minimum Load Pressure Drop in Downflow Panel [Ref. 6]

- **Cross-Over**. During the morning and the afternoon there is a heat absorption difference between East and West sides of the receiver. To minimize the salt flow variation in the parallel salt flow circuits (to maintain a constant salt outlet temperature), a cross-over from East Pass to West Pass and West Pass to East Pass is provided. Consideration was given to omitting the cross-over, so that when there is a significant heat absorption unbalance, a high salt flow rate can be maintained on the hot side of the receiver to provide better tube cooling for the tubes experiencing the high heat flux rates. However, the disadvantage to not having the cross-over is that during the high heat absorption unbalance periods, the low heat absorption circuit flow rate may have to be turned down below the minimum allowable flow rate required for stability. The flow circuit would have to be taken off outlet temperature control and operating time would be lost. Including the cross-over is therefore preferred. If low load operation results in high local tube temperatures, defocusing heliostats can be implemented.

- **Tube Size and Circuitry Arrangement.** For the Phase I study three possible ways to interconnect the receiver panels, as shown in Figure 7, were considered. Different tube diameters were used to maintain a nominal 4 m/s salt velocity for a high heat transfer rate. In each arrangement there is a cross-over from East Pass to West Pass and West Pass to East Pass to minimize the salt flow variation required to maintain a constant salt outlet temperature. The preferred arrangement, and that selected for the Phase I study, was the use of the larger diameter tube [45.7 mm (1.80 in)] with eight (8) panels in series and two(2) parallel flow paths. Advantages included:

- having the flow control valves at the cold salt inlet reduces valve design temperature.
- total number of tubes is minimized which simplifies assembly fabrication.
- not putting pairs of panels in uncontrolled parallel flow reduces temperature gradients across the panel width.
- having more panels in series reduces temperature balances and reduces the salt and tube metal temperature at the location of the peak heat flux.
- larger diameter tubes are structurally more rigid.

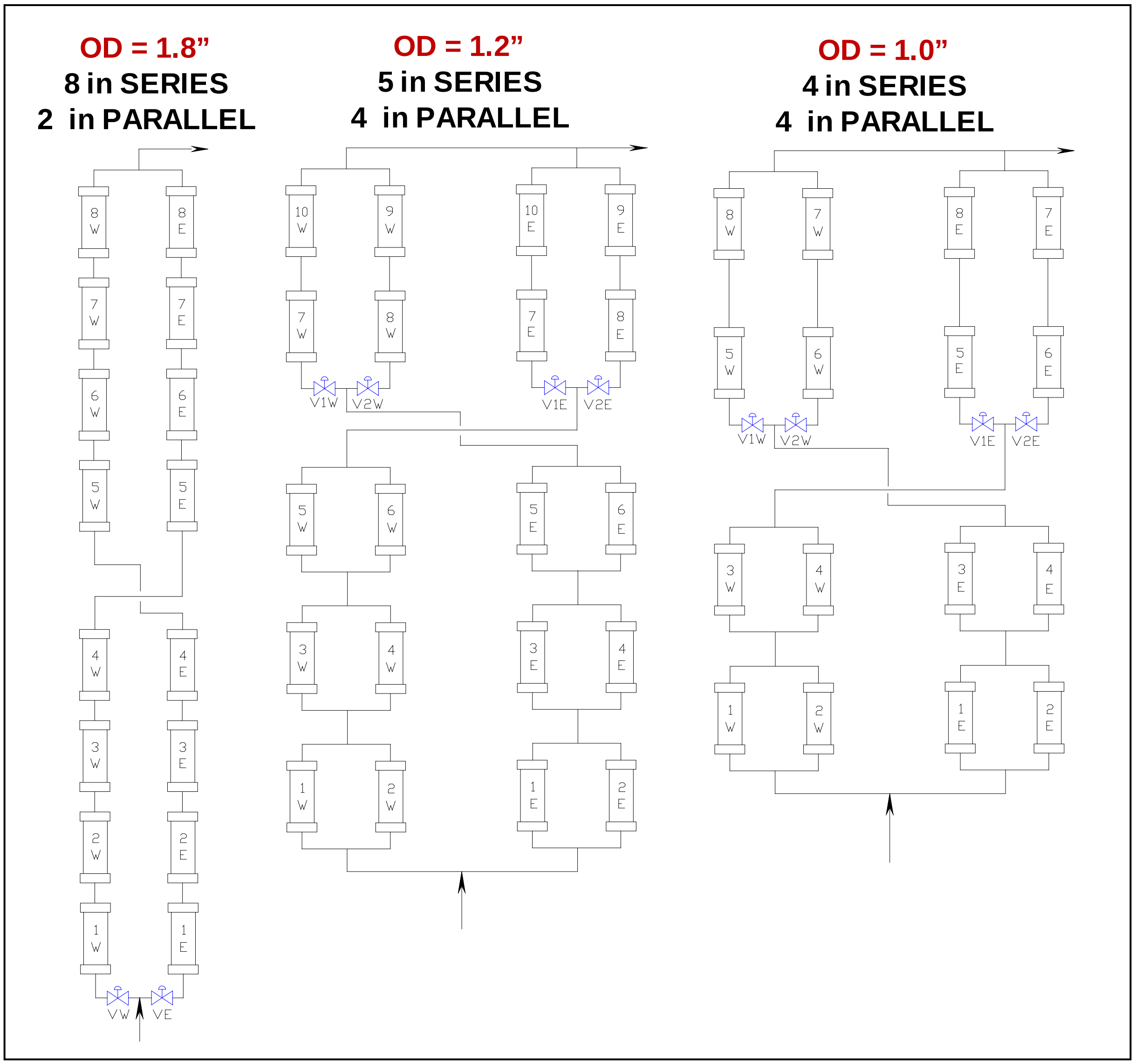

Figure 7. Panel Circuitry Arrangements

For Phase II, the starting point for the design was to use the same approach selected for the Phase I design [i.e., 45.7 mm (1.8 in.) OD tubes, two (2) parallel circuits, ~4 m/s (13 ft./s) molten salt velocity, ~20 bar (300 psi) total pressure drop)]. Limiting the panel width to ~3m (10 ft.) for shipping would require a minimum of 18 panels for the selected receiver diameter. The number of panels per circuit would increase form eight (8) to nine (9). Average velocity through the panels would also increase to ~4.7 m/s (15.5 ft./s) and the resulting total pressure loss would be greater than 28 bar (400 psi).

With the target design parameters exceeded, it was decided to increase the number of panels to 24, have four (4) independently controlled circuits with six (6) panels per circuit as schematically illustrated in Figure 8.

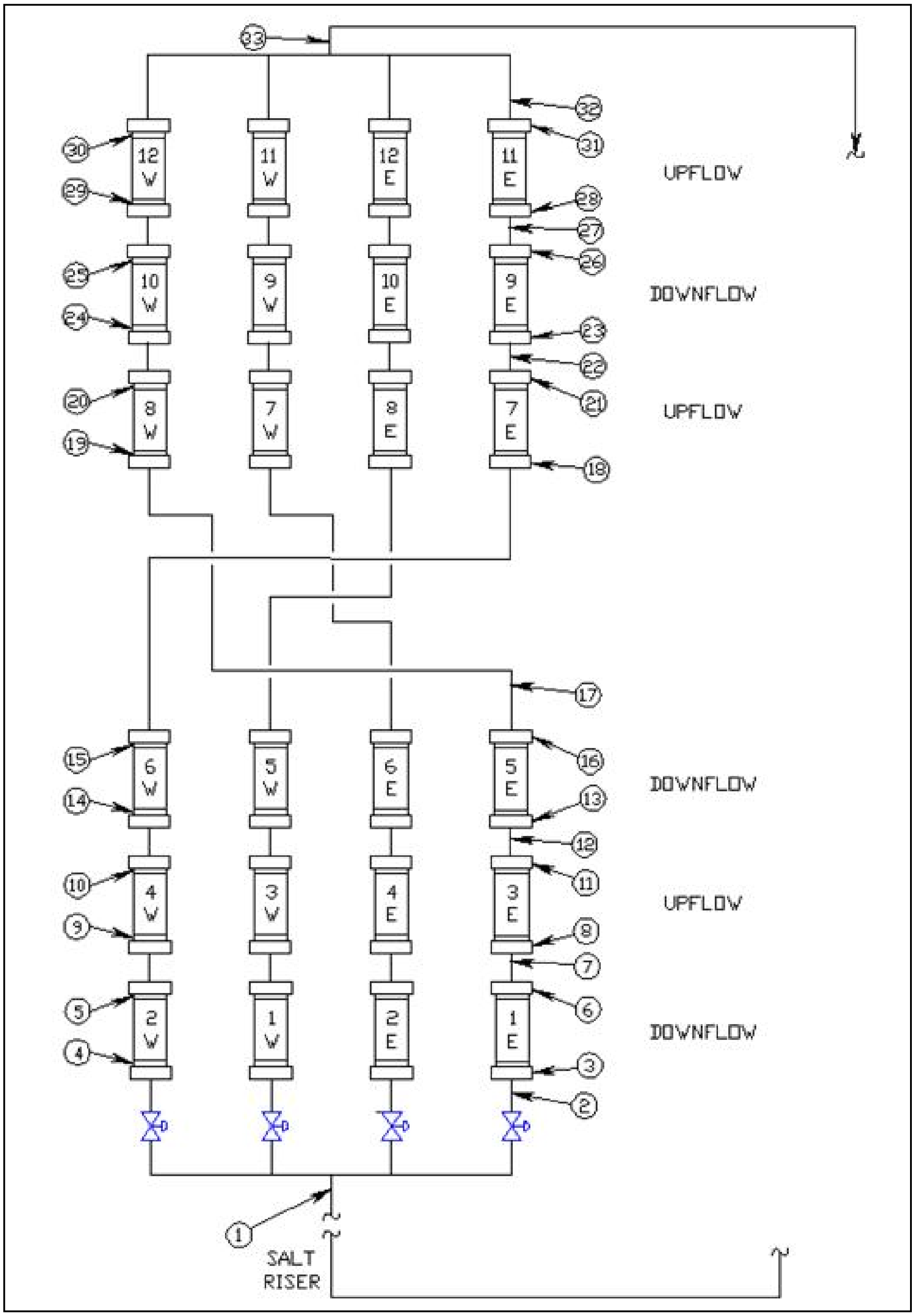

Figure 8. Pressure Part Circuitry

Using the 45.7 mm (1.8 in.) OD tubes, the resulting maximum salt velocity (3.56 m/s) was lower than the nominal target value of ~4 m/s, and the total frictional pressure drop (161 psi) was considerably lower than that for the Phase I design (257 psi).

Since the Phase II salt temperature [600°C (1112°F) is 35°C (63°F) hotter than for Phase I [565°C (1049°F)] and the maximum peak incident heat flux (1287 kW/m^2) is slightly higher than for Phase I (1266 kW/m^2), it was preferred to have at least the same or higher salt velocities for Phase II to give improved cooling to minimize tube metal temperature.

Table 1 compares some of the performance parameter differences between 45.7 mm (1.8 in.) and 40.6 mm (1.6 in.) OD tubes. Advantages of the smaller tube OD include:

- Maximum Metal and Salt Temperature ~11°F cooler
- Receiver Weight ~6.5% lighter
- Minimum Stable Load ~5% lower

		PHASE 1	PHASE II		
OD	in.	**1.8**	**1.8**	**1.6**	**Difference**
Tube Quantity/Panel		60	50	56	6 Tubes
No. of Panels		16	24	24	-
Passes per Circuit		8	6	6	-
Avg Velocity	m/s	3.67	3.38	3.85	14%
Max Velocity	m/s	3.82	3.56	4.06	14%
Frictional dp	bar (psi)	17.73 (257.04)	11.09 (160.77)	14.96 (216.90)	34.9%
Max design Pressure	bar (psi)	25.60 (371.2)	16.47 (238.82)	19.86 (287.97)	20.6%
Film Coefficient @ peak flux node	J/s-m2-C	8,384	7,323	8,294	13.3%
Max IDT (1)	°C (°F)	620 (1148.0)	650 (1202.0)	644 (1191.2)	-6°C (-10.8°F)
Max MMT	°C (°F)	649 (1200.2)	676 (1248.8)	670 (1238.0)	-6°C (-10.8°F)
IDT @ peak flux node	°C (°F)	490 (914.0)	491 (915.8)	472 (881.6)	-19°C (-34.2°F)
MMT @ peak flux node	°C (°F)	553 (1027.4)	560 (1040.0)	542 (1007.6)	-18°C (-32.4°F)
Min Load (2)	%		32	27	5%
Metal Weight (3)	kg	50,080	73,732	74,175	0.6%
Salt Weight (3)	kg	65,361	95,451	84,039	-12.0%
Total Weight (3)	kg	115,441	169,183	158,214	-6.5%

NOTES:

1. Maximum molten salt temperature in boundary layer.
2. Preliminary estimate; further evaluation required.
3. Includes tube panels, headers, and piping.

Table 1. Comparison of 45.7 mm (1.8 in.) and 40.6 mm (1.6 in.) OD Receiver Tubes

The increased pressure drop for the 40.6 mm (1.6 in.) OD tubes also increases the flow stability (refer to Appendix A) for the downflow panels.

3.2.3 Receiver Panel Header Arrangement. The three (3) receiver panel header arrangements illustrated in Figure 9 were considered for the Phase II receiver. Advantages/disadvantages for each arrangement include:

- **Inboard Headers - Common Elevation.** The headers are shorter than the panel width, requiring tubes to be angled to connect to the header, which increases the complexity of the design. With the oven box inside the receiver, a continuous band of sheet metal can be installed on the outside of the receiver which can more readily provide a wind-resistant seal. Another benefit is that flat panels, for the exposed portion of the oven box, can more readily accept spillage flux without deformation. If deformation does occur, the flat panels are easier to repair. With the oven boxes inboard, interior space within the tower is reduced. This option was selected for the Phase I design.

- **Inboard Headers – Staggered Elevations.** The headers are the same width as the panels and are staggered at alternating elevations. This simplifies the tube-to-header arrangement and allows for more access. However, the main disadvantage is that the longer header, on the inward-side of the panel, tends to lock-in the assembly and necessitates partial removal of adjacent receiver panels to allow clearance for the replacement of a single panel assembly which is not desirable from a maintenance perspective.

- **Outboard Header – Common Elevation.** The headers are the same width as the panels, have a simple tube-to-header arrangement, which allows for easier single panel replacement. Access for maintenance would be from the outside of the unit, suspended from a crane-supported man lift. The overhang above and below the heated receiver panels requires the oven boxes to be tapered (not flat) which may be more prone to distortion from spillage fluxes. To seal the oven boxes, neighboring panels must be exactly adjacent, which requires tight fabrication tolerances to prevent air infiltration on windy days. This option also provides more space on the interior of the tower for better inside access. This option was used on Solar Two.

The "Outboard Header – Common Elevation" option was selected for the present Phase II design because it simplifies fabrication, simplifies maintenance, provides more interior tower space, and is the lowest cost approach.

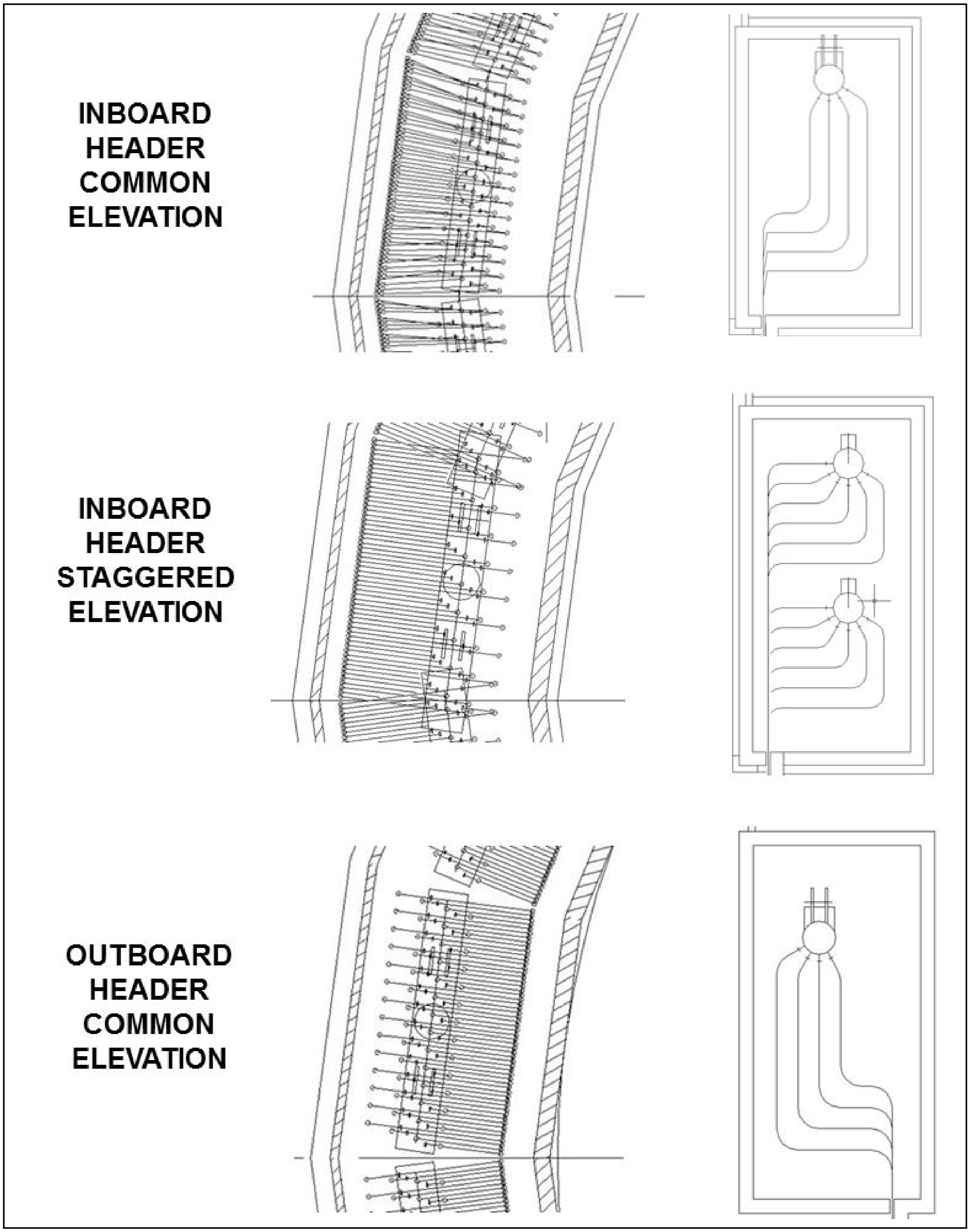

Figure 9. Receiver Panel Header Arrangement Options

3.3 Material Selection.

3.3.1 Tubing. Candidate materials [Ref. 2] included:

- Special Metals Corporation:
  - Inconel 625
  - Inconel 625LCF (proprietary to the Boeing Corporation under USA Patent No. 5,862,800)
- Haynes International:
  - Haynes 230 (UNS No. N06230)
  - Haynes 625
  - Haynes 625SQ (proprietary to the Boeing Corporation under USA Patent No. 5,862,800)

The material selected for the heated receiver panel tubes was Haynes 230 (see Appendix B for properties). Haynes 230 was selected because it has good creep to rupture properties, resistance to stress corrosion cracking, and resistance to corrosion in a potassium nitrate/sodium nitrate environment. The low thermal expansion, compared to 300 series stainless steel, means the thermal expansion and resulting thermal stresses are reduced. The Haynes 230 has also recently been approved for use by the ASME Boiler and Pressure Vessel code, for use in molten salt service, with seam-welded tubing. This is an important change, especially since seamless tubing is not generally available in the relatively thin thicknesses required for receiver tubing.

Haynes 230 has the following advantages over Haynes 625 or 625LCF for this application:

- Lower coefficient of thermal expansion
- Superior thermal Stability
- Excellent LCF properties
- Good oxidation resistance
- 625 embrittles in the temperature region of 593 °C (1100 ^{o}F) and above, due to aging
- Haynes 230 shows the least ductility degradation above 593 °C (1100 ^{o}F) and can survive better in a similar fatigue application.

3.3.2 Piping and Headers. Piping and header material selection depends on the molten salt operating temperature. Per the specification [Ref. 2] seamless piping was used based on:

- Salt Temperature < 400^{o}C (752 °F)
  - Carbon steel
- Salt Temperature > 400^{o}C (752 °F)
  - SA213TP321H
  - SA213TP347H
  - SA213TP316L

Piping and header thicknesses were computed with a corrosion allowance based on a linear relationship with a value of 0.3 mm (1.18 mils) for a salt temperature of 290 °C (554 °F) and 0.7 mm (2.76 mils) at 565 °C (1049 °F) salt temperature.

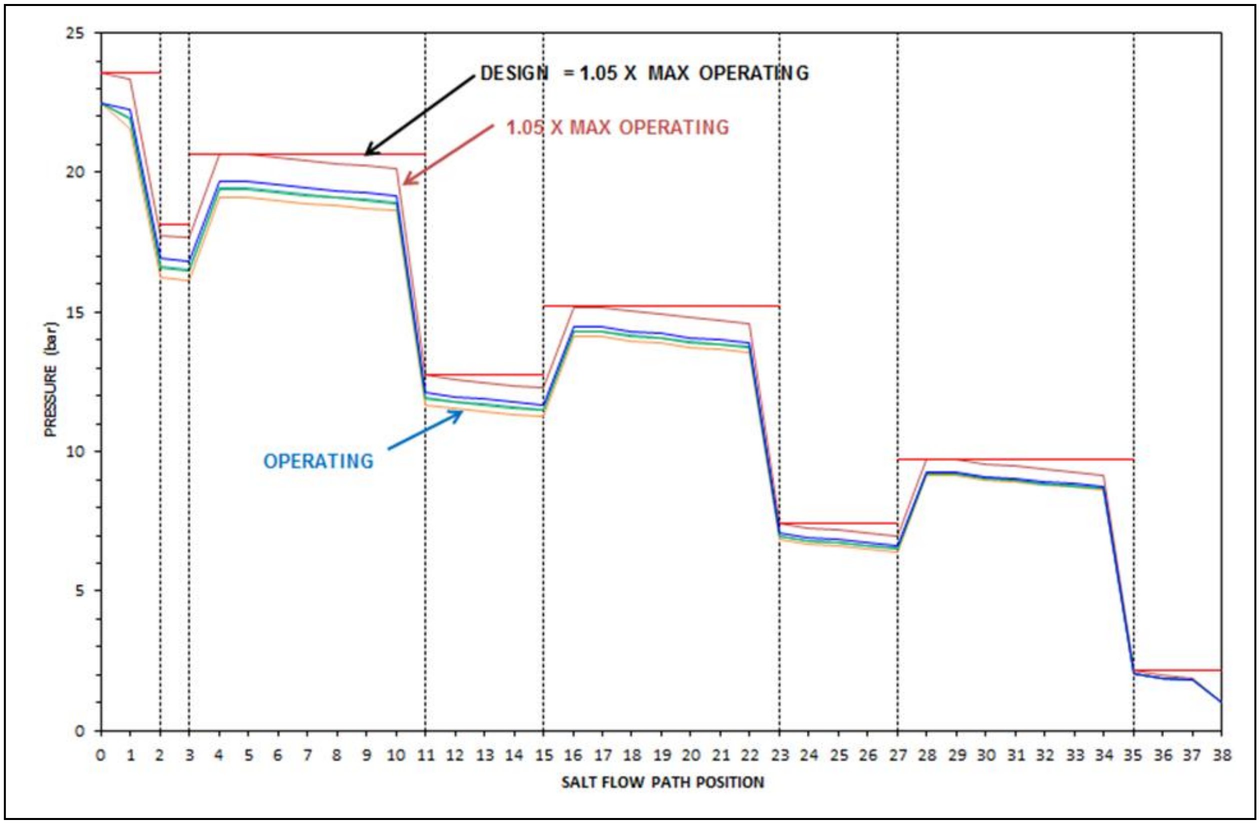

Figure 10. Operating and Design Pressure

3.3.3 Pressure Part Design. Pressure parts were selected for the receiver design, based on the thermal/hydraulic analysis described in Section 3.4, and are summarized in Table 2. Figure 8 identifies the circuitry numbering. Headers were designed with the same material as the connected piping. Tube stubs of the same material as the headers were used to connect to the heated panel tubing. Spool pieces are included (as required) between the header tube stubs and panel tubing to match thermal expansion properties. A variable design pressure, as shown in Figure 10 was used with a 5% margin applied to the computed operating pressure. The operating pressure drop for load case Day 300 12:00:00 was used to determine design pressure. The salt flow path position location numbers are defined in Appendix C.

3.4 Thermal/Hydraulic Design.

3.4.1 Heat Flux Maps. Incident heat flux maps were provided for twenty (20) load cases [five(5) different days and at four (4) different times between early morning and noon]. Table 3 summarizes the load cases and lists significant given and computed performance parameters. A typical incident flux map for the load case with the maximum incident heat flux is shown in Figure 11. Listed in the figure is the total incident heat absorbed (kw) per panel. Table 4 lists the pertinent details for the flux map grid. All incident heat flux maps are included in Appendix D.

Pipe/ Header #	Panel #	Item	Qty	Size (in.)		Thickness (in.)		Material	Length (ft)	Design Pressure (psia)	Design Temp (°F)	Operating Temp (°F)	Metal Weight (lb)	Salt Weight[3] (lb)
				O.D.	I.D.	MW	AW							
1		Main Feed Pipe to Evaporator Circuit	1	22.00	21.500	0.219	0.250	SA106C	109.00	343	622	586	6,579	32,495
2		Transfer Pipe	4	12.75	12.438	0.137	0.156	SA106C	56.01	343	622	586	4,887	22,355
3		Inlet Header	4	14.00	13.500	0.219	0.250	SA106C	7.51	263	622	586	1,147	3,532
4		Inlet Stubs	224	1.75	1.480	0.122	0.135	SA210A1	0.25	263	622	586	136	79
	1E,1W,2E,2W	Tubes	224	1.61	1.480	0.059	0.065	Haynes230	97.11	300	1,134	691	26,729	30,721
5		Outlet Stubs	224	1.75	1.480	0.122	0.135	SA210A1	0.25	300	779	691	136	79
6		Outlet Header	4	14.00	13.250	0.328	0.375	SA106C	7.51	300	777	689	1,705	3,403
7		Transfer Pipe	4	12.75	12.390	0.158	0.180	SA106C	21.33	300	750	689	2,143	8,445
8		Inlet Header	4	14.00	13.250	0.328	0.375	SA335P11	7.51	300	750	689	1,705	3,403
9		Inlet Stubs	224	1.75	1.480	0.122	0.135	SA213T11	0.25	300	750	689	136	79
	3E,3W,4E,4W	Tubes	224	1.61	1.480	0.059	0.065	Haynes230	97.11	300	1,231	797	26,729	30,721
10		Outlet Stubs	224	1.75	1.480	0.122	0.135	SA213T12	0.25	185	910	797	136	79
11		Outlet Header	4	14.00	13.500	0.219	0.250	SA335P12	7.51	185	909	797	1,147	3,532
12		Transfer Pipe	4	12.75	12.438	0.137	0.156	SA335P12	21.33	185	882	797	1,860	8,511
13		Inlet Header	4	14.00	13.500	0.219	0.250	SA335P12	7.51	185	882	797	1,147	3,532
14		Inlet Stubs	224	1.75	1.480	0.122	0.135	SA213T12	0.25	185	882	797	136	79
	5E,5W,6E,6W	Tubes	224	1.61	1.480	0.059	0.065	Haynes230	97.11	220	1,285	903	26,729	30,721
15		Outlet Stubs	224	1.75	1.480	0.122	0.135	SA213T12	0.25	220	1,036	903	136	79
16		Outlet Header	4	14.00	13.500	0.219	0.250	SA376TP347H	7.51	220	1,035	901	1,147	3,532
17		Transfer Pipe (Crossover)	4	12.75	12.438	0.137	0.156	SA376TP347H	63.65	220	1,008	901	5,553	25,402
18		Inlet Header	4	14.00	13.500	0.219	0.250	SA376TP347H	7.51	220	1,008	901	1,147	3,532
19		Inlet Stubs	224	1.75	1.480	0.122	0.135	SA213TP347H	0.25	220	1,008	901	136	79
	7E,7W,8E,8W	Tubes	224	1.61	1.480	0.059	0.065	Haynes230	97.11	220	1,287	973	26,729	30,721
20		Outlet Stubs	224	1.75	1.480	0.122	0.135	SA213TP347H	0.25	108	1,089	973	136	79
21		Outlet Header	4	14.00	13.688	0.137	0.156	SA376TP347H	7.51	108	1,085	973	721	3,631
22		Transfer Pipe	4	12.75	12.438	0.137	0.156	SA376TP347H	21.33	108	1,058	973	1,860	8,511
23		Inlet Header	4	14.00	13.688	0.137	0.156	SA376TP347H	7.51	108	1,058	973	721	3,631
24		Inlet Stubs	224	1.75	1.480	0.122	0.135	SA213TP347H	0.25	108	1,058	973	136	79
	9E,9W,10E,10W	Tubes	224	1.61	1.480	0.059	0.065	Haynes230	97.11	141	1,305	1,044	26,729	30,721
25		Outlet Stubs	224	1.75	1.480	0.122	0.135	SA213TP347H	0.25	141	1,132	1,044	136	79
26		Outlet Header	4	14.00	13.500	0.219	0.250	SA376TP347H	7.51	141	1,130	1,042	1,147	3,532
27		Transfer Pipe	4	12.75	12.438	0.137	0.156	SA376TP347H	21.33	141	1,103	1,042	1,860	8,511
28		Inlet Header	4	14.00	13.624	0.165	0.188	SA376TP347H	7.51	141	1,103	1,042	866	3,598
29		Inlet Stubs	224	1.75	1.480	0.122	0.135	SA213TP347H	0.25	141	1,103	1,042	136	79
	11E,11W,12E,12W	Tubes	224	1.61	1.480	0.059	0.065	Haynes230	97.11	141	1,377	1,116	26,729	30,721
30		Outlet Stubs	224	1.75	1.480	0.122	0.135	SA213TP347H	0.25	31	1,182	1,116	136	79
31		Outlet Header	4	14.00	13.688	0.137	0.156	SA376TP347H	7.51	31	1,175	1,112	721	3,631
32		Transfer Pipe to Outlet Manifold	4	12.75	12.438	0.137	0.156	SA376TP347H	47.00	31	1,139	1,112	4,100	18,757
33		Main Return Pipe to Hot Surge Tank	1	22.00	21.624	0.165	0.188	SA376TP347H	105.00	31	1,139	1,112	4,780	31,665
										Tubing			162,001	185,275
										Piping			33,623	164,651
										Headers & Stubs			13,318	42,492
										Total Weight			**208,942**	**392,418**

Table 2. Pressure Part Summary

Day of year	Time	DNI	Final Incident Power (reported)	Final Incident Power (calculated)	Final Absorbed Power (calculated)	% Load	Receiver efficiency	Molten Salt Total Flow Rate	ID Temp	Max. MM Temp	Max. OD Temp	Max. OD - Bulk Temp	Peak Incident Flux	Inlet Pressure
		W/m2	MWt	MWt	MWt			kg/s	°C	°C	°C	°C	kW/m2	bara
8	8:30:00	799	543	547	487.57	61.33	89.19	1,098	656	678	700	224	859	13.22
8	9:30:00	918	734	738	668.71	84.12	90.58	1,506	656	685	713	264	1,154	18.51
8	10:30:00	937	795	800	727.13	91.46	90.88	1,637	651	679	707	273	1,225	20.47
8	12:00:00	994	863	868	791.70	99.59	91.18	1,782	645	671	697	278	1,287	22.53
81	7:00:00	653	426	429	376.85	47.40	87.92	848	661	681	701	182	670	10.54
81	8:30:00	883	753	758	687.84	86.52	90.80	1,549	666	701	735	247	1,158	18.83
81	10:00:00	930	842	847	771.88	97.09	91.18	1,738	660	694	728	262	1,220	21.81
81	12:00:00	912	804	809	735.36	92.50	90.93	1,656	645	670	695	264	1,186	20.45
154	6:00:00	639	426	428	377.29	47.46	88.13	849	668	689	711	163	665	10.67
154	8:00:00	855	NA	754	685.40	86.21	90.89	1,543	672	709	747	226	1,108	18.56
154	10:00:00	928	865	870	795.00	100.00	91.36	1,790	665	703	741	242	1,167	22.46
154	12:00:00	926	858	862	786.88	98.98	91.24	1,772	651	681	711	256	1,178	22.20
227	6:00:00	491	278	280	236.67	29.77	84.58	533	659	672	685	145	431	8.32
227	8:00:00	820	707	711	644.52	81.07	90.63	1,451	670	704	739	227	1,069	17.21
227	10:00:00	915	846	851	776.94	97.73	91.26	1,749	663	699	735	248	1,171	21.85
227	12:00:00	909	865	870	794.87	99.98	91.35	1,790	657	691	725	235	1,081	22.44
300	7:30:00	560	331	333	286.06	35.98	85.81	644	656	671	685	169	520	9.06
300	9:00:00	887	731	735	666.12	83.79	90.61	1,500	661	692	722	255	1,143	18.34
300	10:30:00	964	851	856	780.71	98.20	91.16	1,758	654	685	716	275	1,275	22.31
300	12:00:00	964	865	870	793.75	99.84	91.22	1,787	647	675	703	271	1,253	22.53
UNHEATED (29.77% LOAD)														8.66

Table 3. Load Case Summary

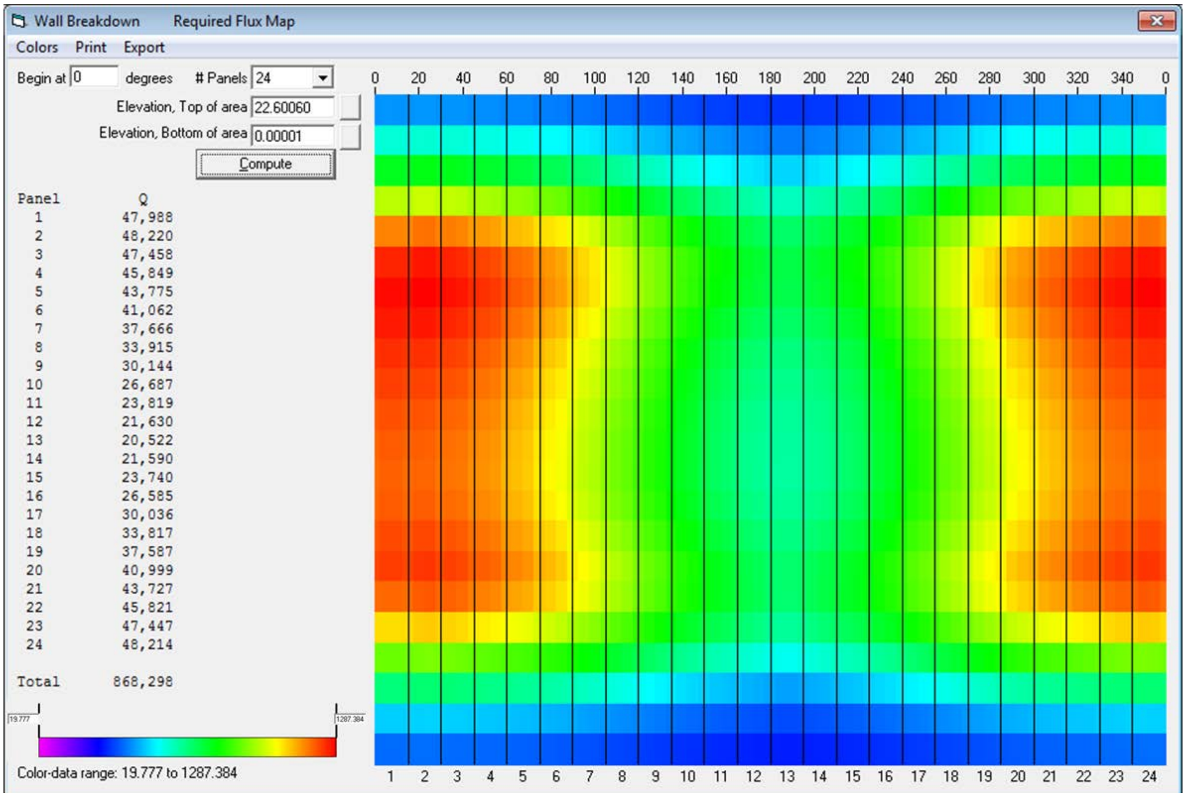

Figure 11. Incident Heat Flux Distribution – Day 8 12:00:00

North Q Max	kW/m2	
South Q Max	kW/m2	
North Q Edge	kW/m2	
South Q Edge	kW/m2	
Q Max	kW/m2	1253
Q Min	kW/m2	61
Diameter	m	57.087
Perimeter	m	
Half Perimeter	m	

Panels		24
Nodes Wide		72
Nodes High		22
Node Width	m	
Height	m	22.6006
Node Height	m	1.027

Table 4. Incident Heat Flux Map Parameters

Each panel was divided vertically into 22 equal height nodes. Horizontally, each panel was divided into four vertical strips that are 1/6th -1/3rd -1/3rd -1/6th of the total panel width. With this arrangement the nodal heat flux values for the outer strips fall on the panel edge and in the center of the two inner strips (Figure 12).

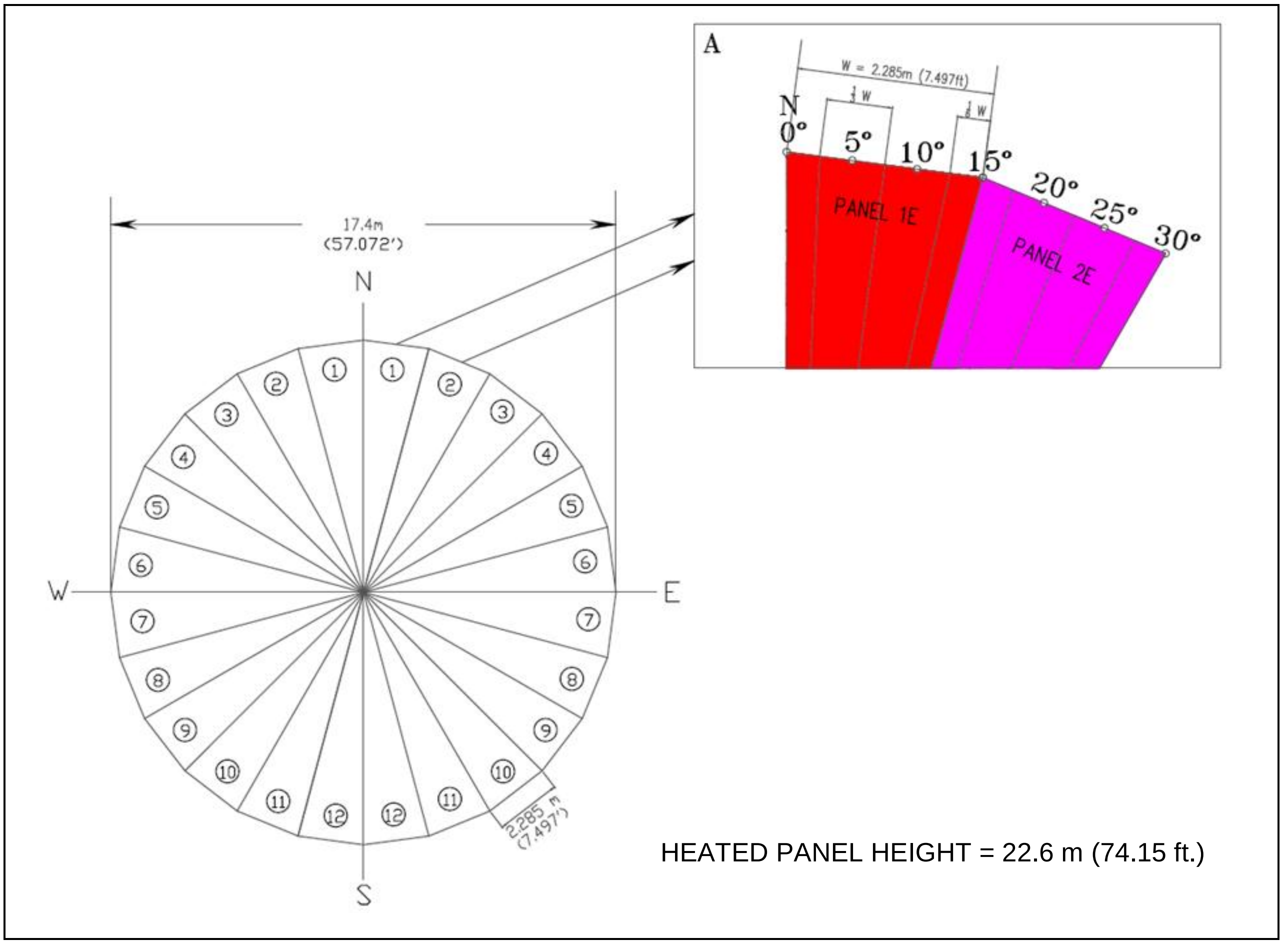

Figure 12. Heat Flux Node Locations

3.4.2 Heat Transfer Correlations. The correlations used for predicting heat transfer to and from the tubing in the receiver panels are summarized in Table 5. The forced, natural, and combined convection correlations in combination with a 0.06 reflectivity were used to determine heat loss from each panel node based on an iterative calculation to determine the node surface temperature and the resultant absorbed heat flux.

3.4.3 Temperatures and Pressure Drop. Based on the heat flux profiles defined for each load case, fluid bulk, tube ID, tube MM (mean metal), and tube OD temperatures as well as tube OD minus fluid bulk temperature differences were computed for each panel node. Figures 13, 14, 15, 16 and 17 illustrate the temperature distribution for each of these parameters for the load case with the maximum value for each parameter. Incident heat flux values and resulting computed temperatures (fluid bulk, tube ID, tube OD) for each node are included in Appendix E for the maximum OD minus bulk fluid temperature load case (Day 8 12:00:00) and in Appendix F for the maximum fluid film and tube metal temperature load case.

The highest temperature differential between the tube outside surface and the bulk fluid temperature occurs at the location with the highest incident heat flux in Panel 1W on Day 8 12:00:00. Figure 18 includes the incident and absorbed heat flux profiles in this section of Panel 1, and also lists the internal film coefficient, maximum fluid temperatures, and absorbed heat flux in each node of this worst case panel strip.

NUSSELT NUMBER CORRELATIONS	
SALT FILM COEFFICIENT	
REVISED MODIFIED HAUSEN EQUATION (1987) For calculating the heat transfer coefficient across the Tube wall – salt fluid interface.	$Nu_{revised\ -mh} = 0.0235\{Re^{0.8} - 230\}[1.8Pr^{0.3} - 0.8]\left(\frac{\mu_{bulk}}{\mu_{film}}\right)^{0.14}$
CONVECTION HEAT LOSS	
NATURAL CONVECTION COEFFICIENT CHURCHILL & CHU CORRELATION (1975) For the heat transfer coefficient calculation based on natural convection with turbulent external flow on a flat vertical surface	$Nu_{nc} = \frac{h_{nc}L}{k} = \left[0.825 + \frac{0.387Ra^{1/6}}{\left[1+\left(\frac{0.492}{Pr}\right)^{9/16}\right]^{8/27}}\right]^2$
FORCED CONVECTION COEFFICIENT SOURCE UNKNOWN	$Nu_{fc} = \frac{h_{fc}D}{k} = 0.0266Re^{0.805}Pr^{1/3}$
MIXED CONVECTION COEFFICIENT SANDIA REPORT: SAND84-8717 (1984)	$h = \left(h_{fc}^{3.2} + h_{nc}^{3.2}\right)^{1/3.2}$

Table 5. Heat Transfer Correlations

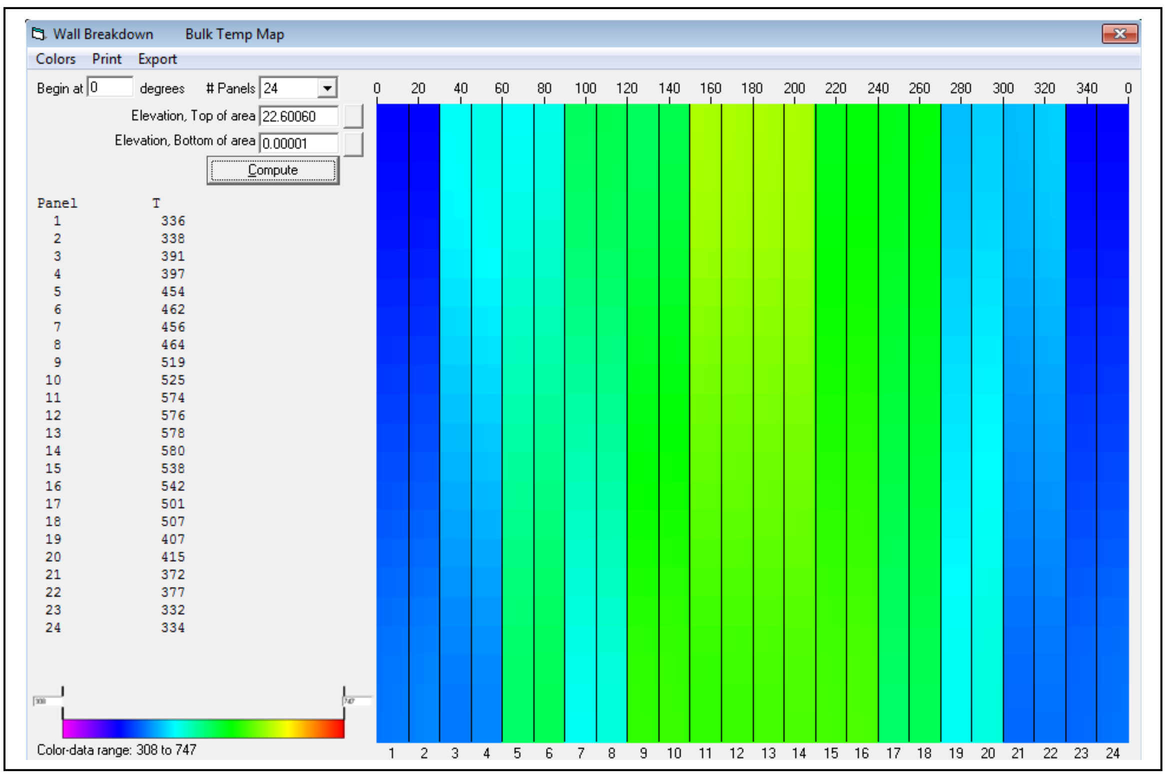

Figure 13. Molten Salt Bulk Fluid Temperature – Day 154 08:00:00

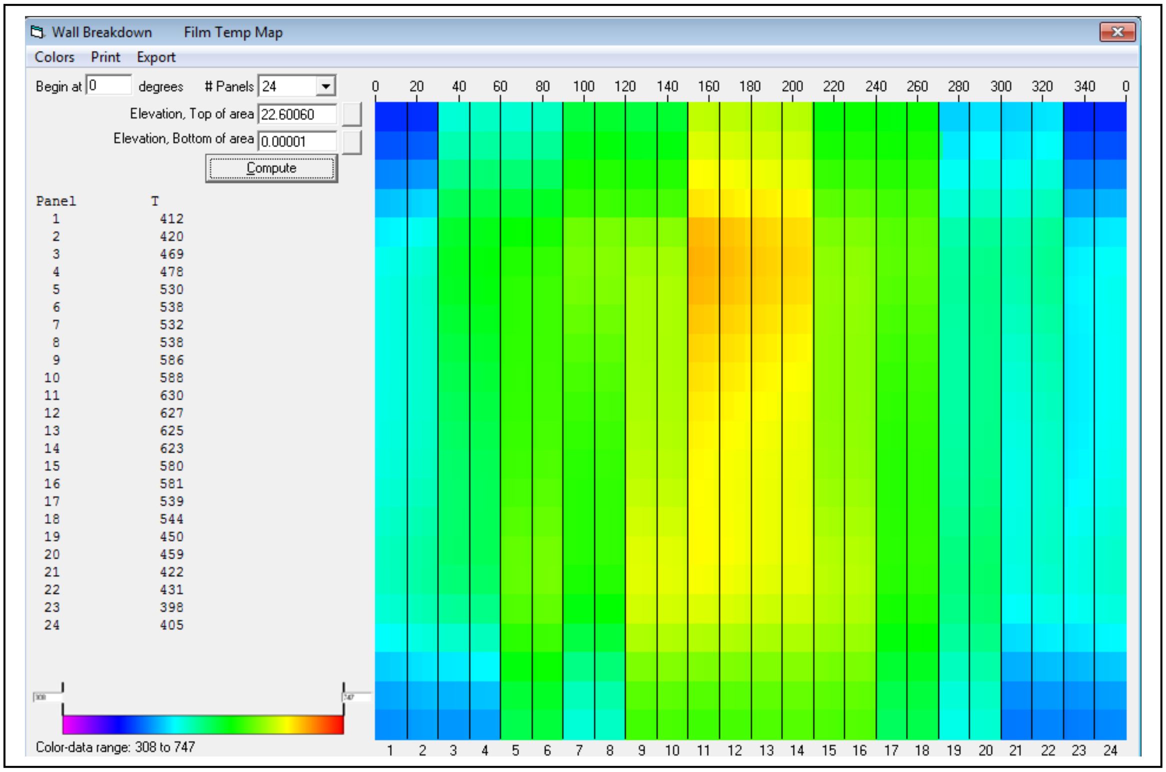

Figure 14. Tube ID Temperature – Day 154 08:00:00

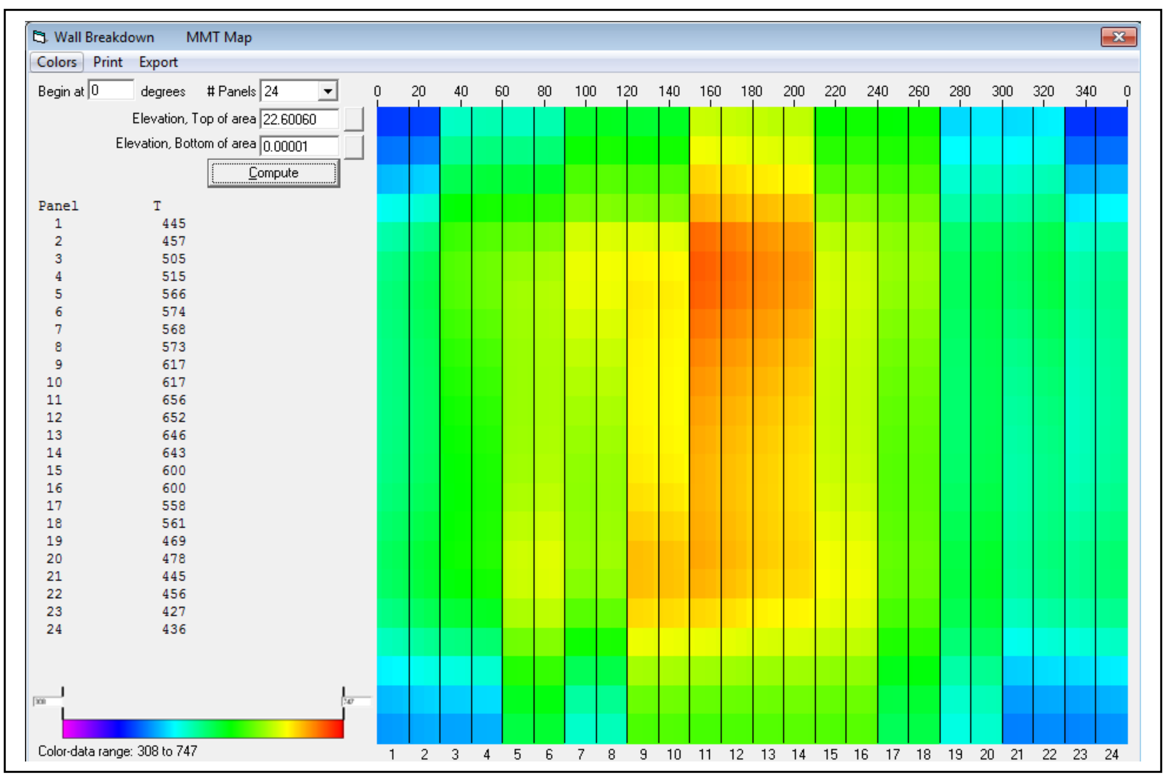

Figure 15. Tube MM Temperature – Day 154 08:00:00

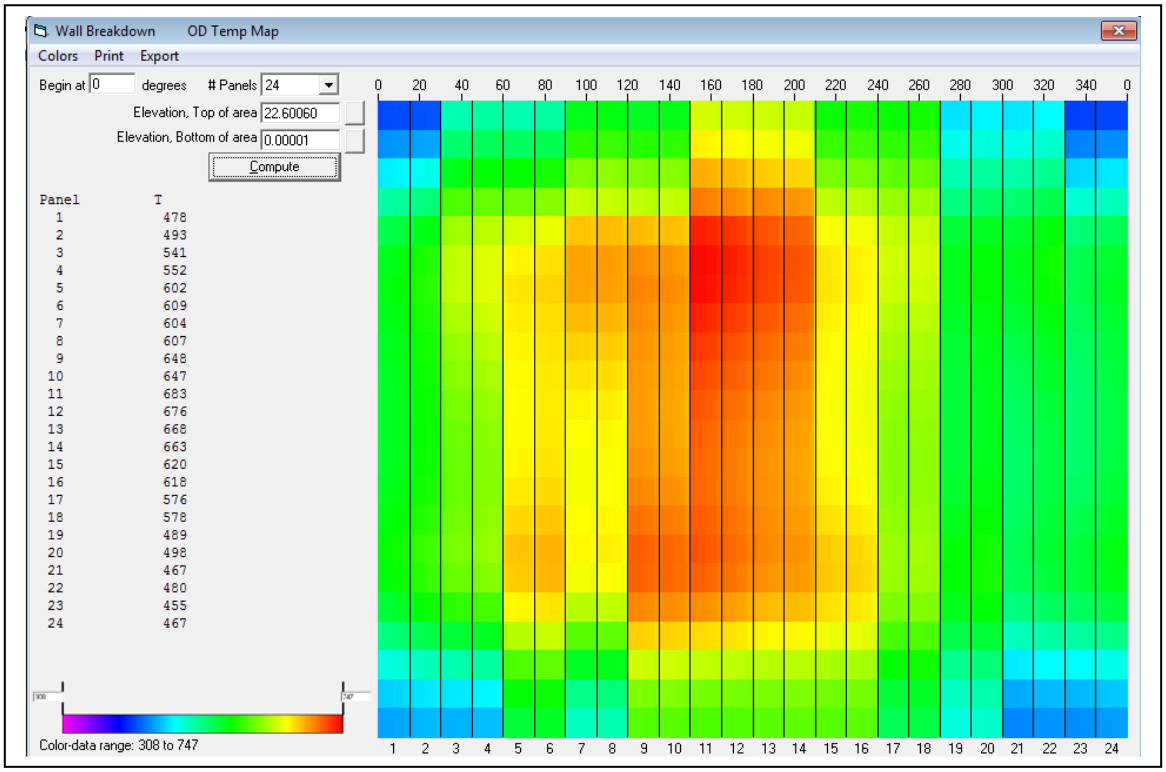

Figure 16. Tube OD Temperature – Day 154 08:00:00

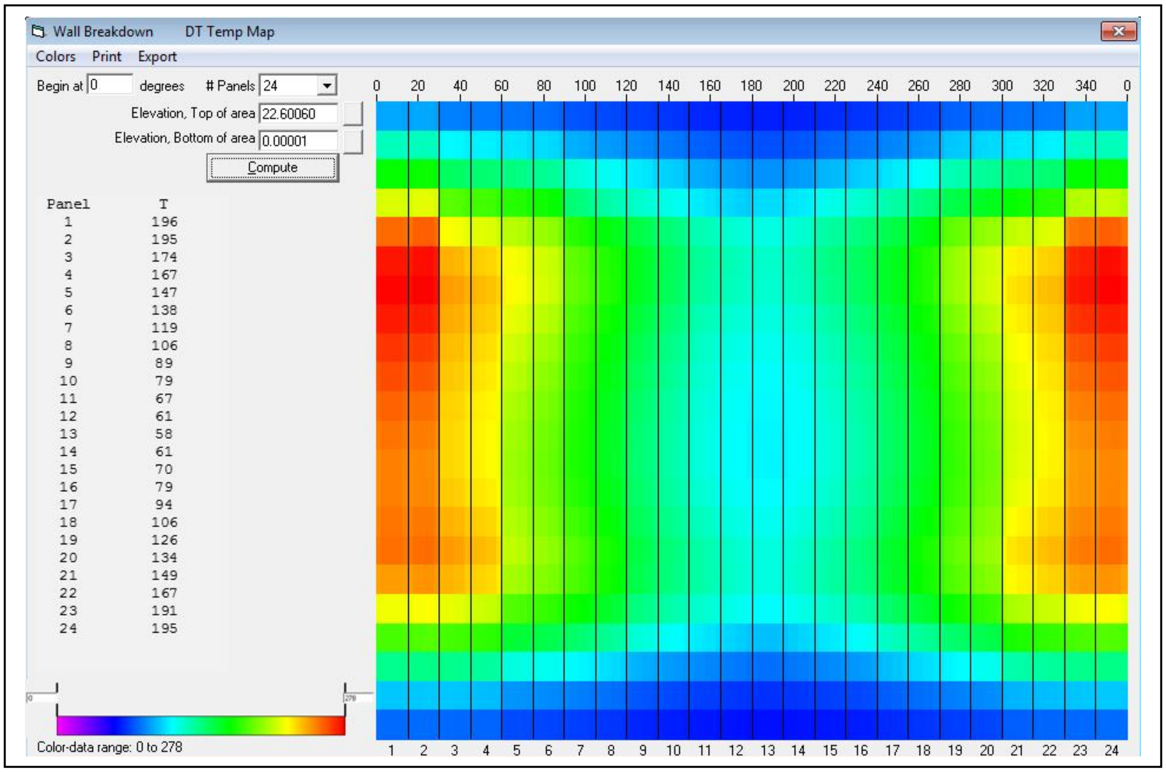

Figure 17. Tube OD Minus Bulk Temperature Difference – Day 8 12:00:00

	Film Coefficient J/s-m²-C	Max Fluid Temp °C	Avg Absorbed Flux kW/m²
Zone 22	7715	309	186
Zone 21	7866	310	361
Zone 20	8045	312	587
Zone 19	8217	315	810
Zone 18	8408	319	1072
Zone 17	8535	323	1180
Zone 16	8628	327	1202
Zone 15	8699	331	1175
Zone 14	8767	335	1145
Zone 13	8835	339	1123
Zone 12	8901	343	1102
Zone 11	8968	347	1089
Zone 10	9036	351	1082
Zone 9	9110	355	1092
Zone 8	9190	358	1118
Zone 7	9270	362	1140
Zone 6	9324	366	1099
Zone 5	9337	370	965
Zone 4	9301	372	748
Zone 3	9215	374	472
Zone 2	9127	375	252
Zone 1	9074	375	133
NOTES:	1, 2	2, 3	2

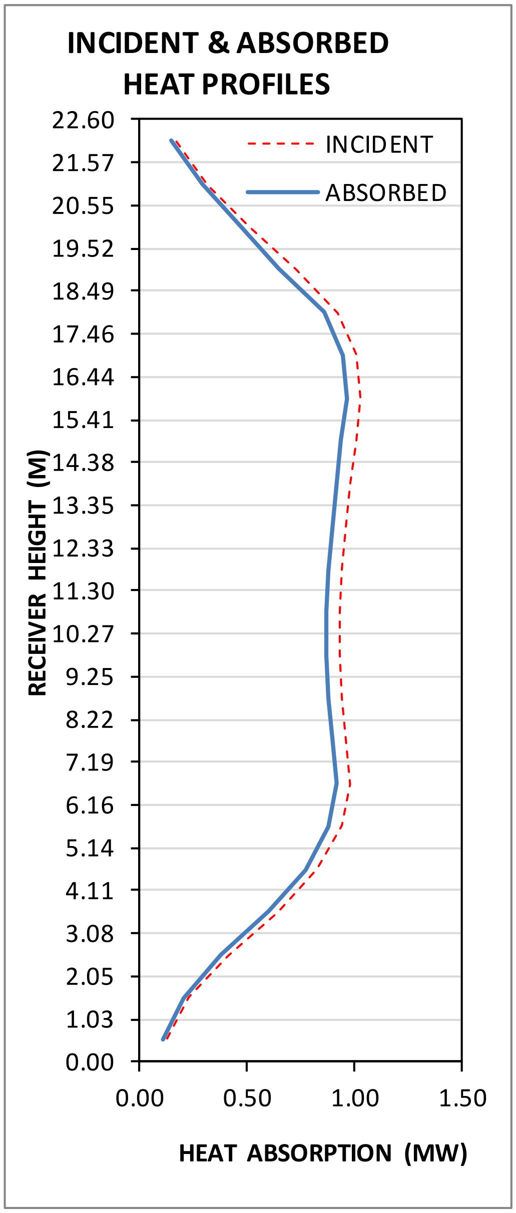

NOTES:
1. Modified Hausen correlation.
2. All values for tube in panel with greatest local incident and absorbed heat flux
3. Max fluid temperature at zone outlet.

Figure 18. Panel 1 Region with Maximum Absorbed Heat Flux - Day 8 12:00:00

Frictional pressure losses through the piping and panel tube are summarized in Table 6. The values listed are for load case Day 300 12:00:00 which had the highest calculated pressure loss.

1.6" TUBES (SERIES 6 PASS)			
Units		BAR	PSI
Main Feed Pipe		0.327	4.74
Transfer Pipe to Pass 2W		0.147	2.12
2W	Inlet Header	0.087	1.26
	Tubes	2.368	34.34
	Outlet Header	0.084	1.22
Transfer Pipe 2W-4W		0.114	1.66
4W	Inlet Header	0.088	1.27
	Tubes	2.303	33.41
	Outlet Header	0.084	1.22
Transfer Pipe 4W-6W		0.107	1.55
6W	Inlet Header	0.089	1.29
	Tubes	2.272	32.96
	Outlet Header	0.086	1.24
Transfer Pipe 6W-7E		0.146	2.12
7E	Inlet Header	0.091	1.32
	Tubes	2.262	32.81
	Outlet Header	0.087	1.26
Transfer Pipe 7E-9E		0.105	1.52
9E	Inlet Header	0.090	1.31
	Tubes	2.260	32.78
	Outlet Header	0.088	1.28
Transfer Pipe 9E-11E		0.106	1.54
11E	Inlet Header	0.091	1.33
	Tubes	2.263	32.82
	Outlet Header	0.089	1.29
Transfer Pipe to Out Manifold		0.133	1.93
Main Return Pipe to Hot Surge Tank		0.322	4.67

UNITS	BAR	PSI
TOTAL PIPING ΔP	1.506	21.84
TOTAL DC ΔP	0.858	12.44
TOTAL FEEDER ΔP	NA	NA
TOTAL RISER ΔP	NA	NA
MAIN FEED & RETURN PIPE ΔP	0.648	9.40
TOTAL PANEL ΔP	14.783	214.41
TUBES	13.729	199.12
INLET HEADERS	0.536	7.77
OUTLET HEADERS	0.518	7.52
TOTAL ΔP	16.289	236.26
AVG VELOCITY FOR FLOW PATH (m/s)	4.068	
MAX VELOCITY FOR FLOW PATH (m/s)	4.234	
AVG VELOCITY (m/s)	4.026	
MAX VELOCITY (m/s)	4.234	

Table 6. Piping and Tubing Frictional Pressure Losses

3.4.4 Thermal Efficiency. The defined incident heat flux map (refer to Section 3.4.1) has each panel divided into a grid of 96 nodes. An iterative calculation was done to match assumed and computed incident and absorbed heat fluxes for each node based on the computed tube surface temperature. Ambient heat losses were based on:

- Ambient Temperature = 25 ^{o}C (77 ^{o}F)
- Wind Velocity = 17.9 m/sec (58.7 ft./s)
- Receiver Surface Emissivity = (Table 7)
- Receiver Surface Reflectivity = 0.0388
- Convection Losses = (refer to natural, forced, and combined convection loss correlations in Table 5)

[**NOTE:** The optical properties of the black absorptive coating applied to the external surface of the heated receiver tubes are based on the coating applied by plasma deposition. It is assumed that vacuum deposition machines that are used for applying a coating to a continuous sheet of stainless steel can be modified to handle a round, rather than a flat, geometry. For sheet application, the supply roll is outside the vacuum chamber, as is the take-up roll. Sliding seals, between the moving sheet and the stationary machine, are available to isolate the vacuum chamber from the ambient. The sliding seals would be modified to handle the round tube geometry.]

TEMP (^{o}C)	EMISSIVITY
0	0.2688
50	0.2737
100	0.2802
150	0.2886
200	0.2991
250	0.3118
300	0.3266
350	0.3434
400	0.3619
450	0.3820
500	0.4033
550	0.4256
600	0.4486

Table 7. Panel Coating Emissivity

The computed efficiency for each load case is included in Table 3.
The maximum efficiency for the cases analyzed was for the nominal full load on Day 154 at 10:00:00:

- Total Incident Heat = 870 MW_t
- Total Absorbed Heat = 795 MW_t
- Receiver Thermal Efficiency = 91.36%

3.4.5 Vent and Overflow Downcomer Design

When filling the receiver with molten salt, air must be vented from the receiver pipes, heated tube panels, and headers**.** The vent system must also be properly sized to allow the receiver to be drained in a reasonable time. The vent lines must be open to the atmosphere and configured in a way to safely discharge molten salt if it is entrained or overflows into the vent system or if there is a partial or complete blockage of the main downcomer pipe that directs hot molten salt to the hot storage tank. The configuration designed to meet these requirements is illustrated in Figure 19.

Vent pipes are connected to the high point in the transfer pipes that interconnect the panel headers at the top of the unit. Each vent line has a globe valve that is closed during normal operation. [Consideration was given to using orifices, with a continuous salt bypass flow, to replace the vent valves. However, this option, as discussed in Appendix I, will result in high fluid and tube metal temperatures.] Vent lines from the east panels are connected to the east vent header; west panels to the west vent header. Each of the vent headers has a discharge vent pipe that is connected to the overflow bottle vent pipe which is open to the atmosphere. The vent lines to and from the vent headers are conservatively sized 4” pipes.

For venting of the outlet transfer pipes, 8” pipes are connected to the high point in each of the four (4) 12” outlet transfer pipes and extend up to a 5’ diameter overflow bottle. The 6” diameter J-shaped vent pipe is open to the atmosphere and is the high point for the receiver flow circuitry. The outlet of the vent pipe is directed to an 8” opening in the top head of the bottle so that any molten salt entrained in the vented air is directed back into the overflow bottle and down the 14” overflow downcomer pipe.

During normal operation, molten salt will rise in the 8” overflow transfer to pipes to a level based on the pressure drop in the 12” outlet transfer pipes to the main 22” downcomer pipe. In the event that there is a partial or total blockage of the main 22” downcomer pipe, the full load flow rate must be maintained through the overflow system to protect the heated panels for at least 20 seconds so that the heliostats can be de-focused from the receiver. The 8” overflow pipe size was selected so that the back-pressure created from the full load flow rate does not exceed the selected pressure part design pressures as shown in Figure 9.

The overflow transfer pipes connect tangentially to the overflow bottle to provide a common elevation point (for equal gravity head loss) and unimpeded momentum for free fall into the overflow downcomer pipe. The overflow downcomer pipe size was selected so that the pipe does not run full with the full load flow for at least 20 seconds.

3.4.6 Preheat/Fill and Drain Analysis

An analysis of the drain piping was conducted to determine the time required to drain the entire system (panels, piping, tanks, etc.). Vent line size will also dictate drain rate. The vent and drain line arrangements are illustrated in Figures 19 and 20.

The drain time was computed using the following formula:

$$t = \frac{V_{element}}{C\ A\ h_{element}} \sqrt{\frac{2}{g}}\ \left[\sqrt{h_{drain} + h_{element}} - \sqrt{h_{drain}}\right] \sqrt{1 + f\,\frac{L}{d}}$$

where,

t = drain time
$V_{element}$ = volume of element to be drained
$h_{element}$ = height of element to be drained
C = coefficient of discharge
A = flow area of drain line
g = gravitational constant
h_{drain} = vertical distance from bottom of element to drain line
f = friction factor
L = equivalent resistance length of element piping
d = inside diameter of drain line

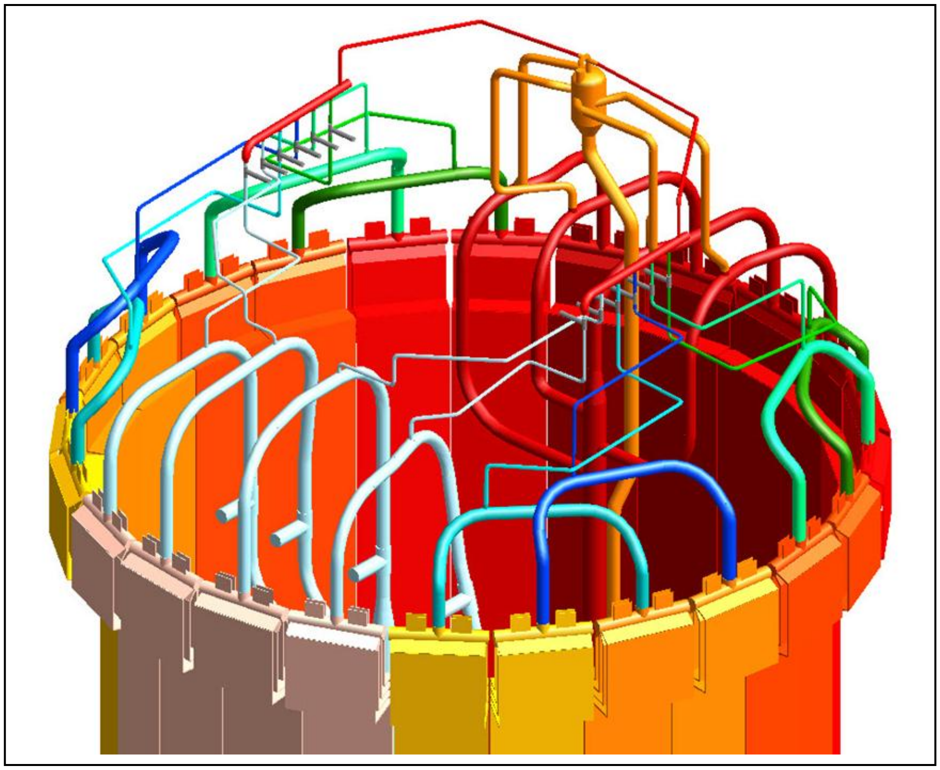

Figure 19. Vent System Arrangement

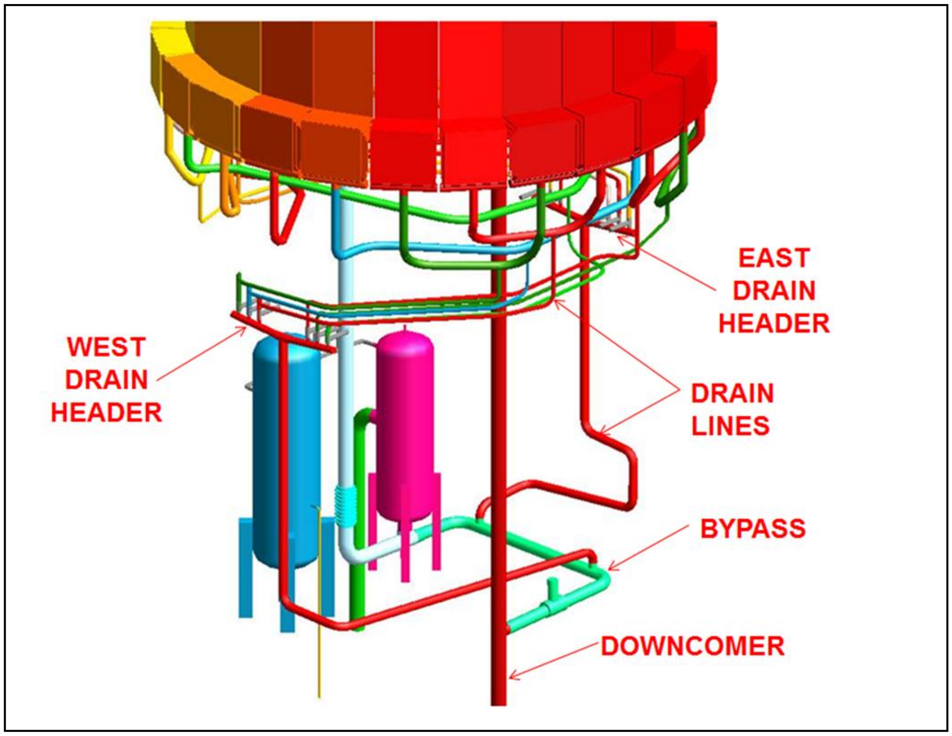

Figure 20. Drain System Arrangement

The drain time is calculated of the minimum of the various elements to be drained. Table 8 shows that the minimum time to drain the entire system is 2.13 minutes. Also shown is the minimum vent size for each system.

no. of panels		1	2	2	2	12	Tank	Tank +24
Weight	lb	12,821	28,399	28,654	29,581	170,069	101,480	493,898
Density	lb/ft3	118	118	118	118	118	118	118
Volume of pipe	ft3		23	26	33	137	132	660
Volume of element	ft3	109	241	243	251	1441	860	4186
distance element to drain line	ft	10.0	9.0	12.0	12.0	12.0	5.0	12.0
height of element	ft	97.1	107.1	107.1	107.1	119.1	23.5	71.3
discharge coefficient		0.6	0.6	0.6	0.6	0.6	0.6	0.6
Inside Diameter of drain line	in	12.0	6.0	6.0	6.0	12.0	22.0	22.0
Inside Diameter of drain line	ft	1.00	0.50	0.50	0.50	1.00	1.83	1.83
Flow area of drain line	ft2	0.79	0.20	0.20	0.20	0.79	2.64	2.64
friction factor		0.03	0.03	0.03	0.03	0.03	0.03	0.03
Equivalent Length	ft	80	119	130	170	175	50	250
g	ft/hr^2	4.17E+08	4.17E+08	4.17E+08	4.17E+08	4.17E+08	4.17E+08	4.17E+08
K1	ft2-hr/lb	0.043	0.043	0.041	0.041	0.039	0.077	0.047
K2	1/ft2	0.004	0.024	0.025	0.028	0.005	0.001	0.001
drain time	hr	0.002	0.029	0.029	0.034	0.036	0.007	0.033
drain time	min	0.13	1.76	1.77	2.06	2.13	0.40	1.97
Overall drain time	min	2.13						
Minimum Vent size	in	1.1	1.6	1.6	1.7	4.0	3.1	

Table 8. Receiver Drain Time

The receiver will be drained each day as part of the daily shutdown process. The drain time is important to prevent the salt from crystallizing and solidifying inside the panels. In addition to a relatively quick drain time, the receiver's electric heating system will be placed in operation to delay the cooling of the salt as it drains through the receiver. The draining will be coordinated with the removal of the incident flux to allow for proper flow without overheating the tubes.

3.4.7 Oven Box Design. It would not be practical to insulate and heat trace the manifolds and tubing connections to the manifolds due to its physical arrangement. Instead, the concept of an oven box is used to heat the manifolds and connecting tubing. This oven box is also used to maintain the manifold and tubing at 35 °C during the evening to allow for minimum start up time in the morning. The oven box is unique in that heat from the box heaters needs to be conserved. However, when the receiver is in operation, overheating due to the spillage of the incident flux must be prevented. A thermal analysis of the oven box was conducted to determine the metal temperatures as shown in Figure 21.

The following assumptions were made:

- Temperature at insulation inside surface = fluid temperature
- Left side of shield and top, right, and bottom of insulation is cooled by natural convection and radiation to ambient
- Shield right side/insulation left side is cooled by buoyancy driven ambient air flow
- Radiation interchange occurs between right side of plate and left side of insulation

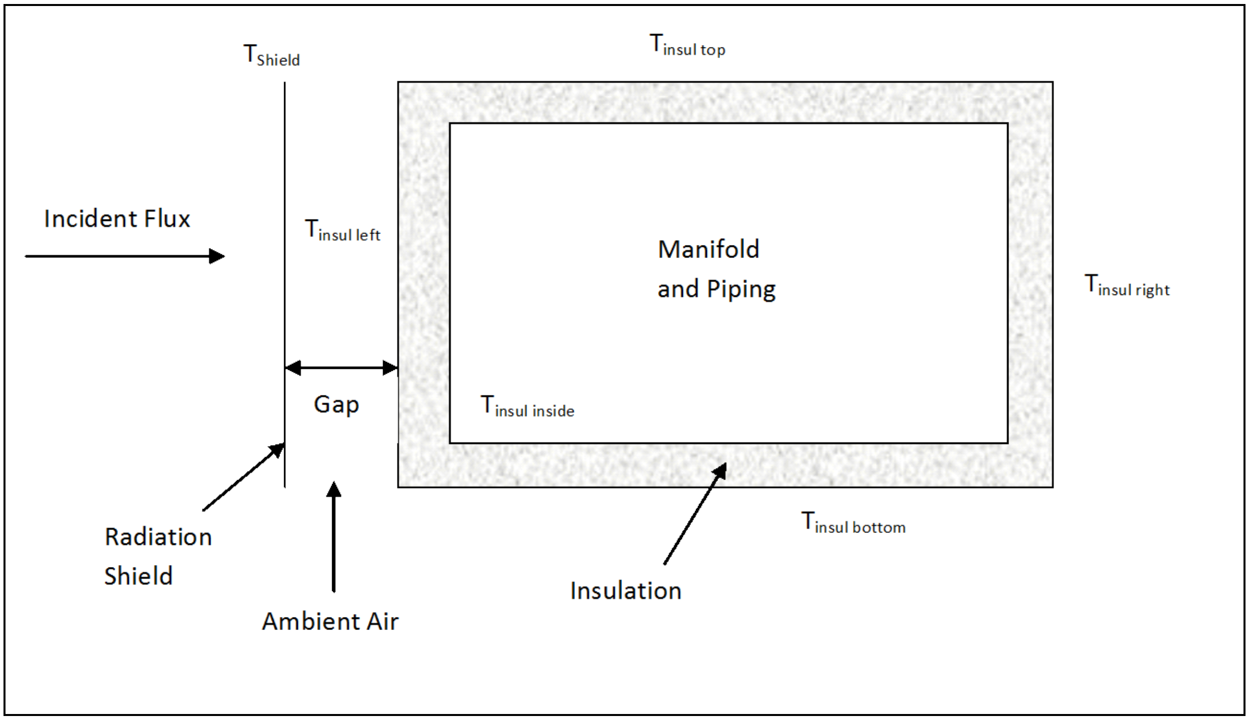

Figure 21. Oven Box Thermal Analysis

The thermal results are presented in the following Table 9. The shield white reflective paint is VHT paint (which uses ceramic particles) and is assumed (limited data available) to have an emissivity comparable to the discontinued Pyromark Series 2400 paint. The reflectivity is expected to be in the 0.8 to 0.9 range. A conservative reflectivity of 0.85 was used for calculations. For reference, the discontinued Pyromark Series 2400 paint reflectivity was 0.7.

Panel		1	3	7	11	Maximum
Fluid Temp.	C	308	442	438	602	
Incident Flux	kw/m2	236	233	186	117	
Shield Reflectivity		0.85	0.85	0.85	0.85	
Ambient Temp.	F	110	110	110	110	
Shield emissivity		0.84	0.84	0.84	0.84	
Insulation emissivity		0.70	0.70	0.70	0.70	
Air gap thickness	in	2.0	2.0	2.0	0.0	
Insulation cond.	Btu/hr-ft-F	0.10	0.10	0.10	0.10	
Insulation thickness	in	4.0	4.0	4.0	4.0	
Skin Temp.						
Shield	F	1034	1031	934	762	1034
Left Insul.	F	926	929	829	670	929
Top/Side Insul.	F	166	192	220	220	220
Bottom Insul.	F	178	207	241	241	241

Table 9. Oven Box Thermal Analysis Results

3.4.8 Inlet Surge Tank Design/Loss of Receiver Pump Analysis

A calculation was conducted to determine the flow rate versus time of the inlet surge tank in the event of a loss of receiver pump.

The following assumptions were made:

- Inlet surge tank size: 7' diameter x 23.5' height (including 2:1 elliptical heads)
- Pressurized air tank size: 8' diameter x 29' height (including 2:1 elliptical heads)
- Static head between vent and surge tank outlet = 102 psi (125 ft.)
- Frictional pressure loss = 223 psi (100% load), 24 psi (30% load)
- Air tank pressure = 490 psia
- Tank level during normal operation = 19.2' (100% load), 12.4' (30% load)
- Minimum required time to maintain normal operating flow = 20 sec
- Salt level should not rise in the upper tank head or fall into the lower tank head (i.e. should remain within the cylindrical portion of the inlet surge tank).

The salt mass flow rate and height of salt in the surge tank are shown in Figure 22.

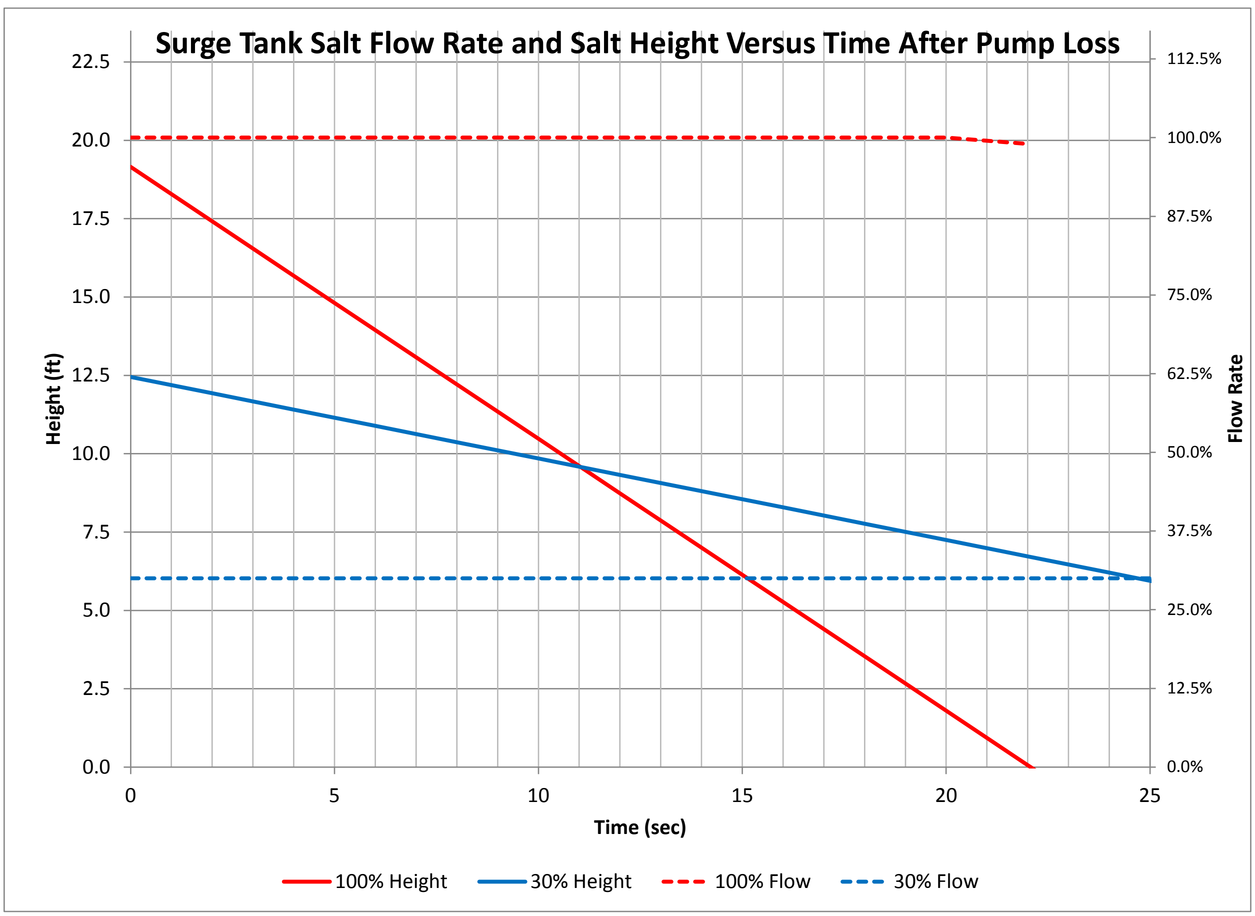

Figure 22. Surge Tank Salt Flow Rate and Height vs. Time After Pump Loss

When filling the receiver:

- The air compressor pressurizes the air inlet tank to the maximum operating pressure [34.5 barg (500 psig)]. If the inlet air tank pressure drops below a defined lower limit [33.8 barg (490 psig)], the air compressor is activated to bring the pressure back to the set point.
- Pressure regulator between air inlet tank and inlet surge tank is set for a downstream pressure (inlet surge tank pressure) a defined increment below the measured receiver inlet pressure, P1. The defined increment is based on the static head of salt from the desired salt level in the inlet surge tank and the elevation of the P1 pressure measurement.
- A radar level detector is mounted on the top of the inlet surge tank to confirm the level set by the defined increment above the measured P1 pressure.
- Salt pump establishes a 30% flow rate to fill the receiver.
- Salt moves into the inlet surge tank and rises to a level that compresses the trapped air in the tank (initially at atmospheric pressure) to a pressure that matches the weight of salt above the required inlet pressure. The inlet pressure P1 is the frictional pressure drop for 30% flow through the receiver plus the static head of salt above the P1 inlet pressure measurement elevation.
- The block valve between the inlet surge tank and pressure regulator is then opened to let the regulator increase the downstream pressure to the set point which should push the salt to the desired level.

For normal operation:

- With heliostats focused and applying heat to the receiver, the required salt flow (and receiver load) increases, increasing the receiver inlet pressure P1.
- The block valve (between the inlet air tank and the inlet surge tank) is kept open for normal operation.
- The pressure regulator set point is switched to be set to be equal to the measured P1 pressure.
- As load increases, P1 increases, and the salt level in the inlet surge tank will start to rise, compressing the trapped air above the salt. The pressure regulator set point will also increase as the P1 pressure increases.
- As load deceases, P1 decreases, and the salt level in the inlet surge tank will start to drop, lowering the pressure of the trapped air above the salt. The pressure regulator set point will also decrease as the P1 pressure decreases.
- If a high level limit is measured by the radar level detector, the pressure level set-point will be reset at a defined pressure increment above the measured P1 pressure to bring the measured level back to the expected level.
- If a low level limit is measured by the radar level detector, the vent valve on the top of the vessel will be opened until the measured level adjusts up to the expected level based on the value of P1.

If the salt pump trips:

- The loss of salt pump signal is activated and a signal is sent to the pressure regulating valve to adjust as required to hold the set point pressure equal to the measured P1 value at the time of loss of the salt pump.
- Air from the air inlet tank will flow into the inlet tank forcing salt flow out of the tank at a rate that will maintain the P1 set pressure.
- By maintaining the P1 set pressure, the salt flow rate at the time of pump loss will be maintained for a minimum of 20 seconds, giving the heliostats time to focus off the receiver.
- The pressure in the air inlet tank will drop and beyond 20 seconds will be equal to the air surge tank pressure as it continues to fall.
- The system was sized to store enough air to provide the required salt flow rates without the need for a continuous air supply form the compressor.
- If the compressor is available, it can be kept active, during the loss of pump event, to maintain the maximum air set pressure in the air tank.

3.4.9 Preheat and Heat Trace System

A calculation was performed to determine the electric heating power to heat the oven box from minus 9.4 °C (15 ^{o}F) to 315.6 °C (600 ^{o}F) in one hour. The power required was calculated as follow:

$$Q_{required} = \sum_{i=1}^{4} \frac{MC_p(T_{final} - T_{initial})}{\Delta t} + Q_{loss}$$

where,

i = elements (manifold, tubes, insulation, air)
M = mass of element
C_p = specific heat of element
T = Temperature
Δt = time period for heat up
Q_{loss} = average heat loss to the environment during heat up

The total power required is 20.68 kw/m (20.34 Btu/hr-ft) as shown in Table 10.

		Manifold	tubes	air	insulation				heat loss		
Length	ft	1	73		1		Length	ft	1		
OD	in	14	1.61				Area	ft2/ft	34.40		
tw	in	0.25	0.065				Wind Vel.	mi/hr	10		
ID	in	13.50	1.48				hconv	Btu/hr-ft2-F	3.71		
Vol	ft3/ft	0.07	0.16	69.96	11.47		hrad	Btu/hr-ft2-F	1.50		
density	lb/ft3	490	490	0.07	8		htot	Btu/hr-ft2-F	5.21		
Mass	lb/ft	37	78	5	92		hins	Btu/hr-ft2-F	0.30		
							htot	Btu/hr-ft2-F	0.28		
Tinit	F	15	15	15	15		Tamb	F	15		
Tend	F	600	600	600	420		Tend	F	600		
cp	Btu/lb-F	0.12	0.12	0.24	0.27		Tavg inside	F	308		
Heat	Btu	2,580	5,502	688	10,031						
time	hr	1	1	1	1					total	
Heat Rate	Btu/hr-ft	2,580	5,502	688	10,031		Qloss	Btu/hr-ft	2,854	21,654	Btu/hr-ft
										6.3	Kw/ft

Table 10. Oven Box Power Requirement

3.4.10 Basket Strainers. Solid material the size of BB's to the size of grapes can accumulate in the molten salt system if contaminated by particles such as sand from nitrate salt handling or rust forming in carbon steel piping as a result of local hot spots from trace heating. Maintenance of molten salt quality is considered a plant wide concern. Strainers are therefore not within the receiver suppliers scope of supply. Potential location of strainers (to be determined by others) is at the salt pump discharge upstream of the check and isolation valves. The goal would be to trap any particles prior to reaching the pump discharge valves and prior to reaching any of the valves in the receiver. A second filter may be installed at the inlet to the steam generator to trap any particles prior to reaching the steam generator control, vent, and drain valves.

3.4.11 Process Flow Diagrams. Figures 23, 24, 25, and 26 summarize the molten salt conditions passing through the receiver system for Day 154 (10:00:00).

3.4.12 Process and Instrument Diagrams

Process and instrumentation diagrams are included in Appendix G.

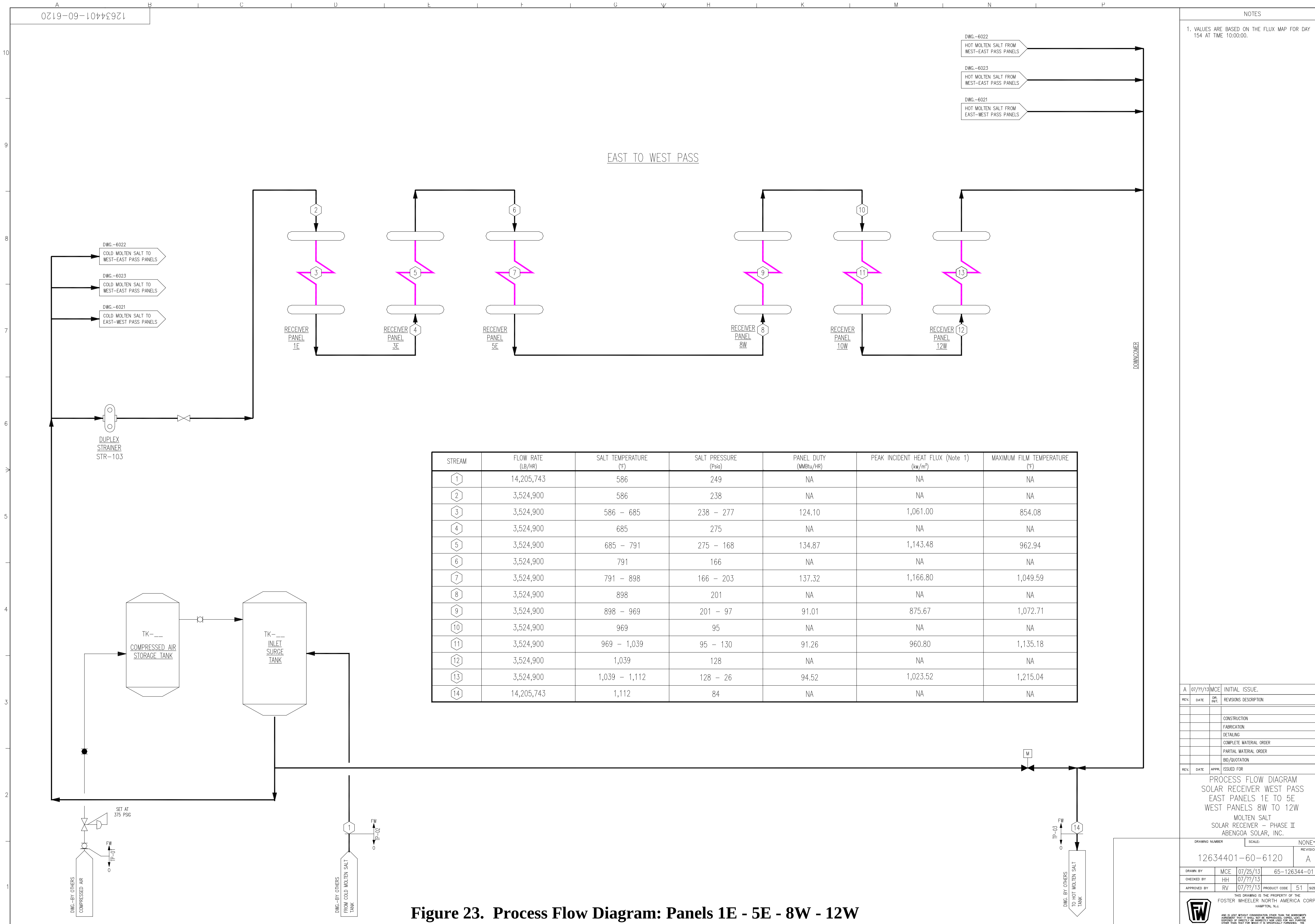

STREAM	FLOW RATE (LB/HR)	SALT TEMPERATURE (°F)	SALT PRESSURE (Psia)	PANEL DUTY (MMBtu/HR)	PEAK INCIDENT HEAT FLUX (Note 1) (kw/m²)	MAXIMUM FILM TEMPERATURE (°F)
1	14,205,743	586	249	NA	NA	NA
2	3,524,900	586	238	NA	NA	NA
3	3,524,900	586 – 685	238 – 277	124.10	1,061.00	854.08
4	3,524,900	685	275	NA	NA	NA
5	3,524,900	685 – 791	275 – 168	134.87	1,143.48	962.94
6	3,524,900	791	166	NA	NA	NA
7	3,524,900	791 – 898	166 – 203	137.32	1,166.80	1,049.59
8	3,524,900	898	201	NA	NA	NA
9	3,524,900	898 – 969	201 – 97	91.01	875.67	1,072.71
10	3,524,900	969	95	NA	NA	NA
11	3,524,900	969 – 1,039	95 – 130	91.26	960.80	1,135.18
12	3,524,900	1,039	128	NA	NA	NA
13	3,524,900	1,039 – 1,112	128 – 26	94.52	1,023.52	1,215.04
14	14,205,743	1,112	84	NA	NA	NA

Figure 23. Process Flow Diagram: Panels 1E - 5E - 8W - 12W

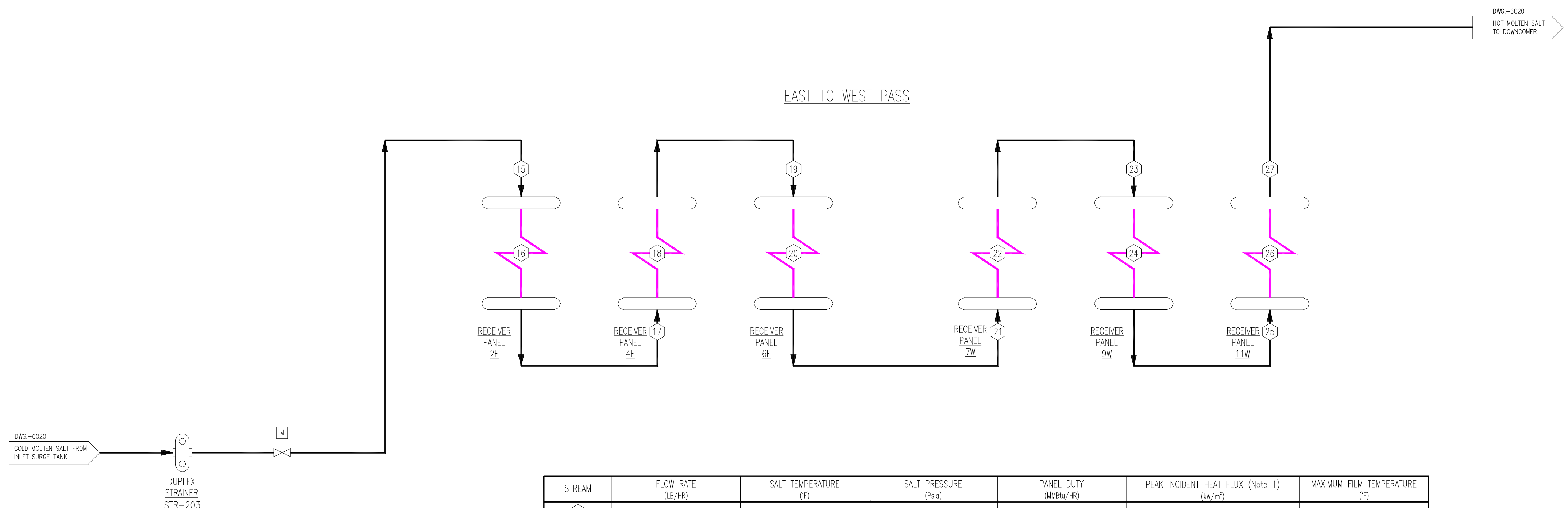

STREAM	FLOW RATE (LB/HR)	SALT TEMPERATURE (°F)	SALT PRESSURE (Psia)	PANEL DUTY (MMBtu/HR)	PEAK INCIDENT HEAT FLUX (Note 1) (kw/m²)	MAXIMUM FILM TEMPERATURE (°F)
15	3,554,759	586	241	NA	NA	NA
16	3,554,759	586 – 689	241 – 279	130.56	1,115.62	865.86
17	3,554,759	689	278	NA	NA	NA
18	3,554,759	689 – 796	278 – 170	137.32	1,161.22	968.75
19	3,554,759	796	168	NA	NA	NA
20	3,554,759	796 – 901	168 – 205	136.11	1,160.66	1,050.58
21	3,554,759	901	202	NA	NA	NA
22	3,554,759	901 – 973	202 – 98	92.48	841.38	1,077.55
23	3,554,759	973	96	NA	NA	NA
24	3,554,759	973 – 1,042	96 – 130	90.21	917.14	1,135.48
25	3,554,759	1,042	129	NA	NA	NA
26	3,554,759	1,042 – 1,112	129 – 26	92.11	1,001.24	1,208.79
27	3,554,759	1,112	26	NA	NA	NA

NOTES

1. VALUES ARE BASED ON THE FLUX MAP FOR DAY 154 AT TIME 10:00:00.

REV.	DATE	DR. INIT.	REVISIONS DESCRIPTION
A	07/??/13	MCE	INITIAL ISSUE.

REV.	DATE	APPR.	ISSUED FOR
			CONSTRUCTION
			FABRICATION
			DETAILING
			COMPLETE MATERIAL ORDER
			PARTIAL MATERIAL ORDER
			BID/QUOTATION

PROCESS FLOW DIAGRAM
SOLAR RECEIVER WEST PASS
EAST PANELS 2E TO 6E
WEST PANELS 7W TO 11W
MOLTEN SALT
SOLAR RECEIVER – PHASE II
ABENGOA SOLAR, INC.

DRAWING NUMBER: 12634401–60–6121
SCALE: NONE=1–0"
REVISION: A

DRAWN BY	MCE	07/25/13	65–126344–01
CHECKED BY	HH	07/??/13	
APPROVED BY	RV	07/??/13	PRODUCT CODE 51 SIZE 5

Figure 24. Process Flow Diagram: Panels 2E – 6E – 7W – 11W

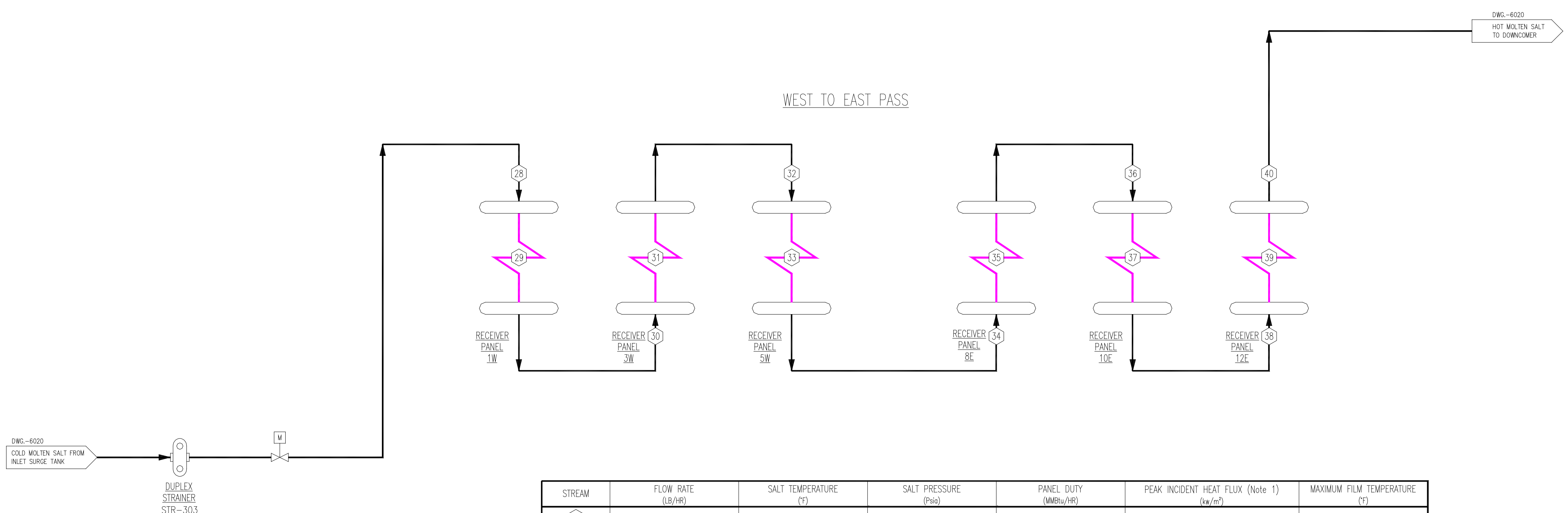

STREAM	FLOW RATE (LB/HR)	SALT TEMPERATURE (°F)	SALT PRESSURE (Psia)	PANEL DUTY (MMBtu/HR)	PEAK INCIDENT HEAT FLUX (Note 1) (kw/m²)	MAXIMUM FILM TEMPERATURE (°F)
28	3,551,547	586	242	NA	NA	NA
29	3,551,547	586 – 681	242 – 280	120.93	864.41	845.02
30	3,551,547	681	278	NA	NA	NA
31	3,551,547	681 – 768	278 – 170	111.19	818.65	917.21
32	3,551,547	768	168	NA	NA	NA
33	3,551,547	768 – 846	168 – 205	100.10	802.65	965.33
34	3,551,547	846	203	NA	NA	NA
35	3,551,547	846 – 945	203 – 98	128.77	1,117.33	1,092.72
36	3,551,547	945	96	NA	NA	NA
37	3,551,547	945 – 1,035	96 – 130	116.32	1.034.15	1,156.81
38	3,551,547	1,035	129	NA	NA	NA
39	3,551,547	1,035 – 1,112	129 – 26	101.36	932.40	1,223.59
40	3,551,547	1,112	26	NA	NA	NA

NOTES

1. VALUES ARE BASED ON THE FLUX MAP FOR DAY 154 AT TIME 10:00:00.

REV.	DATE	DR. INIT.	REVISIONS DESCRIPTION
A	07/??/13	MCE	INITIAL ISSUE.

REV.	DATE	APPR.	ISSUED FOR
			CONSTRUCTION
			FABRICATION
			DETAILING
			COMPLETE MATERIAL ORDER
			PARTIAL MATERIAL ORDER
			BID/QUOTATION

PROCESS FLOW DIAGRAM
SOLAR RECEIVER EAST PASS
WEST PANELS 1W TO 5W
EAST PANELS 8E TO 12E
MOLTEN SALT
SOLAR RECEIVER – PHASE II
ABENGOA SOLAR, INC.

DRAWING NUMBER: 12634401-60-6122 SCALE: NONE=1-0" REVISION: A

DRAWN BY	MCE	07/29/13	65-126344-01
CHECKED BY	HH	07/??/13	
APPROVED BY	RV	07/??/13	PRODUCT CODE 51 SIZE 5

12634401-60-6122

Figure 25. Process Flow Diagram: Panels 1W – 5W – 8E – 12E

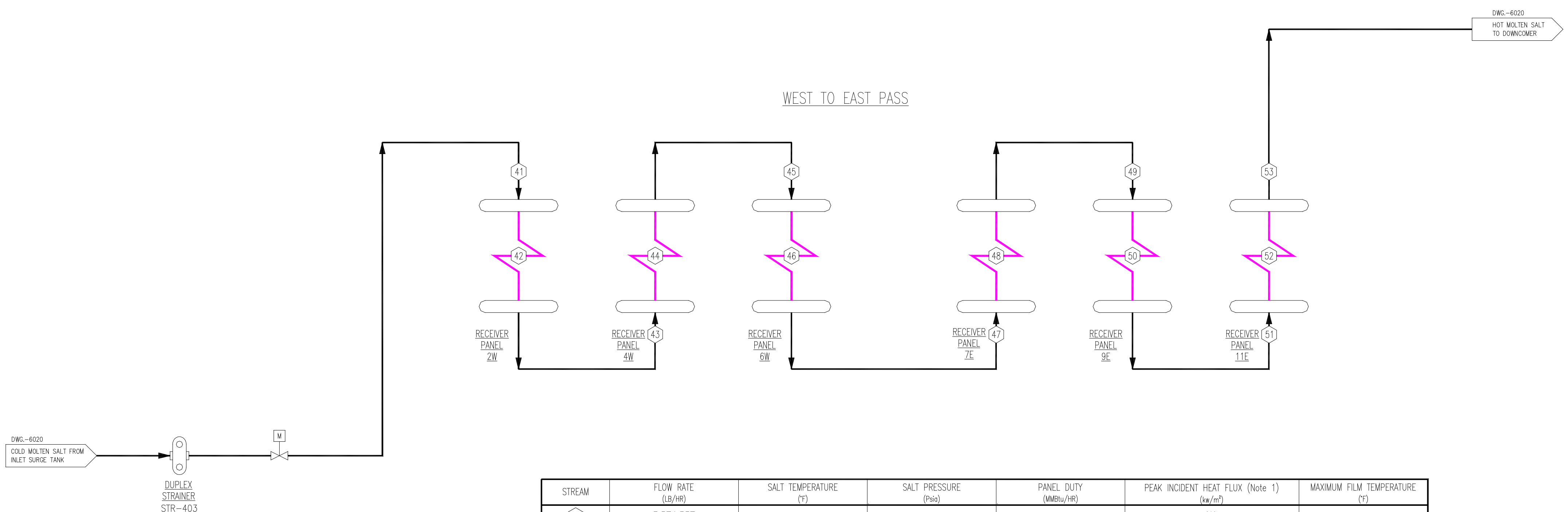

STREAM	FLOW RATE (LB/HR)	SALT TEMPERATURE (°F)	SALT PRESSURE (Psia)	PANEL DUTY (MMBtu/HR)	PEAK INCIDENT HEAT FLUX (Note 1) (kw/m²)	MAXIMUM FILM TEMPERATURE (°F)
41	3,574,537	586	244	NA	NA	NA
42	3,574,537	586 – 678	244 – 282	116.95	829.89	838.77
43	3,574,537	678	280	NA	NA	NA
44	3,574,537	678 – 760	280 – 171	105.80	805.51	902.91
45	3,574,537	760	170	NA	NA	NA
46	3,574,537	760 – 834	170 – 206	95.96	815.48	948.43
47	3,574,537	834	204	NA	NA	NA
48	3,574,537	834 – 936	204 – 98	132.43	1,143.24	1086.52
49	3,574,537	936	97	NA	NA	NA
50	3,574,537	936 – 1,029	97 – 131	122.48	1.080.08	1155.72
51	3,574,537	1,029	129	NA	NA	NA
52	3,574,537	1,029 – 1,112	129 – 26	108.95	984.32	1228.74
53	3,574,537	1,112	26	NA	NA	NA

NOTES

1. VALUES ARE BASED ON THE FLUX MAP FOR DAY 154 AT TIME 10:00:00.

REV.	DATE	DR. INIT.	REVISIONS DESCRIPTION
A	07/??/13	MCE	INITIAL ISSUE.

REV.	DATE	APPR.	ISSUED FOR
			CONSTRUCTION
			FABRICATION
			DETAILING
			COMPLETE MATERIAL ORDER
			PARTIAL MATERIAL ORDER
			BID/QUOTATION

PROCESS FLOW DIAGRAM
SOLAR RECEIVER EAST PASS
WEST PANELS 2W TO 6W
EAST PANELS 7E TO 11E
MOLTEN SALT
SOLAR RECEIVER – PHASE II
ABENGOA SOLAR, INC.

DRAWING NUMBER: 12634401–60–6123 SCALE: NONE=1–0" REVISION: A

DRAWN BY	MCE	07/29/13	65–126344–01
CHECKED BY	HH	07/??/13	
APPROVED BY	RV	07/??/13	PRODUCT CODE 51 SIZE 5

Figure 26. Process Flow Diagram: Panels 2W – 6W – 7E – 11E

3.5 Mechanical Design

This section summarizes the stress analysis calculations performed on the molten salt solar receiver. The scope of the study is to come up with practical and economical design of the solar boiler. The stress analysis calculations are performed with scope of the study in mind. Further detailed analysis is required to complete the design of the solar boiler that is ready to be built.

The receiver tubes within the solar boiler are subjected to high thermal load as well as a large number of cycles. Thus, for this study, stress analysis calculations are focused on the tubes of the solar receiver, and the tube-to-header connections.

This study is a continuation of phase 1 of the same project. Much of the background for this report can be found in report for phase 1 study. The minimum wall thickness (MW) determined from a pressure standpoint per ASME Section 1 for the 40.9 mm (1.61 in) OD Haynes 230 tubes are shown below; the tubes, however, will be provided with a minimum wall thickness of 1.65 mm (0.065").

Pass	Thickness (in.)		Design Pressure (psia)	Design Temp (°F)	Code MW (in)
	MW	AW			
Pass 1	0.059	0.065	300	1,134	0.012
Pass 2	0.059	0.065	300	1,231	0.017
Pass 3	0.059	0.065	220	1,285	0.016
Pass 4	0.059	0.065	220	1,287	0.016
Pass 5	0.059	0.065	141	1,305	0.011
Pass 6	0.059	0.065	141	1,377	0.015

3.5.1 Stress Analysis of Tubes/Panels – Problem Setup and Definition.

Flux maps were provided for 20 different time points, spanning an entire year. In the Phase II design, the molten salt receiver consists of 24 panels. As such, the analysis could be set up for 480 unique cases. An effort was made to consolidate the number of cases.

The solar receiver consists of 6 passes. Each pass consists of 4 panels in parallel flow – 2 north panels and 2 south panels. The design pressure for each panel in the same relative panel location (pass) is the same. Thus, for the pressure load, only one panel in each pass must be analyzed, such that the results may be applied to all 4 panels in the pass.

From the work performed during the Phase I portion of this project, it was determined that the point with the highest strain and stress levels is at the location of highest solar flux. Solar flux values on each pass, for all of the 20 time points, were compared. The time point with the highest solar flux was selected for each individual pass. This was the peak flux for the panel.

It was then assumed that all 4 panels of a given pass experienced peak flux for 12 hours a day for 365 days a year. This is a very conservative assumption and can be safely used for the analysis.

Table 11 below provides the 6 cases that were analyzed in this study. The result of each case can be applied to all the 4 panels of the given pass.

Table 11 : Design Point (with Max Flux) for Each Pass

Pass	DAY	TIME	PANEL	INTERNAL PRESSURE (PSI)	Max Flux (W/m2)
1	8	1200	1W	300	1293
2	300	1030	3E	300	1283
3	300	1030	5E	220	1243
4	81	1000	7E	220	1157
5	154	1000	9E	141	1090
6	154	1000	11E	141	993

Table 12 below summarizes the background data used to make selections in Table 11 above.

Table 12: Maximum Absorbed Heat Flux (W/m2) For All Panel For All Given Time Point.

		Pass 1				Pass 2				Pass 3				Pass 4				Pass 5				Pass 6			
Day	**Time**	**1E**	**2E**	**2W**	**1W**	**3E**	**4E**	**4W**	**3W**	**5E**	**6E**	**6W**	**5W**	**7E**	**8E**	**8W**	**7W**	**9E**	**10E**	**10W**	**9W**	**11E**	**12E**	**12W**	**11W**
8	8:30	782	828	724	752	853	860	610	670	854	839	458	541	793	748	357	394	712	665	348	337	597	534	457	383
8	9:30	1,076	1,135	991	1,023	1,157	1,155	891	953	1,132	1,082	704	805	1,019	968	538	610	918	846	472	489	754	653	557	496
8	10:30	1,182	1,224	1,119	1,145	1,230	1,211	1,022	1,077	1,172	1,121	851	945	1,068	1,009	663	752	930	833	543	591	732	643	564	525
8	12:00	1,279	1,293	1,277	1,293	1,277	1,242	1,193	1,241	1,195	1,136	1,056	1,134	1,059	964	860	961	863	767	682	764	685	621	573	620
81	7:00	565	599	479	515	619	649	359	425	669	671	286	313	662	650	284	273	613	570	368	315	544	515	461	417
81	8:30	1,016	1,078	917	965	1,120	1,149	753	839	1,164	1,154	604	672	1,126	1,081	529	553	1,027	972	596	552	907	826	729	648
81	10:00	1,150	1,201	1,087	1,114	1,224	1,228	964	1,031	1,217	1,193	822	892	1,157	1,107	707	758	1,044	972	670	672	895	819	739	687
81	12:00	1,176	1,192	1,178	1,192	1,179	1,150	1,107	1,149	1,108	1,052	977	1,050	979	895	805	893	808	724	649	721	652	596	552	594
154	6:00	482	538	373	428	581	604	297	325	622	652	294	283	666	661	369	321	649	632	459	421	588	546	524	493
154	8:00	903	986	781	833	1,039	1,074	657	716	1,099	1,115	584	611	1,115	1,099	628	594	1,069	1,028	728	674	979	920	840	775
154	10:00	1,067	1,124	1,010	1,031	1,152	1,170	926	969	1,176	1,170	849	884	1,152	1,127	805	821	1,090	1,044	821	806	993	939	873	834
154	12:00	1,163	1,186	1,179	1,186	1,180	1,157	1,121	1,157	1,122	1,074	1,016	1,073	1,018	957	890	954	893	833	777	829	780	738	702	736
227	6:00	334	370	267	307	392	399	200	225	413	429	184	184	431	424	222	196	417	400	291	263	367	351	337	306
227	8:00	895	966	772	827	1,009	1,041	634	701	1,064	1,076	536	577	1,068	1,045	547	522	1,006	959	643	589	907	846	764	693
227	10:00	1,088	1,142	1,027	1,051	1,168	1,180	928	981	1,179	1,165	826	875	1,142	1,107	756	785	1,060	1,005	755	744	946	884	814	770
227	12:00	1,064	1,089	1,088	1,089	1,089	1,077	1,058	1,077	1,059	1,035	1,005	1,034	1,007	977	940	973	944	913	881	908	885	861	832	858
300	7:30	461	477	407	441	503	518	335	378	521	517	242	279	509	480	205	219	450	431	238	215	405	362	329	278
300	9:00	1,032	1,095	959	985	1,132	1,147	825	905	1,139	1,109	639	730	1,057	999	511	566	947	890	504	483	812	719	619	544
300	10:30	1,228	1,271	1,180	1,202	1,283	1,271	1,063	1,132	1,243	1,202	891	980	1,149	1,082	724	803	999	908	619	660	816	732	651	609
300	12:00	1,240	1,261	1,249	1,261	1,249	1,222	1,178	1,222	1,179	1,119	1,043	1,118	1,045	963	874	960	877	795	721	792	723	668	625	666

The receiver analysis involved the following steps:

- Buckstay stiffener calculation for wind and seismic loading
- Receiver Tube Finite Element Analysis
  - Thermal analysis to determine the temperature distribution
  - Stress analysis to determines the creep and fatigue life of the tubes
- Header to tube connection Analysis
- Full panel flexibility analysis

3.5.2 Buckstay Requirement for Wind and Seismic Loading.

The exact geographic location for the project was not defined. The following typical wind and seismic criteria, were therefore used to design the solar receiver:

- Wind:
  - 40.2 m/sec (90) mph equivalent to 415.0 kg/m^2 (85 pounds per square feet) at the average height of the solar receiver. The exact geometry of the support tower is not known. An estimate for the effects of vortex shedding was made. This needs to be updated for future studies when more specific information (natural frequency) of the support tower is known

  - To avoid damage, the heliostats are designed to quickly go to their horizontal position, when the wind velocity is above 17.9 m/sec (40 mph). Thus the solar receiver will never see combined loading of 100% temperature and 100% wind load.
- Seismic: 0.30 g

A one tube Caesar piping model was built and analyzed to determine the number of buckstays required. The tube was fixed for the two horizontal degrees of freedom and all three rotational degrees of freedom at the two ends at the tube welds to the headers. Six buckstays were placed 4.52 m (14.8 ft.) apart. The vertical tube load was supported at the second bend. As shown in Table 12a, the wind load resulted in larger forces than seismic loads. Two wind conditions were analyzed: 40 mph at operating design temperature and 90 mph at operating temperatures (since the heliostats will not be focused on the tubes).

Table 12a Wind and Seismic Load Calculations

Wind

Velocity (MPH)	89.5	40
Pressure (PSF)	85	17
OD (inch)	1.61	1.61
AW (inch)	0.065	0.065
Wind Load (lb. / linear in)	**0.950**	**0.190**
Seismic Load (g)	0.30	
Metal Density (lb./in^3)	0.324	
Metal Cross Section Area (in^2)	0.315	
Fluid Density (lb./in^3)	0.069	
Fluid Cross Section Area (in^2)	1.720	
Weight / linear ft. of tube (lbs.)	2.651	
Seismic Load (lb. / linear in.)	**0.066**	
GOVERNING LOAD:	**WIND**	

The results from the Caesar analysis shown in Table 12b indicate that six buckstays are sufficient for the given wind and earthquake loads. Further analysis may be required when the exact geographic location of the project is defined and exact wind and seismic loads are known.

40 mph Wind at Operating Condition Allowable Stress at Tube Design (Max Metal) Temperature						
Pass	*Pass 1*	*Pass 2*	*Pass 3*	*Pass 4*	*Pass 5*	*Pass 6*
Tube OD (in)	1.61	1.61	1.61	1.61	1.61	1.61
Wind Pressure (psf)	17	17	17	17	17	17
Linear Load (lb./in)	0.19	0.19	0.19	0.19	0.19	0.19
Design Temp (F)	1,134	1,231	1,285	1,287	1,305	1,377
Design Pressure (psi)	300	300	220	220	141	141
Code Allowable Stress, Sa (psi)	19,608	13,962	11,290	11,198	10,390	7,528
Allowable Stress for Occ Load. = 1.15 Sa (psi)	22,549	16,056	12,984	12,878	11,949	8,657
Occasional Load Stress (psi)	6,416	6,416	5,979	5,979	5,548	5,548
Stress %	**28%**	**40%**	**46%**	**46%**	**46%**	**64%**

89.5 mph (40 m/s) Wind at Operating Condition Allowable Stress at Operating (Max Salt) Temperature						
Pass	*Pass 1*	*Pass 2*	*Pass 3*	*Pass 4*	*Pass 5*	*Pass 6*
Tube OD	1.61	1.61	1.61	1.61	1.61	1.61
Wind Pressure (psf)	85	85	85	85	85	85
Linear Load	0.95	0.95	0.95	0.95	0.95	0.95
Operating (Max Salt) Temp	691	797	903	973	1,044	1,116
Design Pressure (psi)	300	300	220	220	141	141
Code Allowable Stress, Sa (psi)	28,772	28,200	28,200	28,200	28,200	21,856
Allowable Stress for Occ Load.= 1.15 Sa (psi)	33,088	32,430	32,430	32,430	32,430	25,134
Occasional Load Stress	24,740	24,740	24,304	24,304	23,873	23,873
Stress %	**75%**	**76%**	**75%**	**75%**	**74%**	**95%**

Table 12b Wind Stresses

3.5.3 Single Receiver Tube Finite Element Analysis

The first step of the analysis addressed a single tube of the molten salt solar receiver, along with the inlet and outlet headers, supports, and stabilizing reinforcements (buckstays). The arrangement of the single tube model is shown in Figure 27. Only half the tube was modeled to take advantage of symmetry. Shell elements were used to mesh the half tube model, which represented a typical tube in the receiver panel. Shell 132 and Shell 281, both 8 node elements within ANSYS, were used for thermal and structural analysis, respectively. Tubes were terminated in the header. Rotation of header was fixed. Six levels of buckstays were modeled by fixing horizontal translation degree of freedom. Tube was supported in vertical direction at the first buckstay.

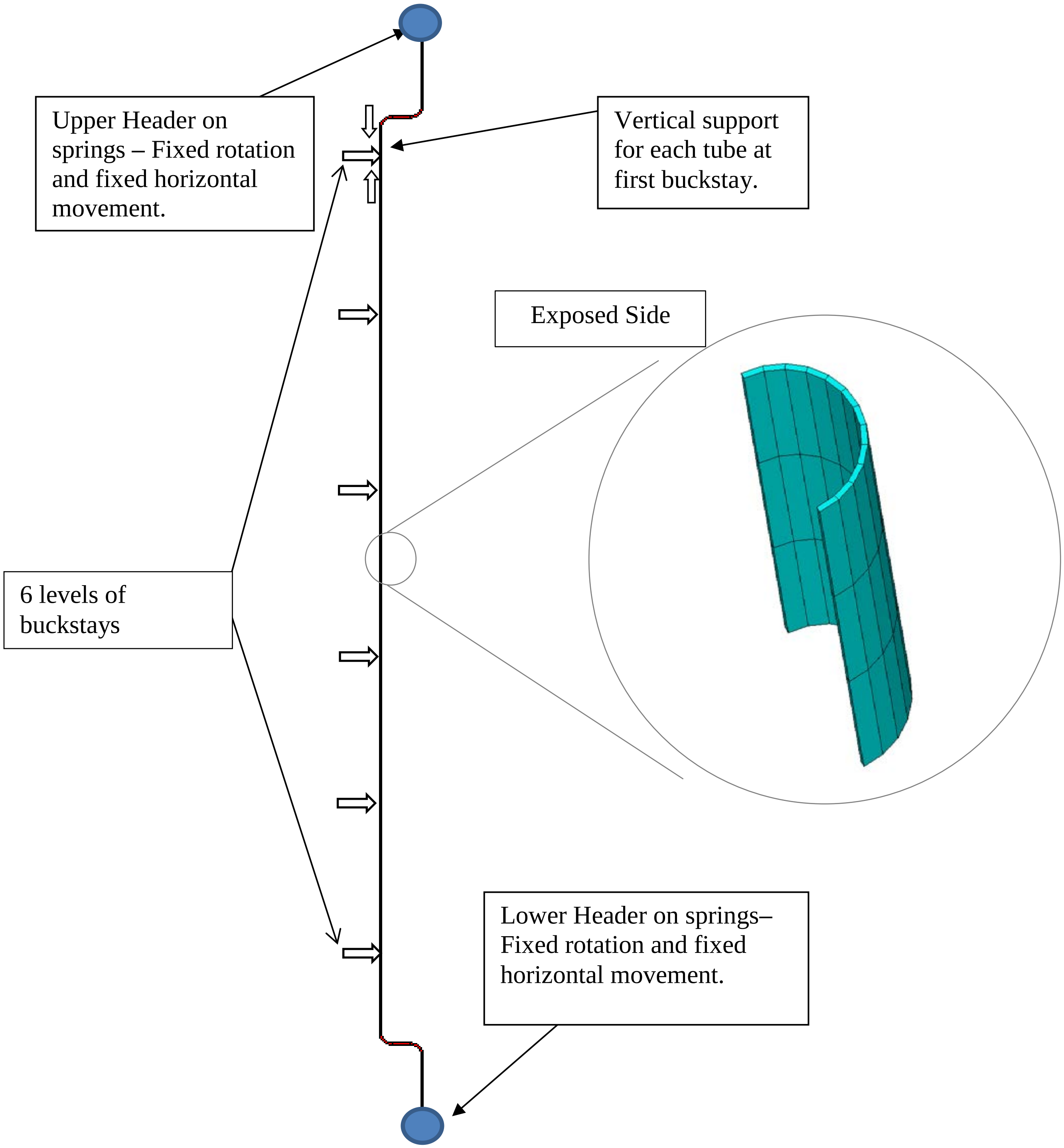

Figure 27: Single Tube Arrangement

3.5.4 Single Receiver Tube Thermal Analysis

For the thermal analysis, a convection condition was applied on the inside of the tube using the temperatures and film coefficients, as calculated based upon the flux map data. A heat flux was applied on the outside of the tube, which was varied both circumferentially and vertically. A view factor was applied in the circumferential direction according to equation given below, to account for shading from adjacent tubes.

$$Q = \frac{3 - 3\sin\theta + 2\cos\theta\sqrt{1 - \sin\theta}}{5 - 4\sin\theta}$$

This distribution is depicted graphically in Figure 28. The heat flux was also varied in the vertical direction, based upon the distribution provided in the flux maps. Vertically, the heat flux was varied, as given in the CI sheet, and as seen in Table 13.

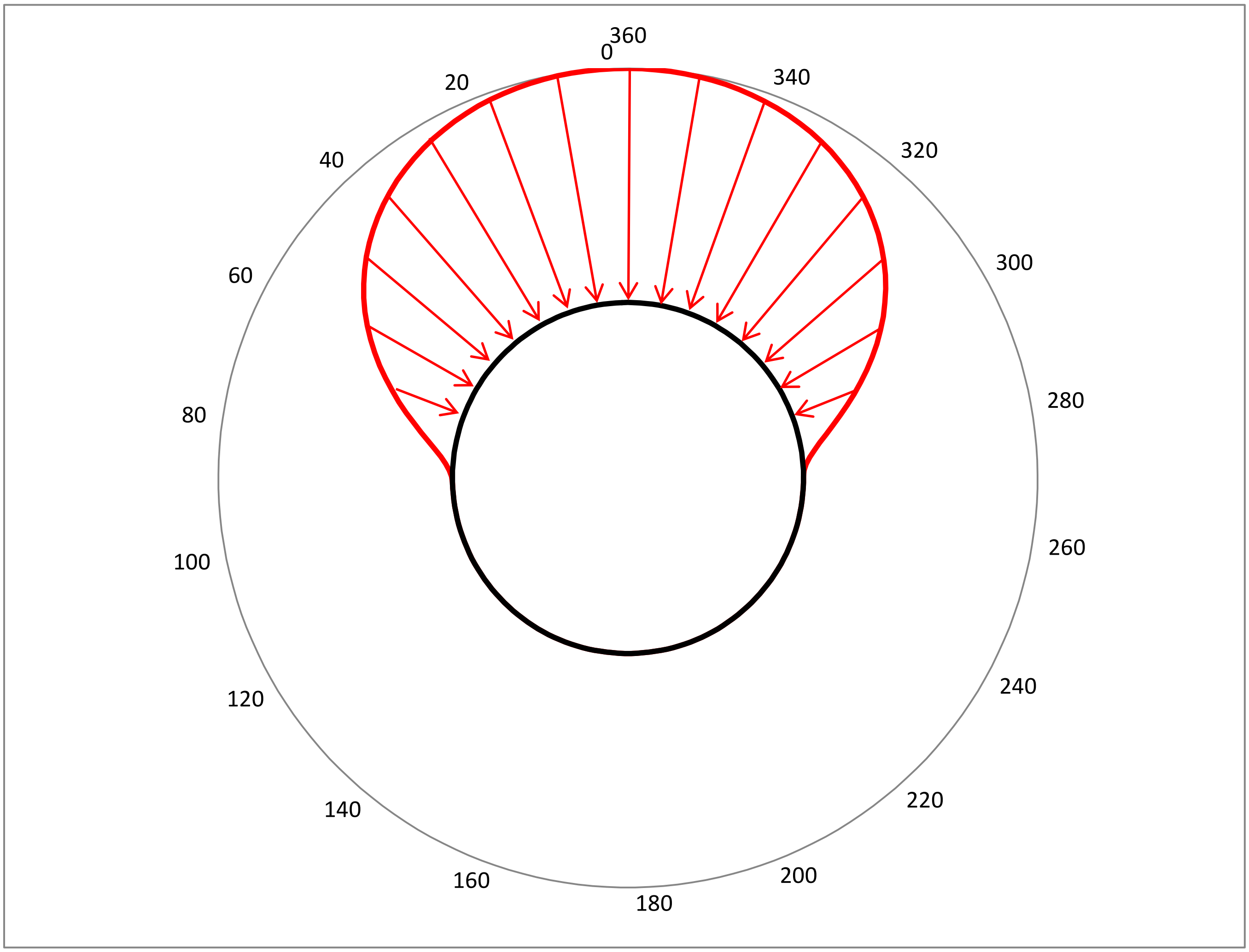

Figure 28: Graphical representation of the circumferential heat flux distribution

Table 13: Typical Absorbed Heat Flux (Btu/hr./in2) Distribution on a Tube. (Day 8 12:00 pm. Panel 1W Shown Here)

Exposed Tube Elevation (inch)	Circumferential Distance. (Degrees) (90 = Crown of the Tube. 0 = Side of the tube)																													
	0	3	6	9	12	15	18	21	24	27	30	33	36	39	42	45	48	51	54	57	60	63	66	69	72	75	78	81	84	87	90
74.2	0	3	13	28	48	71	97	124	151	178	204	229	252	273	292	309	325	339	351	362	371	379	386	392	397	401	404	406	408	408	409
72.5	0	3	13	28	48	71	97	124	151	178	204	229	252	273	292	309	325	339	351	362	371	379	386	392	397	401	404	406	408	408	409
69.1	0	6	25	54	93	138	188	241	294	346	397	445	489	530	567	601	631	658	682	703	721	737	750	761	771	778	784	789	792	793	794
65.7	0	10	40	88	151	225	306	392	479	564	646	724	796	863	923	978	1027	1071	1110	1144	1173	1199	1221	1239	1254	1267	1276	1283	1288	1291	1292
62.4	0	14	56	122	208	310	423	541	661	778	892	999	1098	1190	1274	1350	1418	1478	1532	1579	1619	1655	1685	1710	1731	1748	1761	1771	1778	1782	1783
59.0	0	19	74	161	276	411	560	716	874	1030	1180	1322	1454	1575	1686	1787	1876	1956	2027	2089	2143	2190	2230	2263	2291	2313	2331	2344	2353	2358	2360
55.6	0	21	81	177	303	452	616	788	962	1134	1299	1455	1600	1734	1856	1967	2065	2154	2231	2300	2359	2411	2454	2491	2522	2546	2566	2580	2590	2596	2598
52.2	0	21	83	181	309	461	628	803	981	1155	1323	1482	1631	1767	1891	2004	2105	2194	2274	2343	2404	2456	2501	2538	2570	2595	2614	2629	2639	2645	2647
48.9	0	21	81	177	302	450	613	785	958	1129	1293	1449	1593	1727	1848	1958	2057	2144	2222	2290	2349	2400	2444	2481	2511	2536	2555	2569	2579	2585	2587
45.5	0	20	79	172	295	439	598	765	934	1101	1261	1412	1553	1683	1802	1909	2005	2091	2166	2232	2290	2340	2383	2418	2448	2472	2491	2505	2514	2520	2522
42.1	0	20	77	169	289	430	586	750	916	1079	1236	1385	1523	1650	1767	1872	1966	2050	2124	2189	2245	2294	2336	2371	2400	2423	2442	2456	2465	2470	2472
38.8	0	19	76	166	283	422	575	736	899	1059	1213	1359	1495	1620	1734	1837	1929	2011	2084	2148	2204	2252	2292	2327	2355	2378	2397	2410	2419	2424	2426
35.4	0	19	75	164	280	417	568	727	888	1046	1199	1343	1477	1601	1713	1815	1906	1988	2059	2122	2177	2225	2265	2299	2327	2350	2368	2381	2390	2396	2397
32.0	0	19	74	163	278	415	565	723	883	1040	1192	1335	1468	1591	1703	1804	1895	1976	2047	2110	2165	2212	2252	2286	2314	2336	2354	2367	2376	2382	2383
28.6	0	19	75	164	281	418	570	729	891	1049	1202	1347	1481	1605	1718	1820	1912	1993	2066	2129	2184	2231	2272	2306	2334	2357	2375	2388	2398	2403	2404
25.3	0	20	77	168	287	428	584	747	912	1074	1230	1378	1516	1643	1759	1863	1957	2040	2114	2179	2235	2284	2325	2360	2389	2412	2431	2444	2454	2459	2461
21.9	0	20	78	171	293	437	595	762	930	1096	1256	1406	1547	1676	1794	1901	1997	2082	2157	2223	2281	2330	2373	2408	2438	2462	2480	2494	2504	2509	2511
18.5	0	19	76	165	283	421	574	734	896	1056	1210	1355	1490	1615	1729	1832	1924	2006	2078	2142	2197	2245	2286	2320	2349	2372	2390	2403	2412	2418	2419
15.2	0	17	66	145	248	370	504	645	787	927	1062	1190	1309	1419	1518	1609	1690	1762	1825	1881	1930	1972	2008	2038	2063	2083	2099	2111	2119	2123	2125
11.8	0	13	51	112	192	286	390	499	610	718	823	922	1014	1099	1176	1246	1309	1365	1414	1457	1495	1527	1555	1579	1598	1614	1626	1635	1641	1645	1646
8.4	0	8	32	71	121	181	246	315	385	453	519	582	640	694	742	787	826	861	893	920	944	964	982	996	1009	1019	1026	1032	1036	1038	1039
5.1	0	4	17	38	65	97	132	169	206	243	278	311	342	371	397	421	442	461	477	492	505	516	525	533	540	545	549	552	554	555	556
1.7	0	2	9	20	34	51	69	89	108	128	146	164	180	195	209	222	233	243	251	259	266	272	277	281	284	287	289	291	292	292	293
0.0	0	2	9	20	34	51	69	89	108	128	146	164	180	195	209	222	233	243	251	259	266	272	277	281	284	287	289	291	292	292	293

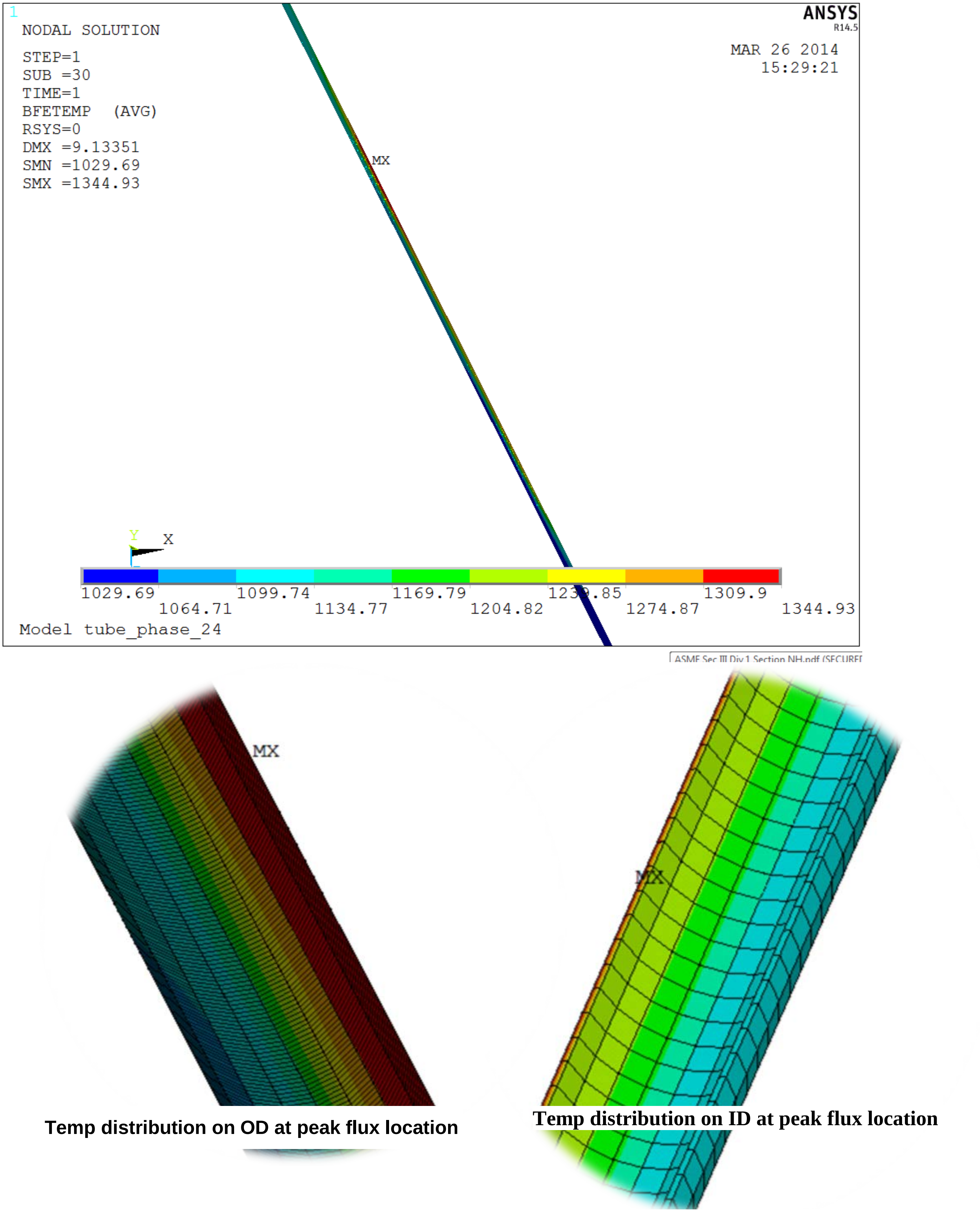

Figure 29: Temperature Distribution on a typical tube (Tube from panel 6 shown here)

Figure 29 shows the temperature distribution on the inside and outside of a typical tube. High metal temperatures are concentrated at the location of the peak flux, as shown in the cross section presented in Figure 30. It can be noted that the temperatures are highest on the crown of the tube. Temperatures drop very quickly along the circumference, and are essentially equal to fluid temperature for the unexposed part of the tube. In the vertical direction, the temperature is proportional to the flux absorbed by the tube.

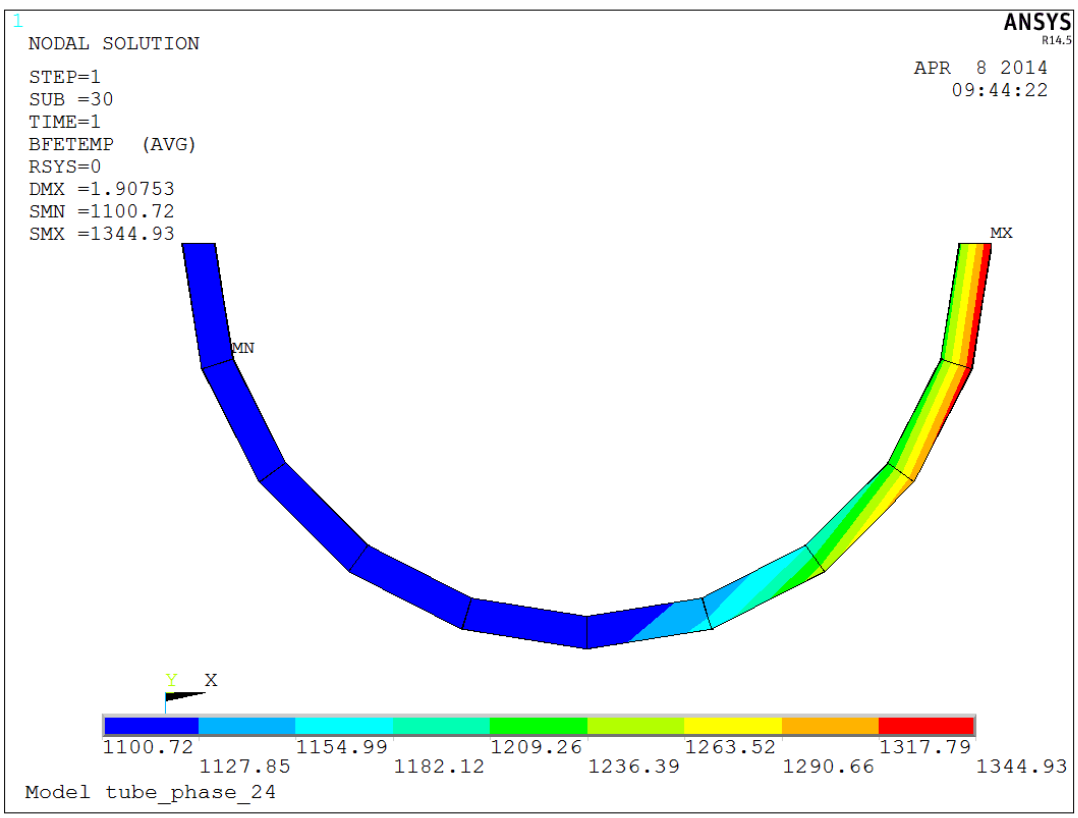

Figure 30: Temperature Distribution on a typical tube cross section (Tube from panel 6 shown here)

Table 14 contains a summary of the thermal analysis results for all 6 panels.

PASS	**DESIGN POINT**		**PANEL**	**MAX FLUX**	**PRESSURE**	**Temperature At Peak Flux Point (F)**		
	DAY	**TIME**		**(kW/m2)**	**(psi)**	OD	ID	T Diff thru Tube Thickness
1	8	1200	1W	1293	300	1082	902	**180**
2	300	1030	3E	1283	300	1181	1014	**168**
3	300	1030	5E	1243	220	1251	1099	**152**
4	81	1000	7E	1157	220	1244	1099	**145**
5	154	1000	9E	1090	141	1282	1154	**128**
6	154	1000	11E	993	141	1345	1228	**117**

Table 14: Thermal Analysis Result Summary

3.5.5 Steady State Stress Finite Element Analysis

Steady state stress analysis was performed on the single tube models, applying internal pressure, gravity and temperature loads. Stress and strain plots are given in Figure 31 below. As expected, high stress and strain is seen at the crown of the tube. High thermal gradient at the crown is the main cause of the high stress and strain at that location.

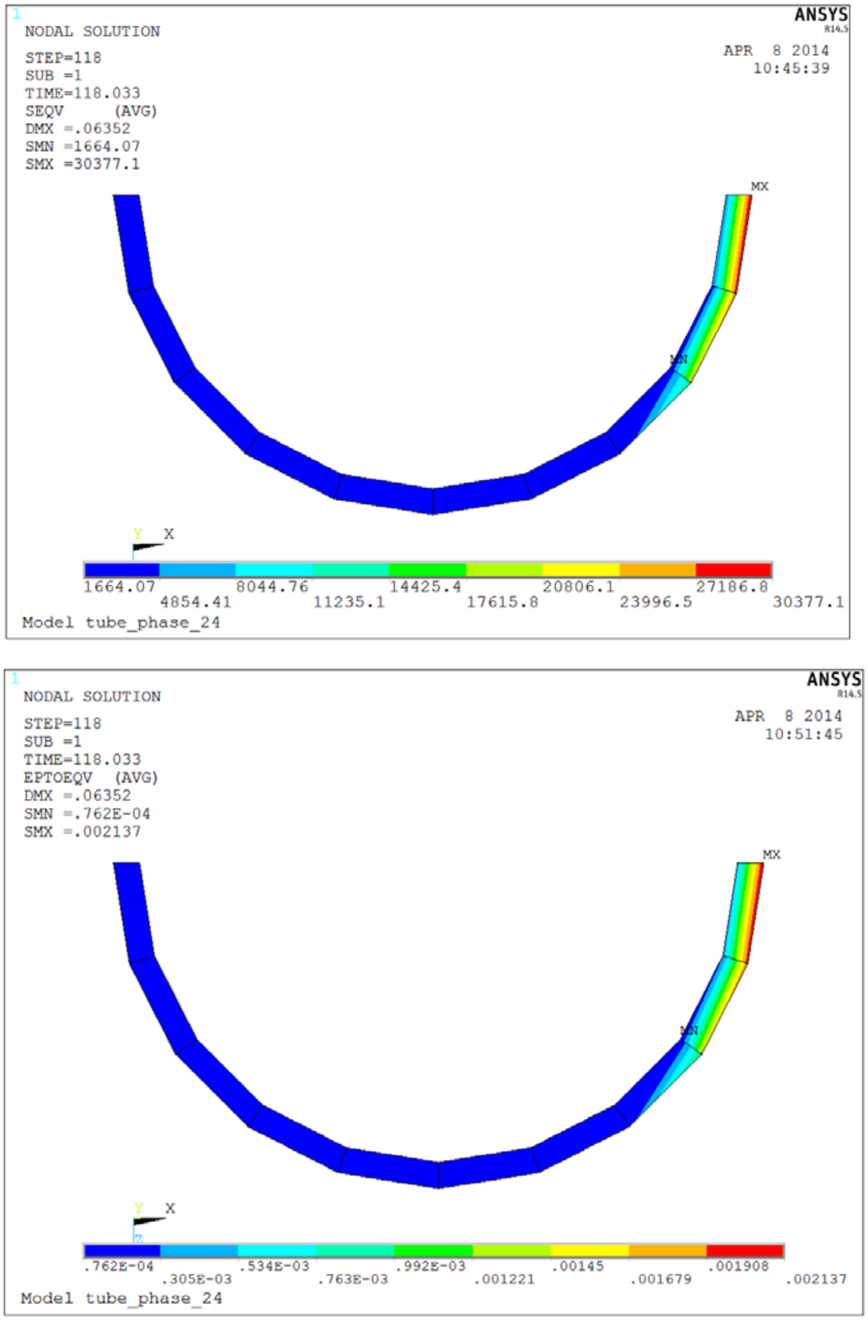

Figure 31: Von Mises Stress and von Misses Strain on a typical tube cross section at peak flux elevation

(Tube from panel 1 shown here)

Figure 32 below shows the Von Misses strain on a vertical portion of the tube exposed to solar flux. A portion of the tube exposed to solar flux experiences local yielding. This yielding is due to the thermal (secondary) loads and is acceptable, upon satisfactory results from further analysis, as shown in cyclical analysis sections below.

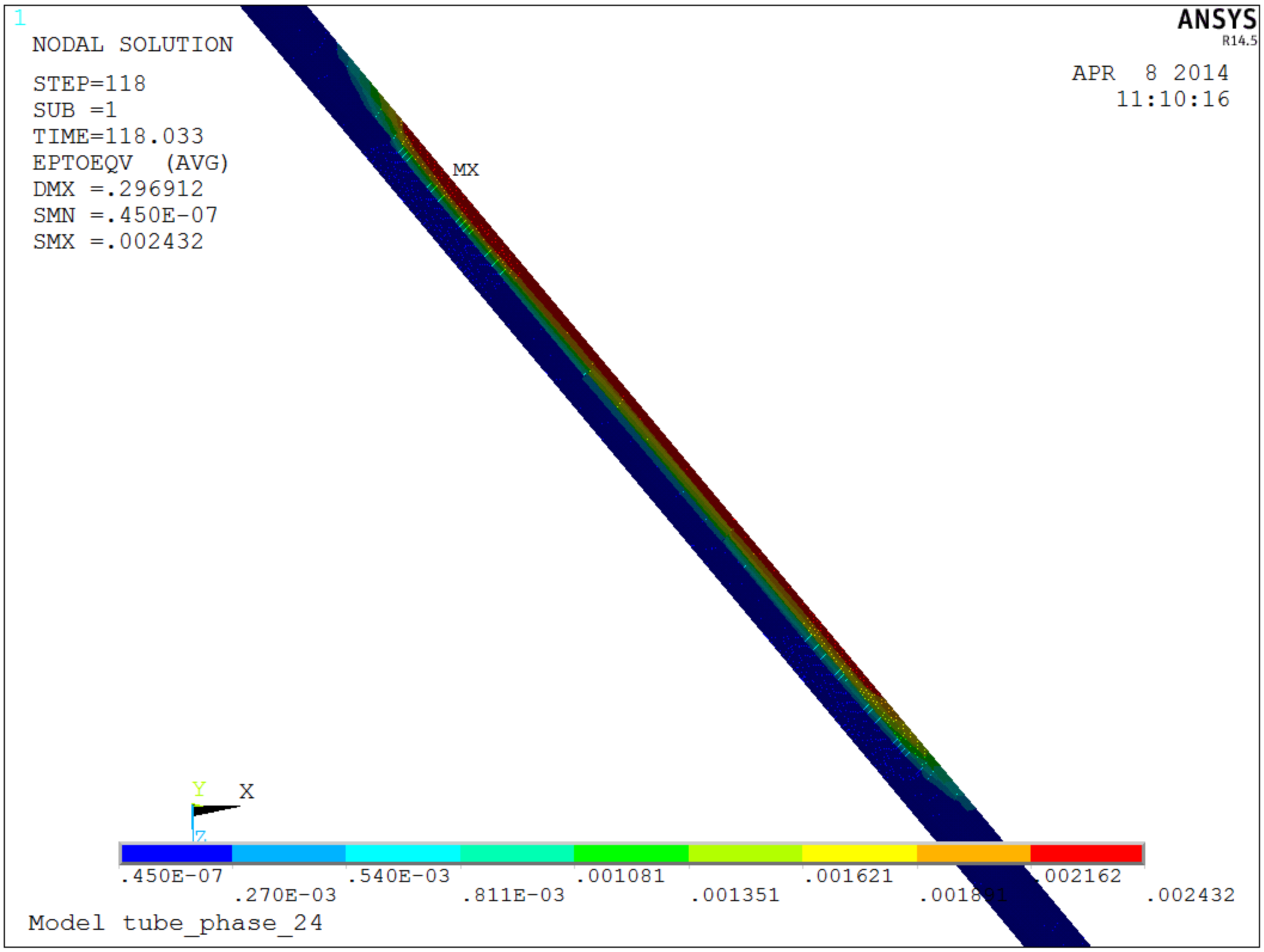

Figure 32: Von Mises Strain on vertical tube exposed to solar flux

(Tube from panel 1 shown here)

3.5.6 Creep Analysis

During normal operation, the crown of the receiver tubes experiences temperatures sufficiently high to be within the material creep regime. Due the cyclical nature of the receiver, fatigue life is also of great concern. The receiver must be designed in such a fashion as to survive the creep and fatigue damage for its design life.

An additional challenge with the receiver tube design and analysis has been the lack of detailed material data required to solve creep-fatigue problems. Very limited data is available for Haynes 230 alloy on creep-fatigue interaction, traditionally used to design pressure parts using ASME Section III, Division 1, Subsection NH methods.

After consultation with experts in the field, Foster Wheeler employed an alternate method, which is a simplification of the method described in Reference 11. This evaluation method may be summarized as follows:

1. Define temperature dependent "pseudo" yield stress.
    a. Pseudo yield stress is the lesser of tabulated yield stress and stress to cause rupture, due to creep, in the time of interest.
2. Use "pseudo" yield stress instead of actual yield stress for finite element analysis.
3. Use elastic-perfectly plastic material model in finite element analysis.
4. Perform cyclic elastic-plastic analysis to demonstrate shakedown.
    a. Shakedown refers to the achievement of cyclic elastic behavior throughout the part based on the pseudo yield stress.

If shakedown is achieved in FEA using pseudo yield stress and elastic-perfectly plastic material model, it can be concluded that the real cyclic rupture time is greater than the selected time. Application of these methods, for the single receiver tube model, resulted in the conclusion that the receiver tubes will meet the design life criteria.

3.5.7 Calculation of Pseudo Yield Stress

Stress to rupture was calculated using the Modified Power Law method in Reference 12. The calculated stress value was multiplied by 0.67, where 0.67 is the safety factor used by ASME.

For temperatures of 1,100 F and below, the yield stress for Haynes 230, as per ASME Section 2, is lower than the stress to rupture. The resultant pseudo yield stress is tabulated in Table15 below.

It is assumed that the solar receiver will be in operation for 12 hours a day. Consequently, 30 years of operation results in approximately 132,000 operating hours.

Temperature (F)	Design Life		
	44,000 Hrs. (10 yrs.)	88,000 hrs. (20 yrs.)	132,000 hrs. (30 yrs.)
100	31.30	31.30	31.30
500	31.30	31.30	31.30
1100	31.30	31.30	31.30
1125	29.66	28.17	27.33
1150	24.28	22.71	21.84
1175	19.84	18.27	17.40
1200	16.52	15.00	14.18
1225	14.25	12.82	12.06
1250	12.77	11.45	10.74
1275	11.78	10.56	9.91
1300	11.01	9.90	9.30
1325	10.31	9.31	8.77
1350	9.62	8.72	8.23

Table 15: Pseudo Yield Strength of Haynes 230 (ksi)

Pseudo yield stress at 132,000 hours used for cyclical analysis in following section. Pseudo yield stress at 44,000 hrs. and 88,000 hrs were calculated but not used.

3.5.8 Cyclical Analysis

A load cycle was constructed of two simple steps.

1. Operating Load: Deadweight of metal and salt, internal pressure and thermal load
2. Shut Down Load: Dead weight of metal only.

Considering one start up and one shut down per day, a 30 year design life would mean 10,950 full cycles in total. This does not account for partial cycles encountered due to cloud cover. A conservative assumption of 3 full cycles per day to account for cloud cover, and any other transient situation, will result in approximately 33,000 cycles during a 30 year design life.

Figure 33 below shows plots of the maximum plastic strain versus the number of load cycles. Strain values associated with only the operating load are plotted for clarity. It can be seen that in all the cases, plastic strain increases for the initial few cycles. However, after a relatively small number of cycles, no increase in plastic strain is seen between two cycles (reach shakedown). Shakedown is reached in all cases in less than 60 cycles.

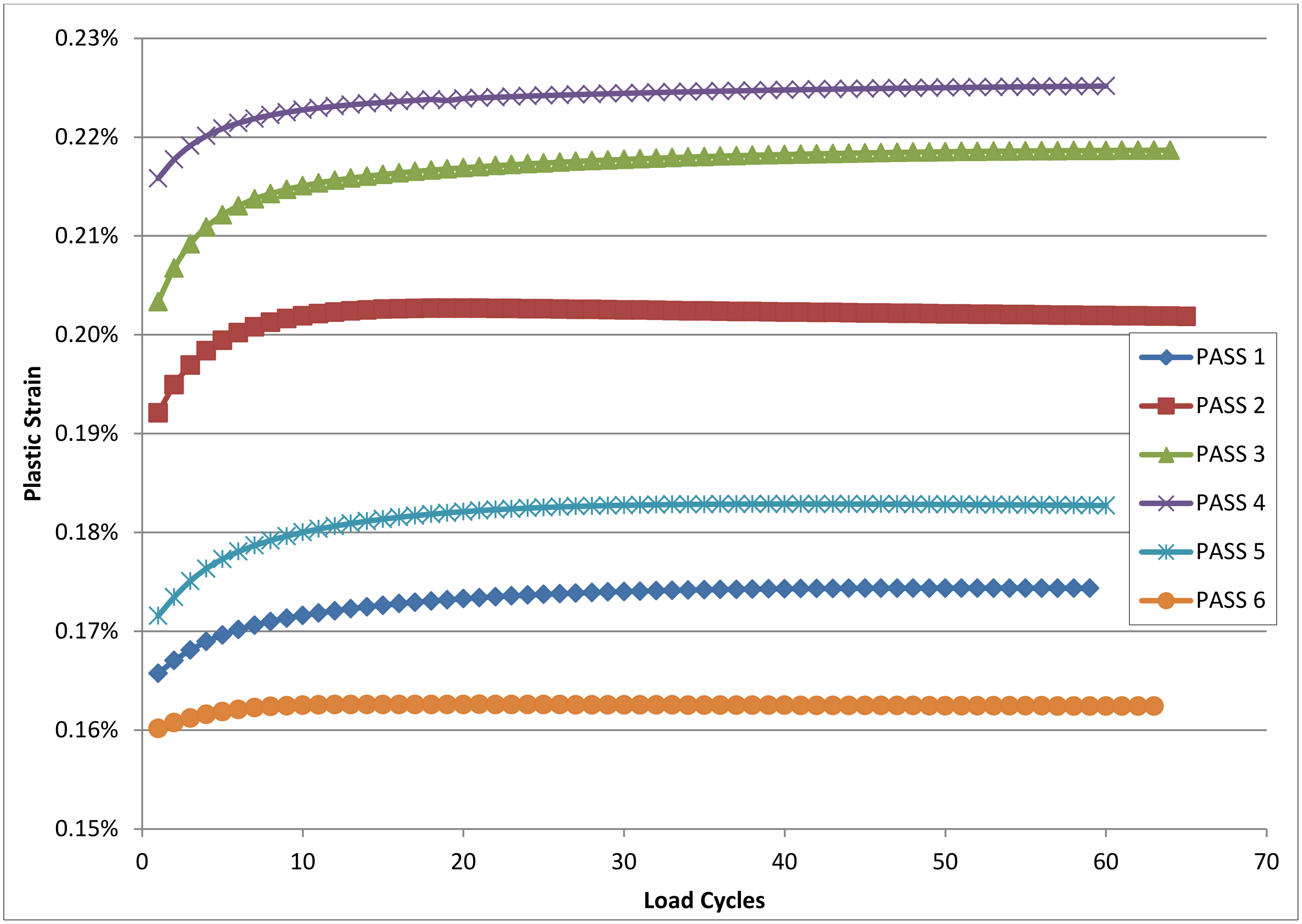

Figure 33: Plastic Strain vs Load Cycles

3.5.9 Fatigue Analysis

Equivalent strain ranges were calculated as per ASME Sec III, Division 1, Subsection NH – Non Mandatory Appendix T – Paragraph T-1414: Equation for Equivalent Strain Range, which is given below.

$$\Delta\epsilon_{\mathrm{equiv}.i} = \frac{\sqrt{2}}{2(1+\nu^*)}\left[\begin{array}{l}(\Delta\epsilon_{xi}-\Delta\epsilon_{yi})^2+(\Delta\epsilon_{yi}-\Delta\epsilon_{zi})^2 \\ +(\Delta\epsilon_{zi}-\Delta\epsilon_{xi})^2 \\ +\frac{3}{2}(\Delta\gamma_{xyi}^2+\Delta\gamma_{yzi}^2+\Delta\gamma_{zxi}^2)\end{array}\right]^{1/2}$$

$$\Delta\epsilon_{xi} = \epsilon_{xi} - \epsilon_{xo}$$
$$\Delta\epsilon_{yi} = \epsilon_{yi} - \epsilon_{yo}$$
etc;

Fatigue life of the receiver tubes was calculated based on the fatigue curve for Haynes 230 given in Figure 34 below.

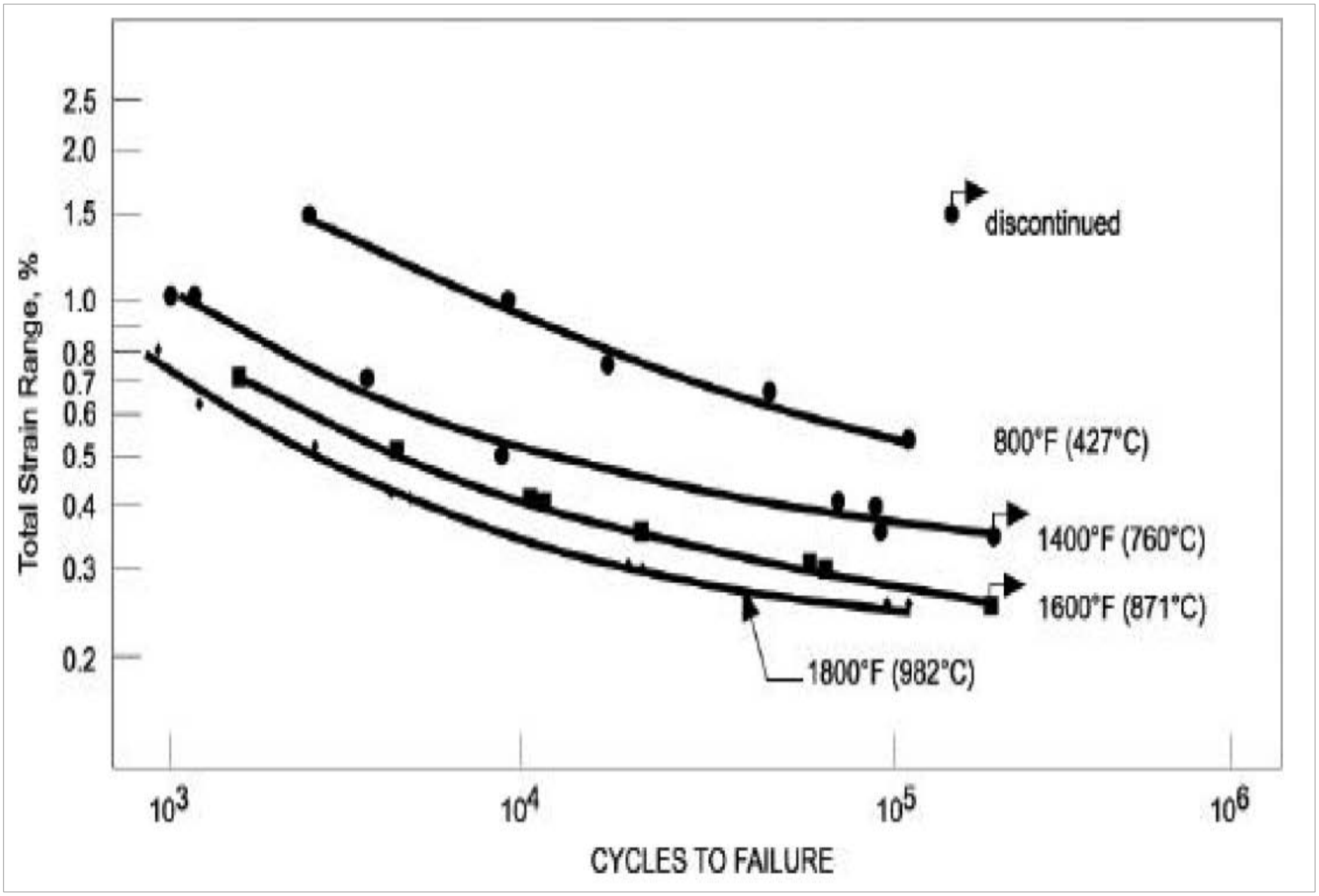

Figure 34: Haynes 230 Fatigue Curve

For each of the receiver panels, two points were selected to evaluate the fatigue life. The first point was selected as the location of highest strain. This point also coincided with peak flux point

on the tube. The second point was the location of highest temperature. For up-flow panels, the second point with highest temperature was the same as first point with highest strain. For the down-flow panels, there were generally two separate points used in the evaluation.
As per the ASME Boiler and Pressure Vessel Code, a factor of two was applied on calculated strain range. For each given temperature and strain range, the fatigue life was estimated, using some interpolation and some extrapolation, from the Haynes 230 fatigue curve given in Figure 34. Results of fatigue life are given the Table 16 below. With the limited material data available, the results presented are considered to be a good approximation. The panels in pass 2 and pass 3 have the shortest life with approximately 30,000 cycles.

<table>
<tr><th colspan="2">DESIGN POINT</th><th rowspan="2">PANEL</th><th colspan="4">Results</th></tr>
<tr><th>DAY</th><th>TIME</th><th></th><th>Temp</th><th>2 x Strain Range</th><th>Life (Cycles)</th></tr>
<tr><td rowspan="2">8</td><td rowspan="2">1200</td><td rowspan="2">1W</td><td>Max Strain Point</td><td>1055</td><td>0.52%</td><td>47,000.00</td></tr>
<tr><td>Max Temp Point</td><td>1082</td><td>0.48%</td><td>65,000.00</td></tr>
<tr><td rowspan="2">300</td><td rowspan="2">1030</td><td rowspan="2">3E</td><td>Max Strain Point</td><td rowspan="2">1181</td><td rowspan="2">0.52%</td><td rowspan="2">31,000.00</td></tr>
<tr><td>Max Temp Point</td></tr>
<tr><td rowspan="2">300</td><td rowspan="2">1030</td><td rowspan="2">5E</td><td>Max Strain Point</td><td>1213</td><td>0.51%</td><td>30,000.00</td></tr>
<tr><td>Max Temp Point</td><td>1251</td><td>0.48%</td><td>35,000.00</td></tr>
<tr><td rowspan="2">81</td><td rowspan="2">1000</td><td rowspan="2">7E</td><td>Max Strain Point</td><td rowspan="2">1244</td><td rowspan="2">0.46%</td><td rowspan="2">42,000.00</td></tr>
<tr><td>Max Temp Point</td></tr>
<tr><td rowspan="2">154</td><td rowspan="2">1000</td><td rowspan="2">9E</td><td>Max Strain Point</td><td>1252</td><td>0.42%</td><td>80,000.00</td></tr>
<tr><td>Max Temp Point</td><td>1282</td><td>0.38%</td><td>160,000.00</td></tr>
<tr><td rowspan="2">154</td><td rowspan="2">1000</td><td rowspan="2">11E</td><td>Max Strain Point</td><td rowspan="2">1345</td><td rowspan="2">0.35%</td><td rowspan="2">260,000.00</td></tr>
<tr><td>Max Temp Point</td></tr>
</table>

Table 16: Fatigue Life of Solar Receiver Tubes

3.5.10 HEADER STUB THERMAL TRANSIENT ANALYSIS

The connection of the Haynes 230 alloy tube to the panel header was analyzed, and was designed to reduce stress due to transient thermal conditions. Two conditions lead to high stress –

1) Rapid thermal transient
2) Dissimilar material properties of header and tube material.

Stepped change in geometry (wall thickness) and material properties were introduced to lower the stress.

3.5.10.1 Rapid Thermal Transient – Header Stub

The tube to header joints were designed to survive the following conditions:

Material temperature at start of transient, C	*Between 309 and 600 (or max operating temperature)*
Material temperature at end of transient, C	*Between 309 and 600 (or max operating temperature)*
Rate of temperature change, C/sec	*5*
Number of cycle	*30,000*
Design life, years	*30*

Header stubs were added to reduce thermal stress on the connection. The stubs were designed to be fabricated of the same material as the header. In order to reduce thermal transient stresses, the thickness of the stub was selected to be approximately the average of the thickness of the tube and the header.

3.5.10.2 Dissimilar Material Properties – Spool Piece

The thermal expansion coefficients of Haynes 230 alloy (tube) and SA 213 TP 347H (Header Stubs for Pass 7 thru 12) vary significantly. The analysis showed that directly welding the tubes to the header stub would generate high stress, even at uniform temperature. In order to resolve this potential for excessive stresses, a spool piece with intermediate thermal expansion material properties was introduced between each tube and header stub. INCONEL 825 was found to be suitable material. To further minimize the stresses due to mismatches in thermal expansion coefficients, associated with material property changes, weld filler materials with intermediate thermal expansion property were selected for use in joining either end of the spool piece.

To keep the design consistent, the spool piece design was used for all the panels. Introducing the spool piece for carbon and alloy steel panels did not adversely affect the design.

Figure 35 below illustrates the detailed arrangement of the tube-to-header connection, and Figure 36 includes the details of the materials selected for each temperature range, across the receiver panels.

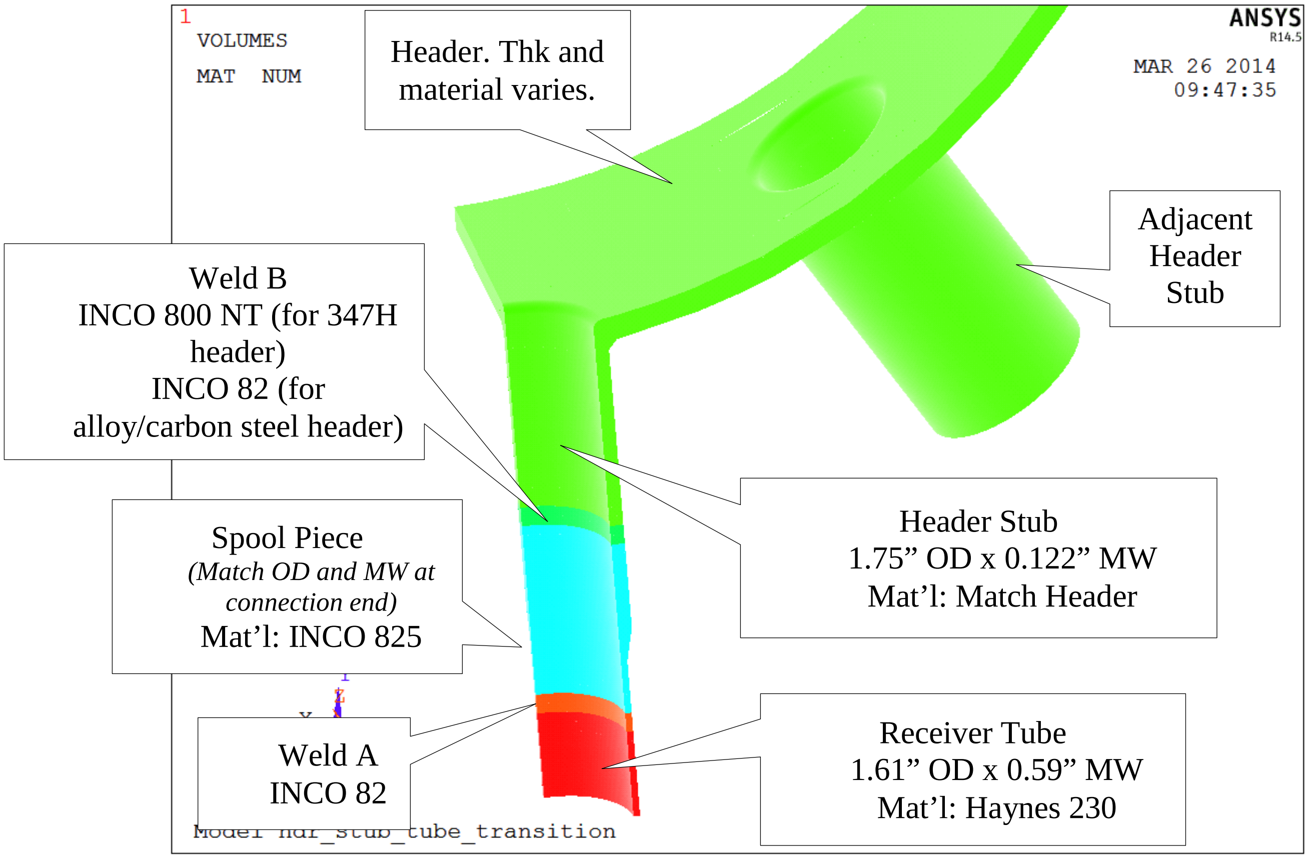

Figure 35: Details of tube-to-header arrangement to reduce stresses

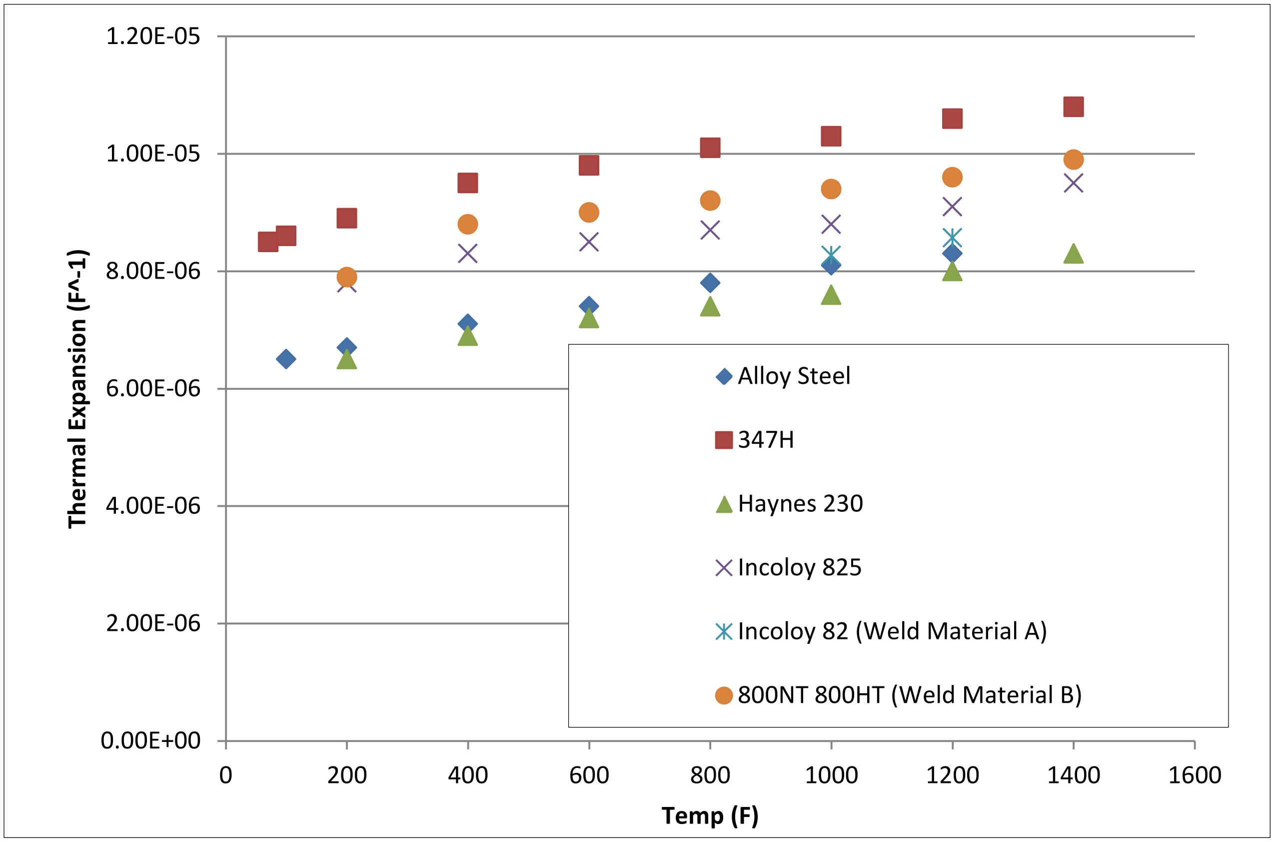

Figure 36: Thermal Expansion for Header to Tube Connection Materials

3.5.10.3 Stress Analysis and Results

Figure 35 above shows the model created for finite element analysis. Taking symmetry into account, a one quarter model of the tube to header connection was created. It includes the receiver tube, spool piece, header stub, header and the joining welds. An adjacent header stub was also modeled to complete the model. Transient thermal and static structural analyses were performed using the ANSYS finite element software.

Transient thermal analysis was performed with an initial condition of uniform temeprature of 588 ^{0}F (309 ^{0}C). The temperature of the ID surface, assumed to be same as fluid temperature, was ramped up to the maximum operating temerature for each panel. The rate of temperature chage was 5 ^{0}C/sec. The temperature profile was captured at the end of the ramp, and a static structural analysis was performed to calculate the resulting thermal stress.

Three separate tube-to-header connections were selected and analyzed to capture all of the variations of thickness, material and temperature.

1. Case A - for header material: Carbon/Alloy Steel
   a. Max operating temp: 797 ^{0}F
   b. Max header thickness: 0.375”
2. Case B – for header material: 347H with thickest header
3. Case C – for header material: 347H with highest operating temperature.

Figure 37 shows the temperature profile at the end time for header-tube connection in case C.

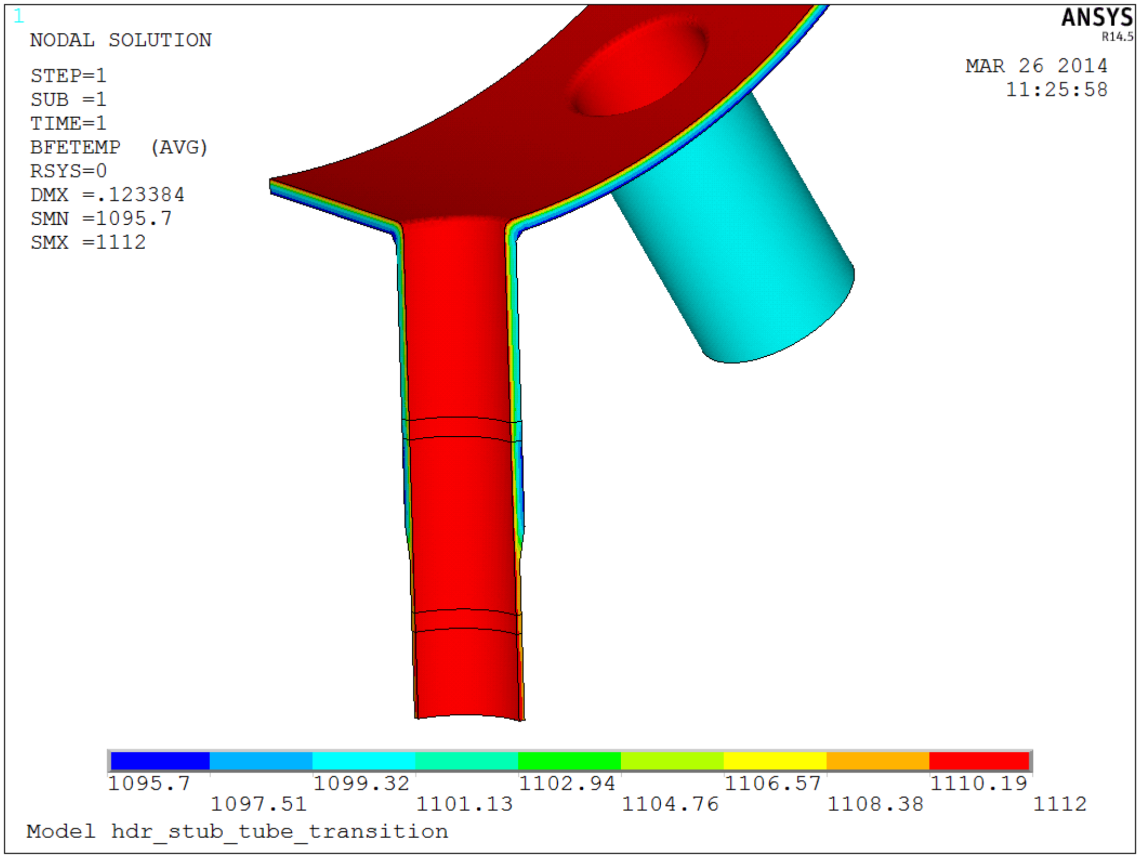

Figure 37: Temperature Plot for Header to Tube Connection (Case C shown here)

Figure 38 below gives the stress distibution of the tube-to-header for case B. Very local high stress are seen at both ends of the spool welds. The abrupt change in geometry and material properties is responsible for these high stress. Additionally, these stress are extremely localized. In reality, the weld metal diffusion inherent in the welding process will crate a region of intermediate material properties, which will provide for a smoother transition. Any of the small local regions of high stress remaining could experince local yielding.

Away from this local region near weld, stress in the entire model are much lower.

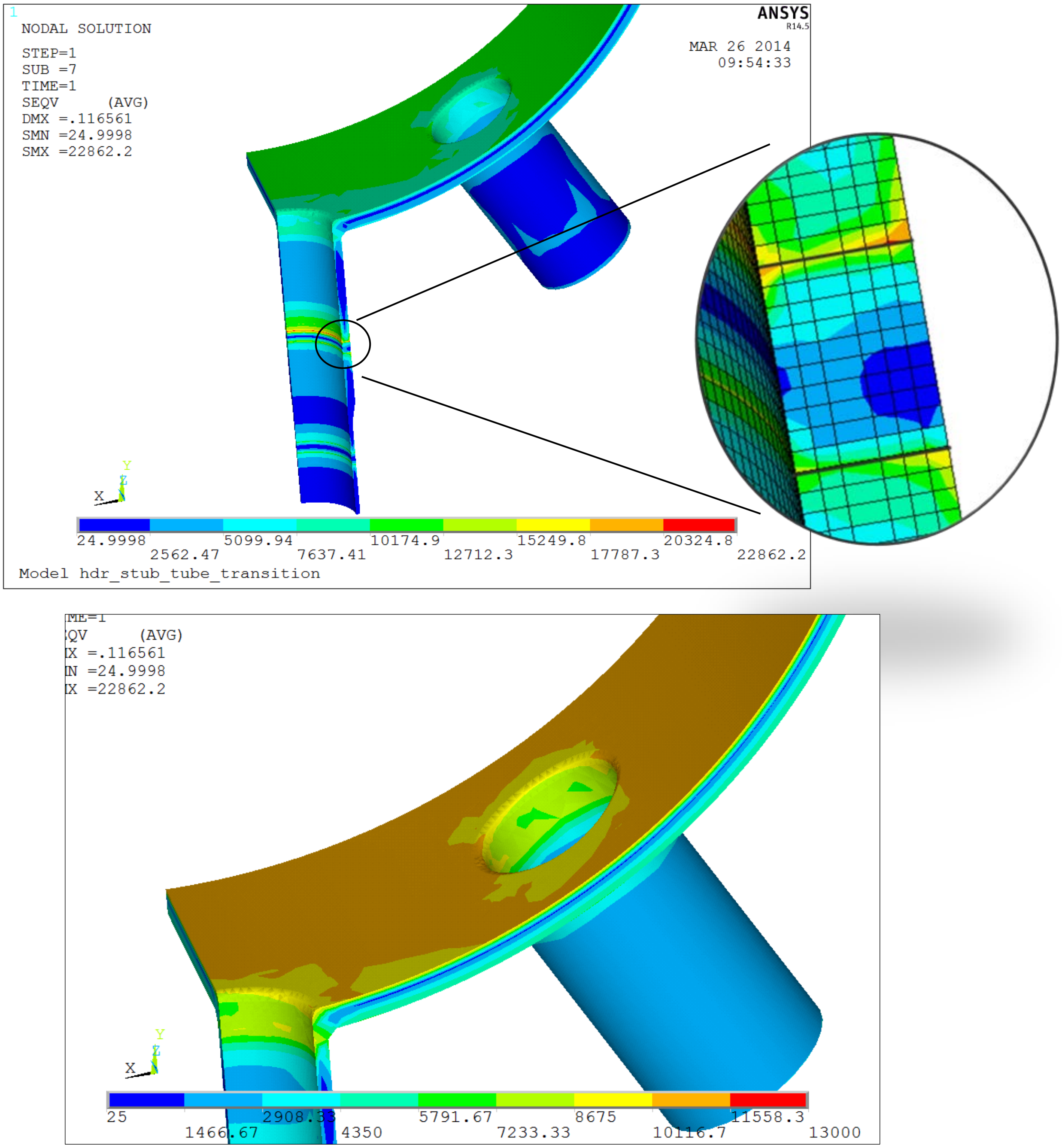

Figure 38: Stress Plot for Header to Tube Connection (Case B shown here)

INPUT						OUTPUT			
CASE	Panel	Header & Stub Material	Header Thk (in)	Time for Temp Change (s)	Max Temp at ID of the HDR, Tube and Stub (^{0}F)	Min Temp at OD of the HDR (^{0}F)	Delta Temp thru thickness (^{0}F)	Max Stress Away from stub / spool / tube weld (ksi)	ASME Code Range Stress for HDR Stub (ksi)
A	1 thru 5/6 (Inlet)	Alloy Steel	0.375	23	797 (425 ^{0}C)	753	44.4	11.6	24.5 @ Design Temp of 910 ^{0}F
B	5/6 (outlet) thru 10	347H	0.25	50	1,042 (561 ^{0}C)	1,000	41.9	13.0	27.2 @ Design Temp of 1182 ^{0}F
C	11 and 12	347H	0.156	58	1,112 (600 ^{0}C)	1,096	16.3	11.1	

Table 17: Stress Analysis Summary for Tube-To-Header Connection

Table 17 above summarizes the results of thermal transient and static stress analyses for the tube-to-header connections.

Ramping the temperature down 5 °C/sec yields similar results. However, with lower temperature at the end point, the allowable stresses are higher, while the predicted actual stress are lower. As a result, only the cases with temperature ramping up are reported.

3.5.11 PANEL ANALYSIS

The solar heat flux incident on the boiler varies both vertically and horizontally. Thus, each panel, consisting of 56 tubes, will experience variations of heat flux across both its width and height. It became necessary to determine acceptable limits of heat flux variation across a given panel. Any potential flow imbalance may also contribute to a temperature difference across the panel.

This problem was solved using CAESAR piping analysis program. A simplified, conservative, approach was taken in setting up the problem, as explained below.

- Model one typical full panel - with upper header, lower header and the 6 levels of stiffeners. Considering symmetry, only half the panel with 28 tubes was modeled.
- Uniform temperature was applied to the whole model – 1300 F
- Temperature of one tube in the center – 1400 F
- Boundary conditions (see Figure 39 for details)
  - Headers fixed for rotational degree of freedom in Z direction (axial direction of headers)
  - Zero point, in Z direction, at mid-point of headers.
  - Translation in X direction fixed for both headers and all buckstays.

The model was analyzed with just temperature load, testing the flexibility of the tube. Summary of results given below:

Uniform Temperature of panel	**1300 ^{0}F**
Temperature of one tube	**1400 ^{0}F**
Internal Pressure (psi)	**300**
Cold Allowable (Sa) psi	**30,000**
Hot Allowable (Sh) psi	**6,700**
Max Stress from analysis (psi)	**5,612**
(Caesar File Name: Abengoa 2 Panel)	**OK**

One tube running 100 ^{0}F hotter than the rest of the panel is an extreme and perhaps an unrealistic scenario. However, the goal of this analysis was to show that if the one tube running 100 °F hotter is flexible enough, and thus does not result in an overstressed condition, then any variation in heat flux or flow imbalance causing a 100 ^{0}F temperature difference across the panel will not overstress the panel.

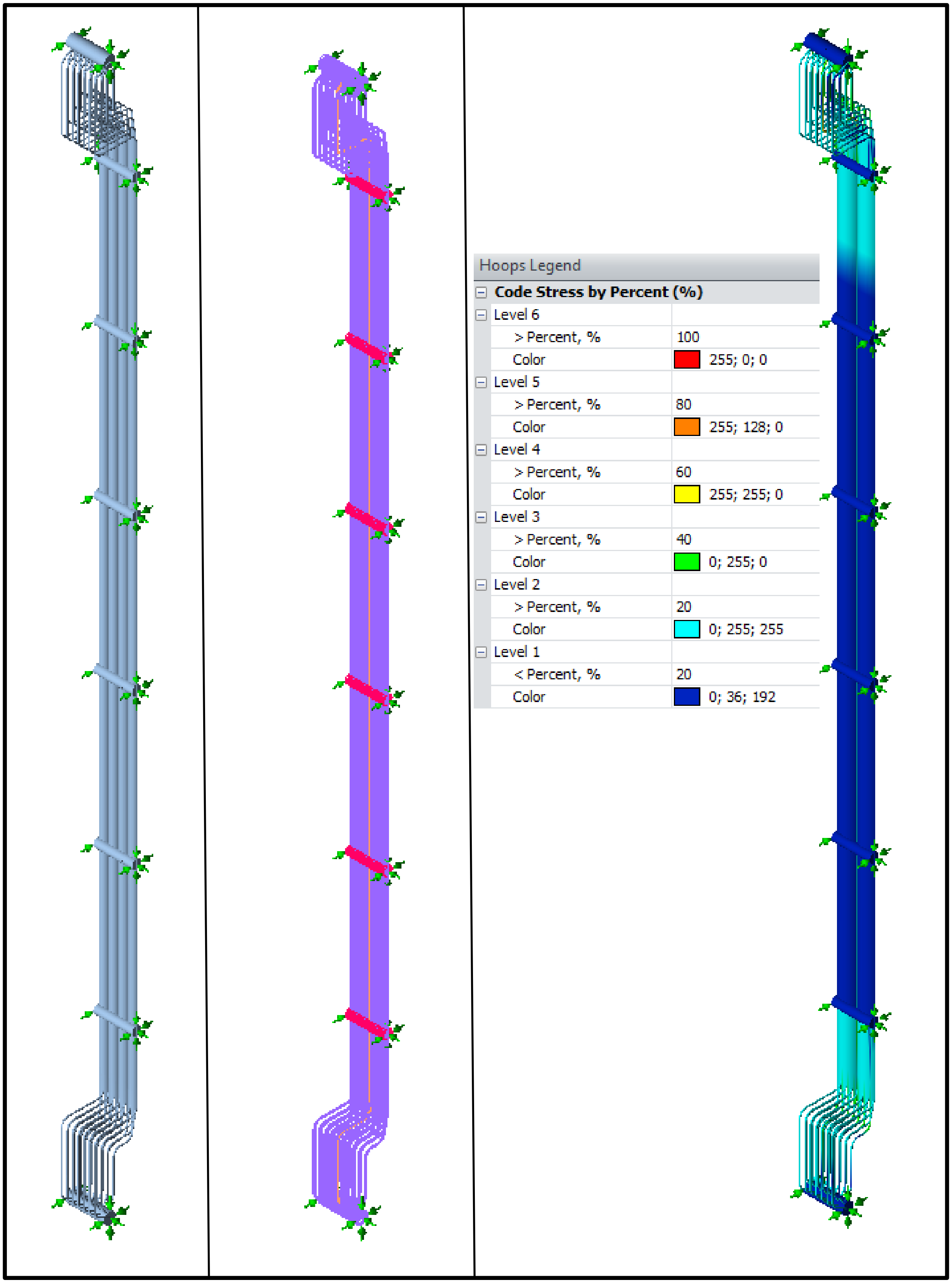

Figure 39: Complete Panel Flexibility Analysis

3.5.12 General Arrangement Drawings. Figures 40 to 45 include side elevation, sectional, and isometric views of the receiver system. Figure 46 illustrates the header oven box. Figure 47 shows the receiver panel strongback location.

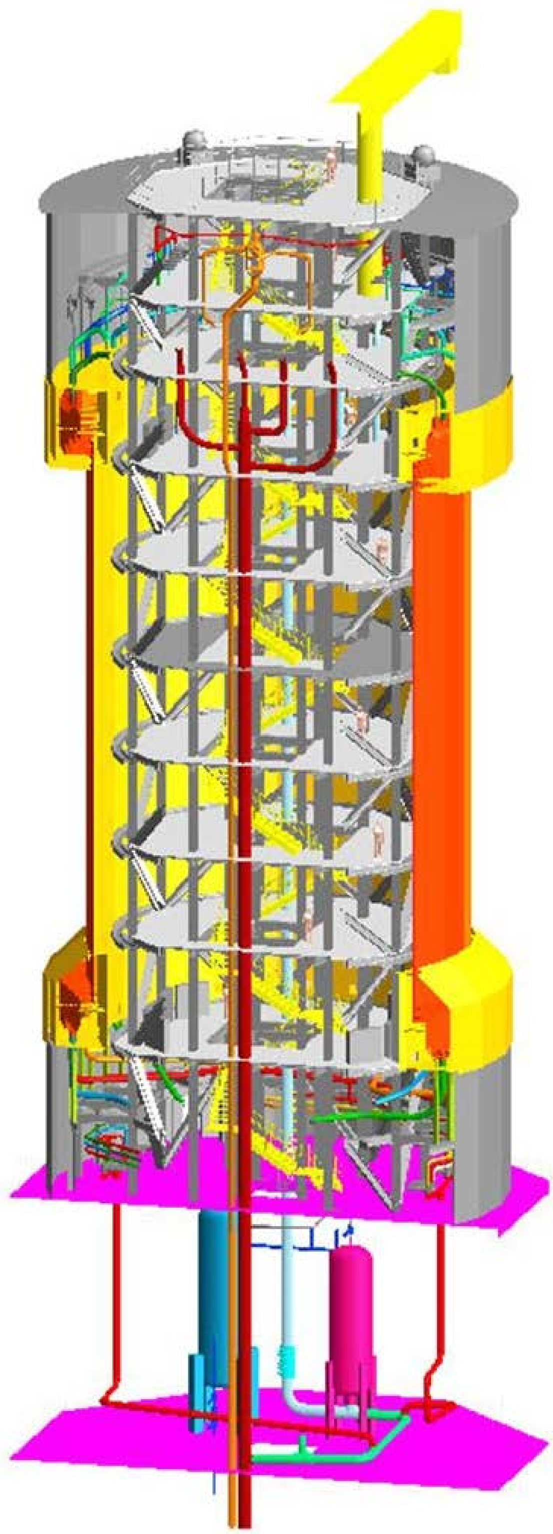

Figure 40 Isometric Cut-Away View of Receiver

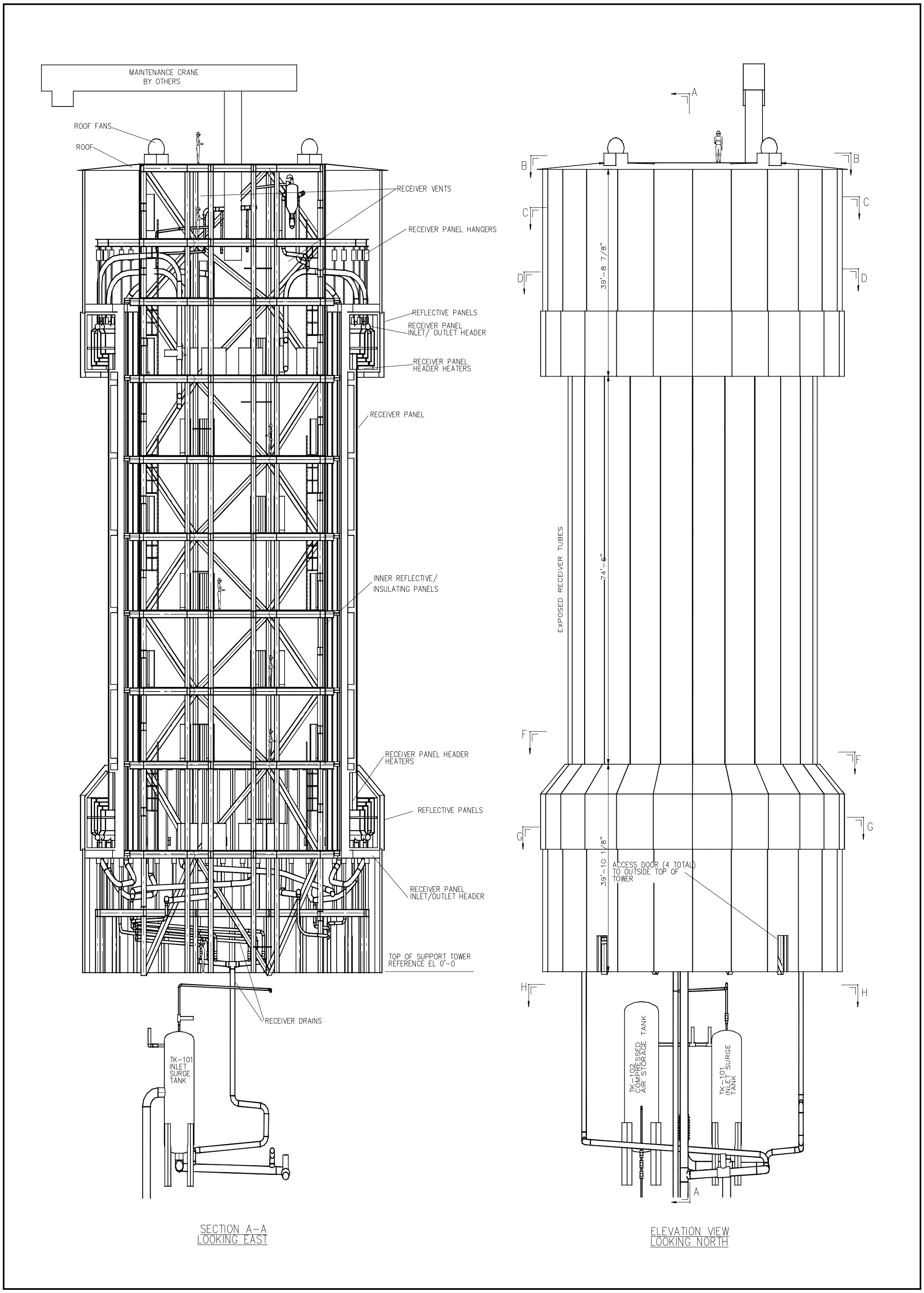

Figure 41. Receiver Side Elevation and Section A-A

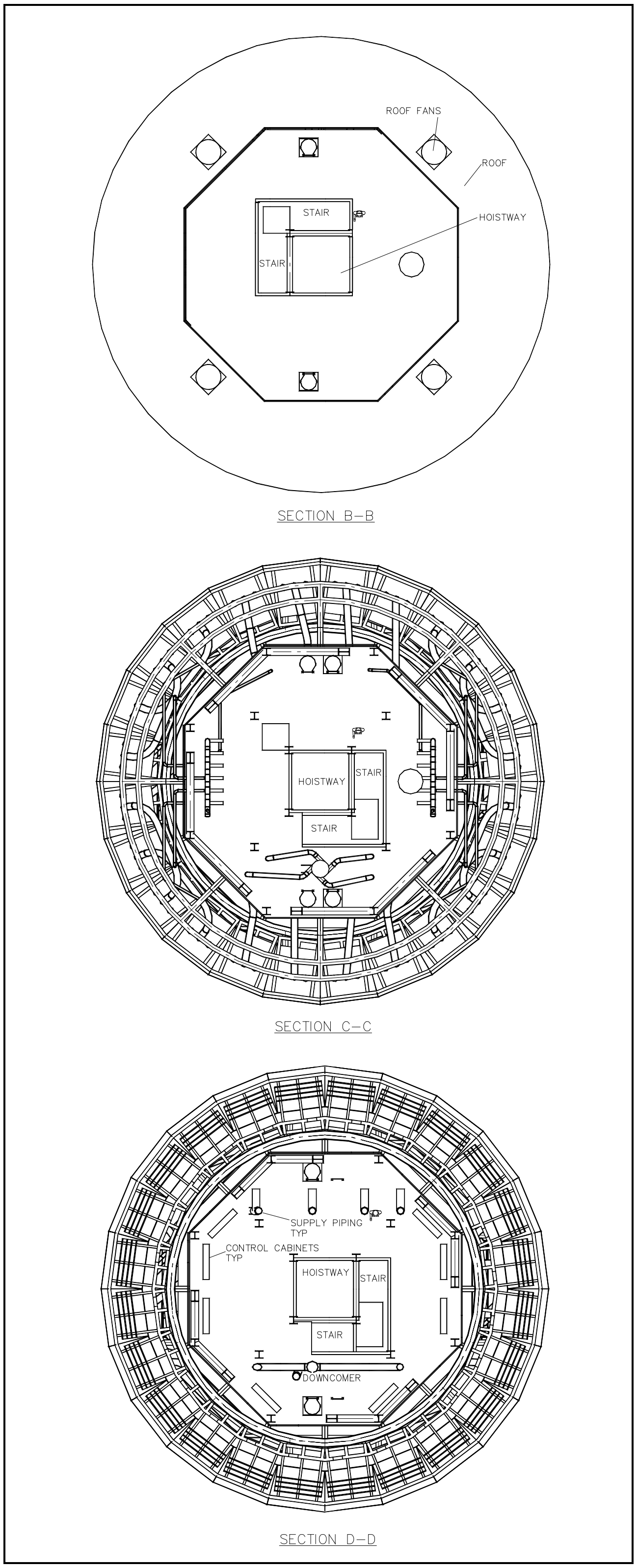

Figure 42. Receiver Section Views B-B, C-C, D-D

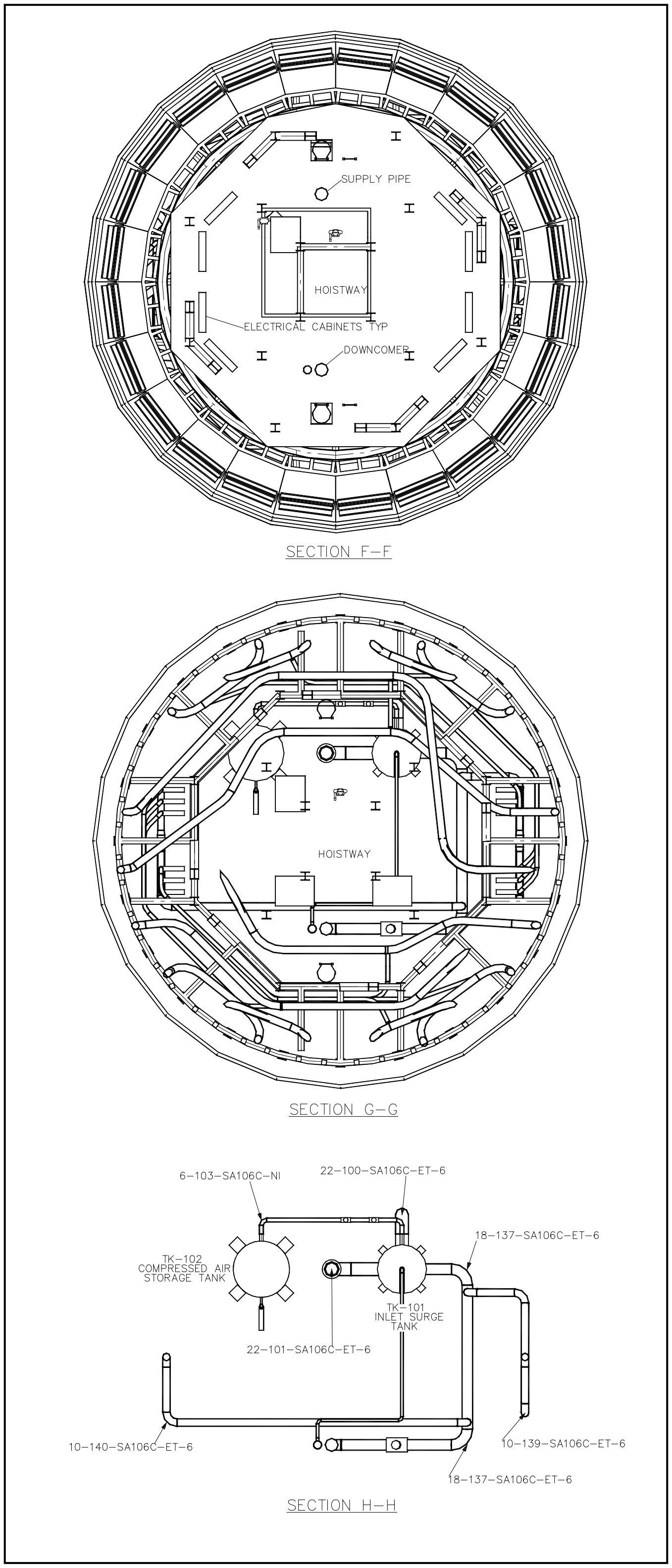

Figure 43. Receiver Section Views F-F, G-G, H-H

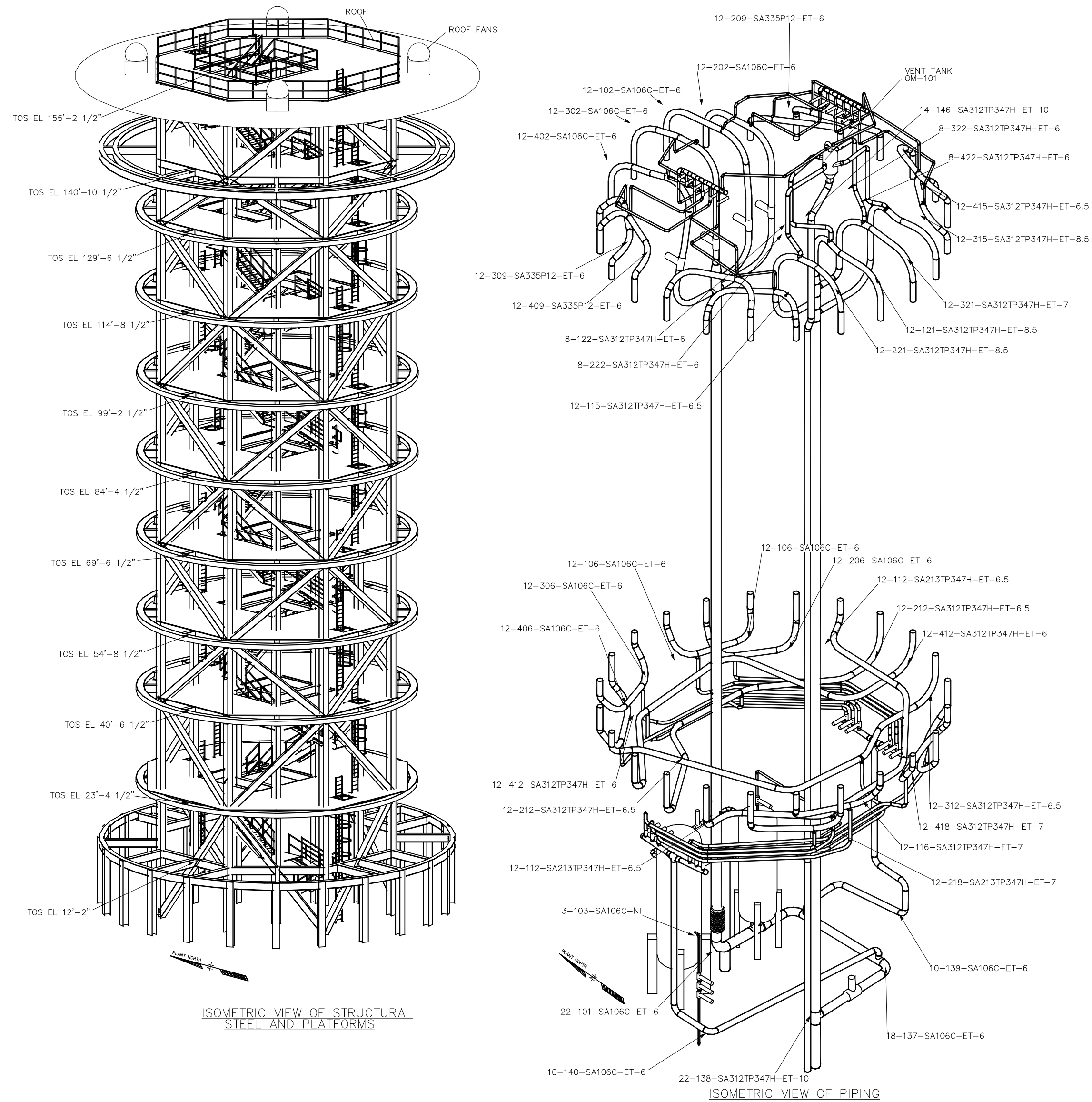

Figure 44. Receiver Structural Steel, Platforms, and Piping

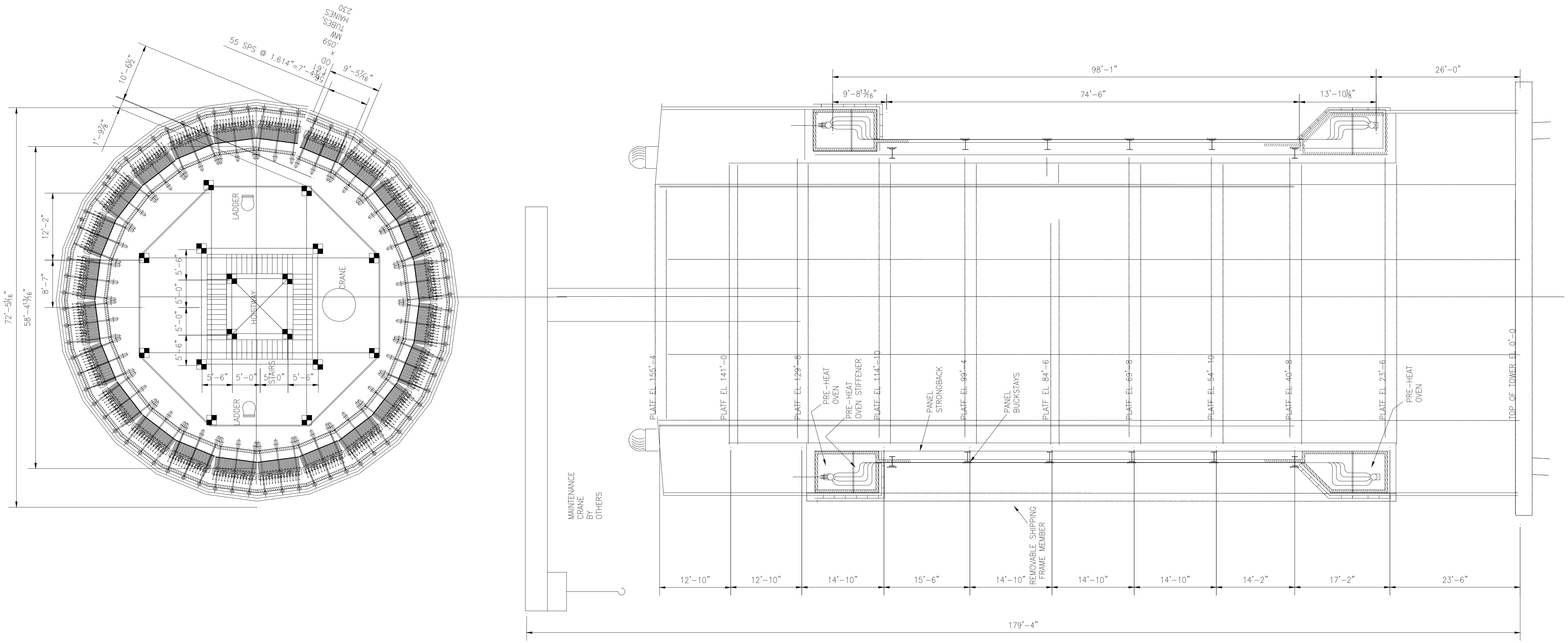

Figure 45. Receiver General Arrangement

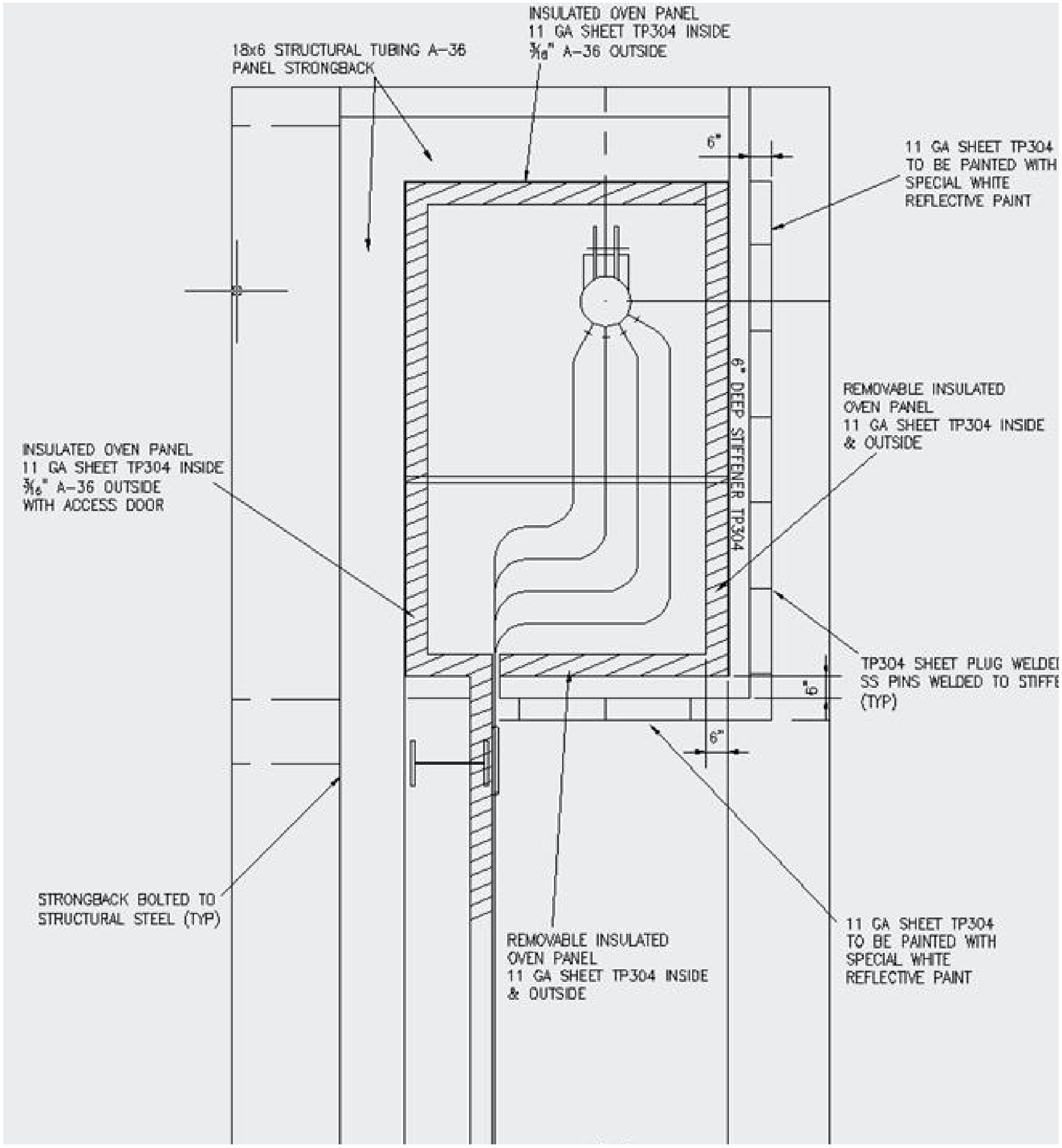

Figure 46. Header Oven Box

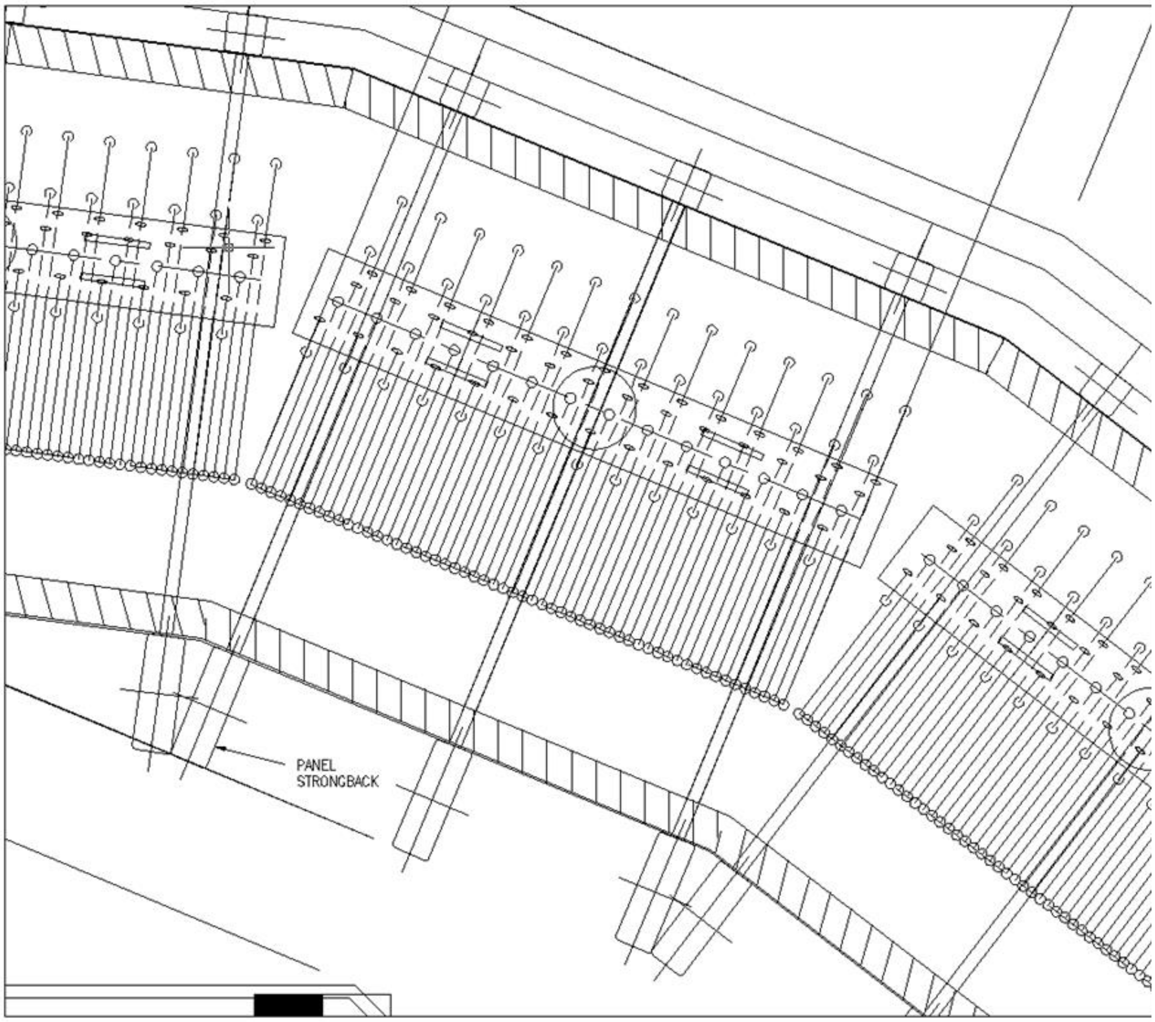

Figure 47. Receiver Panel Strongback

3.6 Electrical and Instrumentation.

3.6.1 Receiver Oven Enclosure Heaters. Electrical radiant heaters will heat the upper and lower receiver oven enclosures (ROE) from 38 to 316 °C (100 to 600 ^{o}F) in less than one (1) hour. All ROE's will be maintained at 38 °C (100 °F) during over-night shutdown; by keeping temperatures above the dew point moisture formation is prevented. Four (4) control panels will be provided for the lower ROE's and another four (4) for the upper ROE's. The following applies to the lower ROE heaters and is the same for the upper ROE heaters:

Each of the twenty four (24) solar panel sections will be heated using ten (10) Inconel sheath radiant heaters rated 5500W, 480V 3-phase. A NEMA 4 control panel will be provided as the terminal point interface and to power / control six (6) solar panel sections. A total of four (4) control panels will be provided for the upper receiver enclosure. Each control panel will have an integral 400A, 480V 3-phase disconnect switch and six (6) silicon control rectifier branch circuits, each capable of handling the load of 10 - 5500W heaters. A digital indicating temperature controller with load management module will be provided to control all four circuits, whereby one temperature sensor will control every four solar panels. In order to minimize wiring from the control panel to the heaters, the power cables from the ten (10) 3-phase heaters will be wired to a local power junction box. One (1) 3-phase feeder will be wired to the junction box incoming terminals and jumpered to the fused branch circuits.

3.6.2 Electric Trace Heat. Transfer pipes, vents, drains and associated valves will be electrically heat traced using 480V 1-phase Inconel sheath mineral insulation heater cables capable of heating the pipes from 38 to 316 °C (100 to 600 ^{o}F) in four (4) hours. All lines will be maintained at 38 °C (100 ^{o}F) during over-night shutdown. By keeping temperatures above the dew point moisture formation is prevented. Each heater cable will be factory terminated with a 4 foot .cold section. Resistance temperature detector line sensors will be provided as required. A NEMA 4 control panel will be provided as the terminal point interface and to power / control the heater cables. Each control panel will have an integral 600A at 480V 3-phase disconnect switch and ground fault interrupter branch circuits. A computer touch screen operator interface will be provided along with RS 485 Modbus communications. A total of three (3) control panels will be provided.

3.6.3 Lighting. The solar receiver will be illuminated using enclosed and gasketed luminaires with 120V high efficiency high pressure sodium lamps providing an average illumination level of 10 foot candles. Each platform will be provided with local on-off switches in order to minimize energy consumption. In addition 120V convenience receptacles will also be provided at each platform for portable task lighting, etc. A 15KVA dry type encapsulated transformer rated 480V-208V/120V will be provided along with a 3-phase distribution panel consisting of a 50A 3-pole main circuit breaker, 18 – 1-pole circuit breakers and 6 - 1-pole GFI circuit breakers.

3.6.4 Power Distribution. A centrally located NEMA 4 Power Panel will be provided to serve as the terminal point interface; rated 400A, 480V 3-phase consisting of 24-15A 3-pole circuit breakers, 2-60A 3-pole circuit breakers and 2-40A 3-pole circuit breakers for powering motor operated valves (with integral starter), power receptacles, lighting transformer, and crane (supplied by others). Two (2) power receptacles rated 480V 3-phase will be centrally located in the solar structure for welding, etc.

3.6.5 Instrumentation. Receiver performance will be controlled and monitored with the following:

- **Flow Meters.** Molten salt flow rate in each of the East and West Passes will be measured using non-intrusive ultrasonic type flow meters. The sensor assembly will be made of dual beam ultrasonic sensors mounted on a 316 Stainless Steel pipe spool piece with ANSI 300 #RF flanged end connections. The signal converter (transmitter) will be remotely mounted from the sensor. The transmitter will have a 4-20 mA signal output and will be wired from the Miscellaneous Power Distribution Panel for 120 VAC power supply. Signal wiring from the transmitter will be terminated at the Analog Junction Box for interface to the Control System.
- **Pressure Transducers.** Process pressure measurement of molten salt will be done using electronic transmitters with remote diaphragms filled with high temperature fill fluid. The transmitters will be 2-wire type with 4-20 mA output with HART protocol. Signal wiring from the transmitter will be terminated at the Analog Junction Box for interface to the Control System.
- **Temperature Indicators.** Process temperature measurement of molten salt will be done using Type K Thermocouple element fitted inside 304H stainless steel protection thermowell. Thermocouple extension wiring from the element will be terminated at the Thermocouple Junction Box for interface to the Control System. Each solar receiver temperature will be measured using an Infrared Camera that will be focused at pre-selected section of the panel. The camera will measure the temperature gradient of the field of view and transmit the image and measured temperature data to the Control System. The camera output signal will be sent to the control system via ETHERNET IP protocol. Ethernet wiring from the camera will be terminated at the Analog Junction Box for interface to the Control System. Power to camera will be supplied over the Ethernet. Each camera will be provided with an IP66 rated enclosure. The camera will be installed locally near the base of the solar receiver.
- **Control Valves.** Pneumatic actuated isolation valves with 120 VAC, 3-way solenoids will be provided for the Compressed Air System. The solenoid valve power and position switches wiring will be terminated to the Digital Control Junction Box for interface to the Controls System. Electric motor operated control and isolation valves will be provided each with integral starter powered from the 480 VAC, 3-phase Power Panel. The control signal wiring, valve position switches and status wiring will be terminated to the Digital Control Junction Box for interface to the Control System.

3.6.6 Instrumentation Wiring. All instruments are wired to strategically located junction boxes which also serve as the interface terminal point. Thermocouples are wired to junction boxes with type K terminal blocks, transmitters are wired to analog junction boxes and motor operated valves are wired to control junction boxes . All junction boxes are NEMA 4.

3.6.7 Lightning Protection and Obstruction Lighting. Lightning protection air terminals and aviation obstruction lighting is provided by the crane supplier. Power for the crane motor if required, and obstruction lighting has not been considered.. Two lightning down-conductors are provided from the crane area to the bottom of the receiver.

3.6.8 Miscellaneous. All cables shall be routed in rigid steel hot dipped galvanized conduits. All power cables shall be rated 600V type XHHW 90^{o}C stranded copper conductor. All lighting cables shall be rated 600V type XHHW 90^{o}C solid copper conductors. All thermocouple extension wire shall be rated 300V type K (chromel-alumel). All analog cable shall be rated 300V single twisted pair shielded. All control cable shall be rated 600V multi-conductor unshielded. Lightning down-conductors shall be bare copper stranded conductors.

3.7 Operational Concepts

3.7.1 Operating States

The operation of the receiver system can be divided into five states that are described in detail in Reference 4; since the five states are applicable to the proposed CSP design, they have been extracted from the referenced document as follows:

- Long Term Hold/Overnight Hold. The heliostats are in the stow position, the receiver is drained, and the electric heat trace circuits are inactive.

- Standby. The heliostats are focused on the standby aim points, and the receiver is in operation. Salt is flowing in the riser, the receiver bypass line, and the downcomer.

- Preheat. The receiver electric heat trace circuits are active, the preheat heliostats are focused on the receiver, and the receiver pump is in operation. Salt is flowing in the riser, the receiver bypass line, and the downcomer.

- Normal Operation. All of the available heliostats are focused on the receiver, the receiver flow rate is controlled to achieve an outlet temperature of 600 °C (1112 °F), and the electric heat trace circuits are de-energized at normal operation temperature set points.

- Cloud Standby. All of the available heliostats are focused on the receiver, the receiver flow rate is controlled to achieve an outlet temperature of 510 °C (950 °F) under theoretical clear sky conditions, and the electric heat trace circuits are de-energized at the normal operation temperature set points.

3.7.2 Transition Between States

There are nine transitions between operating states as follows:

- Long Term Hold to Standby. The operator moves the heliostats from the stow position to tracking the standby aim points. The temperatures of the riser, the receiver bypass line, and the downcomer are raised to 260 °C (500°F). The receiver pump is started, and a flow is established in the riser, the bypass line, and the downcomer.

- Standby to Preheat. The temperatures of the receiver ovens and interpanel piping are raised to 315 °C (599°F). The preheat heliostats are moved from the standby aim points to the preheat aim points.

- Preheat to Standby. The preheat heliostats are moved from the preheat aim points to the standby aim points.

- Preheat to Normal Operation. The transition consists of the following steps: (1) the receiver is filled by flooding, (2) flow is established, (3) a flow rate corresponding to clear sky conditions is established, (4) the heliostats are moved from the standby (or Preheat) aim points to the normal aim points, and (5) the flow rate is controlled to achieve a nominal outlet temperature of 600 °C (1112°F).

- Normal Operation to Standby. Automatic temperature control is suspended, and the flow rate is controlled to achieve an outlet temperature of 510 °C (950 °F) under theoretical clear sky conditions.

- Cloud Standby to Normal Operation. Automatic temperature control is resumed, and the flow rate is controlled to achieve a nominal outlet temperature of 600 °C (1112°F).

- Normal Operation to Standby. The heliostats are moved from the normal aim points to the standby aim points, the inlet vessel is vented to atmosphere, and the receiver is drained.

- Standby to Long Term Hold. The heliostats are moved from tracking the standby aim points to the stow position, the receiver pump is stopped, and the electric heat trace circuits are inactive.

3.7.3 Cloud Transients. There are an infinite number of cloud transients possible. However, the most severe condition is the response of the control system to the cloud transient. For example, assume the receiver has a maximum turndown ratio of 6 to 1. For absorbed powers between 100 percent (795 MWt) and 17 percent (133 MWt), the receiver is in outlet temperature control, with a set point of 600^{o}C. If the absorbed power falls below 133 MWt, outlet temperature control is abandoned, and the salt flow rate increases to a value which would provide an outlet temperature of 600^{o}C if the skies were completely clear. The intent is to prevent outlet temperature overshoot should the cloud transient end more quickly than the receiver pumps can respond.

Assume the receiver is operating with an absorbed power of 133 MWt, and is in outlet temperature control. If the temperature control is abandoned, and if the salt flow rate is increased to 90 percent of design, and if the absorbed power remains at 133 MWt, the rate of temperature change in the panel headers near the inlet of the receiver is about 9.3^{o}C/sec. Near the outlet of the receiver, the rate of temperature change is slightly less at 8.4^{o}C/sec. The calculations are based on a 12 in., Sch 40 pipe connecting the panels.

As an alternate case, if the salt flow rate is increased to only 65 percent of design, and if the absorbed power remains at 133 MWt, the rate of temperature change in the panel headers near the inlet of the receiver is about 6.3^{o}C/sec. Near the outlet of the receiver, the rate of temperature change is 5.6^{o}C/sec.

As another alternate case, if the salt flow rate is increased to only 33 percent of design, and if the absorbed power remains at 133 MWt, the rate of temperature change in the panel headers near the inlet of the receiver is about 1.8^{o}C/sec. Near the outlet of the receiver, the rate of temperature change is 1.4^{o}C/sec.

Items of note include:

- The receiver control logic is within receiver designer's scope of supply. The extent to which receiver designer believes it is necessary to prevent temperature overshoot will determine the speed of the receiver pumps once outlet temperature control is abandoned.

- The speed with which a cloud transient ends will determine the degree of conservatism in the selection of the receiver pump speed. For Southwest desert sites, there are days in which opaque clouds, with well-defined edges, move across the field. For this type of cloud, selecting a pump speed close to the clear sky pump speed is likely needed. In contrast, for hazy days, in which the clouds are not completely opaque, and have poorly defined edges, a relatively low pump speed can be selected, as the risk of temperature overshoot is low.

- Depending on the time of the day, and the day of the year, clear sky conditions will result in a wide range of possible absorbed powers. As such, there will be 1) an annual histogram of pump speeds needed to respond to clear sky conditions, and 2) an annual histogram of rates of temperature change in the inter-panel piping.

- For the purposes of the Phase II design, the assumption is that the receiver is subjected to two(2) cloud transients each day, and that the rate of temperature change in the inter-panel piping is in the range of 3 to 6^{o}C/sec.
- Temperature change in the range of 8 to 9^{o}C/sec may be problematic, and the control system should limit clear sky flow rates to about 65 percent of the design flow rate to prevent very rapid cooling of the inter-panel piping.

- On those days in which the clear sky flow needs to be 65 to 100 percent of the design flow rate, the control system could 1) accelerate the receiver pumps to 65 percent of the design flow rate, and 2) defocus a portion of the field to limit the incident power at the end of the cloud transient. Once the cloud transient ended, the defocused heliostats could be returned to tracking. The effect on the annual plant output from the limited defocusing should be a very small value.

- For reference, at Solar Two, full clear sky flow rates were established on a routine basis during cloud transients. Rates of temperature change in the inter-panel piping was not a concern. This may have been the case because 1) the receiver only had to last 3 years, or 2) the surface to volume ratio of the inter-panel piping was high, which limited the rates of temperature change in the metal.

4.0 Solar Receiver Cost and Fabrication Plan

4.1 Cost Estimates for Design, Fabrication (Table 18) A budgetary estimate for the cost of the Receiver and Boiler exchangers has been prepared based on the use of standard manufacturing techniques and the worldwide supply of materials and labor. We have allowed or the installation of the Pyromark replacement coating and curing in the fabrication shop.

TABLE 18 Cost Summary

Budgetary Equipment Cost Estimate	
Pressure Parts	
Pressure Part Panels	$ 25,698,624
Boiler Piping	$ 607,475
Miscellaneous Boiler Valves	$ 963,793
Buckstays, Hangers & Expansion Bellows	$ 3,023,605
Surge Tanks	$ 208,189
Pressure Part Panel Insulation	$ 978,274
Total Pressure Parts	$ 31,479,959
Support Structure	
Platforms	$ 973,051
Structural Steel	$ 4,091,374
Maintenance Hoist	$ 33,709
Total Support Structure	$ 5,098,134
Remaining Equipment	
Miscellaneous Piping	$ 836,316
Insulation & Lagging	$ 417,090
Internal Insulated Panels	$ 724,981
Oven Enclosure & Sheilds	$ 3,599,982
Instrumentation	$ 1,133,525
Heat Trace & Heaters	$ 2,706,693
Electrical (cabling, lighting, panels)	$ 411,155
Spare Parts	$ 180,652
Roof	$ 291,512
Total Remaining Equipment	$ 10,301,906
Total Solar Receiver	$ 46,880,000
Total Steam Generator Exchangers	$ 20,500,000

4.2 Manufacturing Techniques. All pressure parts will be designed and fabricated according to ASME Section 1.

The panels will be fabricated in modules which will include tubes, header, buckstays, supporting steel and insulation. The steel framework will be used as a shipping frame, and after field modification, will be used as the permanent operational structure.

The tubes will be ordered in maximum available lengths to minimize the amount of welds in the solar heated section. Tube stubs will be welded to their headers with set-on full penetration welds. The high nickel content of the Haynes 230 material requires high purity gases when welding and, the tube ID will be purged during welding to minimize scale build up. Tubes will be inspected using ultrasonic testing with a 5% ID and OD notch and electromagnetically tested with a 0.8 mm diameter drilled hole. Attachments for buckstays will be welded with a double plate so as not to overstress the thin tubes.

Each panel will be heated in the furnace for curing after the painting. This means that all headers must be stubbed and then joined with panels after the flat panel has been painted and cured. The applied thickness of the paint will be measured with dry film thickness testers.

4.3 Maintenance Cost. Typical maintenance costs for this system have been estimated at 2% of the capital cost. This figure is typical for boilers and other thermal equipment. Until long term maintenance data becomes available it is reasonable to use this value.

5.0 Conclusions

Foster Wheeler has designed a 795 MWt Molten Salt Receiver to demonstrate its viability and to develop the associated costs. The design was performed in adequate detail to ensure that the equipment could be classified as commercially available. This involved reviewing various tube sizes, optional flow circuitries, incident flux maps, stress analyses of the absorbing surface (both elastic and non-linear) and materials properties that were deemed appropriate for the service. In addition, manufacturing methods and systems were reviewed based on worldwide availability of material and labor. An internal steel structure was developed to provide proper support for the heat transfer surface and to allow work areas for maintenance personnel. Operational methodology and instrument control philosophy were reviewed to provide safe and consistent operation of the unit. During the design process certain areas were designated as requiring further study. These areas, however, are not considered insurmountable and would not preclude fabrication of a working unit. The current design is sufficient and complete to warrant further study and development of a working unit. The heat exchangers presented in this study have been provided in concept on a commercial basis for existing molten salt projects. These areas where further investigation could produce improvements in efficiency and manufacturing techniques would result in lower capital cost.

8.0 References

1. Cost and Performance Baseline for Fossil Energy Plants, Volume 1: Bituminous Coal and Natural Gas to Electricity, Final Report Revision 1, DOE/NETL-2007/1281, National Energy Technology Laboratory, August 2007

2. Abengoa Solar Inc., "Development of Baseload CSP – Advanced Nitrate Salt Central Receiver Power Plant: Receiver Specification," Contract DE-EE003596, July 18, 2013.

3. K.W. Battleson, "Solar Power Tower Design Guide: Solar Thermal Central Receiver Power Systems. A Source of Electricity and /or Process Heat.", Sandia National Laboratories, Albuquerque, SAND81-8005, April 1981.

4. P.K. Falcone, "A Handbook for Solar Central Receiver Design", Sandia National Laboratories, Livermore, SAND8-80009, December 1986.

5. A.B. Zavoico, "Solar Power Tower Design Basis Document", Sandia National Laboratories, Albuquerque and Livermore, SAND2001-2100, July 2001.

6. G. Carli, "Phase 1 – Final Report, Molten Salt Solar Receiver Subsystem Research Experiment," Report No. TPS-82-S41, Foster Wheeler Solar Development Corporation, Livingston, NJ, November 1982.

7. Abengoa Solar Inc., "Development of Baseload CSP – Advanced Nitrate Salt Central Receiver Power Plant: Steam Generator Specification," Contract DE-EE003596, February 5, 2011.

8. Foster Wheeler North America, Corp., "BASELOAD CONCENTRATING SOLAR POWER GENERATION – Molten Salt Solar Receiver and Steam Generator Design, Analysis, and Cost" DOE Contract DE-EE003596, March 2012.

9. Sandia National Laboratories, Correspondence from D.B. Dawson to Distribution, "Revised Physical Property Values for Molten Nitrate Salts," April 26, 1982.

10. J.E. Pacheco, "Flow Stability in Molten Salt Tube Receivers," Sandia National Laboratories, Albuquerque, SAND-92-2467C, OSTI ID: 6643110; Legacy ID: DE93005374, January 1992.

11. P. Carter, T.-L.Sham, R.I. Jetter, "Application of Shakedown Analysis To Evaluation of Creep-Fatigue Limits," Proceedings of the ASME 2012 Pressure Vessels & Piping Division Conference, Toronto, Ontario, Canada, July 2012,PVP2012-78083, 2012.

12. V.R. Ishwar, M Katcher, L.M. Pike, "Modified Power Law – Ni-22Cr-14W-2Mo-La Alloy Creep Rupture",

9.0 Acronyms and Abbreviations

a	Subscript a Denotes Absolute Pressure
ASME	American Society of Mechanical Engineers
bar	Bars Pressure
Btu	British Thermal Units
c_p	Constant Pressure Specific Heat
C	Coefficient of Discharge
CHF	Critical Heat Flux
CSP	Concentrating Solar Power
d	Diameter
D	Diameter
DOE	Department of Energy
f	Friction Factor
ft	Feet
FEA	Finite Element Analysis
g	Gravitational Constant or Denoting Gage Pressure
k	Thermal Conductivity
h	Heat Transfer Coefficient or Height Depending on Equation
hr	Hour
HEI	Heat Exchanger Institute
HTF	Heat Transfer Fluid
HTRI	Heat Transfer Research Inc.
ID	Inside Diameter
in	Inches
kg	Kilograms
kW	Kilowatt
lb	Pound
L	Length
m	Meter
min	Minute
mm	Millimeter
mph	Miles per Hour
M	Mass
MPa	Mega Pascal
MW	Minimum Wall Thickness
MWt	Megawatts Thermal
NEMA	National Electric Manufacturers Association
Nu	Nusselt Number
OD	Outside Diameter
psi	Pounds per Square Inch
P	Pressure
Pr	Prandtl Number

Q	Heat Loss
Re	Reynolds Number
ROE	Receiver Oven Enclosure
s	Allowable Stress (Subscript a for Cold and h for Hot)
sec	Seconds
t	Time
T	Temperature
TEMA	Tubular Heat Exchanger Manufacturers Association
V	Volume
Vh	Velocity Head
°C	Degrees Centigrade
°F	Degrees Fahrenheit
µ	Viscosity

APPENDIX A

Downflow Stability Analysis

As conceptually shown in Figure A-1 for a downflow panel, the average circuit dictates the total pressure drop (Point 1) between inlet (upper) header and the outlet (lower) header. A strongly heated tube can have a reduced flow (Point 2) and a resulting higher fluid temperature. Another possible pressure balance is a reversed flow (Point 3) where the hot, lighter salt gravity head is less than the total pressure drop and an upward flow is required to achieve the total pressure drop.

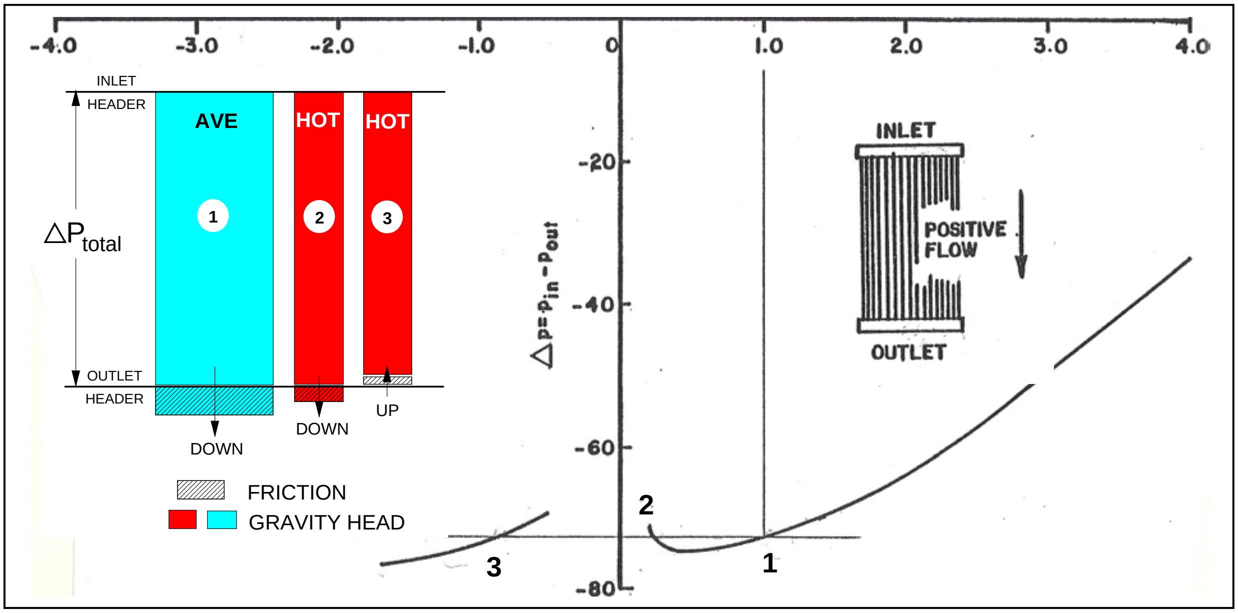

Figure A-1. Minimum Load Pressure Drop in Downflow Panel [Ref. 6]

In 1992 Sandia National Laboratories published a report (Ref. 10) that describes an analysis procedure to determine if a downflow circuit is unstable. The development of the procedure was based on pressure drop characteristic curves similar to the one shown in Figure A-1 for a downflow circuit with a fixed heat input. If the computed pressure drop falls to the left of the minimum pressure drop (point M), i.e., where dP/dW < 0 (negative slope part of the curve), the flow can be unstable.

For a given (fixed) physical configuration of a downflow circuit, a stability map can be plotted that shows the safe operating regimes as shown in Figure A-2. The plotted curve defines the flow rate that results in the minimum pressure drop (point M in Figure A-1) for a given heat flux input (i.e., where dP/dW = 0).

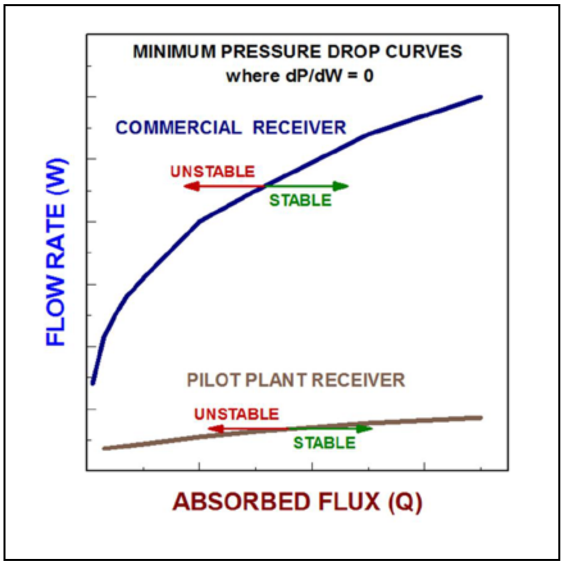

Figure A-2. Stability Map

As described in Reference 10, stability maps for a range of different physical configurations can be represented by one graph using non-dimensional parameters. Similarity analyses of the differential momentum and energy equations shows the relative magnitude of the buoyant Reynolds number, Gr/Re^2. When $Gr/Re^2 << 1$, inertial forces dominate. Conversely, $Gr/Re^2 >> 1$, buoyant forces dominate. Calculating Gr and Re for data used in stability map plots as illustrated in Figure A-2 showed that the data conveniently fits the curve $Gr/Re^2 = 0.08$. Plotting Gr versus Re, Re numbers to the right of the curve have stable flow: to the left, unstable flow (refer to Figure A-7 below).

Following the procedure, pressure characteristic curves were plotted for cold (1E) and hot (10W) panels and for two(2) load points, Day 8 8:30:00 (61.27% load) and Day 227 6:00:00 (29.67% load). The plots and the values used to create the plots are included in Figure A-3, A-4, A-5, and A-6. The vertical dashed red lines shows the location where the molten salt temperature is equal to 621°C (1150°F) which is the maximum data point used for creation of the salt properties equations. Properties beyond this temperature are based on an extrapolation defined by the property equations (refer to Appendix H). The vertical dotted red line shows the minimum pressure drop location where dP/dW = 0.

In all cases, the pressure drop point for the normal operating point (flow multiplier = 1) was on the positive sloped portion of the pressure drop curve indicating stable flow.

The non-dimensional parameters for the cases evaluated are included in Table A-1. The non-dimensional relationship, Gr/Re^2, for the dP/dW = 0 points did not give a constant value (such as 0.08) as described in Reference X. As shown in Figure A-7, only one of the minimum pressure drop points (squares or triangles) was near the $Gr/Re^2 = 0.08$ curve.

The ratio Gr/Re^2 simplifies to a function of the following parameters:

$$\frac{1}{G^2}\Delta T\rho$$

where, G = mass flux
ΔT = ID surface temperature – bulk fluid temperature
ρ = fluid density at bulk temperature

The value for Gr/Re^2 will therefore vary depending on load, heat flux, and panel location (cold inlet on high heat flux north side or hot outlet on low heat flux south side). The non-dimensional plot show in Figure A-7 was therefore not used as the basis for defining flow stability.

For reference Table A-1 includes a Gr/Re^2 comparison for 1.6" OD and 1.8" OD tubes. Because of the higher molten salt velocity for the smaller tube, the non-dimensional ratio is a smaller value indicating that inertial forces are more dominant than the buoyant forces giving more flow stability for the panels with molten salt flow downward. The normal operating points for 25% load (estimated) with the 1.6" OD and 1.8" OD tubes are plotted in Figure A-7 and shows that the 1.6" OD tube in the more stable direction.

	PANEL 1E								
	FLOW MULTIPLIER	Q	M	FRICTION DP	STATIC DP	TOTAL DP	T_{IN}	T_{OUT}
		MW	kg/s	bar	bar	bar	°C	°C
DOWNFLOW	0.175	25.35	45	0.0327	-4.8199	-4.7872	308	679
	0.225	25.35	57	0.0560	-4.8957	-4.8398	308	598
	0.3	25.35	77	0.0941	-4.9615	-4.8674	308	526
	0.35	25.35	89	0.1239	-4.9894	-4.8655	308	495
	0.4	25.35	102	0.1575	-5.0103	-4.8528	308	472
	0.55	25.35	141	0.2804	-5.0501	-4.7697	308	428
	0.7	25.35	179	0.4355	-5.0727	-4.6373	308	402
	0.8	25.35	204	0.5561	-5.0831	-4.5270	308	391
	0.9	25.35	230	0.6903	-5.0911	-4.4008	308	381
	1	25.35	255	0.8377	-5.0976	-4.2599	308	374
	1.1	25.35	281	0.9980	-5.1028	-4.1048	308	368
	0.208	25.35	53	0.0483	-4.8743	-4.8260	308	621
UPFLOW	-1.1	25.35	281	-0.9580	-4.9888	-5.9468	374	434
	-1.0	25.35	255	-0.8043	-4.9836	-5.7879	374	440
	-0.9	25.35	230	-0.6631	-4.9772	-5.6403	374	447
	-0.9	25.35	217	-0.5973	-4.9735	-5.5707	374	451
	-0.8	25.35	204	-0.5346	-4.9693	-5.5039	374	456
	-0.8	25.35	192	-0.4752	-4.9645	-5.4397	374	461
	-0.7	25.35	179	-0.4191	-4.9590	-5.3781	374	468
	-0.7	25.35	166	-0.3662	-4.9527	-5.3189	374	475
	-0.6	25.35	153	-0.3167	-4.9453	-5.2619	374	483
	-0.5	25.35	128	-0.2276	-4.9260	-5.1536	374	505
	-0.5	25.35	115	-0.1882	-4.9131	-5.1013	374	519
	-0.3	25.35	67	-0.0703	-4.8208	-4.8911	374	621

DAY OF YEAR:	8	RECEIVER TOTAL INCIDENT HEAT	525 MW
TIME OF DAY:	8:30:00 AM	RECEIVER TOTAL HEAT ABSORPTION	467 MW
		SALT FLOW	1051 KG/S

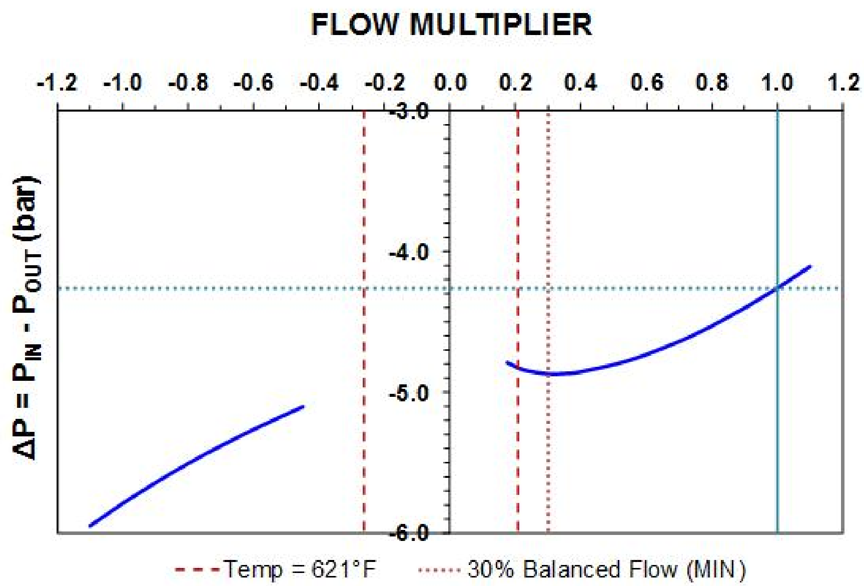

Figure A-3. Pressure Drop Characteristic Plot – Panel 1E – Day 8 8:30:00 (61.27% load)

	PANEL 10W							
	FLOWMULTIPLIER	Q	M	FRICTION DP	STATIC DP	TOTAL DP	T_{IN}	T_{OUT}
		MW	kg/s	bar	bar	bar	°C	°C
DOWNFLOW	0.175	9.79	45	0.0292	-4.6224	-4.5932	544	685
	0.225	9.79	57	0.0501	-4.6502	-4.6002	544	654
	0.3	9.79	77	0.0865	-4.6745	-4.5880	544	627
	0.35	9.79	89	0.1152	-4.6849	-4.5698	544	615
	0.4	9.79	102	0.1473	-4.6927	-4.5454	544	606
	0.55	9.79	141	0.2641	-4.7075	-4.4434	544	589
	0.7	9.79	179	0.4109	-4.7160	-4.3051	544	579
	0.8	9.79	204	0.5250	-4.7198	-4.1948	544	575
	0.9	9.79	230	0.6518	-4.7228	-4.0710	544	572
	1	9.79	255	0.7912	-4.7253	-3.9340	544	569
	1.1	9.79	281	0.9430	-4.7272	-3.7842	544	567
	0.322	9.79	82	0.0987	-4.6795	-4.5808	544	621

UPFLOW	-1.1	9.79	281	-0.9398	-4.6842	-5.6240	569	591
	-1.0	9.79	255	-0.7881	-4.6822	-5.4703	569	594
	-0.9	9.79	230	-0.6489	-4.6798	-5.3287	569	596
	-0.9	9.79	217	-0.5840	-4.6784	-5.2624	569	598
	-0.8	9.79	204	-0.5222	-4.6768	-5.1990	569	600
	-0.8	9.79	192	-0.4637	-4.6750	-5.1387	569	602
	-0.7	9.79	179	-0.4083	-4.6729	-5.0813	569	604
	-0.7	9.79	166	-0.3562	-4.6706	-5.0267	569	607
	-0.6	9.79	153	-0.3073	-4.6678	-4.9751	569	610
	-0.5	9.79	128	-0.2195	-4.6606	-4.8801	569	618
	-0.5	9.79	115	-0.1806	-4.6558	-4.8364	569	624
	-0.5	9.79	121	-0.1996	-4.6583	-4.8578	569	621

DAY OF YEAR: 8
TIME OF DAY: 8:30:00 AM

RECEIVER TOTAL INCIDENT HEAT 525 MW
RECEIVER TOTAL HEAT ABSORPTION 467 MW
SALT FLOW 1051 KG/S

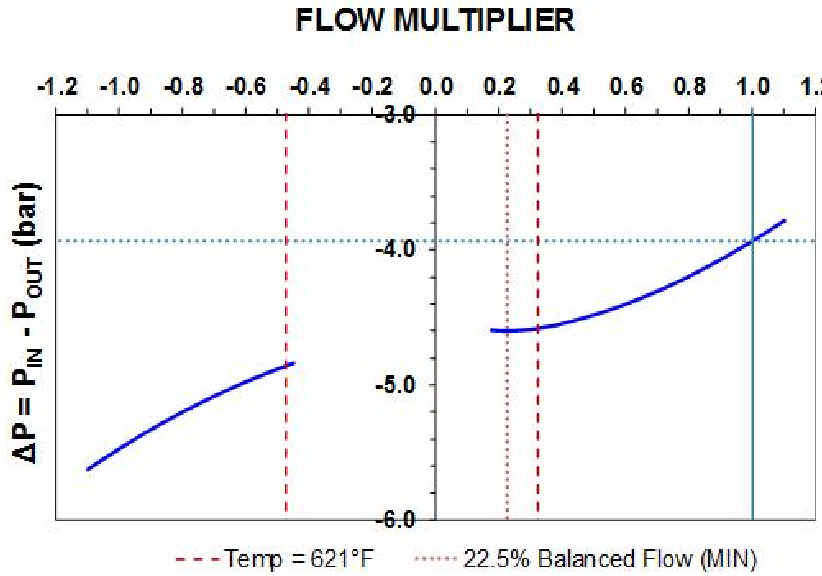

Figure A-4. Pressure Drop Characteristic Plot – Panel 10W – Day 8 8:30:00 (61.27% load)

	PANEL 1E							
	FLOW MULTIPLIER	Q	M	FRICTION DP	STATIC DP	TOTAL DP	T_{IN}	T_{OUT}
		MW	kg/s	bar	bar	bar	°C	°C
DOWNFLOW	0.135	10.23	18	0.0060	-4.8123	-4.8062	308	687
	0.2	10.23	26	0.0140	-4.9255	-4.9115	308	566
	0.3	10.23	39	0.0286	-5.0028	-4.9742	308	481
	0.4	10.23	52	0.0477	-5.0412	-4.9935	308	438
	0.5	10.23	65	0.0713	-5.0641	-4.9928	308	412
	0.6	10.23	78	0.0992	-5.0794	-4.9802	308	395
	0.7	10.23	92	0.1311	-5.0902	-4.9591	308	382
	0.8	10.23	105	0.1671	-5.0984	-4.9313	308	373
	0.9	10.23	118	0.2069	-5.1047	-4.8978	308	366
	1	10.23	131	0.2506	-5.1098	-4.8592	308	360
	1.1	10.23	144	0.2981	-5.1139	-4.8159	308	355
	0.164	10.23	21	0.0097	-4.8743	-4.8646	308	621
UPFLOW	-1.1	10.23	144	-0.2857	-5.0239	-5.3096	360	407
	-1.0	10.23	131	-0.2402	-5.0198	-5.2600	360	412
	-0.9	10.23	118	-0.1984	-5.0148	-5.2131	360	418
	-0.8	10.23	105	-0.1602	-5.0085	-5.1687	360	425
	-0.7	10.23	92	-0.1258	-5.0004	-5.1262	360	434
	-0.6	10.23	78	-0.0952	-4.9896	-5.0848	360	446
	-0.5	10.23	65	-0.0686	-4.9744	-5.0430	360	463
	-0.4	10.23	52	-0.0460	-4.9516	-4.9976	360	489
	-0.3	10.23	39	-0.0276	-4.9134	-4.9410	360	532
	-0.2	10.23	26	-0.0132	-4.8365	-4.8497	360	616
	-0.2	10.23	21	-0.0081	-4.7782	-4.7863	360	679
	-0.2	10.23	26	-0.0128	-4.8322	-4.8449	360	621

DAY OF YEAR:	227		RECEIVER TOTAL INCIDENT HEAT	269 MW
TIME OF DAY:	6:00:00 AM		RECEIVER TOTAL HEAT ABSORPTION	226 MW
			SALT FLOW	509 KG/S

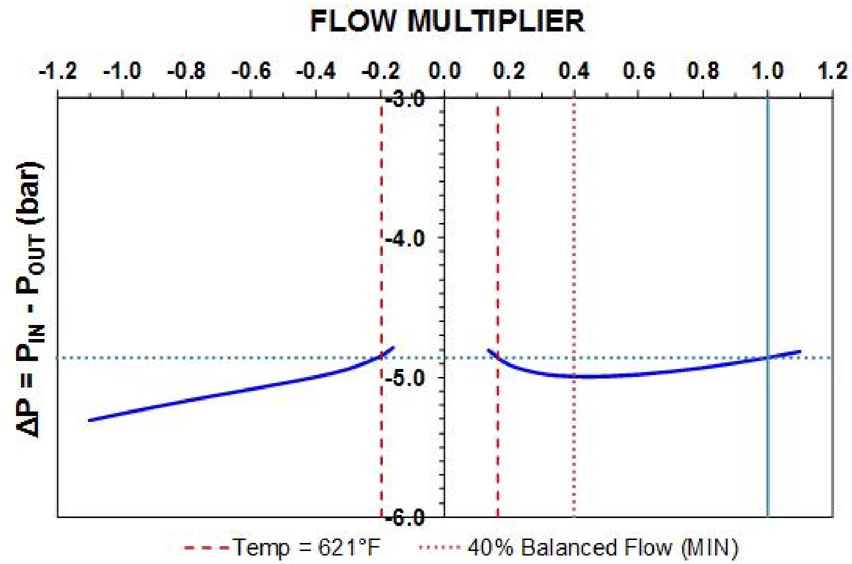

Figure A-5. Pressure Drop Characteristic Plot – Panel 1E – Day 227 6:00:00 (29.67% load)

	PANEL 10W							
	FLOW MULTIPLIER	Q	M	FRICTION DP	STATIC DP	TOTAL DP	T_{IN}	T_{OUT}
		MW	kg/s	bar	bar	bar	°C	°C
DOWNFLOW	0.3	7.95	39	0.0255	-4.6813	-4.6559	515	646
	0.35	7.95	46	0.0342	-4.6980	-4.6638	515	628
	0.37	7.95	48	0.0379	-4.7033	-4.6654	515	622
	0.4	7.95	52	0.0438	-4.7104	-4.6666	515	614
	0.5	7.95	65	0.0659	-4.7278	-4.6619	515	594
	0.6	7.95	78	0.0918	-4.7393	-4.6475	515	581
	0.7	7.95	92	0.1215	-4.7476	-4.6261	515	572
	0.8	7.95	105	0.1549	-4.7538	-4.5989	515	564
	0.9	7.95	118	0.1919	-4.7586	-4.5667	515	559
	1	7.95	131	0.2324	-4.7624	-4.5300	515	555
	1.1	7.95	144	0.2765	-4.7655	-4.4891	515	551
	0.372	7.95	49	0.0383	-4.7039	-4.6656	515	621
UPFLOW	-1.1	7.95	144	-0.2753	-4.6971	-4.9724	555	590
	-1	7.95	131	-0.2312	-4.6940	-4.9252	555	594
	-0.9	7.95	118	-0.1906	-4.6902	-4.8808	555	598
	-0.85	7.95	111	-0.1717	-4.6879	-4.8596	555	601
	-0.8	7.95	105	-0.1536	-4.6854	-4.8390	555	604
	-0.75	7.95	98	-0.1365	-4.6825	-4.8190	555	607
	-0.7	7.95	92	-0.1202	-4.6792	-4.7995	555	611
	-0.65	7.95	85	-0.1049	-4.6755	-4.7804	555	615
	-0.6	7.95	78	-0.0905	-4.6710	-4.7616	555	620
	-0.55	7.95	72	-0.0771	-4.6658	-4.7429	555	626
	-0.5	7.95	65	-0.0645	-4.6595	-4.7241	555	633
	-0.593	7.95	78	-0.0886	-4.6704	-4.7590	555	621

DAY OF YEAR: 227
TIME OF DAY: 6:00:00 AM

RECEIVER TOTAL INCIDENT HEAT 269 MW
RECEIVER TOTAL HEAT ABSORPTION 226 MW
SALT FLOW 509 KG/S

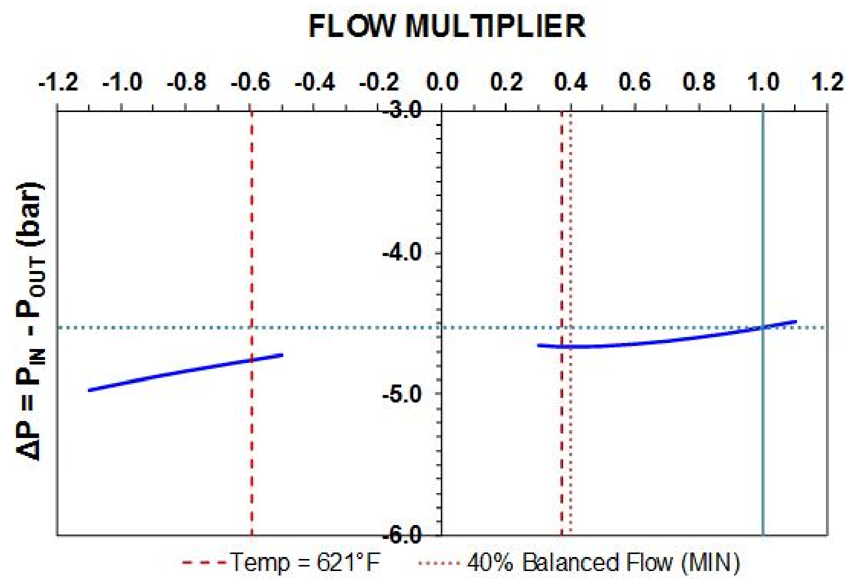

Figure A-6. Pressure Drop Characteristic Plot – Panel 10W – Day 227 6:00:00 (29.67% load)

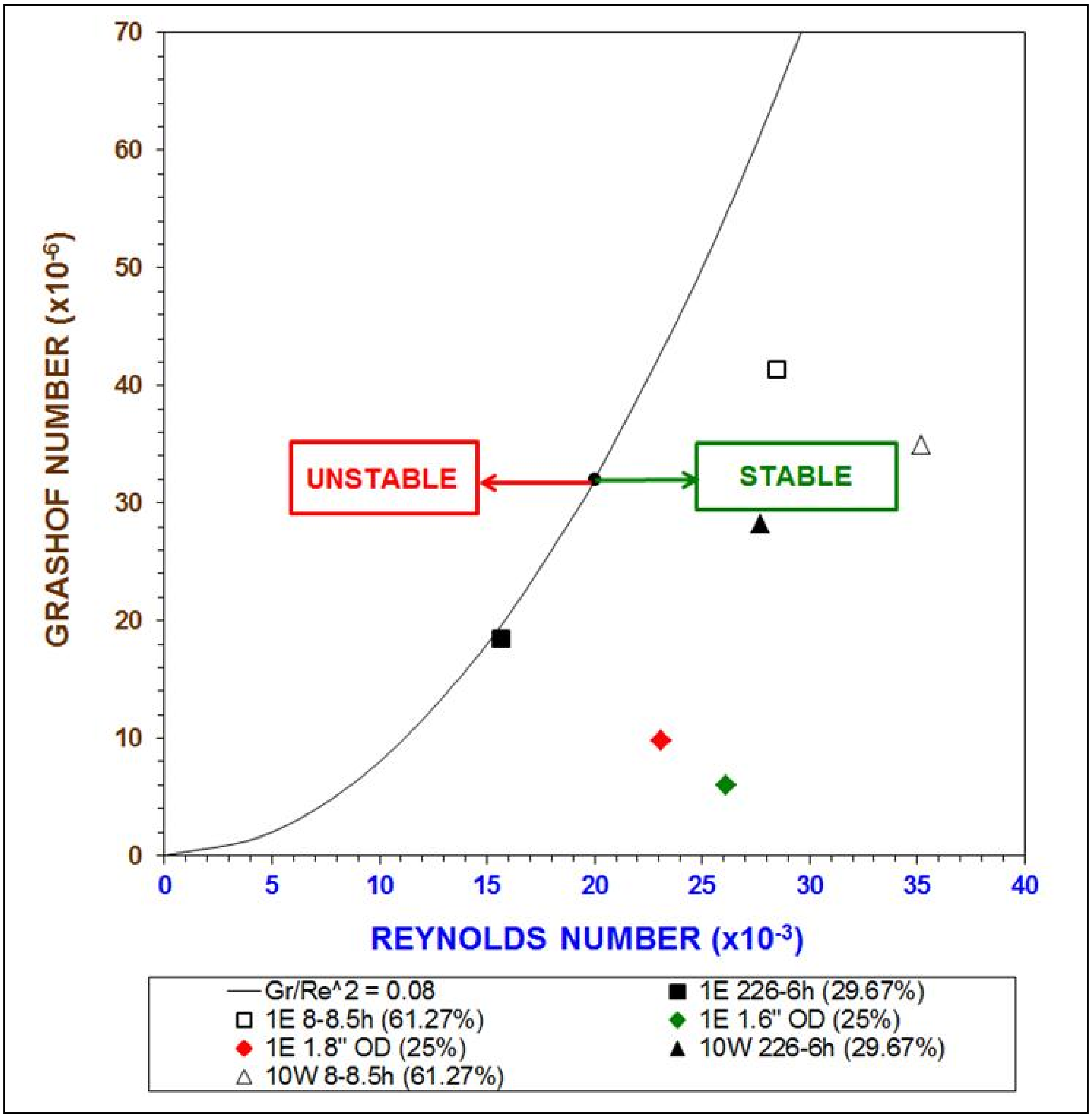

Figure A-7. Stability Map Using Non-Dimensional Parameters

										1.61" OD	1.8" OD
Load	%	29.67%	29.67%	29.67%	29.67%	61.27%	61.27%	61.27%	61.27%	25%	25%
Flux Map Day		227	227	227	227	8	8	8	8	Estimated	Estimated
Flux Map hr		6:00:00	6:00:00	6:00:00	6:00:00	8:30:00	8:30:00	8:30:00	8:30:00	Estimated	Estimated
Panel #		10W	10W	1E	1E	10W	10W	1E	1E	1E	1E
Tube OD	mm	40.894	40.894	40.894	40.894	40.894	40.894	40.894	40.894	40.894	45.7
Tube MW	mm	1.49	1.49	1.49	1.49	1.49	1.49	1.49	1.49	1.49	1.49
Tube ID	mm	37.5862	37.5862	37.5862	37.5862	37.5862	37.5862	37.5862	37.5862	37.5862	42.3922
Flow Multiplier		1	0.4	1	0.4	1	0.225	1	0.3	1	1
Q	MW	7.95	7.59	10.23	9.84	9.79	9.27	25.35	24.26	8.68	8.66
M	kg/s	131	52	131	52	255	57	255	77	110	110
dPf	bar	0.247	0.058	0.265	0.063	0.849	0.112	0.892	0.151	0.194	0.138
dPs	bar	-4.763	-4.573	-5.110	-5.046	-4.725	-4.655	-5.098	-4.970	-5.109	-5.109
dPt	bar	-4.5151	-4.5151	-4.8450	-4.9832	-3.8759	-4.5437	-4.2056	-4.8185	-4.9152	-4.9709
Avg Panel ID Temp	°C	572	630	400	497	582	661	431	601	399	408
Avg Panel Bulk Temp	°C	536	565	336	375	557	601	343	421	336	336
dT	°C	36	64	64	122	25	60	88	181	63	72
Beta		0.000363646	0.000367526	0.000338953	0.000343506	0.000366453	0.000372365	0.000339814	0.000348968	0.000338979	0.000338986
Kin. Viscosity	m2/s	7.02E-07	6.60E-07	1.36E-06	1.09E-06	6.73E-07	5.79E-07	1.30E-06	8.93E-07	1.36E-06	1.36E-06
density	kg/m3	1749	1730	1876	1851	1736	1708	1872	1823	1876	1876
Reynolds #		64	28	31	16	132	35	63	29	26	23
Grashof #		14	28	6	18	11	35	9	41	6	10
Gr/Re^2		0.0033	0.0369	0.0064	0.0748	0.0006	0.0282	0.0023	0.0508	0.0088	0.0184

Table A-1. Non-Dimensional Parameters for Phase II Receiver

APPENDIX B

Haynes 230 Alloy

HAYNES International

HIGH-TEMPERATURE TECH BRIEF

HAYNES® 230® Alloy

"Designing Thinner" with HAYNES® Components

HAYNES® 230® alloy has many design advantages over less robust materials of construction. These include superior oxidation-resistance, metallurgical stability, fatigue strength and repairability. But the stand-out feature of 230 alloy is its excellent strength. You can design higher strength into your component by using the same thickness of construction as for other materials, or you can "design thinner" by reducing thickness, and still gain all of 230 alloy's other advantages. The chart below shows how much gauge reduction you can achieve in comparison to various heat-resistant alloys. So when the mass of your part is important, or if heat transfer needs to be improved, "design thinner" with 230 alloy's strength advantage. Use 2/3 to 3/4 of the thickness required for HASTELLOY® X alloy, or 1/2 to 2/3 of the thickness needed for 800H alloy. Only a third of the thickness of type 310 stainless steel is needed for the same level of strength! The same advantages exist for ASME Vessel Code construction for service up to 1650°F (900°C), although the extent of thickness reduction possible may vary somewhat. Reference to the individual code cases for comparison is recommended.

	Service Temperature		
Alloy	**1400°F (760°C)**	**1600°F (870°C)**	**1800°F (980°C)**
X	25%	34%	26%
800H	47%	51%	39%
601	54%	54%	36%
253 MA	54%	53%	42%
316	56%	64%	60%
RA330	60%	61%	54%
304	63%	68%	63%
310	66%	69%	72%
600	71%	63%	45%
446	90%	90%	88%

*Based on 1000-hour rupture life strength

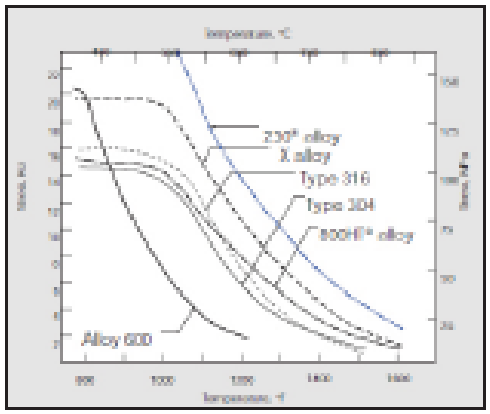

**Allowable design stresses

Product Description:

HAYNES® 556® alloy is an iron-nickel-chromium-cobalt alloy that combines effective resistance to sulfidizing, carburizing, and chlorine-bearing environments at high temperatures with good oxidation resistance, fabricability, and excellent high-temperature strength. It has also been found to resist corrosion by molten chloride salts and molten zinc.

HAYNES 556 alloy is highly useful for service at elevated temperature in moderately to severely corrosive environments. Applications include tubing and structural members in waste heat recuperators, superheaters, and internals in municipal and chemical waste incinerators; power plant burner buckets, cair nozzles, and fluidized bed combustor heat exchangers and internals; high speed furnace fans, galvanizing bath hardware and brazing fixtures; and high-temperature rotary calciners and kilns. There are also additional uses in the chemical petrochemical process and pump and paper industries.

Chemistry: Weight %

Ni*	Co	Cr	Mo	W	Fe	Si	Mn	C	Al	B	La
57	5*	22	2	14	3*	0.4	0.5	0.10	0.3	0.015*	0.02

*As Balance *Maximum

H-3084E

HAYNES International

HIGH-TEMPERATURE TECH BRIEF

HAYNES® 230® Alloy

"Designing Thinner" with HAYNES® Components

HAYNES® 230® alloy has many design advantages over less robust materials of construction. These include superior oxidation-resistance, metallurgical stability, fatigue strength and repairability. But the stand-out feature of 230 alloy is its excellent strength. You can design higher strength into your component by using the same thickness of construction as for other materials, or you can "design thinner" by reducing thickness, and still gain all of 230 alloy's other advantages. The chart below shows how much gauge reduction you can achieve in comparison to various heat-resistant alloys. So when the mass of your part is important, or if heat transfer needs to be improved, "design thinner" with 230 alloy's strength advantage. Use 2/3 to 3/4 of the thickness required for HASTELLOY® X alloy, or 1/2 to 2/3 of the thickness needed for 800H alloy. Only a third of the thickness of type 310 stainless steel is needed for the same level of strength! The same advantages exist for ASME Vessel Code construction for service up to 1650°F (900°C), although the extent of thickness reduction possible may vary somewhat. Reference to the individual code cases for comparison is recommended.

	Service Temperature		
Alloy	1400°F (760°C)	1600°F (870°C)	1800°F (980°C)
X	25%	34%	26%
800H	47%	51%	39%
601	54%	54%	36%
253 MA	54%	53%	42%
316	56%	64%	60%
RA330	60%	61%	54%
304	63%	68%	63%
310	66%	69%	72%
600	71%	63%	45%
446	90%	90%	88%

*Based on 1000-hour rupture life strength

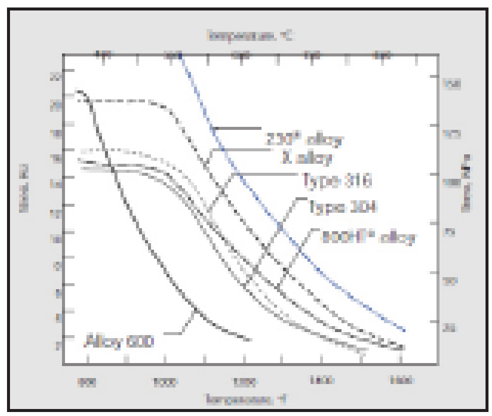

**Allowable design stresses

Product Description:

HAYNES® 556® alloy is an iron-nickel-chromium-cobalt alloy that combines effective resistance to sulfidizing, carburizing, and chlorine-bearing environments at high temperatures with good oxidation resistance, fabricability, and excellent high-temperature strength. It has also been found to resist corrosion by molten chloride salts and molten zinc.

HAYNES 556 alloy is highly useful for service at elevated temperature in moderately to severely corrosive environments. Applications include tubing and structural members in waste heat recuperators, superheaters, and internals in municipal and chemical waste incinerators; power plant burner buckets, cair nozzles, and fluidized bed combustor heat exchangers and internals; high speed furnace fans, galvanizing bath hardware and brazing fixtures; and high-temperature rotary calciners and kilns. There are also additional uses in the chemical petrochemical process and pump and paper industries.

Chemistry: Weight %

Ni*	Co	Cr	Mo	W	Fe	Si	Mn	C	Al	B	La
57	5*	22	2	14	3*	0.4	0.5	0.10	0.3	0.015*	0.02

*As Balance *Maximum

H-3084E

APPENDIX C

Salt Flow Path Position And Design Pressure

#	PIPING/TUBES	P bara	Max P bara	1.05P bara	Calc Pdesign bara	Issued Design P bara
0	Main Feed Pipe	22.47	22.47	23.59	23.59	23.59
1	Transfer Pipe to Pass 1E	21.56	22.26	23.37	23.59	23.59
1	Transfer Pipe to Pass 2E	21.96	22.26	23.37	23.59	23.59
1	Transfer Pipe to Pass 1W	21.91	22.26	23.37	23.59	23.59
1	Transfer Pipe to Pass 2W	22.26	22.26	23.37	23.59	23.59
2	Inlet Header Pass 1E	16.23	16.91	17.76	17.76	18.15
2	Inlet Header Pass 2E	16.62	16.91	17.76	17.76	18.15
2	Inlet Header Pass 1W	16.57	16.91	17.76	17.76	18.15
2	Inlet Header Pass 2W	16.91	16.91	17.76	17.76	18.15
3	Inlet Stubs Pass 1E	16.15	16.83	17.67	17.67	18.15
3	Inlet Stubs Pass 2E	16.54	16.83	17.67	17.67	18.15
3	Inlet Stubs Pass 1W	16.49	16.83	17.67	17.67	18.15
3	Inlet Stubs Pass 2W	16.83	16.83	17.67	17.67	18.15
4	Pass 1E Tubes	19.11	19.69	20.68	20.68	20.68
4	Pass 2E Tubes	19.44	19.69	20.68	20.68	20.68
4	Pass 1W Tubes	19.40	19.69	20.68	20.68	20.68
4	Pass 2W Tubes	19.69	19.69	20.68	20.68	20.68
5	Outlet Stubs Pass 1E	19.11	19.69	20.68	20.68	20.68
5	Outlet Stubs Pass 2E	19.44	19.69	20.68	20.68	20.68
5	Outlet Stubs Pass 1W	19.40	19.69	20.68	20.68	20.68
5	Outlet Stubs Pass 2W	19.69	19.69	20.68	20.68	20.68
6	Outlet Header Pass 1E	18.98	19.56	20.54	20.68	20.68
6	Outlet Header Pass 2E	19.31	19.56	20.54	20.68	20.68
6	Outlet Header Pass 1W	19.27	19.56	20.54	20.68	20.68
6	Outlet Header Pass 2W	19.56	19.56	20.54	20.68	20.68
7	Transfer Pipe 1E-3E	18.90	19.48	20.45	20.68	20.68
7	Transfer Pipe 2E-4E	19.23	19.48	20.45	20.68	20.68
7	Transfer Pipe 1W-3W	19.19	19.48	20.45	20.68	20.68
7	Transfer Pipe 2W-4W	19.48	19.48	20.45	20.68	20.68
8	Inlet Header Pass 3E	18.80	19.36	20.33	20.68	20.68
8	Inlet Header Pass 4E	19.13	19.36	20.33	20.68	20.68
8	Inlet Header Pass 3W	19.09	19.36	20.33	20.68	20.68
8	Inlet Header Pass 4W	19.36	19.36	20.33	20.68	20.68
9	Inlet Stubs Pass 3E	18.72	19.27	20.24	20.68	20.68
9	Inlet Stubs Pass 4E	19.04	19.27	20.24	20.68	20.68
9	Inlet Stubs Pass 3W	19.00	19.27	20.24	20.68	20.68
9	Inlet Stubs Pass 4W	19.27	19.27	20.24	20.68	20.68
10	Pass 3E Tubes	18.63	19.18	20.14	20.68	20.68
10	Pass 4E Tubes	18.95	19.18	20.14	20.68	20.68
10	Pass 3W Tubes	18.91	19.18	20.14	20.68	20.68
10	Pass 4W Tubes	19.18	19.18	20.14	20.68	20.68
11	Outlet Stubs Pass 3E	11.69	12.14	12.75	12.75	12.75
11	Outlet Stubs Pass 4E	11.95	12.14	12.75	12.75	12.75
11	Outlet Stubs Pass 3W	11.92	12.14	12.75	12.75	12.75
11	Outlet Stubs Pass 4W	12.14	12.14	12.75	12.75	12.75
12	Outlet Header Pass 3E	11.53	11.98	12.57	12.75	12.75
12	Outlet Header Pass 4E	11.79	11.98	12.57	12.75	12.75
12	Outlet Header Pass 3W	11.76	11.98	12.57	12.75	12.75
12	Outlet Header Pass 4W	11.98	11.98	12.57	12.75	12.75

#	PIPING/TUBES	P bara	Max P bara	1.05P bara	Calc Pdesign bara	Issued Design P bara
13	Transfer Pipe 3E-5E	11.45	11.89	12.49	12.75	12.75
13	Transfer Pipe 4E-6E	11.71	11.89	12.49	12.75	12.75
13	Transfer Pipe 3W-5W	11.68	11.89	12.49	12.75	12.75
13	Transfer Pipe 4W-6W	11.89	11.89	12.49	12.75	12.75
14	Inlet Header Pass 5E	11.35	11.78	12.37	12.75	12.75
14	Inlet Header Pass 6E	11.60	11.78	12.37	12.75	12.75
14	Inlet Header Pass 5W	11.57	11.78	12.37	12.75	12.75
14	Inlet Header Pass 6W	11.78	11.78	12.37	12.75	12.75
15	Inlet Stubs Pass 5E	11.26	11.70	12.28	12.75	12.75
15	Inlet Stubs Pass 6E	11.51	11.70	12.28	12.75	12.75
15	Inlet Stubs Pass 5W	11.48	11.70	12.28	12.75	12.75
15	Inlet Stubs Pass 6W	11.70	11.70	12.28	12.75	12.75
16	Pass 5E Tubes	14.10	14.46	15.19	15.19	15.19
16	Pass 6E Tubes	14.31	14.46	15.19	15.19	15.19
16	Pass 5W Tubes	14.29	14.46	15.19	15.19	15.19
16	Pass 6W Tubes	14.46	14.46	15.19	15.19	15.19
17	Outlet Stubs Pass 5E	14.10	14.46	15.19	15.19	15.19
17	Outlet Stubs Pass 6E	14.31	14.46	15.19	15.19	15.19
17	Outlet Stubs Pass 5W	14.29	14.46	15.19	15.19	15.19
17	Outlet Stubs Pass 6W	14.46	14.46	15.19	15.19	15.19
18	Outlet Header Pass 5E	13.97	14.33	15.04	15.19	15.19
18	Outlet Header Pass 6E	14.17	14.33	15.04	15.19	15.19
18	Outlet Header Pass 5W	14.15	14.33	15.04	15.19	15.19
18	Outlet Header Pass 6W	14.33	14.33	15.04	15.19	15.19
19	Transfer Pipe 5E-8W	13.89	14.24	14.95	15.19	15.19
19	Transfer Pipe 6E-7W	14.09	14.24	14.95	15.19	15.19
19	Transfer Pipe 5W-8E	14.07	14.24	14.95	15.19	15.19
19	Transfer Pipe 6W-7E	14.24	14.24	14.95	15.19	15.19
20	Inlet Header Pass 8W	13.75	14.09	14.80	15.19	15.19
20	Inlet Header Pass 7W	13.94	14.09	14.80	15.19	15.19
20	Inlet Header Pass 8E	13.92	14.09	14.80	15.19	15.19
20	Inlet Header Pass 7E	14.09	14.09	14.80	15.19	15.19
21	Inlet Stubs Pass 8W	13.66	14.00	14.70	15.19	15.19
21	Inlet Stubs Pass 7W	13.86	14.00	14.70	15.19	15.19
21	Inlet Stubs Pass 8E	13.83	14.00	14.70	15.19	15.19
21	Inlet Stubs Pass 7E	14.00	14.00	14.70	15.19	15.19
22	Pass 8W Tubes	13.57	13.91	14.61	15.19	15.19
22	Pass 7W Tubes	13.76	13.91	14.61	15.19	15.19
22	Pass 8E Tubes	13.74	13.91	14.61	15.19	15.19
22	Pass 7E Tubes	13.91	13.91	14.61	15.19	15.19
23	Outlet Stubs Pass 8W	6.87	7.09	7.45	7.45	7.45
23	Outlet Stubs Pass 7W	7.00	7.09	7.45	7.45	7.45
23	Outlet Stubs Pass 8E	6.98	7.09	7.45	7.45	7.45
23	Outlet Stubs Pass 7E	7.09	7.09	7.45	7.45	7.45
24	Outlet Header Pass 8W	6.70	6.92	7.27	7.45	7.45
24	Outlet Header Pass 7W	6.83	6.92	7.27	7.45	7.45
24	Outlet Header Pass 8E	6.82	6.92	7.27	7.45	7.45
24	Outlet Header Pass 7E	6.92	6.92	7.27	7.45	7.45
25	Transfer Pipe 8W-10W	6.62	6.84	7.18	7.45	7.45
25	Transfer Pipe 7W-9W	6.75	6.84	7.18	7.45	7.45
25	Transfer Pipe 8E-10E	6.73	6.84	7.18	7.45	7.45
25	Transfer Pipe 7E-9E	6.84	6.84	7.18	7.45	7.45

#	PIPING/TUBES	P bara	Max P bara	1.05P bara	Calc Pdesign bara	Issued Design P bara
26	Inlet Header Pass 10W	6.52	6.73	7.07	7.45	7.45
26	Inlet Header Pass 9W	6.64	6.73	7.07	7.45	7.45
26	Inlet Header Pass 10E	6.63	6.73	7.07	7.45	7.45
26	Inlet Header Pass 9E	6.73	6.73	7.07	7.45	7.45
27	Inlet Stubs Pass 10W	6.43	6.64	6.97	7.45	7.45
27	Inlet Stubs Pass 9W	6.55	6.64	6.97	7.45	7.45
27	Inlet Stubs Pass 10E	6.54	6.64	6.97	7.45	7.45
27	Inlet Stubs Pass 9E	6.64	6.64	6.97	7.45	7.45
28	Pass 10W Tubes	9.14	9.27	9.73	9.73	9.73
28	Pass 9W Tubes	9.21	9.27	9.73	9.73	9.73
28	Pass 10E Tubes	9.20	9.27	9.73	9.73	9.73
28	Pass 9E Tubes	9.27	9.27	9.73	9.73	9.73
29	Outlet Stubs Pass 10W	9.14	9.27	9.73	9.73	9.73
29	Outlet Stubs Pass 9W	9.21	9.27	9.73	9.73	9.73
29	Outlet Stubs Pass 10E	9.20	9.27	9.73	9.73	9.73
29	Outlet Stubs Pass 9E	9.27	9.27	9.73	9.73	9.73
30	Outlet Header Pass 10W	9.00	9.12	9.58	9.73	9.73
30	Outlet Header Pass 9W	9.07	9.12	9.58	9.73	9.73
30	Outlet Header Pass 10E	9.06	9.12	9.58	9.73	9.73
30	Outlet Header Pass 9E	9.12	9.12	9.58	9.73	9.73
31	Transfer Pipe 10W-12W	8.91	9.03	9.48	9.73	9.73
31	Transfer Pipe 9W-11W	8.98	9.03	9.48	9.73	9.73
31	Transfer Pipe 10E-12E	8.97	9.03	9.48	9.73	9.73
31	Transfer Pipe 9E-11E	9.03	9.03	9.48	9.73	9.73
32	Inlet Header Pass 12W	8.81	8.93	9.37	9.73	9.73
32	Inlet Header Pass 11W	8.88	8.93	9.37	9.73	9.73
32	Inlet Header Pass 12E	8.87	8.93	9.37	9.73	9.73
32	Inlet Header Pass 11E	8.93	8.93	9.37	9.73	9.73
33	Inlet Stubs Pass 12W	8.72	8.84	9.28	9.73	9.73
33	Inlet Stubs Pass 11W	8.79	8.84	9.28	9.73	9.73
33	Inlet Stubs Pass 12E	8.78	8.84	9.28	9.73	9.73
33	Inlet Stubs Pass 11E	8.84	8.84	9.28	9.73	9.73
34	Pass 12W Tubes	8.63	8.74	9.18	9.73	9.73
34	Pass 11W Tubes	8.69	8.74	9.18	9.73	9.73
34	Pass 12E Tubes	8.68	8.74	9.18	9.73	9.73
34	Pass 11E Tubes	8.74	8.74	9.18	9.73	9.73
35	Outlet Stubs Pass 12W	2.05	2.07	2.17	2.17	2.17
35	Outlet Stubs Pass 11W	2.06	2.07	2.17	2.17	2.17
35	Outlet Stubs Pass 12E	2.06	2.07	2.17	2.17	2.17
35	Outlet Stubs Pass 11E	2.07	2.07	2.17	2.17	2.17
36	Outlet Header Pass 12W	1.88	1.89	1.99	2.17	2.17
36	Outlet Header Pass 11W	1.89	1.89	1.99	2.17	2.17
36	Outlet Header Pass 12E	1.89	1.89	1.99	2.17	2.17
36	Outlet Header Pass 11E	1.89	1.89	1.99	2.17	2.17
37	Transfer Pipe to Out Manifold	1.80	1.81	1.90	2.17	2.17
37	Transfer Pipe to Out Manifold	1.80	1.81	1.90	2.17	2.17
37	Transfer Pipe to Out Manifold	1.80	1.81	1.90	2.17	2.17
37	Transfer Pipe to Out Manifold	1.81	1.81	1.90	2.17	2.17
38	Main Return Pipe	1.00	1.00	1.05	2.17	2.17

APPENDIX D

Incident Heat Flux Maps

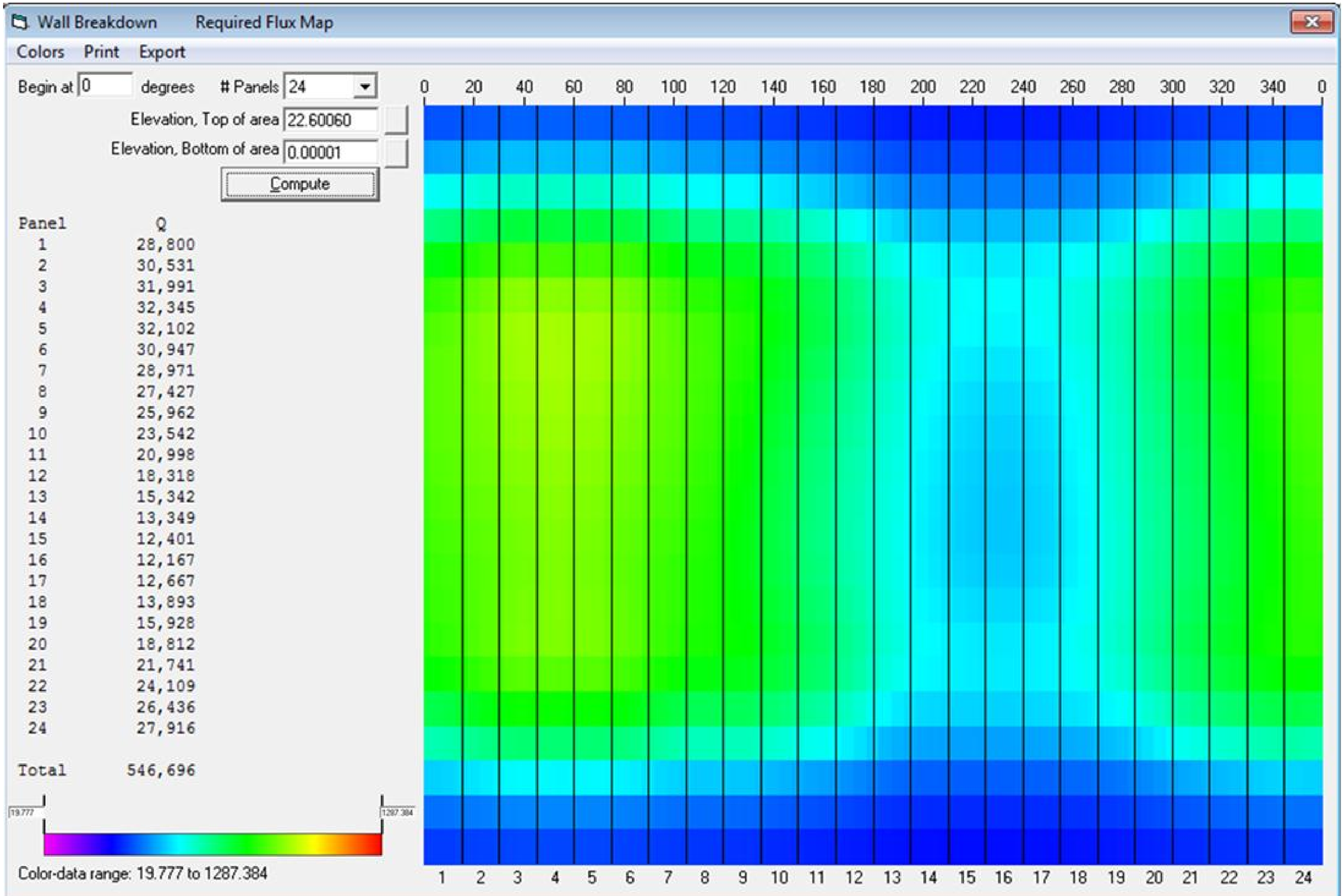

INCIDENT HEAT FLUX DISTRIBUTION – DAY 8 8:30:00

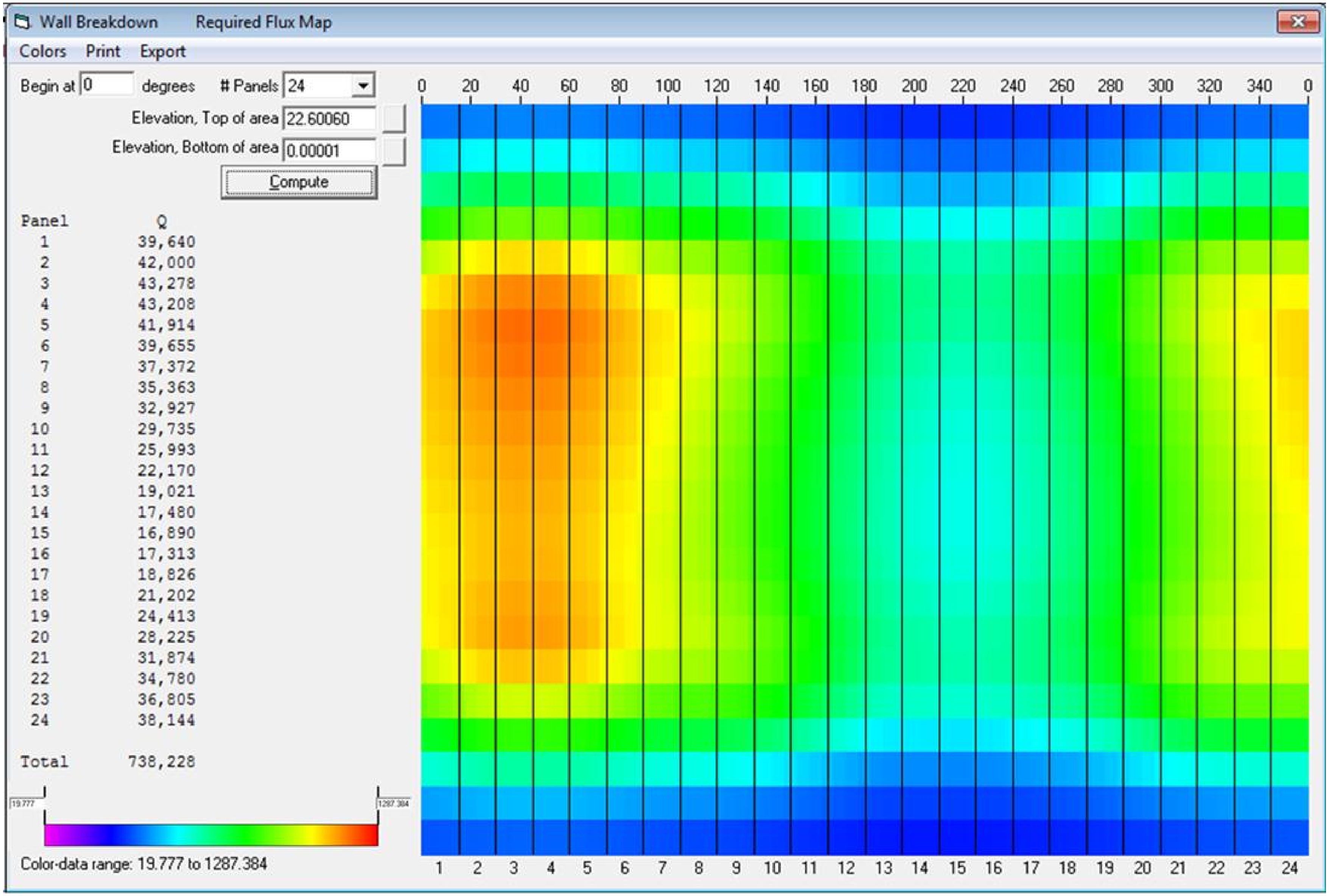

INCIDENT HEAT FLUX DISTRIBUTION – DAY 8 9:30:00

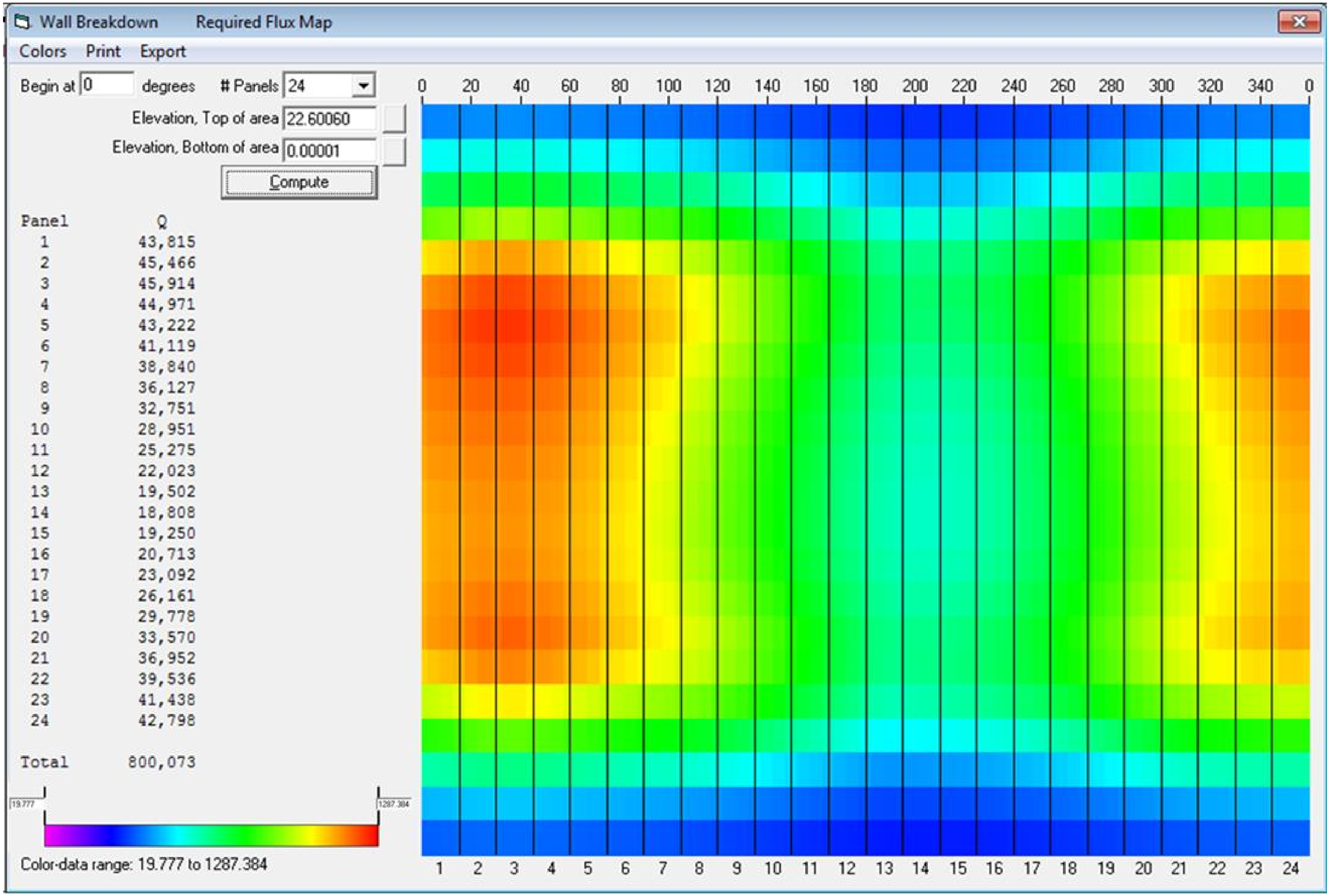

INCIDENT HEAT FLUX DISTRIBUTION – DAY 8 10:30:00

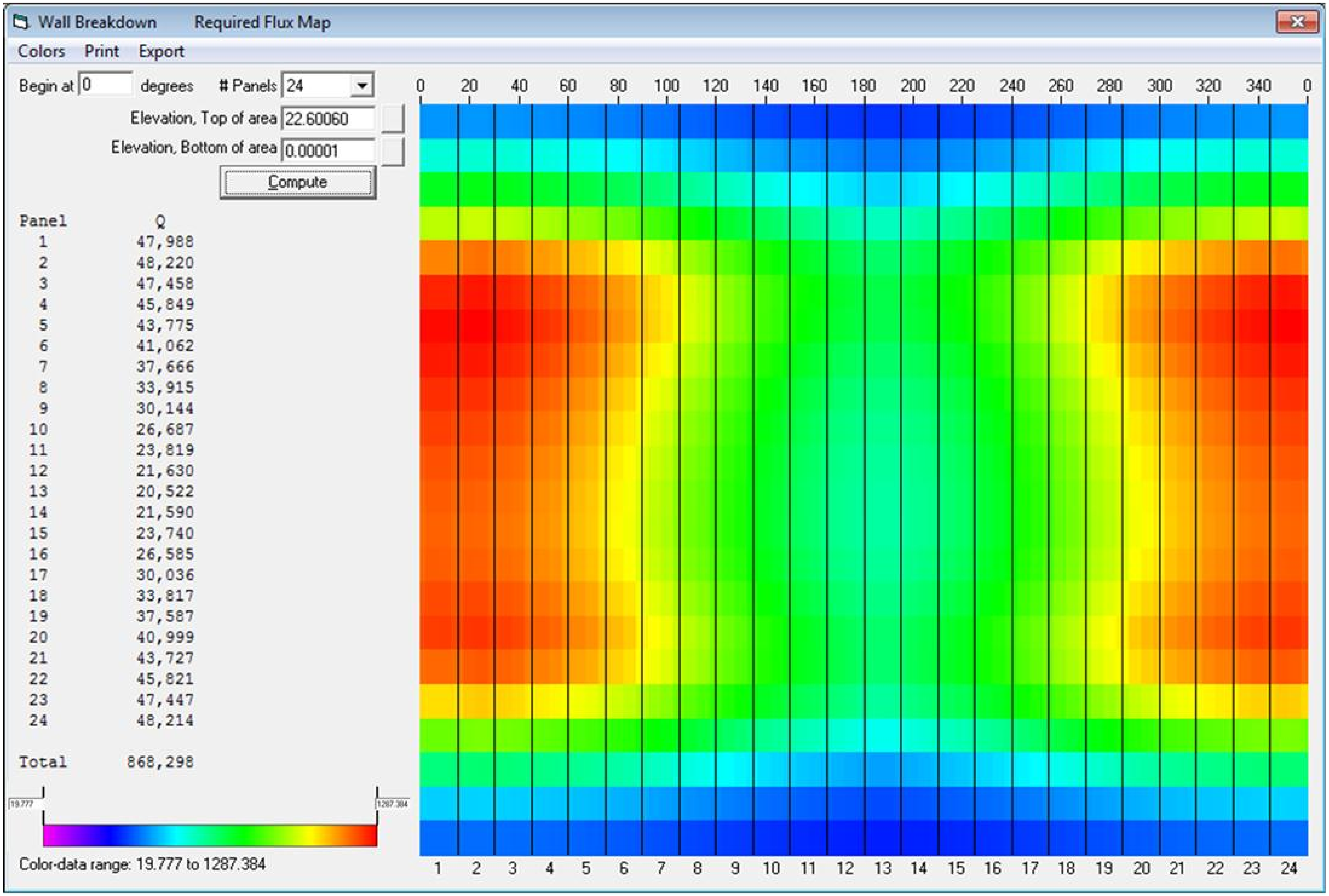

INCIDENT HEAT FLUX DISTRIBUTION – DAY 8 12:00:00

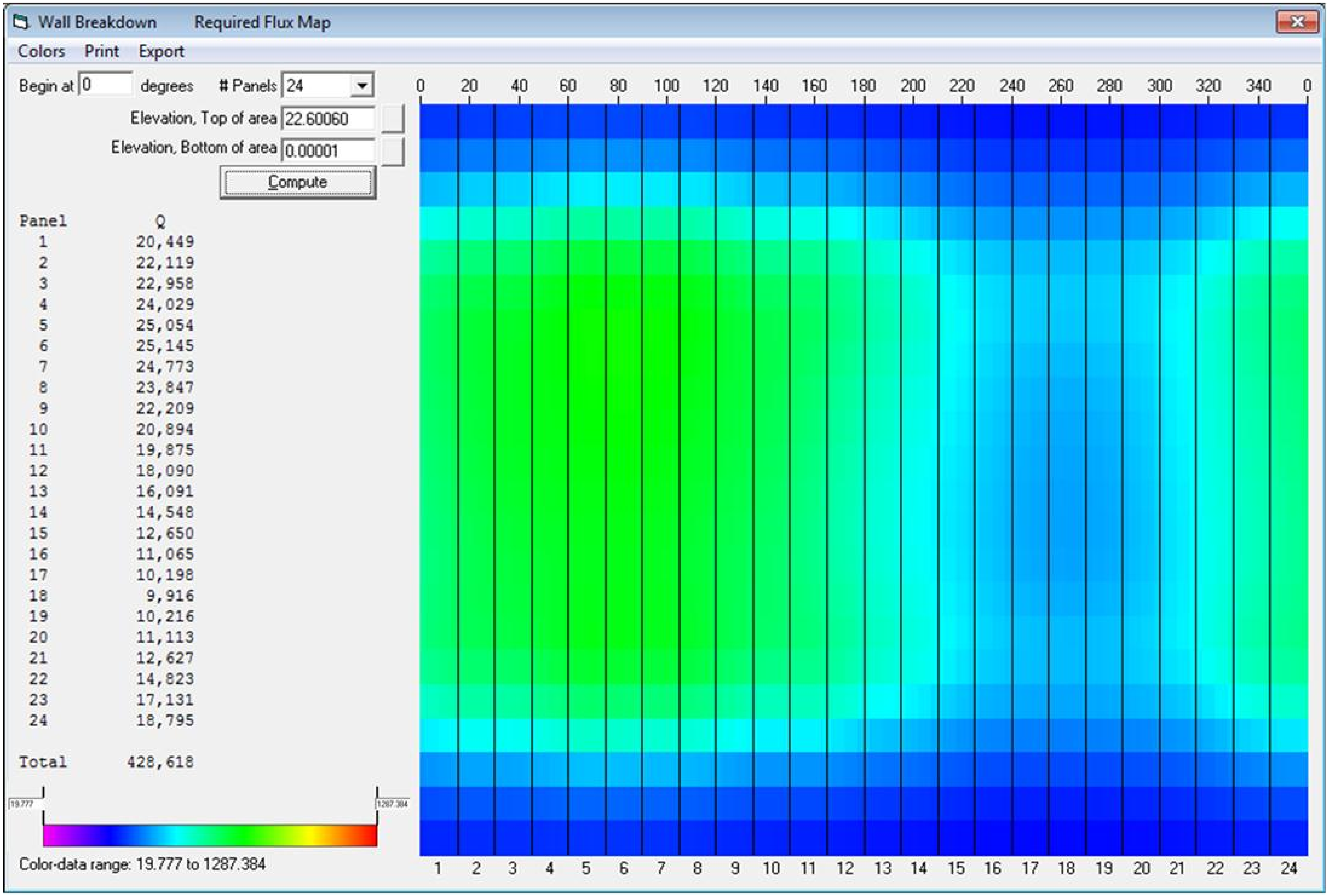

INCIDENT HEAT FLUX DISTRIBUTION – DAY 81 7:00:00

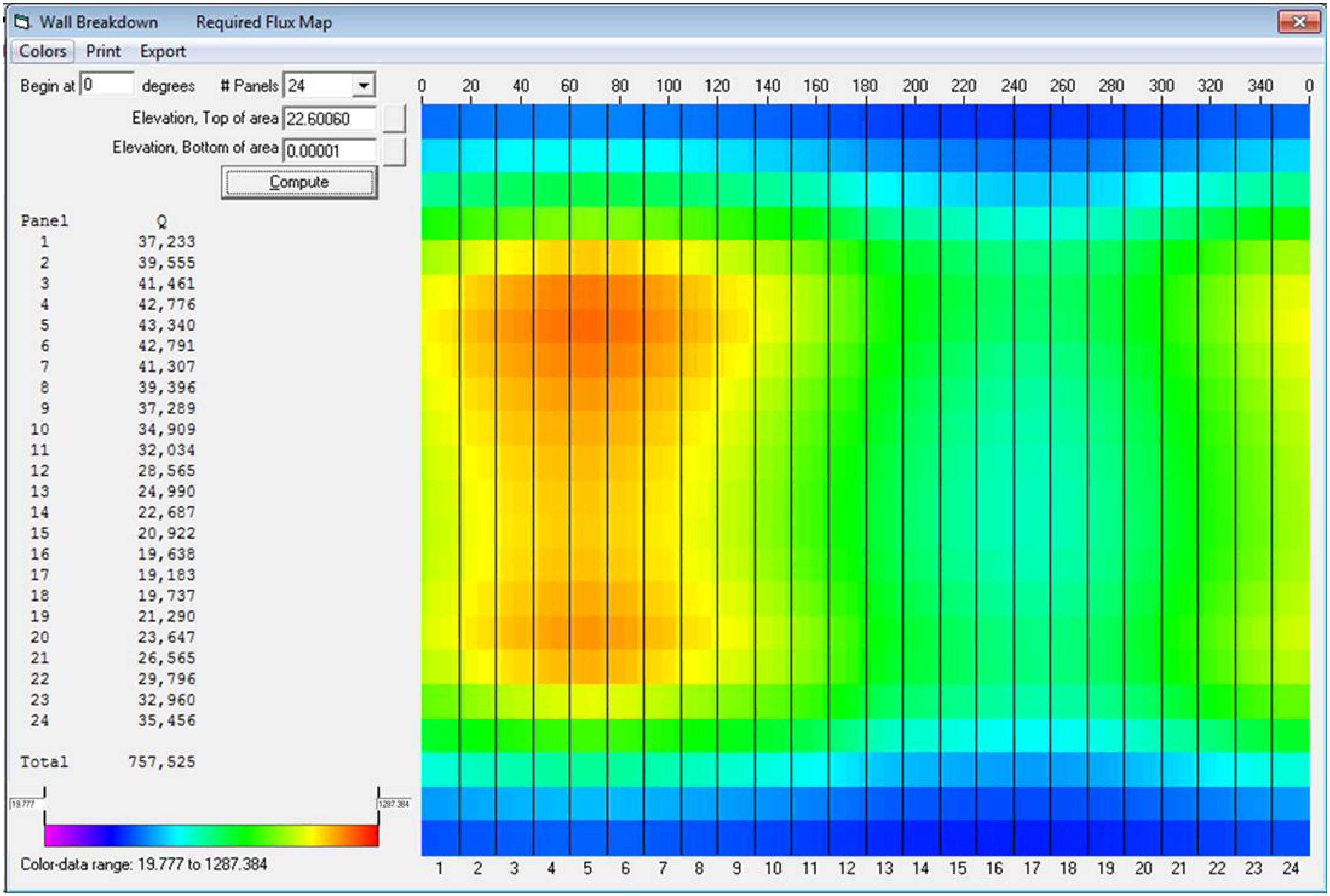

INCIDENT HEAT FLUX DISTRIBUTION – DAY 81 8:30:00

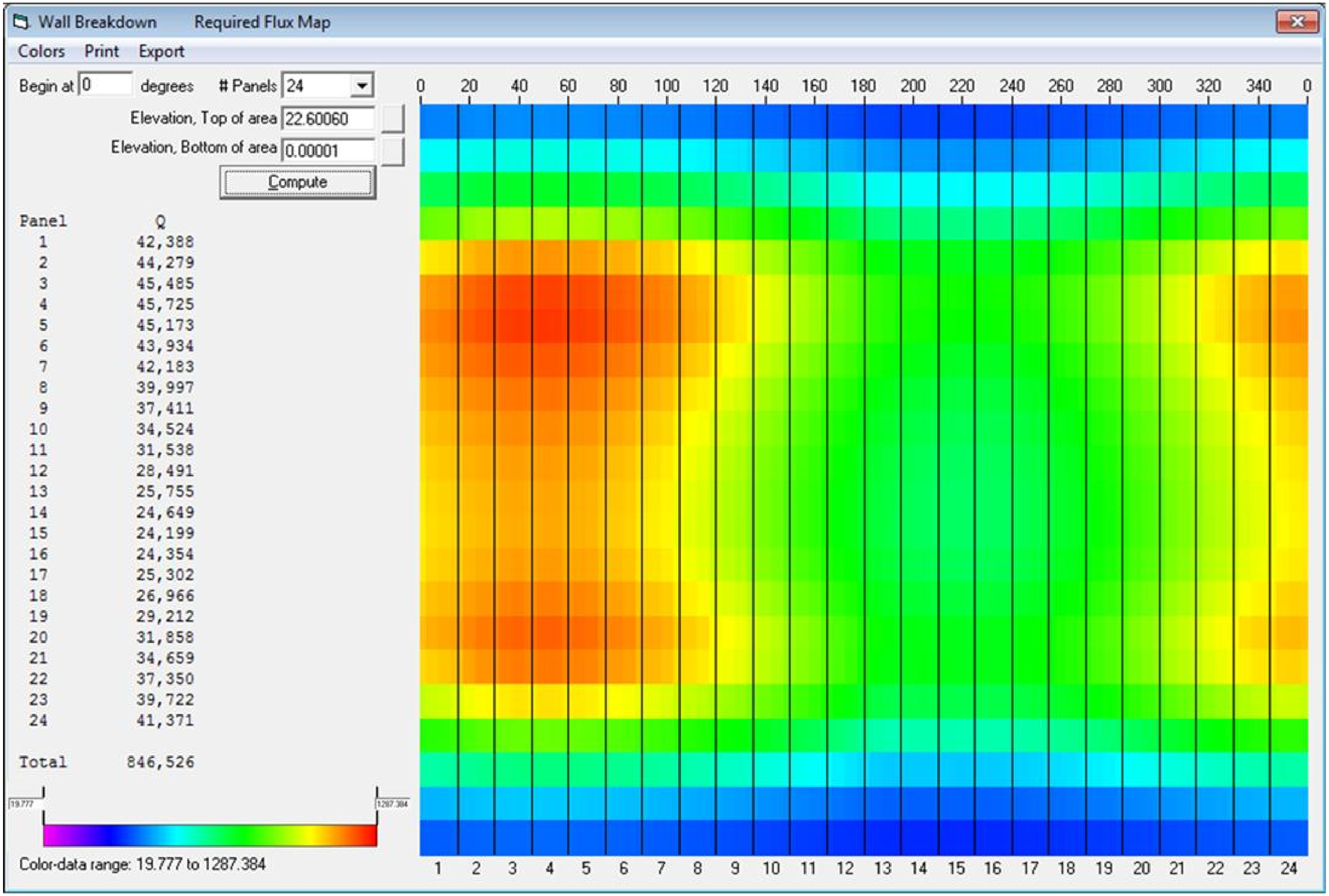

INCIDENT HEAT FLUX DISTRIBUTION – DAY 81 10:00:00

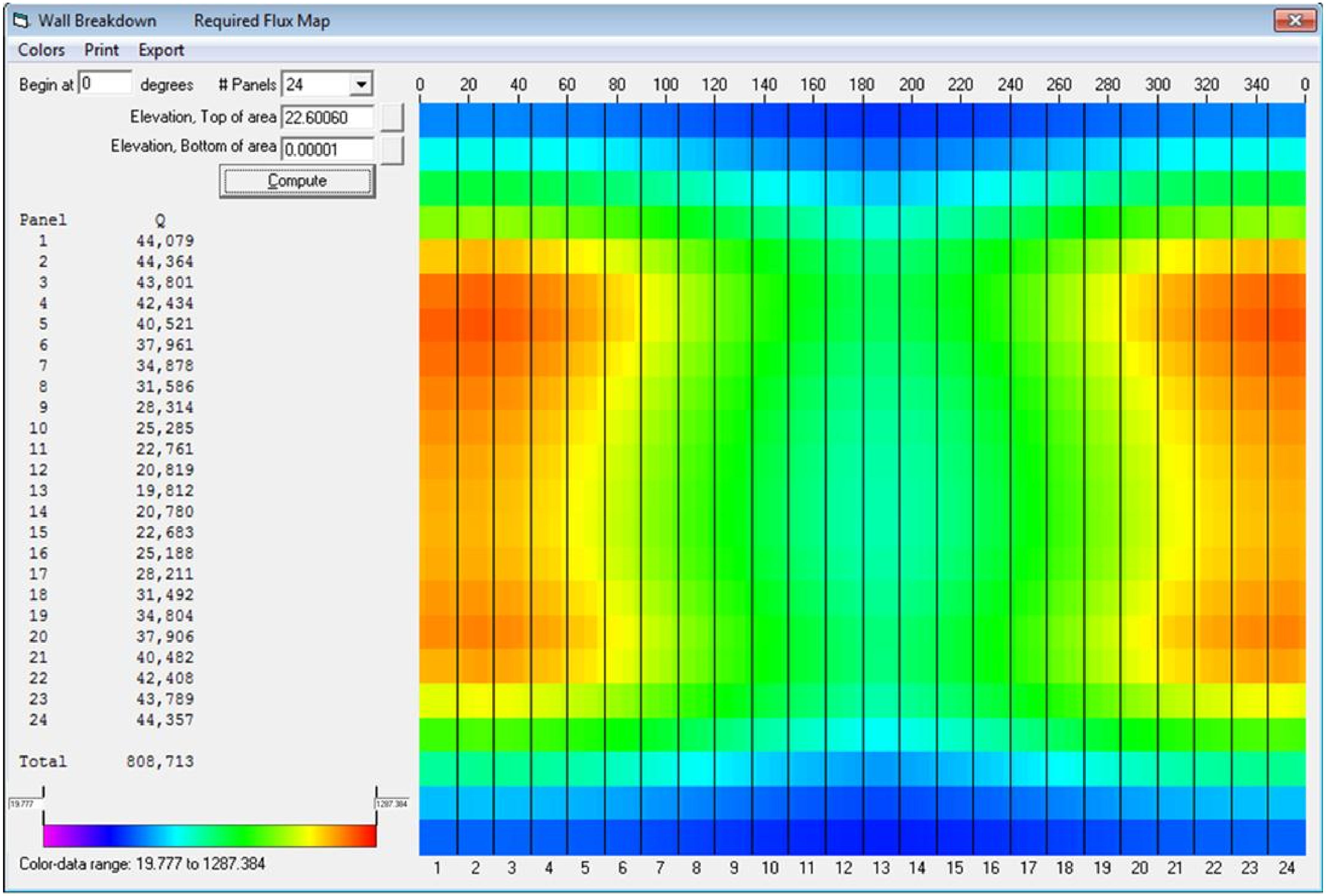

INCIDENT HEAT FLUX DISTRIBUTION – DAY 81 12:00:00

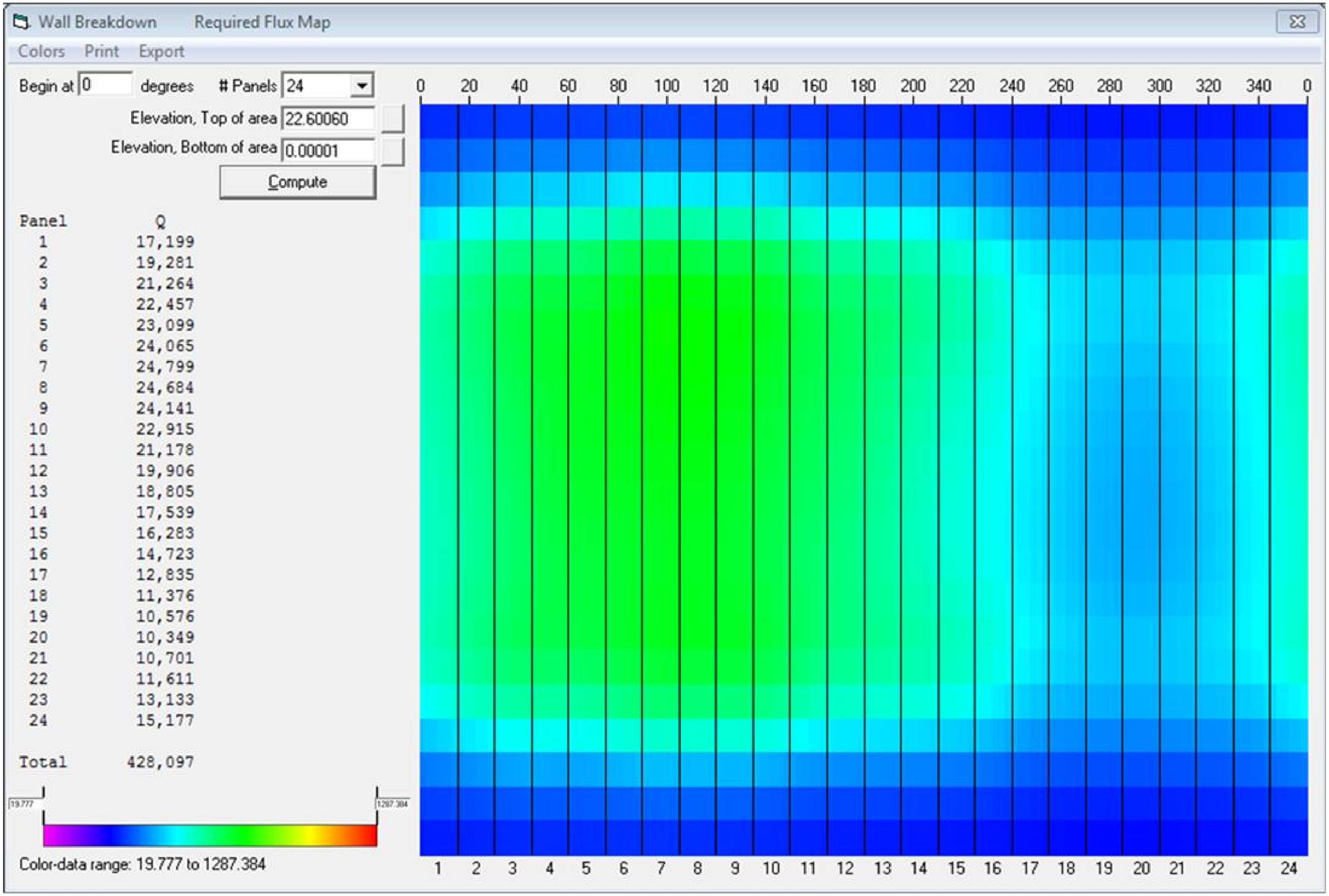

INCIDENT HEAT FLUX DISTRIBUTION – DAY 154 6:00:00

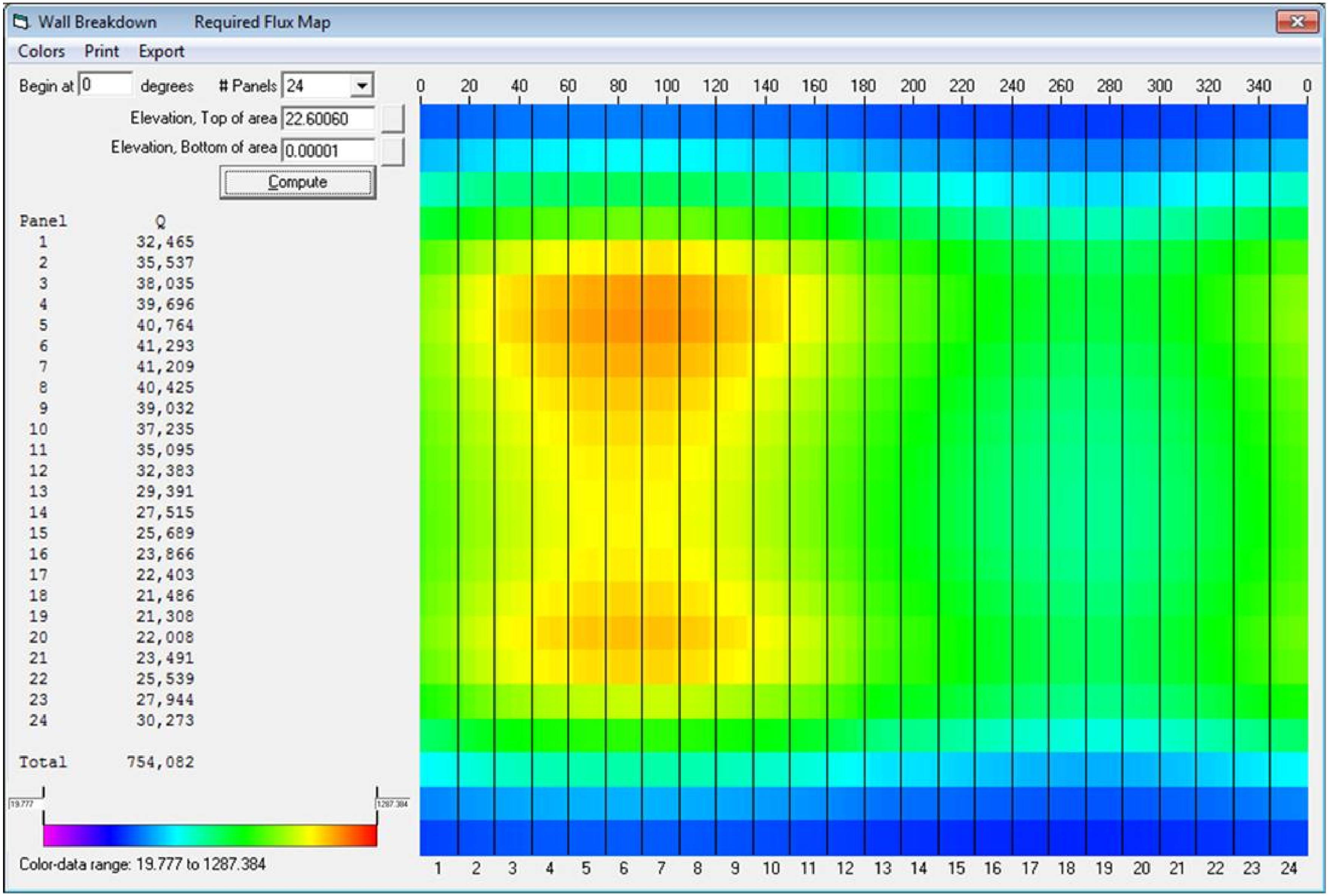

INCIDENT HEAT FLUX DISTRIBUTION – DAY 154 8:00:00

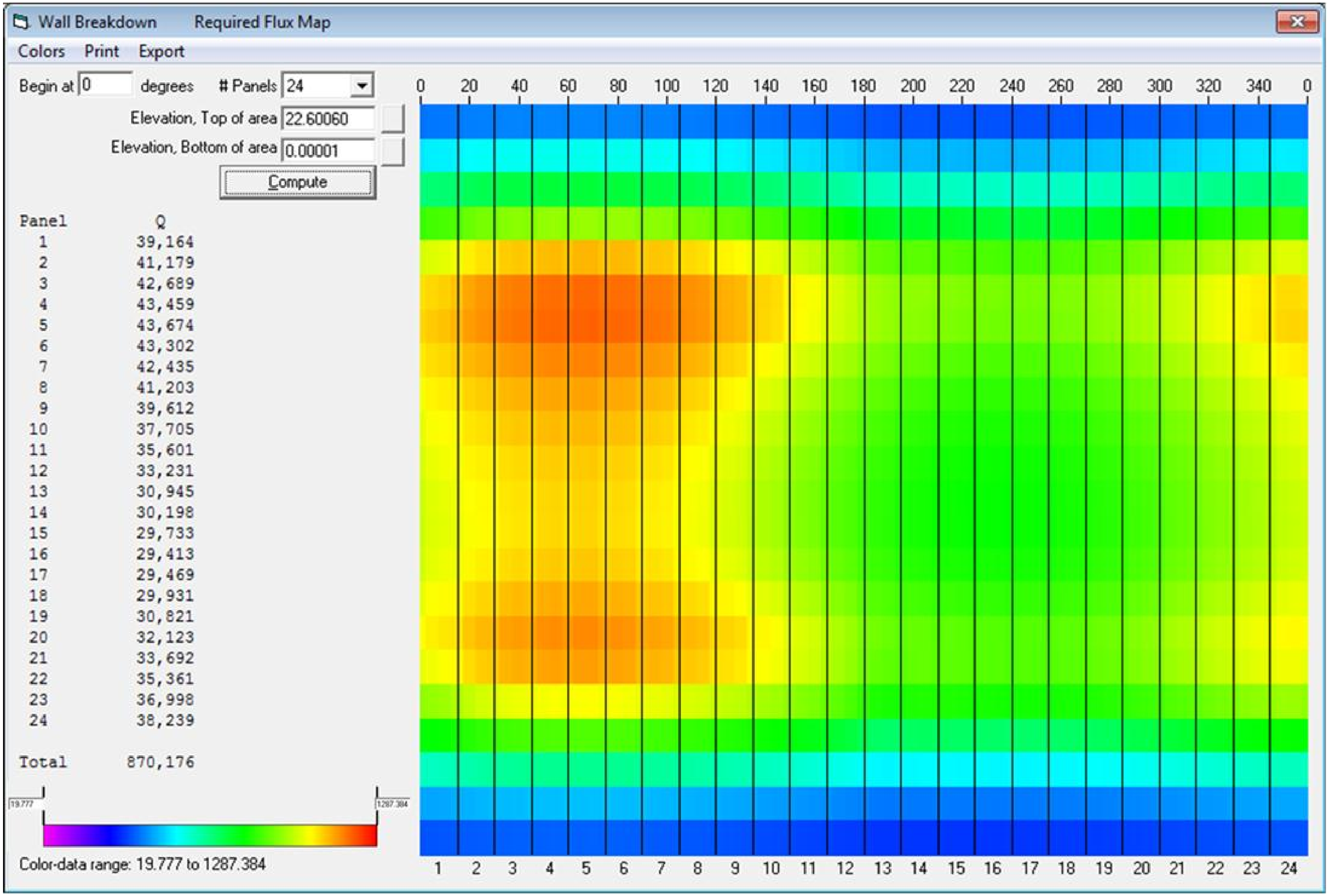

INCIDENT HEAT FLUX DISTRIBUTION – DAY 154 10:00:00

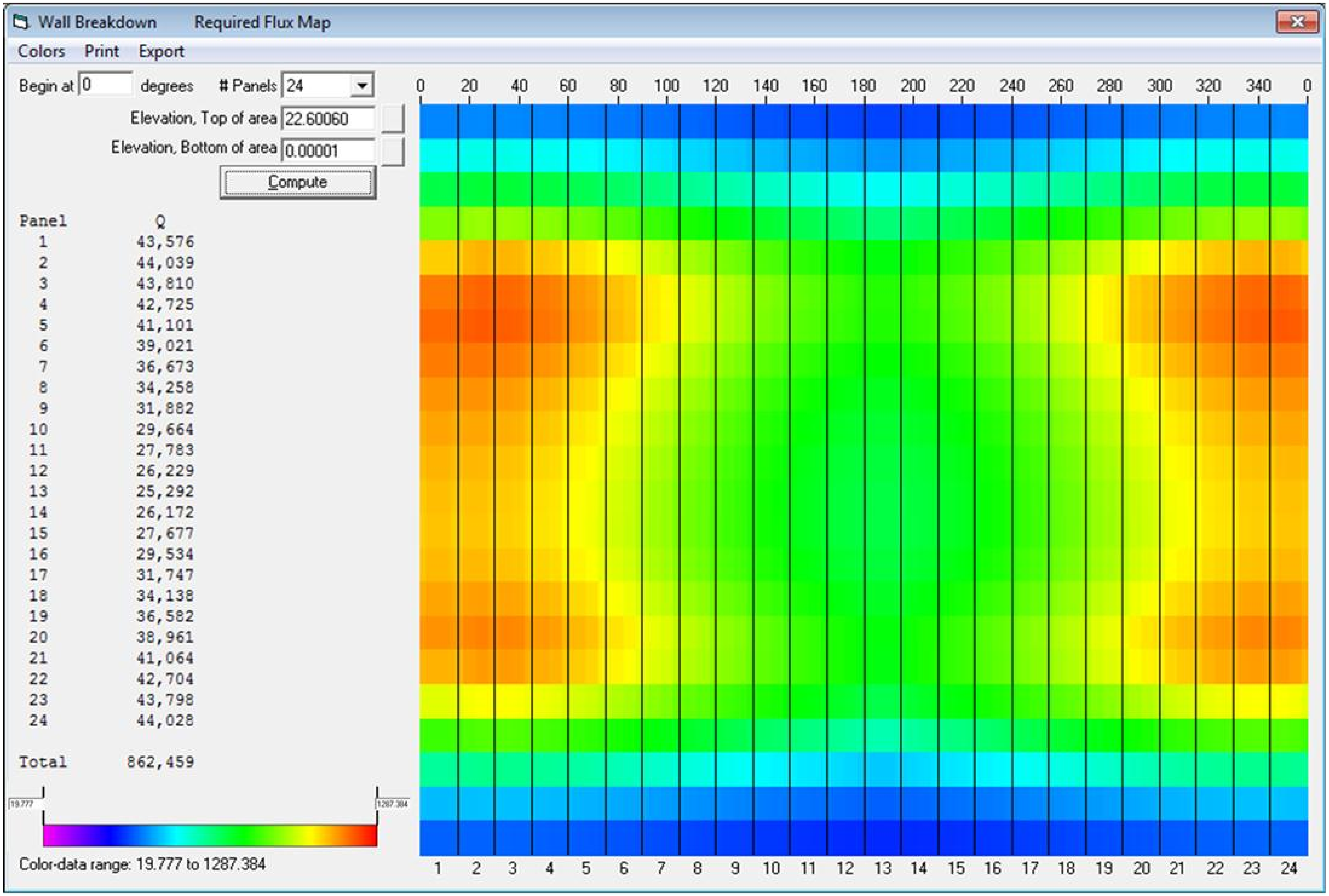

INCIDENT HEAT FLUX DISTRIBUTION – DAY 154 12:00:00

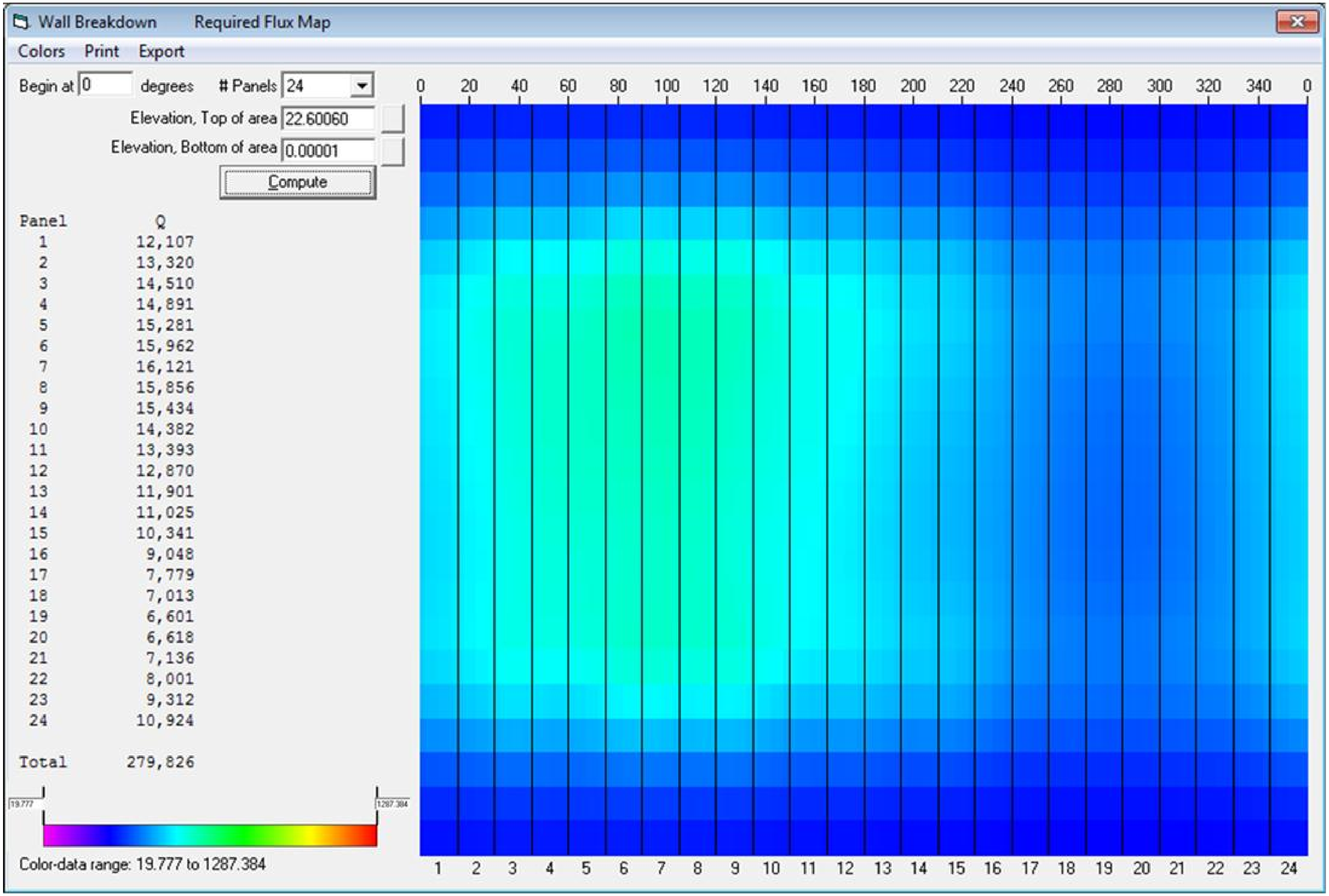

INCIDENT HEAT FLUX DISTRIBUTION – DAY 227 6:00:00

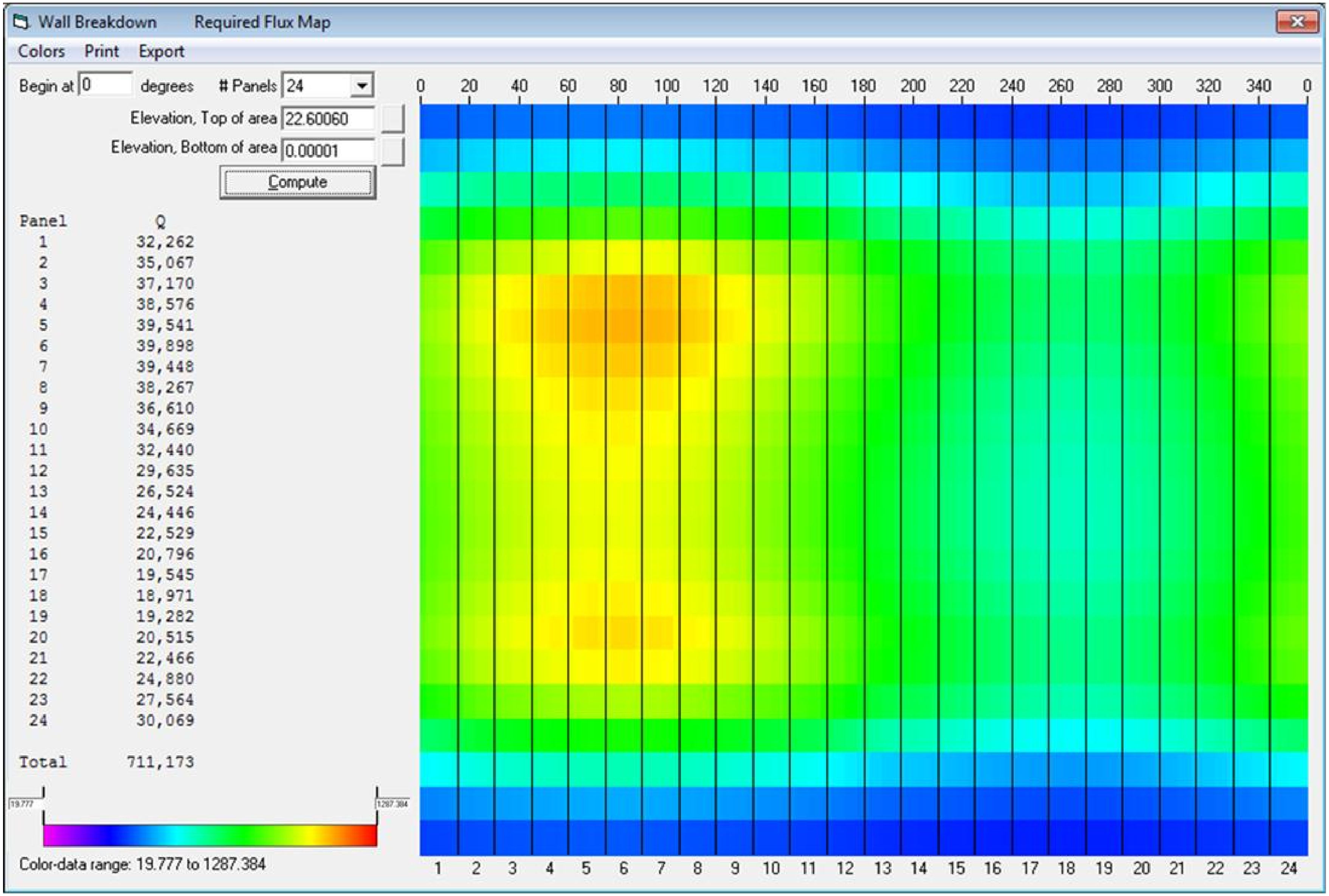

INCIDENT HEAT FLUX DISTRIBUTION – DAY 227 8:00:00

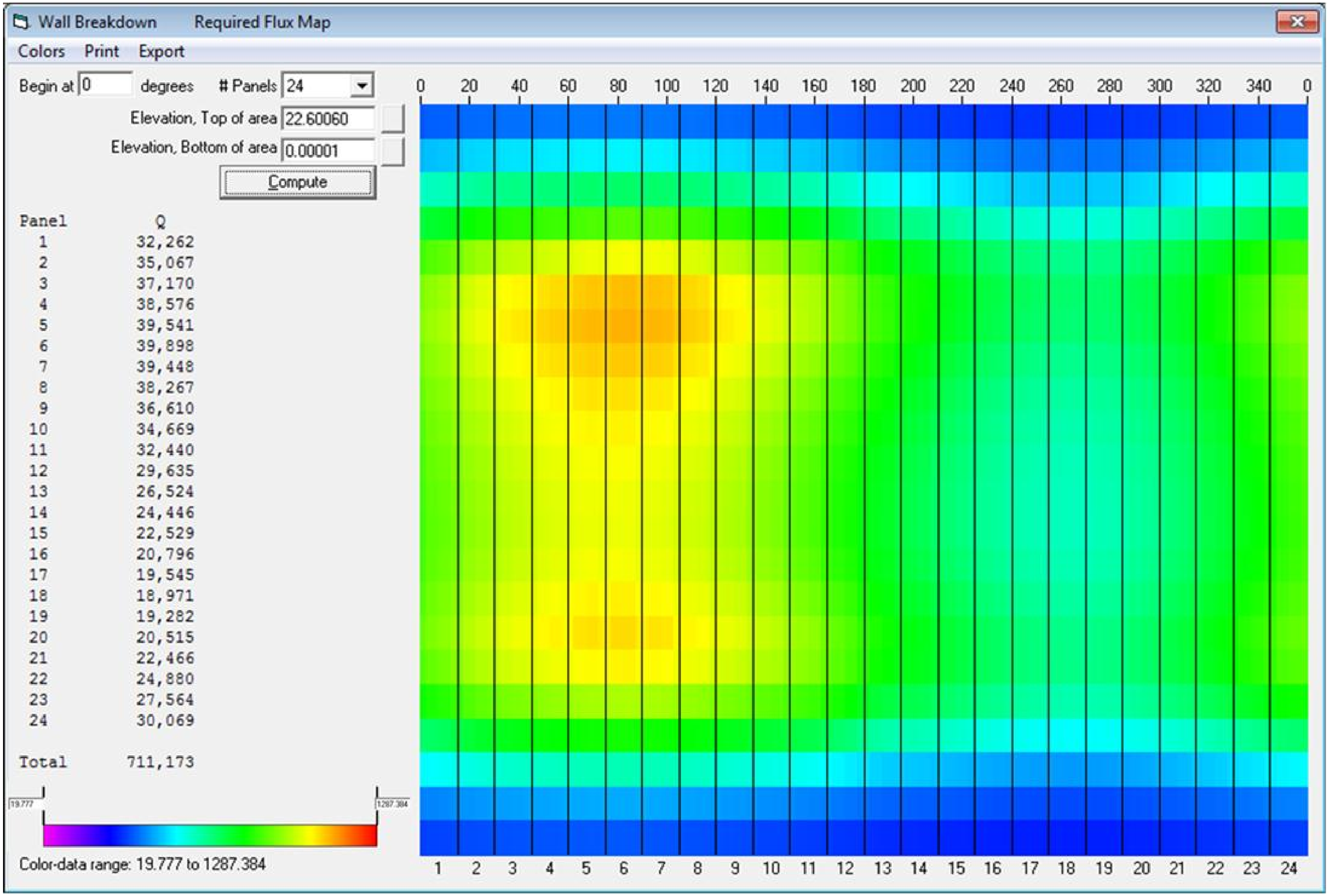

INCIDENT HEAT FLUX DISTRIBUTION – DAY 227 8:00:00

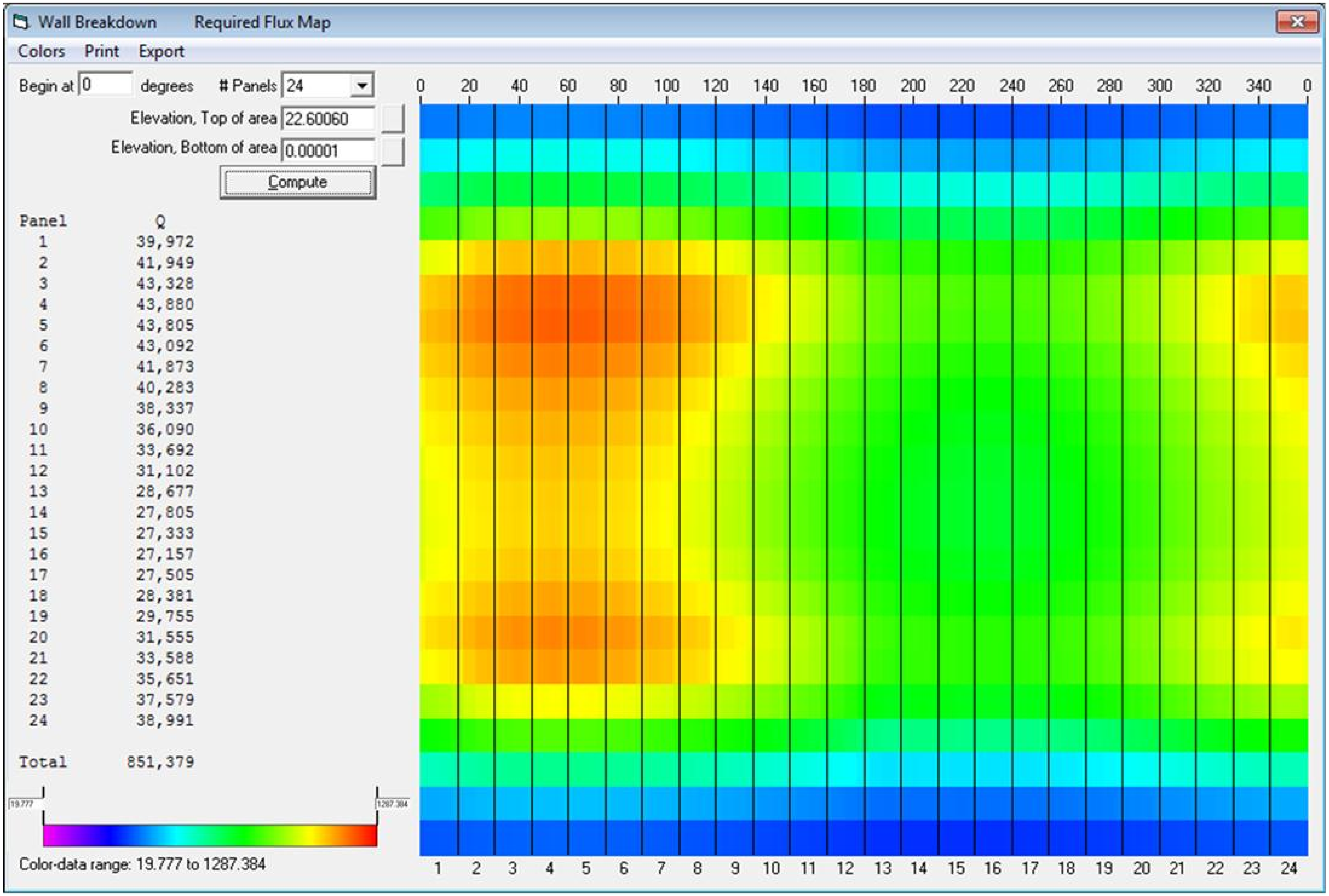

INCIDENT HEAT FLUX DISTRIBUTION – DAY 227 10:00:00

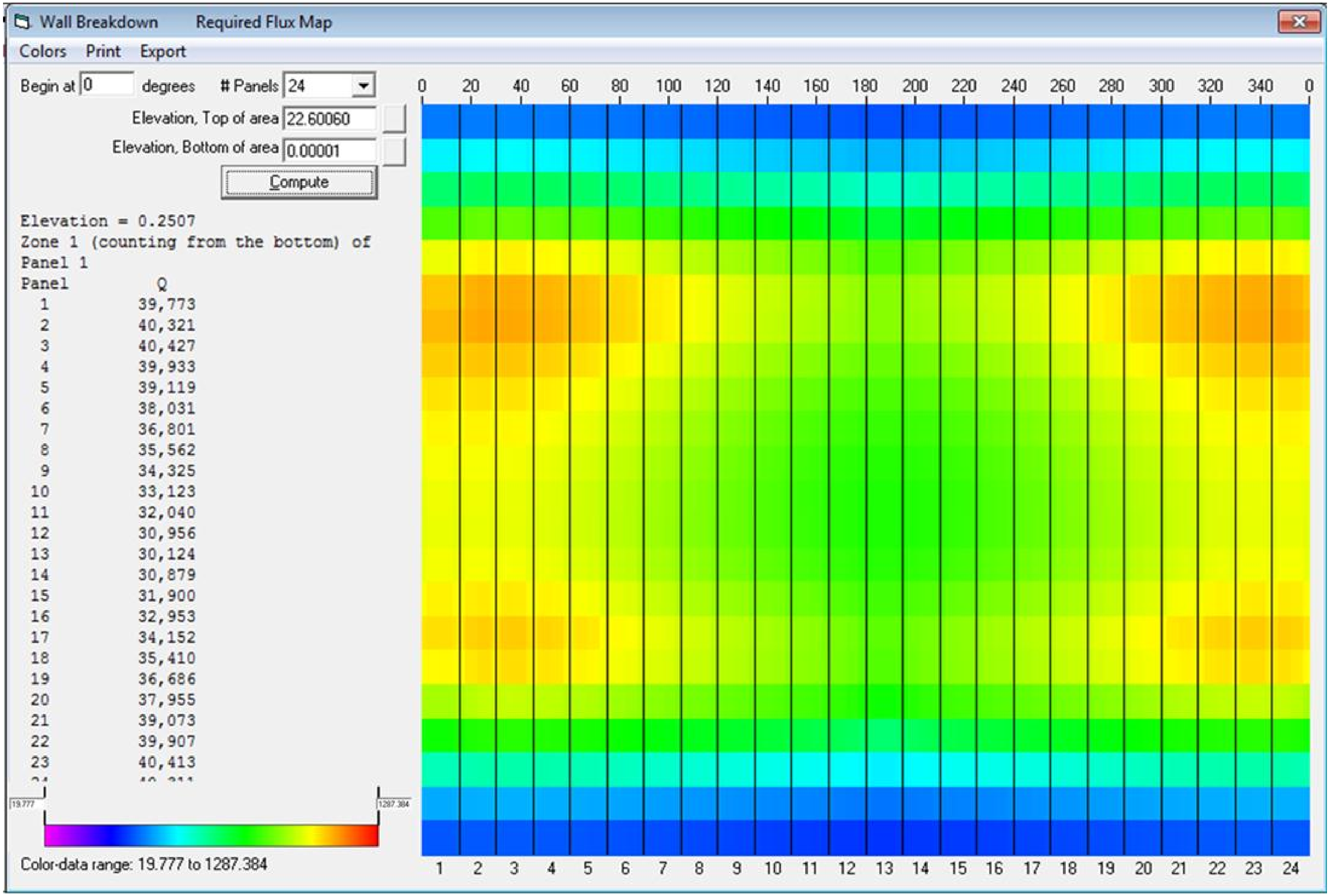

INCIDENT HEAT FLUX DISTRIBUTION – DAY 227 12:00:00

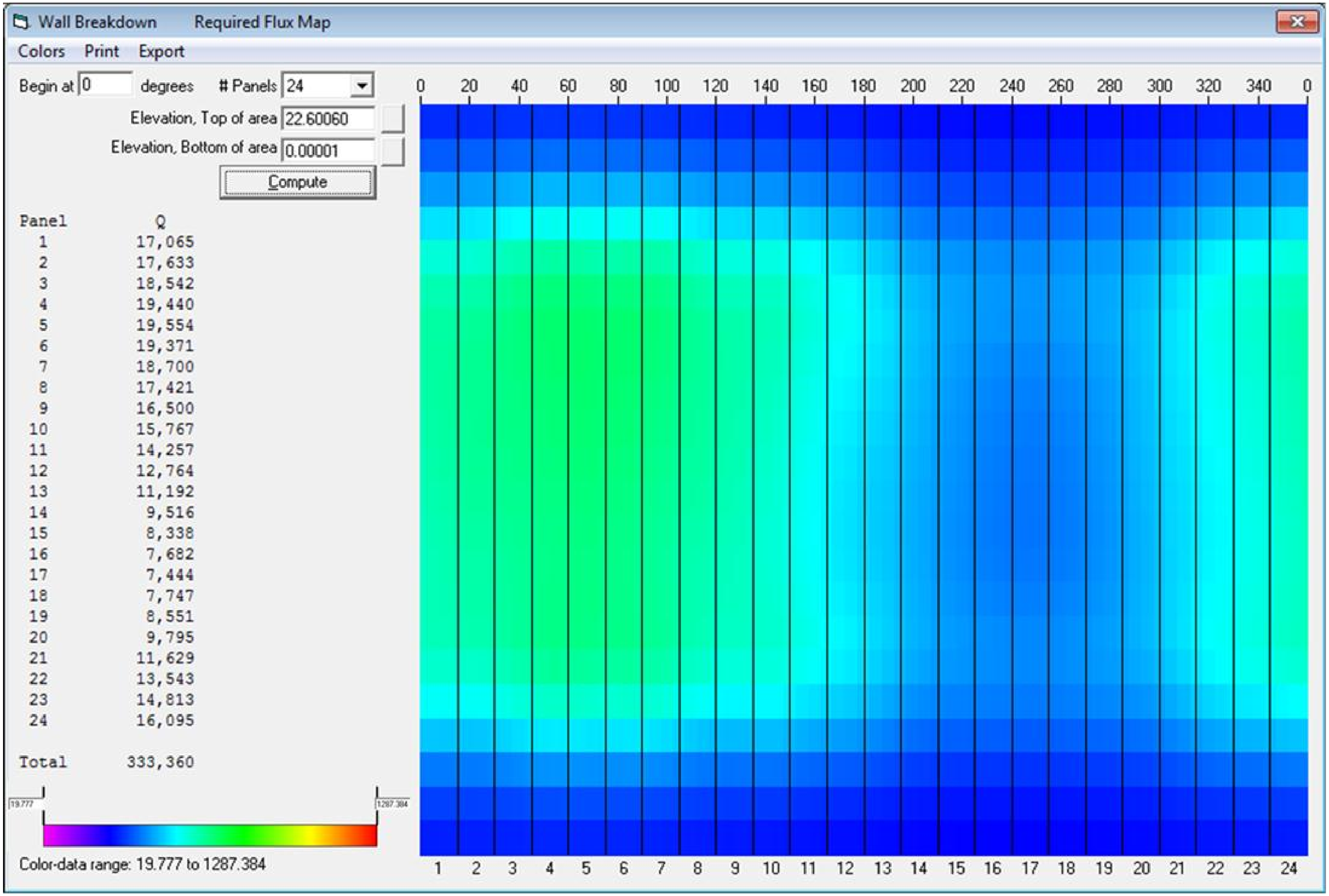

INCIDENT HEAT FLUX DISTRIBUTION – DAY 300 7:30:00

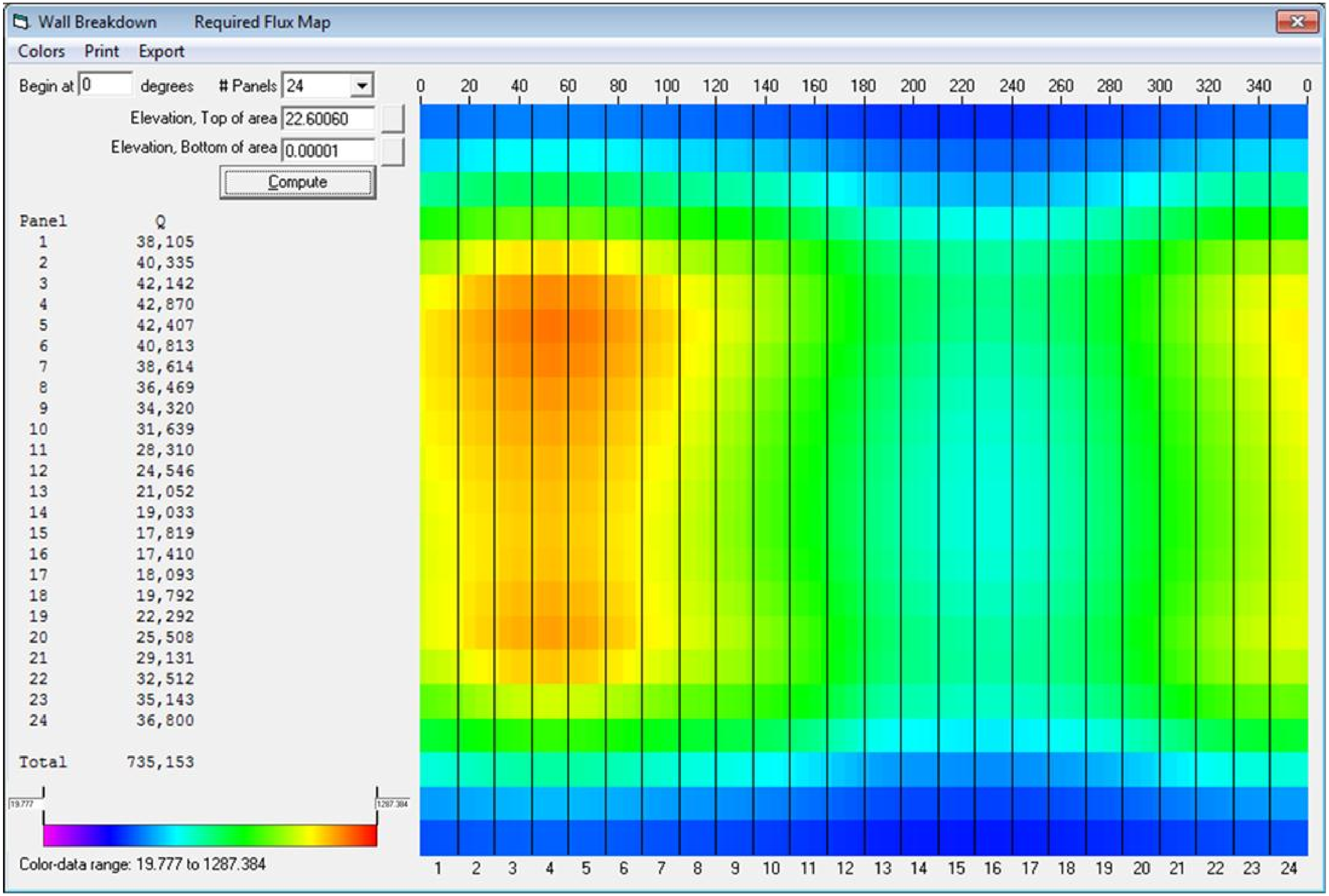

INCIDENT HEAT FLUX DISTRIBUTION – DAY 300 9:00:00

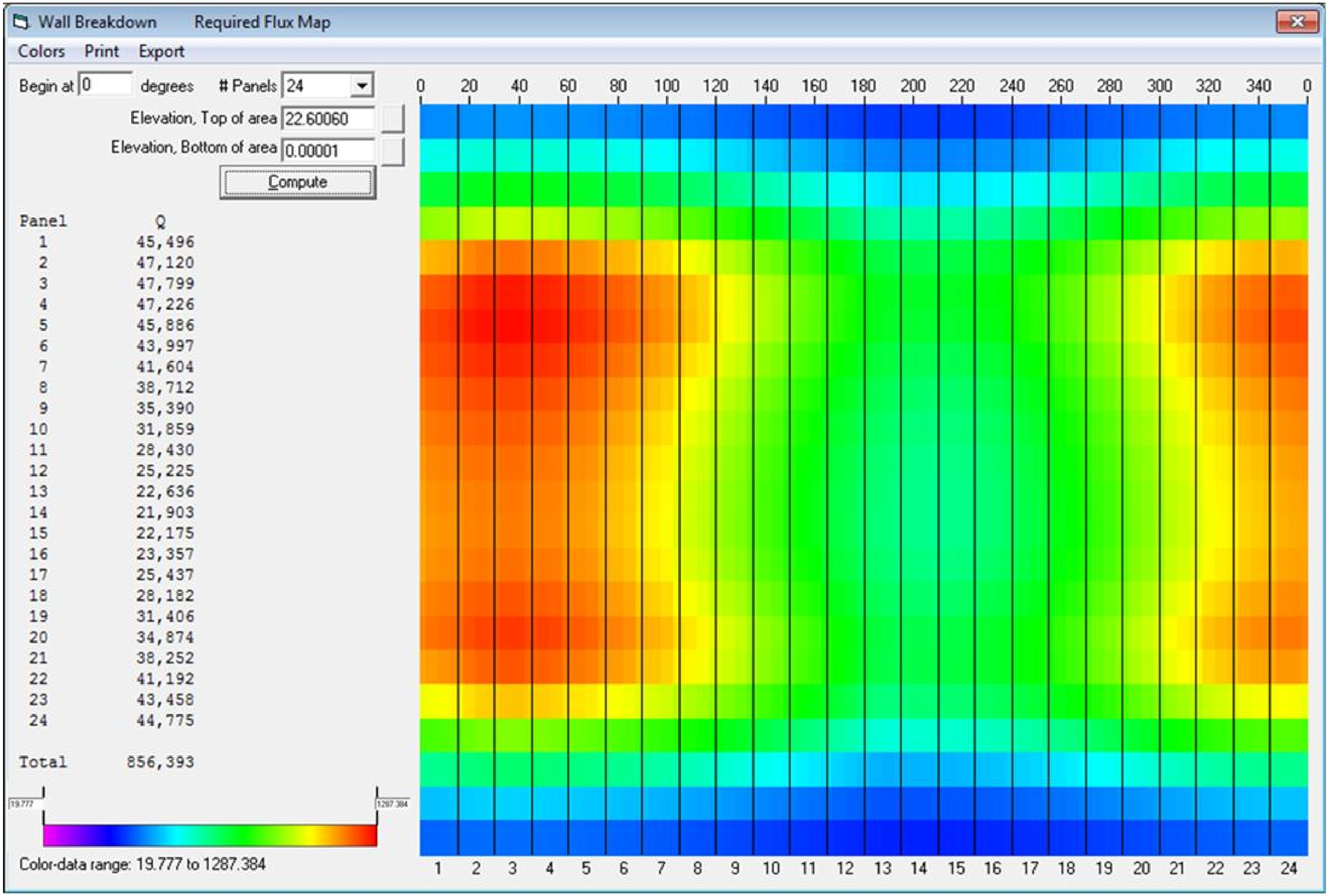

INCIDENT HEAT FLUX DISTRIBUTION – DAY 300 10:30:00

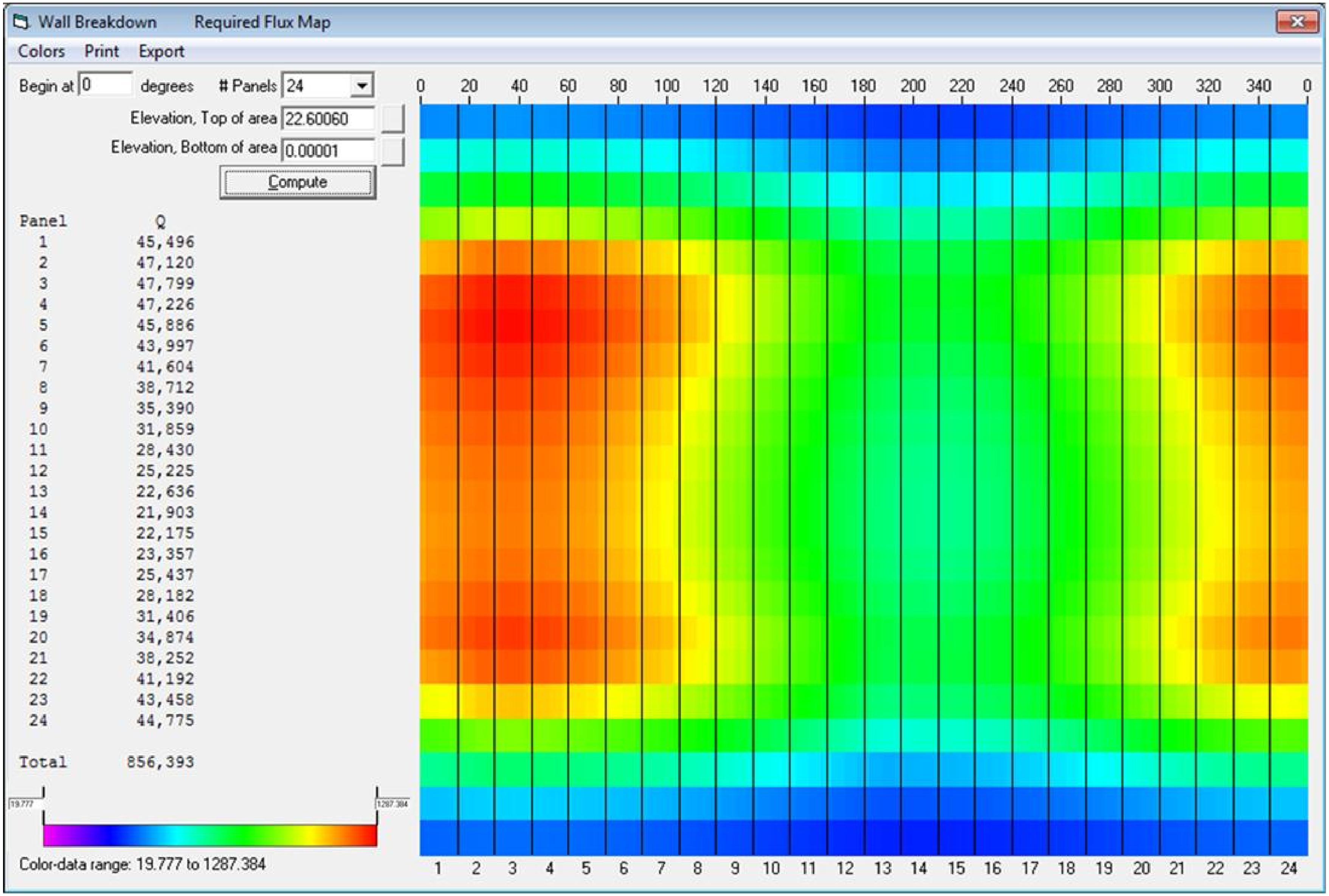

INCIDENT HEAT FLUX DISTRIBUTION – DAY 300 10:30:00

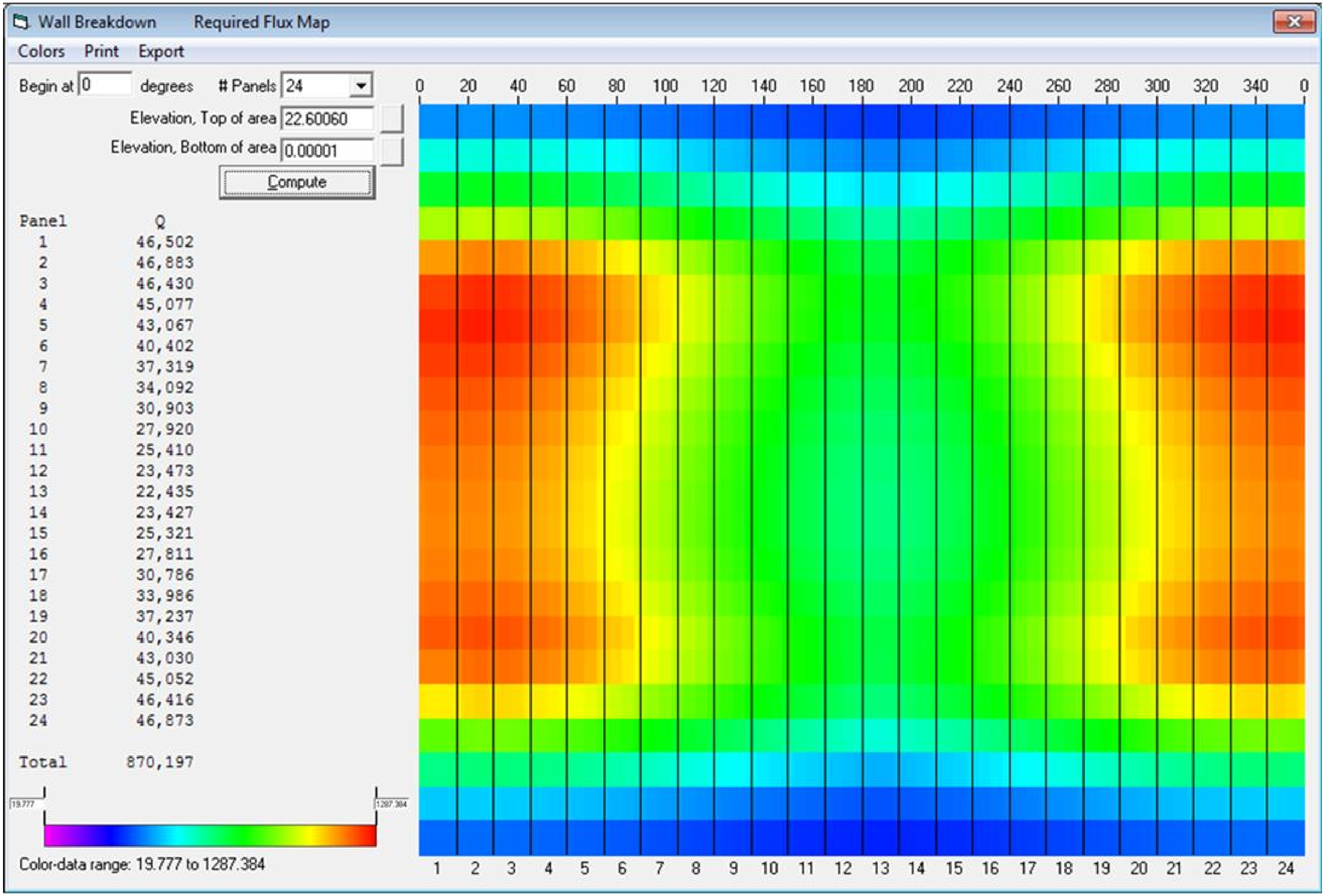

INCIDENT HEAT FLUX DISTRIBUTION – DAY 300 12:00:00

APPENDIX E

Day 8 12:00:00
Incident Heat Flux
&
Calculated Temperatures

Heat Flux Distribution

INCIDENT HEAT FLUX MAP Day of Year: 8 Time of Day: 12:00:00

3/1/2013 Rev E2

	PANEL 1E				PANEL 2E				PANEL 3E				PANEL 4E			
Radial Position (4)	0.0	5.0	10.0	15.0	15.0	20.0	25.0	30.0	30.0	35.0	40.0	45.0	45.0	50.0	55.0	60.0
Elevation (3)																
22.087	201	206	205	201	201	207	208	201	201	205	203	196	196	198	196	188
21.060	379	386	385	379	379	391	392	381	381	387	384	370	370	374	370	356
20.032	610	619	618	611	611	629	631	615	615	623	618	597	597	602	596	576
19.005	880	887	887	880	880	903	906	887	887	895	886	861	861	865	856	831
17.978	1120	1125	1125	1121	1121	1144	1148	1128	1128	1132	1123	1096	1096	1095	1084	1056
16.950	1240	1244	1243	1240	1240	1260	1263	1245	1245	1246	1236	1210	1210	1204	1193	1165
15.923	1272	1276	1276	1272	1272	1286	1287	1272	1272	1269	1260	1236	1236	1228	1216	1189
14.896	1250	1257	1257	1250	1250	1259	1258	1243	1243	1241	1233	1209	1209	1200	1189	1160
13.869	1221	1232	1231	1221	1221	1229	1227	1210	1210	1209	1202	1178	1178	1170	1159	1128
12.841	1199	1210	1210	1199	1199	1206	1203	1186	1186	1186	1179	1154	1154	1146	1135	1103
11.814	1177	1189	1189	1177	1177	1184	1181	1163	1163	1164	1157	1132	1132	1125	1114	1082
10.787	1162	1175	1175	1162	1162	1170	1167	1149	1149	1150	1144	1119	1119	1112	1101	1069
9.759	1155	1168	1167	1155	1155	1163	1161	1142	1142	1144	1138	1112	1112	1107	1096	1064
8.732	1161	1175	1175	1161	1161	1173	1171	1151	1151	1155	1148	1121	1121	1118	1107	1074
7.705	1183	1197	1197	1183	1183	1199	1199	1177	1177	1183	1176	1147	1147	1146	1134	1100
6.677	1201	1212	1212	1201	1201	1221	1223	1202	1202	1209	1199	1170	1170	1170	1158	1125
5.650	1153	1158	1158	1153	1153	1174	1179	1162	1162	1165	1156	1130	1130	1128	1117	1089
4.623	1013	1011	1012	1014	1014	1031	1037	1026	1026	1024	1016	997	997	991	981	962
3.596	789	784	784	790	790	800	806	801	801	795	789	777	777	769	762	750
2.568	506	501	501	506	506	511	514	512	512	507	502	497	497	489	485	479
1.541	280	276	277	280	280	281	282	282	282	278	275	273	273	268	266	263
0.514	156	154	154	156	156	156	156	156	156	153	152	151	151	148	147	145
	(1)	(2)	(2)	(1)												

INCIDENT HEAT FLUX MAP Day of Year: 8 Time of Day: 12:00:00

3/1/2013 Rev E2

	PANEL 5E				PANEL 6E				PANEL 7E				PANEL 8E			
Radial Position (4)	60.0	65.0	70.0	75.0	75.0	80.0	85.0	90.0	90.0	95.0	100.0	105.0	105.0	110.0	115.0	120.0
Elevation (3)																
22.087	188	189	187	178	178	178	175	165	165	164	160	149	149	147	142	132
21.060	356	359	355	340	340	341	336	318	318	316	308	289	289	285	277	258
20.032	576	580	574	552	552	553	544	518	518	514	502	473	473	466	453	425
19.005	831	833	825	797	797	795	782	749	749	740	722	685	685	672	652	616
17.978	1056	1054	1043	1012	1012	1004	988	950	950	933	911	869	869	847	823	781
16.950	1165	1157	1145	1113	1113	1098	1080	1041	1041	1017	994	950	950	922	896	852
15.923	1189	1176	1162	1129	1129	1109	1091	1051	1051	1024	1000	956	956	924	899	855
14.896	1160	1145	1131	1096	1096	1073	1054	1014	1014	985	962	919	919	886	862	819
13.869	1128	1113	1098	1061	1061	1039	1020	978	978	950	928	884	884	852	830	786
12.841	1103	1088	1073	1035	1035	1013	994	952	952	924	904	859	859	828	807	762
11.814	1082	1067	1052	1014	1014	992	973	931	931	904	883	839	839	809	788	743
10.787	1069	1055	1039	1001	1001	980	961	918	918	892	871	827	827	798	777	733
9.759	1064	1050	1035	996	996	976	956	914	914	888	867	823	823	796	774	731
8.732	1074	1064	1048	1008	1008	990	970	926	926	903	881	835	835	810	788	744
7.705	1100	1093	1077	1037	1037	1022	1001	956	956	936	912	865	865	843	819	774
6.677	1125	1121	1106	1067	1067	1055	1034	989	989	970	945	899	899	877	852	806
5.650	1089	1084	1071	1039	1039	1027	1008	969	969	950	926	884	884	862	837	796
4.623	962	955	945	921	921	908	892	862	862	843	821	788	788	766	744	711
3.596	750	742	734	719	719	706	694	674	674	655	639	616	616	595	578	555
2.568	479	472	467	459	459	448	440	428	428	414	403	390	390	375	364	350
1.541	263	257	255	250	250	243	238	232	232	222	217	210	210	200	194	187
0.514	145	141	140	137	137	132	129	125	125	120	116	112	112	106	103	99
	(1)	(2)	(2)	(1)												

INCIDENT HEAT FLUX MAP Day of Year: 8 Time of Day: 12:00:00

3/1/2013 Rev E2

	PANEL 9E				PANEL 10E				PANEL 11E				PANEL 12E			
Radial Position (4)	120.0	125.0	130.0	135.0	135.0	140.0	145.0	150.0	150.0	155.0	160.0	165.0	165.0	170.0	175.0	180.0
Elevation (3)																
22.087	132	129	125	116	116	114	110	102	102	101	98	92	92	91	89	84
21.060	258	254	246	230	230	226	220	205	205	203	198	186	186	186	180	171
20.032	425	417	405	380	380	373	363	342	342	338	330	312	312	310	301	286
19.005	616	602	584	552	552	540	525	498	498	490	478	456	456	450	437	418
17.978	781	758	736	698	698	679	661	630	630	615	601	575	575	564	550	528
16.950	852	824	799	760	760	735	715	682	682	663	646	621	621	606	592	572
15.923	855	823	799	759	759	730	709	676	676	653	637	611	611	595	582	565
14.896	819	786	763	722	722	692	672	637	637	613	597	572	572	556	545	530
13.869	786	754	732	690	690	660	641	605	605	581	566	540	540	525	515	502
12.841	762	731	709	668	668	638	619	584	584	560	545	518	518	504	495	481
11.814	743	713	692	650	650	621	602	566	566	543	528	502	502	488	479	466
10.787	733	704	683	641	641	613	594	559	559	536	521	495	495	481	472	458
9.759	731	702	681	640	640	613	594	558	558	536	521	494	494	481	471	457
8.732	744	718	696	654	654	630	609	573	573	553	537	508	508	496	485	468
7.705	774	750	727	684	684	661	640	603	603	585	568	538	538	527	514	494
6.677	806	784	759	716	716	696	674	637	637	621	604	574	574	563	547	523
5.650	796	773	748	710	710	690	670	637	637	622	605	578	578	567	549	524
4.623	711	687	665	635	635	616	598	573	573	557	543	523	523	510	493	471
3.596	555	534	517	496	496	478	464	447	447	433	422	408	408	395	383	367
2.568	350	335	324	312	312	298	289	279	279	268	261	253	253	244	236	228
1.541	187	177	171	164	164	156	151	145	145	138	134	130	130	124	120	117
0.514	99	93	90	85	85	80	77	74	74	70	67	65	65	62	60	58
	(1)	(2)	(2)	(1)												

INCIDENT HEAT FLUX MAP Day of Year: 8 Time of Day: 12:00:00

3/1/2013 Rev E2

	PANEL 12W				PANEL 11W				PANEL 10W				PANEL 9W			
Radial Position (4)	180.0	185.0	190.0	195.0	195.0	200.0	205.0	210.0	210.0	215.0	220.0	225.0	225.0	230.0	235.0	240.0
Elevation (3)																
22.087	84	85	85	83	83	88	90	91	91	97	100	101	101	109	112	114
21.060	171	172	172	170	170	180	185	185	185	197	202	204	204	218	224	228
20.032	286	288	287	286	286	301	309	311	311	329	336	340	340	362	371	378
19.005	418	418	417	417	417	437	449	455	455	477	488	496	496	524	537	549
17.978	528	525	525	528	528	549	563	574	574	599	613	627	627	659	676	696
16.950	572	567	567	571	571	591	605	619	619	644	660	679	679	712	732	757
15.923	565	560	560	565	565	581	594	610	610	634	650	673	673	706	727	756
14.896	530	527	527	530	530	544	554	570	570	594	610	634	634	668	689	719
13.869	502	500	499	501	501	514	523	538	538	563	578	602	602	637	657	686
12.841	481	480	480	481	481	494	502	516	516	542	557	580	580	615	635	664
11.814	466	465	465	465	465	478	486	500	500	526	541	564	564	599	618	647
10.787	458	457	457	457	457	471	479	493	493	519	534	556	556	591	610	638
9.759	457	456	456	456	456	470	479	492	492	519	534	556	556	591	611	637
8.732	468	468	468	468	468	485	495	507	507	535	551	571	571	607	627	652
7.705	494	493	493	493	493	514	526	537	537	567	584	601	601	639	660	682
6.677	523	521	521	523	523	547	562	573	573	603	620	636	636	673	695	715
5.650	524	518	518	524	524	549	567	578	578	605	621	637	637	669	690	709
4.623	471	461	462	471	471	493	510	522	522	543	557	572	572	597	616	635
3.596	367	356	357	367	367	382	396	408	408	421	432	446	446	463	478	495
2.568	228	220	220	228	228	236	244	253	253	261	268	279	279	288	298	311
1.541	117	112	112	117	117	120	124	130	130	133	138	145	145	150	155	164
0.514	58	56	56	58	58	59	61	65	65	67	69	73	73	77	80	85
	(1)	(2)	(2)	(1)												

INCIDENT HEAT FLUX MAP Day of Year: 8 Time of Day: 12:00:00

3/1/2013 Rev E2

	PANEL 8W				PANEL 7W				PANEL 6W				PANEL 5W			
Radial Position (4)	240.0	245.0	250.0	255.0	255.0	260.0	265.0	270.0	270.0	275.0	280.0	285.0	285.0	290.0	295.0	300.0
Elevation (3)																
22.087	114	124	128	130	130	141	145	147	147	158	162	164	164	174	177	177
21.060	228	245	252	256	256	275	283	287	287	307	314	316	316	334	339	338
20.032	378	403	414	423	423	451	464	471	471	500	512	516	516	543	551	550
19.005	549	582	599	614	614	650	669	683	683	721	737	747	747	781	792	795
17.978	696	733	755	778	778	820	844	866	866	909	930	948	948	986	1001	1010
16.950	757	796	820	849	849	893	919	947	947	991	1015	1039	1039	1078	1096	1111
15.923	756	796	820	852	852	896	921	953	953	997	1021	1048	1048	1088	1107	1127
14.896	719	759	782	815	815	859	882	915	915	959	982	1011	1011	1052	1071	1094
13.869	686	728	750	782	782	826	849	880	880	925	947	975	975	1017	1036	1059
12.841	664	706	727	758	758	803	825	856	856	901	922	950	950	992	1011	1034
11.814	647	688	709	740	740	784	805	836	836	881	901	928	928	971	990	1012
10.787	638	680	701	730	730	774	795	825	825	869	890	917	917	959	978	1000
9.759	637	678	700	728	728	772	793	821	821	865	886	912	912	955	975	995
8.732	652	694	716	742	742	787	809	834	834	879	901	925	925	969	989	1008
7.705	682	725	748	772	772	818	842	864	864	911	935	955	955	1001	1022	1037
6.677	715	758	783	805	805	851	877	898	898	945	970	989	989	1034	1055	1067
5.650	709	748	772	795	795	837	862	884	884	925	950	969	969	1008	1028	1039
4.623	635	665	687	710	710	743	766	788	788	821	843	863	863	892	909	921
3.596	495	516	534	555	555	578	595	616	616	638	656	674	674	694	707	719
2.568	311	323	335	350	350	363	375	390	390	403	414	428	428	439	448	459
1.541	164	170	177	186	186	193	200	209	209	216	222	232	232	237	243	250
0.514	85	89	92	98	98	102	106	112	112	116	119	125	125	129	132	136
	(1)	(2)	(2)	(1)												

INCIDENT HEAT FLUX MAP Day of Year: 8 Time of Day: 12:00:00

3/1/2013 Rev E2

	PANEL 4W				PANEL 3W				PANEL 2W				PANEL 1W			
Radial Position (4)	300.0	305.0	310.0	315.0	315.0	320.0	325.0	330.0	330.0	335.0	340.0	345.0	345.0	350.0	355.0	360.0
Elevation (3)																
22.087	177	186	188	187	187	195	197	195	195	203	204	201	201	208	207	201
21.060	338	355	357	355	355	370	373	369	369	384	386	380	380	392	391	379
20.032	550	573	578	574	574	596	601	596	596	618	622	615	615	632	629	610
19.005	795	824	831	829	829	856	863	861	861	887	894	887	887	907	902	880
17.978	1010	1042	1051	1055	1055	1084	1093	1095	1095	1123	1132	1128	1128	1148	1143	1120
16.950	1111	1143	1155	1164	1164	1193	1203	1209	1209	1236	1245	1245	1245	1263	1260	1240
15.923	1127	1161	1174	1187	1187	1215	1227	1235	1235	1260	1269	1271	1271	1287	1286	1272
14.896	1094	1129	1143	1159	1159	1188	1199	1208	1208	1232	1240	1242	1242	1258	1259	1250
13.869	1059	1096	1111	1127	1127	1158	1168	1177	1177	1202	1209	1210	1210	1227	1229	1221
12.841	1034	1072	1087	1102	1102	1134	1145	1153	1153	1179	1185	1185	1185	1203	1206	1199
11.814	1012	1051	1066	1081	1081	1113	1124	1131	1131	1156	1163	1163	1163	1181	1184	1177
10.787	1000	1039	1054	1068	1068	1101	1111	1118	1118	1143	1150	1149	1149	1167	1170	1162
9.759	995	1034	1050	1063	1063	1095	1106	1112	1112	1138	1144	1142	1142	1161	1163	1155
8.732	1008	1047	1063	1074	1074	1107	1118	1121	1121	1149	1155	1151	1151	1171	1173	1161
7.705	1037	1077	1093	1100	1100	1134	1146	1147	1147	1176	1184	1177	1177	1199	1199	1183
6.677	1067	1106	1120	1125	1125	1159	1170	1170	1170	1200	1209	1202	1202	1223	1221	1201
5.650	1039	1071	1084	1089	1089	1117	1128	1130	1130	1156	1166	1163	1163	1179	1174	1153
4.623	921	944	955	962	962	981	991	997	997	1016	1025	1026	1026	1037	1031	1013
3.596	719	734	742	750	750	761	770	777	777	789	796	801	801	806	801	789
2.568	459	466	472	479	479	485	490	497	497	502	507	513	513	513	511	506
1.541	250	254	257	263	263	265	268	273	273	275	278	282	282	282	281	280
0.514	136	139	141	145	145	146	148	151	151	152	153	155	155	156	156	156
	(1)	(2)	(2)	(1)												

NOTES:

(1) Incident heat flux at panel edge (kw/m2)

(2) Incident heat flux at third points across panel width (kw/m2)

(3) Node mid point elevation (m)

(4) Flux point radial position from North (degrees)

Diameter	m	17.4
Perimeter	m	54.664
Perimeter (USE)	m	55.0
Half Perimeter	m	27.481
Panels		24
Nodes High		22
Height	m	22.6
Node Height	m	1.0273
Node Height (USE)	m	1.0273
Height (USE)	m	22.601
Outer Angle		5.00
Inner Angle		5.00

Molten Salt Bulk Fluid Temperatures

Node Width (4)	0.3680	0.7770	0.7770	0.3680	0.3680	0.7770	0.7770	0.3680	0.3680	0.7770	0.7770	0.3680	0.3680	0.7770	0.7770	0.3680
22.087	309	309	309	309	309	309	309	309	442	442	442	441	439	438	438	436
21.060	310	310	310	310	310	310	310	310	442	442	441	440	438	438	437	435
20.032	312	312	312	312	312	312	312	312	441	441	440	439	437	437	436	434
19.005	315	315	315	315	315	315	315	315	439	439	438	437	435	435	434	433
17.978	319	319	319	319	318	319	319	318	436	436	435	434	432	432	431	430
16.950	323	323	323	323	322	323	323	323	432	432	432	430	429	428	428	426
15.923	327	327	327	327	327	327	327	327	428	428	428	426	425	424	424	423
14.896	331	331	331	331	331	331	331	331	424	424	423	422	421	420	420	419
13.869	335	335	335	335	335	335	335	335	420	420	419	418	417	417	416	415
12.841	339	339	339	339	339	339	339	339	416	416	415	415	413	413	412	411
11.814	343	343	343	343	343	343	343	342	412	412	411	411	409	409	409	408
10.787	347	347	347	347	346	347	347	346	408	408	408	407	406	405	405	404
9.759	351	351	351	351	350	351	351	350	404	404	404	403	402	402	402	401
8.732	355	355	355	355	354	355	355	354	400	400	400	400	398	398	398	397
7.705	359	359	359	359	358	358	358	358	397	397	396	396	395	395	394	394
6.677	363	363	363	363	362	362	362	362	393	393	392	392	391	391	391	390
5.650	366	367	367	366	365	366	366	365	389	389	389	388	387	387	387	387
4.623	370	370	370	370	369	370	370	369	385	385	385	385	384	383	383	383
3.596	372	373	373	372	371	372	372	371	381	381	381	381	380	380	380	380
2.568	374	375	375	374	373	374	374	373	379	379	379	379	378	378	378	378
1.541	375	375	375	375	374	375	375	374	377	377	377	377	376	376	376	376
0.514	375	376	376	375	374	375	375	374	376	376	376	376	375	375	375	375
Elevation (3)	PANEL 1E				PANEL 2E				PANEL 3E				PANEL 4E			
Avg Temp (°C)	344	344	344	344	343	344	344	343	410	410	410	409	408	407	407	406
Max Temp (°C)	375	376	376	375	374	375	375	374	442	442	442	441	439	438	438	436
Panel Avg Temp (°C)	344				344				410				407			
Panel Max Temp (°C)	376				375				442				439			
	(1)	(2)	(2)	(1)												

Node Width (4)	0.3680	0.7770	0.7770	0.3680	0.3680	0.7770	0.7770	0.3680	0.3680	0.7770	0.7770	0.3680	0.3680	0.7770	0.7770	0.3680
22.087	443	443	443	443	438	438	438	438	533	532	531	529	540	539	538	535
21.060	444	444	444	444	439	439	439	439	533	532	530	528	540	538	537	535
20.032	446	446	446	445	441	441	441	441	532	531	530	527	539	538	536	534
19.005	448	448	448	448	444	444	444	443	530	529	528	526	538	536	535	533
17.978	452	452	452	451	447	447	447	446	528	527	526	524	536	534	533	531
16.950	455	455	455	455	450	450	450	450	525	524	523	521	533	532	531	529
15.923	459	459	459	459	454	454	454	453	522	521	520	518	530	529	528	526
14.896	463	463	463	462	458	457	457	456	519	518	517	515	527	526	525	523
13.869	467	467	466	466	461	461	460	459	516	515	514	512	524	523	522	521
12.841	470	470	470	469	464	464	463	462	513	512	511	510	521	520	520	518
11.814	474	474	473	472	468	467	467	465	510	509	508	507	519	518	517	516
10.787	477	477	477	476	471	470	470	468	507	506	505	504	516	515	515	513
9.759	481	481	480	479	474	473	473	471	504	503	503	502	513	513	512	511
8.732	484	484	483	482	477	477	476	474	501	501	500	499	511	510	510	509
7.705	488	488	487	485	480	480	479	477	498	498	497	497	508	508	507	506
6.677	492	491	491	489	484	483	482	480	495	495	494	494	505	505	505	504
5.650	495	495	494	492	487	486	486	483	492	492	491	491	502	502	502	501
4.623	498	498	497	495	490	489	488	486	489	489	489	488	500	499	499	499
3.596	501	500	499	498	492	492	491	488	486	486	486	486	497	497	497	497
2.568	502	502	501	499	494	493	492	490	484	484	484	484	495	495	495	495
1.541	503	502	502	500	495	494	493	490	483	483	483	483	494	494	494	494
0.514	503	503	502	500	495	494	493	491	482	482	482	482	493	493	493	493
Elevation (3)	PANEL 5E				PANEL 6E				PANEL 7E				PANEL 8E			
Avg Temp (°C)	475	475	474	473	468	468	467	466	508	508	507	506	517	517	516	515
Max Temp (°C)	503	503	502	500	495	494	493	491	533	532	531	529	540	539	538	535
Panel Avg Temp (°C)	474				467				507				516			
Panel Max Temp (°C)	503				495				533				540			
	(1)	(2)	(2)	(1)												

Node Width (4)	0.3680	0.7770	0.7770	0.3680	0.3680	0.7770	0.7770	0.3680	0.3680	0.7770	0.7770	0.3680	0.3680	0.7770	0.7770	0.3680
22.087	532	532	532	532	538	538	538	538	602	600	600	598	601	600	600	599
21.060	532	532	532	532	539	539	539	539	601	600	599	598	601	600	600	598
20.032	534	534	534	533	540	540	540	540	601	600	599	598	600	600	599	598
19.005	535	535	535	535	542	542	541	541	600	599	598	597	600	599	598	597
17.978	538	538	537	537	544	544	544	543	598	597	597	595	598	598	597	596
16.950	540	540	540	539	546	546	546	545	597	596	595	594	597	596	595	594
15.923	543	543	542	542	549	548	548	547	594	594	593	592	595	594	593	593
14.896	546	545	545	544	551	550	550	549	592	592	591	590	593	592	592	591
13.869	548	547	547	546	553	553	552	551	591	590	589	588	591	591	590	589
12.841	550	550	549	548	555	554	554	553	589	588	587	587	589	589	589	588
11.814	553	552	551	550	557	556	556	555	587	586	586	585	588	587	587	586
10.787	555	554	553	552	559	558	558	557	585	585	584	584	586	586	586	585
9.759	557	556	555	554	561	560	560	558	584	583	583	582	585	584	584	584
8.732	559	558	558	556	563	562	561	560	582	581	581	581	583	583	583	582
7.705	562	561	560	558	565	564	563	562	580	580	580	579	582	582	581	581
6.677	564	563	562	560	567	566	565	564	578	578	578	577	580	580	580	579
5.650	567	565	564	562	570	568	568	566	576	576	576	576	578	578	578	578
4.623	569	568	566	564	572	570	569	568	574	574	574	574	577	576	576	576
3.596	571	569	568	566	573	572	571	569	573	573	573	572	575	575	575	575
2.568	572	570	569	567	574	573	572	570	571	571	571	571	574	574	574	574
1.541	572	571	569	567	574	573	572	570	571	571	571	571	573	573	573	573
0.514	572	571	570	567	575	573	572	570	570	570	570	570	573	573	573	573
Elevation (3)	PANEL 9E				PANEL 10E				PANEL 11E				PANEL 12E			
Avg Temp (°C)	553	552	552	551	558	557	556	555	586	586	585	584	587	587	586	586
Max Temp (°C)	572	571	570	567	575	573	572	570	602	600	600	598	601	600	600	599
Panel Avg Temp (°C)	552				557				585				587			
Panel Max Temp (°C)	572				575				602				601			
	(1)	(2)	(2)	(1)												

Node Width (4)	0.3680	0.7770	0.7770	0.3680	0.3680	0.7770	0.7770	0.3680	0.3680	0.7770	0.7770	0.3680	0.3680	0.7770	0.7770	0.3680
22.087	600	600	600	600	599	600	600	601	543	543	543	543	538	538	538	538
21.060	600	600	600	600	598	600	600	601	543	543	543	543	539	539	539	539
20.032	600	599	599	600	598	599	600	600	544	544	544	544	540	540	540	540
19.005	599	598	598	599	597	598	599	600	546	546	546	546	541	542	542	542
17.978	597	597	597	597	596	597	598	598	547	548	548	548	543	544	544	544
16.950	596	596	596	596	594	595	596	596	549	550	550	550	546	546	546	546
15.923	594	594	594	594	593	593	594	595	551	552	552	552	548	548	548	549
14.896	592	592	592	592	591	592	592	593	553	554	554	554	550	550	551	551
13.869	591	590	590	591	589	590	590	591	555	555	556	556	551	552	553	553
12.841	589	589	589	589	588	588	589	589	556	557	557	558	553	554	555	555
11.814	588	587	587	588	586	587	587	588	558	559	559	560	555	556	557	557
10.787	586	586	586	586	585	586	586	586	559	560	561	561	557	558	558	559
9.759	585	585	585	585	584	584	584	585	561	562	562	563	558	560	560	561
8.732	583	583	583	583	582	583	583	583	563	564	564	565	560	561	562	563
7.705	582	582	582	582	581	581	582	582	564	565	566	567	562	563	564	565
6.677	580	580	580	580	579	580	580	580	566	567	568	569	564	566	566	567
5.650	579	579	579	579	578	578	578	578	568	569	570	571	566	568	569	570
4.623	577	577	577	577	576	576	576	577	569	571	572	573	568	569	570	572
3.596	576	576	576	576	575	575	575	575	571	572	573	574	569	571	572	573
2.568	575	575	575	575	574	574	574	574	571	573	574	575	570	572	573	574
1.541	574	574	574	574	573	573	573	573	572	573	574	575	570	572	573	574
0.514	574	574	574	574	573	573	573	573	572	573	574	575	570	572	573	575
Elevation (3)	PANEL 12W				PANEL 11W				PANEL 10W				PANEL 9W			
Avg Temp (°C)	587	587	587	587	586	586	587	587	558	559	560	560	555	556	557	558
Max Temp (°C)	600	600	600	600	599	600	600	601	572	573	574	575	570	572	573	575
Panel Avg Temp (°C)	587				587				559				557			
Panel Max Temp (°C)	600				601				575				575			
	(1)	(2)	(2)	(1)												

Node Width (4)	0.3680	0.7770	0.7770	0.3680	0.3680	0.7770	0.7770	0.3680	0.3680	0.7770	0.7770	0.3680	0.3680	0.7770	0.7770	0.3680
22.087	540	542	543	545	535	538	539	540	432	432	432	432	438	438	438	438
21.060	539	542	543	544	535	537	539	540	433	433	433	433	439	439	439	439
20.032	539	541	542	544	534	536	538	539	435	435	435	435	441	441	441	441
19.005	538	540	541	542	533	535	536	538	437	437	437	437	443	443	443	443
17.978	536	538	539	540	531	533	534	536	439	440	440	440	446	447	447	447
16.950	534	536	537	538	529	530	532	533	442	443	443	443	449	450	450	450
15.923	531	533	534	535	526	528	529	530	445	446	446	447	453	454	454	454
14.896	529	530	531	533	523	525	526	527	448	449	450	450	456	457	457	457
13.869	527	528	529	530	521	522	523	524	451	452	453	453	459	460	461	461
12.841	524	526	527	527	518	520	520	521	454	455	455	456	462	463	464	464
11.814	522	523	524	525	516	517	518	519	456	458	458	459	465	466	467	467
10.787	520	521	522	523	513	515	515	516	459	460	461	462	468	470	470	471
9.759	518	519	520	520	511	512	513	513	462	463	464	465	471	473	473	474
8.732	516	517	517	518	509	510	510	511	464	466	467	468	474	476	476	477
7.705	514	515	515	516	507	507	508	508	467	469	470	471	477	479	480	480
6.677	512	512	513	513	504	505	505	505	470	472	473	474	480	482	483	484
5.650	510	510	510	511	502	502	502	503	473	475	476	477	483	485	486	487
4.623	507	508	508	508	499	499	500	500	475	477	478	480	486	488	489	490
3.596	505	506	506	506	497	497	497	497	477	479	480	482	488	490	491	492
2.568	504	504	504	504	495	495	495	495	478	480	482	483	490	492	493	494
1.541	503	503	503	503	494	494	494	494	479	481	482	484	490	493	494	494
0.514	502	502	502	502	493	493	494	494	479	481	483	484	491	493	494	495
Elevation (3)	PANEL 8W				PANEL 7W				PANEL 6W				PANEL 5W			
Avg Temp (°C)	521	523	523	524	515	516	517	517	457	458	459	460	466	467	468	468
Max Temp (°C)	540	542	543	545	535	538	539	540	479	481	483	484	491	493	494	495
Panel Avg Temp (°C)	523				516				459				467			
Panel Max Temp (°C)	545				540				484				495			
	(1)	(2)	(2)	(1)												

Node Width (4)	0.3680	0.7770	0.7770	0.3680	0.3680	0.7770	0.7770	0.3680	0.3680	0.7770	0.7770	0.3680	0.3680	0.7770	0.7770	0.3680
22.087	430	432	433	433	436	438	438	439	309	309	309	309	309	309	309	309
21.060	429	431	432	433	435	437	438	438	310	310	310	310	310	310	310	310
20.032	428	430	431	431	434	436	437	437	312	312	312	312	312	312	312	312
19.005	427	428	429	430	433	434	435	435	314	315	315	315	315	315	315	315
17.978	424	426	427	427	430	431	432	432	318	318	318	318	318	319	319	318
16.950	421	423	423	424	427	428	428	429	322	322	322	322	322	323	323	322
15.923	417	419	420	420	423	424	425	425	326	326	326	326	327	327	327	327
14.896	414	415	416	416	419	420	421	421	330	330	330	330	331	331	331	331
13.869	410	412	412	413	415	416	417	417	334	334	334	334	335	335	335	335
12.841	407	408	409	409	412	413	413	413	337	338	338	338	339	339	339	339
11.814	404	405	405	405	408	409	409	409	341	342	342	342	342	343	343	343
10.787	400	401	402	402	405	405	406	406	345	345	346	346	346	347	347	346
9.759	397	398	398	399	401	402	402	402	348	349	349	349	350	351	351	350
8.732	394	395	395	395	398	398	398	398	352	353	353	353	354	355	354	354
7.705	391	391	392	392	394	395	395	395	355	357	357	357	358	358	358	358
6.677	388	388	388	388	391	391	391	391	359	360	361	361	362	362	362	362
5.650	384	384	385	385	387	387	387	387	363	364	365	364	365	366	366	365
4.623	381	381	381	381	383	383	384	384	366	367	368	368	369	370	370	369
3.596	378	378	378	378	380	380	380	380	369	370	370	370	371	372	372	371
2.568	376	376	376	376	378	378	378	378	370	372	372	372	373	374	374	373
1.541	374	374	374	374	376	376	376	376	371	372	373	373	374	375	375	374
0.514	373	373	373	373	375	375	375	375	371	373	373	373	374	375	375	374
Elevation (3)	PANEL 4W				PANEL 3W				PANEL 2W				PANEL 1W			
Avg Temp (°C)	402	403	403	404	406	407	407	408	342	343	343	343	343	344	344	343
Max Temp (°C)	430	432	433	433	436	438	438	439	371	373	373	373	374	375	375	374
Panel Avg Temp (°C)	403				407				343				344			
Panel Max Temp (°C)	433				439				373				375			
	(1)	(2)	(2)	(1)												

NOTES:

(1) Bulk Fluid Temperature at panel edge nodes (°C)
(2) Bulk Fluid Temperature at third points across panel width (°C)
(3) Node mid point elevation (m)
(4) Width of Node (m), required for Solar Square program

Tube ID Temperatures
(Salt Film Temperatures)

Node Width (4)	0.3680	0.7770	0.7770	0.3680	0.3680	0.7770	0.7770	0.3680	0.3680	0.7770	0.7770	0.3680	0.3680	0.7770	0.7770	0.3680
22.087	332	333	333	332	332	333	333	332	459	460	459	457	455	455	454	452
21.060	355	356	355	355	354	356	356	354	475	476	475	473	470	470	470	467
20.032	383	384	384	383	382	385	385	383	496	496	495	492	490	490	489	486
19.005	416	417	417	416	414	417	417	415	518	519	518	514	512	512	510	507
17.978	445	445	445	445	443	445	446	444	537	538	536	533	530	530	528	525
16.950	460	461	461	460	458	460	461	459	544	544	543	540	537	536	535	531
15.923	466	467	467	466	464	466	466	464	543	543	542	539	536	535	534	530
14.896	467	468	468	467	465	466	466	464	537	537	536	533	530	529	528	524
13.869	467	468	468	467	465	466	466	464	531	531	530	527	524	523	522	518
12.841	467	469	469	467	465	466	466	464	526	526	525	522	519	518	517	513
11.814	468	469	469	468	466	467	467	464	520	520	520	517	514	513	512	508
10.787	469	471	471	469	467	468	468	466	516	516	515	512	510	509	508	504
9.759	471	473	473	471	469	470	470	468	512	512	512	509	506	506	504	501
8.732	475	477	477	475	473	474	474	472	510	510	509	507	504	504	502	499
7.705	480	482	482	480	478	480	480	477	509	510	509	506	503	503	502	498
6.677	485	486	486	485	482	485	485	482	508	509	508	505	503	502	501	498
5.650	483	484	484	483	481	483	484	481	501	502	501	498	496	495	494	492
4.623	472	472	472	472	470	472	473	471	485	485	484	482	480	480	479	477
3.596	452	452	452	452	450	452	452	451	461	460	460	458	456	456	455	454
2.568	425	425	425	425	423	425	425	424	430	429	429	428	427	426	426	425
1.541	403	403	403	403	401	402	402	401	405	405	404	404	403	402	402	402
0.514	390	391	391	390	389	390	390	389	391	391	391	391	389	389	389	389
Elevation (3)	PANEL 1E				PANEL 2E				PANEL 3E				PANEL 4E			
Avg Temp (°C)	442	443	443	442	441	442.19	442.31	440	496	496	496	493	491	490	489	486
Max Temp (°C)	485	486	486	485	482	484.93	485.14	482	544	544	543	540	537	536	535	531
Panel Avg Temp (°C)	443				441				495				489			
Panel Max Temp (°C)	486				485				544				537			
	(1)	(2)	(2)	(1)												

Node Width (4)	0.3680	0.7770	0.7770	0.3680	0.3680	0.7770	0.7770	0.3680	0.3680	0.7770	0.7770	0.3680	0.3680	0.7770	0.7770	0.3680
22.087	458	458	458	457	453	453	453	452	545	543	542	539	550	549	547	544
21.060	475	475	475	473	469	469	468	467	556	555	553	549	561	559	557	554
20.032	497	497	496	494	490	490	489	486	571	570	568	563	575	573	571	566
19.005	522	522	521	519	514	514	512	509	583	581	578	573	585	582	579	575
17.978	545	544	543	540	535	535	533	529	602	600	597	592	603	600	597	592
16.950	557	557	555	552	547	546	544	540	606	604	601	596	607	604	601	595
15.923	563	561	560	557	552	550	548	544	604	601	598	593	605	601	598	593
14.896	563	562	561	557	552	550	548	544	598	595	593	588	599	596	593	588
13.869	564	562	561	557	552	550	548	543	593	590	587	582	594	590	588	583
12.841	565	563	562	558	553	550	548	544	588	585	583	578	589	586	584	579
11.814	566	565	563	559	554	551	549	545	584	581	578	574	585	582	580	575
10.787	568	567	565	561	555	553	551	546	580	577	575	570	582	579	577	572
9.759	571	569	568	563	558	555	553	548	577	574	572	568	579	576	574	570
8.732	575	573	572	567	562	559	557	552	575	573	571	566	578	575	573	569
7.705	580	579	577	572	567	565	563	557	575	573	571	566	578	575	573	569
6.677	585	584	583	578	572	571	568	563	575	573	571	567	578	576	573	569
5.650	585	585	583	579	573	571	569	564	571	569	567	563	574	572	570	566
4.623	578	577	575	572	566	564	562	558	559	558	556	553	564	562	560	557
3.596	562	561	560	557	551	549	547	544	541	540	538	536	547	545	544	542
2.568	541	540	539	536	531	529	527	524	519	518	517	515	527	525	524	523
1.541	523	522	521	519	514	512	511	508	501	500	500	499	510	509	509	508
0.514	514	513	512	510	505	503	502	500	491	491	490	490	501	501	500	500
Elevation (3)	PANEL 5E				PANEL 6E				PANEL 7E				PANEL 8E			
Avg Temp (°C)	548	547	546	543	537	536	534	530	568	566	564	560	571	569	567	563
Max Temp (°C)	585	585	583	579	573	571	569	564	606	604	601	596	607	604	601	595
Panel Avg Temp (°C)	546				534				564				568			
Panel Max Temp (°C)	585				573				606				607			
	(1)	(2)	(2)	(1)												

Node Width (4)	0.3680	0.7770	0.7770	0.3680	0.3680	0.7770	0.7770	0.3680	0.3680	0.7770	0.7770	0.3680	0.3680	0.7770	0.7770	0.3680
22.087	540	540	540	539	546	545	545	544	607	606	605	603	606	605	604	603
21.060	551	551	550	549	555	555	555	553	614	613	612	610	613	612	611	609
20.032	566	565	564	562	569	568	567	565	624	623	621	619	622	621	619	617
19.005	577	576	574	572	579	578	577	575	632	630	628	625	629	628	626	624
17.978	598	596	594	590	597	596	594	591	643	641	639	636	639	638	636	634
16.950	606	603	601	597	604	602	600	598	645	643	641	638	641	639	638	635
15.923	608	605	603	599	607	604	602	599	643	640	638	635	639	637	635	633
14.896	608	605	603	599	606	603	601	598	638	635	633	631	634	632	631	629
13.869	607	604	602	598	605	603	601	597	634	631	629	627	630	628	627	625
12.841	608	605	603	598	606	603	601	597	630	628	626	623	627	625	624	622
11.814	608	605	603	599	606	603	601	597	627	625	623	621	624	622	621	620
10.787	610	607	604	600	607	604	602	598	625	623	621	619	622	620	619	618
9.759	612	609	606	602	609	606	604	600	624	621	620	617	620	619	618	616
8.732	615	612	609	605	612	609	607	603	623	621	620	617	620	619	618	616
7.705	619	616	614	609	616	614	611	607	624	622	620	618	621	620	618	617
6.677	624	621	618	614	621	618	616	611	625	623	622	619	622	621	619	617
5.650	626	623	620	615	622	620	617	613	623	621	620	618	621	620	618	616
4.623	621	618	615	611	619	616	614	610	616	615	613	612	615	614	612	610
3.596	611	608	606	602	609	607	605	602	605	604	603	602	604	603	602	601
2.568	596	594	592	589	596	594	592	589	591	590	589	589	591	590	590	589
1.541	584	582	580	578	585	583	581	579	580	579	579	578	581	580	580	580
0.514	578	576	574	572	579	577	576	574	574	573	573	573	575	575	575	575
Elevation (3)	PANEL 9E				PANEL 10E				PANEL 11E				PANEL 12E			
Avg Temp (°C)	599	596	594	591	598	596	594	591	620	618	617	615	618	617	616	614
Max Temp (°C)	626	623	620	615	622	620	617	613	645	643	641	638	641	639	638	635
Panel Avg Temp (°C)	595				595				618				616			
Panel Max Temp (°C)	626				622				645				641			
	(1)	(2)	(2)	(1)												

Node Width (4)	0.3680	0.7770	0.7770	0.3680	0.3680	0.7770	0.7770	0.3680	0.3680	0.7770	0.7770	0.3680	0.3680	0.7770	0.7770	0.3680
22.087	604	604	604	604	603	604	605	606	548	549	549	549	544	545	545	546
21.060	611	611	611	611	609	611	612	612	556	557	558	558	553	555	555	555
20.032	619	619	619	619	617	619	621	622	567	569	569	570	565	567	568	568
19.005	628	628	628	628	626	629	630	631	580	582	583	584	579	581	583	584
17.978	635	635	635	635	634	636	638	639	591	594	595	596	591	594	596	597
16.950	637	637	637	637	635	637	639	641	597	599	601	602	597	600	602	604
15.923	635	634	634	635	633	635	637	638	598	600	602	604	599	602	604	606
14.896	631	630	630	631	629	631	632	633	596	599	600	603	598	601	603	606
13.869	627	627	627	627	625	627	628	629	596	598	600	602	597	600	602	605
12.841	624	624	624	624	622	624	625	626	595	598	600	602	597	600	602	605
11.814	621	621	621	621	620	621	622	624	596	598	600	602	597	601	603	606
10.787	619	619	619	619	618	619	620	622	596	599	601	603	598	602	604	607
9.759	618	618	618	618	616	618	619	620	598	601	603	605	600	604	606	609
8.732	617	617	617	617	616	618	619	620	600	604	606	608	603	607	609	612
7.705	618	618	618	618	616	618	620	621	604	608	610	612	607	611	613	616
6.677	619	619	619	619	617	619	621	622	609	612	614	617	611	616	618	621
5.650	617	617	617	617	616	618	619	620	611	614	616	618	613	617	620	622
4.623	612	611	611	612	610	612	613	615	608	611	613	615	610	613	616	618
3.596	602	601	601	602	601	602	603	604	600	603	605	607	601	605	607	609
2.568	590	590	590	590	589	590	590	591	589	591	592	594	589	592	594	596
1.541	581	580	581	581	580	580	580	581	580	581	583	584	579	581	583	585
0.514	576	576	576	576	575	575	575	575	575	576	577	579	574	576	577	579
Elevation (3)	PANEL 12W				PANEL 11W				PANEL 10W				PANEL 9W			
Avg Temp (°C)	616	615	615	616	614	616	617	618	591	593	594	596	591	594	596	598
Max Temp (°C)	637	637	637	637	635	637	639	641	611	614	616	618	613	617	620	622
Panel Avg Temp (°C)	615				616				593				595			
Panel Max Temp (°C)	637				641				618				622			
	(1)	(2)	(2)	(1)												

Node Width (4)	0.3680	0.7770	0.7770	0.3680	0.3680	0.7770	0.7770	0.3680	0.3680	0.7770	0.7770	0.3680	0.3680	0.7770	0.7770	0.3680
22.087	547	550	552	553	544	547	549	550	444	445	446	446	452	453	453	453
21.060	556	559	561	563	554	557	559	561	458	460	461	461	467	468	469	469
20.032	567	572	574	576	566	571	573	575	476	479	480	480	486	489	490	490
19.005	580	585	587	590	580	585	588	590	491	495	496	497	504	507	508	508
17.978	590	595	598	601	592	597	600	603	515	519	521	523	529	533	534	535
16.950	593	598	601	605	595	600	603	607	525	529	532	534	540	544	546	547
15.923	591	596	599	602	593	598	601	604	528	532	535	537	544	548	550	552
14.896	586	590	593	597	587	592	595	599	527	532	534	537	543	548	550	552
13.869	581	586	588	592	582	587	590	593	527	532	534	537	543	548	549	552
12.841	577	582	584	588	578	583	586	589	527	532	534	537	544	548	550	552
11.814	574	578	581	584	574	579	582	585	528	533	535	538	544	549	551	553
10.787	571	576	578	581	572	576	578	581	529	534	537	539	546	551	553	555
9.759	569	573	576	579	569	574	576	579	531	536	539	542	548	553	555	558
8.732	569	573	575	578	568	573	575	577	535	540	543	545	552	557	559	562
7.705	569	573	575	578	569	573	575	578	540	545	548	551	557	563	565	567
6.677	570	574	576	578	569	573	576	578	545	551	554	556	563	568	571	572
5.650	567	571	573	575	566	570	572	574	546	552	555	557	564	569	571	573
4.623	559	562	564	566	557	560	562	564	540	545	548	551	558	562	564	566
3.596	545	547	549	551	542	544	545	547	528	532	534	537	544	547	549	551
2.568	528	529	531	532	523	524	525	526	510	513	515	518	524	527	529	531
1.541	515	515	516	517	508	509	509	510	495	498	500	502	508	511	512	514
0.514	508	508	508	509	500	500	501	501	487	490	491	493	499	502	503	505
Elevation (3)	PANEL 8W				PANEL 7W				PANEL 6W				PANEL 5W			
Avg Temp (°C)	564	568	570	572	563	567	569	571	516	519	521	524	530	534	536	537
Max Temp (°C)	593	598	601	605	595	600	603	607	546	552	555	557	564	569	571	573
Panel Avg Temp (°C)	569				568				520				534			
Panel Max Temp (°C)	605				607				557				573			
	(1)	(2)	(2)	(1)												

Node Width (4)	0.3680	0.7770	0.7770	0.3680	0.3680	0.7770	0.7770	0.3680	0.3680	0.7770	0.7770	0.3680	0.3680	0.7770	0.7770	0.3680
22.087	445	447	448	449	452	454	455	455	331	332	332	332	332	333	333	332
21.060	459	462	463	464	467	470	470	470	352	354	354	354	354	356	356	354
20.032	477	481	482	482	486	489	490	490	380	382	383	382	383	385	385	382
19.005	493	497	499	499	503	507	508	508	407	409	410	409	411	413	413	410
17.978	515	519	520	521	525	529	530	530	439	442	443	442	444	446	446	443
16.950	521	525	527	528	531	535	537	537	453	456	457	457	459	461	461	458
15.923	519	524	525	527	530	534	535	536	459	461	462	463	464	466	466	464
14.896	513	518	519	521	525	528	530	531	459	461	462	462	464	466	466	465
13.869	507	512	513	515	519	522	524	525	458	461	462	462	464	466	466	465
12.841	502	507	508	510	513	517	518	519	458	462	462	462	464	466	466	465
11.814	497	502	504	505	509	512	513	514	459	462	463	463	465	467	467	466
10.787	494	498	500	501	504	508	509	510	460	463	464	464	466	468	468	467
9.759	491	495	496	498	501	505	506	506	462	466	466	466	468	470	471	469
8.732	489	493	495	496	499	503	504	504	466	469	470	470	472	474	474	473
7.705	489	493	495	496	499	502	504	504	471	475	476	475	477	480	480	478
6.677	489	493	495	495	498	502	503	503	476	480	481	481	483	485	485	483
5.650	484	487	488	489	492	495	496	496	475	479	480	480	482	484	484	481
4.623	470	472	473	474	477	479	480	481	465	468	469	469	471	473	472	470
3.596	448	450	450	451	454	455	456	457	446	448	449	450	451	453	452	450
2.568	421	421	422	423	425	426	426	427	420	421	422	423	424	425	425	424
1.541	398	399	399	400	402	402	402	403	398	399	400	400	402	402	402	401
0.514	386	386	386	387	389	389	389	390	386	387	388	388	389	390	390	389
Elevation (3)	PANEL 4W				PANEL 3W				PANEL 2W				PANEL 1W			
Avg Temp (°C)	478	481	482	483	486	489	490	491	435	438	439	439	440	442	442	441
Max Temp (°C)	521	525	527	528	531	535	537	537	476	480	481	481	483	485	485	483
Panel Avg Temp (°C)	481				489				438				441			
Panel Max Temp (°C)	528				537				481				485			

NOTES:

(1) Film (ID) Temperature at panel edge nodes (°C)
(2) Film (ID) Temperature at third points across panel width (°C)
(3) Node mid point elevation (m)
(4) Width of Node (m), required for Solar Square program

Tube OD Temperatures

Node Width (4)	0.3680	0.7770	0.7770	0.3680	0.3680	0.7770	0.7770	0.3680	0.3680	0.7770	0.7770	0.3680	0.3680	0.7770	0.7770	0.3680
22.087	353	355	354	353	353	355	355	353	477	477	477	474	472	472	471	468
21.060	396	397	397	396	395	398	398	396	510	511	510	506	504	504	503	499
20.032	450	452	452	450	449	453	454	450	552	554	552	547	545	546	544	539
19.005	512	514	514	512	511	516	517	512	601	602	600	594	592	592	590	584
17.978	567	568	568	567	565	570	571	567	643	643	641	636	633	632	630	624
16.950	595	595	595	595	593	597	598	594	662	662	659	654	651	650	648	642
15.923	603	604	604	603	601	605	605	601	664	663	661	656	653	652	649	643
14.896	601	602	602	601	599	601	601	597	655	655	653	648	646	644	641	635
13.869	597	599	599	597	595	597	596	593	647	646	645	640	637	635	633	627
12.841	594	597	597	594	592	594	594	590	639	639	638	633	630	628	626	620
11.814	592	595	595	592	590	592	591	587	632	632	631	626	623	622	620	613
10.787	591	594	594	591	589	591	590	586	627	627	626	621	618	617	615	608
9.759	592	595	595	592	590	592	591	587	623	624	622	617	615	614	611	605
8.732	595	598	598	595	593	596	596	591	622	623	622	616	614	613	611	604
7.705	602	605	605	602	600	604	604	599	625	626	624	619	616	616	614	607
6.677	608	611	611	608	606	610	611	606	627	628	627	621	618	618	616	609
5.650	601	602	602	601	599	603	604	600	617	617	615	610	608	608	605	600
4.623	575	575	575	575	573	577	578	575	588	587	586	582	580	578	576	573
3.596	532	531	531	532	530	533	534	532	541	540	538	536	534	532	531	529
2.568	476	475	475	476	474	476	476	475	481	480	479	478	476	475	474	473
1.541	430	430	430	430	429	430	430	429	432	431	431	430	429	428	428	427
0.514	405	405	405	405	403	404	404	403	405	405	405	404	403	403	403	402
Elevation (3)	PANEL 1E				PANEL 2E				PANEL 3E				PANEL 4E			
Avg Temp (°C)	539	541	541	539	538	540.56	540.77	537	585	585	584	579	577	576	574	569
Max Temp (°C)	608	611	611	608	606	610.36	610.80	606	664	663	661	656	653	652	649	643
Panel Avg Temp (°C)	540				539				583				574			
Panel Max Temp (°C)	611				611				664				653			
	(1)	(2)	(2)	(1)												

Node Width (4)	0.3680	0.7770	0.7770	0.3680	0.3680	0.7770	0.7770	0.3680	0.3680	0.7770	0.7770	0.3680	0.3680	0.7770	0.7770	0.3680
22.087	474	474	474	472	468	468	468	466	556	555	553	549	561	559	557	553
21.060	507	507	507	504	499	500	499	495	581	580	577	572	583	581	579	574
20.032	549	550	549	544	540	540	539	534	614	612	609	602	613	610	607	600
19.005	598	598	597	591	587	587	584	578	639	636	632	624	634	631	626	619
17.978	641	641	639	633	629	627	624	617	681	678	673	664	675	670	665	657
16.950	664	662	660	654	649	647	643	636	694	689	684	676	686	680	675	666
15.923	671	668	666	660	655	651	648	640	693	688	683	674	685	678	673	665
14.896	668	666	663	656	651	647	644	636	684	679	674	665	676	670	665	656
13.869	665	663	660	653	648	644	640	632	676	670	666	657	668	662	657	649
12.841	664	661	658	651	646	642	638	630	669	664	660	651	661	655	651	643
11.814	663	660	657	649	645	640	637	628	663	658	654	645	656	650	646	637
10.787	663	660	657	650	645	641	637	628	658	654	650	641	652	646	642	634
9.759	665	662	659	651	646	642	639	630	655	651	647	638	649	644	640	631
8.732	669	667	664	656	651	647	643	634	655	651	647	638	649	644	640	632
7.705	676	675	672	664	659	656	651	642	658	654	650	641	652	647	643	635
6.677	684	682	679	671	666	664	659	650	661	658	653	645	655	651	646	638
5.650	680	679	676	669	664	662	658	649	655	652	647	640	650	646	642	634
4.623	661	659	657	651	646	643	640	633	635	631	627	621	631	627	623	618
3.596	626	625	623	619	613	610	607	602	600	596	594	589	600	596	593	589
2.568	581	579	578	575	570	567	565	561	555	553	551	549	559	556	554	552
1.541	545	543	542	539	534	532	530	527	520	518	517	516	527	525	524	523
0.514	524	523	522	520	515	513	512	509	500	499	499	498	509	508	507	507
Elevation (3)	PANEL 5E				PANEL 6E				PANEL 7E				PANEL 8E			
Avg Temp (°C)	632	623	621	615	610	608	605	598	632	628	625	618	629	624	621	614
Max Temp (°C)	684	682	679	671	666	664	659	650	694	689	684	676	686	680	675	666
Panel Avg Temp (°C)	621				605				626				622			
Panel Max Temp (°C)	684				666				694				686			
	(1)	(2)	(2)	(1)												

Node Width (4)	0.3680	0.7770	0.7770	0.3680	0.3680	0.7770	0.7770	0.3680	0.3680	0.7770	0.7770	0.3680	0.3680	0.7770	0.7770	0.3680
22.087	549	549	548	547	553	553	552	551	612	611	610	607	610	610	608	607
21.060	571	570	569	566	573	572	571	569	628	627	625	622	625	624	623	620
20.032	600	598	596	592	599	597	596	592	649	647	645	641	644	643	641	638
19.005	622	620	616	611	619	617	614	610	665	663	660	656	660	658	655	652
17.978	662	658	654	648	654	651	648	642	691	688	685	680	683	680	678	673
16.950	675	671	666	660	666	662	658	653	697	693	690	685	688	685	683	679
15.923	678	673	668	661	668	663	659	654	694	690	687	682	685	682	679	676
14.896	674	669	665	657	664	659	655	649	687	682	679	674	677	674	672	669
13.869	671	666	662	654	661	655	652	645	680	675	673	668	671	668	666	663
12.841	669	664	660	652	659	654	650	644	675	671	668	663	666	663	661	659
11.814	668	663	659	651	658	653	649	642	671	666	664	659	662	659	658	655
10.787	669	663	659	651	658	653	649	643	668	664	661	656	659	657	655	652
9.759	670	665	661	653	660	655	651	644	666	662	660	655	658	655	654	651
8.732	674	669	665	657	664	659	655	648	667	664	661	656	659	657	655	651
7.705	681	676	672	663	670	666	662	655	670	667	664	659	662	660	658	654
6.677	688	684	679	671	677	673	669	662	674	671	668	663	666	664	662	657
5.650	689	684	679	672	678	674	670	664	672	670	667	662	665	663	660	656
4.623	677	672	668	661	668	664	660	655	660	658	656	652	655	653	650	646
3.596	654	650	646	640	647	644	640	636	639	637	635	633	635	633	631	628
2.568	623	619	616	612	619	616	613	610	611	609	608	607	610	608	607	605
1.541	597	594	592	589	596	593	591	589	589	588	587	587	589	588	587	587
0.514	583	581	579	576	583	581	580	577	577	577	576	576	578	578	577	577
Elevation (3)	PANEL 9E				PANEL 10E				PANEL 11E				PANEL 12E			
Avg Temp (°C)	648	643	640	634	641	637	634	629	657	654	651	647	650	648	646	643
Max Temp (°C)	689	684	679	672	678	674	670	664	697	693	690	685	688	685	683	679
Panel Avg Temp (°C)	641				635				652				647			
Panel Max Temp (°C)	689				678				697				688			
	(1)	(2)	(2)	(1)												

Node Width (4)	0.3680	0.7770	0.7770	0.3680	0.3680	0.7770	0.7770	0.3680	0.3680	0.7770	0.7770	0.3680	0.3680	0.7770	0.7770	0.3680
22.087	608	608	608	608	607	608	609	610	553	554	555	555	551	552	553	553
21.060	622	622	622	622	620	622	624	625	570	572	572	573	568	571	572	572
20.032	639	639	639	639	638	641	643	644	591	594	596	596	592	595	597	598
19.005	659	659	659	659	657	661	664	665	616	620	622	623	619	624	626	628
17.978	675	674	674	675	673	677	680	682	637	642	644	647	642	647	650	654
16.950	680	679	679	680	678	682	685	688	647	651	654	657	652	658	661	666
15.923	678	677	677	678	676	679	682	685	647	651	654	658	653	659	663	668
14.896	671	670	670	671	669	672	674	677	642	646	649	653	649	655	658	663
13.869	665	664	664	665	663	666	667	670	638	643	645	650	645	651	655	660
12.841	660	660	660	660	658	661	663	665	636	641	644	648	643	650	653	658
11.814	656	656	656	656	655	657	659	661	635	640	642	647	642	648	652	657
10.787	654	654	654	654	652	655	656	659	635	640	643	647	642	649	652	658
9.759	652	652	652	652	651	653	655	657	636	641	644	649	644	650	654	659
8.732	653	653	653	653	651	654	656	658	640	646	649	653	648	655	659	663
7.705	656	655	655	656	654	658	660	662	646	652	656	659	654	661	666	670
6.677	659	658	658	659	657	661	664	666	654	660	663	666	662	669	673	677
5.650	658	656	656	658	656	660	663	665	656	662	665	668	663	670	674	678
4.623	648	646	646	648	646	650	653	655	649	653	656	660	655	660	664	668
3.596	630	628	628	630	628	631	633	635	632	635	638	641	636	640	643	647
2.568	606	605	605	606	605	607	608	609	607	610	612	615	610	613	616	619
1.541	588	587	587	588	587	587	588	589	588	590	591	593	589	591	593	596
0.514	578	578	578	578	577	577	578	578	577	579	580	582	577	580	581	583
Elevation (3)	PANEL 12W				PANEL 11W				PANEL 10W				PANEL 9W			
Avg Temp (°C)	574	569	645	645	621	615	644	646	605	598	624	628	625	618	629	634
Max Temp (°C)	649	643	680	679	679	671	678	682	659	650	656	662	684	676	663	670
Panel Avg Temp (°C)	645				647				629				635			
Panel Max Temp (°C)	680				688				668				678			
	(1)	(2)	(2)	(1)												

Node Width (4)	0.3680	0.7770	0.7770	0.3680	0.3680	0.7770	0.7770	0.3680	0.3680	0.7770	0.7770	0.3680	0.3680	0.7770	0.7770	0.3680
22.087	554	558	560	562	553	557	559	560	457	459	459	460	466	467	468	468
21.060	573	578	580	583	573	579	581	583	484	487	489	489	495	498	499	499
20.032	597	603	607	609	600	607	610	613	519	525	527	528	534	539	540	540
19.005	625	632	636	640	631	638	643	646	549	555	558	560	567	573	575	576
17.978	647	655	660	665	656	665	670	674	596	604	608	611	617	624	627	628
16.950	656	664	669	675	666	674	680	685	613	621	625	630	635	643	646	649
15.923	653	661	666	673	664	673	678	684	616	624	629	634	640	647	651	655
14.896	645	653	658	664	655	664	669	675	611	620	624	630	635	643	647	651
13.869	638	646	650	657	648	656	661	667	607	616	620	626	631	640	643	648
12.841	632	640	645	651	642	650	655	661	605	614	618	623	629	638	641	646
11.814	627	635	640	645	637	645	649	655	604	613	617	622	628	636	640	644
10.787	624	632	636	642	633	641	646	651	604	613	617	622	628	637	640	645
9.759	622	630	634	639	631	639	643	648	605	614	619	624	630	638	642	646
8.732	623	631	635	640	631	639	644	648	610	619	623	628	634	643	647	651
7.705	626	634	638	643	634	643	647	651	617	627	632	636	642	651	656	659
6.677	630	638	642	646	638	646	651	655	625	635	640	644	650	660	664	666
5.650	627	634	638	643	634	641	646	650	625	634	639	643	649	658	662	664
4.623	613	618	622	626	618	623	627	631	610	618	623	627	633	640	643	646
3.596	587	591	594	597	589	593	596	600	582	588	592	596	602	607	611	613
2.568	554	556	558	561	552	554	556	559	543	548	551	554	561	565	567	570
1.541	527	528	530	531	523	524	525	527	512	515	518	521	527	530	532	534
0.514	513	514	514	515	507	507	508	509	495	498	500	502	509	511	513	515
Elevation (3)	PANEL 8W				PANEL 7W				PANEL 6W				PANEL 5W			
Avg Temp (°C)	621	614	609	615	619	623	614	621	625	629	577	584	588	591	597	604
Max Temp (°C)	675	666	656	664	669	675	666	674	680	685	625	635	640	644	650	660
Panel Avg Temp (°C)	616				622				585				601			
Panel Max Temp (°C)	675				685				644				660			
	(1)	(2)	(2)	(1)												

Node Width (4)	0.3680	0.7770	0.7770	0.3680	0.3680	0.7770	0.7770	0.3680	0.3680	0.7770	0.7770	0.3680	0.3680	0.7770	0.7770	0.3680
22.087	460	463	464	465	468	471	472	472	351	353	354	353	353	355	355	353
21.060	490	494	496	496	499	503	504	504	392	396	396	395	396	398	398	395
20.032	528	534	536	536	539	544	545	545	445	450	451	449	450	454	453	449
19.005	562	569	572	572	577	583	585	585	496	502	503	502	504	508	507	503
17.978	610	617	620	621	624	630	632	633	558	564	566	565	567	571	570	565
16.950	627	634	636	638	642	648	650	651	584	590	592	592	594	598	597	593
15.923	627	634	637	640	643	649	652	654	592	597	599	600	602	605	605	602
14.896	618	626	629	632	635	642	644	646	588	594	595	596	597	601	601	599
13.869	609	617	620	624	627	633	636	637	584	589	591	591	593	597	597	595
12.841	602	610	613	617	620	626	629	630	581	587	588	588	590	594	594	593
11.814	596	604	607	610	613	620	622	624	578	584	586	586	587	591	592	590
10.787	591	599	602	605	608	615	617	619	578	584	585	585	587	591	591	589
9.759	588	596	599	602	605	611	614	615	579	585	586	586	587	592	592	590
8.732	588	596	599	602	604	611	614	614	583	589	591	590	591	596	596	594
7.705	592	600	603	604	607	614	616	617	590	597	599	597	599	604	604	600
6.677	595	603	606	607	610	616	619	619	597	604	606	605	606	611	611	606
5.650	587	594	596	597	600	606	608	608	591	597	600	599	601	605	604	599
4.623	562	567	569	570	573	577	579	580	567	572	574	574	576	578	577	573
3.596	520	523	525	526	529	531	533	534	525	528	530	531	532	534	533	530
2.568	466	468	469	470	473	474	475	476	469	472	473	474	475	476	476	474
1.541	422	423	424	425	427	428	428	429	424	426	427	428	429	430	430	429
0.514	398	399	399	400	402	403	403	403	400	401	402	402	403	404	404	403
Elevation (3)	PANEL 4W				PANEL 3W				PANEL 2W				PANEL 1W			
Avg Temp (°C)	607	610	556	562	569	574	576	577	530	535	536	536	537	541	540	537
Max Temp (°C)	664	666	627	634	643	649	652	654	597	604	606	605	606	611	611	606
Panel Avg Temp (°C)	584				574				534				539			
Panel Max Temp (°C)	666				654				606				611			
	(1)	(2)	(2)	(1)												

NOTES:

(1) Tube OD Temperature at panel edge nodes (°C)
(2) Tube OD Temperature at third points across panel width (°C)
(3) Node mid point elevation (m)
(4) Width of Node (m), required for Solar Square program

APPENDIX F

Day: 154 08:00:00
Incident Heat Flux
&
Calculated Temperatures

Heat Flux Distribution

INCIDENT HEAT FLUX MAP Day of Year: 154 Time of Day: 8:00:00

3/1/2013 Rev E2

	PANEL 1E				PANEL 2E				PANEL 3E				PANEL 4E			
Radial Position (4)	0.0	5.0	10.0	15.0	15.0	20.0	25.0	30.0	30.0	35.0	40.0	45.0	45.0	50.0	55.0	60.0
Elevation (3)																
22.087	132	138	141	143	143	152	155	155	155	163	165	163	163	170	171	168
21.060	250	262	267	271	271	289	297	297	297	311	315	312	312	324	326	321
20.032	405	422	431	439	439	467	480	482	482	504	510	506	506	524	528	521
19.005	585	605	618	633	633	671	690	696	696	723	732	731	731	753	758	753
17.978	742	764	781	804	804	847	871	883	883	913	924	927	927	951	958	956
16.950	815	839	858	884	884	927	952	968	968	998	1011	1018	1018	1041	1050	1051
15.923	828	854	872	898	898	938	960	979	979	1008	1022	1032	1032	1054	1063	1068
14.896	805	833	850	874	874	909	928	947	947	975	988	1000	1000	1022	1032	1037
13.869	781	812	828	849	849	882	898	915	915	945	957	968	968	992	1001	1005
12.841	763	796	811	830	830	862	877	894	894	924	935	945	945	969	978	981
11.814	748	780	795	813	813	845	860	875	875	904	916	925	925	950	958	961
10.787	739	771	786	803	803	835	850	864	864	893	905	914	914	939	948	950
9.759	734	766	782	799	799	831	847	860	860	890	903	911	911	936	944	946
8.732	742	775	791	807	807	842	859	872	872	903	917	923	923	949	958	958
7.705	763	795	813	829	829	868	888	899	899	933	947	951	951	979	988	986
6.677	783	814	833	851	851	893	917	929	929	963	977	980	980	1007	1017	1013
5.650	762	786	805	826	826	868	894	909	909	938	953	956	956	979	988	986
4.623	675	691	708	731	731	767	792	808	808	830	843	849	849	865	872	874
3.596	526	536	550	571	571	597	617	632	632	646	657	664	664	673	678	682
2.568	336	341	350	365	365	379	392	403	403	410	417	423	423	427	431	435
1.541	184	186	191	200	200	207	213	220	220	223	226	231	231	232	235	238
0.514	101	103	105	110	110	113	116	120	120	122	124	126	126	127	128	130
	(1)	(2)	(2)	(1)												

INCIDENT HEAT FLUX MAP Day of Year: 154 Time of Day: 8:00:00

3/1/2013 Rev E2

	PANEL 5E				PANEL 6E				PANEL 7E				PANEL 8E			
Radial Position (4)	60.0	65.0	70.0	75.0	75.0	80.0	85.0	90.0	90.0	95.0	100.0	105.0	105.0	110.0	115.0	120.0
Elevation (3)																
22.087	168	174	175	171	171	176	177	171	171	175	175	168	168	171	169	162
21.060	321	332	334	327	327	338	339	330	330	338	337	326	326	331	328	315
20.032	521	537	541	532	532	547	549	538	538	550	549	534	534	541	536	518
19.005	753	772	777	769	769	787	791	779	779	792	792	773	773	780	774	752
17.978	956	976	983	977	977	995	999	990	990	1001	1001	983	983	987	980	956
16.950	1051	1070	1077	1075	1075	1090	1095	1087	1087	1096	1095	1079	1079	1079	1072	1050
15.923	1068	1085	1092	1091	1091	1103	1108	1101	1101	1107	1106	1091	1091	1089	1083	1062
14.896	1037	1054	1060	1059	1059	1070	1073	1066	1066	1070	1069	1054	1054	1051	1045	1025
13.869	1005	1023	1028	1026	1026	1037	1039	1030	1030	1035	1033	1018	1018	1015	1010	988
12.841	981	999	1005	1001	1001	1013	1014	1004	1004	1009	1007	991	991	989	984	962
11.814	961	979	984	980	980	992	993	982	982	987	985	968	968	967	962	940
10.787	950	968	973	968	968	980	981	970	970	975	973	956	956	955	950	928
9.759	946	965	969	964	964	976	977	965	965	971	969	951	951	952	947	925
8.732	958	978	983	976	976	989	990	976	976	985	983	964	964	967	963	939
7.705	986	1007	1013	1004	1004	1020	1021	1006	1006	1017	1015	995	995	1001	996	971
6.677	1013	1035	1041	1032	1032	1049	1052	1037	1037	1049	1048	1028	1028	1034	1029	1004
5.650	986	1005	1011	1005	1005	1020	1023	1012	1012	1022	1021	1005	1005	1009	1003	981
4.623	874	887	892	890	890	900	904	898	898	904	903	892	892	892	887	871
3.596	682	689	694	695	695	699	703	701	701	702	702	696	696	692	688	679
2.568	435	437	440	443	443	443	445	446	446	444	444	442	442	436	434	429
1.541	238	238	240	241	241	240	241	242	242	239	239	238	238	234	232	230
0.514	130	130	131	132	132	131	131	131	131	129	129	128	128	125	124	122
	(1)	(2)	(2)	(1)												

INCIDENT HEAT FLUX MAP Day of Year: 154 Time of Day: 8:00:00

3/1/2013 Rev E2

	PANEL 9E				PANEL 10E				PANEL 11E				PANEL 12E			
Radial Position (4)	120.0	125.0	130.0	135.0	135.0	140.0	145.0	150.0	150.0	155.0	160.0	165.0	165.0	170.0	175.0	180.0
Elevation (3)																
22.087	162	163	161	153	153	154	152	144	144	144	142	133	133	133	129	120
21.060	315	318	315	301	301	304	300	286	286	288	283	268	268	268	260	243
20.032	518	522	516	497	497	500	494	475	475	477	470	448	448	445	431	405
19.005	752	754	747	723	723	724	717	692	692	692	682	655	655	647	628	593
17.978	956	955	946	920	920	917	907	881	881	875	863	832	832	819	795	755
16.950	1050	1044	1035	1009	1009	1002	991	964	964	954	940	909	909	891	867	827
15.923	1062	1053	1044	1020	1020	1008	997	970	970	955	941	911	911	890	869	832
14.896	1025	1016	1007	982	982	969	958	930	930	913	899	868	868	848	830	797
13.869	988	981	972	946	946	933	921	892	892	875	861	830	830	811	794	763
12.841	962	954	946	919	919	906	894	865	865	848	834	803	803	784	769	737
11.814	940	932	924	897	897	884	873	842	842	826	813	780	780	762	747	716
10.787	928	922	913	886	886	874	863	832	832	817	803	770	770	752	737	706
9.759	925	920	911	884	884	873	862	831	831	816	802	769	769	752	736	703
8.732	939	937	928	900	900	892	880	848	848	836	821	786	786	770	752	717
7.705	971	971	962	933	933	928	916	883	883	873	857	821	821	806	785	746
6.677	1004	1005	995	966	966	963	951	919	919	911	895	859	859	844	819	776
5.650	981	980	971	946	946	942	931	904	904	896	881	849	849	833	806	763
4.623	871	866	858	840	840	833	824	804	804	795	783	758	758	741	715	678
3.596	679	671	665	654	654	645	638	626	626	616	607	590	590	573	554	526
2.568	429	422	418	412	412	404	400	393	393	384	378	369	369	356	344	329
1.541	230	225	222	219	219	213	211	207	207	201	197	193	193	185	179	171
0.514	122	119	117	115	115	111	110	107	107	103	101	98	98	94	91	87
	(1)	(2)	(2)	(1)												

INCIDENT HEAT FLUX MAP Day of Year: 154 Time of Day: 8:00:00

3/1/2013 Rev E2

	PANEL 12W				PANEL 11W				PANEL 10W				PANEL 9W			
Radial Position (4)	180.0	185.0	190.0	195.0	195.0	200.0	205.0	210.0	210.0	215.0	220.0	225.0	225.0	230.0	235.0	240.0
Elevation (3)																
22.087	120	119	117	111	111	112	110	105	105	106	103	98	98	99	97	93
21.060	243	240	235	224	224	227	224	213	213	215	210	199	199	201	197	188
20.032	405	399	390	374	374	378	374	358	358	358	350	334	334	334	327	313
19.005	593	581	568	548	548	550	544	524	524	521	510	488	488	485	475	457
17.978	755	737	720	698	698	696	688	665	665	657	642	618	618	611	597	578
16.950	827	805	787	764	764	757	747	723	723	710	695	671	671	659	645	625
15.923	832	809	792	767	767	755	743	719	719	704	688	666	666	652	638	620
14.896	797	775	759	733	733	717	704	680	680	664	650	628	628	614	602	584
13.869	763	743	728	700	700	684	671	646	646	631	618	596	596	583	572	554
12.841	737	719	704	676	676	660	647	622	622	608	596	574	574	562	551	533
11.814	716	698	684	656	656	641	628	603	603	590	579	557	557	546	536	518
10.787	706	689	674	647	647	632	620	595	595	583	571	550	550	539	529	511
9.759	703	687	672	644	644	631	619	595	595	583	572	550	550	540	529	511
8.732	717	701	685	657	657	647	635	610	610	601	589	565	565	557	545	525
7.705	746	729	712	685	685	678	667	642	642	634	621	596	596	589	576	554
6.677	776	757	739	714	714	712	702	677	677	670	656	630	630	623	609	586
5.650	763	740	722	704	704	704	697	675	675	668	653	630	630	621	607	587
4.623	678	653	637	626	626	626	621	606	606	597	583	565	565	556	544	528
3.596	526	503	491	486	486	485	481	472	472	463	452	441	441	431	422	412
2.568	329	312	305	303	303	301	298	294	294	287	281	275	275	267	262	257
1.541	171	162	158	157	157	155	153	152	152	147	145	142	142	138	135	134
0.514	87	82	80	80	80	78	77	76	76	74	73	72	72	70	68	68
	(1)	(2)	(2)	(1)												

INCIDENT HEAT FLUX MAP Day of Year: 154 Time of Day: 8:00:00

3/1/2013 Rev E2

	PANEL 8W				PANEL 7W				PANEL 6W				PANEL 5W			
Radial Position (4)	240.0	245.0	250.0	255.0	255.0	260.0	265.0	270.0	270.0	275.0	280.0	285.0	285.0	290.0	295.0	300.0
Elevation (3)																
22.087	93	94	93	89	89	92	91	89	89	92	92	91	91	95	96	96
21.060	188	190	187	180	180	183	181	176	176	182	182	179	179	187	188	187
20.032	313	315	310	299	299	303	300	292	292	299	299	295	295	306	309	308
19.005	457	456	449	435	435	438	433	424	424	431	431	427	427	440	444	445
17.978	578	573	563	549	549	549	543	534	534	540	540	538	538	551	557	561
16.950	625	618	607	593	593	591	584	577	577	582	581	582	582	594	600	608
15.923	620	610	600	587	587	583	577	571	571	574	574	576	576	588	594	604
14.896	584	574	564	552	552	548	542	537	537	541	541	544	544	556	562	573
13.869	554	545	536	523	523	521	516	510	510	515	515	518	518	530	536	546
12.841	533	525	517	504	504	502	497	492	492	497	498	500	500	513	519	529
11.814	518	511	502	490	490	488	484	478	478	484	484	486	486	500	506	515
10.787	511	504	496	483	483	482	477	471	471	477	477	479	479	493	499	508
9.759	511	504	496	482	482	481	476	470	470	475	476	478	478	492	498	507
8.732	525	520	510	495	495	495	489	481	481	488	488	488	488	503	510	518
7.705	554	550	539	522	522	523	516	506	506	514	514	512	512	529	536	542
6.677	586	582	571	553	553	554	547	536	536	544	544	541	541	558	565	570
5.650	587	582	571	555	555	554	548	538	538	543	543	542	542	556	563	569
4.623	528	521	512	500	500	497	491	484	484	487	488	488	488	498	505	511
3.596	412	404	398	391	391	387	382	379	379	379	380	382	382	388	393	401
2.568	257	251	247	245	245	241	238	238	238	237	237	240	240	243	247	253
1.541	134	130	128	128	128	125	124	125	125	124	124	127	127	128	130	135
0.514	68	66	65	65	65	64	64	65	65	64	65	66	66	67	69	71
	(1)	(2)	(2)	(1)												

INCIDENT HEAT FLUX MAP Day of Year: 154 Time of Day: 8:00:00

3/1/2013 Rev E2

	PANEL 4W				PANEL 3W				PANEL 2W				PANEL 1W			
Radial Position (4)	300.0	305.0	310.0	315.0	315.0	320.0	325.0	330.0	330.0	335.0	340.0	345.0	345.0	350.0	355.0	360.0
Elevation (3)																
22.087	96	102	103	104	104	110	112	113	113	120	123	123	123	131	132	132
21.060	187	197	201	201	201	213	217	218	218	231	236	237	237	250	252	250
20.032	308	322	328	329	329	346	353	356	356	376	383	386	386	405	408	405
19.005	445	463	471	475	475	497	508	514	514	539	551	557	557	581	586	585
17.978	561	581	591	600	600	624	638	650	650	678	693	705	705	732	740	742
16.950	608	628	639	652	652	677	692	708	708	737	753	770	770	798	808	815
15.923	604	623	635	650	650	675	691	710	710	738	755	774	774	803	815	828
14.896	573	592	603	619	619	645	659	679	679	708	724	744	744	774	788	805
13.869	546	567	577	593	593	619	633	652	652	682	697	717	717	748	762	781
12.841	529	549	560	575	575	601	615	634	634	664	679	698	698	730	744	763
11.814	515	536	547	561	561	588	601	619	619	649	663	683	683	714	729	748
10.787	508	529	540	554	554	580	594	611	611	641	655	674	674	705	720	739
9.759	507	528	539	553	553	579	592	609	609	639	654	671	671	702	717	734
8.732	518	540	551	563	563	591	605	620	620	651	666	682	682	713	728	742
7.705	542	565	577	588	588	616	631	645	645	677	693	706	706	738	752	763
6.677	570	594	606	616	616	644	660	672	672	705	722	734	734	764	777	783
5.650	569	589	601	611	611	636	652	665	665	693	710	722	722	748	758	762
4.623	511	527	538	548	548	567	581	595	595	617	632	645	645	664	671	675
3.596	401	411	419	429	429	442	453	465	465	481	492	505	505	517	522	526
2.568	253	258	264	272	272	279	286	295	295	304	312	321	321	328	331	336
1.541	135	137	140	146	146	149	153	159	159	163	168	174	174	177	180	184
0.514	71	73	75	78	78	80	82	86	86	88	91	94	94	96	98	101
	(1)	(2)	(2)	(1)												

NOTES:

(1) Incident heat flux at panel edge (kw/m2)

(2) Incident heat flux at third points across panel width (kw/m2)

(3) Node mid point elevation (m)

(4) Flux point radial position from North (degrees)

Diameter	m	17.4
Perimeter	m	54.664
Perimeter (USE)	m	55.0
Half Perimeter	m	27.481
Panels		24
Nodes High		22
Height	m	22.6
Node Height	m	1.0273
Node Height (USE)	m	1.0273
Height (USE)	m	22.601
Outer Angle		5.00
Inner Angle		5.00

Molten Salt Bulk Fluid Temperatures

Node Width (4)	0.3680	0.7770	0.7770	0.3680	0.3680	0.7770	0.7770	0.3680	0.3680	0.7770	0.7770	0.3680	0.3680	0.7770	0.7770	0.3680
22.087	308	308	308	309	309	309	309	309	418	420	421	421	426	427	428	428
21.060	309	309	309	310	309	310	310	310	417	419	420	420	425	427	427	427
20.032	311	311	311	311	311	311	311	311	416	418	419	419	424	425	426	426
19.005	313	313	313	314	314	314	314	314	414	416	417	417	422	423	424	424
17.978	316	316	316	317	317	317	317	317	412	414	414	415	419	421	421	421
16.950	319	319	320	320	320	321	321	321	409	410	411	411	416	417	418	418
15.923	322	323	323	323	323	324	325	325	405	406	407	408	412	413	414	414
14.896	325	326	326	327	327	328	328	328	401	403	403	404	408	409	410	410
13.869	328	329	329	330	330	331	331	332	398	399	400	400	405	406	406	406
12.841	331	332	332	333	333	334	335	335	394	396	396	396	401	402	402	402
11.814	334	335	335	336	336	337	338	338	391	392	393	393	397	398	399	399
10.787	337	338	338	339	339	340	341	342	388	389	389	389	394	395	395	395
9.759	339	341	341	342	342	344	344	345	385	385	386	386	391	391	391	392
8.732	342	343	344	345	345	347	348	348	381	382	382	383	387	388	388	388
7.705	345	346	347	348	348	350	351	352	378	379	379	379	384	384	384	384
6.677	348	349	350	351	351	353	354	355	375	375	375	376	380	381	381	381
5.650	351	352	353	354	354	357	358	358	371	372	372	372	377	377	377	377
4.623	353	355	356	357	357	359	361	361	368	368	368	368	373	373	373	373
3.596	355	357	358	359	359	362	363	364	365	365	365	365	370	370	370	370
2.568	357	358	359	361	361	363	364	365	362	362	363	363	367	367	367	367
1.541	357	359	360	361	361	364	365	366	361	361	361	361	366	366	366	366
0.514	357	359	360	362	362	364	365	366	360	360	360	360	365	365	365	365
Elevation (3)	PANEL 1E				PANEL 2E				PANEL 3E				PANEL 4E			
Avg Temp (°C)	334	335	336	337	337	338.05	338.76	339	390	390	391	391	396	397	397	397
Max Temp (°C)	357	359	360	362	362	364.12	365.50	366	418	420	421	421	426	427	428	428
Panel Avg Temp (°C)	336				338				391				397			
Panel Max Temp (°C)	362				366				421				428			
	(1)	(2)	(2)	(1)												

Node Width (4)	0.3680	0.7770	0.7770	0.3680	0.3680	0.7770	0.7770	0.3680	0.3680	0.7770	0.7770	0.3680	0.3680	0.7770	0.7770	0.3680
22.087	420	421	421	420	428	428	428	428	487	487	487	486	494	494	494	493
21.060	422	422	422	422	429	429	429	429	486	487	487	486	494	494	494	492
20.032	424	424	424	424	431	431	431	431	485	486	485	484	493	493	492	491
19.005	426	427	427	426	434	434	434	434	483	484	483	482	491	491	490	489
17.978	430	430	430	430	437	437	438	437	481	481	481	480	488	488	488	487
16.950	434	434	434	434	441	442	442	441	477	477	477	476	485	485	484	483
15.923	438	438	438	438	445	446	446	445	473	473	473	472	481	481	480	479
14.896	442	442	442	442	449	450	450	449	469	469	469	468	477	477	476	475
13.869	445	446	446	446	453	453	453	453	465	465	465	464	473	473	473	472
12.841	449	450	450	450	457	457	457	457	461	461	461	461	469	469	469	468
11.814	452	453	453	453	460	461	461	461	457	458	457	457	465	465	465	464
10.787	456	457	457	457	464	464	464	464	454	454	454	453	462	462	462	461
9.759	459	460	461	460	467	468	468	468	450	450	450	450	458	458	458	457
8.732	463	464	464	464	471	472	472	471	446	447	447	446	455	455	455	454
7.705	467	468	468	468	475	475	475	475	443	443	443	443	451	451	451	451
6.677	470	471	472	471	478	479	479	479	439	439	439	439	447	447	447	447
5.650	474	475	475	475	482	483	483	482	435	435	435	435	443	443	443	443
4.623	477	478	479	478	485	486	486	486	431	431	431	431	440	440	440	440
3.596	480	481	481	481	488	489	489	488	428	428	428	428	436	436	436	436
2.568	481	482	483	482	489	490	491	490	426	426	426	425	434	434	434	434
1.541	482	483	484	483	490	491	491	491	424	424	424	424	432	432	432	432
0.514	482	484	484	484	491	492	492	491	423	423	423	423	431	431	431	431
Elevation (3)	PANEL 5E				PANEL 6E				PANEL 7E				PANEL 8E			
Avg Temp (°C)	453	454	454	454	461	462	462	461	456	456	456	455	464	464	463	463
Max Temp (°C)	482	484	484	484	491	492	492	491	487	487	487	486	494	494	494	493
Panel Avg Temp (°C)	454				461				456				463			
Panel Max Temp (°C)	484				492				487				494			
	(1)	(2)	(2)	(1)												

Node Width (4)	0.3680	0.7770	0.7770	0.3680	0.3680	0.7770	0.7770	0.3680	0.3680	0.7770	0.7770	0.3680	0.3680	0.7770	0.7770	0.3680
22.087	488	488	488	488	495	495	495	495	601	601	600	598	602	601	600	597
21.060	489	489	489	489	496	496	496	496	601	600	599	597	602	601	599	597
20.032	491	491	491	490	497	497	497	497	600	599	598	596	601	600	598	596
19.005	493	493	493	493	500	500	500	499	598	598	597	595	599	598	597	595
17.978	496	496	496	496	503	503	503	503	596	595	595	593	597	596	595	593
16.950	500	500	500	500	507	507	507	506	593	592	592	590	594	593	592	590
15.923	504	504	504	503	511	511	510	510	590	589	588	587	591	590	589	587
14.896	508	508	508	507	514	514	514	513	586	585	585	583	588	587	586	584
13.869	512	512	511	511	518	517	517	516	583	582	582	580	584	584	583	581
12.841	515	515	515	514	521	521	520	520	579	579	578	577	581	581	580	578
11.814	519	518	518	517	524	524	524	523	576	576	575	574	579	578	577	576
10.787	522	522	521	520	528	527	527	526	573	573	572	572	576	575	574	573
9.759	525	525	525	524	531	530	530	529	570	570	570	569	573	572	572	571
8.732	529	529	528	527	534	534	533	532	567	567	567	566	570	570	569	568
7.705	532	532	532	530	537	537	537	535	564	564	564	563	567	567	566	566
6.677	536	536	535	534	541	541	540	538	561	561	561	560	564	564	564	563
5.650	540	539	539	537	544	544	543	542	558	558	557	557	561	561	561	560
4.623	543	543	542	540	547	547	546	545	554	554	554	554	558	558	558	557
3.596	545	545	544	543	550	549	549	547	552	551	551	551	555	555	555	555
2.568	547	546	546	544	551	551	550	548	549	549	549	549	553	553	553	553
1.541	547	547	547	545	552	551	551	549	548	548	548	548	552	552	552	552
0.514	548	548	547	545	552	552	551	549	547	547	547	547	551	551	551	551
Elevation (3)	PANEL 9E				PANEL 10E				PANEL 11E				PANEL 12E			
Avg Temp (°C)	519	519	519	518	525	525	524	523	575	575	574	573	577	577	576	575
Max Temp (°C)	548	548	547	545	552	552	551	549	601	601	600	598	602	601	600	597
Panel Avg Temp (°C)	519				525				574				576			
Panel Max Temp (°C)	548				552				601				602			
	(1)	(2)	(2)	(1)												

Node Width (4)	0.3680	0.7770	0.7770	0.3680	0.3680	0.7770	0.7770	0.3680	0.3680	0.7770	0.7770	0.3680	0.3680	0.7770	0.7770	0.3680
22.087	602	601	600	598	601	600	600	598	518	518	518	518	524	524	524	524
21.060	602	600	599	598	601	600	600	598	518	518	518	518	524	524	524	524
20.032	601	599	598	597	600	599	599	597	520	520	520	520	526	526	526	525
19.005	599	598	597	596	599	598	598	596	522	522	521	521	527	527	527	527
17.978	597	596	595	594	597	596	596	594	524	524	524	523	530	530	529	529
16.950	595	593	593	591	594	594	593	592	527	526	526	526	532	532	532	531
15.923	592	591	590	589	592	591	591	590	529	529	529	528	534	534	534	534
14.896	589	588	587	586	589	588	588	587	532	531	531	531	537	536	536	536
13.869	586	585	584	583	586	586	585	585	534	534	533	533	539	539	538	538
12.841	583	582	582	581	584	583	583	582	536	536	535	535	541	540	540	540
11.814	580	580	579	578	581	581	581	580	538	538	537	537	543	542	542	541
10.787	578	577	577	576	579	579	579	578	540	540	540	539	545	544	544	543
9.759	575	575	574	574	577	577	576	576	543	542	542	541	547	546	546	545
8.732	573	572	572	572	575	574	574	574	545	544	544	543	549	548	548	547
7.705	570	570	570	569	572	572	572	572	547	546	546	545	551	550	550	549
6.677	568	567	567	567	570	570	570	569	549	549	548	547	553	553	552	551
5.650	565	565	564	564	567	567	567	567	552	551	551	549	555	555	554	553
4.623	562	562	562	562	565	565	565	565	554	553	553	551	557	557	556	555
3.596	560	560	559	559	563	562	562	562	556	555	554	553	559	558	557	556
2.568	558	558	558	558	561	561	561	561	557	556	555	554	560	559	558	557
1.541	557	557	557	557	560	560	560	560	557	556	556	554	560	559	559	557
0.514	556	556	556	556	559	559	559	559	557	557	556	554	560	560	559	558
Elevation (3)	PANEL 12W				PANEL 11W				PANEL 10W				PANEL 9W			
Avg Temp (°C)	579	579	578	577	580	580	580	579	539	538	538	537	543	543	542	542
Max Temp (°C)	602	601	600	598	601	600	600	598	557	557	556	554	560	560	559	558
Panel Avg Temp (°C)	578				580				538				543			
Panel Max Temp (°C)	602				601				557				560			
	(1)	(2)	(2)	(1)												

Node Width (4)	0.3680	0.7770	0.7770	0.3680	0.3680	0.7770	0.7770	0.3680	0.3680	0.7770	0.7770	0.3680	0.3680	0.7770	0.7770	0.3680
22.087	518	518	517	516	524	524	523	523	390	390	390	390	397	397	397	397
21.060	518	518	517	516	524	524	523	523	390	390	390	390	398	398	398	398
20.032	517	517	516	515	523	523	523	522	392	392	392	392	399	399	399	399
19.005	516	516	515	514	522	522	522	521	393	393	393	393	400	400	400	400
17.978	515	514	514	513	521	520	520	520	395	395	395	395	402	402	402	402
16.950	513	512	512	511	519	518	518	518	397	397	397	397	404	405	405	405
15.923	510	510	509	509	516	516	516	516	399	399	399	399	407	407	407	407
14.896	508	508	507	507	514	514	514	514	401	401	401	401	409	409	409	409
13.869	506	506	505	505	512	512	512	512	403	403	403	403	410	411	411	411
12.841	504	504	503	503	511	510	510	510	405	405	405	405	412	413	413	413
11.814	502	502	502	501	509	509	508	508	407	407	407	407	414	415	415	415
10.787	500	500	500	499	507	507	507	506	408	409	409	409	416	416	417	417
9.759	498	498	498	498	505	505	505	505	410	410	410	410	418	418	418	419
8.732	497	496	496	496	504	503	503	503	412	412	412	412	419	420	420	421
7.705	495	495	494	494	502	502	502	501	414	414	414	414	421	422	422	423
6.677	493	493	492	492	500	500	500	500	416	416	416	416	423	424	424	425
5.650	491	490	490	490	498	498	498	498	418	418	418	418	425	426	426	427
4.623	488	488	488	488	496	496	496	496	419	420	420	420	427	428	428	429
3.596	487	486	486	486	494	494	494	494	421	421	421	421	429	429	430	430
2.568	485	485	485	485	493	493	493	493	422	422	422	422	429	430	431	431
1.541	484	484	484	484	492	492	492	492	422	422	423	423	430	431	431	432
0.514	484	484	484	484	492	492	492	492	422	423	423	423	430	431	431	432
Elevation (3)	PANEL 8W				PANEL 7W				PANEL 6W				PANEL 5W			
Avg Temp (°C)	501	501	501	500	508	508	508	508	407	407	407	407	415	415	415	415
Max Temp (°C)	518	518	517	516	524	524	523	523	422	423	423	423	430	431	431	432
Panel Avg Temp (°C)	501				508				407				415			
Panel Max Temp (°C)	518				524				423				432			
	(1)	(2)	(2)	(1)												

Node Width (4)	0.3680	0.7770	0.7770	0.3680	0.3680	0.7770	0.7770	0.3680	0.3680	0.7770	0.7770	0.3680	0.3680	0.7770	0.7770	0.3680
22.087	388	389	390	391	395	396	397	398	308	308	308	308	308	308	308	308
21.060	388	389	390	391	394	396	397	398	309	309	309	309	309	309	309	309
20.032	387	388	389	390	394	395	396	397	311	311	311	311	311	311	311	311
19.005	386	387	388	389	393	394	395	396	312	313	313	313	313	313	313	313
17.978	384	385	386	387	391	392	393	394	315	315	315	315	315	316	316	316
16.950	382	383	384	385	389	390	391	392	318	318	318	318	318	319	319	319
15.923	380	381	382	382	386	387	388	389	320	321	321	321	321	322	322	322
14.896	378	379	379	380	384	385	386	386	323	323	324	324	324	325	325	325
13.869	376	376	377	378	381	382	383	384	325	326	326	327	327	328	328	328
12.841	374	374	375	375	379	380	381	381	328	329	329	329	330	330	331	331
11.814	372	372	373	373	377	378	378	379	330	331	332	332	332	333	334	334
10.787	370	370	371	371	375	376	376	377	332	333	334	335	335	336	336	337
9.759	368	368	369	369	373	374	374	374	335	336	336	337	337	338	339	339
8.732	366	366	367	367	371	371	372	372	337	338	339	340	340	341	342	342
7.705	364	364	365	365	369	369	369	370	339	341	342	342	342	344	345	345
6.677	362	362	362	363	366	367	367	367	342	344	344	345	345	347	348	348
5.650	360	360	360	360	364	364	365	365	344	346	347	348	348	350	350	351
4.623	358	358	358	358	362	362	362	362	347	348	349	350	350	352	353	354
3.596	356	356	356	356	360	360	360	360	348	350	351	352	352	354	355	356
2.568	354	354	354	354	358	358	358	358	349	351	352	353	353	355	356	357
1.541	353	353	353	353	357	357	357	357	350	352	353	354	354	356	357	357
0.514	353	353	353	353	357	357	357	357	350	352	353	354	354	356	357	358
Elevation (3)	PANEL 4W				PANEL 3W				PANEL 2W				PANEL 1W			
Avg Temp (°C)	371	371	372	372	376	377	377	378	331	332	332	333	333	334	334	335
Max Temp (°C)	388	389	390	391	395	396	397	398	350	352	353	354	354	356	357	358
Panel Avg Temp (°C)	372				377				332				334			
Panel Max Temp (°C)	391				398				354				358			
	(1)	(2)	(2)	(1)												

NOTES:

(1) Bulk Fluid Temperature at panel edge nodes (°C)
(2) Bulk Fluid Temperature at third points across panel width (°C)
(3) Node mid point elevation (m)
(4) Width of Node (m), required for Solar Square program

Tube ID Temperatures
(Salt Film Temperatures)

Node Width (4)	0.3680	0.7770	0.7770	0.3680	0.3680	0.7770	0.7770	0.3680	0.3680	0.7770	0.7770	0.3680	0.3680	0.7770	0.7770	0.3680
22.087	325	326	326	327	327	328	328	328	433	435	436	437	441	443	444	444
21.060	342	344	344	345	345	347	348	348	447	451	452	452	456	459	459	459
20.032	364	366	367	368	368	372	374	374	466	470	471	471	475	478	479	479
19.005	388	391	393	395	395	400	402	403	486	491	492	493	496	500	501	500
17.978	410	413	415	418	418	423	427	428	503	508	510	510	514	517	518	518
16.950	421	424	427	430	430	436	439	441	509	513	515	517	520	523	525	525
15.923	425	429	431	434	434	439	442	445	507	511	513	515	518	522	523	523
14.896	425	428	431	434	434	439	441	443	501	505	507	508	512	515	516	517
13.869	424	428	430	433	433	438	440	442	495	499	501	502	506	509	510	511
12.841	424	429	431	433	433	438	440	442	490	494	495	497	500	503	505	505
11.814	425	429	431	434	434	438	441	443	485	489	490	492	495	498	500	500
10.787	426	430	432	435	435	440	442	444	481	485	487	488	491	494	496	496
9.759	427	432	434	437	437	442	444	446	478	482	483	485	488	491	492	493
8.732	430	435	438	440	440	445	448	450	477	481	482	483	487	490	491	491
7.705	435	440	443	445	445	451	454	456	477	481	483	483	487	490	491	491
6.677	440	444	447	450	450	456	460	462	477	481	483	483	487	490	491	491
5.650	440	444	447	450	450	456	460	462	472	476	478	478	482	484	485	485
4.623	432	435	438	441	441	447	451	453	459	461	463	464	467	469	470	470
3.596	416	419	421	425	425	430	433	436	437	438	439	440	444	445	446	446
2.568	395	397	399	402	402	406	409	411	408	409	410	411	415	416	416	417
1.541	378	380	381	384	383	387	389	390	386	386	386	387	391	392	392	392
0.514	368	370	371	373	373	376	378	379	373	373	373	374	378	378	379	379
Elevation (3)	PANEL 1E				PANEL 2E				PANEL 3E				PANEL 4E			
Avg Temp (°C)	407	411	413	415	415	419.66	422.17	424	466	469	470	471	475	478	479	479
Max Temp (°C)	440	444	447	450	450	456.16	459.78	462	509	513	515	517	520	523	525	525
Panel Avg Temp (°C)	411				420				469				477			
Panel Max Temp (°C)	450				462				517				525			
	(1)	(2)	(2)	(1)												

Node Width (4)	0.3680	0.7770	0.7770	0.3680	0.3680	0.7770	0.7770	0.3680	0.3680	0.7770	0.7770	0.3680	0.3680	0.7770	0.7770	0.3680
22.087	437	437	437	437	444	444	444	444	501	502	502	500	508	509	508	506
21.060	454	455	455	455	461	462	463	462	516	517	517	515	523	524	523	520
20.032	476	478	479	478	484	486	486	485	535	536	536	534	542	542	542	538
19.005	502	505	505	504	510	512	513	511	549	550	549	547	554	554	553	550
17.978	526	528	529	528	534	536	536	535	573	575	575	572	580	580	579	576
16.950	539	541	541	541	547	549	549	548	579	580	580	578	585	585	584	581
15.923	544	546	546	546	552	553	554	553	577	578	578	576	583	583	582	579
14.896	544	546	546	546	552	553	554	553	570	571	571	569	576	576	575	572
13.869	544	546	547	546	552	554	554	553	563	564	564	562	569	569	568	565
12.841	545	547	548	547	553	554	555	553	558	558	558	556	563	563	563	560
11.814	546	548	549	548	554	556	556	554	552	553	553	551	558	558	557	554
10.787	548	550	551	550	556	558	558	556	548	549	548	546	554	554	553	550
9.759	550	553	554	553	559	560	561	559	544	545	545	543	550	550	550	547
8.732	555	557	558	557	563	565	565	563	542	543	543	541	548	549	548	545
7.705	560	563	564	563	569	571	571	569	542	543	543	541	548	549	548	545
6.677	566	569	570	569	575	577	577	575	542	543	543	541	548	549	548	546
5.650	567	570	570	570	575	577	578	576	536	537	537	536	543	543	543	540
4.623	559	561	562	562	568	569	570	569	522	522	522	521	528	528	528	526
3.596	543	545	546	546	552	553	553	553	499	499	499	499	506	506	505	504
2.568	521	523	523	523	530	530	531	530	471	470	470	470	478	477	477	477
1.541	503	504	505	505	511	512	512	512	448	448	447	447	455	455	455	455
0.514	493	494	495	494	501	502	502	501	435	435	435	435	443	443	443	442
Elevation (3)	PANEL 5E				PANEL 6E				PANEL 7E				PANEL 8E			
Avg Temp (°C)	528	530	531	530	536	538	538	537	532	533	533	531	538	538	538	535
Max Temp (°C)	567	570	570	570	575	577	578	576	579	580	580	578	585	585	584	581
Panel Avg Temp (°C)	530				537				532				537			
Panel Max Temp (°C)	570				578				580				585			
	(1)	(2)	(2)	(1)												

Node Width (4)	0.3680	0.7770	0.7770	0.3680	0.3680	0.7770	0.7770	0.3680	0.3680	0.7770	0.7770	0.3680	0.3680	0.7770	0.7770	0.3680
22.087	501	501	501	500	507	507	507	506	611	610	609	606	611	609	608	605
21.060	517	517	517	516	522	523	522	521	623	622	621	618	622	621	619	615
20.032	538	538	538	536	542	543	542	540	638	637	636	632	636	635	632	628
19.005	554	554	553	551	558	558	557	555	649	648	646	642	647	645	642	637
17.978	584	584	583	580	587	587	586	583	668	667	665	661	665	663	660	654
16.950	596	596	595	592	598	598	596	594	672	670	669	664	668	666	663	658
15.923	601	600	599	596	603	601	600	597	669	667	666	662	666	663	660	656
14.896	601	600	599	596	602	601	600	597	663	661	659	655	659	656	654	650
13.869	601	600	599	596	602	601	600	596	656	654	653	649	653	651	648	644
12.841	601	600	599	596	603	601	600	597	651	649	648	644	648	646	644	640
11.814	602	602	601	597	604	602	601	597	646	645	643	639	643	641	639	635
10.787	604	604	603	599	606	604	603	599	643	641	639	636	640	638	636	632
9.759	607	606	605	602	608	607	606	602	640	638	637	633	637	635	633	629
8.732	611	611	610	606	613	612	610	606	639	637	636	632	636	634	632	628
7.705	617	617	616	612	619	618	616	612	639	638	636	632	636	635	632	628
6.677	624	624	622	618	625	624	623	618	639	638	637	633	637	635	633	628
5.650	625	625	623	620	626	626	624	620	635	634	632	629	633	632	629	625
4.623	618	617	616	613	620	619	617	614	623	622	621	619	623	621	618	615
3.596	603	603	601	599	606	604	603	600	605	604	603	601	605	604	602	599
2.568	583	582	581	579	586	584	583	581	582	581	581	580	584	583	582	580
1.541	566	565	564	562	569	568	567	565	564	564	563	563	567	566	566	565
0.514	556	556	555	553	560	559	558	556	555	554	554	554	558	557	557	557
Elevation (3)	PANEL 9E				PANEL 10E				PANEL 11E				PANEL 12E			
Avg Temp (°C)	587	586	585	583	589	589	587	584	632	631	630	627	631	629	627	623
Max Temp (°C)	625	625	623	620	626	626	624	620	672	670	669	664	668	666	663	658
Panel Avg Temp (°C)	585				587				630				627			
Panel Max Temp (°C)	625				626				672				668			
	(1)	(2)	(2)	(1)												

Node Width (4)	0.3680	0.7770	0.7770	0.3680	0.3680	0.7770	0.7770	0.3680	0.3680	0.7770	0.7770	0.3680	0.3680	0.7770	0.7770	0.3680
22.087	609	608	607	605	608	607	606	605	525	525	525	525	531	531	530	530
21.060	619	618	616	614	617	617	616	613	536	536	536	535	541	541	540	539
20.032	632	631	629	626	629	629	628	625	550	551	550	548	554	554	553	552
19.005	647	644	642	639	642	642	641	638	567	567	566	564	570	569	568	566
17.978	658	656	653	650	653	652	651	648	582	582	580	578	583	583	581	579
16.950	662	659	657	653	656	655	654	651	590	589	587	585	590	589	588	586
15.923	659	656	654	651	654	652	651	648	592	591	589	586	592	591	589	587
14.896	654	651	649	646	648	647	645	642	591	589	588	585	591	589	588	586
13.869	648	646	644	641	643	642	640	637	590	588	587	584	590	588	587	585
12.841	644	641	639	636	639	637	636	633	590	588	587	584	590	588	587	585
11.814	639	637	635	632	635	633	632	629	590	589	587	585	590	589	588	585
10.787	636	634	632	629	632	631	629	627	591	590	588	586	591	590	589	586
9.759	634	631	630	627	630	628	627	625	593	592	590	588	593	592	591	588
8.732	632	630	629	626	629	628	626	624	597	596	594	591	596	595	594	591
7.705	632	631	629	626	629	628	627	625	602	601	599	596	601	600	598	596
6.677	633	630	629	626	629	629	628	625	607	606	604	601	606	605	603	600
5.650	629	626	625	623	626	626	625	623	609	608	606	603	608	607	605	602
4.623	619	617	615	614	617	617	616	615	605	604	602	599	604	603	601	599
3.596	604	601	600	600	603	602	602	601	595	594	592	589	595	594	592	590
2.568	585	583	582	582	585	585	585	584	580	579	578	576	581	580	579	577
1.541	570	569	568	568	571	571	571	571	568	567	566	564	570	569	568	567
0.514	562	561	561	561	564	564	564	564	562	561	560	558	564	563	562	561
Elevation (3)	PANEL 12W				PANEL 11W				PANEL 10W				PANEL 9W			
Avg Temp (°C)	628	625	624	622	624	624	623	621	582	581	580	578	583	582	581	579
Max Temp (°C)	662	659	657	653	656	655	654	651	609	608	606	603	608	607	605	602
Panel Avg Temp (°C)	625				623				580				581			
Panel Max Temp (°C)	662				656				609				608			
	(1)	(2)	(2)	(1)												

Node Width (4)	0.3680	0.7770	0.7770	0.3680	0.3680	0.7770	0.7770	0.3680	0.3680	0.7770	0.7770	0.3680	0.3680	0.7770	0.7770	0.3680
22.087	525	524	524	522	530	530	530	529	398	399	399	398	405	406	406	406
21.060	533	533	532	531	538	538	538	537	409	409	409	409	416	417	417	417
20.032	544	544	543	541	548	549	548	547	423	424	423	423	430	431	431	431
19.005	556	556	555	553	560	560	559	558	435	436	436	435	442	444	444	445
17.978	566	565	564	562	569	568	568	566	452	453	453	453	459	461	462	462
16.950	568	567	566	564	571	570	570	569	459	459	459	459	466	467	468	469
15.923	566	564	563	561	568	568	567	566	460	461	461	461	467	469	469	471
14.896	560	559	558	556	563	563	562	561	458	459	459	459	466	467	468	469
13.869	556	554	553	552	559	558	558	557	457	458	458	458	465	466	467	468
12.841	552	551	550	548	555	555	554	553	457	457	457	458	464	466	467	468
11.814	549	548	547	545	552	552	551	551	457	458	458	458	465	466	467	468
10.787	546	545	544	543	550	550	549	548	458	458	459	459	465	467	468	469
9.759	544	544	543	541	548	548	547	547	459	460	460	460	467	469	470	471
8.732	544	543	542	541	548	548	547	546	462	463	463	463	470	472	473	474
7.705	545	545	543	542	549	549	548	547	466	467	467	467	474	476	477	478
6.677	546	546	545	543	550	550	549	548	471	472	472	472	479	481	482	483
5.650	544	544	543	541	548	548	547	546	473	474	474	474	480	483	484	485
4.623	537	536	535	534	541	541	540	539	469	470	470	470	477	478	479	480
3.596	524	523	523	522	529	529	528	528	459	460	460	460	467	468	469	470
2.568	508	507	507	507	514	514	513	513	445	446	446	446	453	454	455	456
1.541	495	495	495	494	502	502	502	502	434	434	434	434	441	442	443	444
0.514	488	488	488	488	496	496	496	496	427	428	428	428	435	436	437	437
Elevation (3)	PANEL 8W				PANEL 7W				PANEL 6W				PANEL 5W			
Avg Temp (°C)	541	540	539	538	545	545	544	543	452	450	450	450	457	459	459	460
Max Temp (°C)	568	567	566	564	571	570	570	569	473	474	474	474	480	483	484	485
Panel Avg Temp (°C)	539				544				451				459			
Panel Max Temp (°C)	568				571				474				485			
	(1)	(2)	(2)	(1)												

Node Width (4)	0.3680	0.7770	0.7770	0.3680	0.3680	0.7770	0.7770	0.3680	0.3680	0.7770	0.7770	0.3680	0.3680	0.7770	0.7770	0.3680
22.087	397	399	400	401	405	407	408	409	323	324	324	324	324	325	325	325
21.060	407	410	411	412	415	418	420	421	338	339	340	340	340	342	342	342
20.032	420	423	424	425	429	432	434	435	357	360	361	361	361	364	364	364
19.005	432	435	436	438	442	445	447	449	377	380	381	382	383	386	386	386
17.978	446	449	451	452	456	460	462	464	398	402	404	405	406	409	410	411
16.950	449	452	454	456	459	463	466	468	408	411	414	416	416	420	421	422
15.923	447	450	452	454	457	461	463	466	410	414	416	418	419	422	424	426
14.896	441	444	446	448	452	456	458	461	408	412	414	417	417	421	423	425
13.869	437	440	441	443	447	451	453	455	407	411	413	416	416	420	422	425
12.841	433	436	437	439	443	447	449	451	406	411	413	416	416	420	422	425
11.814	430	432	434	436	440	443	445	448	406	411	413	416	416	420	423	425
10.787	427	430	431	433	437	441	442	445	407	412	414	417	417	422	424	426
9.759	425	428	430	431	435	438	440	443	409	414	416	418	419	423	425	428
8.732	425	428	429	431	434	438	440	442	412	417	419	422	422	427	429	431
7.705	426	429	430	432	435	439	441	443	417	422	425	427	427	432	434	436
6.677	427	430	432	433	437	440	442	444	422	428	430	432	432	437	439	440
5.650	425	428	429	431	434	437	439	441	424	428	431	433	433	438	439	440
4.623	417	419	420	421	425	427	429	431	417	421	424	426	426	430	431	432
3.596	402	404	405	406	409	411	412	414	404	407	409	411	412	415	416	417
2.568	383	384	385	386	389	390	391	392	384	387	389	391	391	393	395	396
1.541	368	369	369	370	373	374	374	375	368	370	372	374	374	376	377	378
0.514	360	360	360	361	365	365	365	366	359	361	363	364	364	366	367	368
Elevation (3)	PANEL 4W				PANEL 3W				PANEL 2W				PANEL 1W			
Avg Temp (°C)	419	422	423	425	428	431	433	435	394	397	399	401	401	405	406	408
Max Temp (°C)	449	452	454	456	459	463	466	468	424	428	431	433	433	438	439	440
Panel Avg Temp (°C)	422				432				398				405			
Panel Max Temp (°C)	456				468				433				440			
	(1)	(2)	(2)	(1)												

NOTES:

(1) Film (ID) Temperature at panel edge nodes (°C)
(2) Film (ID) Temperature at third points across panel width (°C)
(3) Node mid point elevation (m)
(4) Width of Node (m), required for Solar Square program

Tube OD Temperatures

Node Width (4)	0.3680	0.7770	0.7770	0.3680	0.3680	0.7770	0.7770	0.3680	0.3680	0.7770	0.7770	0.3680	0.3680	0.7770	0.7770	0.3680
22.087	338	340	341	341	341	344	344	344	446	449	451	451	455	458	459	458
21.060	369	372	373	374	374	378	380	380	474	479	481	480	484	488	489	488
20.032	408	412	414	416	416	423	426	426	511	517	519	518	522	527	528	527
19.005	452	457	460	464	464	473	477	479	553	559	562	562	565	571	572	571
17.978	491	496	500	506	505	516	521	524	588	595	598	599	602	608	609	609
16.950	510	516	520	526	526	536	542	546	602	610	613	614	617	623	625	625
15.923	515	521	525	531	531	541	546	550	602	609	612	615	617	623	625	626
14.896	511	518	522	528	528	536	541	545	593	600	603	605	608	614	616	617
13.869	508	515	519	524	524	532	536	540	584	591	594	596	599	605	607	608
12.841	506	513	517	522	522	530	533	537	577	584	587	589	592	598	600	600
11.814	504	512	516	520	520	528	531	535	571	578	581	583	586	591	593	594
10.787	504	512	515	520	520	528	531	535	567	573	576	578	581	587	589	589
9.759	505	513	517	521	521	529	533	536	563	570	573	575	578	583	585	586
8.732	508	516	521	525	524	533	538	541	564	571	574	575	578	584	586	586
7.705	515	523	527	532	531	541	546	549	567	574	578	578	581	587	590	589
6.677	521	529	534	538	538	549	554	558	571	578	581	582	585	591	593	592
5.650	519	525	530	535	535	545	552	555	564	571	574	575	578	583	584	584
4.623	501	506	511	517	516	526	532	536	541	546	548	550	553	556	558	558
3.596	470	474	478	483	483	490	496	500	501	504	506	508	511	513	514	515
2.568	429	432	435	439	439	444	448	451	449	451	452	454	457	458	459	460
1.541	396	398	400	403	403	407	409	412	407	408	409	410	414	414	415	415
0.514	377	379	381	383	383	386	388	390	384	384	385	385	390	390	390	391
Elevation (3)	PANEL 1E				PANEL 2E				PANEL 3E				PANEL 4E			
Avg Temp (°C)	471	476	480	484	484	491.52	495.72	499	535	541	543	545	548	552	554	554
Max Temp (°C)	521	529	534	538	538	548.65	554.49	558	602	610	613	615	617	623	625	626
Panel Avg Temp (°C)	478				492				541				552			
Panel Max Temp (°C)	538				558				615				626			
	(1)	(2)	(2)	(1)												

Node Width (4)	0.3680	0.7770	0.7770	0.3680	0.3680	0.7770	0.7770	0.3680	0.3680	0.7770	0.7770	0.3680	0.3680	0.7770	0.7770	0.3680
22.087	451	452	453	452	459	460	460	459	515	516	516	513	521	522	521	518
21.060	483	486	486	485	491	493	493	492	544	546	545	542	550	551	550	546
20.032	525	528	529	527	533	536	537	534	581	584	584	580	587	588	587	583
19.005	573	577	578	576	582	586	586	584	610	612	611	607	613	613	611	606
17.978	616	620	621	620	625	628	629	627	661	663	663	659	665	666	665	659
16.950	637	641	642	642	646	650	651	649	676	677	677	674	680	680	679	674
15.923	643	647	648	648	652	655	656	654	675	677	676	673	679	679	678	673
14.896	640	643	645	644	649	652	652	651	666	667	666	663	670	669	668	663
13.869	636	640	641	641	646	648	649	647	656	657	657	653	660	659	658	654
12.841	635	638	640	639	644	646	647	645	648	649	649	646	652	652	651	646
11.814	633	637	638	638	643	645	646	643	641	643	642	639	645	645	644	639
10.787	634	638	639	638	643	646	646	644	636	637	637	633	640	640	639	634
9.759	636	640	641	640	645	648	648	645	633	634	634	630	636	636	636	631
8.732	641	645	646	645	650	653	653	650	632	634	634	630	636	637	636	631
7.705	649	654	655	653	658	661	662	659	635	637	637	633	639	640	639	634
6.677	657	662	663	661	666	670	670	667	638	641	641	636	643	644	643	638
5.650	655	659	660	659	664	667	668	666	631	633	633	629	636	636	635	631
4.623	636	640	641	640	646	648	649	647	606	607	607	605	611	611	610	607
3.596	603	605	606	606	612	614	614	613	565	565	565	564	570	570	569	567
2.568	559	560	561	561	567	568	569	568	512	511	511	511	518	517	517	516
1.541	523	524	524	524	531	532	532	531	469	469	469	469	476	476	475	475
0.514	503	504	504	504	511	512	512	511	446	446	446	445	453	453	453	452
Elevation (3)	PANEL 5E				PANEL 6E				PANEL 7E				PANEL 8E			
Avg Temp (°C)	605	602	603	602	607	610	610	608	603	605	604	602	608	608	607	603
Max Temp (°C)	657	662	663	661	666	670	670	667	676	677	677	674	680	680	679	674
Panel Avg Temp (°C)	601				609				604				607			
Panel Max Temp (°C)	663				670				677				680			
	(1)	(2)	(2)	(1)												

Node Width (4)	0.3680	0.7770	0.7770	0.3680	0.3680	0.7770	0.7770	0.3680	0.3680	0.7770	0.7770	0.3680	0.3680	0.7770	0.7770	0.3680
22.087	514	514	513	512	519	519	518	517	620	619	618	614	619	617	615	612
21.060	543	544	543	541	547	548	547	544	643	642	641	636	640	639	637	632
20.032	582	583	582	578	584	585	584	580	673	672	670	665	669	668	664	658
19.005	611	611	609	605	613	612	610	606	696	694	691	686	691	689	684	677
17.978	667	667	665	660	666	665	663	658	736	734	731	725	729	726	721	712
16.950	687	686	684	679	685	683	681	676	747	744	741	735	739	735	730	722
15.923	692	690	688	684	689	687	685	680	745	742	739	733	736	732	728	720
14.896	688	687	685	680	686	683	681	676	735	732	729	723	726	722	719	712
13.869	685	683	681	676	682	680	677	671	726	723	720	714	717	714	710	704
12.841	683	681	679	674	680	678	675	669	719	716	713	707	710	707	703	697
11.814	682	680	678	673	679	676	674	668	713	710	707	701	704	701	698	691
10.787	682	681	679	674	679	677	675	669	708	705	703	696	700	697	694	687
9.759	684	683	682	676	682	680	677	671	706	703	700	694	698	694	691	685
8.732	690	689	687	681	687	686	683	676	706	704	701	694	698	695	692	685
7.705	698	698	696	690	696	694	692	685	709	707	705	698	702	699	695	687
6.677	707	707	705	698	704	703	701	694	713	711	708	702	705	703	698	690
5.650	706	705	703	698	704	703	700	694	707	706	703	698	701	698	693	686
4.623	689	688	686	682	688	686	684	680	688	686	684	680	683	680	676	669
3.596	658	657	655	652	658	656	654	651	655	653	651	648	652	649	646	641
2.568	617	615	614	611	618	616	615	612	613	611	610	608	612	610	608	605
1.541	583	582	581	578	585	584	583	580	579	578	577	577	581	579	578	577
0.514	564	563	563	561	567	566	565	563	561	561	560	560	564	563	562	562
Elevation (3)	PANEL 9E				PANEL 10E				PANEL 11E				PANEL 12E			
Avg Temp (°C)	650	650	648	644	650	649	647	642	686	684	682	677	681	678	675	669
Max Temp (°C)	707	707	705	698	704	703	701	694	747	744	741	735	739	735	730	722
Panel Avg Temp (°C)	648				647				682				676			
Panel Max Temp (°C)	707				704				747				739			
	(1)	(2)	(2)	(1)												

Node Width (4)	0.3680	0.7770	0.7770	0.3680	0.3680	0.7770	0.7770	0.3680	0.3680	0.7770	0.7770	0.3680	0.3680	0.7770	0.7770	0.3680
22.087	616	615	613	611	614	613	613	610	532	532	532	531	537	537	537	536
21.060	636	634	633	629	632	632	631	628	552	553	552	550	556	556	555	553
20.032	662	660	657	653	656	656	655	651	579	579	578	575	580	581	579	577
19.005	691	688	685	681	683	683	682	677	610	610	608	604	609	609	607	603
17.978	716	712	708	704	706	705	704	699	637	636	633	629	634	633	630	626
16.950	725	721	717	712	715	713	711	706	650	648	645	640	645	643	641	637
15.923	724	719	715	710	713	710	708	703	651	649	646	641	646	644	641	638
14.896	715	711	708	702	705	702	699	695	647	644	641	637	642	639	637	633
13.869	707	703	700	695	697	694	692	687	643	640	637	633	638	636	633	630
12.841	701	697	694	689	691	688	686	681	640	638	635	631	636	634	632	628
11.814	695	691	689	683	686	683	681	676	639	637	634	630	635	633	631	627
10.787	691	688	685	680	682	680	677	673	640	637	635	630	635	633	631	627
9.759	688	685	682	677	680	677	675	671	641	639	636	632	637	635	633	629
8.732	689	685	682	677	680	678	676	671	646	644	641	636	642	640	637	633
7.705	691	688	685	680	682	681	679	675	653	652	649	643	649	647	644	640
6.677	694	690	687	683	685	685	683	679	661	660	657	651	656	655	652	647
5.650	689	685	682	679	681	681	680	676	663	661	658	653	658	656	654	649
4.623	673	668	665	663	666	666	665	662	653	651	648	644	649	647	644	641
3.596	645	641	639	638	640	640	640	638	632	630	627	624	629	627	625	622
2.568	609	607	605	605	608	607	607	606	602	600	599	596	602	600	598	596
1.541	581	580	579	579	582	581	581	581	578	577	576	574	580	578	577	576
0.514	566	566	565	565	568	568	568	567	566	564	563	562	568	567	566	564
Elevation (3)	PANEL 12W				PANEL 11W				PANEL 10W				PANEL 9W			
Avg Temp (°C)	554	554	673	670	603	602	666	665	610	608	624	622	604	602	621	619
Max Temp (°C)	625	626	725	721	663	661	715	713	670	667	663	661	677	674	658	656
Panel Avg Temp (°C)	668				663				620				618			
Panel Max Temp (°C)	725				715				663				658			
	(1)	(2)	(2)	(1)												

Node Width (4)	0.3680	0.7770	0.7770	0.3680	0.3680	0.7770	0.7770	0.3680	0.3680	0.7770	0.7770	0.3680	0.3680	0.7770	0.7770	0.3680
22.087	530	530	529	528	535	536	535	534	405	406	406	406	413	414	414	414
21.060	547	547	546	544	551	552	551	550	425	426	426	425	432	434	434	434
20.032	569	569	568	565	572	572	572	570	450	452	452	451	458	460	461	460
19.005	594	593	591	588	595	595	594	592	472	474	474	473	480	483	484	484
17.978	614	613	611	607	614	614	612	610	504	505	505	505	511	514	515	516
16.950	621	619	617	613	620	619	618	616	515	516	516	516	522	524	526	527
15.923	618	616	613	610	617	616	615	614	515	516	516	516	522	525	526	528
14.896	609	607	605	602	609	608	607	606	510	511	511	511	517	520	521	524
13.869	602	600	598	596	602	602	600	599	506	507	507	508	514	517	518	520
12.841	597	595	593	590	597	597	596	594	504	505	505	505	512	515	516	518
11.814	592	591	589	586	593	593	592	590	502	504	504	504	510	513	515	517
10.787	589	588	586	583	590	590	589	588	502	504	504	504	510	514	515	517
9.759	588	586	585	582	588	588	587	586	504	505	505	505	512	515	516	518
8.732	589	588	586	583	589	589	588	586	507	509	509	509	515	519	520	522
7.705	592	591	589	586	593	593	591	589	514	516	516	516	522	526	527	529
6.677	596	596	593	590	597	597	595	593	522	523	524	523	529	533	535	536
5.650	595	594	592	589	595	595	594	592	524	525	525	525	531	534	536	538
4.623	582	581	579	577	584	583	582	580	514	515	515	516	522	524	526	528
3.596	559	558	556	555	562	561	560	560	494	495	495	495	502	504	505	507
2.568	529	528	527	527	534	533	533	533	467	467	467	468	474	476	477	478
1.541	505	504	504	504	511	511	511	511	444	444	444	445	452	453	454	455
0.514	492	492	492	492	499	499	499	499	432	432	432	433	440	441	441	442
Elevation (3)	PANEL 8W				PANEL 7W				PANEL 6W				PANEL 5W			
Avg Temp (°C)	607	603	578	577	575	573	579	579	578	577	488	489	489	489	495	498
Max Temp (°C)	679	674	621	619	617	613	620	619	618	616	524	525	525	525	531	534
Panel Avg Temp (°C)	575				578				489				497			
Panel Max Temp (°C)	621				620				525				534			
	(1)	(2)	(2)	(1)												

Node Width (4)	0.3680	0.7770	0.7770	0.3680	0.3680	0.7770	0.7770	0.3680	0.3680	0.7770	0.7770	0.3680	0.3680	0.7770	0.7770	0.3680
22.087	405	408	409	410	413	416	418	419	334	336	336	336	336	338	339	339
21.060	425	428	429	430	434	438	440	441	361	364	365	365	365	369	369	369
20.032	450	454	456	457	460	465	468	469	396	400	402	403	403	408	409	408
19.005	472	477	480	482	486	492	495	497	430	436	439	440	441	447	448	447
17.978	501	506	509	511	514	521	524	528	469	476	479	482	482	489	491	491
16.950	509	514	517	520	524	530	534	538	484	491	495	499	499	506	509	510
15.923	507	512	514	518	521	528	531	536	487	494	497	502	502	509	512	515
14.896	498	503	506	510	513	519	523	528	481	488	492	497	497	504	508	512
13.869	491	496	499	502	506	512	515	520	477	484	488	493	493	500	504	508
12.841	486	491	493	497	500	506	510	514	474	482	485	490	490	498	502	506
11.814	481	486	489	492	495	502	505	509	472	480	484	488	488	496	500	504
10.787	478	483	486	489	492	498	502	506	472	480	484	488	488	496	500	504
9.759	476	481	484	487	490	496	500	504	473	481	485	489	489	497	501	505
8.732	477	482	485	488	491	497	501	504	478	486	489	493	494	502	505	509
7.705	481	486	489	491	494	501	505	508	485	493	497	501	501	509	513	515
6.677	485	491	494	496	499	505	509	512	493	501	506	509	509	517	520	522
5.650	483	488	491	493	496	502	505	508	493	501	505	508	508	515	518	519
4.623	469	473	475	477	480	485	488	491	479	485	489	493	493	499	501	502
3.596	443	445	447	449	453	456	458	461	451	456	460	463	463	468	469	471
2.568	409	410	411	413	416	418	420	422	414	418	420	423	423	426	428	429
1.541	381	382	382	383	387	388	389	390	383	386	388	390	391	393	394	396
0.514	366	366	367	367	371	372	372	373	367	369	371	373	373	375	376	377
Elevation (3)	PANEL 4W				PANEL 3W				PANEL 2W				PANEL 1W			
Avg Temp (°C)	499	501	462	466	474	479	482	485	448	454	457	460	461	466	469	471
Max Temp (°C)	536	538	509	514	524	530	534	538	493	501	506	509	509	517	520	522
Panel Avg Temp (°C)	482				480				455				467			
Panel Max Temp (°C)	538				538				509				522			
	(1)	(2)	(2)	(1)												

NOTES:

(1) Tube OD Temperature at panel edge nodes (°C)
(2) Tube OD Temperature at third points across panel width (°C)
(3) Node mid point elevation (m)
(4) Width of Node (m), required for Solar Square program

APPENDIX G

Receiver
Process and Instrument Diagrams

12634401-60-6100

NOTES

PROCESS AND INSTRUMENTATION DIAGRAMS

ABENGOA SOLAR, INC.
MOLTEN SALT SOLAR RECEIVER – PHASE II
FWNAC CONTRACT No.: 65–126344–01

DRAWING INDEX

REV.	DRAWING NO.	TITLE	REMARKS
B	12634401–60–6100	DRAWING INDEX	
A	12634401–60–6101	SYMBOLS AND LEGEND	
B	12634401–60–6103	SOLAR RECEIVER WEST PASS – EAST PANELS 1E, 3E, 5E TO WEST PANELS 8W, 10W, 12W	
B	12634401–60–6104	SOLAR RECEIVER WEST PASS – EAST PANELS 2E, 4E, 6E TO WEST PANELS 7W, 9W, 11W	
B	12634401–60–6105	SOLAR RECEIVER EAST PASS – WEST PANELS 1W, 3W, 5W TO EAST PANELS 8E, 10E, 12E	
B	12634401–60–6106	SOLAR RECEIVER EAST PASS – WEST PANELS 2W, 4W, 6W TO EAST PANELS 7E, 9E, 11E	

REV.	DATE	DR. INIT.	REVISIONS DESCRIPTION
B	02/06/14	MCE	REVISED AS NOTED.
A	12/12/13	MCE	INITIAL ISSUE.

REV.	DATE	APPR.	ISSUED FOR
			CONSTRUCTION
			FABRICATION
			DETAILING
			COMPLETE MATERIAL ORDER
			PARTIAL MATERIAL ORDER
			BID/QUOTATION

PROCESS & INSTRUMENTATION DIAGRAM
SOLAR RECEIVER
DRAWING INDEX

MOLTEN SALT
SOLAR RECEIVER – PHASE II
ABENGOA SOLAR, INC.

DRAWING NUMBER	SCALE: NONE=1–0"	REVISION
12634401–60–6100		B

DRAWN BY	MCE	07/25/13	65–126344–01	
CHECKED BY	HH	12/12/13		
APPROVED BY	RV	12/12/13	PRODUCT CODE 51	SIZE 5

12634401-60-6101

INSTRUMENT SYMBOLS AND NOTES

INSTRUMENT SYMBOLS

- INSTRUMENT MOUNTED LOCALLY IN THE FIELD.
- CONTROL PANEL MOUNTED (LOCATED IN CONTROL ROOM).
- REAR PANEL MOUNTED (LOCATED IN CONTROL ROOM).
- LOCAL PANEL MOUNTED (IN THE FIELD).
- REAR LOCAL PANEL MOUNTED (IN THE FIELD).
- DATA AQUISITION CONTROL SYSTEM. MONITOR LOCATED IN CONTROL ROOM.
- BINARY CONTROL FUNCTION (DCS)
- DISTRIBUTED CONTROL SYSTEM
- PROGRAMMABLE LOGIC CONTROLLER
- EMERGENCY SHUTDOWN SYSTEM
- BURNER MANAGEMENT SYSTEM
- MOTOR PROTECTION RELAY
- INSTRUMENT W/FREEZE PROTECTION ENCLOSURE

INSTRUMENT TAG DESIGNATION

ABBB CCCC DDDDE GGG

A = UNIT CODE IDENTIFICATION
BBB = SYSTEM CODE
CCCC = FUNCTION IDENTIFICATION
DDDDD= CONTROL LOOP NUMBER
F = UNIQUE SUFFIX MODIFIER (OPTIONAL)
GGG = BUS TECHNOLOGY
FF = FOUNDATION FIELDBUS
DN = DeviceNet
CN = ControlNet

NOTATIONS

DESIGNATION	DESCRIPTION
FW	SUPPLIED BY FOSTER WHEELER NORTH AMERICA CORP.
FO	FAIL OPEN (AIR OR CONTROL SIGNAL)
FL	FAIL LOCKED LAST POSITION (AIR OR CONTROL SIGNAL)
FAI	FAIL AS IS (AIR OR POWER SUPPLY)
FC	FAIL CLOSED (AIR OR CONTROL SIGNAL)
BC	BOILER CODE TERMINAL POINT
NO	NORMALLY OPEN
NC	NORMALLY CLOSED
HR	HALF RETRACT SOOTBLOWER
LR	LONG RETRACT SOOTBLOWER
WB	WALL BLOWER SOOTBLOWER
O	SUPPLIED BY OTHERS
LO	LOCKED OPEN
LC	LOCKED CLOSED
GO	GEAR OPERATED
CHOP	CHAIN OPERATED
VTR	VENT THROUGH ROOF
(V)	SUPPLIED BY EQUIPMENT VENDOR

RUPTURE DISCS

- PRESSURE
- VACUUM

ACTUATORS

- PNEUMATIC SOLENOID OPERATED DIAPHRAGM VALVE (S, IA, VT)
- PNEUMATIC SINGLE SOLENOID OPERATED SINGLE-ACTING PISTON VALVE WITH SPRING RETURN (S, IA, VT)
- PNEUMATIC DOUBLE SOLENOID OPERATED DOUBLE-ACTING PISTON VALVE (IA, S, S, VT)
- PNEUMATIC DIAPHRAGM ACTUATOR WITH POSITIONER AND INTERGRAL POSITION TRANSMITTER (IA)
- PNEUMATIC DOUBLE-ACTING PISTON OPERATOR WITH POSITIONER AND INTERGRAL POSITION TRANSMITTER (IA)
- SOLENOID OPERATOR (S)
- SOLENOID OPERATOR WITH MANUAL OVERRIDE (S)
- MOTOR OPERATOR (M)
- DIAPHRAGM ACTUATOR WITH EXTERNAL TAP (PRESSURE REDUCING VALVE)
- SPRING DIAPHRAGM ACTUATOR (PRESSURE REDUCING REGULATOR)
- DIAPHRAGM ACTUATOR WITH EXTERNAL TAP (BACK PRESSURE REGULATOR)
- SPRING DIAPHRAGM ACTUATOR (BACK PRESSURE REGULATOR)
- HYDRAULIC ACTUATOR (H)
- ELECTRIC MOTOR DRIVE (M)
- AIR MOTOR DRIVE (A)

RELIEVING DEVICES

- PRESSURE SAFETY RELIEF VALVE
- VACUUM RELIEF VALVE
- SOLENOID OPERATED RELIEF VALVE (S)
- HYDROSTATIC RELIEF VALVE
- RELIEF VALVE WITH OPEN VENT STACK

BOILER CODE BREAK (A | B)

A– BOILER PROPER – THE ASME BOILER AND PRESSURE VESSEL CODE (ASME BPVC) HAS TOTAL ADMINSTRATIVE JURISDICTION AND TECHNICAL RESPONSIBILITY (REFER TO SECTION 1 PREAMBLE).

B– BOILER EXTERNAL PIPING AND JOINT – THE ASME BPVC HAS TOTAL ADMINISTRATIVE JURISDICTION (MANDATORY CERTIFICATION BY CODE SYMBOL STAMPING. ASME DATA FORMS. AND AUTHURIZED INSPECTION) OF BOILER EXTERNAL PIPING AND JOINT. THE ASME SECTION COMMITTEE B31.1 HAS BEEN ASSIGNED TECHNICAL RESPONSIBILITY.

C– NON-BOILER EXTERNAL PIPING AND JOINT – NOT SECTION 1 JURISDICTION (SEE APPLICABLE ASME B31. CODE) CODE BREAK AT FIRST BUTT WELD/SOCKET WELD.

D– ASME B31.3

E– ASME SECTION VIII DIV.1

INSTRUMENTATION CATEGORIES

LETTER	FIRST	SECOND	THIRD	FOURTH
A	ANALYZER	ANALYZER, AUTO OR ALARM	ALARM	ALARM
B	FLAME SCANNER	—		—
C	CONDUCTIVITY	CONTROL	CONTROL, CONVERTER, COLUMN OR CLOSED	CONTROL
D	DENSITY	DIFFERENTIAL	DAMPER	—
E	ELECTRIC	ELEMENT	ELEMENT	—
F	FLOW	FEEDER OR FLOW	FLOW	—
G	GAGE	GLASS OR GAGE	—	—
H	HAND (ACTUATED)	HUMIDITY	HAND OR HIGH	HIGH
I	CURRENT	INDICATING	INDICATOR	—
J	—	MULTI-POINT	—	—
K	COMPUTING OR TIME	—	—	—
L	LEVEL	LEVEL OR LIGHT	LOW	LOW
M	MOTOR	METER	MISCELLANEOUS	—
N	—	NOT	—	—
O	OXYGEN	OPERATOR	OPERATOR OR OPEN	—
P	PRESSURE OR PILOT	PNEUMATIC, TEST POINT	POSITIONER	—
Q	—	INTEGRATOR	INTEGRATOR	—
R	RADIATION	RECORDER OR RATIO	RECORDER	—
S	SPEED OR SOLENOID	SOLENOID, SWITCH OR SAFETY	SWITCH	SWITCH
T	TEMPERATURE	TRANSMITTER	TRANSMITTER	—
U	ULTRASONIC OR UNIT	ULTRASONIC	UNIT	—
V	VIBRATION	VALVE	VALVE	—
W	WEIGHT	WELL OR WATER	WINDOWS	—
X	SPECIAL (ON-OFF)	—	—	TRANSMITTER
Y	—	RELAY	RELAY	—
Z	LIMIT	POSITIONER/DRIVE	—	—

LINE TYPES

- MAIN PROCESS PIPING AND MAIN EQUIPMENT OUTLINES
- OTHER PROCESS OR UTILITY PIPING, EQUIPMENT OUTLINES, INSTRUMENT PIPING, ETC.
- SOFTWARE LINK
- PNEUMATIC INSTRUMENT LINE
- CAPILLARY TUBING
- ELECTRICAL/ELECTRONIC SIGNALS
- ET = ELECTRIC HEAT TRACED PIPING
  ST = STEAM HEAT TRACED PIPING
  HC = INSULATED ONLY FOR HEAT CONSERVATION
  NI = NOT INSULATED
- VENDOR SKID/EQUIPMENT BOUNDARY

LINE NUMBERING

14"–137–SA106C–ET–3.5"

- NOMINAL LINE SIZE (INCHES)
- SEQUENCE NUMBER
- PIPE MATERIAL
- HEAT TRACING TYPE / INSULATION REQUIREMENT
- INSULATION THICKNESS (INCHES)

EQUIPMENT

- ROTARY OR SCREW PUMP (MOTOR DRIVEN)
- DUPLEX BASKET STRAINER
- SIMPLEX BASKET STRAINER
- AIR BUSTLE
- ATTEMPERATOR
- COLLECTING SCREW/W MOTOR
- ROTARY SOOTBLOWER
- FULL RETRACTABLE SOOTBLOWER
- HALF RETRACTABLE SOOTBLOWER
- RAKE TYPE SOOTBLOWER
- WATER COLUMN
- SHOWER
- EYEWASH
- CENTRIFUGAL FAN WITH INTEGRAL INLET GUIDE VANES
- CENTRIFUGAL FAN OR PUMP
- BLOWER
- EJECTOR, EDUCTOR OR INJECTOR
- UNCLASSIFIED EQUIPMENT
- ROTARY BLOWER
- FILTER
- SILENCER W/SCREEN
- SILENCER
- TANK
- ELECTRIC HEATER
- FILTER/WATER TRAP
- COLUMN W/LEVEL GAUGE

PROCESS SYMBOLS

VALVES AND DAMPERS

- NEEDLE VALVE, NO
- NEEDLE VALVE, NC
- GATE VALVE, NO
- GATE VALVE, NC
- GLOBE VALVE, NO
- GLOBE VALVE, NC
- BLEED & BLOCK ISOLATION VALVE
- Y-PATTERN GLOBE VALVE
- BALL VALVE, NO
- BALL VALVE, NC
- PLUG VALVE, NO
- PLUG VALVE, NC
- BUTTERFLY VALVE OR DAMPER
- CHECK
- STOP CHECK VALVE
- FLAPPER CHECK VALVE
- FOUR-WAY VALVE
- THREE-WAY VALVE (FLOW & INJECTION INDICATED)
- PETCOCK
- SLIDE GATE VALVE
- ANGLE GATE VALVE
- ANGLE GLOBE VALVE
- LOUVER DAMPER
- OPPOSED BLADE DAMPER
- POPPET DAMPER
- EXCESS FLOW VALVE
- W/SAFETY RELEASE CABLE EMERGENCY SHUTOFF VALVE

PIPING

- SOLIDS INLET MANIFOLD
- REDUCER
- SCREWED CAP
- HOSE CONNECTION
- BREAKAWAY COUPLING
- VENT STACK
- WELDED CAP
- FLOOR DRAIN
- UNION
- SPECIALTY ITEM (SP)
- BLIND FLANGE
- SIGHT GLASS (SG)
- DIAPHRAGM SEAL
- EXPANSION JOINT
- QUICK DISCONNECT
- FIGURE 8 SPECTACLE BLIND (CLOSED)
- FIGURE 8 SPECTACLE BLIND (OPEN)
- PADDLE BLIND
- "Y" STRAINER
- STEAM TRAP OR SELF-ACTING CONDENSATE DRAIN VALVE (T)
- TRANSFER SAFETY VALVE
- FLEXIBLE HOSE
- FILTER/REGULATOR (F/R)
- PIGTAIL
- VENT

MISC. INSTRUMENTS

- PURGE REGULATOR ASSEMBLY (P)
- AVERAGING PITOT TUBE
- VENTURI TUBE OR FLOW NOZZLE
- ORIFICE PRIMARY ELEMENT
- ROTAMETER

DRAWING NOTATIONS

- FW | O — SCOPE BREAK IDENTIFICATION
- FW — SUPPLIED BY FWNAC
- O — SUPPLIED BY OTHERS

BUILDING BREAKS

BB – BOILER BUILDING
TB – TURBINE BUILDING
YD – YARD
UG – UNDERGROUND

XX–XX XX–XX XX–XX XX–XX

NOTES

REV.	DATE	DR. INT.	REVISIONS DESCRIPTION
A	12/12/13	MCE	INITIAL ISSUE.

ISSUED FOR: CONSTRUCTION, FABRICATION, DETAILING, COMPLETE MATERIAL ORDER, PARTIAL MATERIAL ORDER, BID/QUOTATION

PROCESS & INSTRUMENTATION DIAGRAM
SOLAR RECEIVER
SYMBOLS AND LEGEND

MOLTEN SALT
SOLAR RECEIVER – PHASE II
ABENGOA SOLAR, INC.

DRAWING NUMBER: 12634401-60-6101 | SCALE: NONE | REVISION: A

DRAWN BY	MCE	07/25/13	65-126344-01
CHECKED BY	HH	12/12/13	
APPROVED BY	RV	12/12/13	PRODUCT CODE 51

THIS DRAWING IS THE PROPERTY OF THE FOSTER WHEELER NORTH AMERICA CORP. CLINTON, N.J.

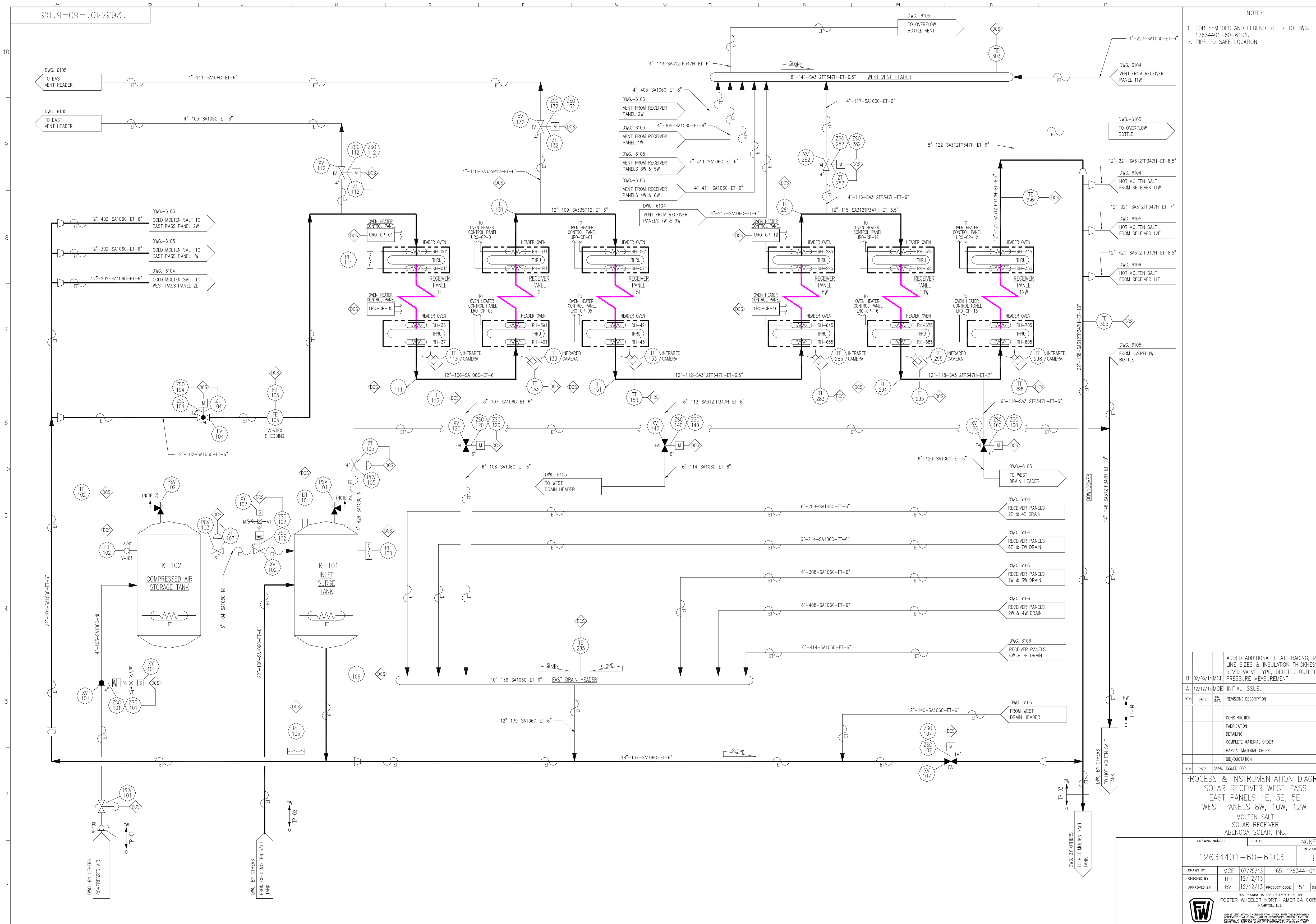

12634401-60-6103
TK-102
COMPRESSED AIR STORAGE TANK
TK-101
INLET SURGE TANK
EAST DRAIN HEADER
WEST VENT HEADER
DOWNCOMER
NOTES
1. FOR SYMBOLS AND LEGEND REFER TO DWG. 12634401-60-6101.
2. PIPE TO SAFE LOCATION.
B 02/06/14 MCE ADDED ADDITIONAL HEAT TRACING, REV'D LINE SIZES & INSULATION THICKNESS, REV'D VALVE TYPE, DELETED OUTLET PRESSURE MEASUREMENT.
A 12/12/13 MCE INITIAL ISSUE.
REV. DATE DR. INIT. REVISIONS DESCRIPTION
CONSTRUCTION
FABRICATION
DETAILING
COMPLETE MATERIAL ORDER
PARTIAL MATERIAL ORDER
BID/QUOTATION
REV. DATE APPR. ISSUED FOR
PROCESS & INSTRUMENTATION DIAGRAM
SOLAR RECEIVER WEST PASS
EAST PANELS 1E, 3E, 5E
WEST PANELS 8W, 10W, 12W
MOLTEN SALT
SOLAR RECEIVER
ABENGOA SOLAR, INC.
DRAWING NUMBER
SCALE: NONE=1-0"
12634401-60-6103
REVISION B
DRAWN BY MCE 07/25/13 65-126344-01
CHECKED BY HH 12/12/13
APPROVED BY RV 12/12/13 PRODUCT CODE 51 SIZE 5
THIS DRAWING IS THE PROPERTY OF THE
FOSTER WHEELER NORTH AMERICA CORP.
HAMPTON, N.J.
AND IS LENT WITHOUT CONSIDERATION OTHER THAN THE BORROWER'S AGREEMENT THAT IT SHALL NOT BE REPRODUCED, COPIED, LENT, OR DISPOSED OF DIRECTLY OR INDIRECTLY NOR USED FOR ANY PURPOSE OTHER THAN THAT FOR WHICH IT IS SPECIFICALLY FURNISHED. THE APPARATUS SHOWN IN THE DRAWING IS COVERED BY PATENTS.

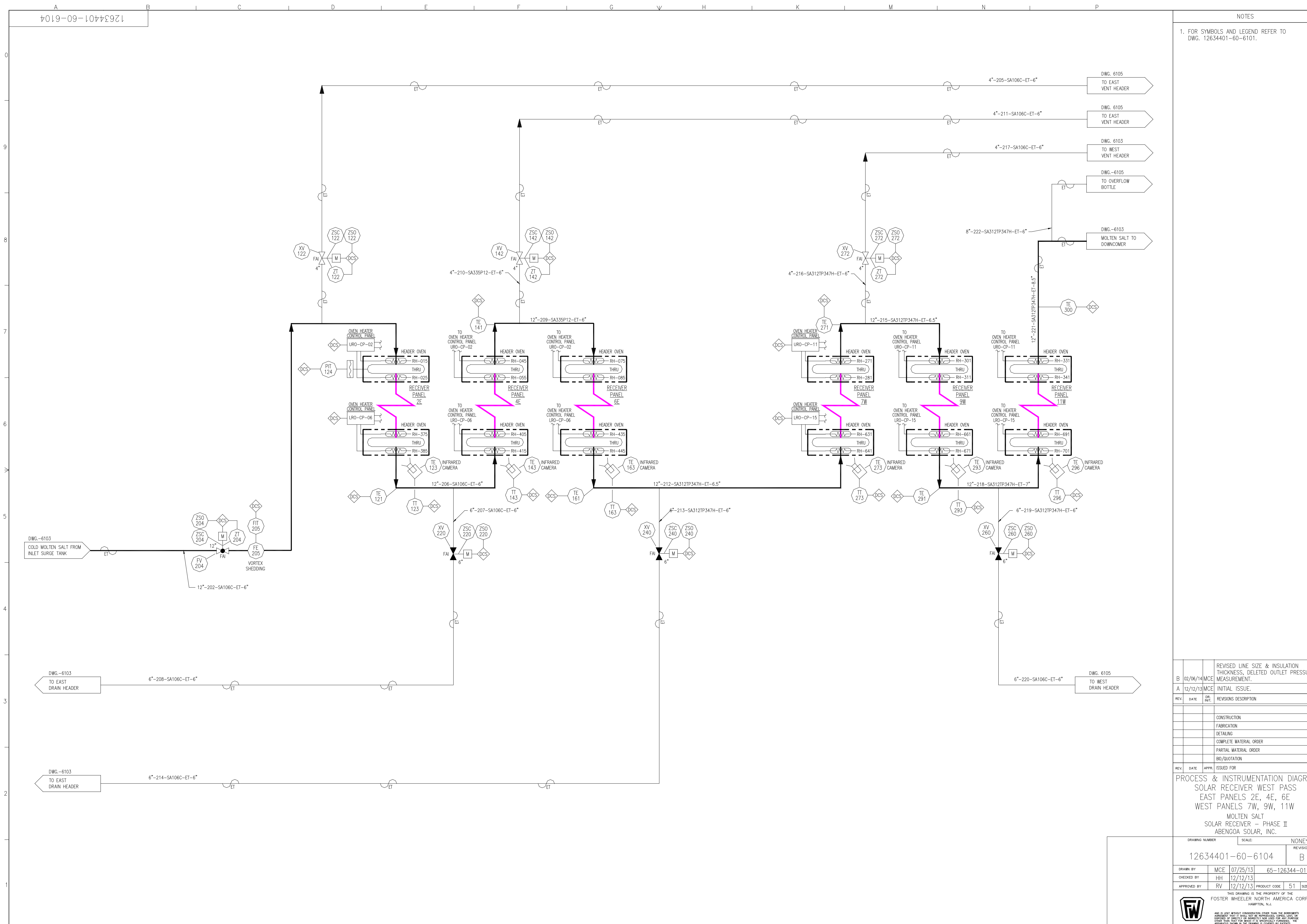

12634401-60-6104
NOTES
1. FOR SYMBOLS AND LEGEND REFER TO DWG. 12634401-60-6101.
DWG. 6105 TO EAST VENT HEADER
4"-205-SA106C-ET-6"
DWG. 6105 TO EAST VENT HEADER
4"-211-SA106C-ET-6"
DWG. 6103 TO WEST VENT HEADER
4"-217-SA106C-ET-6"
DWG.-6105 TO OVERFLOW BOTTLE
DWG.-6103 MOLTEN SALT TO DOWNCOMER
8"-222-SA312TP347H-ET-6"
4"-210-SA335P12-ET-6"
4"-216-SA312TP347H-ET-6"
12"-209-SA335P12-ET-6"
12"-215-SA312TP347H-ET-6.5"
12"-221-SA312TP347H-ET-6.5"
OVEN HEATER CONTROL PANEL
HEADER OVEN
THRU
RECEIVER PANEL 2E
RECEIVER PANEL 4E
RECEIVER PANEL 6E
RECEIVER PANEL 7W
RECEIVER PANEL 9W
RECEIVER PANEL 11W
INFRARED CAMERA
12"-206-SA106C-ET-6"
12"-212-SA312TP347H-ET-6.5"
12"-218-SA312TP347H-ET-7"
6"-207-SA106C-ET-6"
6"-213-SA312TP347H-ET-6"
6"-219-SA312TP347H-ET-6"
DWG.-6103 COLD MOLTEN SALT FROM INLET SURGE TANK
12"-202-SA106C-ET-6"
VORTEX SHEDDING
DWG.-6103 TO EAST DRAIN HEADER
6"-208-SA106C-ET-6"
DWG. 6105 TO WEST DRAIN HEADER
6"-220-SA106C-ET-6"
DWG.-6103 TO EAST DRAIN HEADER
6"-214-SA106C-ET-6"
B 02/06/14 MCE REVISED LINE SIZE & INSULATION THICKNESS, DELETED OUTLET PRESSURE MEASUREMENT.
A 12/12/13 MCE INITIAL ISSUE.
REV. DATE DR. INIT. REVISIONS DESCRIPTION
CONSTRUCTION
FABRICATION
DETAILING
COMPLETE MATERIAL ORDER
PARTIAL MATERIAL ORDER
BID/QUOTATION
REV. DATE APPR. ISSUED FOR
PROCESS & INSTRUMENTATION DIAGRAM
SOLAR RECEIVER WEST PASS
EAST PANELS 2E, 4E, 6E
WEST PANELS 7W, 9W, 11W
MOLTEN SALT
SOLAR RECEIVER – PHASE II
ABENGOA SOLAR, INC.
DRAWING NUMBER 12634401-60-6104
SCALE: NONE=1-0"
REVISION B
DRAWN BY MCE 07/25/13 65-126344-01
CHECKED BY HH 12/12/13
APPROVED BY RV 12/12/13 PRODUCT CODE 51 SIZE 5
THIS DRAWING IS THE PROPERTY OF THE
FOSTER WHEELER NORTH AMERICA CORP.
HAMPTON, N.J.
AND IS LENT WITHOUT CONSIDERATION OTHER THAN THE BORROWER'S AGREEMENT THAT IT SHALL NOT BE REPRODUCED, COPIED, LENT, OR DISPOSED OF DIRECTLY OR INDIRECTLY NOR USED FOR ANY PURPOSE OTHER THAN THAT FOR WHICH IT IS SPECIFICALLY FURNISHED. THE APPARATUS SHOWN IN THE DRAWING IS COVERED BY PATENTS.

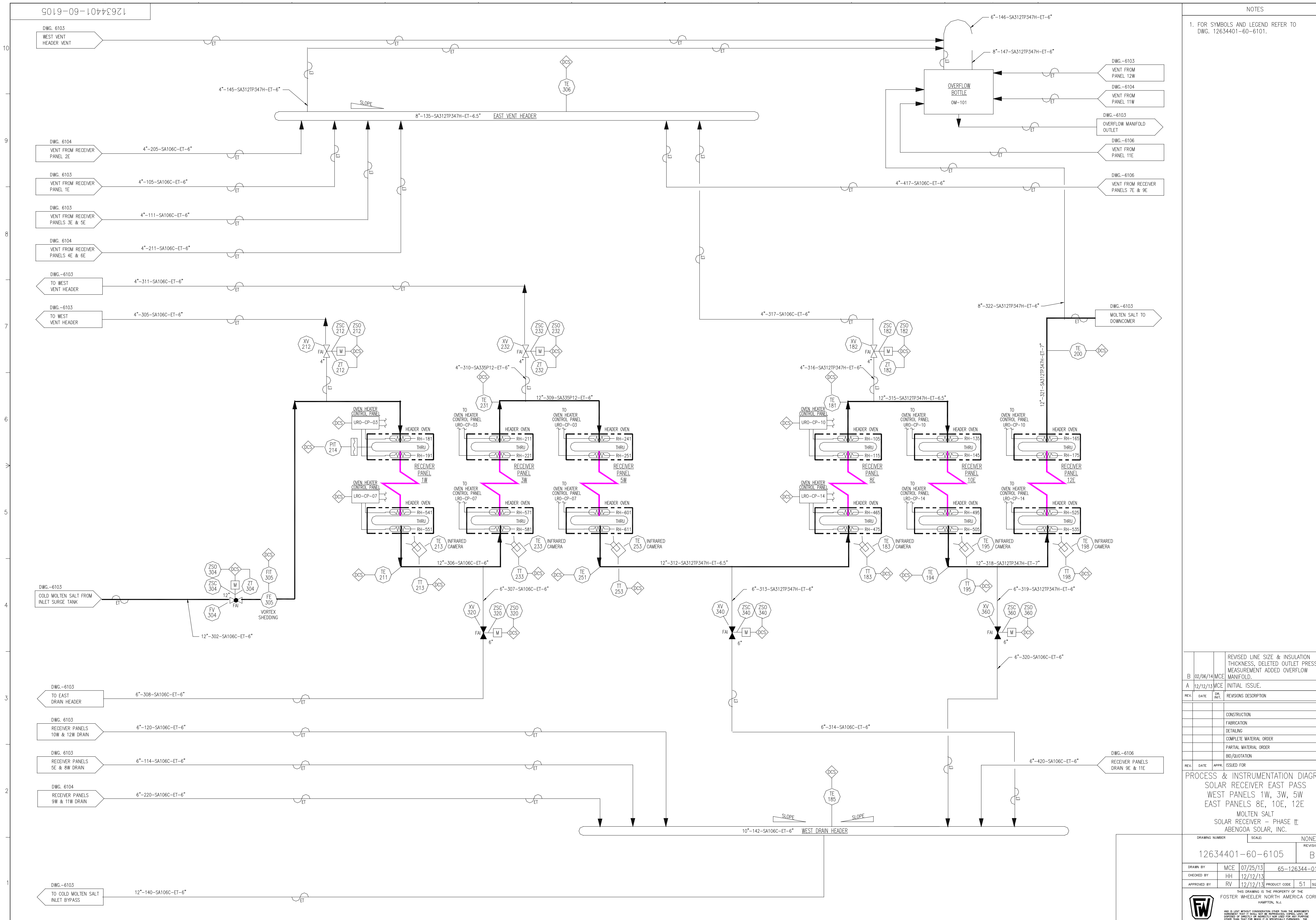

NOTES
1. FOR SYMBOLS AND LEGEND REFER TO DWG. 12634401-60-6101.
EAST VENT HEADER
WEST DRAIN HEADER
OVERFLOW BOTTLE
OM-101
RECEIVER PANEL 1W
RECEIVER PANEL 3W
RECEIVER PANEL 5W
RECEIVER PANEL 8E
RECEIVER PANEL 10E
RECEIVER PANEL 12E
COLD MOLTEN SALT FROM INLET SURGE TANK
MOLTEN SALT TO DOWNCOMER
TO COLD MOLTEN SALT INLET BYPASS
VORTEX SHEDDING
INFRARED CAMERA
B 02/06/14 MCE REVISED LINE SIZE & INSULATION THICKNESS, DELETED OUTLET PRESSURE MEASUREMENT ADDED OVERFLOW MANIFOLD.
A 12/12/13 MCE INITIAL ISSUE.
PROCESS & INSTRUMENTATION DIAGRAM
SOLAR RECEIVER EAST PASS
WEST PANELS 1W, 3W, 5W
EAST PANELS 8E, 10E, 12E
MOLTEN SALT
SOLAR RECEIVER - PHASE II
ABENGOA SOLAR, INC.
12634401-60-6105
B
65-126344-01
FOSTER WHEELER NORTH AMERICA CORP.

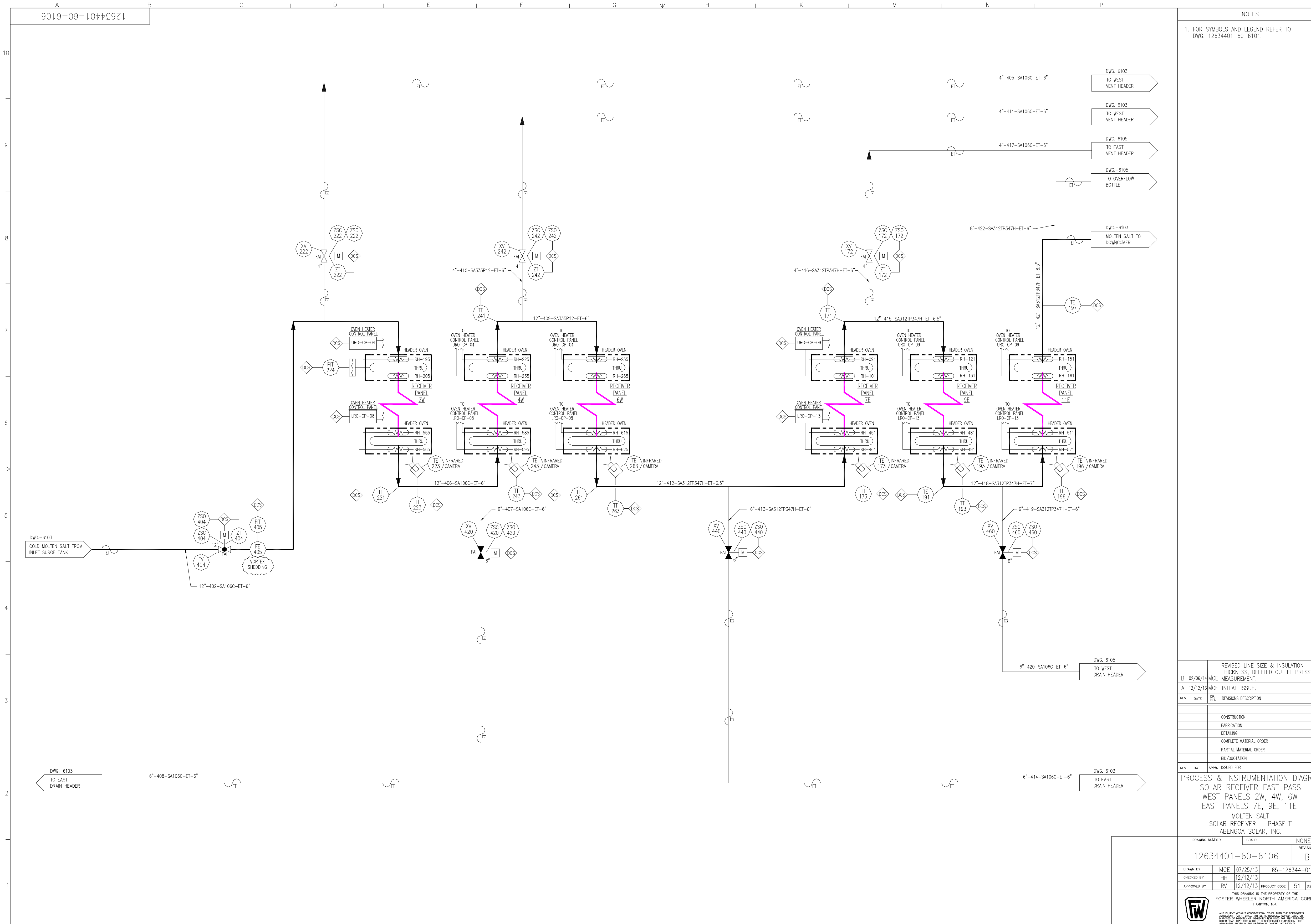
12634401-60-6106
NOTES
1. FOR SYMBOLS AND LEGEND REFER TO DWG. 12634401-60-6101.
DWG. 6103 TO WEST VENT HEADER
DWG. 6103 TO WEST VENT HEADER
DWG. 6105 TO EAST VENT HEADER
DWG.-6105 TO OVERFLOW BOTTLE
DWG.-6103 MOLTEN SALT TO DOWNCOMER
DWG.-6103 COLD MOLTEN SALT FROM INLET SURGE TANK
DWG.-6103 TO EAST DRAIN HEADER
DWG. 6105 TO WEST DRAIN HEADER
DWG. 6103 TO EAST DRAIN HEADER
4"-405-SA106C-ET-6"
4"-411-SA106C-ET-6"
4"-417-SA106C-ET-6"
8"-422-SA312TP347H-ET-6"
12"-402-SA106C-ET-6"
6"-408-SA106C-ET-6"
6"-420-SA106C-ET-6"
6"-414-SA106C-ET-6"
RECEIVER PANEL 2W
RECEIVER PANEL 4W
RECEIVER PANEL 6W
RECEIVER PANEL 7E
RECEIVER PANEL 9E
RECEIVER PANEL 11E
VORTEX SHEDDING
INFRARED CAMERA
B 02/06/14 MCE REVISED LINE SIZE & INSULATION THICKNESS, DELETED OUTLET PRESSURE MEASUREMENT.
A 12/12/13 MCE INITIAL ISSUE.
REV. DATE REVISIONS DESCRIPTION
CONSTRUCTION
FABRICATION
DETAILING
COMPLETE MATERIAL ORDER
PARTIAL MATERIAL ORDER
BID/QUOTATION
ISSUED FOR
PROCESS & INSTRUMENTATION DIAGRAM
SOLAR RECEIVER EAST PASS
WEST PANELS 2W, 4W, 6W
EAST PANELS 7E, 9E, 11E
MOLTEN SALT
SOLAR RECEIVER - PHASE II
ABENGOA SOLAR, INC.
DRAWING NUMBER 12634401-60-6106
REVISION B
DRAWN BY MCE 07/25/13
CHECKED BY HH 12/12/13
APPROVED BY RV 12/12/13
65-126344-01
THIS DRAWING IS THE PROPERTY OF THE FOSTER WHEELER NORTH AMERICA CORP.

APPENDIX H

Molten Salt Properties

Molten salt properties defined in the Abengoa receiver specification were:

The Receiver coolant is nitrate salt, which is a nominal mixture of 60 percent by weight $NaNO_3$ and 40 percent by weight KNO_3.

The nominal Receiver inlet and outlet temperatures are 290 °C and 565 °C, respectively.

Temperature range The salt mixture can be used over a temperature range of 260 °C to approximately 621 °C.

Freezing point As temperature decreases, the mixture starts to crystallize at 238 °C, and is completely solid at 221 °C.

Isotropic compressibility ($NaNO_3$) at the melting point $2 * 10^{-10}$ m^2 / N.

Heat of fusion (based on the average of heat of fusion of each component) h_{sl} = 161 kJ/kg

Change in density upon melting $\Delta V / V_{solid} = 4.6\% \Rightarrow V_{liquid} = 1.046\ V_{solid}$

A list of fluid properties, over a range of temperatures, is shown in Table 1.

Table 1. Nitrate Salt Properties for a Range of Temperatures

Temperature, F	Density, lb_m/ft^3	Specific heat, Btu/lb_m-F	Absolute Viscosity, lb_m/ft-hr	Thermal Conductivity, Btu/hr-ft-F
500	120.10	0.356	10.5058	0.284557
550	118.98	0.358	8.6073	0.287692
600	117.87	0.359	7.0853	0.290827
650	116.76	0.360	5.8940	0.293962
700	115.65	0.361	4.9873	0.297097
750	114.54	0.362	4.3196	0.300232
800	113.43	0.363	3.8450	0.303367
850	112.32	0.364	3.5175	0.306502
900	111.21	0.366	3.2913	0.309637
950	110.10	0.367	3.1206	0.312771
1,000	108.99	0.368	2.9596	0.315906
1,050	107.88	0.369	2.7623	0.319041
1,100	106.77	0.370	2.4830	0.322176

The fluid properties of nitrate salt, each as functions of temperature between 300 °C and 600 °C, are described below. The properties are nominally independent of pressure.

Density, as a function of temperature:

ρ (lb_m / ft^3) = 131.2 - 0.02221 * T (°F)

ρ (kg / m^3) = 2090 - 0.636 * T (°C)

Specific heat, as a function of temperature:

c_p (Btu / lb_m- °F) = 0.345 + (2.28*10^{-5}) * T (°F)

c_p (J / kg - °C) = 1443 + 0.172 * T (°C)

Absolute viscosity, as a function of temperature:

μ (lb_m / ft - hr) = 60.28440 - 0.17236 * T (°F) + (1.76176*10^{-4}) * $(T (°F))^2$ - (6.11408*10^{-8}) * $(T (°F))^3$

μ (mPa - sec) = 22.714 - 0.120 * T (°C) + (2.281 * 10^{-4}) * $(T (°C))^2$ - (1.474*10^{-7}) * $(T (°C))^3$

Thermal conductivity, as a function of temperature:

k (Btu / hr - ft - °F) = 0.253208 + 6.26984 * 10^{-5} * T (°F)

k (W / m - °C) = 0.443 + 1.9 * 10^{-4} * T (°C)

Properties of solid salt are as follows:

Density, ρ

$NaNO_3$	2,260 kg / m^3 at ambient temperature
KNO_3	2,190 kg / m^3 at ambient temperature

Heat capacity, c_p

$NaNO_3$	37.0 cal / °C - mol = 1,820 J / kg - °C near the melting point
KNO_3	28.0 cal / °C - mol = 1,160 J / kg - °C near the melting point

Thermal conductivity, k

KNO_3	2.1 W / m - °C

These equations are the same as described in Sandia National Laboratories correspondence from 1982 (Ref. 9) which indicates that the data has a maximum value of 600°C. Using these equations and extrapolating beyond 600°C may not be valid. For example, with reference to Figure H-1, the absolute viscosity equation goes negative at a temperature of about 696°C. The revised absolute viscosity equation used in this study was:

μ (mPa - sec) = 840.75 *[T (°C) – 360]^(-0.897)

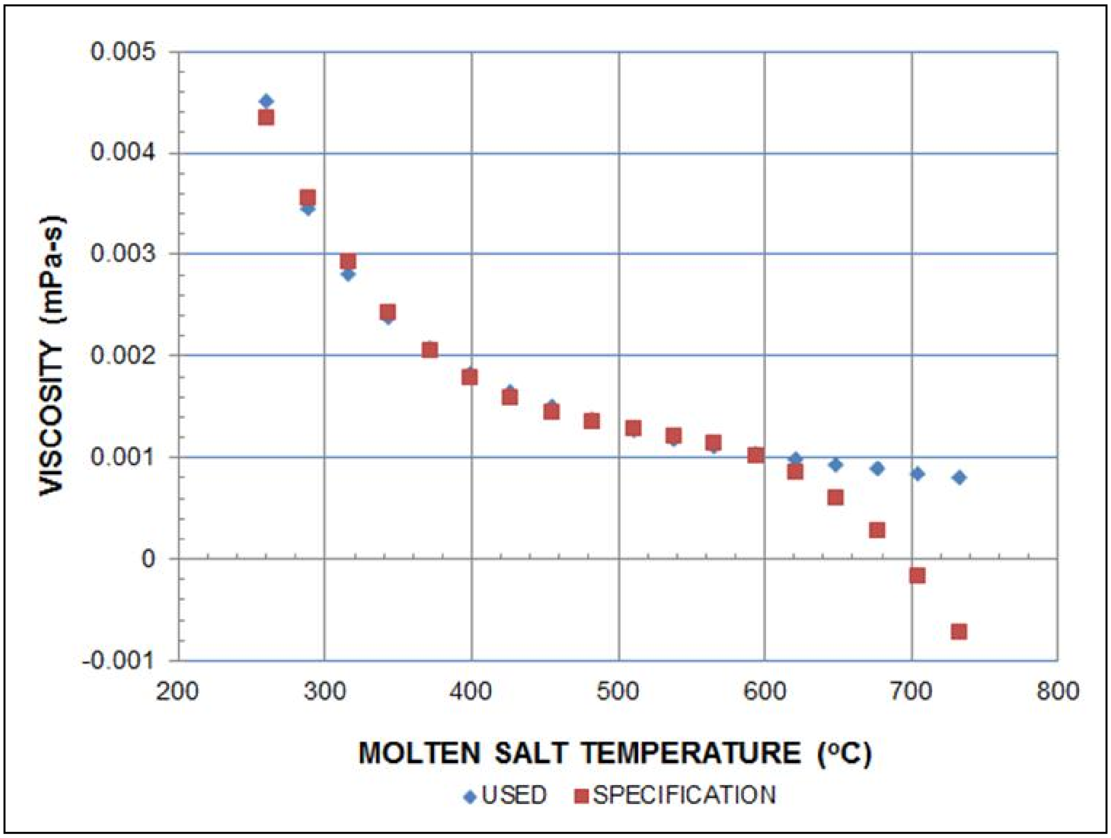

Figure H-1. Absolute Viscosity of Molten Salt

APPENDIX I

Flow Bypass Using Orifices in Receiver Vent System

If orifices are used in the receiver vent lines to eliminate valves, some molten salt will bypass the receiver panels and flow directly to the receiver outlet pipes. In order to estimate the quantity of salt bypassing and the impact of the bypass on maximum salt and tube metal temperatures, the following analysis was conducted:

1. **Load Case:** DJ 300 – 12h (99.77% load)
2. **Circuit:** 2E-4E-6E-7W-9W-11W (refer to Figure I-1)
3. **Vent Orifice Size:** 3/8" (initial assumption and minimum practical size; size used in Solar Two)
4. **Vent Flow Rate:** Circuit pressure drop calculations through the circuit gave an initial estimate for the molten salt pressure profile through the circuit. Knowing the pressure at the inlet to the vent line and the pressure at the receiver outlet, the approximate pressure drop required across the orifice was known. With the orifice resistance coefficient, the flow rate that would yield the required pressure loss could be computed.

Panel	Bypass (% of Circuit Inlet Flow)
2E	1.2
4E	1.0
7W	0.7
Total	2.8

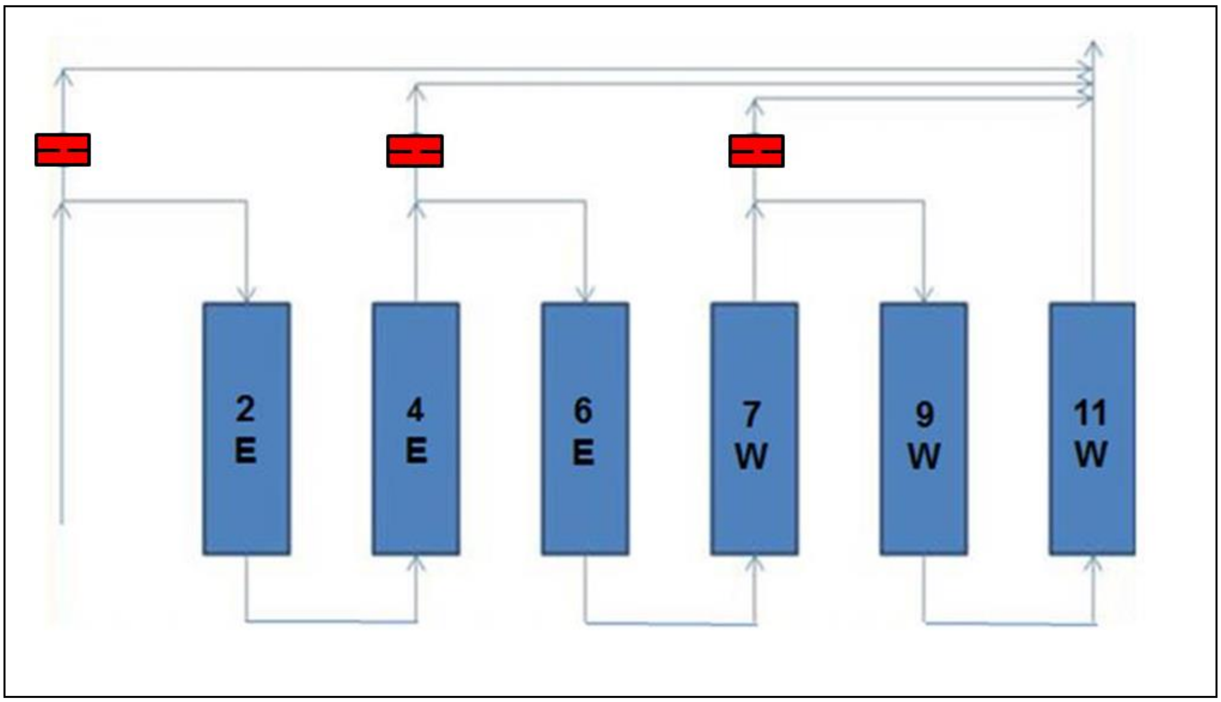

Figure I-1. Vent Orifice Location in Circuit 2E-4E-6E-7W-9W-11W

5. **Temperature Changes**: With some molten salt bypassing the receiver panels, the salt bulk and film temperature will increase as shown in Table I-1. The salt temperature leaving the last receiver increases to 605°C and is quenched with the bypass flow back to

	WITHOUT BYPASS FLOW			WITH BYPASS FLOW			
Panel #	Bulk Tin °C	Bulk Tout °C	Max Tid °C	Bulk Tin °C	Bulk Tout °C	Max Tid °C	Δ Tid °C
2E	308	373	486	308	374	488	2
6E	435	489	571	436	492	575	4
9W	534	570	623	538	575	628	5
11W	570	600	643	575	605	649	6

Table I-1. Fluid Temperatures With and Without Vent Orifices

The highest calculated ID temperature among the full load cases is 665°C (DJ 154 – 10h refer to Table 2 in Section 3.3.3). Based on the example calculation, with vent orifice bypass flow, the ID temperature will increase to ~671°C with the bypassed flow. This exceeds the target molten salt temperature limit of 670°C limit. Also, at this location, the computed tube mean metal temperature (709°C) without salt bypassing is a few degrees above the ASME (Code Case 2665-1) maximum temperature of 704°C (1300°F) for Haynes 230 alloy. Heliostat defocusing at this location will be required to reduce the incident heat flux about 5%. As a result, vent orificing, with a continuous amount of salt bypassing the receiver panels, is not recommended. Additional calculations to quantify the receiver drain rate using the minimum practical orifice size (3/8") were therefore not done.

SANDIA REPORT

SAND2014-18103
Printed September 2014
Unlimited Release

Loop for the Observation of Film Temperature Effects on Decomposition (LOFTED)

Alan M. Kruizenga, William Kolb, Ron J. Briggs, Joshua Christian, Daniel Ray, David Gill, John Kelton, Kye Chisman

Prepared by
Sandia National Laboratories
Albuquerque, New Mexico 87185 and Livermore, California 94550

Sandia National Laboratories is a multi-program laboratory managed and operated by Sandia Corporation, a wholly owned subsidiary of Lockheed Martin Corporation, for the U.S. Department of Energy's National Nuclear Security Administration under contract DE-AC04-94AL85000.

Sandia National Laboratories

Issued by Sandia National Laboratories, operated for the United States Department of Energy by Sandia Corporation.

SAND2014-18103

Printed September 2014

Loop for the Observation of Film Temperature Effects on Decomposition (LOFTED)

Alan M. Kruizenga[1], William Kolb[2], Ron J. Briggs[2], Joshua Christian[2], Daniel Ray[2], David Gill[2], John Kelton[2], Kye Chisman[2]

1. 8223: Materials Chemistry
2. 6223: Concentrating Solar Technologies Department

Sandia National Laboratories
P.O. Box 969
Livermore, California 94550-MS9403

Abstract

Molten nitrate salt Loop for the Observation of Film Temperature Effects on Decomposition (LOFTED) was designed, fabricated, and tested. This unique experimental arrangement allowed a 60/40 molten nitrate salt to be continuously pumped through a Haynes 230 pipe, allowing simulation of a solar receiver. The wall temperature was held at 670°C during the test and the bulk temperature range from 600-610°C for approximately 1200 hours. Salt decomposition was tested using a calibrated total alkalinity methodology to assess oxide content over time. Several alloys (347SS, HR-224, In625-SQ, Haynes 230) were tested for corrosion performance over the duration of the study and compared to previous static tests. Results yielded nearly a tenfold increase in corrosion rate as compared to 600°C, owing to the need to understand the effects of flow and mass transport on corrosion in molten salt environments.

ACKNOWLEDGMENTS

Authors' gratefully want to thank colleagues Bruce Kelly and Drake Tilley at Abengoa Solar for aide in calculations, discussions and suggestions over the course of this work. Discussions such as these are immensely valued for guiding work toward a solution that useful to all parties involved.

Authors' also gratefully thank Ryan Nishimoto and Andrew Gardea for the metallography preparation and electron microscopy. Kye Chisman was invaluable in the testing and operation of LOFTED.

This work was funded through award DE-EE0003596 "Development of Baseload CSP Advanced Nitrate Salt Central Receiver Power Plant"

CONTENTS

FIGURES

TABLES

NOMENCLATURE

CSP	Concentrated Solar Power
DOE	Department of Energy
EDS	Energy Dispersive Spectroscopy
EPA	U.S. Environmental Protection Agency
GPM	Gallons per minute
LOFTED	Loop for the Observation of Film Temperature Effects on Decomposition
NSTTF	National Solar Thermal Test Facility
MSTL	Molten Salt Test Loop
SEM	Scanning Electron Microscopy
SNL	Sandia National Laboratories
TC	Thermocouple

1. INTRODUCTION

Sandia has designed and fabricated a pumped-salt test loop that will flow molten nitrate salt through a heated test section of pipe and past a variety of material samples. The test rig operates to simulate a 30-year plant life (estimated based on total salt volume and salt flow rate), with salt samples removed throughout the duration of the test. The salt samples, metal samples, and heated "receiver" tube were evaluated to study both salt decomposition over time and the effects of the salt on the metals.

The receiver outlet temperature in Phase II of the DOE study is 600°C. The Reynolds number in the last panels of the receiver is a nominal 250,000. To achieve a bulk salt temperature of 600°C with a Reynolds number of 250,000, the salt film temperature must be approximately 670°C.

At 670°C, the salt will thermally decompose, as discussed in Section 2. However, the residence time of the salt in the film region is believed to be too short for the decomposition reaction to proceed to completion.

In Phase II of the plant design, the capacity of the thermal storage system is 14 hours. Over the 30-year life of the project, the salt inventory passes through the receiver some 16,200 times, and exposing the inventory to the flux, and to the temperature conditions in the last panel, for a cumulative period of approximately 33 hours.

Decomposition of salt is temperature dependent. The decomposition process accelerates when the salt moves from the bulk region to the film region, and the temperature of the salt increases to 670°C. The decomposition process then slows when the salt moves from the film region back to the bulk region, and the temperature of the salt decreases to 600°C. An experiment will be developed to simulate the rate of decomposition that will be experienced in a commercial project, one example of which is described below in Section 3. The proposed experiment emulates the temperature and hydraulic conditions found in the last panel of a commercial receiver.

This page intentionally left blank.

2. TEST PLAN, SYSTEM DESCRIPTION, AND SEQUENCE OF OPERATION

2.1 Interpolation of the Experimental Results

The average fluid pressure in the last panel in a commercial receiver is approximately 5 bar. However, the fluid pressure in the experiment is approximately 7 bar, based on the pump curve shown in Figure 4. The pump uses a constant-speed motor drive.

When considering the equilibrium between nitrate and nitrite, in the equation below, an increase in fluid pressure, resulting in an increase in the partial pressure of oxygen, will suppress nitrite formation:

$$\boldsymbol{NO_2^- \rightleftharpoons NO^- + \frac{1}{2}O_2} \qquad \textbf{Equation 1}$$

To the extent that a reduction in the nitrite concentration reduces the rate of oxide formation, the higher fluid pressures in the experiment could, in principle, result in a lower production of oxides and nitrogen oxides than in a commercial plant. However, if the salt is exposed to a step change in temperature, the time required to establish a new equilibrium nitrite concentration is on the order of 30 hours, based on the quantity of salt in kilograms [1]. Presumably, a comparable time may be required to establish a new equilibrium nitrite concentration in response to a change in pressure. The rate may also depend on the diffusion time of oxygen through the bulk fluid, which would be a function of the distance from the nitrate ion to the free surface of the liquid. Because the residence time of the salt in the receiver is on the order of minutes, rather than tens of hours, the equilibrium nitrite concentration in a commercial plant is likely to be determined by the combination of the following:

1) the average temperature of the hot and cold storage tanks (~450 °C),
2) the average fluid pressure in the storage tanks (~1.6 bar), and
3) the oxygen partial pressure in the storage tanks (0.21 bar).

The storage vessels in the proposed experiment operate under a combination of temperature (600°C), fluid pressure (1.2 bar), and oxygen partial pressure (0.21 bar), which will result in an equilibrium nitrite concentration higher than in a commercial plant. This, in turn, should lead to an oxide formation rate higher than that observed in a commercial plant, and, therefore, the results of the thermal stability experiment may be viewed as conservative.

2.2 Requirements for the Salt Thermal Stability Experiment

2.2.1 Thermal Characteristics

To emulate the conditions in a commercial receiver, the thermal stability experiment should have the following characteristics:

1) Haynes 230 nickel alloy tube,
2) 670°C salt film temperature,

3) A temperature profile across the tube diameter that is as similar as possible to the temperature profile across a commercial receiver tube, and
4) A cumulative exposure time of 33 hours, based on heating around the full circumference of the tube.

During the 30-year life of the project, the salt inventory is exposed to the flux and temperature conditions in the last panel of the actual receiver for a total of 33 hours. During this period, the salt is heated from only the outer surface of the tube. The experiment should replicate the exposure time of salt in the last panel of the receiver.

2.2.2 Salt Characteristics

The salt will be a nominal mixture of 60 percent by weight sodium nitrate, and 40 percent by weight potassium nitrate. (See Attachment 1.)

The sodium nitrate will be a typical industrial grade, with a maximum total chloride content of 0.6 percent, and a maximum magnesium content of 0.1 percent.

The potassium nitrate will be a typical technical grade, with a maximum total chloride content of 0.2 percent, and a maximum magnesium content of 0.02 percent.

2.3 Equipment Considerations for the Experiment: Conceptual Design

During the 30-year life of a commercial receiver, the salt passes through the receiver some 16,200 times. The annual average salt velocity is on the order of 3 m/sec, and the annual average residence time in the last panel of the receiver is about 22 m/3m/sec = 7.3 seconds. Thus, over the life of the project, the total residence time of the salt in the last panel is approximately 33 hours.

The conceptual arrangement for the experiment includes a circulation pump, a heated test section, various instruments, and a control system. A representative piping and instrument diagram is shown in Figure 1.

The pump draws suction from a pump sump, circulates the salt through the pipe to the heated test section, and returns the salt to the pump sump. A chiller fan circulates air around the pump sump to reduce the temperature of the heated salt to the nominal bulk salt temperature. The pump sump is maintained at a nominal temperature of 600°C by balancing the heat input from the test section with the heat removed by the fan.

The experiment is designed to use a tube (representative of the actual receiver) with an inside diameter equal to that of the commercial receiver (41 mm), and to operate with a nominal salt velocity of 3 m/sec. An unheated section of pipe, with a diameter of 41 mm and a length of 11 m, is installed upstream of the test section. The purpose of the 11 m unheated section is to establish a hydraulic boundary layer, similar to that at the mid-point of a commercial receiver panel. As such, the commercial receiver and the test section will have comparable values for the Reynolds number, the velocity profile across the tube diameter, the fluid temperature profile across the tube diameter, and the oxide production rate per kg of flow. A conceptual equipment arrangement is shown in Figure 2.

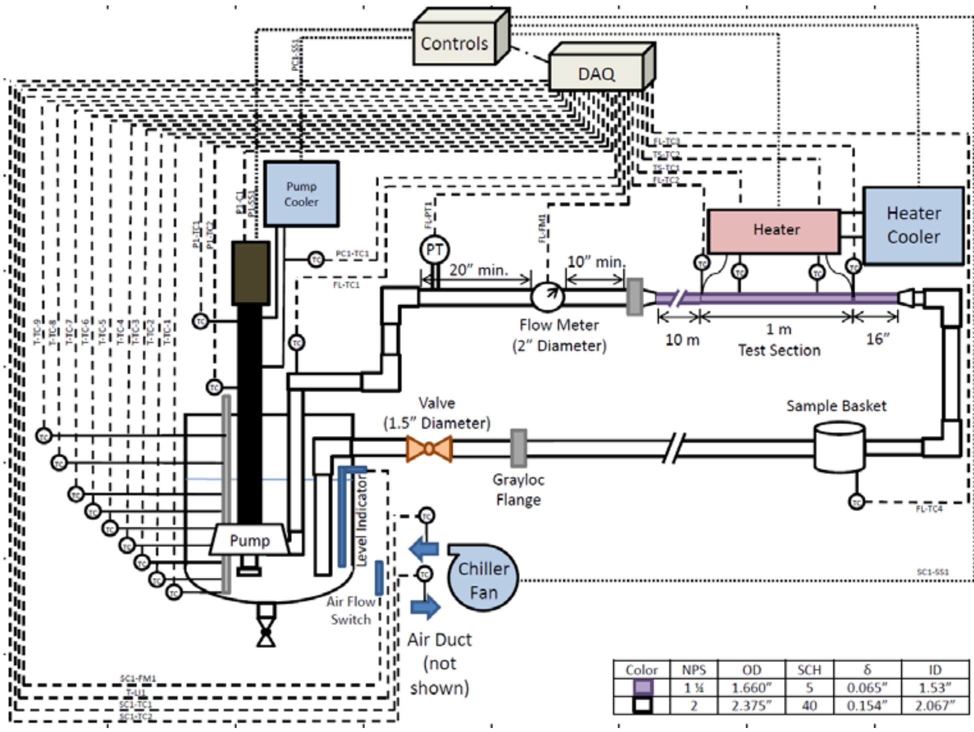

Figure 1: Representative Piping and Instrument Diagram

The method used to heat the test section of receiver is to pass a high-frequency, oscillating current through an electric coil surrounding the tube. This establishes a film temperature of 670°C, for which a nominal power input power of 75 kWe per meter (39.37 in) of heated length is required.

Continuing with the example, the salt inventory in the experiment would need to pass through the test section 16,000 times to replicate the exposure of the salt in a commercial plant (16,000 * (22 m (24.05 ft) commercial tube length / 1 m (39.37 in) experiment tube length) * (0.4 heated circumference in commercial tube / 1.0 heated circumference in experiment tube) = 141,000 times). The factor of 0.4 / 1.0 accounts for both partial circumferential heating in a commercial receiver tube, and full circumferential heating in the experiment tube.

Based on a heated test section length of 1.0 m, the volume of the salt in the test section is about 0.0011 m^3. A conceptual experiment arrangement has a salt inventory of 0.143 m^3. Thus, the ratio of the salt inventory in the experiment to the salt inventory in the test section is about 0.0143 / 0.0011 = 130. To simulate the exposure of the salt to the conditions in a commercial project, the duration of the experiment needs to be 141,000 passes * (1 m / 3 m/sec) * 130 = 6,100,000 seconds, or 71 days.

A preliminary schedule, developed by Sandia, shows a test duration of 60 days. With a duration of 60 days, the experiment will represent the first 25 years of commercial plant operation (60 / 71 * 30 years = 25 years). This is judged to be adequate for the purposes of the DOE study.

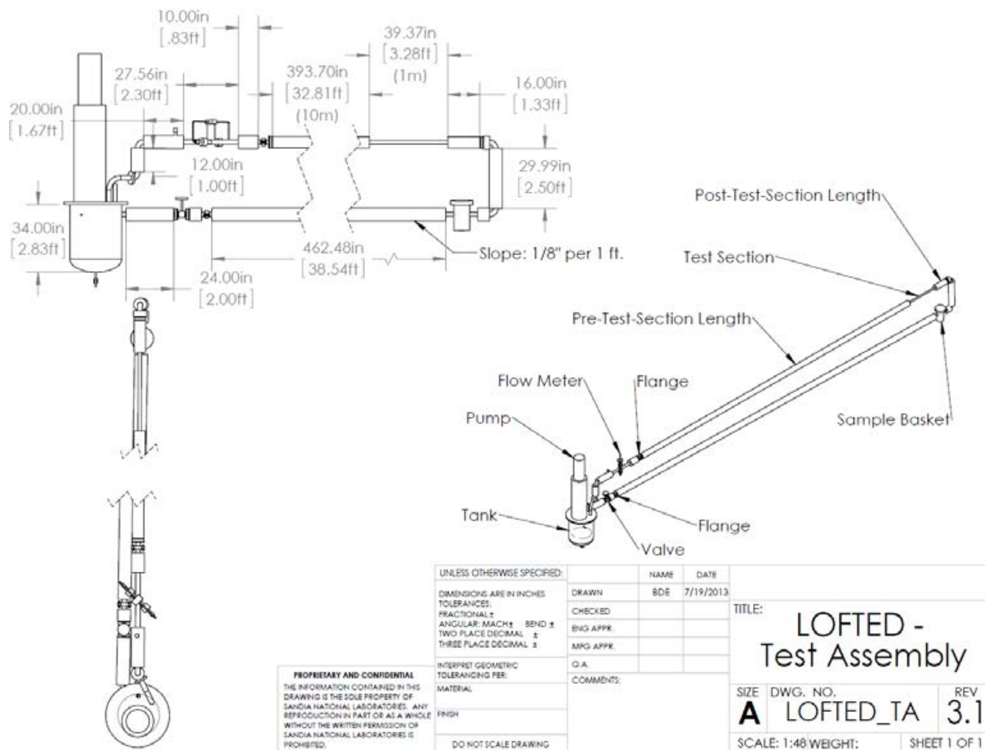

Figure 2: Conceptual Equipment Arrangement (not the final constructed piping layout)

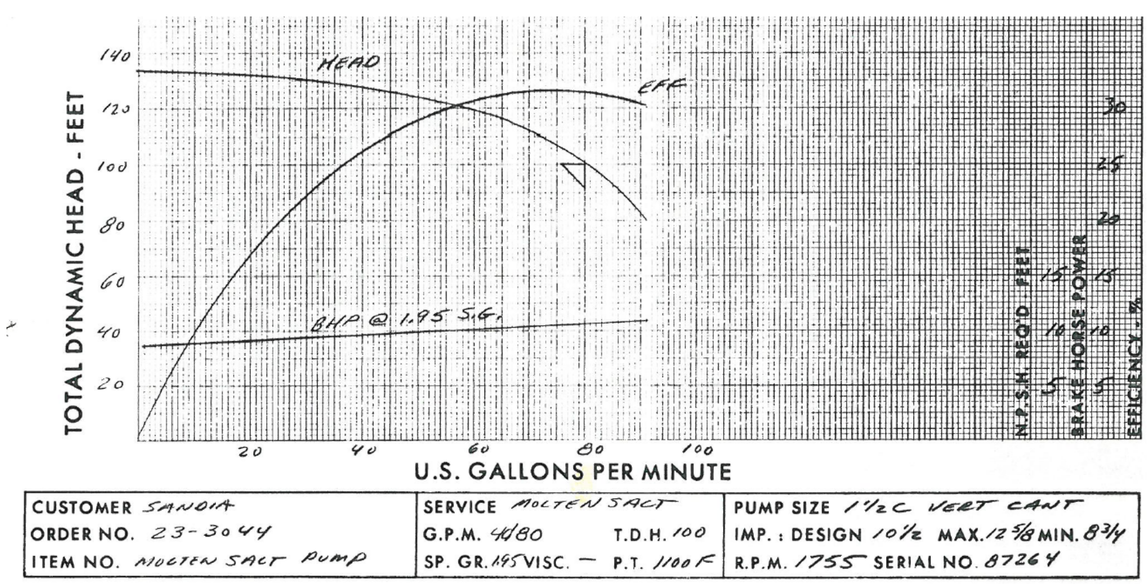

Figure 3: Characteristics of the Salt Circulation Pump

2.4-System Description

2.4.1 Initial concepts to support the test requirements:

The initial concept for the design and construction of the system consisted of two hot-salt tanks (600°C), a small section of tubing located between these two tanks, and the sample coupons. Coupons are nominally rectangular shaped and are approximately 2 inches long and are 0.5-1 inch in length. These coupons were based on a previous study of materials to use in a commercial project include the following: Alloy 230; Type 347H stainless steel; Inconel 625SQ; and Alloy HR224.

A total of 16 corrosion coupons would be placed in a sample basket, located within the salt flow in the bottom portion of one of the tanks. The tubing would have represented the receiver test section, and would have been externally heated to 670°C when salt was flowing through the tubing. The heater would have been deenergized when the salt flow stopped, due to the change in direction (as described below).

In the initial test design, the molten salt would have been pushed from one tank to the other using dry compressed air. As one tank was pressurized, the salt in that tank would be displaced and pushed through the tube test section, at which time the test section heater would be energized. When the tank was empty of salt, the heater would deenergize, the air in the first tank would be bled off, and, at the same time, the second tank would be pressurized. The salt would then be pushed from the second tank to the third tank using compressed dry air, then pushed through the tube test section, at which time the test section heater would be energized. This would complete two cycles through the system. The cycle would continue until the test was completed. As mentioned above, the sample coupons would have been placed on the bottom of one of the tanks in the salt flow path. In this case, the coupons would be exposed during half of the cycles.

As this design concept was analyzed, we discovered that the intent of the test would be difficult to fulfill, because the salt flow would momentarily stop while the flow transitioned, and would change directions between cycles. This meant that the coupons would see only half of the cycles. The belief was the salt in the tube would overheat during this transition and that the velocity through the test section would be impossible to determine and maintain. We briefly looked at a few other configurations and found similar issues. To adequately meet the intent of the test, it was determined that a pumped system would be required.

2.4.2 Overall description of pumped system

The system that was designed and constructed needed to address the requirements of the test plan. This system needed to 1) have a flow rate that met a Reynolds number similar to that for a CSP tower plant, 2) have the wall temperature maintained at 670 °C at the internal receiver wall, 3) the coupons exposed to the outlet bulk-salt temperature of the heated receiver, and 4) ensure that the salt inventory of the entire system would be as minimal as possible, such that the entire salt inventory could flow past the heated test section a predetermined number of cycles, so as to represent a 30-year power plant lifespan. During the 30-year life of the project, the salt inventory is exposed to the flux and temperature conditions found in the last panel for a total of 33 hours.

Again, to meet this intent, it was determined that a pumped system would be required.

2.4.3 Test Rig Construction

The system can be seen in the figures presented below. A view of the pump and test section at the end of the system is seen in Figure 4. The figure shows a platform that was modified to support the tank, pump, pump motor, and pump bearing cooler. A set of stairs was constructed for safe access to the platform during salt sampling. The pump was placed on an interface plate, which was attached to a small molten salt tank built from a .66 m (26") diameter 316 SS pipe. The salt within the tank was electrically heated by externally mounted mineral-insulated (MI) heat traces. There were Thermocouples TCs mounted internally to the tank, which allowed for monitoring the salt levels, as well as the molten salt temperatures and the upper air temperatures within the tank. The level was also measured using a bubbler system.

The pump feeds the supply piping, where the salt flows past a pressure transducer and through a flow meter (Figure 5). The supply side is 2" NPS schedule 40 stainless steel (316) pipe. After turning through two long-radius elbows at the end of the pipe, the salt returns to the tank through Haynes 230, 1.5" tubing. Attached to the second elbow is a reducer measuring 2 inches to 0.5-inches. The Haynes 230 1.5-inch, schedule 5 tubing was attached to the reducer. This tubing represents a section of an actual commercial receiver. There were three sections within the Haynes 230 receiver: the pretest section, measuring 10.97 meters (m) (36 ft.) in length; the 1 m (39.37 in.) test section; and a 0.41 m (16 in.) post-test section. The Haynes 230 was welded using Haynes filler rod. The tubing has a 10.97 m (35.9') free flowing zone, simulating a half-length of receiver piping, before entering the 1 m (39.37") induction heated zone (inside the protective shed), where heat is added through the surface of the pipe to achieve a higher film temperature. This coil, along with the associated electrical and controls, provided the required thermal input to the receiver tube to obtain the 670°C internal wall temperature. The post-test tubing continues to maintain a steady flow before passing through a control valve and the metal sample test section, before being sent back into the tank.

The pump, pump motor, control valve, and blower already existed on-site, and were repurposed for this test.

Figure 5 shows a wider angle view of the test, and includes the flow meter and turn-around sections of the piping, as well as the pipe hangers. Because the pipe length increases by 8.9 cm (3.5") during heating to temperature, the pipe hangers are all made to be compliant to longitudinal motion. The supply pipe is much stronger than the return tubing, so the supply pipe uses more traditional pipe hangers welded to the pipe. The return tubing is supported in hanging pipe cradles,, first, because the tubing is quite flexible, and, second, because of the desire to have a smooth, free-flowing tubing for developing the flow regime,. In all of the piping, the slope of the pipe is evident, giving positive flow for the salt to drain back to the tank when the system is shut down.

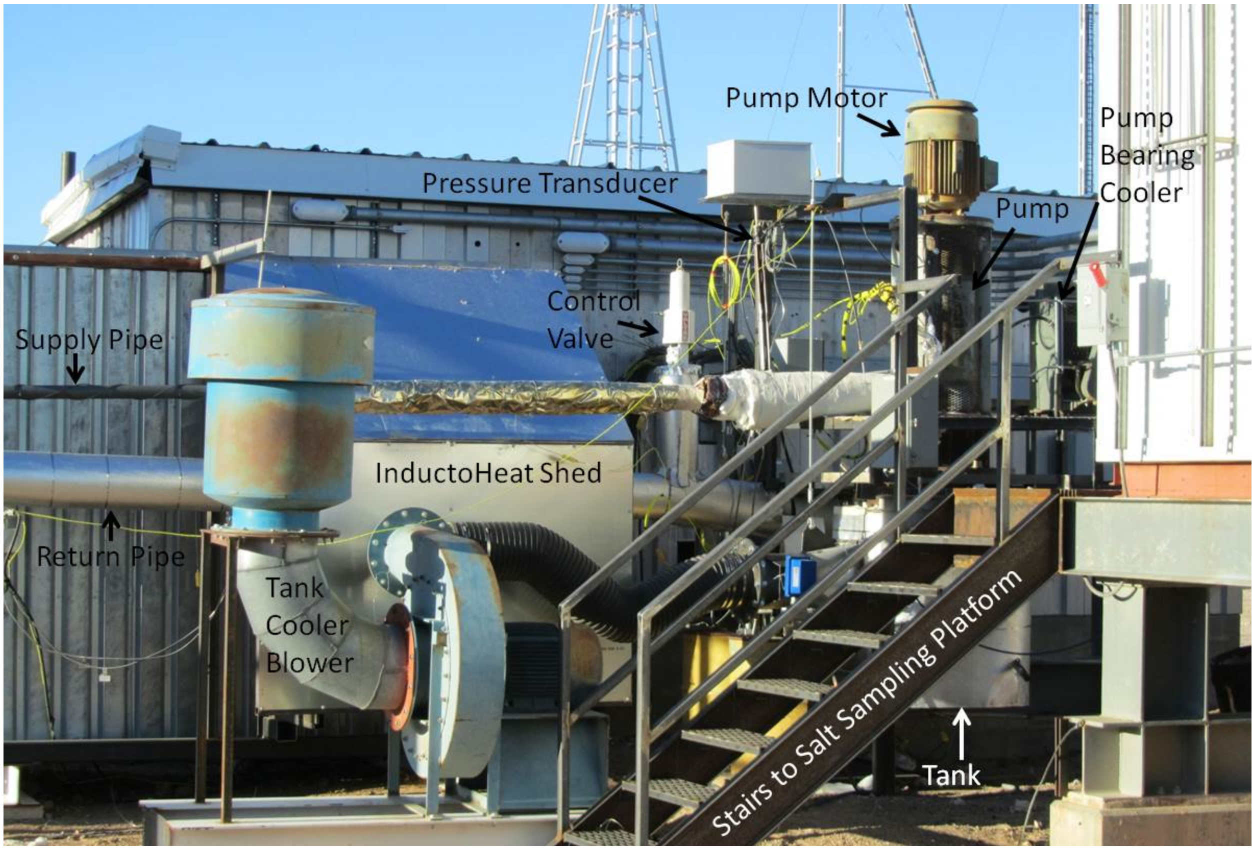

Figure 4: The Pump and Test Section Installed On-Site

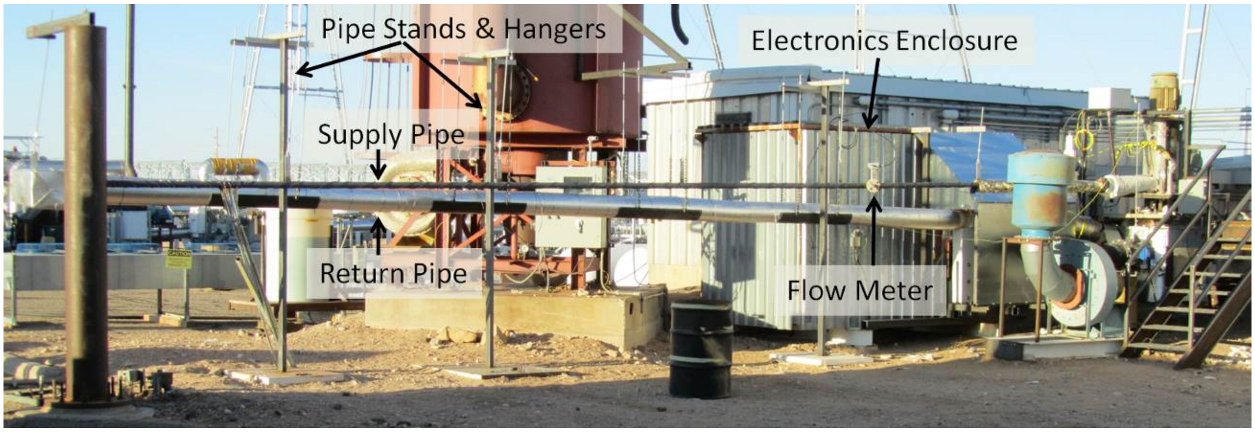

Figure 5 - A Wider View of LOFTED Shows the Full Piping System and Pipe Hangers

In the figures above, it is evident that the supply line <u>is not</u> insulated, while the return line <u>is</u> insulated. The system was originally constructed with both lines insulated and heat-traced. The system was brought to temperature and flow was started in the system. However, it then became necessary to de-insulate the supply line to achieve additional cooling to reject the heat generated by the induction heating system.

Figure 6 shows the back side of the electronics enclosure. which contains the controller and pyrometer for the Inductoheat unit. The enclosure protects these items from rain. The Inductoheat requires substantial cooling for the coil and the control electronics, therefore the enclose is equipped with a primary cooling loop that cools these items, as well as with a heat exchanger on a secondary loop. The secondary loop consists of a pump cart with a large volume of coolant and an air-to-water fin-fan heat exchanger. All of these items, including the electronics enclosure, existed onsite at Sandia, and were repurposed and adapted for use during this test.

Figure 6 - The Electronics enclosure 1) contains the InductoHeat controller, pyrometer, and heat exchanger (left), and 2 is attached to the Cooling Loop and Cooler (right).

Although it is difficult to see due to the presence of the insulation, hangers, stands, and platforms, there was a significant amount of work required during the creation of the tank and piping. The tanks and piping all were heat-traced with mineral-insulated resistive heat trace. Stainless steel shimstock was used to secure the heat trace in place, and a layer of shimstock was wrapped around each vessel to isolate the heat trace from the insulation. Only then was the insulation installed. The primary insulation is Pyrogel XT, in 5 and 10mm thicknesses, with some Thermal Ceramics Superwool used to fill small gaps. A layer of shimstock was installed partway through the insulation layers to reflect IR emissions back into the piping system. Finally, the vessels were covered with a layer of aluminum cladding for weather protection.

2.4.4 Sub Systems

The subsystems required to support both the electronics apparatus and the environmental control systems are described in this section.

- **Tank**

The tank, with an NPS 26-inch diameter, is constructed of 316 SS. The tank temperature tree indicates the internal salt and air temperature at 4-inch intervals from the bottom to the top of the tank, with additional TCs spaced ½-inch apart between 15 and 18 inches from the tank bottom. This lower region has more T/Cs to provide additional sensing at the operational salt level during normal operations, nominally 17 inches. A pipe flange is welded to the upper portion of the 26-in. pipe, which was bolted to the SS Interface Plate.

Figure 7:The Tank Positioned in the Assembly Stand, with Flow Control Valve and Cooling Ductwork Attached.

- **Salt Pump**
  Lawrence 25 HP cantilever molten salt pump flow rate of 100 GPM, 100 PSI at 600°C. A cross the line full voltage started was utilized, the pump did not control flow or pressure in the system. The pump has a pipe flange welded to the pump base. This flange was bolted to the SS Interface Plate. The pump would automatically shut down if any of the set-point values outlined in the alarm matrix are reached. See figure 3 for the associated pump curve.

- **Salt Pump Cooler**
  The Lawrence pump requires an auxiliary radiator and water pump, which flow water through the thrust bearings to keep them cool. This pump cooler system ran 24/7. An automatic trip of the salt pump would occur if the water temperature rose higher than the set-point value in the alarm matrix.

- **Pump and Tank Interface Plate**
  The pump and tank interface plate, made of 347 stainless steel, was needed to isolate the carbon steel pump flange-plate from the high temperature salt. Figure 7 shows a drawing of this plate.

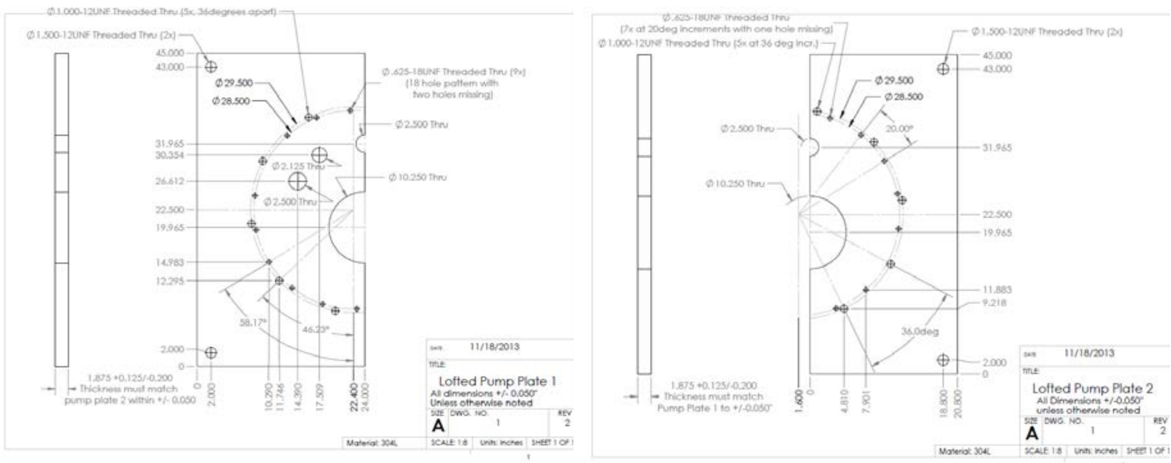

Figure 8: The 347 SS Plate Supports the Pump and the Tank; plate is configured as two halves that slide together around the assembled pump.

- **Piping**
  The piping system consists of several types of material: all NPS two-inch pipe is 316 SS schedule 40; flow meter is 321 SS; PT extension is 316 SS; the pretest, test, and posttest sections are Haynes 230, 1.5 inch, schedule 5 tube. A 4inch 316 SS pipe held metal test section coupon samples.

- **Pressure Transducer**
  GEFRAN 750 PSI NAK pressure transducer with 6-inch flexible stem; Model/Product Number KE2-6-M-P75D-4-4-B-S-XMD05. The pressure transducer provides a 4-20 ma analog input to the N.I. control system. The pressure transducer was mounted to a 316 SS extension standoff pipe, 30 inches long, with a ¾ inch diameter. (See Figure 9, below.) This extension is intended to lower the temperature of the salt within the 2-in pipe (600 °C to 300 °C at the diaphragm of the pressure transducer). The pressure transducer electronics a located in a NEMA 4 box containing an electric heater controlled by thermostat to maintain 55°C. This was necessary to provide a constant temperature to the electronics and helped eliminate daily shifts in data due to temperature swings in the ambient environment. The pump and heater would automatically shut down if any of the values outlined in the alarm matrix were reached.

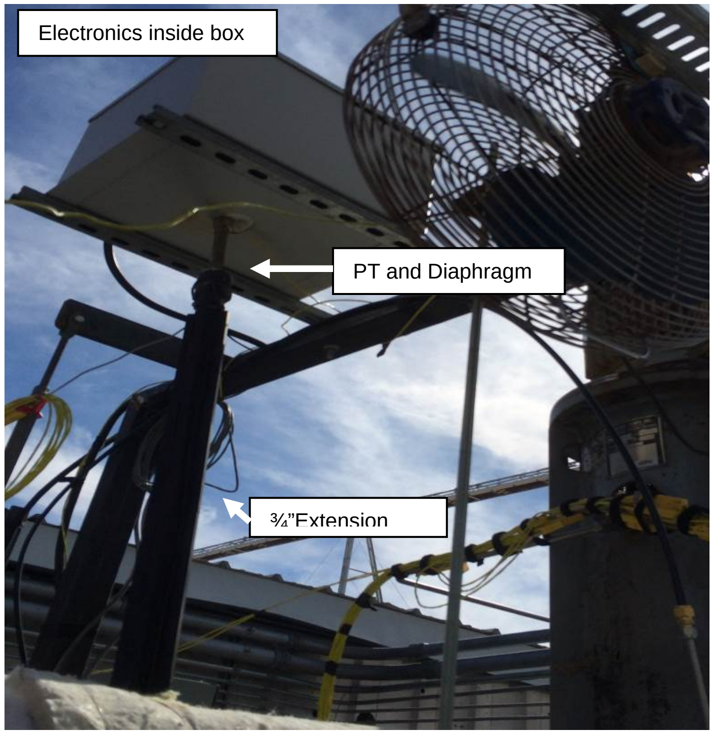

Figure 9: Pressure Transducer mounted on 30" extension

- **Flowmeter**
  Krohne ultrasonic 2in molten salt flowmeter,321 H SS; Model # S39447X303D00100 for the flow tube; Converter: VN5045D0032300010. The flowmeter provides a 4-20 ma analog input to the N.I. control system. The flowmeter is welded into the 2-in piping system; the converter is mounted approximately 4 m away, within a building. The pump and heater automatically shut down if any alarm matrix values are reached.

Figure 10: Flowmeter electronics are mounted separately, away from the heat.

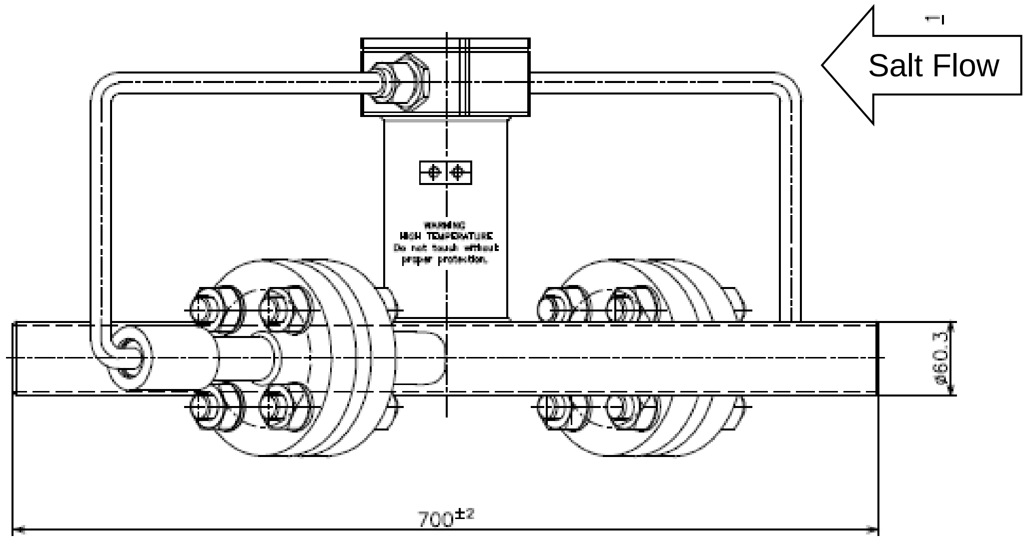

Figure 11: Flow Meter Factory Drawing

- **Test Section**
  Haynes 230, 1.5-inch schedule 5 tube, 1 M (39.37”) in length. Figure 13 shows the test section encapsulated by the InductoHeat coil.

- **Coupon Sample Holder**
  Figure 12 shows the sample tree that holds the metal samples in the flow stream. The samples will be used for comparison of the corrosion effects of the high temperature salt on different materials as shown in the figure.

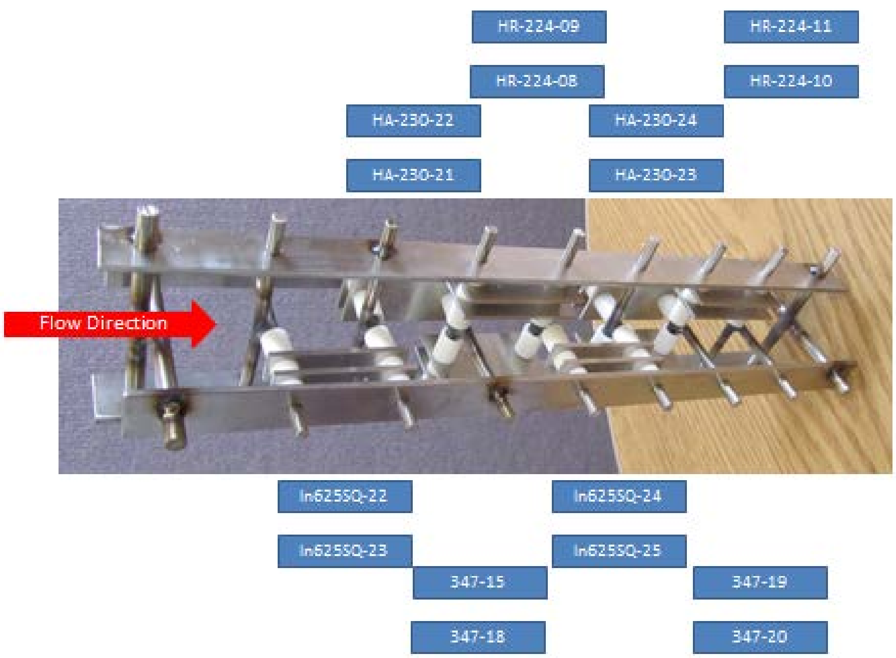

Figure 12 : The Sample Tree Holds The Metal Samples In The Flow Stream for Corrosion Analysis.

- **Inductoheat**

  The 1-meter, NPS 1-1/2 inch Haynes 230 (1.6 inch OD) test section was heated via the 150 KW Inductoheat induction heating unit. The unit heated the surface temperature of the test section to a set point of 670°C, which was controlled via the Labview PID controls. (See the alarm matrix for the induction heater trip setpoints for numerous conditions.) The induction heater was controlled using a 0-10 VDC signal input.

  The Inductoheat was selected because it can apply a large amount of thermal energy to a very small area of material. The system, designed by Inductoheat for the exact application, is 1m (39.37") of Haynes 230 1.5 tube. The Inductoheat unit and coil were comparatively expensive, with low efficiency, but it is available on a commercial basis, provides a uniform heat flux around the circumference of and along the length of the tube, and is known to work. Resistive heat trace could not achieve the watt density needed in the small area. Radiant heaters presented problems with flux uniformity and lamp cooling.

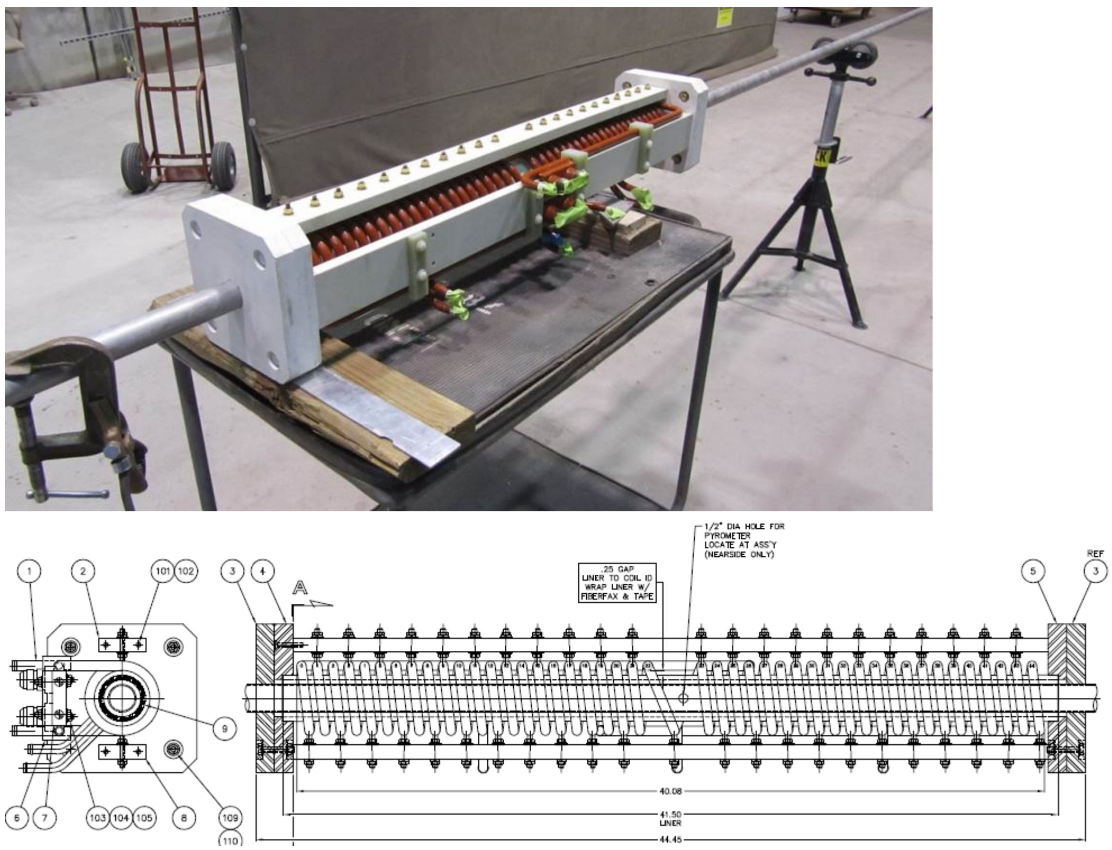

**Figure 13: The Inductoheat coil purchased for this project.
The 1m coil is supported by insulation board. The Haynes tube is surrounded by rigid insulation board that includes a hole to allow the pyrometer to view the pipe inside and to measure the temperature of the pipe wall.**

- **Pyrometer**
  Williamson Corporation Pro 91 Dual-wavelength fiber optic sensor with interface module. 4-20 ma analog output signal. The pyrometer was used to monitor the test section wall temperature through a ½-in hole located mid-coil.

Figure 14: The Williamson Pyrometer

- **Flanges**
  Grayloc hubs 2-in, 316 SS, Schedule 40, with 2-piece, 4-bolt clamps and seal ring, inconcel 718, silver. These were used in four places:
  - Pump discharge post pressure transducer
  - Pre receiver test section
  - Post receiver test section
  - Post coupon sample holder

- **Heat trace**
  The piping system is heated using five separate electrical IM heat trace cables: Zones 1, 2, 3, 4, and 7.
  1. Zone 1 has been designed to heat from the pump discharge to the pre-test section 2 inch line. This includes the 2 inch flow meter. 120 VAC, 328 watt. The cable was 15.3m in length.
  2. Zone 2 has been designed to heat the PT extension. 208 VAC, 1870 watt for each cable with two cables installed. One energized one spare. Each cable was 2.2m in length.
  3. Zone 3 has been designed to heat from the pre-test section the Haynes 230 1.5 inch tube schedule 5. 208 VAC, 2090 watt for each cable with two cables installed. One energized one spare. Each cable was 17.1m in length.
  4. Zone 4 has been designed to heat the valve bonnet. 120 VAC, 250 watt for each cable with two cables installed. One energized one spare. Each cable was 1.5m in length.
  5. Zone 7 has been designed to heat from the test section to the tank inlet. This includes the coupon sample holder and the valve body. 120 VAC, 390 watt for each cable with two cables installed. Both were energized. Each cable was 2.4m in length.

The tank is heated using two separate electrical IM heat trace cables, Zones 5 and 6.

6. Zone 5 has been designed to heat the 17 inches inside the cooling duct portion; this is the upper portion of the round tank and where the salt resides. 208 VAC, 3060 watt for each cable with two cables installed. Both are energized. Each cable is 23.5m in length.
7. Zone 6 the bottom cone and a portion of the drain line; this portion is also where the salt resides. 208 VAC, 1700 watt for each cable, with two cables installed. Both are energized. Each cable is 12.5m in length.

Each Zone is controlled via a separate Chromolox on/off controller with a set point that can be changed at each controller.

Figure 15: Trace Control System

- **Salt Cooler**
  A 17-in high by 1.5-in deep, 347 SS ductwork encapsulated the bottom 17 inches of the tank. A 10- inch diameter carbon steel pipe and plastic hose connected this ductwork to a 5 hp blower located approximately 3 m away from the tank. An actuated air flow damper was inserted into this 10-in pipe to control air flow to the ductwork. The salt pump outlet temperature (FL-TC1) was maintained at 600°C, and was accomplished by blowing ambient air over the bottom 17 inches of the tank surface. The volume of air to the salt cooler was controlled by the inlet damper, which was modulated via a 4- 20 MA control signal.

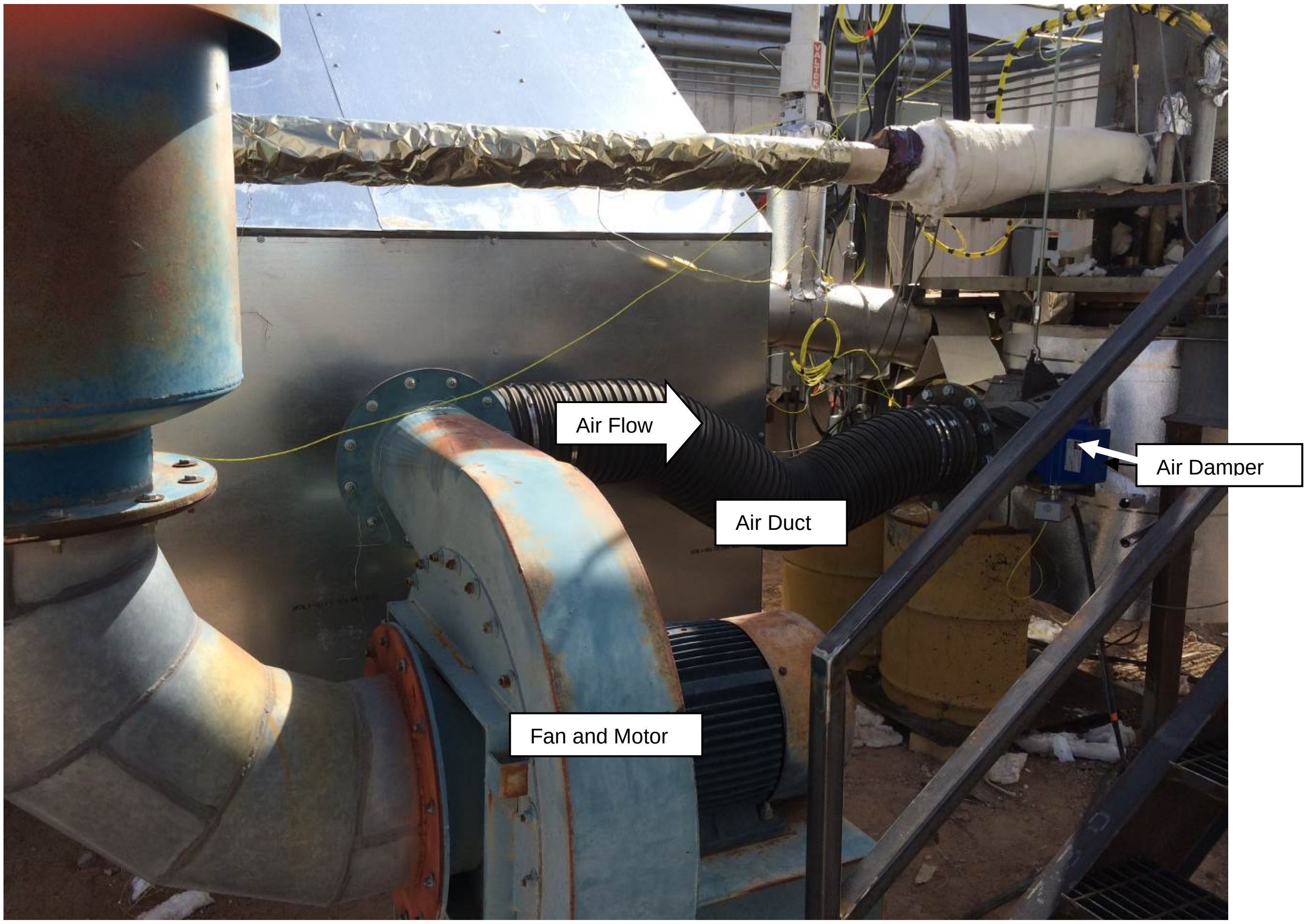

Figure 16: Salt Cooler System

- **Controls and Data Acquisition System, National Instruments**
  The controls sub-system supports both automatic and manual control and monitoring of the Lofted system. Data was downloaded to an Excel© spreadsheet at 30 sec intervals; each entire day's information was saved to a unique spreadsheet at 12 midnight. The system was composed of the following components:
  - Desk-top computer and monitor
  - Network connected National Instruments (NI) Compact RIO (cRIO-9072)
  - NI C-series modules to support digital and analog IO to/from the Lofted hardware.
  - Signal isolation modules (where appropriate) to protect the NI modules from surge damage.
  - Uninterruptable Power supply to maintain control and monitor of the system, over short (10-15 min) power out periods.

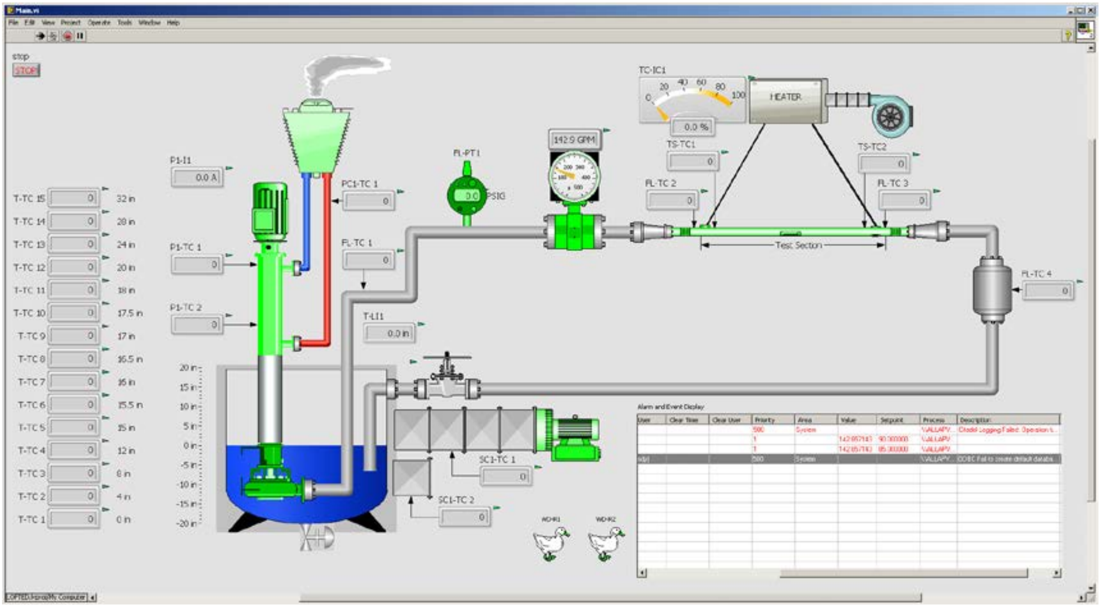

Figure 17: Main User Interface

Table 1 : Control and Data Taglist

Tag Name	Description	DO/DI/ AO/AI/TC	Type of Signal
T-TC 1	Tank temperature 1 -3/8 inches off bottom	TC	Type K -MV
T-TC 2	Tank temperature 3 -1/4 inches off bottom	TC	Type K -MV
T-TC 3	Tank temperature 8 inches off bottom	TC	Type K -MV
T-TC 4	Tank temperature 12 inches off bottom	TC	Type K -MV
T-TC 5	Tank temperature 15 inches off bottom	TC	Type K -MV
T-TC 6	Tank temperature 15 ½ inches off bottom	TC	Type K -MV
T-TC-7	Tank temperature 16 inches off bottom	TC	Type K -MV
T-TC 8	Tank temperature 16 ½ inches off bottom	TC	Type K -MV
T-TC 9	Tank temperature 17 inches off bottom	TC	Type K -MV
T-TC 10	Tank temperature 17 ½ inches off bottom	TC	Type K -MV
T-TC 11	Tank temperature 18 inches off bottom	TC	Type K -MV
T-TC 12	Tank temperature 20 inches off bottom	TC	Type K -MV
T-TC 13	Tank temperature 24 inches off bottom	TC	Type K -MV
T-TC 14	Tank temperature 28 inches off bottom	TC	Type K -MV
T-TC 15	Tank temperature 32 inches off bottom	TC	Type K -MV
SC1-TC 1	Salt Tank cooler inlet temperature	TC	Type K -MV
SC1-TC 2	Salt Tank cooler outlet temperature	TC	Type K -MV
P1-TC 1	Salt pump oil temperature	TC	Type K -MV
PT-TC1	Pressure Transducer TC	TC	Type K -MV
PPC1-TC 1	Salt pump cooling temperature outlet	TC	Type K -MV

Tag Name	Description	DO/DI/ AO/AI/TC	Type of Signal
FL-TC 1	Flow Loop Pre test section temperature	TC	Type K -MV
FL-TC 2	Flow Loop Post test section temperature	TC	Type K -MV
AMB-TC 1	Ambient Temp	TC	Type K -MV
EMO-1	EMO turn off inductoheat and pump -	DI	NC contacts
T-LI1	Level Indicator	AI	4-20 MA
FL-PT1	Flow Loop Pump discharge pressure	AI	4-20 MA
FL-FM1	Flow Loop flow meter	AI	4-20 MA
TS-TT1	Pyrometer Test section Temperature	AI	4-20 MA
TC-IC1	Inductoheat controls	AO	0-10 VDC
P1-SS1	Salt pump start stop	DO	24 VDC coil contactor
PC1-SS1	Salt pump cooler start stop	DO	24 VDC coil contactor
SC1-SS1	Salt cooler start stop	DO	24 VDC coil contactor
IC-SS1	Inductoheat on/off	DO	24 VDC coil contactor
WD-R1	Watchdog Relay #1	DO	24 VDC coil contactor
WD-R2	Watchdog Relay #2	DO	24 VDC coil contactor
SC1-V1	Damper -- Salt Tank Cooler Blower	AO	4-20 ma

2.5 Sequence of Operations

2.5.1 Pre-heat

- **Piping**
  Each Zone is controlled by a separate Chromolox on/off controller, which has a set point that can be changed at each controller. The set points for Zones 1, 3, 4, and 7 will be 300°C deadband of +/- 5°C. The set point for Zone 2 will be 275°C deadband of +/- 5°C. Once the temperatures of all of these zones have reached their set points the date and time will be recorded by the test operator.

- **Tank**
  Each Zone is controlled via a separate Chromolox on/off controller with a set point that can be changed at each controller. The set point for Zones 5 and 6 will be 300°C deadband of +/- 5°C. Once the temperatures of all of these zones have reaches their set points the test operator will document.

2.5.2 Salt Fill

1. Tank
   Prior to heating the tank, the Salt Pump Cooler shall be turned on via the Start/Stop point (PC1-SS1). The Salt Pump Cooler shall run 24/7 while salt is molten in the system.

2. Each Zone is controlled via a separate Chromolox on/off controller, which has a set point that can be changed at each controller. The set point for Zones 5 and 6 will be 300°C deadband of +/- 5°C. Once the temperatures of both of these zones have reached their set points, the test operator will record the date and time when the final zone reached its set point.

   For this procedure, the tank temperature tree shall indicate the air temperature within the tank every 4 inches from the bottom to the top of the tank, with additional TC at a spacing of ½-inch in the zone between 15 and 18 inches. Once the air temperature reaches 300°C, the tank temperatures shall be monitored to ensure that the pump, the air, and the environment have reached the required temperature. The tank will then be allowed to "bake-out" for 24 hours after all TC have stabilized. Once this bake-out process is complete, the salt will be added.

2.5.3 Pre-Test Salt Heat-up and Conditioning

1. Tank

Once the tank has been loaded with salt, the set points for the external heat trace in Zones 5 and 6 shall be set to maintain a minimum temperature of 565°C deadband of +/- 5°C. Once the temperatures of both of these zones, and of all the TCs in the TC tree, have reached this temperature, the test operator will record the date and time the final zone reached its set point. This temperature shall be maintained for a minimum of 48 hours.

The level sensor shall automatically display the current salt fluid level, in inches from bottom of furnace, and the useable salt fluid level in inches. (Note: The bottom 14.25 inches of salt are not useable, therefore subtract 14.25 inches from the total salt height to obtain the useable salt level.)

Warning Level: At a salt operating level of 17 inches from the bottom of the tank, an alarm will sound and send out an email to the test engineers.

Alarm Point: If the salt level drops below 14.25 inches, safety interlocks in the control system shall first de-energize the Inductoheat, and then de-energize and disable the pump. An alarm will sound and send out an email to the test engineers in response to the low-level condition.

2.5.4 Pre-Test Salt Cool-down

1. Tank

Once the salt has been conditioned, the set points for the external heat trace (Zone 5 and Zone 6) shall be lowered to maintain a minimum temperature of 300°C deadband of +/- 5°C. Once the temperatures of both of these zones, and of all of the TCs in the TC tree, have reached this temperature, the test operator will record the date and time when the final zone has reached the set point.

2.5.5 Test Operation

The following sequence outlines the safety steps to be completed prior to test operations:

1. Establish the exclusion area.
2. Verify that no combustibles are within the test exclusion area.
3. Turn on the red beacon west of 9980-A.
4. Make a site announcement that testing will begin at LOFTED, and that the site is off-limits to non-test personnel.

The following sequence outlines the control functions for the system during test operations:

5. Data shall be saved to a test data file. All data shall be collected at a rate of every 30 seconds.
6. Prior to initiating salt flow the operator shall verify that the pre-heat temperatures of the salt in the tank and in the piping system, including the valve bonnets, have been reached by reviewing the Chromolox controllers and the TC tree temperatures.
7. Turn on the Inductoheat cooling system.
8. Open the Flow Control Valve to “100% open”.
9. Verify that the level of salt is at or within operational limits
10. Verify that the water temperature through the Salt Pump Cooler system is within operational limits.
11. The operator shall then initiate the test by pressing a screen button on the operator workstation.
12. Start the pump, and begin monitoring salt level, pressure, and flow.
13. Adjust the air to the Flow Control Valve to obtain the desired flow (37 GPM). Using PPE, lock the valve in place.
14. Monitor the salt temperature and level in the tank.
15. After 10 minutes of the system being stabilized at the desired values initiate the induction heating system. Initial induction heating system set point shall be 585°C. Slowly raise set point to 610°C controlling off of TC-2 “TC-IC1 SP”

16. Raise the set points for the external tank heat trace Zones 5 and 6 to maintain a minimum temperature of 560°C deadband of +/- 5°C. Once the temperatures of both of these zones and all TCs in the TC tree have reaches this temperature the test operator will document.
17. Turn on the salt cooler (fan is in "Auto" mode; the program needs to be placed in AUTO at the control system in 9980-A.); verify the set point is 598°C and that "SC-V1 SP" is controlling off of TC-1. The control system modulates the inlet damper between minimum and maximum using a PID control loop to maintain the salt discharge temperature at 598°C. If the salt discharge temperature drops below 597°C, the inlet damper will close, however, the fan will stay on.

    Note: Salt cooling shall be automatically regulated at 598°C based on FL-TC1 (pump salt discharge temperature).

    The test counter will run when the pump is on, and the Inductoheat is energized, and the outlet temperature (FL-TC2) is 605°C or greater.

2.5.6 Normal Test Shutdown

The following sequence outlines the control functions for the system during Normal Test termination.

1. Turn off the Inductoheat using the unit's controls.
2. De-energize the Inductoheat.
3. Continue to flow the salt through the system for 10 minutes to allow residual heat from the Inductoheat and the test section to be dissipated. Once the test section outlet and inlet temperatures (FL-TC2 and FL-TC3) are equal, proceed to next step.
4. De-energize the pump.

The following sequence outlines the safety steps to be completed <u>after</u> test operations:

1. Remove the exclusion area.
2. Turn off the red beacon west of 9980-A.
3. Make a site announcement that testing has been completed at LOFTED.

2.5.7 Emergency Test Shutdown

The following sequence outlines the control functions for the system during Emergency Test Shutdown:

1. If any of the following conditions occurs during a test, the test system shall immediately be terminated.
    a. The emergency shutdown switch is activated. – The switch will be hard-wired into both the Inductoheat and the pump control circuits. The other contacts will be wired into the control system
    b. The emergency shutdown button on the operator workstation is activated.

c. Any condition identified in the "Alarm Matrix" as a "Critical Alarm" is reached. See the Alarm Matrix in section 2.5.10, below.

1. The controls system shall automatically turn off the Inductoheat.
2. The controls system shall turn off the pump.
3. The controls system shall turn off the salt cooler fan.
4. The Chromolox shall control the heat trace zones to maintain the temperatures at the default setpoints.
5. De-energize the Inductoheat.
6. De-energize the pump.

2.5.8 Loss of Power Shutdown

The following sequence outlines the control functions for the system during a loss of power to the system. The control computer is supplied with UPS power to ensure that the following sequence occurs:

1. The control system shall lock out the Inductoheat to prevent automatic restart.
2. The control system shall lock out the pump to prevent automatic restart.
3. Once power is restored, the Chromolox controllers shall resume control of the tank and heat trace systems to maintain the temperatures at the default set points.

2.5.9 Recovery

The following sequence outlines the control functions to recover from a salt freeze.

1. Piping

   The set point for Zones 1, 3, 4, and 7 will be 300°C deadband of +/- 5°C. The set point for Zone 2 will be 275°C deadband of +/- 5°C. Once the temperature of each of these zones has reached its set point, the test operator will document the time the final zone reached its set point.

2. Tank

   Prior to heating the tank, the Salt Pump Cooler shall be turned on using the Start/Stop point (PC1-SS1). The Salt Pump Cooler shall run continuously (24/7) while salt is molten in the system.

   The set point for Zones 5 and 6 will be 300°C deadband of +/- 5°C. Once the temperature of each of these zones has reached its set point, the test operator will document the time the set point was reached.

   Once the tank has reached 300°C, the set points for the external heat trace Zones 5 and 6 shall be set to maintain a minimum temperature of 565°C, deadband of +/- 5°C. Once the temperatures of both of these zones, and all of the TCs in the TC tree, have reached this temperature, the test operator will document the time the temperature was reached.

Once the piping system reaches the required temperature, and the tank dwells at the prescribed isothermal condition, test operation can proceed.

2.5.10 Alarm Matrix

Point Name	**Description**	**Low Alarm**	**High Alarm**	**Critical Alarm Set Point**
FL-FM1	Flow Rate	<30 GPM		<25 GPM
FL-PT1	Pressure	10	100	None
T-LI1	Salt Tank Level	<17 inches		<14.25 Inches
PC1-TC1	Salt Pump Cooler-Water Temp		82	88
P1-TC2	Pump Bearings Temp		82	88
TS-IC1	Test section temperature via the Pyrometer		>680	> 690

This page intentionally left blank.

3. COMMISSIONING, OPERATIONS, AND TEST EXPERIENCE

3.1 Start-up and Commissioning

Each control and data signal was tested from end-to-end, and the functionality of the control and data acquisition systems was confirmed. The tank was heated and salt was introduced and melted using the tank heaters. A total of 775 lbs. of solar salt was added to the tank through the vent line located on top of the tank. A combination of 475 lbs. of sodium nitrate (NaNO3) prills (60%), and 300 lbs. of potassium nitrate (KNO) prills (40%), were added. The solar salt used for this test consisted of 60 % NaNO3 Industrial Grades Prills and 40% KNO Technical Grade Prills purchased from SQM North America Corporation. Once all of the salt had been introduced and was melted, the temperature was raised above 500°C for 48 hours, then raised to 585°C to decompose any magnesium nitrate to magnesium oxide. The pipe heat trace was turned on and, once the pipe had been heated, the salt pump was turned on and salt flowed through the system. Tuning then began on the flow rate, using the flowmeter and the valve to adjust salt flow. The induction heater was checked for its ability to heat the salt, and the blower was checked for its ability to cool the salt.

The salt cooling system was designed to operate during the cool period of the year; initial plans were to start and end the testing in the winter months. However, the system was started up and operated during warmer periods. Because the cooling capacity of the system was marginal, it was necessary to reduce and remove the insulation from both the pump plate and a portion of the pump discharge piping.

During the final commissioning, it was determined that the Pyrometer reading, which was reading the wall temperature at the center of the 1m test section, was not accurate, most likely due to ambient losses at the coil. Initially, this temperature reading was to be used control 1) the output of the induction heater, and 2) the wall temperature. After analyzing the issue, a decision was made to control the heater using the Flow Loop Posttest section temperature, FL-TC2. A calculation was performed using this TC. The result showed that the FL-TC2 set point would need to be 610°C to result in a 670°C temperature in the wall section.

The initial plan called for a salt flow of 55 GPM to accomplish the goal of 30 years of accelerated testing. At start-up, the flow rate was set using the 1 ½" flow control valve at 55 GPM, which resulted in 60 PSIG. However, the induction heater was in an overload condition and would not allow the wall temperature, or the Posttest outlet temperature, to be reached. To rectify this issue, two items needed to be addressed. First, both the transformer tap settings and the capacitor bank internal to the Inductoheat needed to be adjusted. Second, the flow rate needed to be lowered. Once these two adjustments were completed, the flow rate was set to 37 GPM using the flow control valve. The average test flow rate was 38.8 GPM.

The Inductoheat has a maximum output power of 150 kWe, while the calculated power put into heating the salt was 64 kWth. The discrepancy can be traced to the fraction of electric power that goes into heating the salt, the fraction of the electric power that goes into heating the cooling water for the Inductoheat electronics and the Inductoheat coil, and the losses to ambient surroundings.

Since the film temperature cannot be measured directly it was necessary to perform a series of approximations and calculations to determine this value. Inductoheat losses precluded the use of this power directly, thus it was necessary to rely upon independent variables to calculate the film temperature. Ultimately, a flow rate was the variable controlled to set the film temperature. The method employed to select the flow rate was as follows:

a) A trial volume flow rate was selected, from which the mass flow rate was calculated.

b) A velocity was calculated, from which the internal convection heat transfer coefficient was calculated using the standard Dittus-Boelter equation with a correction factor on the Nusselt number for values of tube length/diameter ratios less than 400.

c) The temperature rise across the test section was measured, which corresponded to a given thermal power into the salt. (i.e. $Q = \dot{m}C\Delta T$, where Q is thermal power, $\dot{m}$ is mass flow, C is heat capacity, and ΔT is the temperature change from inlet to outlet).

d) Given the convection coefficient and the thermal power input, the film temperature required to accomplish the necessary heat transfer was calculated.

$T_{film} = \frac{\dot{m}C(T_{outlet} - T_{inlet})}{hA} + T_{bulk}$, where A is the circumferential pipe area

e) The trial volume flow rate was adjusted until the calculated film temperature reached the desired value of 670°C. The flow rate of 38 GPM was selected.

During the test, the bulk salt in the tank was maintained at 600°C, either by removing heat using the salt cooling system or by adding heat using the Inductoheat system. The heat trace, Zones 5 and 6, were not energized while the test was operational.

3.2 Operations and Test Experience

The test was initiated on April 8, 2014. On April 14, six days later, a salt leak was discovered in the system. The test had to be shut down until a solution could be identified and implemented. Due to the high operating temperatures, the bolted connection between the tank and the Tank Interface Plate expanded, stretching the bolts, and creating a large gap between the tank and the plate. In addition, the two separate pieces of the Tank Interface Plate had expanded, causing an approximate 3/8-inch gap. The two gap areas allowed molten salt to exit the tank, which lowered the salt inventory and caused a system trip as a result of the low salt levels. To correct the situation, a stainless steel catch pan was designed and fabricated, then welded to the outer surface of the tank. This “catch pan” surrounds the tank’s entire upper flange and the bolted connections of the tank, and captures the leaking salt. A ¾-inch stainless steel pipe was run from the catch pan back into the bottom of the tank. The idea was that the majority of the salt would be captured by the catch pan, then reintroduced into the salt inventory in the tank.

Figure 18: Catch pan attached to tank and ¾-in drain line

Figure 19: Catch pan attached to tank

Figure 20: ¾-inch drain line attached to bottom of tank to reintroduce salt to tank inventory

Due to this leak, the salt inventory decreased to 20.7 inches, which is approximately 629 pounds of salt; the pre-start inventory was 25.5 inches / 775 pounds of salt. The test was restarted on April 21, 2014, and ran until April 30, when it tripped due to the low flow (i.e., low salt level), which caused the pump to draw air. The system was restarted, but continued to tripped the next day. On May 5, 100 pounds of salt was added. (See Table 2: Salt Additions) On May 7, during salt sampling, another salt leak was discovered at the flanged connection to the pump discharge. The insulation around that flange was removed, exposing the flange and bolts. The bolts had stretched and the clamps were loose. All four bolts were inspected and re-torqued. On May 27, the system again tripped due to low salt level. At that time it was determined that the other three sets of flanges had leaked. It was not obvious prior to this trip that the flanges were leaking, because the salt had not leaked through either the insulation or the outer aluminum jacket, which covered the entire flange(s). All of the associated bolts had stretched and the clamps were loose. From this point forward, flange inspections and re-torque became a process that was conducted each time the system was shut down for salt sampling.

A timer was implemented as part of the control and data acquisition system. This timer was activated when the following three conditions were true: 1) the pump is on, 2) the induction heater is on, and 3) the posttest section temperature (FL-TC 2) is >= 605°C. There were times when the pump and the induction heater were on, but the temperature of the posttest section was below 605°C, in which case the timer would not actuate. The final test duration time was 61 days, 15 hours, and 49 minutes. This represents approximately 12 years of operational plant life.

Table 2: Salt Additions

Date	Total Amount Lbs.	Potassium Nitrate Lbs.	Sodium Nitrate Lbs	Timer Days / hrs / mins
March 12, 2014	775	475	300	Initial Salt fill
May 15, 2014	100	40	60	21 / 7 / 6
May 22, 2014	173	73	100	26 / 1 / 33
May 27, 2014	350	140	210	29 / 7 /

The Inductoheat heater system included a primary cooling system and a secondary cooling system to cool the electronics and the induction coil. This secondary cooling system was a water/glycol-to-air cooler, and could only cool the system to a minimum of the ambient temperature. The Inductoheat controller had multiple trips designed into the system to protect the electronics, as well as the entire package, from overheating.

One of these trips was cooling water temperature. As stated above, the system was designed to operate in the cool period of the year, and initial plans were to start and end operations in the winter months. However, the system was started and operated during warmer periods, so the cooling capacity of the system was marginal; during warmer periods the ambient temperature would shut down the Inductoheat system, stopping the test timer. It became necessary to add additional cooling capacity to the secondary air cooler.

A water spray was added to the air cooler fins to help lower the water/glycol temperature. Once this was completed, and the salt issues had been resolved (after the end of May), the system operated reasonably well, which allowed additional testing to occur. The testing was stopped on July 8, 2014, to allow enough time for the coupon corrosion analyses to be completed prior to the end of the fiscal year.

As stated in Section 3.1 of this report, the goal of this test was to reach an equivalent of a 30 year plant life, or 33 hours of equivalent wall temperature exposure, i.e., salt in direct contact with the last panel in a commercial receiver, at temperatures up to 670°C. Due to the salt leaks, the Inductoheat cooling issue, and a few other issues, including a computer crash and power outages, this goal was not achieved. The final time elapsed on the test system timer was 61 days, 15 hours, 49 minutes. At an average salt flow rate of 38.8 GPM, as documented below in Figure 21, the test resulted in a plant operations of 12 years Figure 21 also shows a days' worth of key data which was used to verify the system's operations.

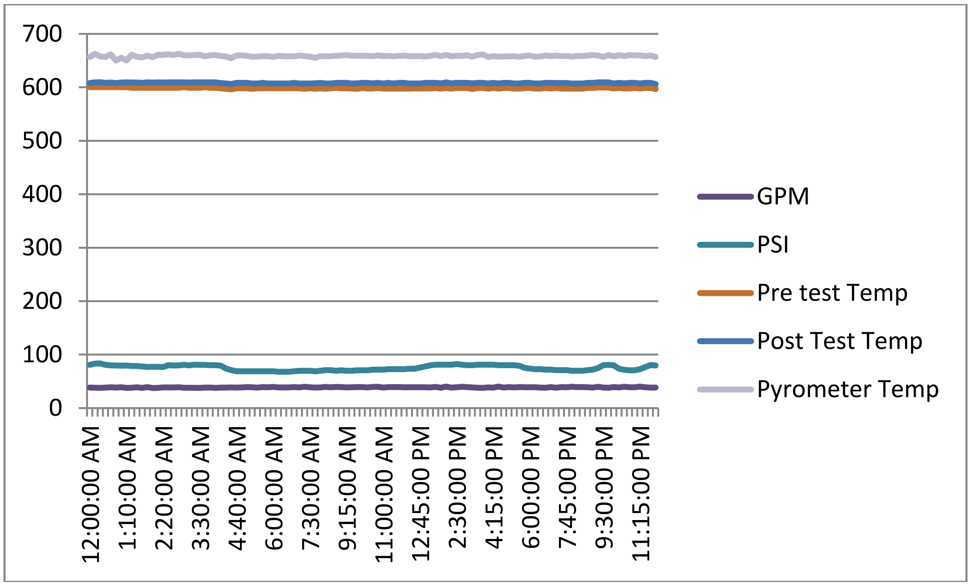

Figure 21: July 1, 2014

Average Flow –	38.8 GPM
Average Pressure –	74.9 PSI
Average Pre-test Temp –	598.4°C
Average Post-test Temp –	608.1°C
Average Test Wall Temp –	658.4°C

a. Flowmeter

The Krohne flow meter operated continuously with a salt inventory at 600°C. The reading from the meter appeared to be very consistent over the entire test period. The electric heat trace and the thermal insulation were installed around both of these systems. The heat trace and insulation could be installed up to the flow meter's flanges, but could not include these flanges. These areas need to be kept cooler than the salt. After initial start-up, all of the insulation was removed and the heat trace on this meter was shut off. The insulation was removed due to salt cooling, as described in other sections of this report. Below is the factory calibration.

Test equipment data / Kalibrierstanddaten / Données du banc d'étalonnage

Serial Number / Seriennummer / Numéro de série	: AF
Fluid / Flüssigkeit / Fluide	: Water / Wasser / Eau
Uncertainty calibration circuit / Unsicherheit Kalibrierstand / Incertitude du banc d'etalonnage	: 0.02%

Calibration Results / Kalibrier Resultats / Résultats d'étalonnage

Flow rate Durchflussmenge Débit [%]	Set flow rate Gewählte Durchfluss Débit réglé [m3/h]	Deviation Abweichung Ecart [%]
101	40.376	-0.21
51	20.304	+0.06

Figure 22: Flow Meter factory calibration

b. Pressure Transducer:

The GEFRAN NaK-filled pressure transducer has an upper operation temperature of 538°C. The diaphragm and the body of the sensor were mounted on a 30" extension pipe to reduce the temperature from 600°C to an acceptable range. Sandia National Laboratories has these identical pressure transducers with the extensions installed on the Molten Salt Test Loop MSTL and have experienced what is believed to be a vacuum, similar to a venturi. To address this, a ¼ " SS tube was placed internal to the extension. This tube protruded into the salt flow in the 2" pipe and extended up to the pressure transducer diaphragm. This would allowed salt to fill the entire ¾" pipe and allowed a constant flow of salt up to the diaphragm. The threaded connections, which are between the ¾" extension and the pressure transducer body, have leaked in all of the installations at the NSTTF. This threaded connection was intended to be frozen following initial start-up and once the system pressure was known. The reason for freezing was to create a salt plug, thus stopping any leak. The insulation was removed and the heat trace was turned off, however, the salt did not freeze. The belief is the internal ⅛" tube allowed hot salt to flow through the ¾" extension, keeping the inventory molten. The pressure transducer leaked a small amount of salt, but did not impact the system's salt inventory. The extension was mounted straight up, so that when the system was shut down, the salt drained back into the tank. The published factory technical specification lists the accuracy at .25%.

3.3 Salt sampling

Initially, salt samples were taken three days per week. However, once the salt leaks were discovered, the samples were taken once a week. This decision was made due to the increase in stress on the entire system. Each time a salt sample was taken, the induction heater and the salt pump had to be shut down and the system made safe. When the system was shut down, portions of the system quickly cooled down. The 2 in. piping at the pump discharge would contract, because it was not well insulated, while the 1.5 in. receiver tube would stay at approximately the same test temperatures and at the same heated length. The 2-in pipe was observed to have shortened by a few inches, even during very short time periods. The average time needed for salt sampling was 15 minutes. Also, due to the thermal cycling, the bolts on the flange connections stretched, causing the flanges to separate and leak. Once we identified these as “leaking” issues, the flange connections were torqued during the system shutdown.

The salt samples were drawn using a ¼-inch 316 SS tube. The molten salt was taken from the tank through the sump vent line. The molten salt in the tube was lowered into a nitrogen-purged container. When the salt had frozen, which took a few minutes, the sample was placed into a glass vial, which was located in the nitrogen-purged container. The foil-lined top was securely placed on the top of the glass vial, then tape was placed around the top and the glass to add additional protection for the atmosphere within the vial. Once this was completed, the samples were stored in a separate container.

4. ANALYTICAL RESULTS AND DISCUSSION

4.1 Nitrate Salt Equilibrium and Decomposition Chemistry: Salt Analysis

The nitrate ions in the salt are in chemical equilibrium with the nitrite ions, based on the following reversible reaction:

$$NO_3^- \leftrightarrow NO_2^- + ½\ O_2 \qquad \textbf{Equation 2}$$

The nitrite concentration is a function of the salt temperature and the partial pressure of oxygen in the cover gas above the salt. At 600°C, and with an oxygen partial pressure of 0.21 bar, the equilibrium nitrite concentration is in the range of 5 to 6 percent.

The nitrite ion thermally decomposes to form the oxide and nitrogen oxides, as follows:

$$NO_2^- \rightarrow O^{--} + NO(g) \qquad \textbf{Equation 3}$$

The oxide ions remain in solution, while the nitrogen oxide leaves the salt in the form of a gas. Because the NO does not remain in solution, the reverse reaction, which would generate the nitrite ion from the oxide ion, proceeds only at a very limited rate. As such, Reaction 2 is nominally a decomposition reaction, rather than an equilibrium reaction.

(Note: In the discussion, the generic term ‘oxide ion’ refers to a range of potential oxide species, including the oxide ion (O^{--}), the perioxide ion (O_2^{--}), and the superoxide ion (O^-). Currently, the relative concentrations of the three species have yet to be determined.)

It can be noted that the nitrite decomposition reaction is always underway. The reaction rate is modest at a temperature of 600°C, but is believed to be significant at a temperature of 670°C.

The oxide ions are a major source of corrosion. Specifically, the oxide ion migrates through the protective metal oxide layer that forms on iron and nickel alloys. The oxide ion then reacts with the chromium in the parent metal to form a soluble form of chromium oxide, which then migrates back out through the protective oxide layer. This chromium leaching process represents a major loss in the corrosion resistance of the parent metal. Nonetheless, not all of the oxide ions formed are available for reaction with the chromium. Competing oxidation reactions include the formation of iron oxide, sodium carbonate, and nickel oxide.

4.2 Salt Chemistry Wet Chemistry Analysis

Currently, there are no reliable methods for determining oxide concentrations in the salt. A multi-pronged approach undertaken in this study consisted of 1) performing a total alkalinity measurement, and 2) storing samples that are periodically removed and stored in sealed containers to prevent oxygen, carbon dioxide, and water vapor from reacting with the salt. Salt samples were taken periodically during the course of the experiment.

LOFTED Total Alkalinity Analysis

Because no standard methods exist for measuring oxide in nitrate salts, it was necessary to develop some preliminary methodologies for such quantification. To this end, known concentrations of oxide in mixtures of 60/40 solar salt were formulated using Na_2O_2 as the oxide. Sodium peroxide was chosen over sodium oxide (Na_2O) on the basis of available purity, with the ultimate goal to have certainty around the initial chemistries. Na_2O_2 reagent grade (97%) was obtained from Sigma-Aldrich, in contrast to 80% Na_2O (impurities are 20% Na_2O_2). Salts were mixed at room temperature, then heated to 500°C for 24 hours prior to extracting samples.

Eight mixtures of 60/40 binary salt and sodium peroxide were used, ranging in concentration from 500ppm to 5000ppm (Figure 9). Each mixture was added to water, where the following equilibrium was established [2, 3]:

$$\boldsymbol{H_2O + O^{2-} \rightleftharpoons 2OH^-} \qquad \textbf{Equation 4}$$

Alkalinity method SM 2320B was utilized for this analysis. SM 2320B is a standard EPA method that is used to quantify wastewater alkalinity. Autotitration is performed through the addition of a standard acid to an aqueous solution of salt mixture until the final pH is 4.5. The amount of titrant consumed can then be used to calculate the total alkalinity, which is reported as $CaCO_3$. One sample concentration was repeated using six duplicates (refer to the peroxide content of 2634ppm in Figure 9), and the scatter was determined to be 3.8%. The lower bound on this measurement is ~300ppm Na_2O_2 in a 60/40 melt.

Increasing the concentration of sodium peroxide in the melt had a linear effect, as shown in Figure 23. Total Alkalinity (TA) is now correlated to oxide concentration in the melt, and the data yields the following equation:

$$\boldsymbol{Oxide[ppm] = 0.695(TA) + 1751} \qquad \textbf{Equation 5}$$

This equation is used in the measurements in the following section to determine the projected oxide content in the LOFTED system over time.

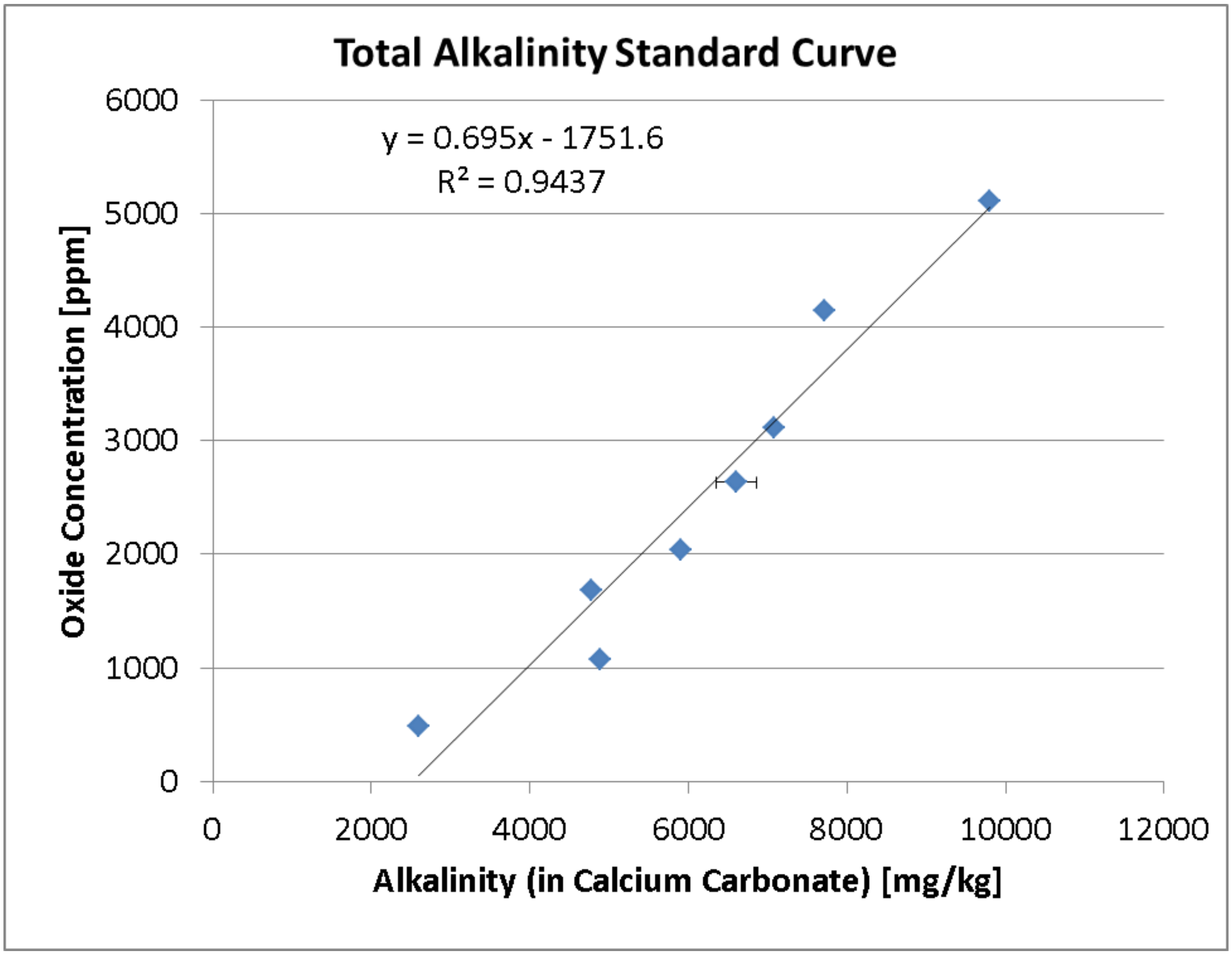

Figure 23: Sodium peroxide concentration in 60/40 salt vs. total alkalinity measurement.

Salt samples were removed, as provided in Table 3. Given the large number of samples, only nine samples were analyzed (Figure 24). It was found that the concentration data varied wildly over time, due to changes in salt quantity in the system over time. Make-up salt had to be added over the duration of the test, as a result of leaks in the system, which dilute the amount of accumulated oxide. By taking into account the accumulated amount of salt, as noted per comments in Table 1, there was a clear trend of increasing oxide over time (Figure 25) until reaching a plateau, which was followed by a decrease in oxide content. The reason for the decrease observed in sample 23 is unclear.

Oxide concentration in the melt is the difference between the rate of oxide production and the rate of oxide consumption. Oxide production arises from the thermal decomposition of the nitrite ion [3, 4], which is a function of temperature, relative stability of the cation [5], and relative concentration of nitrite/nitrate anion. Oxide consumption is based on several competing reactions in the LOFTED experiment: oxidation of the containment forming solid corrosion products, soluble corrosion products (i.e., chromate formation), and carbon dioxide in the head space combining with oxide to form carbonate. The decrease in oxide concentration at the final time of the test is related to an imbalance between production and consumption.

Table 3: Salt sample pull schedule and addition of salt

Sample Number	Date Taken	Temperature	Pump/Inductor Heat Hours	Comments
1	3/27	300	0	775 lbs of salt initial
2	4/10	600	2 days 9 hrs	
3	4/14	230	4 days 18 hrs	Took sample from spill
4	4/23	600	6 days 10 hrs	
5	4/25	600	7 days 19 hrs	
6	4/28	600	10 days 18hrs	
7	4/30	600	11 days 20 hrs	
8	5/2	600	12 days 11 hrs	
9	5/5	460	12 days 11 hrs	Salt added May 5, 100lbs
10	5/7	600	14 days 2 hrs	outlet flange leaked-tightened
11	5/9	600	16 days 4 hrs	outlet flange leaked-tightened
12	5/12	490	18 days 7 hrs	Tripped due to power outage
13	5/14	600	20 days 7 hrs	
14	5/16	600	22 days 5 hrs	Salt added May 15, 100lbs
15	5/19	519	23 days 13 hrs	Tripped
16	5/21	593	24 days 20 hrs	
17	5/27	550	29 days 7 hrs	Salt added May 22, 173lbs; Salt added May 27, 350lbs
18	6/2	600	33 days 14 hrs	
19	6/9	600	39 days 6 hrs	
20	6/16	600	45 days 12 hrs	
21	6/23	600	52 days 11 hrs	
22	6/30	600	54 days 9 hrs	
23	7/7	600	60 days 17 hrs	Tripped, Temp 455C

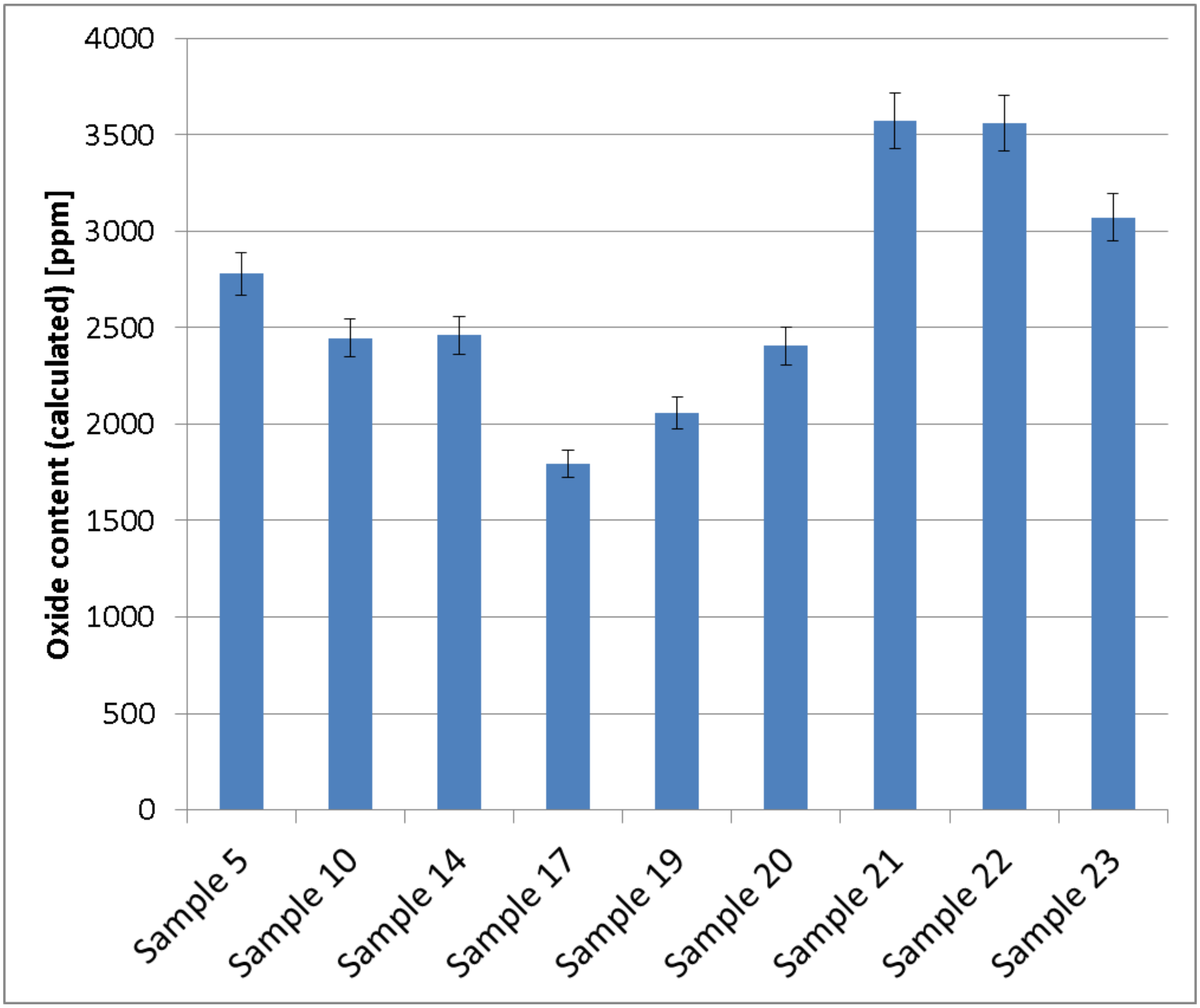

Figure 24: Calculated oxide concentration for select LOFTED salt samples. Error bars are set at 4% based on repeatability measurements.

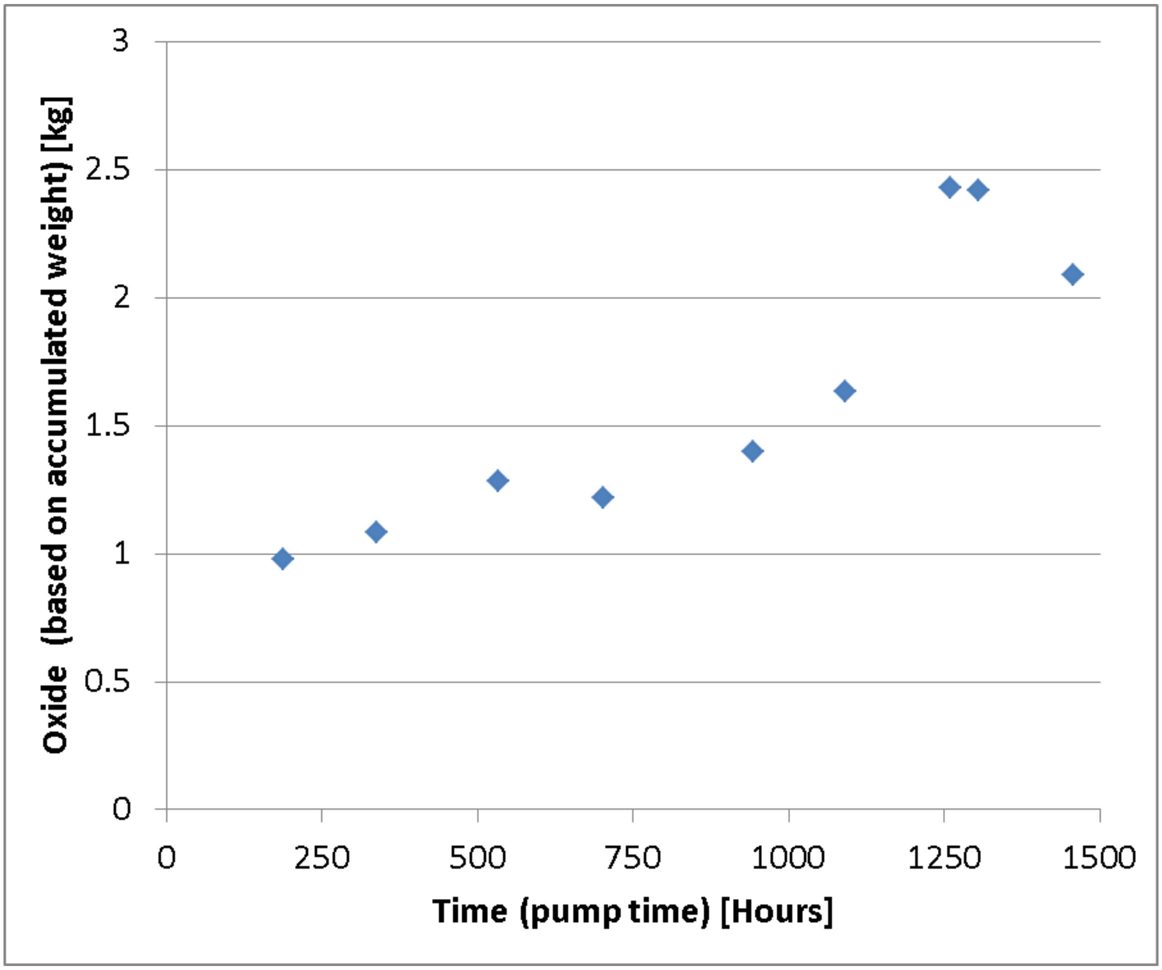

Figure 25: Accumulated oxide content over time.

4.3 Corrosion Results

Sandia has recently completed a corrosion survey of 13 iron and nickel alloys in nitrate salt at a temperature of 600°C [6-8]. Based on the study, candidates for use in a commercial project include the following: Alloy 230; Type 347H stainless steel; Inconel 625SQ; and Alloy HR224. The last is a Ni-Fe-Cr alloy, which has shown low corrosion rates due to relatively high aluminum content.

A total of 16 corrosion coupons were placed in a sample basket, where the salt temperature is a uniform 600°C. The corrosion tests include four coupons of each of the four alloys. The coupons were used in the 'as received' condition, and not subjected to welding, heat treating, or ageing after receipt.

The coupons were removed at the end of the experiment, and analyzed for weight loss and chemical composition of the corrosion layer. As discussed below in the section related to Equipment Considerations, the duration of the experiment was relatively short, and the combination of time and oxide concentrations in the sample basket did not duplicate the conditions in a commercial project. As such, the corrosion tests will be, to some degree, only qualitative in nature, looking for characteristics such as pitting, spalling, or delamination that may eliminate a candidate alloy from further consideration.

Corrosion Rates

Static corrosion experiments using the same salt composition, grade, and supplier (both salt and metal coupons) have been done recently at 400, 500, 600, and 680°C for In625, Haynes 230, and 347SS [6-9], however, the only data available at 600°C is for HR-224. Corrosion rates and metallographic analysis will frequently refer back to these studies for meaningful comparisons.

ASTM G1-03 practices were used as the general guide for oxide removal techniques [10]. The tenacious oxide formed on high-nickel-content alloys is not easily removed using mechanical or chemical techniques alone. Therefore, combinations of both methods were employed.

Excess salt was removed from the samples prior to oxide removal. Samples were placed in deionized water and cleaned via bath ultrasonication for ten minutes, or until the samples appeared visually clear of deposits. Samples masses, with the oxide layer intact, were measured.

Stainless steel alloys (347SS and HR-224) used ASTM G1-03 Designation C.7.4 for oxide removal guidance [10]. Samples were washed for five minutes in a boiling $NaOH/KMnO_4$ bath, rinsed for one minute in a room temperature diammonium citrate ($(NH_4)_2HC_6H_5O_7$) bath, then rinsed with deionized water. They were dried with lint-free cotton wipes, weighed, and the process was repeated for a total of four bath cycles. This proved to remove oxide layers satisfactorily.

Oxide layers on nickel based alloys were especially tenacious. Previous attempts, as guided by the ASTM method, to chemically remove the oxide layer were ineffective. Therefore, a modification of the stainless steel method was developed for nickel alloys. Samples were washed for an hour in boiling $NaOH/KMnO_4$ bath, then washed for an additional hour in a boiling diammonium citrate bath, and, finally, rinsed with deionized water. Samples were dried with lint-free cotton wipes and weighed. All samples were then abraded using glass beads (grit 60), until the oxide layer was completely removed. All corrosion samples were compared to pristine base samples, which were also subjected to chemical baths and abrasion to determine whether the mass loss was strictly due to the loss of the oxide layer.

Calculations to assess corrosion damage were performed as depicted in various standards [10, 11] using the following equation:

$$\frac{\mu m}{yr} = \frac{87600(\Delta M'')}{\rho T} \qquad \textbf{Equation 6}$$

ρ is alloy density (g/cm^3), T is time in hours, and $\Delta M''$is the area of normalized mass loss.

The alloys investigated have been sorted into several sections, primarily by the main elemental constituents. An attempt was made to make relevant comparisons in each section using weight gain, descaled loss (corrosion rate), and electron microscopy along with any pertinent discussion.

Table 4: Nominal composition of alloys

Alloy	Cr	Mo	Ni	Mn	Si	Fe	Co	W	Al	Other
347SS	17.45	0.32	9.43	1.57	0.63	69.72	-	-	-	Nb (0.62), Cu (0.26)
HR-224	20.50	0.21	46.44	0.33	0.31	27.62	0.38	-	3.86	Ti(0.35)
In625-SQ**	21	9	62b	0.5*	0.15*	5*	1*	-	0.4*	Nb+Ta(3.7), Ti (0.4*)
Haynes 230	22.37	1.27	59.41	0.49	0.42	1.32	0.19	14.16	0.32	Cu(0.05)

**Nominal composition
*Maximum
b-balance

Table 5: Corrosion coupon rate data from LOFTED test with nominal fluid temperature at 610°C. Triplicate samples used to determine corrosion rates.

Alloy	Alloy Density [g/cm^3]	Exposure Duration [Hours]	Weight Loss* [mg/cm^2]	Metal Loss** [µm/year]
347SS	8.03	1200	18.0±2.4	163 ± 22
HR-224	8	1200	7.0±0.1	64.2 ± 1.3
In625SQ	8.44	1200	12.8±3.8	111 ± 27
Haynes 230★	8.97	1200	49.5±8.8	403 ± 71

*Average using triplicate samples
**From Equation 4
★ Internal oxidation observed loss rate does not include internal attack.

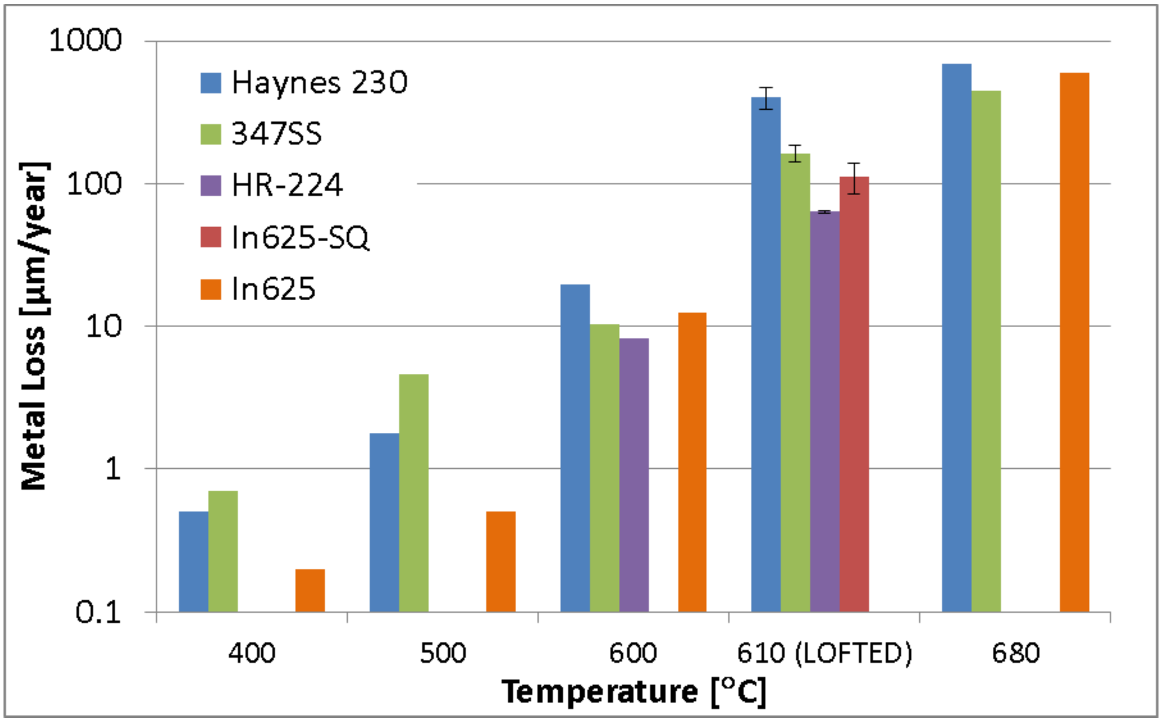

Figure 26: Corrosion rate of alloys from current test and previous experiments [7, 9]. Note the use of logarithmic scale, which indicates a factor of ten increase in corrosion from static experiments at 600°C to LOFTED tests at about 610°C.

Metallography

Scanning electron microscopy (SEM) and energy dispersive spectroscopy (EDS) were performed on the JEOL JSM 840A, using the EDS system from Thermo Electron Corp. All plan and x-ray mapping analyses were performed on this instrument.

Sample number 347SS exhibited some oxide spallation upon removal. Previous studies, which ranged from 400-680°C in a static configuration, yielded no spallation behavior, which may indicate this behavior has some dependence on flowing systems. Despite evidence of surface exfoliation, the overall corrosion morphology appeared to be consistent with static exposures, with two noteworthy differences (Figure 26). First, magnesium was present in the outermost corrosion scale. A thin layer of Mg was present in all of the alloy analyses, as will be shown in subsequent figures. Second, little sodium was present in the surface oxide, whereas previous results identified mixed phases of sodium ferrite ($NaFe_2O_4$) and hematite (Fe_2O_3) [6]. It is not clear why sodium ferrite was not particularly present on the outermost oxide layer here, although previous authors indicate the transition to sodium ferrite formation occurs above 615°C [12]. The exact conditions leading to sodium ferrite formation is largely temperature dependent, but may also be linked to oxide concentration in the melt. Most of the oxide thickness, roughly 5-8 µm, was iron oxide, with mixed oxides of chromium, nickel, and iron near the interface between the base alloy and the oxide.

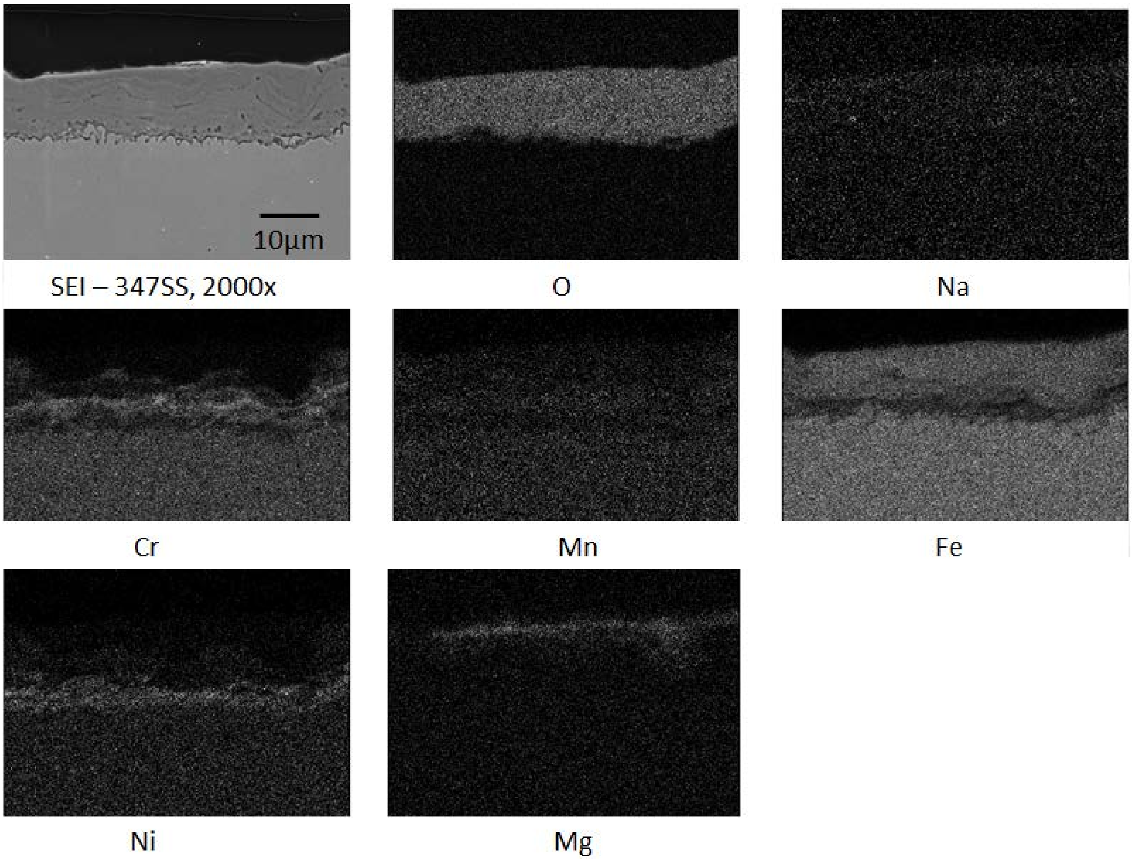

Figure 27: EDS x-ray map of 347SS cross section. Outermost oxide layer consists of a Mg, Fe oxide, with an inner layer of mixed oxides of chromium and iron. Nickel enrichment is observed on the alloy/oxide interface due to chromium depletion.

HR-224 had the lowest corrosion rate of all samples tested, and was found to have incomplete oxidation even after more than 1000 hours of exposure (Figure 27). In regions where oxidation occurs, iron oxide was the corrosion product. These results were consistent with previous 600°C static corrosion studies.

Figure 28 is the cross-sectional x-ray map of HR-224 in a region of continuous oxidation layer. The corrosion layer is primarily a thin iron oxide. Low corrosion rates may be tied to the presence of aluminum in the alloy, as observed in the enriched aluminum content at the oxide interface. Slight chromium depletion was observed directly below the oxide/base alloy interface, indicating that any layer forming at the interface does not fully inhibit chromium dissolution from the alloy. Furthermore, in locations of discontinuous oxide growth, nodule-like iron oxides were observed (Figure 29), and it is unclear how oxide growth would continue over long timeframes. HR-224 has been proven to be resistant in high temperature oxidizing environments [13], and exposures in higher temperature nitrate salts may prove insightful for receiver tube applications, which has merit for further study.

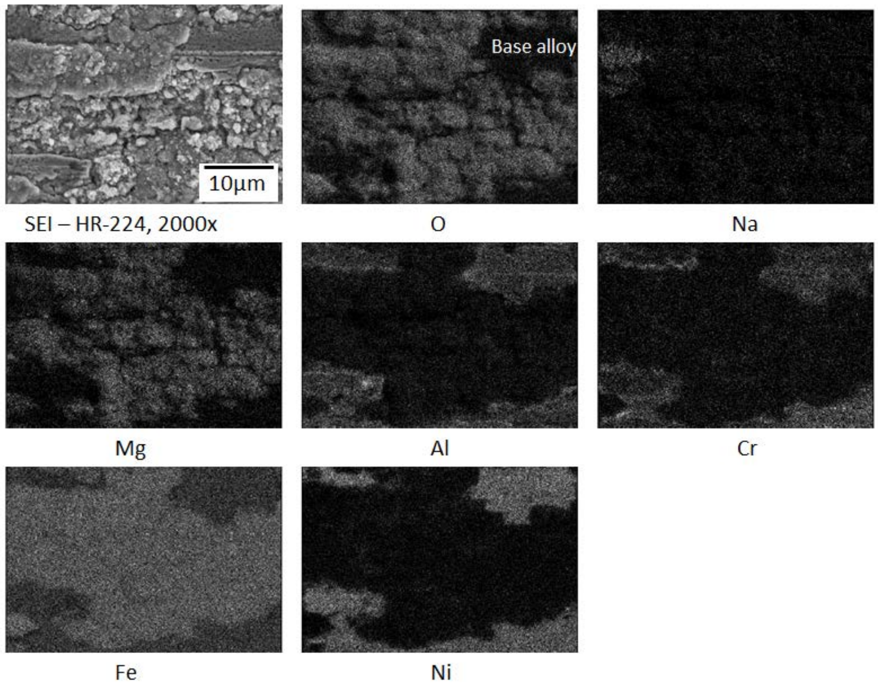

Figure 28: HR-224 had incomplete surface oxidation after more than 1000 hours of exposure. This result is consistent with previous static 600°C tests [7]. Where oxidation is observed, the oxide appears to be an iron oxide with a thin layer of Mg.

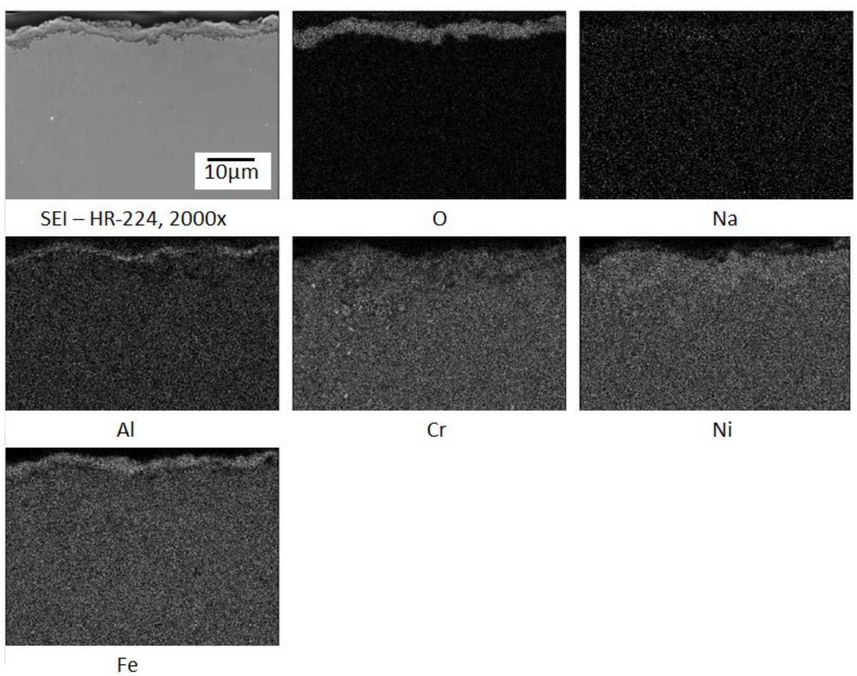

Figure 29: HR-224 had the smallest corrosion observed in the study. Oxide formation appeared to be primarily iron oxide, although aluminum enrichment was observed in the oxidation layer.

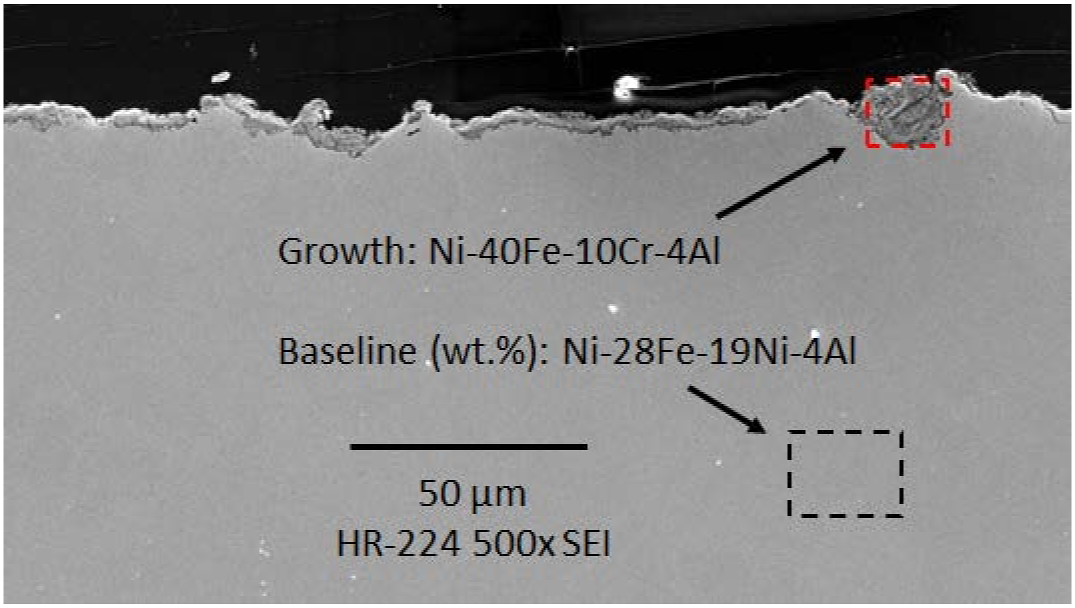

Figure 30: Iron oxide nodules were observed in various locations on HR-224.

Haynes 230 was investigated in two locations and two geometries in the LOFTED test. Flat coupons were co-located with all other alloys that were exposed at a nominal temperature of 610°C; the test section was Haynes 230 pipe, at a nominal temperature of 670°C. Figures were labelled either as "coupon" or "pipe" to differentiate between conditions.

The mechanisms and morphologies of coupon exposures were consistent with previous exposures, in that NiO is the primary outer oxide, with an internal oxidation layer occurring (Figure 31). One key difference was observed here: a localized form of corrosion was observed on the surface, shown in Figure 30. This localized corrosion, which appeared to be shallow pit-like structures, was found in multiple locations on the Haynes 230 coupons. Due to the sparse and sporadic nature of the localized corrosion, locating instances for cross sectional analysis was difficult. However, Figure 32 is thought to be a cross sectional view of the localized attack, where the corrosion morphology was unusual, having high levels of sodium and iron present.

Pipe analysis, Figure 33, had a markedly different morphology and corrosion product composition as compared to coupon samples. Nickel was shown to be relatively depleted in the corrosion layer, while chromium was comparatively enriched. Furthermore, no internal oxidation stringers were present. This change in morphology cannot simply be a function of temperature, as in Figure 34, which was exposed at 680°C, and had similar corrosion morphology as compared to Figure 30 – an outer layer of NiO with a chrome oxide internal oxidation layer beneath.

Assuming that a flowing medium will increase corrosion rates (as shown by the factor of an 8-10 time increase in corrosion from 600 (static) to 610°C (flowing) in Figure 25), the pipe corrosion rates may be higher than the 600 µm/year rate found in static studies at 680°C. It is possible that, if corrosion rates are high enough, rapid dissolution of chromium and tungsten may result in a oxidation layer that lacks mechanical integrity. Such a layer would be completely non-protective. Thus, a uniform removal of pipe wall material would be the resulting observed behavior.

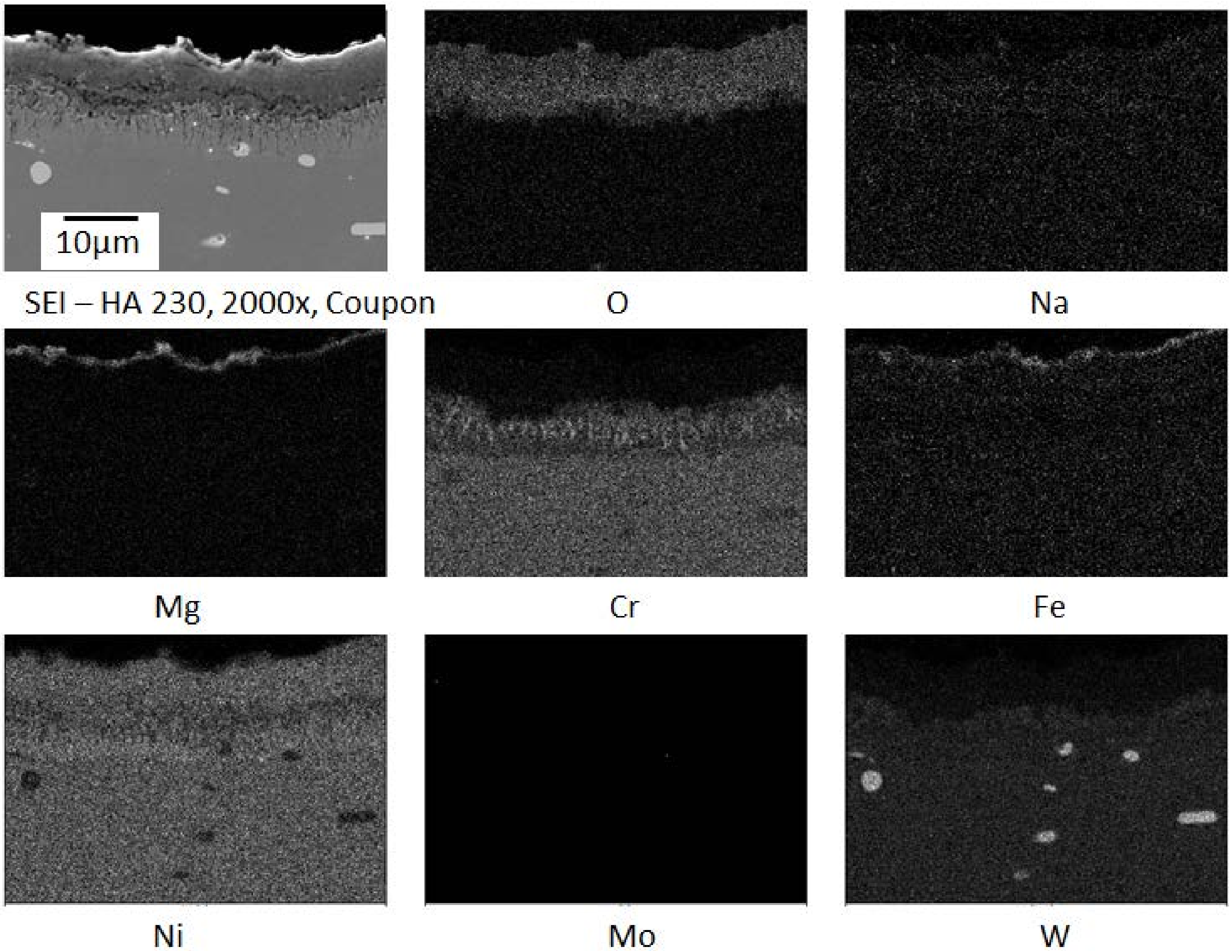

Figure 31: Haynes 230 coupons had an internal oxidation attack that consisted of an external oxide layer of NiO followed by an internal chrome oxide. Similar behavior was observed for static tests at 600 and 680°C [7, 9].

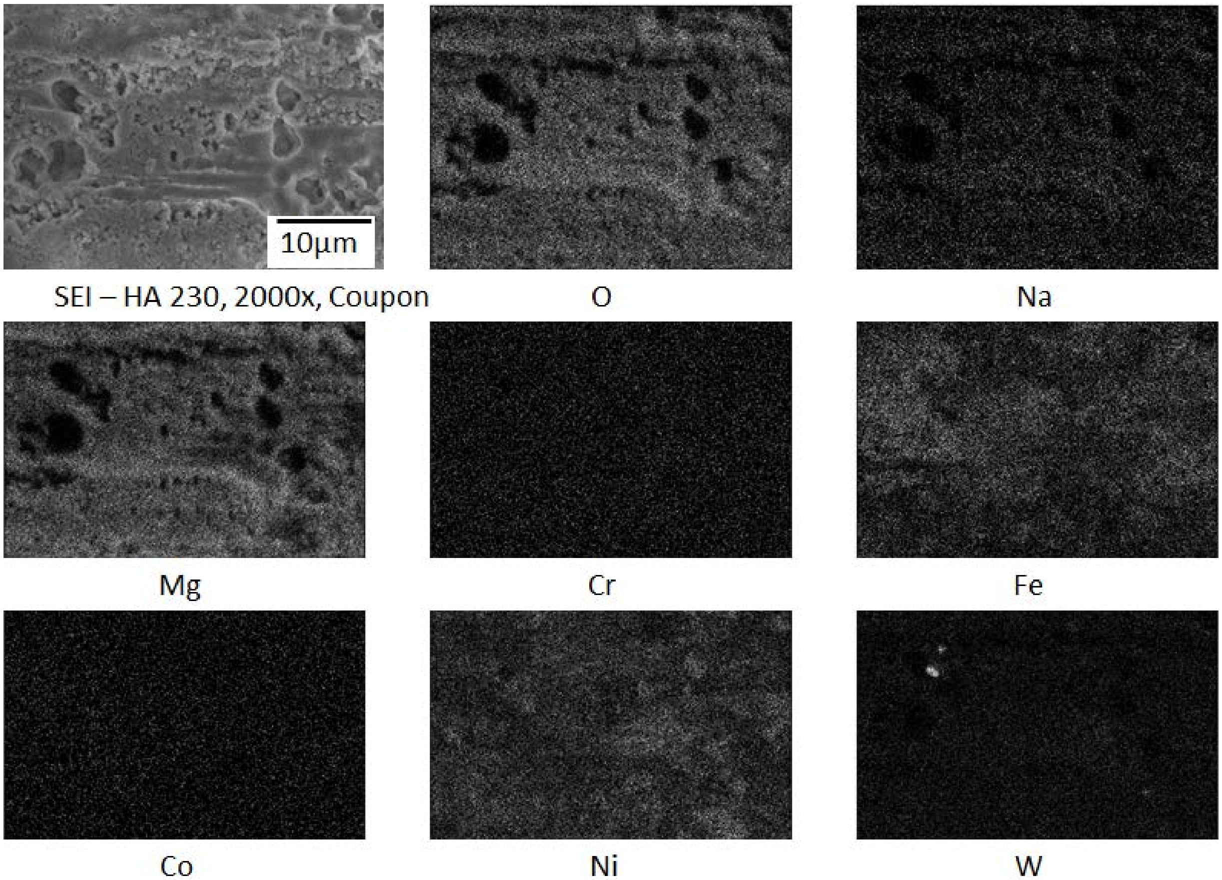

Figure 32: Haynes 230 had trace indications of pitting on the surface of the sample, which had not been observed in previous studies.

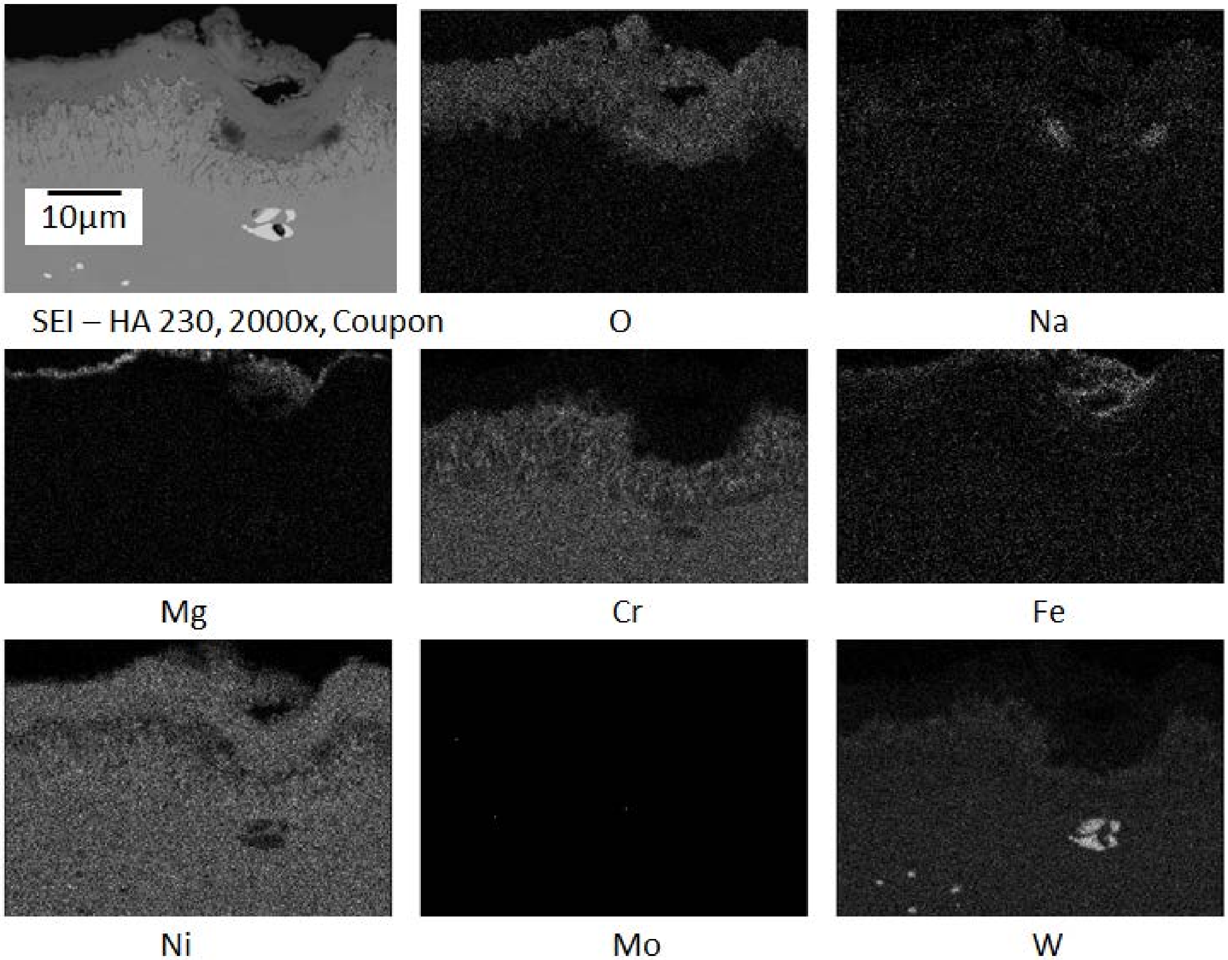

Figure 33: Haynes 230 cross-section, which is thought to be of a localized corrosion area. Note the sodium and iron enrichment of the area.

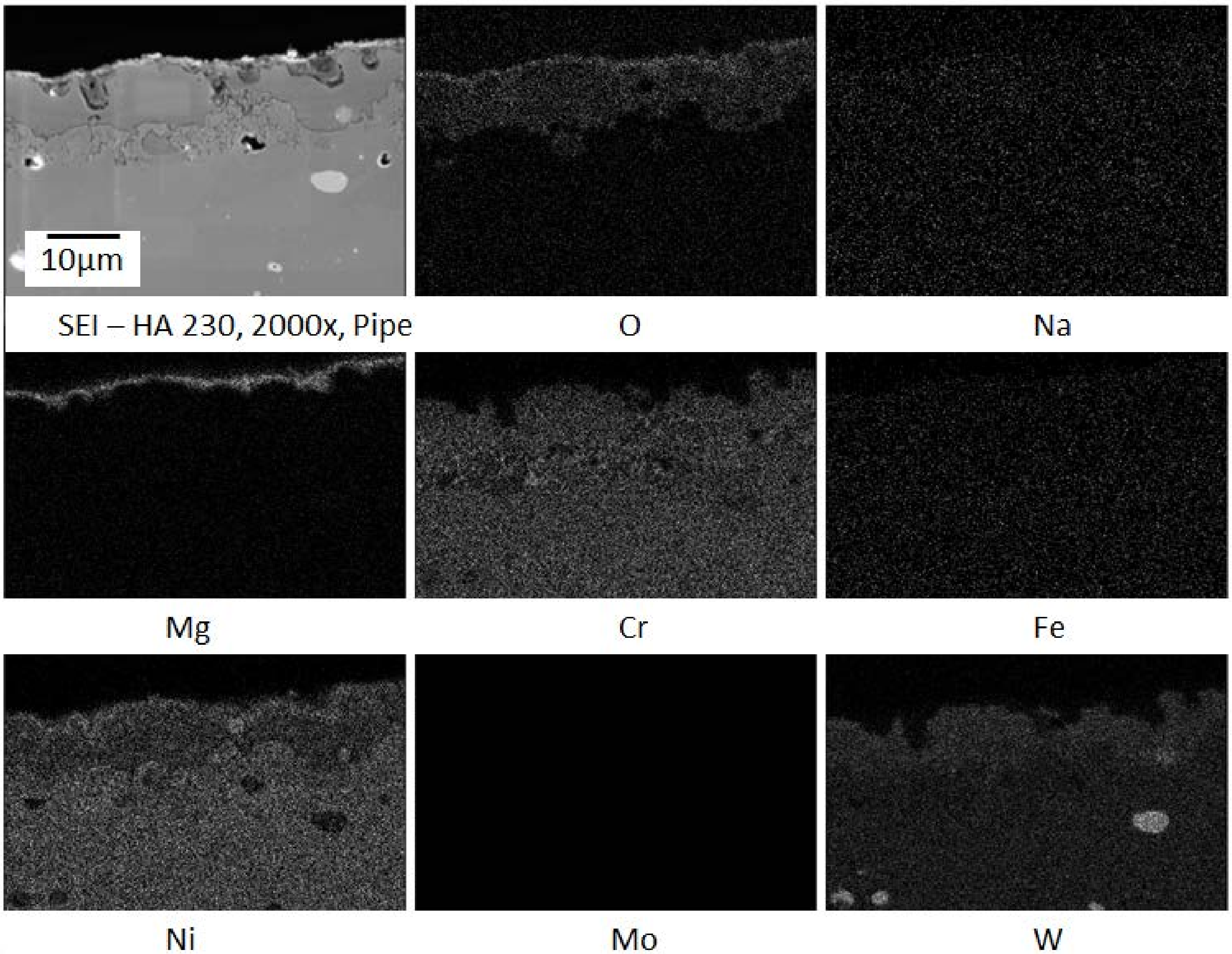

Figure 34: Haynes 230 pipe had a different microstructure as compared to HA230 coupons. The pipe had a tungsten-enriched oxidation layer, with no oxide stringers penetrating into the base alloy.

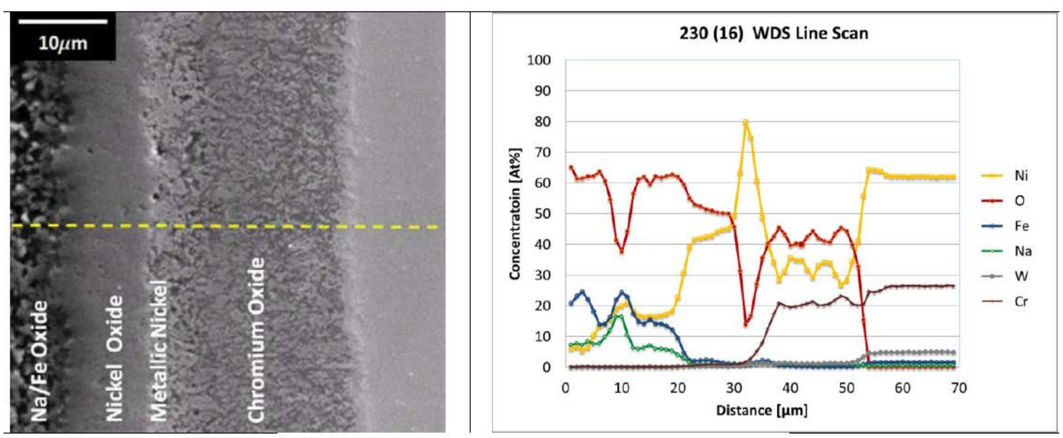

Figure 35: Haynes 230 after 500-hour static exposure in a 680°C binary salt (from [9]).

In625-SQ behaved in a similar fashion to grade In625 at 600°C, as shown in Figure 36, where NiO formed on the surface is the primary oxidation product. In the flowing environment, In625-SQ corroded more slowly, thus outperforming 347SS. This is likely due to the protective nature of NiO, which is more compact and adherent than iron oxides. Some localized attack was noted (see Figure 35), and appeared to be of a similar nature to Haynes 230. However, this behavior was only observed in a couple of locations and was difficult to even find during analysis.

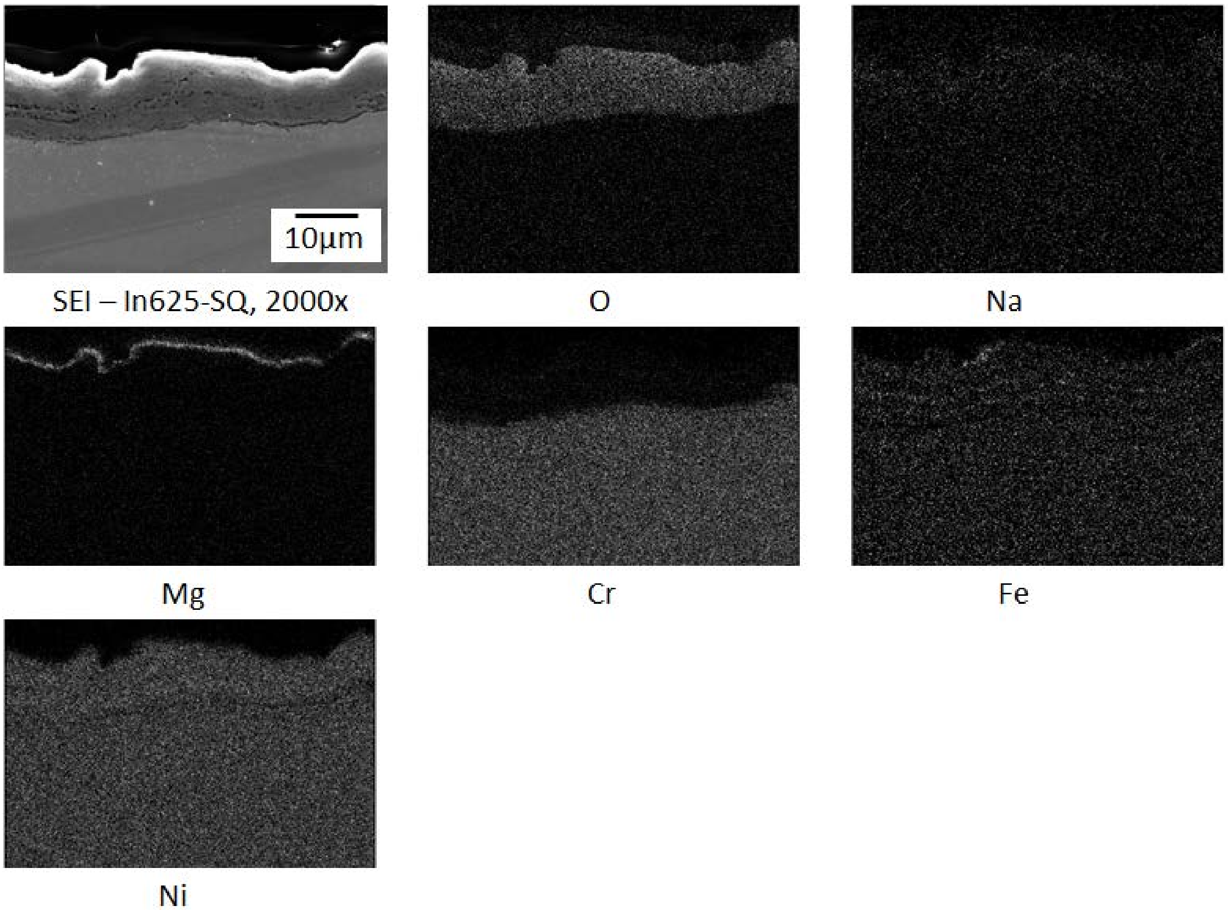

Figure 36: In625-SQ had similar microstructure as observed in previous studies [7], with the formation of a relatively thick NiO layer.

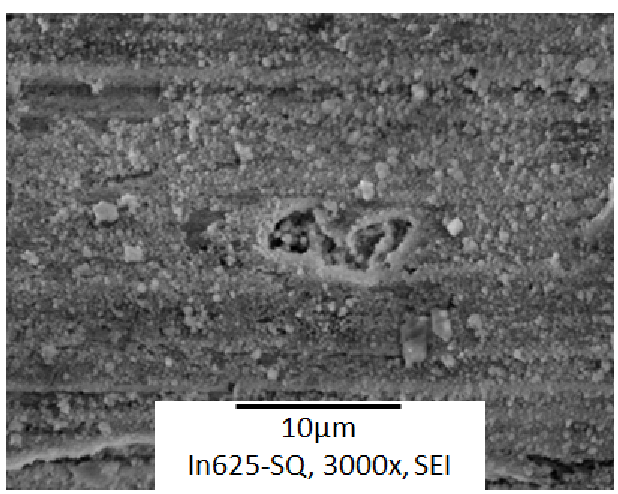

Figure 37: Small holes were observed that may indicate the presence of pitting.

Discussion of Results

Several trends emerged from the LOFTED corrosion tests. First, all alloys experienced higher corrosion in the flowing experiment than in the static tests. Exposure temperatures were slightly higher, approximately 10°C, however, this should not exclusively account for an order of magnitude increase in corrosion. Furthermore, this test also had high wall temperatures, at approximately 670°C. It is still unclear what the concentration of oxide in solution is in this arrangement versus in an isothermal, static melt at 600°C. It is expected that the LOFTED arrangement had a higher oxide concentration, therefore, coupled with flow, mass transport of species for reaction should be increased.

Second, corrosion morphologies on samples appear to have similar structures, as compared to static 600°C tests. Haynes 230 and In625-SQ did have some localized attack that may require further study to understand any root cause, although, after roughly 1000 hours, these structures were relatively sparse and quite shallow in comparison to the uniform corrosion.

Third, magnesium was found as a thin outer layer on all samples. Magnesium was likely in the form of MgO, as it is well known that 1) any magnesium nitrate decomposes above 480°C, and 2) standard practice in the operation of Solar Two was to hold at 540°C to further decompose the impurity[14]. Refined grade salt obtained from SQM had 0.02% - max magnesium (typical values of 0.006% magnesium), thus, using the maximum, approximately 0.3 lbm of Mg could be present in the melt. The Mg source may be the impurity content in the salt, which, with temperature and agitation, may be more soluble in the melt. Figure 37 indicates that MgO is, by far, the most thermodynamically stable, with the formation of mixed Cr/Mg oxides possible. The role of Mg in corrosion is still unclear, however a test to quickly assess this may be as simple as creating a solution of binary nitrate salt saturated with MgO, exposing samples for 500 hours, and then comparing to static 600°C tests.

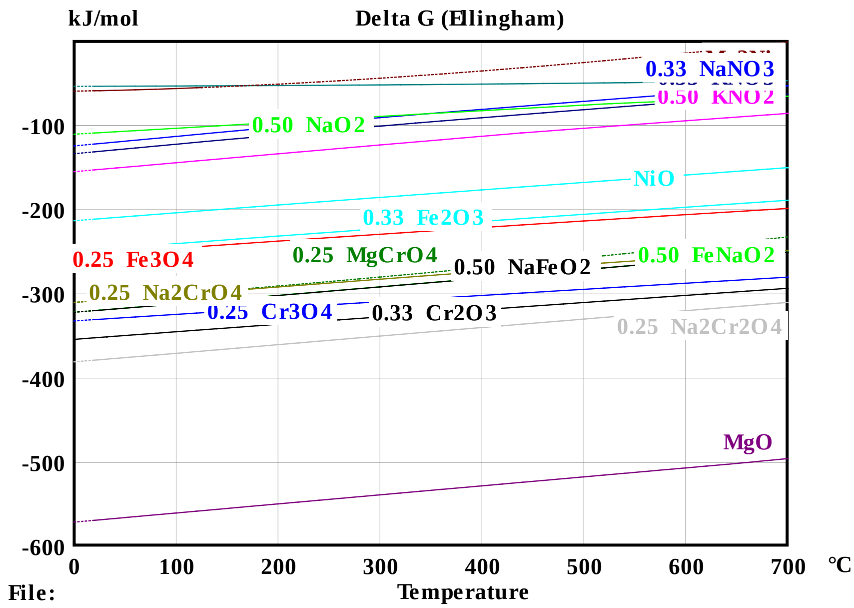

Figure 38: Ellingham diagram of a Na-K-Mg-Fe-Cr-Ni-O system. Only products of interest were included. The thermodynamic driving force for formation becomes larger as the Gibb's free energy becomes more negative.

This page intentionally left blank.

5. CONCLUSION

Flange and bolted connections in molten salt systems are known to be causes of salt leaks. This is mainly due to incompatible materials used for gasket materials and the elongation of bolts due to the heating and cooling (i.e. expansion and contraction of the metals). Bolt growth causes a leak path to form which salt permeates. Salt technology surveys, prior to designing the LOFTED system, led to the selection and use of Grayloc hubs, 316 SS, Schedule 40, 2-piece, 4-bolt clamps and seal ring, Inconel 718, silver. Operational experience from this test indicates that current salt technology has not adequately addressed this leak issue and all connections should continue to be welded in the future.

Similarly a pump and tank interface plate was designed allowing separation of the carbon steel pump plate from the 600 °C molten salt. This plate was bolted to both the tank and to the carbon steel pump plate. This interface plate also allowed placement of the pump into the tank. The plate should be welded to both the carbon steel pump plate and to the tank to avoid leaking issues.

The GEFRAN pressure transducers have not operated well in our other system at the NSTTF due to excessive heat at the diaphragm and the electronic components. These issues resulted in leaks at the bolted connection, inaccurate readings. Past attempts to thermally isolate the transducer from the molten salt by placement of a long standoff tube resulted in a Venturi-effect, causing a vacuum, which caused the diaphragm to fail.

This problem was solved by placing connecting a ¼ inch tube from the diaphragm and extending approximately 1/8 inch into the molten salt flow. The ¼ inch was placed inside of a 30 inch long ¾ inch diameter pipe that was allowed to leak slightly at the cold connection. Operational experience indicated that these design changes alleviated heat and vacuum issues, however more testing is needed to verify any resultant changes in accuracy.

The Krohne flow meter operated continuously with a salt inventory at 600°C. The reading from the meter appeared to be very consistent over the entire test period. The flow meter was not insulated, which allowed it be in thermal contact with surrounding and operate at temperatures lower than 600°C.

Total alkalinity (TA) methods to determine oxide content over time, using Na_2O_2 as a surrogate oxide, might be considered a first step in quantifying and evaluating the evolving salt chemistry, which inevitably happens during the course of operation. The TA method did not result in a one-to-one comparison of oxide unless a calibration curve was created to provide the correct conversion offset. TA data from the LOFTED test indicate a steady increase in oxide production over the course of the test, with the exception of the last measurement. At this point, the TA method should be used with caution. Although it is a viable methodology for correlating corrosion to oxide content, it is unclear which species dominate the reaction.

Corrosion rates in the flowing LOFTED set-up at approximately 610°C are 8 to 20 times more corrosive by comparison to 600°C static tests. The increased rate is attributed to oxide generation and mass transport specific to the LOFTED experimental design.

Metallographic results indicate that flat coupons have similar morphologies as compared to static, isothermal tests. Localized corrosion was noted on the Haynes 230 and In625-SQ, but more investigation is needed to understand the nature of this attack.

6. REFERENCES

1. Nissen, D.A., and D.E. Meeker, *NITRATE NITRITE CHEMISTRY IN NANO3-KNO3 MELTS.* INORGANIC CHEMISTRY, 1983. **22**(5): p. 716-721.

2. Lovering, D.G., *Molten salt technology*. 1982, New York: Plenum Press.

3. Nissen, D.A., *Chemistry of the binary nano-3/KNO-3 sodium-nitrate/potassium-nitrate system*, 1981, SAND81-8007, Sandia National Laboratories, Livermore, CA.

4. Cordaro Joseph, G., *Chemical Perspectives on Alkali and Earth Alkaline Nitrate and Nitrite Salts for Concentrated Solar Power Applications*, in *Green*2013. p. 9.

5. Stern, K.H., *EFFECT OF CATIONS ON THERMAL DECOMPOSITION OF SALTS WITH OXYANIONS - A SEMI-EMPIRICAL CORRELATION.* JOURNAL OF CHEMICAL EDUCATION, 1969. **46**(10): p. 645.

6. Kruizenga, A., and D. Gill, *Corrosion of Iron Stainless Steels in Molten Nitrate Salt.* Energy Procedia, 2014. **49**(0): p. 878-887.

7. Kruizenga, A.M., D.D. Gill, and M. LaFord, *Materials Corrosion of High Temperature Alloys Immersed in 600°C Binary Nitrate Salt*, 2013, SAND2013-2526, Sandia National Laboratories, Livermore, CA.

8. Kruizenga, A., D. Gill, and M. Laford. *Corrosion of austenitic alloys in binary 60/40 nitrate salt at 600°C*. in *ASME 2013 7th International Conference on Energy Sustainability, ES 2013 Collocated with the ASME 2013 Heat Transfer Summer Conference and the ASME 2013 11th International Conference on Fuel Cell Science, Engineering and Technology, July 14, 2013 - July 19, 2013*. 2013. Minneapolis, MN, United States: American Society of Mechanical Engineers.

9. Kruizenga, A.M., D.D. Gill, and M.E. LaFord, *Corrosion of high temperature alloys in solar salt at 400, 500, and 680°C*, 2013, SAND2013-8256, Sandia National Laboratories, Livermore, CA.

10. *Standard Practice for Preparing, Cleaning, and Evaluating Corrosion Test Specimens*, in *G1-03*2003, ASTM International.

11. Jones, D.A., *Principles and prevention of corrosion*. 1996, Upper Saddle River, NJ: Prentice Hall.

12. Bradshaw, R.W., and S.H. Goods, *Corrosion of alloys and metals by molten nitrates*, 2001, SAND2000-8727, Sandia National Laboratories, Livermore CA.

13. Deodeshmukh, V.P., S.J. Matthews, and D.L. Klarstrom, *High-temperature oxidation performance of a new alumina-forming Ni–Fe–Cr–Al alloy in flowing air.* International Journal of Hydrogen Energy, 2011. **36**(7): p. 4580-4587.

14. Pacheco, J.E., et al., *Final test and evaluation results from the Solar Two project*, 2002, SAND2002-0120, Sandia National Laboratories, Albuquerque, N. M.

This page intentionally left blank.

7. APPENDICES

PRODUCT DATA SHEET - INDUSTRIAL CHEMICALS

POTASSIUM NITRATE — Technical Grade - Prilled

CAS N°7757- 79 - 1

GENERAL DESCRIPTION	
CHEMICAL FORMULA	KNO_3
APPEARANCE	White Prills
INTERNAL CODE	NPP-T

CHEMICAL SPECIFICATIONS GUARANTEED				
PURITY	KNO_3	%	99.3	min
CHLORIDE	Cl	%	0.2	max

CHEMICAL SPECIFICATIONS TYPICAL			
SULFATE	SO_4	%	0.02
NITRITE	NO_2	%	< 0.002
IRON	Fe	ppm	< 5
COPPER	Cu	ppm	< 1
CHROMIUM	Cr	ppm	< 1
LEAD	Pb	ppm	< 5
ARSENIC	As	ppm	< 0.1
INSOLUBLES		%	0.02

TYPICAL SIEVE ANALYSIS (CUMULATIVE %)			
SIZE GUIDE NUMBER (SGN)			210 - 230
US Standard Sieve	Tyler	mm	
+ 7	+ 7	2.81	10%
+ 10	+ 9	2.00	65%
+ 16	+ 14	1.20	99%
- 20	- 20	< 0.85	< 1%

PHYSICAL PROPERTIES	
MOLECULAR WEIGHT	101.1
MELTING POINT	333 ℃
SOLUBILITY (in water at 20 ℃)	31.6 g/ 100 cm^3
DENSITY (Bulk)	1.28 ton (metric) /m^3
SPECIFIC GRAVITY	2.110

Code No. 0033 Version Nov-09

PRODUCT DATA SHEET - INDUSTRIAL CHEMICALS

SODIUM NITRATE — Industrial Grade - Prilled

CAS N°7631 - 99 - 4

GENERAL DESCRIPTION	
CHEMICAL FORMULA	$NaNO_3$
APPEARANCE	White Prills
INTERNAL CODE	SSI

CHEMICAL SPECIFICATIONS GUARANTEED				
PURITY (*)	$NaNO_3$	%	98	min
CHLORIDE	Cl	%	0.48	max

(*) Purity corresponds to N content expressed as NaNO3

CHEMICAL SPECIFICATIONS TYPICAL			
SULFATE	SO_4	%	0.15
NITRITE	NO_2	%	< 0.02
PERCHLORATE	ClO_4	%	0.1 - 0.3
POTASSIUM	K	%	1.35
IRON	Fe	ppm	< 5
COPPER	Cu	ppm	< 1
CHROMIUM	Cr	ppm	< 1
LEAD	Pb	ppm	< 5
ARSENIC	As	ppm	< 0.1
INSOLUBLES		%	0.1
MOISTURE		%	0.1

SCREEN ANALYSIS TYPICAL			
SIZE GUIDE NUMBER (SGN)			200
UNIFORMITY INDEX (UI)			48
US Standard Sieve	Tyler	mm	
+ 7	+ 7	2.81	5%
+ 8	+ 8	2.36	35%
+10	+ 9	2.00	63%
+12	+10	1.68	86%
+16	+14	1.20	97%
- 20	- 20	< 0.85	< 1%

Note: Measured at manufacturing site. Particle size can be affected by handling and transportation

PHYSICAL PROPERTIES		
MELTING POINT		308 ºC
SOLUBILITY (in water at 20 ºC)		88 g/100 cm3
DENSITY (Bulk)	Free Fall	1.22 ton (metric)/m3
	Tapped	1.30 ton (metric)/m3
ANGLE OF REPOSE		28°
SPECIFIC GRAVITY		2.257

Before using this product, please read the product specifications, the material safety data sheet and any other applicable product literature.
The conditions of your use and application of our products, technical assistance and information (whether verbal, written, or by way of production evaluations), including any suggested formulations and recommendations, are beyond our control. Therefore, it is imperative that you test our products, technical assistance and information to determine to your own satisfaction whether they are suitable for your intended uses and applications. This application-specific analysis at least must include testing to determine suitability from a technical as well as health, safety, and environmental standpoints. It is also not recommended that the product be used for any described purpose without verification by the user of compliance with all applicable laws, regulations and registration requirements. No warranty is made as to the accuracy of any data or statements contained herein. While this product is furnished in good faith, this product is provided to you without any representation or warranty, expressed or implied, as to quality, condition, utility, merchantability, completeness, suitability or fitness for any particular purpose or use or any other matter or thing whatsoever and without recourse against SQM in any event. Without limiting the generality of the foregoing, SQM specifically disclaims any responsibility or liability relating to the use of this product and shall not in any event, be liable for any special, incidental or consequential damages arising from such use.

Code No. 45 Version Jul-10

Figure 39: Refined grade salt used in LOFTED experiment.

7.1 Suggested follow on testing

To better simulate the corrosion characteristics expected in a commercial plant, a separate set of corrosion tests may be conducted after the conclusion of the experiment. The corrosion test might consist of the following steps:

1) An oxide level representing, for example, Year 5 in a commercial project is established in a salt bath. Corrosion tests are conducted on the candidate alloys for a representative period; perhaps 1000 hours.
2) The oxide level is increased to represent, for example, Year 10 in a commercial project. Corrosion tests are conducted on the candidate alloys for a second representative period.

These steps are repeated until the 30-year duration of a commercial project has been simulated, or until the corrosion rates are determined to be excessive.

As an adjunct to the supplemental corrosion tests, experiments in methods to reduce the oxide content of the salt might also be conducted. Potential approaches include the following:

1) Mix CO_2 with the salt to form sodium carbonate, as follows:

$$2\ Na^{+} + CO_2 + O^{--} \rightarrow Na_2CO_3$$

The solubility of the carbonate is relatively low, and the carbonate will precipitate from the salt inventory.

2) Mix the salt with nitric oxide (NO), which converts the oxide ion back to the nitrite ion, as follows:

$$O^{--} + NO \rightarrow NO_2^{-}$$

3) Expose the salt to carbon steel to form various iron oxides, as follows:

$$3\ O^{--} + 2\ Fe \rightarrow Fe_2O_3$$

The solubility of iron oxides is very low, and the iron oxides will precipitate from the salt inventory.

DISTRIBUTION

1 Bruce Kelly
Abengoa Solar LLC
One Kaiser Plaza, Suite 1675
Oakland, California 94612

1 Drake Tilley
Abengoa Solar LLC
1250 Simms Street, Unit 101
Lakewood, CO 80401

1 Mark Lausten
SunShot Initiative, U.S. Department of Energy
1000 Independence Avenue, SW EE-4S
Washington, DC 20585

1 Thomas Rueckert
SunShot Initiative, U.S. Department of Energy
1000 Independence Avenue, SW EE-4S
Washington, DC 20585

1	MS1127	William Kolb	6123
1	MS1127	Subhash Shinde	6123
1	MS1127	Joshua Christian	6123
1	MS9153	Timothy Shepodd	8220
1	MS9403	Alan Kruizenga	8223
1	MS9403	Adam Rowen	8223

1	MS0899	Technical Library	9536 (electronic copy)

Sandia National Laboratories